Sensing Issues in Civil Structural Health Monitoring

Edited by
Farhad Ansari

Springer

CSHM
UIC 2004

SENSING ISSUES IN CIVIL STRUCTURAL HEALTH MONITORING

Sensing Issues in Civil Structural Health Monitoring

Edited by

FARHAD ANSARI
University of Illinois,
Chicago, IL, U.S.A.

Springer

A C.I.P. Catalogue record for this book is available from the Library of Congress.

ISBN 1-4020-3660-4 (HB)
ISBN 1-4020-3661-2 (e-book)
ISBN 978-1-4020-3660-6 (HB)
ISBN 978-1-4020-3661-3 (e-book)

Published by Springer,
P.O. Box 17, 3300 AA Dordrecht, The Netherlands.

www.springeronline.com

Printed on acid-free paper

Printed in the Netherlands.

TABLE OF CONTENTS

FOREWORD

Civil infrastructure systems are generally the most expensive assets in any country, and these systems are deteriorating at an alarming rate. In addition, these systems have a long service life in comparison to most other commercial products. As well, the introduction of intelligent materials and innovative design approaches in these systems is painfully slow due to heavy reliance on traditional construction and maintenance practices, and the conservative nature of design codes. Feedback on the "state of the health" of constructed systems is practically nonexistent.

In the quest for lighter, stronger and corrosion-resistant structures, the replacement of ferrous materials by high-strength fibrous ones is being actively pursued in several countries around the world, both with respect to the design of new structures as well as for the rehabilitation and strengthening of existing ones. In North America, active research in the design of new highway bridges is focused on a number of specialty areas, including the replacement of steel reinforcing bars in concrete deck slabs by randomly distributed low-modulus fibers, and the replacement of steel prestressing cables for concrete components by tendons comprising super-strong fibers. Research is also being conducted on using FRPs to repair and strengthen existing structures.

By and large, today's bridges and roads are "deaf, dumb and blind"; and they are also in a state of disrepair due to inadequate maintenance, excessive loading, and adverse environmental conditions, both natural

and man-made. In the United States alone, there are more than 200,000 deficient bridges, and in Canada there are approximately 30,000. The first bridges instrumented with integrated FOSs were built in Germany about 15 years ago; these first-generation gauges only provided information about the change in total length of the instrumented component, and had very limited strain resolution. The current Fiber Bragg Grating (FBG) sensors, based on a passive spectral ratiometric approach using a low power and broad bandwidth light source, provide more detailed information. Now it is possible to interrogate many FOS sensors by using a novel multiplexing system to provide even dynamic data at a micro level.

In the past, the monitoring of structures was carried out by means of portable measuring devices carried to the site each time a set of readings was required. In recent years, remote monitoring techniques have been developed using lasers, FOSs and remote data collection and processing techniques. A researcher or maintenance engineer can now collect data without leaving the office. ISIS Canada has developed a software package for monitoring structures that can be accessed via the Internet. Using this technology, a number of structures, including bridges, overpasses, columns, and a parking structure, are currently being monitored in Canada.

The new discipline of Civionics is being developed by Civil Structural Engineers and Electrophotonics Engineers in order to lend validity and integrity to this process. Civionics will produce engineers with the knowledge to build "smart" structures containing the necessary structural health monitoring (SHM) equipment to provide much needed information related to the health of structures before major structural failures. This discipline will, thereby, assist engineers and others to realize the full benefits of monitoring civil engineering structures.

Realistically, it is true that consulting engineers and contractors will only invest in the development of the expertise created by graduates of the Civionics discipline when they can be assured that the prospects for business, both short term and long term, are good in this field. The ISIS Canada experience of integrating fiber optic sensors (FOS) and fiber reinforced polymers (FRP) into innovative structures that have been built across Canada demonstrates that these opportunities do exist.

For SHM to be successful and useful, specifications must be written on the entire process, starting from the system design to data collection. The Civionics specifications include the technical requirements for the SHM system including fiber optic sensors, cables, conduits, junction boxes and the control room. A specification for data collection and storage is currently being developed as well. This workshop will be a forum for reviewing the evolution of Civionics specifications as a result of several case studies of structural health monitoring projects in Canada.

There is an urgent need to take advantage of emerging technologies that have the potential for increasing the life of civil engineering structures and reducing maintenance costs. This workshop is in a position to make a substantial contribution toward this goal. The workshop should create an international network that intends to expend its resources over the next several years in advancing the widespread use of new technologies in infrastructure projects, mainly by judicious and innovative use of smart materials and intelligent sensing to build intelligent structures using the Civionics discipline to monitor these structures for their health.

My congratulations to the organizing committee of the workshop and, in particular, to Professor Farhad Ansari for inviting researchers, practitioners and owners to donate their precious time to become involved in the discussions to formulate a winning strategy to build the intelligent structures of the 21st century that will be economical to build and require less maintenance.

Aftab Mufti,
President
ISIS Canada
16th September 2004

PREFACE

Structural health monitoring (SHM) is emerging as an important element in managing the public works infrastructure systems such as bridges, tunnels, buildings, dams, and power plants. To a greater extent, infrastructure has become more reliant on SHM for myriads of reasons that include increased number of aging structures, bold concepts in design of innovative structures, use of new materials, increased costs associated with the maintenance, safety, and security as well as the need for effective post disaster condition surveys. A successful civil structural health-monitoring (CSHM) program involves selection and placement of sensors suitable for measurement of key parameters that influence the performance and health of the structural system. Survey of literature reveals development of a number of conventional and novel sensors for this purpose including optical fibers, MEMS, PZT and magnetic based sensors.

Despite recent developments in the engineering of innovative sensors a number of issues has limited their applications to civil engineering structures. Civil structures are inherently large in dimension, geometrically complex with different elements and joints, and composed of diverse materials. The response of structural elements is due to an assortment of perturbations and therefore the measurements of interest are not limited to strains and vibrations. For instance, measurement of importance in cable stays is force and the condition of strands, i.e. rupturing of the strands. Whereas detection of cracks, excessive deflections and corrosion in reinforcing bars is important in concrete elements and structural systems. Moreover, a number of major application areas in civil structures such as post seismic and disaster monitoring have received very little attention. It turns out that many of the novel sensor systems that have been developed over the past decade have the potential for effective health monitoring of

civil structures. In certain instances, the advanced sensory systems have been effectively employed for health monitoring of structural systems. However, in the majority of cases these successes have been sporadic mainly due to issues involved in practical adaptation of the new technologies in civil structural systems. The primary technological challenges that need to be resolved prior to full adaptation of the sensor systems for CSHM are highlighted below:

- Configuring the sensor for sensing parameters of relevance, i.e. cracks, forces, corrosion, deflections, etc.
- Sensor packaging for a diverse set of materials and structural elements such as concrete decks, rebars, steel cables, structural steel, FRP sheets and tendons
- Installation problems due to harsh construction environment
- Calibration and referencing for long term sensing
- Sensor packaging and durability
- Long-term stability and survivability
- Long term reliability
- Multiplexing and distributed sensing
- Dynamic range, spatial resolution and sensitivity
- Data acquisition, processing, and interpretation
- Sensor leads, junction boxes, monitoring stations, and other periphery systems for consideration during the construction process design
- Calibration and referencing for permanently embedded sensors

This list is not exhaustive, but it serves to illustrate some of the characteristic problems that need to be addressed for practical implementation of advanced sensing technologies to large structural systems. In essence, addressing these issues requires:

1) Synthesis of available sensing technologies and verification of their relevance to structural systems
2) Determination of the developmental stage of the technologies
3) Evaluation of the barriers that prevent implementation
4) Development of timelines for a coordinated R&D plan
5) Identification of appropriate test beds for demonstration projects
6) Development of Standards and Specifications

To accomplish this, an international organizing committee composed of leaders in CSHM technologies was asked to invite experts from their countries to gather at a workshop to present the current status of CSHM and to develop plans for applications of these technologies for condition monitoring of constructed facilities. This book is compilation of the state-of-the art as presented by these experts during the first CSHM workshop that was convened in Oahu, Hawaii in November 2004. Three separate technical committees worked on the development of R&D plans. Syntheses of their deliberations were presented to the workshop steering committee at the conclusion of the workshop. The members of the steering committee comprised of government decision makers, engineers, scientists and academicians with expertise in construction and maintenance of the public works infrastructure systems.

I am pleased to introduce the members of the international organizing committee, steering committee, and the technical committees of the workshop:

International Organizing Committee

Alessandro De Stefano, Politecnico di Torino, Italy
Wolfgang Habel, BAM, Germany
Hyun-Moo Koh, Seoul National University , Korea
Sung Kon Kim, Seoul National University of Technology, Korea
Aftab Mufti, ISIS Canada, University of Manitoba, Canada
JinPing Ou, Harbin Institute of Technology, China
Zhishen Wu, Ibaraki University, Japan

Steering Committee Members

Perumalsamy N. Balaguru, Committee Chair, Rutgers University, USA
Yukio Adachi, Hanshin Expressway Public Corporation, Japan
Steven Chase, Federal Highway Administration, USA
Hamid Ghasemi, Federal Highway Administration, USA
Bernd Hillemeier, Technical University of Berlin, Germany
Andrew Horosko, Ministry of Transportation, Canada
Sun Kon Kim, Seoul National University, Korea
Qingbin Li, Tsinghua University, China
Bojidar Yanev, New York City Department of Transportation, USA

Technical Committee Members

COMMITTEE - 1 SENSOR ATTRIBUTES AND PLACEMENT ISSUES	**COMMITTEE - 2** SENSOR RELIABILITY FOR LONG TERM MONITORING	**COMMITTEE - 3** STANDARDS AND SPECIFICATIONS
CO-CHAIRS: **B. BAKHT** AND **K. KAGEYAMA**	CO-CHAIRS **E. AKTAN** AND **S. NAZARIAN**	CO-CHAIRS **M. MOTAVELLI** AND **B. TALJSTEN**
LOREN CARD	**JINPING OU**	**IAN N. ROBERTSON,**
GAUR P. JOHNSON	**VISTASP M. KARBHARI**	**KONRAD BERGMEISTER**
MOHSEN A. ISSA	**WOLFGANG R. HABEL**	**INADA HIROSHI**
FRITZ BRUNNER	**ALEXIS MENDEZ**	**QINGBIN LI**
KARA PETERS	**ZHIJUN ZHANG**	**KAZUO HOTATE**
CHANGSEN SUN	**K. YOKOYAMA**	**SOHEIL NAZARIAN**
K. TATEISHI	**AKIRA TODOROKI**	**HIROSHI INADA**
SUMITRO SONARYO	**MING L. WANG**	**AHMAD SHUAIB**
SAIID SAIIDI	**HIROSHI KOBAYASHI**	**BERND HILLEMIEIER**
TAKASHI MATSUMOTO	**PETER CHANG**	**ZHISHEN WU**
DE STEFANO A.	**NABIL F. GRACE**	**PAOLO CLEMENTE**
PIERRE LABOSSIÈRE	**GAMIL TADROS**	**AFTAB A. MUFTI**
YUKIO ADACHI	**J.F. CHOO**	**STEVEN B. CHASE**
BOJIDAR YANEV	**SUNGKON KIM**	**JUNGWHEE LEE**
ROGER CHENG	**FRITZ K. BRUNNER**	**J.H. JANG**

Results from the work of technical committees will be synthesized in a report and disseminated to the public through a report to the National Science Foundation. The financial support of the National Science Foundation (NSF) for this workshop is greatly acknowledged. I am indebted to a number of organizations for their support and sponsorship of the workshop. These organizations include the American Concrete Institute (ACI), Canadian network of excellence, Intelligent Sensing for Innovative Structures (ISIS Canada), National Natural Sciences Foundation of China (NNSFC), and the newly formed International Society for Health Monitoring of Intelligent Infrastructure (ISHMII). The primary goal of ISHMII is to advance the understanding and the application of Structural Health Monitoring (SHM) in civil engineering infrastructure. In this respect, ISHMII provides the desirable forum for exchange of ideas. One of the recommendations of the workshop steering committee pertained to future sponsorships of the CSHM workshops by ISHMII. It takes motivated engineers to further the state-of-the-art in CSHM and I am sure that we are on the right path towards advancing our goals. I am grateful for the

enthusiastic support of the civil engineering community in making this workshop a success.

Farhad Ansari

Smart Sensors & NDT Laboratory
November 2004

Chapter I

Global Perspectives on Structural Health Monitoring of Civil Structures

ARE CIVIL STRUCTURAL ENGINEERS "RISK AVERSE"? CAN CIVIONICS HELP?

Aftab A. Mufti, Baidar Bakht, Gamil Tadros, Andrew T. Horosko, and Gordon Sparks

ISIS Canada Research Network, JMBT Structures Inc., SPECO Engineering, Deputy Minister, Manitoba Transportation & Government Services, Professor, Department of Civil Engineering, University of Saskatchewan

Abstract: This paper discusses the reasons civil engineers have for being conservative in their design and argues that structural health monitoring will assist in providing data that could realistically be used to calibrate load and strength factors leading to more efficient and economical designs.

Key words: conservative, data, decision, designs, efficient, risk, structural engineers, structural health monitoring, SHM.

1. RISK ASSOCIATED WITH CIVIL STRUCTURES

Before we try to answer the two questions posed in the title of our paper, we would like to consider the degrees of risks involved in various human endeavours, which are considered 'acceptable' by the society. For example, the table of the risk of death involved in various activities, as proposed by Melchers [**1**], is reproduced below in Table 1.

Notwithstanding the accuracy of the risk values given in Table 1, it is clear that the risk involved in the failure of completed civil structures is significantly smaller than that involved, for example, in air travel. It is

Farhad Ansari (ed.), Sensing Issues in Civil Structural Health Monitoring, 3–12.

Table 1. Risks involved in various activities (Melchers, 1987)

Activity	**Risk (/ million / year)**
Alpine Climbing	1500 – 2000
Swimming	120
Smoking	1000
Air Travel	24
Car Travel	200
Coal Mining	300
Construction	150 – 440
Manufacturing	4000
Building Fires	8 – 24
Structural Failures	0.1

recalled that the civil structures include bridges, public buildings, dams, offshore platforms and power plants. The glaring differences between risks involved in various endeavours of the human society lead to another set of questions:

- Are the low levels of risks associated with completed civil structures fixed by the society?

- Or are these risk levels fixed by the designers of civil structures themselves because they are wary of taking undue risks?

It is true that the public does not expect civil structures to ever fail. However, we suspect that the low risk levels associated with completed civil structures are a result of a combination of both the demands of society and also the awareness of the structural engineer. Unlike manufactured machines with usually well tested prototypes, each structure is unique and nearly always without means to monitor its performance during its service life under loads and circumstances, which are more difficult to forecast than those for machines. We would like to make a case for the structural health monitoring (SHM) of important civil structures, such as large bridges and public buildings. They could be monitored on a continuous basis, thus eliminating certain unknowns about their performance, which could and

does change with time. In making a case for the SHM of important civil structures, we foresee the slight increase in the notional, rather than the actual, risk of failure in these structures, but a significant reduction in the capital cost that society has to incur partly to construct and largely to maintain its infrastructure.

2. CIVIL STRUCTURAL DESIGN PROCESS

Traditionally, structural components had been designed by the working stress method, which requires that the maximum stress due to nominal dead loads and live 'service' loads is a fraction of the maximum stress that the component can withstand. The ratio of the failure stress to the 'actual' stress was and is still known as the factor of safety. As long as the factor of safety was a sufficiently large number, say 2 or 3, the design was deemed to be safe. While the working stress design has served the engineering community well for a long time, it has led to structures with non-uniform margins of safety. For example, if long- and short-span components were designed to the same design specifications, or codes, the long-span components would have considerably larger margins of safety than their short-span counterparts. This would be so because the designs of large span components are governed by dead loads, which can be forecast with more certainty than live loads, which govern the design of short-span components.

Works of researchers such as Cornell and Lind in the late 1960's and early 1970's laid the foundations for modern structural design codes, which are based on the concept of structural reliability [**2**]. In some parts of Europe and in Canada, the philosophy incorporating probabilistic-based design is referred to as the limit states design method; and in the USA, the same method is referred to the load and resistance factor design (LRFD) method. The first limit states design code for bridge design in Canada was the Ontario Highway Bridge Design Code [**3**], introduced in 1979, followed by two editions, and then by the Canadian Highway Bridge Design Code [**4**]. The LRFD method was introduced for bridge design by the AASHTO Specifications in 1994 [**5**].

It is important to note that the working stress method, which is still practiced in many parts of the USA as well as many other countries, was used to design a very large part of the current stock of infrastructure in practically every country. The earlier working stress design methods, requiring manual calculations and based on simplifying assumptions, were usually quite conservative. Today, the benefits of such conservatism can be exploited after they have been identified especially by careful use of SHM.

Similar to several other modern limit states design codes, the Canadian and American bridge design codes relate only to the notional safety margin

of individual components. The safety margin, quantified by the dimensionless safety index β, relates to probability of failure of the component, and is determined by the statistical properties of variable resistance *R* of the component, and those of *S*, the effects of the combination of loads, which are also subjected to statistical variations.

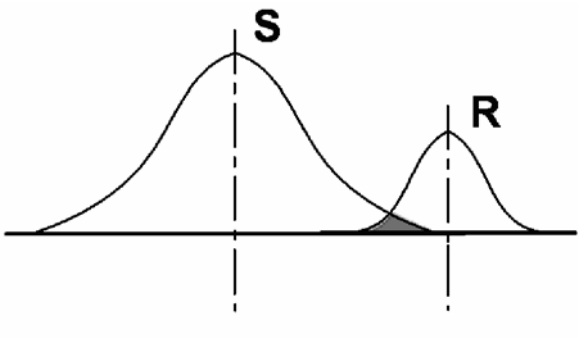

Figure 1. Probability of failure of a structural component

As illustrated in Figure 1, the distributions of *R* and *S* are likely to overlap, indicating a certain probability of failure. The load and resistance factors specified in a structural design code determine the value of β for the components of structures designed by the code. After determining by back calculations that the value of β for components of existing bridges are 3.5 or greater, it was agreed amongst the experts in the field that components of new bridges should be designed for β = about 3.5. Both the Canadian and American bridge design codes are generally calibrated to β = 3.5 (see Fig. 2), which corresponds to the notional probability of failure of a component of 1 in nearly 2,000 during the lifetime of the bridge. Considering the lifetime of a bridge to be 75 years, the probability of failure corresponding to β = 3.5 translates to one failure in about 150,000/year. The fact that this probability of failure is significantly larger than the probability of failure of one in 10 million/year for completed structures (Table 1), underscores two very important points with respect to bridges, in particular:

- β relates only to the notional failure of a component; the failure of the combination of components, being a system, has a much smaller probability of failure; and

- since most failures are caused by extreme events, such as those relating to hydraulics, β should not be taken as the real measure of the safety of the structure.

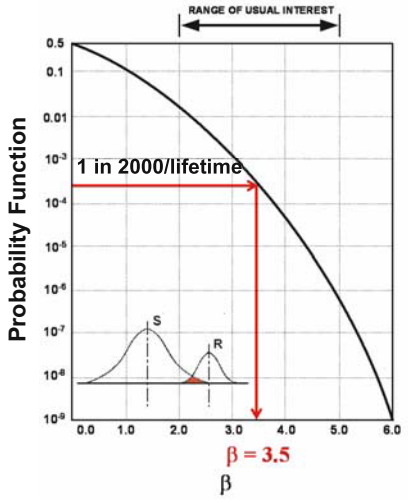

Figure 2. Safety index beta and probability of failure

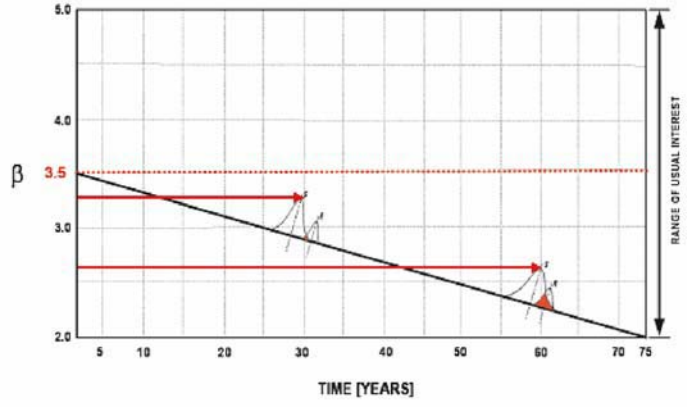

Figure 3. Reduction in safety index with time

The resistance of a structure, say a bridge, can reduce with time, due to environmental and other time dependent effects, with the result that the *R* distribution shown in Figure 1 moves to the left. Similarly, the live loads that a bridge is called upon to carry can also increase with time, and has been experienced in Canada with changes in vehicle weight regulations demanded by the economics of weight hauling by highway trucks. The increase in vehicle weights causes the *S* curve in Figure 1 to move to the right. As illustrated in Figure 3, the net result of the decrease of resistance and increase of loads over time is the increase of the overlapping areas of two curves. Hence, it can be seen that the notional safety indices of the

components of a bridge can decrease with time. Should such a reduction in the safety index always give us a cause for concern? Fortunately, we can continue to use a bridge even if its safety index is smaller than, say 3.5, but only if we have reliable knowledge about the structure. In pioneering and ground breaking work, Bakht and Jaeger [**6**] pointed out that each time a bridge was tested surprising results were observed. Its true behaviour was different than the original design.

The CHBDC (2000) has a section on the evaluation of bridges, which is based on the concept of a target reliability index that can change with (a) system behaviour, (b) component behaviour, and (c) the level of inspection. The system behaviour relates to the effect of the failure of a component to the failure of the whole structure; the component behaviour corresponds to the ductility of its failure; and the inspection level refers to degree of confidence in the inspection process in determining the actual condition of the bridge and its components. The effect of the three factors on the target reliability index can be explained with the help of two examples.

In the first example, the component under consideration is critical to the safety of the entire structure. It can fail suddenly, such as in shear or by buckling. The component is also not inspectable, possibly because it is hidden. For such a component, the target reliability index β is required by the CHBDC (2000) to be 4.00. For normal traffic, the live load factor α_L corresponding to β of 4.00 is 1.77.

For the second example, the component is such that its failure does not affect the failure of the whole structure. Also, it is subjected to gradual failure with warning of probable failure. The inspection of the component is carried out by the evaluator and the calculations for the final evaluation account for all information during this inspection. For such a component, the target reliability index β is required by the CHBDC (2000) to be 2.50 with the live load factor α_L for normal traffic being 1.35.

It can be seen that depending upon the system and element behaviour and confidence on inspection, the difference between two useable live load capacities can be as large as about 24%. If the condition of a component of a structure were determined with the help of sensors in an SHM system, the degree of confidence in the determination will be greater than in any visual inspection, with the consequence that the evaluator of the component will be able to utilize a larger portion of its live load capacity.

The concept of the target reliability index changing with the inspection level does not exist in design of new structures. Yet, it can be appreciated that the level of risk that a designer takes with a new design can be suitably increased, and the capital cost of the structure decreased, if he/she were confident that the condition of the structure and the load that it receives will

be determined continually and accurately by an SHM system. Drawing upon the comparison between a fully instrumented aerospace structure and civil structure without any instruments, we state confidently that the designers of civil structures are risk-averse to an extent because of the absence of information about the field performance of these structures.

3. STRUCTURAL HEALTH MONITORING SYSTEMS

The second question posed in the title of our paper – Can civionics help (in making designers of civil structure less risk-averse)? – is also answered affirmatively by the above discussion. The term 'civionics' was coined recently to be parallel to 'avionics,' which is defined in American English language dictionaries to denote the application of electronics to aviation and astronautics. 'Civionics' refers to the application of electronics to civil structures (to determine the state of their health). The use of sensors to monitor the response of a structure or its model is not new, nor is bridge evaluation by field testing, which includes both diagnostic and proof testing. What is new, however, is SHM through the use of civionics. It is recalled that the purpose of SHM, according to Mufti [**7**], is to monitor the in-situ behaviour of a structure accurately and efficiently to determine its health or condition. SHM is the integration of a sensory system, a data acquisition system, a data processing system, an archiving system, a communications system, and a damage detection and modelling system to acquire knowledge, either on demand or on a continual basis, regarding the in-service performance of structures.

In the past, civil engineers have maintained the integrity of civil structures by means of a system of manual inspection, nondestructive evaluation (NDE) and interpretation of data using conventional technologies. The profession has relied heavily on evaluation parameters given in codes of practice that lead to conservative and often costly conclusions. The current practice has resulted in a North American stock of the civil structures whose health is not easy to monitor. For example, many bridges and large buildings constructed in earthquake-prone areas cannot be opened immediately after a seismic event due to the time and cost involved in performing extensive safety checks. The result is that we cannot be sure how safe these structures are and whether they should continue to be in service.

In order to remain competitive in today's global economic environment, the owners of civil structures need to minimize out-of-service time for their structures. This is true whether a service disruption results from periodic inspections to detect deterioration resulting from normal operations or from inspections following extreme events, such as strong-motion earthquakes,

hurricanes, or flash floods. In the evaluation of any structural system, it is important to be able to assess specific performance issues related to serviceability, reliability and durability. To effectively quantify the system's performance requires a means to monitor and evaluate the integrity of these large civil structures while in service. This information will allow owners to allocate resources towards repair, replacement or rehabilitation of their structures. This information will also aid in future projects, as it will help to estimate the life cycle costs of the structural system compared to the initial cost. The essence of the SHM technology, therefore, is to develop autonomous systems for continuous monitoring, inspection and damage detection of structures. The results of structural conditions should be automatically reported through a local network or to a remote monitoring centre. Clearly, the development of such a system will involve many disciplines including structures, materials, damage detection, sensors, data collection and intelligent processing, computers, and communication as is shown in Figure 4.

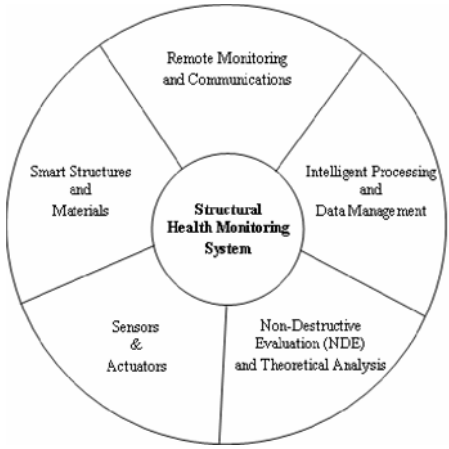

Figure 4. The basic components of SHM Systems

Although conventional NDE can be considered within the framework of SHM, there is a difference in terms of data interpretation between the traditional NDE and SHM. The traditional NDE techniques tend to use direct measurements at discrete time intervals to determine the physical condition of structures. For example, bridge testing could either be diagnostic or involve proof loading. For this type of evaluation, a history data is generally not required. SHM techniques use continuous monitoring and assess the change in the measurements at the same location at two different times to identify the condition of a structure. Hence, a history of data is crucial to the

technique. The direct benefit potential from SHM systems is enormous and includes:

- monitoring and evaluating structures in real-time under service conditions;
- reducing downtime;
- improving safety and reliability; and
- reducing maintenance costs.

With the reduced downtime and improved reliability, in-service structures can be used more productively with less cost.

The following example highlights a statue that itself is a simple structure but embodies the concept of SHM.

4. CIVIONICS INTO PRACTICE

For SHM to become part of civil structural engineering, it should include civionics. Formal definition are given below to encourage the development of Civionics as an academic discipline in Canadian universities and technical colleges.

The new discipline of civionics must be developed by civil structural engineers and electrophotonics engineers to lend validity and integrity to the process. Civionics will provide engineers with the knowledge to build "smart" structures containing the necessary SHM equipment to provide much needed information related to the health of structures before things go wrong. This discipline will, thereby, assist engineers and others to realize the full benefits of monitoring civil engineering structures.

Realistically, it is true that consulting engineers and contractors will only invest in the development of the expertise created by graduates of the civionics discipline when they can be assured that the prospects for business are good in this field. The ISIS Canada experience of integrating FOSs and FRPs into innovative structures that have been built across Canada demonstrates that these opportunities do exist.

5. CONCLUSIONS AND RECOMMENDATIONS

The answer to the question, *"Would civionics help to change the "risk shy" culture of civil structural engineers?"* is a conditional yes. However, the civionics discipline needs to be further developed.

As mentioned earlier, ISIS Canada intends to significantly change the design and construction of civil engineering structures. For changes in design and construction to be accepted, it is compulsory that innovative structures be monitored for their health so that the necessary data store can be developed. To assist in achieving this goal, ISIS Canada is developing a new discipline, which integrates Civil Engineering and Electrophotonics under the combined banner of Civionics. In addition, ISIS Canada is developing new Civionics specifications and guidelines for construction engineers [**10**].

We also believe the change in culture would lead to new innovations in civil engineering technologies and methods.

ACKNOWLEDGMENTS

The financial assistance of NCE, ISIS Canada and NSERC is gratefully acknowledged. The assistance of Ms. Nancy Fehr, Executive Assistant to the President of ISIS Canada is also acknowledged with gratitude.

REFERENCES

1. Melchers, R.E., Structural Reliability and Analysis Prediction, Ellis Horwood Ltd., (Division of John Wiley & Sons), UK, 1987.
2. Nowak, A.S. and Collins, K.R., Reliability of Structures, McGraw-Hill, New York, USA, 2000.
3. OHBDC, Ontario Highway Bridge Design Code, Ontario, Canada, 1979.
4. (CHBDC) Canadian Highway Bridge Design Code, Canadian Standard Association, Ontario, Canada, 2000.
5. AASHTO, AASHTO LRFD Bridge Design Specifications, American Association of State Highway and Transportation Officials, Washington, D.C., 1994.
6. Bakht, B. and Jaeger, L.G., Bridge Testing – a surprise every time. ASCE Journal of Structural Engineering, 115(5), 1990.
7. Mufti, A.A. "Guidelines for Structural Health Monitoring", Winnipeg, Manitoba: ISIS Canada, 2001.
8. www.isiscanada.com, ISIS Canada Research Network Web Site, Winnipeg, Manitoba, Canada, 2003.
9. Mufti, A.A., "Integration of Sensing in Civil Engineering Structures: Development of the New Discipline of Civionics," Proceedings for the First International Conference on Structural Health Monitoring and Intelligent Infrastructure (SHMII-1), November 13-15, 2003.
10. Rivera, E., Mufti A.A. and Thomson, D., Civionics Specifications, Design Manual, ISIS Canada Research Network, Winnipeg, Manitoba, Canada, 2004.

MONITORING TECHNOLOGIES FOR MAINTENANCE AND MANAGEMENT OF URBAN HIGHWAYS IN JAPAN

A Case of Hanshin Expressway Public Corporation

Yukio Adachi
Hanshin Expressway Public Corporation, Japan

Abstract: The development of inspection and monitoring techniques for civil infrastructure systems, such as highway viaducts, is an urgent need to diagnose the condition of the deteriorating structures or seismically damaged structures. This paper introduces the advanced non-destructive inspection techniques for seismically damaged structure by 1995 Hyogo-ken Nanbu earthquake and also advanced maintenance monitoring system for deteriorating structures developed by Hanshin expressway public corporation, Japan.

Key words: Highway structures, Monitoring, Inspection, Maintenance, Seismic damage

1. INTRODUCTION

Since its foundation in 1962, the Hanshin Expressway Public Corporation (HEPC) has built urban highways in the Osaka and Kobe metropolitan area in Japan for 42 years. The expressway network currently expands 233.8 km in total length and is traveled by about 900,000 vehicles or about 1,300,000 people on average per day. As shown in Figures 1 and 2, of the 233.8 km currently in service 86% are elevated structures and sections in service for 20 years or longer account for more than 50% of the Hanshin Expressway structures. With these structures getting older, maintenance becomes increasingly important in order to consistently keep them sound. Photo 1 and 2 show the typical examples of the deterioration of structures. Based on the background above, development of inspection and monitoring techniques for deteriorating structures are urgent need for maintenance activities.

Farhad Ansari (ed.), Sensing Issues in Civil Structural Health Monitoring, 13–22.

Development of inspection and monitoring techniques is also needed for risk management. HEPC experienced tremendous seismic damage shown in Photo 3 due to 1995 Hyogo-ken Nanbu earthquake. One third of the piers in Kobe area were needed to be re-constructed. The number of the piers for reconstruction is over 300. The damage assessment of the structure is the essential activity for the restoration. Damage information was obtained by the eye-inspection. Eve-inspection is a reliable method but it needs much time and no meaning for under ground part of the structure such as piles and underground part of the pier as shown in Photo 4. Therefore, development of inspection and monitoring techniques for seismically damaged structures are also urgent need for risk management of expressway network.

This paper introduces the monitoring technologies for maintenance and management of urban highways developed by Hanshin expressway public corporation.

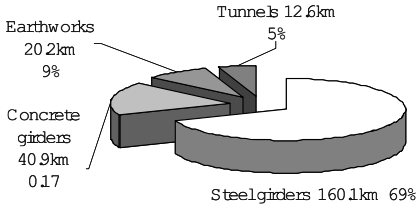

Figure 2. Hanshin expressway by age

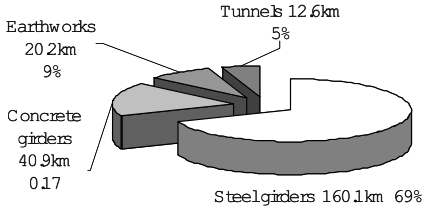

Figure 2. Structural types

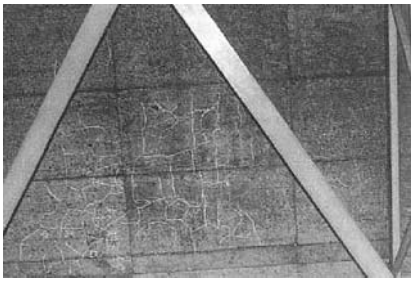

Photo 2. Deterioration of slab panels

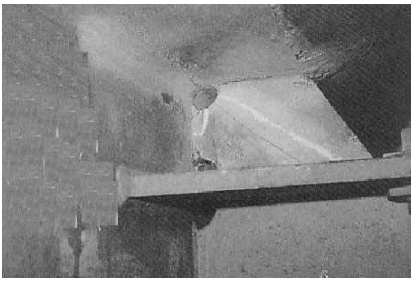

Photo 2. Fatigue cracks of steel girders

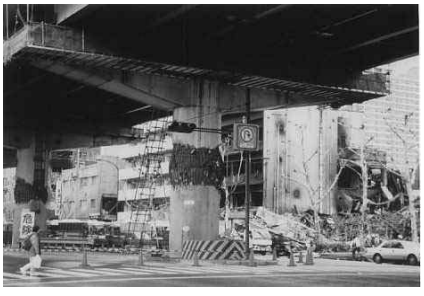

Photo 3. Seismically damaged bridge

Photo 4. Hidden seismic damage of column

2. MAINTENANCE TECHNIQUES

2.1 Intelligent road surface inspection system

Pavement cracks, potholes, ruts, and other road surface damages can greatly impair driving safety and comfort traffic flow, causing hydroplaning or slipping of the steering wheel. These also allow water to collect beneath the pavement, which accelerates the deterioration of the pavement and the bridge deck. Thus finding and repairing such damage at an early stage is extremely important in maintaining bridges in good condition.

Daily inspection patrols involving visual inspection of the road surface has been carried out for road surface inspection, but is reliant on the skill level of inspectors. Therefore HEPC developed intelligent road surface inspection system for intelligent and reliable inspection.

Figure 3 shows the system configuration. The inspection vehicle is mounted with a CCD camera, laser emitter equipment, and image processing unit, as well as VICS (Vehicle Information Communication System) receivers and wheel speed sensors to get position information. The inspection vehicle travels along the roadway according to traffic flow and assesses the condition of the road surface in real time. Data on the road surface—information on the type and location of damage and images of damage—are stored on the road damage collection terminal. The inspector transfers to the Maintenance Management Database System in the form of inspection data via the road damage confirmation terminal.

Images received from the CCD camera mounted to the inspection vehicle are analyzed using image processing to identify road damage such as cracks and potholes. Figure 4 shows the road damage detection procedure. Images

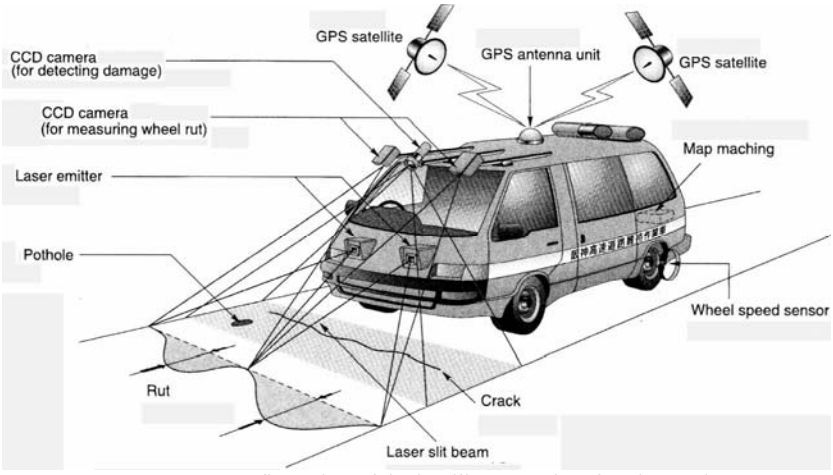

Figure 3. System configuration of the intelligent road surface inspection system

of the road surface are separated by gradation conversion processing into the white/yellow painted sections and differential images. The differential images are masked using the painted section, then the remaining differential images are analyzed for damage by area-based analysis and horizontal/vertical profiling. Ruts in the road surface are measured with a laser using the light section method as shown in Figure 5. The light source is a laser beam diffused into a fan shape. The camera measures distortions in the laser.

2.2 Inspection robot

For the maintenance of highway structures, the inspection activities are the most important. There are four categories of inspection: initial, daily, periodic and extra. The purpose of daily inspection is to obtain general conditions of damaged road structures at an early stage, and periodic inspection looks into details of the detected damage to estimate functional

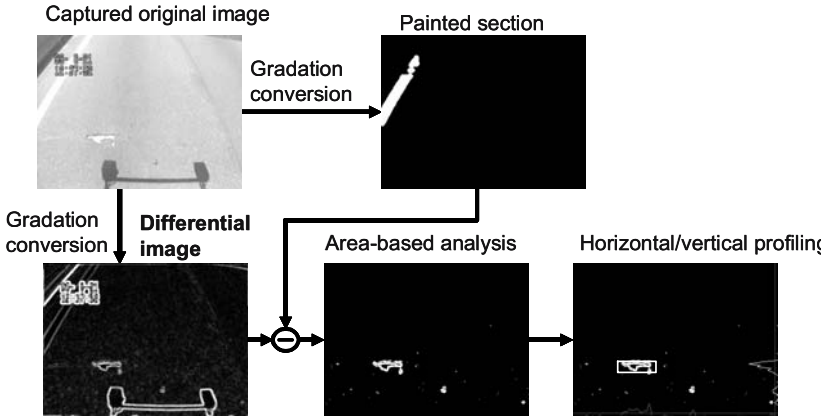

Figure 4. Road surface damage detection flow

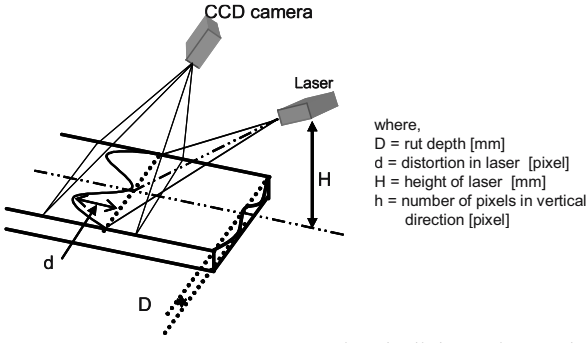

Figure 5. Measurement using the light section method

deterioration of the structures. The maintenance activities are performed mainly based on the periodical inspection results.

However, over 40% percent of the cost of the periodic inspection as shown in Figure 6 is for temporary facility just for performing inspection. In order to reduce the inspection cost, inspection robot has been developed. The robot shown in Photo 5 which is a trial production for steel I shaped girders as shown in Figure 7 can inspect the crack distribution and damage level of concrete slabs and crack propagation at the steel girder by CCD camera and also can move to the inspection point by itself by traveling with hanging on the lower flange of the girder.

2.3 Database system

Road structure maintenance activities by the HEPC consist of inspection, judgment of necessity for repair, and implementation of repair. For this, accumulation of repair and inspection data is very important, while as-built data of individual structures is also essential. Repair and maintenance of road structures require a wide variety of information, and the amount of information to be stored increases rapidly as new routes are opened for service.

As a part of electronic data processing for efficient management of maintenance information, the HEPC started to create a database of basic maintenance information in the fiscal year 1990 and completed a first-phase database system in the fiscal year 1993. As put into practical use, the system was found to be significantly poor in data compatibility and also to lack

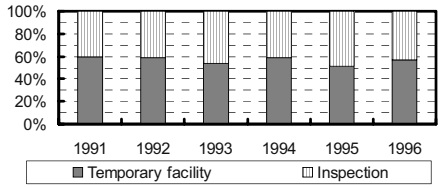

Figure 6. Measurement using the light section method

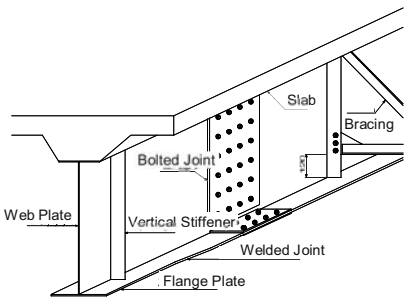

Figure 7. Steel I-shaped girder

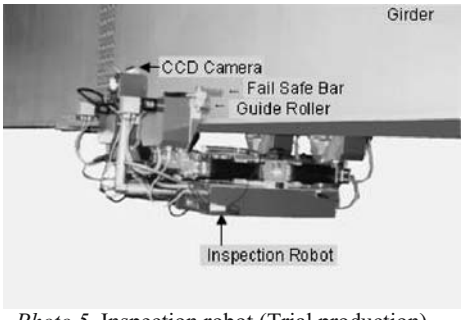

Photo 5. Inspection robot (Trial production)

capacity for general application which is needed for promoting effective use of the system in the future. To address these issues, the original database was enhanced by making use of significant progress in computer technology to the current maintenance information management system which consists of the maintenance information database and the management system. Figure 7 shows the configuration of the current maintenance information management system. This database system stores all information about assets, inspection results and repair works in electronic forms for the maintenance management of the structures. The data is exchanged with related offices through a client-server system.

3. SEISMIC DAMAGE DETECTION TECHNIQUES

3.1 Pile damage detection techniques

A lot of elevated structures suffered significant damage from the Great Hanshin Earthquake in January 1995. The size of the region affected and severity were extensive. What is the most notable in this event is that a lot of damage was found to the piles of viaducts. There is no inspection technique firmly developed yet at that time. Therefore the damage of the pile had to be inspected without sufficient preparation in terms of both inspection and evaluation methods. Three inspection methods were primary employed. The most reliable method of inspection was direct visual inspection which was expensive and took time, so two advanced non-destructive inspection techniques; bored-hole camera inspection and pile integrity inspection that

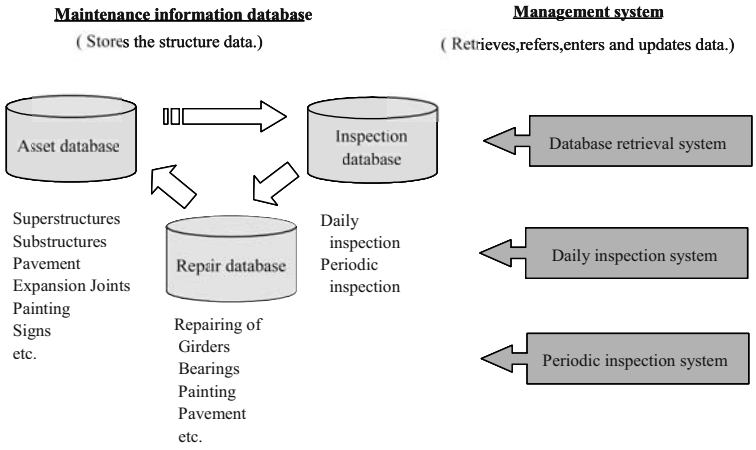

Figure 8. Maintenance information management system configuration

required much less time, were mostly employed.

Direct visual inspection was the most direct and reliable way in determining the damage because it allows their direct observation by excavating and exposing the pile top section, though only externally. Orientation and intensity of cracks in the piles can be indispensable in determining the degree of damage. On the other hand, due to the need for excavation, the benefits of this inspection method depend on the labor and equipment available for excavation, and inspection area is only limited to the pile top section, not the entire length.

An alternative method was an indirect visual method using a bored-hole camera, which allows inexpensive, rapid investigation to piles to a similar extent to direct visual inspection. Here, a hole is bored down the center of the target pile and a small camera is inserted in the hole to allow assessment of the conditions inside based on observed inside crack width and inside crack density.

The principle of the pile integrity test is to generate an impact wave at the pile top with a plastic hammer and measure the reflected wave with an accelerometer. And the basic idea of this test method is to analyze a reflected

Photo 6. Direct inspection for pile damage

Photo 7. Typical pile damage

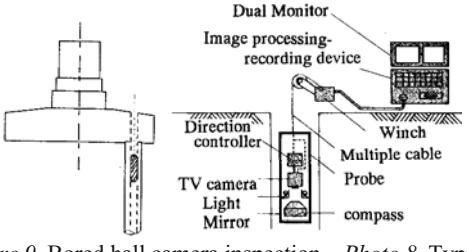

Figure 9. Bored hall camera inspection

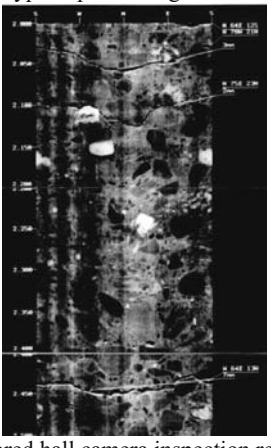

Photo 8. Typical bored hall camera inspection result

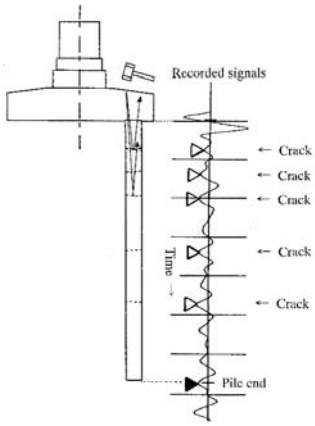

Figure 10. Pile integrity test

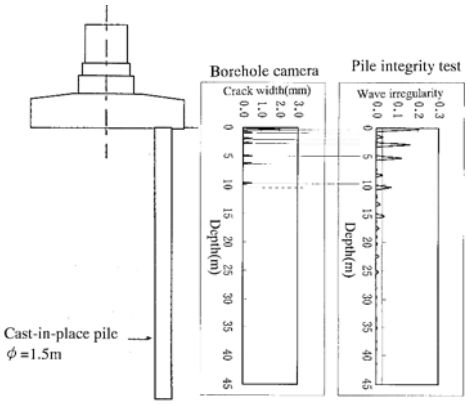

Figure11. Comparison of bored hall camera test and pile integrity test

elastic wave, which can be achieved rapidly and at a fairly low cost. It is a very useful, effective way of roughly assessing the damage to a pile.

3.2 Real-time earthquake damage estimation system

In case of seismic event, immediate action is very important in order to prevent secondary disaster and to collect damage data for immediate restoration policy making. But in the case of Hyogo-ken Nanbu earthquake, it was very difficult to make immediate actions because no system to collect damage information had been developed. Based on the lessons from the 1995 Hyogo-ken Nanbu earthquake, seismic damage estimation system has been developed to approximately grasp the damage of structures in order to estimate the damage of the expressway network.

The system obtains the strong motion data recorded along the expressway network shown in Figure 12. Using the strong motion data, the seismic intensity of the each branch route are roughly estimated in the divided zone with considering the site ground condition of each divided zone as shown in Figure 13. The seismic intensity of each divided zone of each route is calculated as the following way.

1) Conversion from SI at the ground surface of the observation point to seismic intensity at the bed rock surface of the observation point.
2) Estimation of seismic intensity at the bed rock surface of the evaluation point by the interpolation of seismic intensity at the bed rock surface of the observation point.
3) Conversion from seismic intensity at the bed rock surface of the evaluation to seismic intensity at the ground surface of the evaluation point.

Using the seismic intensity of the evaluation point, the damage level of the structure is evaluated. The evaluation is conducted by the fragility curve method. The relation between the damage level, "response ductility" in this system, and the seismic intensity of the earthquake waves," spectrum intensity" in this system is defined in accordance with the earthquake response analysis using structural database and seismic wave database. The fragility curve (cumulative hazard curve) for the damage level A through D as shown in Figure 14 and Table 1 approximated by logarithmic normal distribution is also shown in Figure 15. The application of the fragility curve enables to estimate the damage percentage for each damage rank of piers in certain spectrum intensity.

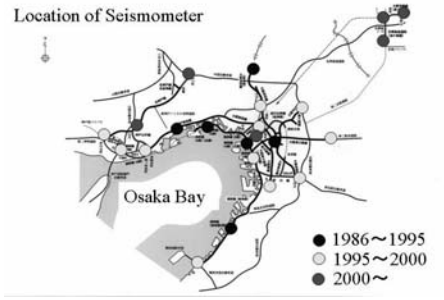

Figure 12. Location of implemented seismometer

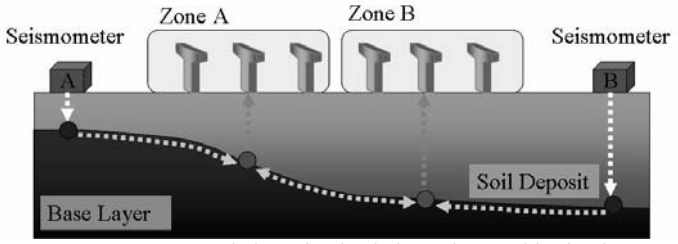

Figure 13. Interpolation of seismic intensity at arbitral point

Table 1. Damage assessment criteria

Damage rank	Damage discription	Criteria
E	No damage	
D	Joints and bearings are damaged	GPA>300gal
C	Minor damage (Needs ductility emhancement)	μ r> 1
B	Major damage (Needs Strenoth retrofit)	μ r > 2
A	Seriour damage (Needs reconstruction)	μ r > μ u

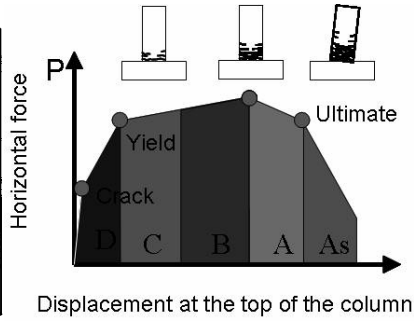

Figure 14. Idea of the damage assessment

Figure 16 shows the sample output of the seismic damage of certain assumed event. This will be helpful for immediate action at the future event.

4. CONCLUSION

The inspection and monitoring activities using intelligent technologies developing at the Hanshin expressway public corporation are introduced in this paper. Repair and maintenance budgets per service length are being reduced due to the current social and economic circumstances in general. Without intelligent inspection and monitoring techniques, further rationalization in maintenance can not be performed. Moreover, development of inspection and monitoring techniques is also needed for risk management. Further study is needed for the development in these fields.

REFERENCES

1. Adachi Y, Momozawa M, Hasegawa Y, Horie R. " Intelligent Inspection System for Road surface Deterioration", Proceedings of second international conference on intelligent traffic system, Orland, U.S.A., September, 1996.
2. Okada H, Ishizaki Y, Shirao K, Hagiwara H. "A proposal of a new inspection technique for highway bridges", Proceedings of the conference on nondestructive inspection, 2000. (In Japanese)
3. Ueda K, Hirose T. "Development of a periodic inspection system", Proceedings of second international conference on bridge maintenance, safety and management, Kyoto, Japan, October, 2004.(In press)
4. Adachi Y, Unjoh S. "Inspection Methods of Damaged Structurs Caused by Earthquakes", Proceedings of US/Japan Joint Seminar on Civil Infrastructure System, Honolulu, U.S.A., August, 1997.
5. Miyawaki K, Kagayama T, Okunishi F. "The system of Real-time Earthquake Damage Estimation in Hanshin Expressway", Proceedings of US/Japan Bridge workshop, Tsukuba, Japan, October, 2000.

THE ROLE OF SENSING AND MEASUREMENT IN ACHIEVING FHWA'S STRATEGIC VISION FOR HIGHWAY INFRASTRUCTURE

Steven B. Chase
Federal Highway Administration, United States

Abstract: Like many countries, the United States has implemented a bridge inspection program to collect information on bridges. In the US, the Federal Highway Administration's (FHWA) National Bridge Inventory database is one of the most comprehensive sources of long-term bridge information in the world. In the US the majority of the States have implemented element level inspection programs to support State and local level bridge management programs. A basic limitation of both the NBI and element level approach is that the data collected relies almost totally upon visual inspection techniques. Visual inspection is not quantitative and hidden or otherwise invisible deterioration damage is missed. The non-quantitative, subjective, highly variable, and nonspecific nature of this data makes it inadequate for comprehensive long-term decision support. Essential research necessary to support the information needs for bridge management for the future is a Long-Term Bridge Performance (LTBP) program. Sensing and measurement technologies play an essential role in this program.

Key words: Sensing, Measurement, Bridges, Bridge Management.

1. INTRODUCTION

In the United States as of 2003, 26.6% of the US bridges were structurally deficient or functionally obsolete, as reported by the Federal Highway Administration (FHWA). This assessment of the structural and functional condition of the nation's highway bridges is based upon data reported to the FHWA by bridge owners across the country and maintained

Farhad Ansari (ed.), Sensing Issues in Civil Structural Health Monitoring, 23–32.

by FHWA in the National Bridge Inventory (NBI) database. Bridge owners have been reporting this data since 1972 when FHWA established the National Bridge Inspection Program. The National Bridge Inspection Program was established in response to the collapse of the "Silver" Bridge in 1967 and the program focuses on the safety of highway bridges. The bridge inspection program requires that qualified inspectors inspect highway bridges at least once every two years and that the results are reported to the FHWA. This data is used to report the condition of the nation's highway bridges to Congress every two years and to administer the Highway Bridge Replacement and Rehabilitation Program (HBRRP). Last year the HBRRP provided more than $3.5 billion to replace or rehabilitate deficient bridges.

2. BACKGROUND AND NEED

The type of data collected and reported for the National Bridge Inspection Program is adequate for managing and administering a national program aimed at eliminating deficient bridges but it is inadequate for some other purposes. The data is not detailed enough to support bridge maintenance programs. The NBI does not record the condition of paint systems, joints or provide information on local damage or deterioration. The data is too general, subjective and qualitative to be used to develop plans and estimates for repair or rehabilitation work. For example, the NBI records condition data for the entire supersructure of the bridge with a subjective rating ranging from excellent to failed as a integer from 9 to 0. In response to these limitations, many states augment the NBI by collecting additional information or use a different, more refined, approach to collection and recording of bridge condition data. The more refined approach characterizes a bridge as a collection of elements, such as girders and piers, and records quantitative condition data on each element. Standardized elements have been defined for highway bridges and automated methods are used to translate the element level data into the NBI data required by the FHWA.

Although the element level inspections provide more detailed and useful information for network level bridge management, especially at the state and local level, the information collected is still very limited in several respects. The most significant limitation is that the data collected is based solely upon visual inspection, augmented with limited mechanical methods such as hammer sounding or prying. Visual inspection is highly variable. The FHWA's Nondestructive Evaluation Validation Center recently completed the first comprehensive and quantitative study of the reliability of visual inspection and the NBI condition rating system. The results of that study indicate that a range of condition ratings of 3 or 4 categories can be expected

routinely with different inspectors reporting results for same bridge in the same condition. This variability is in addition to the inherent limitation of visual inspection to fail to detect invisible deterioration, damage or distress. There are many types of damage and deterioration that need to be detected and measured in order to determine if a bridge is safe or to decide if repairs are required. Many of these are difficult or impossible to detect visually unless the damage or deterioration is severe. For example, it is not possible to look at a bridge and determine if it has been overloaded or if it has settled unless the damage is so severe as to cause the lines of the bridge to change. Frozen bearings, corrosion and fatigue damage can exist with no visible indications. Routine visits by bridge inspectors also do not collect information on the operational performance of bridges such as congestion, accident history or fatigue of structural members. The life-cycle of a bridge is commonly described as the sequence of initial construction and the intermittent maintenance, repair, rehabilitation actions ending in the replacement or retirement of the bridge. Clearly, a sequence of actions, the timing and extent of which are based solely upon visual inspections, are very different from a sequence of actions based upon more quantitative and reliable damage detection methods.

The implementations of customer driven quality improvement programs or asset management supported by true engineering economic analysis are also hindered by the lack of necessary information. We currently guess at average daily traffic values. We do not know the size, number and weight of the trucks our bridges carry. The actual stresses, strains, deflections and displacements the bridges experience are unknown. There is a need to more accurately quantify the operational performance of highway bridges. The performance measures, which are of most immediate interest and importance to the traveling public, are congestion, accidents, and service. These same performance measures can help to quantify the value of bridge as assets in terms of user costs and benefits.

Such quantitative measures are also needed to implement true life cycle cost analysis or performance based specifications. FHWA, like all federal agencies in the United States, is directed by executive order to consider life cycle cost for major projects. However, the life cycle of bridges has not been defined. The deterioration rates of different materials, structural systems in different environments of loading and climate have not been measured. There is a specific need to integrate quantitative performance measures into the management systems for the highway infrastructure. Some of the measurement and detection needs currently not met by our standard practice of visual inspections are tabulated below. These measurement and detection needs exist at many levels and can serve many purposes.

Table 1 Sensing and Measurement Needs

Damage	Deterioration	Operation	Service
Impact	Corrosion	Traffic counts	Congestion
Overload	Fatigue	Weight of trucks	Accidents
Scour	Water absorption	Maximum stress	Reduced traffic capacity
Seismic	Loss of prestress force	Stress cycles	Delay
Microcracking	Unintended structural behavior	Deflection	Unreliable travel time
Settlement	Chemical changes (e.g. ASR, DEF)	Displacement	Reduced load capacity
Movement			
Lack of Movement			

3. SUMMARY OF RECENT RESEARCH

The FHWA and others have conducted research and development in sensing and measurement technologies that can help meet these needs. Several examples illustrating the application of this technology to monitor and measure bridges are described in this article. This summary is not comprehensive. It is intended to demonstrate that technology exists to meet the needs identified and to stimulate interest in application and further development of innovative technologies to measure and monitor the long term performance of bridges.

Global health monitoring has evolved to the point where a number of large systems have been implemented on large bridges in many parts of the world. One such system has been installed and is operating on the Commodore Barry Bridge over the Delaware River in Pennsylvania. Although promising, the full potential of this technology has not been realized or defined and significant issues remain to be researched. The information technology component is one such issue. In spite of these limitations, the information these types of systems already provide has proven to be very useful to the owners of the bridges where they have been installed. One example of the type of information these systems provide is the detection and quantification of unexpected bending of tension elements due to differential solar radiation exposure

Non-intrusive load capacity measurement is one of the needs identified above. Substandard load capacity is the single most frequent reason for a bridge to be classified as structurally deficient in the United States. One technology, which the FHWA has adapted to meet this need, is a laser measurement system for bridge load testing. The system uses a computer-

controlled mirror to aim an invisible, eye safe, infrared laser beam at a point on the bridge. The laser measures the range to the point on the bridge and reports the three-dimensional spherical coordinates of that point, relative to the local origin set by the laser system. The system can repeat this measurement at different points on the bridge hundreds of times in a few minutes. The system has a measurement range of about 30 meters and an accuracy, resolution and repeatability of a fraction of a millimeter. The system does not require special targets and works well on ordinary steel, concrete and timber surfaces. Using this system it is possible to rapidly measure the three dimensional deflection response of a bridge to a heavy truck. The system can also be used to rapidly and quantitatively measure if any part of the bridge has moved since the last time the bridge was scanned, with an accuracy, precision and repeatability of a fraction of a millimeter. This system is also capable of early detection of subsidence or loss of prestress. This example demonstrates that long-term monitoring does not always require a dedicated and permanently installed monitoring system for each bridge.

The detection and measurement of fatigue and vulnerability to fracture continue to be a pressing need for the hundreds of thousands of steel bridge in the nation. The National Bridge Inspection Program was initiated in 1971 in response to a bridge failure caused by a brittle fracture. The brittle fracture of a welded plate girder resulted in complete bridge failure in Milwaukee, Wisconsin in December 2001 demonstrates that this vulnerability still exists. This bridge had been visually inspected a few weeks prior to the failure and there was no visual indication of the impending failure at the fracture site.. Subsequent forensic analysis has confirmed vulnerability to sudden brittle fracture due to welding practices and details that produced high residual stress and triaxial restraint. Visual inspection alone is not capable of detecting or quantifying these conditions. FHWA is researching the use of thermographic stress imaging to detect such conditions.

Although fatigue was not a contributing factor to the brittle fracture in Milwaukee, it continues to be a major problem on aging steel bridges. The measurement and characterization of the random, variable amplitude cyclic stress that brides are subjected to is an essential measurement need. Technology has been developed to help manage fatigue. Numerous examples of portable, battery powered, data acquisition systems now exist. These systems offer very high dynamic range, very low noise and adaptive digital spread spectrum radio network telemetry capabilities. Using this technology it is possible to rapidly instrument a bridge at fatigue prone or critical details and measure what happens under traffic and wind loading.

The wireless network technology can quantify the fatigue-loading regime at a fatigue prone detail but it cannot measure if a fatigue crack is growing under that load. These cracks do not grow continuously but advance in microscopic steps. The advance of the crack front is accompanied by release of potential energy that produces ultrasonic stress waves. This is similar in concept to the release of energy associated with an earthquake but on a microscopic scale. The stress waves can be detected using special sensors tuned for this purpose. The method is call acoustic emission (AE) and it has been used for many years in the energy and process industries. However, prior AE instruments were not practical for long term monitoring of fatigue cracks on highway bridges. The lack of electrical power on most bridges, the difficulty in accessing the details on the bridge, the very high background noise environment, and perhaps most importantly, the random loadings with rare high load events driving crack extension all worked against successful application of AE on bridges. A new battery powered, eight channel AE instrument specifically designed for the bridge monitoring need was developed in cooperation with the FHWA's NDE Validation Center. These systems can also telemetry information via modem or radio link.

While the two prior systems are very useful, they are expensive (10's of $K), and they are still limited by battery power to relatively short term monitoring. A totally passive and inexpensive fatigue measurement sensor has also been developed to meet the need for very long duration fatigue measurement. This sensor is attached to the bridge and strains along with the bridge. The sensor is based upon a special passive strain amplification design and two, pre-cracked, coupons with integral analog crack length gages. The two coupons are fabricated with materials that have different crack growth properties. These manufactured fatigue cracks grow in response to the random variable amplitude strains on the bridge. By periodically measuring the crack lengths in the two coupons with a special reader, the effective number of cycles at a predetermined stress range can be quantified. This sensor can be likened to a fatigue odometer. Using this technology, it is possible to measure how the fatigue life of a highway bridge is being consumed.

Another example of new technology applied to help collect essential performance information is the development of a smart bridge bearing. Non-operating bearings, and the tremendous stresses that result, are a common factor in bridge failures. They are also a very common maintenance requirement. In addition, the distribution of live and dead loads to the bearings through the structural systems of the bridges is a possible diagnostic and damage detection capability that this technology will enable. If there is a significant change in stiffness of a structural member due to fracture, impact or other reason, it is likely that the distribution of the loads to the

bearings will change. A smart bearing could "feel" the damage in the bridge. The enabling technologies are sophisticated but the concept is simple. The intelligence for the bearing is provided by multi-axis fiber optic strain sensors, capable of measuring both vertical and shear strains, that have been integrated into a composite panel. The panel can be integrated into the bearing. The panel could be laminated between the neoprene bearing pads commonly used on highway bridges and can measure the vertical and lateral forces transmitted from/to the bridge.

There are an almost unlimited number of possible applications for sensing and measurement technologies for highway bridges. The technology does not need to be expensive and sophisticated. Another example concerns a wing wall that was moving due to excessive hydrostatic pressure. Remedial measures were taken and the owner wanted to monitor the movement of the wall relative to the abutment. The environment is severe and an inexpensive but reliable sensor was needed. The NDE Validation Center conceived, designed, built and installed an inexpensive displacement sensor in a few weeks. The sensor has been monitoring the wall for three years and has proven that the remedial measures were effective. Over the years FHWA has developed a versatile modular instrumentation concept that facilitates rapid prototyping and deployment of specialized sensing applications. This lends itself to specialized and critical component monitoring where unique features or requirements can be readily accommodated.

An illustration of this versatility is another application on a fracture critical hanger on a pin and hanger detail. The hanger is being monitored using the same modular system that was used to monitor the wing wall. The sensors in use are welded resistive foil strain gages. The hanger is supposed to freely rotate about the pin as the bridge expands and contracts due to temperature changes. The hanger transfers vertical load and is designed as a tension element. If the pin and hanger interface corrodes, a very common occurrence, the friction between the pin and hanger can cause significant bending in the hanger. In addition, the sudden slippage of the pin hanger interface can result in tremendous dynamic stress. The fatigue and possible fracture consequences of this phenomenon were not considered in the design of these details. The response of the hanger was measured during a load test. In addition to bending in the expected direction, unexpectedly transverse bending of the hanger was also measured. Detection and measurement of unintended structural behavior is a major benefit of this type of monitoring.

Steel bridges are not the only bridges vulnerable to sudden failure and collapse. A number of prestressed concrete bridges have collapsed due to undetected corrosion of tendons. One recent example was the collapse of a

pedestrian bridge in the summer of 2000 after only seven years of service. The failure was caused by corrosion and failure of the high strength steel tendons that helped support the bridge. The localized corrosion of the tendons was attributed to calcium chloride unexpectedly found its way into the grout used to fill in holes created during the fabrication of the precast girders. The source of the calcium chloride is still unknown but undetected corrosion of prestressing steel has led to the failure of a number of bridges.

When such a wire breaks there is a sudden and significant release of potential energy. Such wire breaks generate stress waves which propagate outward from the structure and which can be detected by sensors, such as accelerometers. By analyzing the arrival times of the signals, it is not only possible to detect the wire breaks but to also locate where the break occurred. The method is similar to a network of seismometers to locate and quantify earthquakes. Such systems are commercially available and are installed on a number of bridges.

Detecting wire breaks is certainly useful, but a potentially more useful technology is the detection and quantification of corrosion before failure occurs. The most common cause of corrosion in highway bridges is the salt placed on the bridges to keep the bridge open during winter storms. The corrosion of structural steel is usually visible. However, the corrosion of reinforcing and prestressing steel in concrete structures is not visible until significant damage has occurred. A new device, developed in cooperation with the FHWA, is an embeddable corrosion sensor. The sensor is designed to be placed inside of concrete structures and to measure corrosion rate, concrete conductivity and chloride ion concentration. The instrument is small and eventually will be powered and interrogated by wireless radio frequency methods. If the size and cost can be reduced, hundreds or thousands of these sensors could be economically embedded in a bridge to provide quantitative information about the state of corrosion well before severe damage has occurred.

4. FUTURE DIRECTIONS

Much of the sensing and measurement technology to monitor bridges is already available. This technology can provide the quantitative and objective information necessary to move beyond our current subjectively based bridge management systems. There is a need to evolve to a more quantitatively driven management approach. This need has been identified and emphasized by the United States National Academies of Science and Engineering.

Several workshops have been held where stakeholders from the public, private and academic communities have been bought together to identify the most pressing and highest priority research needs for dealing with an aging highway infrastructure. The result was a National Infrastructure Renewal Research Agenda. The need for reliable and timely data and information is recognized as critical to the efficient management of the nation's highways. The agenda also identifies the need for much improved decision support tools as well as to integrate probabilistic life-cycle analysis into infrastructure management. The need to value infrastructure assets and quantify the benefits of the system is also specifically mentioned. Quantitative, relevant and useful measures of performance are emphasized.

The safety assurance of highway structures for extreme events would also be greatly enhanced by short and long term monitoring and measurement of the loading and structural response during extreme events. As already demonstrated, assessment and management of bridges and other structures demand the quantitative measurements provided by the monitoring of structures. It is not possible to develop enhanced specifications without long-term observation and quantitative measurement of structural behavior and deterioration. Finally, the basic information necessary to support the automation of design, construction and maintenance, identified as a national priority for infrastructure research and development must be provided by sensing and measurement technology.

For all of the reasons outlined, the Federal Highway Administration is proposing to begin a Long Term Bridge Performance Monitoring Program. This program would be similar to the Long Term Pavement Performance Program that has been underway for more than 15 years. The program will include detailed inspections and periodic evaluations conducted on a representative sample (in the thousands) of bridges to monitor and measure their performance over an extended period of time (at least 20 years). These inspections and evaluations would be much more standardized, quantitative and detailed than the routine bridge inspections conducted in support of the National Bridge Inspection program. This is envisioned to be a federally funded and managed program that will not impose additional data collection burdens upon the bridge owners. It is anticipated that the resulting database will provide high quality, quantitative, performance data for highway bridges to support improved designs, improved predictive models, and better bridge management systems. A second component of this long-term bridge performance program will be to instrument a subset of these sample bridges (in the hundreds) to provide continuous long-term structural bridge performance data. The third component of the program will include detailed forensic autopsies of several hundred bridges each year (out of the several

thousand bridges that are decommissioned each year). These forensic autopsies could also be conducted for bridges that fail unexpectedly. The intent is to collect valuable performance data and quantitative statistics on corrosion, overloads, alkali-silicate reaction, and all other important deterioration processes from these bridges.

The long-term bridge performance program will be designed to accommodate and develop both general trend information, and information specific to a variety of bridge types, locations, and environmental exposures.

5. CLOSURE

To summarize, the application of sensing and measurement technologies to long term bridge monitoring can provide quantitative data for network and bridge level management. This would contribute to a much greater level of accuracy, reliability and utility of data necessary for asset management. Bridge safety, especially during extreme events, is enhanced by measurement and monitoring of critical bridge components. Enhanced safety, reliability and efficient maintenance can result from improved incident detection and assessment. Global bridge health and performance assessment in support of asset management, enhanced specifications and realistic life-cycle cost analysis must be, and arguably can only be, accomplished using quantitative measurement methods. Subjective assessment simply is not adequate to meet these needs. Sensing and measurement technologies will play an essential role in the proposed Long-term Bridge Performance Program.

RECENT DEVELOPMENT OF BRIDGE HEALTH MONITORING SYSTEM IN KOREA

H.M. Koh 1, S. Kim 2, and J.F. Choo 3

1, 3 Department of Civil Engineering, Seoul National University, Korea
Korea Bridge Design & Engineering Research Center (KBRC), Korea
2 Department of Structural Engineering, Seoul National University of Technology, Seoul

Abstract: Since bridge structures constitute the very vulnerable part of civil transportation system that affect directly the public safety, focus has been done on the active development of bridge health monitoring in Korea since 1990's. Gathering of field data for design verification and monitoring of long-term performance of bridges were performed in the scope of systematic and scientific inspection and management programs. Actually, modern and integrated monitoring systems are introduced in newly-built bridge structures since their design stage. This paper reviews recent development of bridge health monitoring systems in Korea in newly-built bridges with their objectives and major characteristics.

Key words: Structural health monitoring, bridge management system, integrated monitoring system.

1. BRIDGE MANAGEMENT SYSTEM IN KOREA

1.1 Road system in Korea

The Korean road system can be classified into 5 groups according to the management authorities: the national expressway network, the national highway network, the metro-city road network, the provincial road network and the city-county road network. Among these networks, the national expressway and national highway networks constitute the major road

Farhad Ansari (ed.), Sensing Issues in Civil Structural Health Monitoring, 33–42.

transportation axes in the peninsula and represent nearly 50% of the whole Korean bridge stock.

The national expressway network is managed by the Korea Highway Corporation (KHC), which is responsible of the construction, operation, maintenance and repair of the expressway network. The network is constituted by 23 expressways developing a length of 2,778 km of which 609 km are composed by a total of 5,389 bridges. On the other hand, regional construction management offices are managing the 14,524 km of the national highway network including 4,309 bridges for a length of 384 km. And, the remaining 3 classes average a total length of about 79,027 km comprising 10,569 bridges developing a length of about 800 km.

1.2 The Korean Bridge Management System: KOBMS

It has been seen that bridge structures occupy a large proportion of the transportation network and, since bridges constitute the very vulnerable part of civil infrastructures affecting directly public transportation and safety, attention has been focused on the development of a total bridge management system since early of 1990s.

Total bridge management system (BMS) attempts to include inspection, evaluation, estimation and rehabilitation of bridges in a systematized organization, which integrates structural health monitoring (SHM) systems installed in bridges [**1 – 2**]. BMS is an information-oriented system, which aims the global supervision of all the information gathered in every bridge so as to help the supervisor deciding current and future requirements for optimal management and rehabilitation of bridges. Following, to perform scientific and rational management and rehabilitation of bridges, the Korean Ministry of Construction and Transportation (MOCT) together with the Korea Institute of Construction Technology (KICT) developed since 1995 the Korean BMS (KOBMS), which is operating for ordinary road bridges [**3**].

The hardware of KOBMS is constituted by regional networks and, high-performance and high-capacity computers to manage efficiently the huge volume of data gathered in bridges. Such network operates interactively by linking the KICT, road facilities of the MOCT, 5 regional offices, 1 R&D office and 18 road management offices since 1996 (Fig. 1).

The software of the KOBMS is composed by a database (DB) recording archives related to bridges, a program computing the investment priorities, a rehabilitation and retrofit techniques DB, a tunnel DB, a program outputting the current state of bridges, a decision-making system performing the essential functions of the BMS (Fig. 1). Especially, the BMS DB stores and compiles about 230 items per bridges including their characteristics, structures, inspection records, load carrying capacity, etc. Investment

priorities, as a basic function of the BMS, stand for the process by which one decides the sequence of bridges to be considered for management and rehabilitation in the budget planning. The KOBMS DB arranges 64 basic rehabilitation and retrofit techniques for bridge and defines 120 types of damage that may occur in bridge, so as to select automatically an appropriate rehabilitation and retrofit basic technique for each type of damage. Using the KOBMS DB, a report on the current state of the bridges is published annually and, provides statistics of the basic parameters of the bridges and their current state according to their classification.

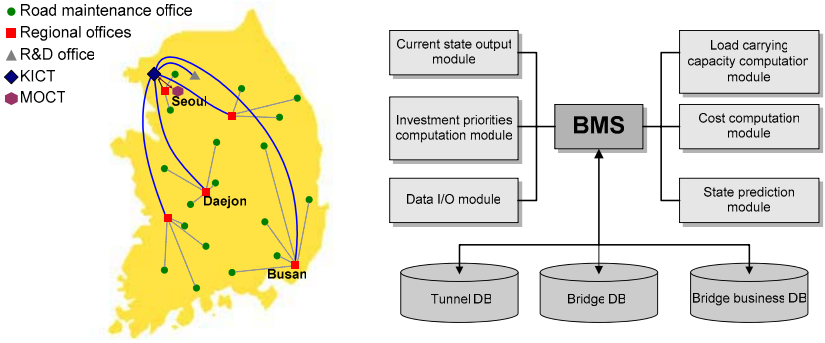

Figure 1. Hardware and software of the KOBMS

The KOBMS made it possible to manage efficiently the huge volume of bridge data in a systematic and effective organization. Moreover, it made it possible to systematize the state evaluation and records management of rehabilitation and retrofit for each bridge as well as for the whole bridge stock. The state of bridges has seen significant improvement while large reduction of the budget invested for their management, being rationally shared, has been obtained [**4**].

2. HEALTH MONITORING SYSTEMS FOR BRIDGES IN KOREA

Installation of SHM systems in Korea began since 1995 in order to collect field data by full-scale load capacity tests for design verification of existing bridges and, subsequently, evaluate the health of the structures using stand-alone field system consisting of sensors, field hardware and online transmission to a computer on field. Thereafter, modern technologies were introduced in SHM systems since the design stage to evolve onto an overall bridge management integrated system for the monitoring of long-term

performance and durability of newly-built bridges in the scope of systematic inspection and maintenance programs. More recently, efforts intend to increase and upgrade the monitoring efficiency and performance through sensor-based bridge monitoring systems (SBBMS). Such system will provide advanced innovative functions like sensor fusion using new sensing techniques, reliable massive signal transmission via web-based operating system or wireless signal transmission, automated surveillance, adaptive signal processing, etc. [**1** – **2**]. Figs. 2 and 3 and Table 1 summarize major and representative bridges equipped with SHM systems in Korea.

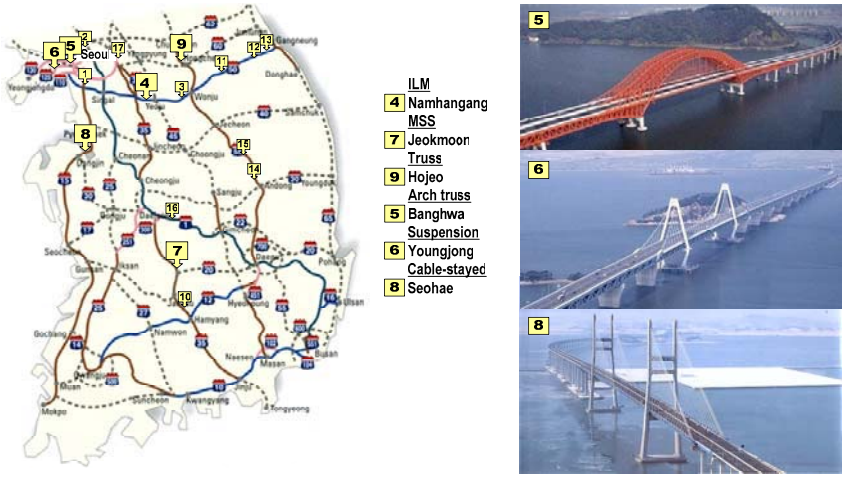

Figure 2. Major instrumented bridges in national expressway network

Figure 3. Major instrumented bridges in national highway network

Table 1. List of recent and major instrumented bridges in Korea

Name	Type	Length (m)	Completion date	No. of sensors*	Managing authorities
Jeokmoon	MSS	1,000	2000.12	112 (102+10)	KHC
Hojeo	Truss	80+120+80	2001.08	76 (69+7)	KHC
Banghwa	Steel arch	540 of 2,559	2000.11	137 (115+22)	KHC
Youngjong	Suspension	125+300+125	2000.11	380 (209+171)	KHC
Seohae	Cable-stayed	60+200+470+200+60	2000.12	183 (44+139)	KHC
Samcheonpo	Cable-stayed	103+230+103	2003.04	66 (15+51)	KICT
Gwangan	Suspension	200+500+200	2000.04	51 (21+30)	KICT

* Total No. of sensors (No. of static sensors + No. of dynamic sensors)

3. APPLICATION OF INTEGRATED SHM SYSTEMS IN NEW BRIDGES

Most of the long-span bridges newly built in Korea is instrumented with modern monitoring systems. Recent systems adopted in new bridges exploit modern technologies from sensing to processing, i.e. many sensors and data acquisition systems that measure the behavior of the bridge during its construction become part of the long-term health monitoring system.

An attempt to integrate health monitoring systems of several bridges together has been achieved to reduce costs and increase significantly the management efficiency management. This integrated system includes BMS as well for inspection, estimation and rehabilitation. The integrated system for the Seohae, Youngjong and Banghwa bridges may be cited as the best example of the current monitoring system. The data collected at each bridge are processed exclusively at each field station for real-time monitoring and alarming sudden abnormal behavior. But data that are useful for long-term evaluation of bridge condition, as well as periodical inspection data, can be transmitted through high-speed internet line to the management center located far away from the site. Once data are collected at the center, integrated BMS handles them to classify, store and retrieve. This integrated BMS is able to itemize bridge maintenance details, not only physical information but also knowledge. And, based on the inspection results, it may manage status assessment, rating, repair and strengthening history.

3.1 Youngjong bridge

Youngjong bridge is a self-anchored suspension bridge with a double-deck warren truss girder carrying both railway and roadway linking Incheon International Airport to Seoul (point 6 in Fig. 2).

The SHM system installed in the bridge has been exploited to identify its dynamic properties before opening by means of field loading test using two

vibrators, which generated flexural and torsional vibrations of the bridge (Fig. 4). Comparison of the measured data such as natural frequencies, vibration modes and damping ratios with design values showed good correspondence attesting for the reliability of the bridge (Table 2).

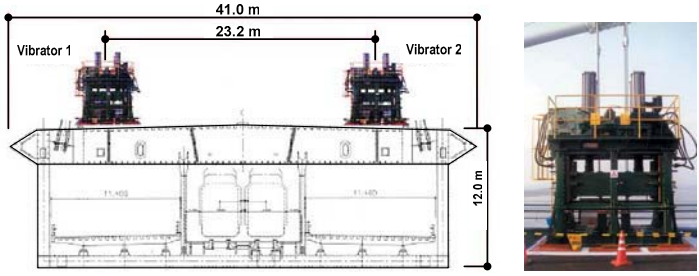

Figure 4. Disposition of the vibrators installed on Youngjong bridge for field loading test

Table 2. Dynamic characteristics of Youngjong bridge identified by forced vibration test

Dynamic characteristics	Natural frequency (Hz)		Damping ratio	
	Design	Measured	Design	Measured
Flexure 1st mode	0.422	0.487	0.03	0.06
Antisymmetric flexure 1st mode	0.716	0.810	0.03	0.03
Torsion 1st mode	0.781	1.060	0.02	0.023
Antisymmetric torsion 1st mode	1.195	1.700	0.02	0.05

3.2 Seohae bridge

Seohae bridge is the longest cable-stayed bridge in Korea, which links Pyoengtaek and Dangjin by crossing the Asan bay (point 8 in Fig. 2). Its five spans are constituted by stiffened steel girders with precast slab. And, more than 10 types of sensors for a total of 180 units are actually installed in the major parts of the cable-stayed (Fig. 5), PSM and FCM bridges.

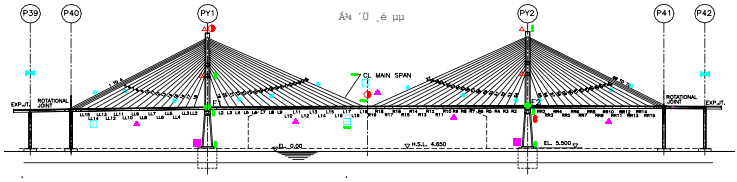

Figure 5. Location of sensors in the cable-stayed bridge of Seohae bridge [**1 – 2**]

The structural behavior of the cable-stayed bridge has been observed and analyzed during 2 years after its completion. Results showed that the annual variation of the vertical deflection in the stiffening girder satisfies the

allowable design limit with a range of -320 to 30 mm and that deflection due to live load presents a range of 189.7 mm, which represents only 25% of 808.8 mm, the design limit (Fig. 6). The stress range in the stiffening girder due to live loads showed good correlation with the volume of traffic monitored during 2 years and, since it represents only 5 to 12% of the design stress, stress margin appears to remain considerable. It could thus be said that actual highway bridge design specifications are producing excessively conservative structures.

The thermal deformation of expansion joints at the extremities of the bridge is also shown to correspond accurately with theoretical predictions (Fig. 6). And, tensioning force in the cables ranged within 95 to 104% of the initial value attesting for the stability of the bridge. Seohae bridge appears thus to be healthy in view of its long-term behavior [**5**].

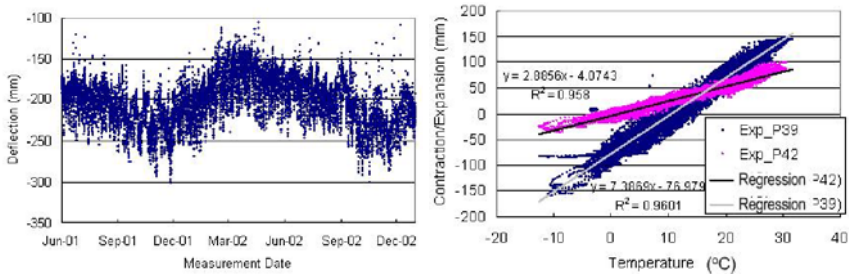

Figure 6. Annual variation of vertical deflection at the center of the main span and thermal expansion/contraction of expansion joints of Seohae bridge [**5**]

4. APPLICATION OF SENSOR BASED BRIDGE MONITORING SYSTEM

Recently, SBBMS has been proposed and effectively applied on newly built bridges to increase monitoring efficiency and performance by exploiting new sensor technologies [**2** – **6**]. The purposes of SBBMS are providing information (1) to assess the behavior of the bridge, (2) to ensure serviceability and safety during its service life and (3) to help design, construction and maintenance. Application of SBBMS can be found in Gwangan and Samcheonpo bridges.

The hardware system performs measurement and data acquisition of the bridge behavior by remote sensing using sensors and data loggers, and the software system achieves data processing, storage, analysis and display in customized form (Fig. 7).

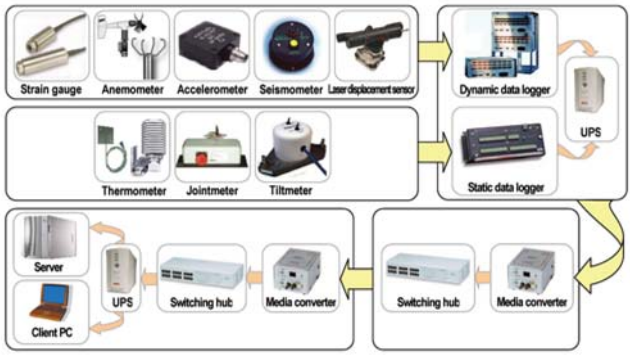

Figure 7. Organization chart of the monitoring system installed in Gwangan bridge

4.1 Gwangan bridge

Gwangan bridge is located in front of Gwangan town beach (point 6 in Fig. 3) and is the longest suspension bridge in Korea. It is an earth-anchored suspension bridge with a double-deck warren truss girder carrying roadways. The pylons are steel towers where the main cables are sustained with the stiffening girder at 105 m height.

The monitoring hardware system (Figs. 7 and 8) has been designed to perform real time monitoring of the structural behavior of the bridge.

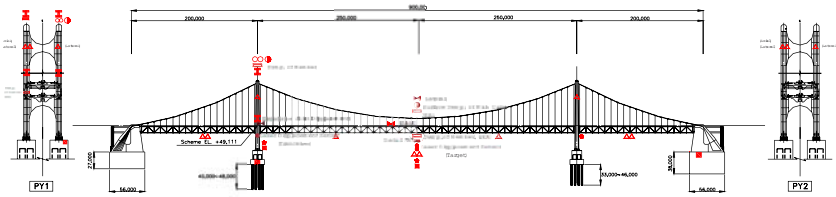

Figure 8. Location of sensors in Gwangan bridge [**1 – 2**]

The SHM system was used to produce alarm/warning during the crossing of Maemi typhoon in September, 2003. Measurement of the wind speed at the pylon and midspan of the bridge (Fig. 9) helped to make decision of blocking and reopening of the bridge to traffic so as to ensure public safety during the typhoon.

Health monitoring after the crossing of the typhoon was also performed using the measured inclination of the pylon (Fig. 9) and displacement at the expansion joints. The corresponding natural frequencies were computed and results showed that natural frequencies remained within safety limits, which made it possible to conclude that the bridge was not affected by the typhoon.

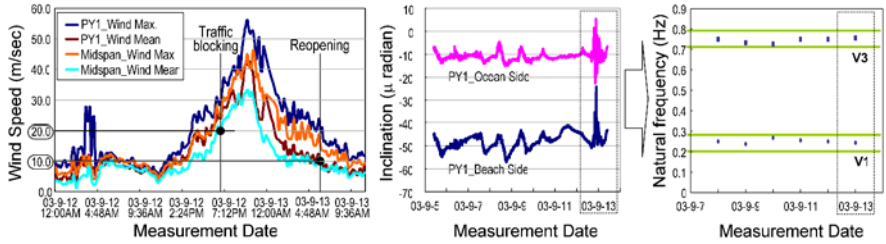

Figure 9. Wind speeds measured in the pylon and midspan, and inclination of the pylon with corresponding natural frequencies of Gwangan bridge during Maemi typhoon

4.2 Samcheonpo bridge

Samcheonpo bridge is a three-span cable-stayed bridge with composite girder, located in the Hallyeo maritime national park and connecting Sacheon city to Changsung Island (point 4 in Fig. 3). The health monitoring hardware system for the management of Samcheonpo bridge (Fig. 10) is similar to Gwangan bridge.

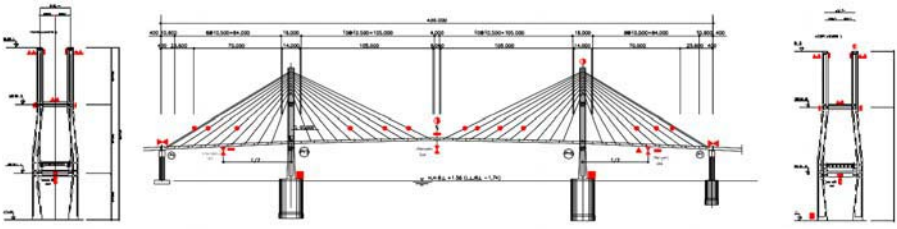

Figure 10. Location of sensors in Samcheonpo bridge

A forced vibration test was performed on the cable-stayed bridge for system identification purpose just after its completion and before opening. The objective was to determine the initial values of the dynamic properties of the bridge for comparison with design values and calibration of the analytic model.

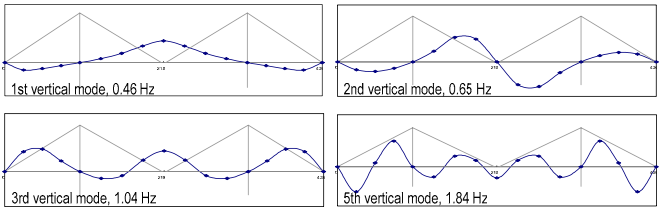

Figure 11. Mode shapes measured through forced vibration test at Samcheonpo bridge

The excitation force was induced by the sudden braking of a fully loaded truck of 29.7 ton and acceleration responses were measured at 14 points. According to the number of measuring points and loading characteristics, vibration modes up to the 7th mode could be distinguished (Fig. 11). Experimental results were shown to correspond accurately with design values and calibration of the analytic model made it possible to reduce RMS error to 2.61% [**7**].

5. CONCLUSIONS

Recent development and applications of SHM for newly built bridges in Korea have been addressed. Observations obtained through integrated SHM system as well as SBBMS were seen to be exploited effectively and diversely like system identification of bridge characteristics for design verification or calibration of analytic model, assessment of long-term behavior, and giving alarm when abnormal behavior is detected.

Current researches focus on developing systematic decision algorithm for repair and strengthening, and improving SHM hardware performance so as to lengthen service life of bridges and ensure serviceability and safety.

REFERENCES

1. Koh HM, Choo JF, Kim CY, Kim S, Park CM. "Progress of research and applications in structural health monitoring of bridges in Korea", *Proceedings of the International Workshop on Structural Health Monitoring of Bridges / Colloquium on Bridge Vibration*, Kitami Institute of Technology, Japan, Sept. 1-2, 2003, pp. 89-100.
2. Koh HM, Choo JF, Kim S, Kim CY. "Recent application and development of structural health monitoring systems and intelligent structures in Korea", *Proceedings of the First International Conference on Structural Health Monitoring and Intelligent Infrastructure*, Tokyo, Japan, Nov. 12-15, 2003, pp. 99-112.
3. Korea Institute of Construction Technology. "Current status of bridge management system", *Workshop on Maintenance System of Public Facilities*, Korea, June, 1996.
4. Korean Ministry of Construction and Transportation. "Records of the current status of bridges", 2002.
5. Park CM, Park JC. "Evaluation of structural behavior using full scale measurements on the Seohae cable-stayed bridge", *Proceeding of the Annual Conference of the Korean Society of Civil Engineers (KSCE)*, Korea, 2003, pp. 571-576.
6. Jang JH, Kim S, Kim WJ. "Sensor based bridge monitoring system", *Proceedings of the International Workshop on Structural Health Monitoring of Bridges / Colloquium on Bridge Vibration*, Kitami Institute of Technology, Japan, Sept. 1-2, 2003, pp.117-120.
7. Yoon JG, Lee J, Kim JI. "FVT signal processing for structural identification of cable-stayed bridge", *Proceedings of 2003 Fall Workshop of the Korean Society for Noise and Vibration Engineering (KNSVE)*.

A STRATEGY TO IMPLEMENT STRUCTURAL HEALTH MONITORING ON BRIDGES

Charles Sikorsky
Division of Enginering Services, California Department of Transportation USA

Abstract: Previously researchers in the area of non-destructive damage evaluation (NDE) envisioned a bridge management system where sensors fed measured responses such as strain and acceleration into a damage identification algorithm. While significant advances have been made toward achieving this goal, the area of non-destructive damage evaluation is hardly ready for implementation. Based on a previously developed Level IV NDE Method, a strategy is proposed to incorporate this method into a structural health monitoring system and to investigate the economic feasibility of implementing structural health monitoring on bridges.

Key words: Damage Index Method, modal-based non-destructive damage detection, damage evaluation, remaining service life

1. INTRODUCTION

Previously researchers in the area of non-destructive damage evaluation (NDE) envisioned a bridge management system where sensors fed measured responses such as strain and acceleration into a damage detection algorithm. This algorithm would then determine if the bridge had deteriorated to the point where safety to the traveling public had been compromised, and notify the appropriate public officials [1]. While significant advances have been made toward achieving this goal, the area of NDE is hardly ready for implementation. Capitalizing on this perceived failure, the area of structural health monitoring (SHM) has emerged as a relatively simple technology to implement, since all that is required is an instrumentation system permanently mounted to the structure. Structural health monitoring has been

Farhad Ansari (ed.), Sensing Issues in Civil Structural Health Monitoring, 43–53.

defined by some as "the use of in-situ, nondestructive sensing and analysis of structural characteristics, including the structural response, for detecting changes that may indicate damage or degradation" [2]. To satisfy this definition, there is no requirement for a SHM System to estimate structural capacity or remaining service life. All that is required is an ability to collect as much data as possible and as quickly as possible which is not as important to a State Bridge Engineer as estimating structural capacity or remaining service life.

Prior to reviewing the current status of structural health monitoring, let us first reexamine the need for structural health monitoring of bridges. That need is based on the introduction of new materials in bridge construction, serviceability of the bridge after an extreme event, and the continued deterioration of the infrastructure.

Initially, fibre-reinforced polymer (FRP) composite materials were introduced to the bridge community as an effective material for strengthening structures subjected to seismic events. Since then these materials have also been investigated as a means to rehabilitate or strengthen a bridge. Rehabilitation is taken here as the restoration of the structure to its original design condition, whereas strengthening implies the live-load capacity of the structure is increased. While there are benefits to these materials (such as high strength-to-weight and stiffness-to-weight ratios), there are limitations as well. One such limitation is the lack of data to evaluate the long-term performance of bridges rehabilitated with these materials [3]. Although experimental work in the laboratory has demonstrated that FRP composites can be used to strengthen a reinforced concrete member, it is difficult to realistically quantify strength in the laboratory, since as a minimum, deterioration is a result of the interaction between the manufacturing process, environment and stress due to load [4]. With the increasing use of FRP composites for rehabilitation of bridge decks and girders, a methodology to evaluate the rehabilitated structure's performance is necessary.

In addition, events over the past decade have forced State Bridge Engineers to consider the effects of extreme events other than earthquakes on the response of a bridge. The most visible of these events has been the series of tragic terrorist attacks against the U.S., both nationally and abroad. While not as sensational as the terrorist attacks, recent barge mishaps on the nation's waterways have brought identified other bridge vulnerabilities. For example, a barge accident in June 2002 caused one-third of the 1988-foot long structure carrying I-40 across the Mississippi River to collapse. A renewed interest among bridge engineers to mitigate the effects of extreme events on bridges, as well as reopen the structures immediately after such an

event, identifies a need the area of structural health monitoring could potentially satisfy.

Lastly, deterioration and increasing functional deficiency of civil infrastructure continue to pose some of the more significant challenges to civil engineers. It should be noted that this was the argument to support initial development of non-destructive damage evaluation methods. In the United States alone, 27.5% of bridges were structurally deficient or functionally obsolete in 2000 [5]. The deterioration and functional deficiencies of highway infrastructure are attributed to aging, weathering of materials (i.e. corrosion of steel), accidental damage (i.e., natural disasters), and increased traffic and industrial needs. In order to mitigate deterioration and efficiently manage maintenance efforts on bridges, a methodology is still needed to monitor and evaluate their safety.

2. STRUCTURAL HEALTH MONITORING UPDATE

Over the past several decades, a significant research effort has focused on the development of algorithms to locate and quantify structural damage using non-destructive methods. Damage is defined here as a loss or change in structural stiffness. Work has focused on systems identification algorithms as well. System identification is taken here as the construction of a numerical model from input/output data. The area of structural health monitoring has gained notoriety as a complementary technology to system identification and non-destructive damage detection methods [6].

2.1 Review of Recent Work

In an effort to rapidly assess the state of structural health monitoring, a workshop was held at the University of California, San Diego to develop a preliminary consensus of the state of the technology [7]. The Workshop included attendees who have worked in different areas of structural health monitoring for the past decade or longer. Researchers in such areas as sensors, system identification, non-destructive damage detection, data acquisition and transmission, and visualization were invited to discuss their work. A brief summary is provided below.

Several papers on sensors were included that discussed accelerometers and fiber optic strain gauges. Specifically, a general review of fiber optic sensors was provided, as well as a system to detect debonds in concrete reinforcement utilizing a smart sensor. Another paper presented a review of fibre optic sensor applications. Included in that paper were results from a pipeline that was monitored to predict its remaining service life based on a

corrosion model of the pipe. Another researcher discussed the development of a low-cost wireless sensing unit for deployment in a structural health monitoring system, and pointed out that installation costs for a monitoring system can represent up to 25% of the total system cost. Lastly, performance requirements for sensor networks were emphasized. It was pointed out that performance requirements of the sensor network need to be defined early to drive development of a useful and economic sensor system.

Another important area of structural health monitoring discussed at the Workshop was damage detection and system identification advances. A general overview of several structural health monitoring approaches useful for the detection of changes in civil infrastructure systems and components, using both local and global system identification techniques was presented. Another researcher pointed out that baseline updating is the first step for model-based structural health monitoring of civil infrastructure. A stochastic optimization technique was used to construct a reliable baseline model of an instrumented highway bridge. In another work, the Damage Index Method was used to evaluate a reinforced concrete T-girder bridge rehabilitated using FRP composite materials. The Damage Index Method successfully identified changes in stiffness resulting from the structural rehabilitation. Lastly, the application of adaptive computing algorithms to the problem of damage detection and localization in structural systems was presented. In the first approach, damage was defined as changes to the material and / or geometric properties of systems including changes to the boundary conditions and system connectivity, which adversely affect the system's performance. In this application, the algorithms refer to systems identification approaches that determine if changes in system parameters are significant and indicative of damage to the structure. In comparison, applied adaptive computing algorithms were applied to an aircraft. That work concluded such an approach could serve as a Level III damage detection method; however it was unclear how it could be used to evaluate damage and predict remaining service life of a structure.

Included in the Workshop were two papers describing structural health monitoring efforts in Japan and Canada. More specifically, ISIS Canada is focusing on the integration of new materials such as fibre reinforced polymer (FRP) composites in civil applications and the need for structural health monitoring to demonstrate the importance of these new materials. An in-depth summary of structural health monitoring in Japan was provided as well. More specifically, the application of vibration-based techniques on large-scale structures was reviewed, as well as recent innovation in sensory and monitoring technology.

Two areas which have received limited attention are the areas of data transmission and visualization. A need will arise to rapidly transmit data to

a central location, as well as quickly view the results once health monitoring systems are ready for wide spread implementation. To satisfy that need the ROADNet (real-time observatories, application and data management network) Program, as well as novel system architecture for exploiting distributed video array in automated motion detection, analysis, and event recognition was provided.

Lastly, two researchers presented integrated structural health monitoring systems. For example, one paper provided an in-depth description of a health monitoring system developed and implemented by the authors for a long span bridge. While the paper discussed several important concepts related to health monitoring, the method did not provide any means to locate and quantify damage, estimate remaining service life nor load rate the bridge. Another health monitoring system was described that envisioned a framework that will network and integrate real-time sensor data, database and archiving systems, computer vision, data analysis and interpretation, physics based numerical simulation of complex structural systems, visualization, reliability and risk analysis, and rational statistical decision making procedures. The authors premise their work on the idea that the main issue facing structural health monitoring is not the lack of measurements per se, but rather how to measure, acquire, process, and analyze the massive amount of data to extract useful information concerning the condition assessment of the monitored structures. Unfortunately neither demonstrated a method to detect and evaluate damage.

Lastly, a summary of the AISC-ASCE benchmarking study was presented. Phase 1 of the study focused on modeling error and the lack of input information. Phase II will focus on an actual structure.

2.2 Weaknesses

Current work toward development of structural health monitoring systems can be classified either as a data-driven approach or a physics-driven approach. In a physics-driven approach, a physical model of the structure is developed, typically using finite elements. Experimental results from the health monitoring system are used to update this model, and then locate and quantify damage. A data-driven approach develops a model as well; however the model is based more on statistical mechanics than structural mechanics. Most health monitoring systems collect data that is compared with results from some numerical model. The weakness with the data-driven approaches is a focus on identifying a change based on the large quantities of data extracted from the structure, rather than identifying what information is needed and then collecting the experimental data from the structure in service. While some systems incorporate a system identification

or non-destructive damage evaluation algorithm to rapidly process the data, these are the exception, not the rule. The issue of evaluation of bridge capacity and estimation of remaining service was mentioned by several authors, however no one demonstrated a methodology by which capacity and remaining service life could be obtained.

In summary, there are at least three major weaknesses from the perspective of a bridge owner, associated with the current focus of structural health monitoring. First, the cost to install and maintain the infrastructure associated with a database system is enormous. Second, a database system is not mobile and is limited to permanently instrumented bridges. Third, the ability of a data-based monitoring system to evaluate safety is limited to the events seen by the monitoring system. Even more frustrating to a State Bridge Engineer is the lack of consensus among researchers and a failure to evaluate differing systems [7]. An owner needs a SHM System that can evaluate the ability of the structural system to function as designed and estimate the remaining service life of the structural system.

3. PROPOSED STRATEGY

In order to be of value to a transportation agency for wide spread application, a structural health monitoring system must satisfy the following attributes. First, the system must be mobile as well as fixed and utilize the minimum number of sensors possible. That is, the sensors can be permanently mounted or temporarily mounted on the bridge to gather sufficient data to evaluate the structure as needed. Second, it must be able to rapidly locate and quantify damage on a global basis. Third, it must incorporate local NDT techniques to enable an Inspector to physically locate the defect identified by the damage detection algorithm. Lastly, the system must be able to estimate structural capacity and remaining service life.

In an effort to determine which work is beneficial to the development of a structural health monitoring system, a strategy is proposed to investigate the economic feasibility of implementing structural health monitoring on bridges in general. First a previously developed Level IV NDE method is reviewed. Based on this, a plan is formulated to investigate the economic feasibility of implementing this technology.

3.1 A Level IV Damage Assessment Method

Over the past ten years, a group at Texas A&M University has been funded by the Federal Highway Administration and the California Department of Transportation to develop a general methodology to non-

destructively evaluate the structural safety of bridges [8]. Key elements of the methodology are listed below:

1. determine the questions the owner would like answered;
2. develop the necessary instrumentation plan;
3. measure structural response of the existing structure;
4. use systems identification and measured modal parameters to generate an estimate of a baseline structure;
5. use modal parameters of baseline and existing structures to identify stiffness properties of the existing structure;
6. identify loading environments for analysis (e.g., wind, traffic, or seismic);
7. develop system failure models for the structure;
8. extract resistance capacities of the elements from the identified structure, and
9. perform a system reliability analysis.

A key step in the procedure is the capability to relate the resistances of the components of the structural system (as they are used in the reliability sense) to the measured dynamic response of the existing structure by means of a damage localization and severity estimation scheme. This "Level IV Damage Assessment" methodology has been successfully demonstrated using several types of bridges subjected to a variety of loading types. The structural capacity and useful life of a structure can be estimated by integrating nondestructive testing, damage localization and severity estimation, structural and system reliability, and fatigue analysis [9, 10].

3.2 Development of an Implementation Plan

Using the above methodology as a guide, a plan is formulated to investigate the economic feasibility of implementing structural health monitoring on bridges. As a start, the plan must investigate the following:

1. What output does a bridge owner expect from a structural health monitoring system?
2. What algorithms are available to provide this output?
3. What measurements are needed as input to these algorithms?
4. What sensors are available to measure this response?
5. Can the SHM System cost be reduced significantly?

As noted earlier by others, identification of the requirements expected from the SHM System is critical [7]. As a minimum, a State Bridge Engineer needs to know whether the bridge can continue to carry the load for

which is was designed, as well as for how long. Based on these requirements, are existing algorithms sufficient to provide this information? In addition, criteria are needed to evaluate the performance of these algorithms; such as probability of detection, probability of false positives, data processing needs of the algorithm and the complexity of the algorithm. Once an algorithm is identified, what measurements of structural response are needed and can they be collected using existing instrumentation? Are there issues related to multiplexing and distributed sensing, as well as the reliability and durability of the instrumentation and data transmission systems. Lastly, how much of the data reduction and damage assessment can or should be done on-site?

4. APPLICATION OF THE METHODOLOGY

Two examples are provided where this damage assessment methodology was applied to structures in service. In both instances the capacity of a bridge in-service was evaluated.

4.1 Byron Road Bridge

The bridge selected for rehabilitation was built in 1964 and is a 340 foot long, 5 span, two-lane highway bridge spanning an aqueduct canal. The superstructure consists of a cast in-place, continuous, reinforced concrete T-girder, monolithically connected to the bents. The 6-1/4 inch (158.75 mm) thick reinforced concrete deck spans transversely between the 7.25 feet (2209.8 mm) center-to-center spaced girders.

In the spring of 1998, this bridge experienced punching shear failures at two locations on the bridge superstructure. After analysis of the structure, a strengthening measure was proposed that included carbon fibre reinforcement bonded directly to the bottom soffit with an epoxy adhesive. Table 1 presents the results of the damage assessment showing a maximum increase in stiffness after strengthening of over 20%. The resultant flexural demand – capacity ratios were calculated for each span, based on the December 2000 results. A demand/capacity ratio of 1.0 or less is considered acceptable.

Table 1. Results of Damage Assessment

Span	Average Increase in Stiffness			Flexure
	Baseline	December 1999	December 2000	D/C
1	0	-0.04	-0.01	0.81
2	0	-0.24	-0.02	0.92
3	0	-0.12	-0.01	0.85
4	0	-0.16	-0.02	0.87
5	0	-0.03	-0.03	0.81

4.2 Kings Stormwater Crossing Bridge

The bridges carrying State Route 86 across the Kings Stormwater Channel near the Salton Sea are two span structures carrying two lanes of traffic and are 13.0m (42.5 feet) wide. The bridge carrying northbound traffic is constructed using fiber-reinforced polymer (FRP) composite materials and is 20.1m (66.0 feet) in length. The bridge system consists of a two-span beam-and-slab superstructure with a multicolumn intermediate pier. The superstructure is composed of 6 longitudinal carbon shell girders with a wall thickness of 10 mm (3/8 inch) and a 343 mm (13.5 inch) inside diameter. They are connected across their tops with a modular FRP deck system. The damage localization results in Figures 2 and 3 indicate the development of separation of the deck panels between 26 Sep 01 and 05 May 02. For these data sets, the severity estimation approached 1.0 indicating a complete loss of capacity at those elements. This “damage” was easily verified by field investigation and deemed insignificant.

5. CONCLUSIONS

An owner needs a SHM System that can evaluate the ability of the structural system to function as designed and estimate the remaining service life of that system. A strategy was proposed to investigate the economic feasibility of implementing structural health monitoring on bridges that satisfies that need. To accomplish this, an existing Level IV NDE method was reviewed and the weakness of existing work that is not advancing implementation of a SHM System was reviewed. Lastly, examples were provided to demonstrate the technical feasibility of the SHM System using a Level IV NDE Method. What remains is to evaluate the economic feasibility of implementing such a system. To accomplish this, a consensus must be developed among academia, industry and government.

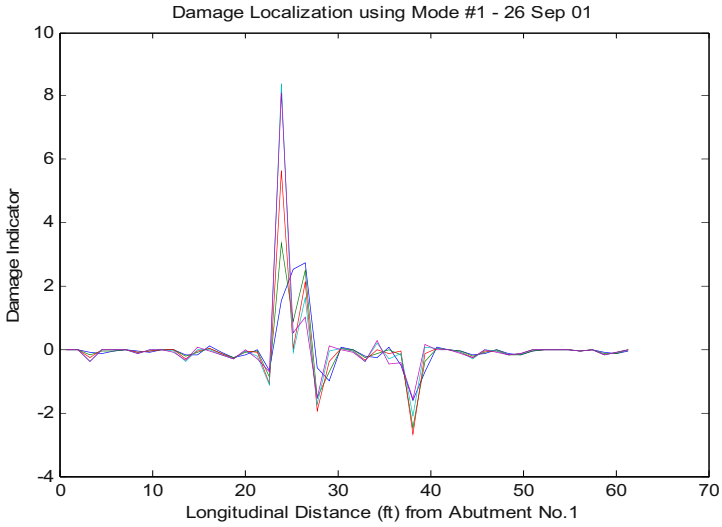

Figure 2. Damage Localization using Mode #1 – 26 Sep 01

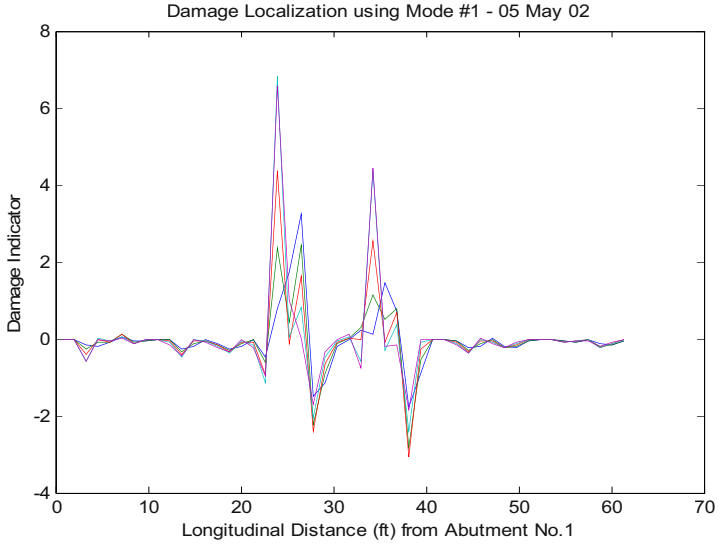

Figure 3. Damage Localization using Mode #1 – 05 May 02

ACKNOWLEDGEMENTS

The Author wishes to acknowledge the support of the California Department of Transportation. Also, the Author wishes to acknowledge Mike Keever for his critical review of this paper. Views and opinions presented here are those of the Author and should not be interpreted as official policy of the Department or the State of California.

REFERENCES

1. Farrar, C. and D. Jauregui. Damage Detection Algorithms Applied to Experimental and Numerical Modal Data from the I-40 Bridge. Los Alamos National Laboratory Report #LA-13074-MS, Los Alamos, New Mexico, January, 1996.
2. Housner, G.W., L.A. Bergman, T.K. Caughey, A.G. Chassiakos, R.O. Claus, S.F. Masri, R.E. Skelton, T.T. Soong, B.F. Spencer, and J.T.P. Yao. "Structural control: past, present, and future." Journal of Engineering Mechanics, ASCE 123(9), September 1997, pp. 897-971.
3. Karbhari, V.M., Chin, J. W., and D. Reynaud. “Critical Gaps in Durability Data for FRP Composites in Civil Infrastructure.” Proceedings, 45th International SAMPE Symposium, SAMPE, Long Beach, California, May 21-25, 2000.
4. Concrete Society, “Design Guidance for Strengthening Concrete Structures Using Fibre Composite Materials,” Concrete Society Technical Report No. 55, 2000.
5. ASCE 2003 Progress Report (2003).
6. Chang, F.-K., (ed). Proceeding of the International Workshop on Structural Health Monitoring. Stanford, CA, September, 2001.
7. Charles Sikorsky and Vistasp Karbhari (ed.), *Structural health monitoring and diagnostics of bridge infrastructure*; *Proc. Workshop, La Jolla, California, 7-8 March 2003*.
8. Stubbs, N., Park, S., Sikorsky C., and S. Choi. “A Global Non-destructive Damage Assessment Methodology for Civil Engineering Structures.” *International Journal of Systems Science*, Vol 31 (11), 2000 pp. 1361-1372.
9. Park, S., N. Stubbs, and C. Sikorsky. "Linkage of nondestructive damage evaluation to structural system reliability." Proceeding, Smart Structure and Material Symposium, SPIE, San Diego, March 1997, pp. 234-245.
10. Lee, L., C. Sikorsky and V. Karbhari. “Remaining Service Life of FRP Rehabilitated Structures.”, SAMPE National Convention, San Diego, CA November 2004 (to be presented).

SENSORS – NOT JUST FOR RESEARCH ANYMORE

Nicholas P. Vitillo
New Jersey Department of Transportation, Bureau of Research, 1035 Parkway Avenue, Trenton, NJ 08625, USA

Abstract: The use of sensors for research applications is commonplace. But the need and use of sensors has made the transition for the realm of the highly scientific research world to mainstream of engineering applications. This migration is due in part to the improvement or enhancement of the sensor itself and in part to the enhancement of related technologies – computers, cellular technology, and wireless technology. The other reason for the migration is based on need. Mainstream engineering recognizes the benefit of the senor technology to address their need for reliable data to assist with decision making, incident management, validation of assumptions, safety, and security enhancements. The paper provides a summary of the sensor uses outside of the research community and identifies some emphasis need in sensor technology and related technologies.

Key words: Sensors, Safety, Management Systems, Security

1. INTRODUCTION

New Jersey Department of Transportation (NJDOT) like many states has been using sensor technology in their research program to collect a wide variety of data element for their research projects. We considered these sensors as elements in our research toolbox. The advances in sensor technology (e.g., size, cost, capabilities), computers, cell phone technology, and wireless technology has attracted the attention of other transportation

Farhad Ansari (ed.), Sensing Issues in Civil Structural Health Monitoring, 55–64.

sectors. Our research tools have made a successful transition to the mainstream engineering and operations applications.

Sensor technology is cited as one of the hottest trends for 2004. [1] The use of sensor technology has broadened beyond the research realm. It has found its way into the areas of safety, operations, environment, infrastructure management, goods movement, and security,

The reasons for using sensors has also expanded. Sensor had been primarily used to collect research data as part of discovery. Now the sensors are being used for verification of assumptions, continuous monitoring 24/7, sensing what cannot be seen, monitoring long-term effects, and providing tools for a more secure life. [2,3]

2. MAINSTREAM APPLICATIONS

2.1 Bridge Design, Materials, and Construction Linkages

The use of the sensor technology has provided tools for the research, bridge, materials, and construction engineers to verify assumptions made during design, to visualize concrete strength development over time in three-dimensions, to confirm in-situ properties and temperatures, and to provide an objective means for early stripping of forms or opening to traffic. The sensor tools also open up lines of communications between these engineers in a way that has rarely been done before. The bridge engineer in headquarters can view the same data as the regional materials engineer and the on-site construction engineer. Decision or changes can be made in real time.

Sensors were incorporated in a multi-phased construction project using the first Load Resistance Factor Designed (LRFD) bridge in New Jersey. The research project principal investigator and bridge design offices worked together to perform a 3-D Finite Element Analysis (FEM) of the bridge and of the optimal sensors locations in the bridge. During construction sensor data provide information on concrete temperature, beam deflection, deck strains, and more. After construction, various weighted trucks were used to calibrate the weigh-in-motion sensors and to verify design assumptions. Modifications were made to the design based on the data. In phase 2, a latex modified overlay was placed on the deck after modeling with the 3-D Finite

Element Analysis. The sensors in the overlay and phase 1 deck construction helped to verify the results of the FEM analysis for the LRFD bridge.

The same project also incorporated a new bridge approach design. Adding sensors to the original and modified designs provided verification that the new design was nearly four times stronger than the original design and the remainder of the approach slabs were changed to the new design based on these results. In addition, the bridge engineer changed approach slabs on other projects to reflect the observed improvement on the research project due to the strong evidence provided by the sensor technology.

The use of wireless sensors to record in-situ concrete maturity and strength gain has improved the quality control and efficiency at pre-stressed concrete plant and for in-place concrete operations. It provides a tool to verify the assumed concrete strengths used in the design, but adds three-dimensional capabilities that were not easily available with concrete cylinders. The technology also provides the contractor and resident engineer with an in-situ estimate of strength and concrete temperatures for stripping forms, especially important during winter concreting operations.

Sensor technology is also finding innovative applications in lesser engineering focused applications. The New York State Thruway Authority coordinated the development of an electronic system that detects vehicles that are too tall for the network. The system uses sensors to monitor the height of trucks traveling on the New York State Thruway. [4]

The familiarity with the technology has also led to the incorporation of sensors for long-term monitoring of the structural integrity into the structure during design and construction, not as an-add on element. [5]

2.2 Pavement Design, Materials, and Construction Linkages

The NJDOT has been conducting a series of research project under a Mechanistic Pavement Design “umbrella” to collect data necessary for a rapid implementation of the new AASHTO guide. The studies have collaborated laboratory and field testing with strategically placed pavement temperature, moisture, ground water level, and freeze-thaw depth sensors that will continue to provide the pavement designer, materials engineer, and management engineer with data for more accurate assessment of pavement properties, and remaining life. The long-term data will be used by the design engineer and management engineers to modify current pavement design equations, performance equations, and for adjustment a pavement properties based on the temperature and moisture conditions. The seasonal variation research project incorporated two of NJ’s Long Term Pavement Performance

(LTPP) Specific Pavement Study (SPS) sites [SPS 5 and SPS 9]. The data from these sites will also be used to make model adjustments for Superpave implementation at the State and local levels.

In an article for Better Roads Magazine, Kuennen, reported on the use Smart structures and the FHWA's nanotechnology initiative. "Some inspectors are querying sensor systems embedded in, or attached to, specific locations on the structure using a mobile device for interfacing with these various sensors. The inspectors are able to access the loading conditions and corresponding structural responses, and any changes in local material properties, of the structure since the last inspection period. Several wireless maturity meters, attached to rebar and about the size of a candy bar, were imbedded in the newly placed pavement. Using a handheld computer, data were collected and analyzed to provide a concrete strength value. Recorded data include current temperature of the pour, date and temperature when poured, and dates on which it was last checked. Because the wireless meter provides immediate and continuous data, on the progress of the strength gain Michigan DOT was able to open the pavement without delays." [1]

The use of temperature, moisture, and strain sensors in pavements that use Accelerated Load Facilities (ALF) to rapidly assess pavement material performance in Kansas and Turner Fairbank Highway Research Center provide for improved modeling of pavement stresses, strains and material properties and condition for the non-homogeneous, anisotropic, and climatically affected pavement materials. [6] Other applications, like Smart Roads in Virginia provide a blue print for expanding the use of sensor technology to everyday pavement applications and monitoring.

2.3 Safety Linkages

In a comprehensive article, Karr summarized the most dramatic use of sensors under the Intelligent Vehicle Initiative, a program that is targeted at high-frequency crashes. They include: 1)a forward collision warning and adaptive cruise control system that uses electronic sensors, Global Positioning System, and radar to provide audio and visual warnings on a head-up display to a driver who follows another vehicle too closely; 2) radar-based lane-change and road- departure warning technology; 3) a rollover stability advisor/controller system to aid truck drivers in avoiding rollovers; 4) a bundled safety package comprised of electronically-controlled braking, disc brakes, and a commercial rear-end collision avoidance system (CAS) for trucks; 5) collision warning systems for transit buses; 6)

"intelligent intersection" technology; and, 7) radar detectors at rural unsignalized intersections. [7]

In some recent studies, NJDOT Research used sensors to verify information from traffic simulations models for transit bus prioritization and enhancement of round abouts. The traffic and safety engineers plan to continue to use sensors to verify results from traffic simulations models at other locations. Truck location tracking with global positioning systems is common, and prototype systems exist for characterizing surrounding traffic and roadway conditions. This technology is being used to monitor flow patterns for traffic operations centers along with traffic speed and incident location information to optimize timing and evaluation of alternative route information. [8]

A report by the SRF Consulting Group [9] summarizes the use of sensor technology to detect the presence of non-motorized traffic – bicycles and pedestrians. "The majority of traffic detection technology and sensor research has focused on the detection of "motorized" traffic. This has left a need for objective information on the performance of "non-motorized' traffic detectors. Bicycles and pedestrians are the two most common types of non-motorized traffic. In recent years, sensors have been developed to detect the presence of pedestrians and the speed and presence of bicycles. This has been accomplished with a variety of technologies, including microwave, infrared, video and inductive loops. These applications optimize intersection operations and improve safety by reducing the conflicts between vehicles and pedestrians. Similarly, bicycle detectors are being used to provide detection inputs to traffic signals for call and extend functions."

These types of sensor have been incorporated into lighted crosswalk technology in NJ to activate the flashing crosswalk when the presence of a bicyclist or pedestrian is detected.

Workzone safety has received increased attention. The use of GPS and sensors in workzones have been identified as tool that can have a significant effect on improving worker and traveler safety in workzones. Fontaine [10] illustrated the use of the Work zone intelligent transportation systems (WZITSs) program as a way to improve safety and reduce congestion at work zone locations. These systems usually integrate portable changeable message signs and speed sensors with a central control system that automatically determines appropriate messages that are based on current traffic conditions to warn drivers of downstream congestion, alert drivers to slower speeds ahead, and suggest alternate routes on the basis of prevailing conditions.

The use of pavement sensors coupled with cameras provides the means for traveler information on alternate routes and rapid deployment of emergency response units. Expanding the system with RWIS sensors to measure pavement and bridge temperatures and anti-icing chemical concentrations through the traffic operations centers provides a means of ensuring traveler safety during inclement weather by deploying salt and chemical unit when and where they are needed. [11]

Tuan reported on the use of sensors in an innovative conductive concrete application in Nebraska. Conductive concrete is a relatively new material technology developed to achieve high electrical conductivity and high mechanical strength. Temperature sensors and a microprocessor-based controller system were installed to monitor and control the deicing operation of the inlay. The sensors help to control the system allowing sufficient power to maintain an ice-free deck. [12]

Swearingen also explored the balance of environmental factors with traveler safety in a study for the Ohio Department of Transportation (ODOT), which already had 72 Road Weather Information Systems (RWIS) sites in place, recently expanded its reporting station coverage to 160 sites, with more than 400 pavement sensors on the state's highways. The new Environmental Sensing Stations (ESS) are totally wireless, using a combination of wireless pavement sensors with solar panels power and cellular communications. The RWIS has been shown to be a system that is useful year round, as the pavement sensors can also monitor traffic speed, traffic volumes, and wind speeds. [13]

2.4 Management System Linkages

Pavement, Bridge, Asset, Maintenance, and Safety Management Systems have increased the use of sensors in their program to collect a variety of data elements on a periodic or continuous basis. Data from sensors incorporated in these systems can be shared to form and integrated or overall management system.

Casas credited advances in the production of optical fibers made possible the recent development of innovative sensing systems for the health monitoring of civil structures. The main reasons cited are the reduced weight and dimensions of fiber optic sensors, the strong immunity to electromagnetic interference, the improved environmental resistance and the scale flexibility for small-gauge and long-gauge measurements. These systems can provide high-resolution and measurement capabilities that are not feasible with conventional technologies. In addition, they are

manufactured at a low cost and they offer a number of key advantages, including the ability to multiplex an appreciable number of sensors along a single fiber and interrogate such systems over large distances. “For these reasons, it is evident that fiber optic sensors will change the instrumentation industry in the same way fiber optics has revolutionized communications.” [14]

To facilitate an efficient bridge management system, knowledge is required of the state of health of bridge structures. over 10 percent of bridges in the U.S. have been found to be structurally deficient. Electronic monitor of bridge structure constitutes a major advance in industry technology, as it integrates processing electronics with sensors, a combination that enables it to use digital communications. [15-17]

The use of sensors will increase with the implementation of the new AASTHO Mechanistic-Empirical Design of Pavement Structures. Kim describes a new method for estimating the axle weight of a moving vehicle that will help to improve the traffic weight data and allow the development of improved load spectra curves. It uses two piezoelectric sensors and an adaptive-footprint tire model. The method is less sensitive to variable factors that influence the axle weight of a moving vehicle. [18]

2.5 Security Linkages

The events of September 11, 2001 forced the United State to take a new look at homeland security at the National, State, and local levels. The security of the transportation industry is at the center of this effort. The movement of people, goods, utilities, and pipelines as well as natural resources - rivers and water reservoirs are the cornerstone of our economy and way of life. These events emphasized the need to use all means available to ensure the safety of our citizens and visitors. The security umbrella will greatly accelerate the development and implementation of new sensor technology. [19]

Hundreds of thousands of cargo container arrive on ships everyday from foreign countries. One of the most important problems facing the U.S. Department of Transportation is the detection of illegal chemicals and explosives entering this country. There is a major concern for the security risk that this presents. One solution presented by Tyler looked at the concept of smart cargo containers fitted with sensors that can detect intrusion and radiation. The sensors feature two-way communications devices that can alert security personnel. Bosco also addressed these concerns. He cited the limitations of the current methods used by governments to detect harmful substances by means of physical inspections, sophisticated detection

instrumentation and trained "sniffing" dogs. He discussed the feasibility of integrating a variety of microcantilever sensors into a hand-held sensor system capable of sensing and identifying illegal explosives. Researchers at the University of Alabama at Huntsville have developed the capability to design, fabricate and test microcantilever devices that can detect trace amounts of most organic and inorganic chemicals. These sensors are so sensitive that, in some cases, they can exceed the sensitivity of trained dogs. The sensors are small enough that many sensors can be placed on a single silicon chip. "[20-22]

Security around airports is particularly sensitive. Many high tech innovations have been pressed into service within the terminal complexed, but less has been done to secure the extent of the airport property. The size of most airports makes perimeter security extremely difficult. Aloni described the use of a new technology for airport security on the runways and taxiways. Perimeter security requires "smart" fences that can detect attempts to breech them. The sensors can be calibrated to only respond to stimuli above a certain threshold in intensity to avoid false positives. [23]

While airport have received much attention, the security of our natural resources deserves as much focus. Shenkiryk discusses concerns for our nation's water systems and the associated supply, treatment and distribution infrastructure. He discusses an automated infrastructure surveillance technology that was developed and implemented.. This centralized information management system integrates and provides surveillance information using a single universal interface that allows the display of all monitoring devices within a water agency's inventory to include the management of input from videocameras, motion detectors, acoustic sensors, and other like devices. [24]

3. CONCLUSIONS

Sensors have made a successful transition to the mainstream engineering and operations areas. The transition will continue to increase as the sensor and related technologies improve and the needs expand.

REFERENCES

1 Kuennen, T. "Hottest Trends for the New Year: Here's a Quick Rundown on Some of 2004's Cutting-Edge Themes in

Transportation Infrastructure Construction, Maintenance", Better Roads, Volume: 73 Issue: 12, pp 20-26, 28, 30, 32-33, 2003.

2 "High-Tech Future Begins to Take Shape with Tampa Expressway", Engineer News Record. Volume: 250 Issue: 17, 2003.

3 Sinha, SK . "State-of-the-Art in Sensor Technologies", Proceedings of the ASCE International Conference on Pipeline Engineering and Construction. Baltimore, Maryland, Volume 2 pp 1592-02, 2003.

4 Breskin, Ira. "Wiggle Room at Highway Bridges", New York Times. 05/25/2003.

5 Grivas, DA; Garlock, M. "Sensing Systems for Bridges: An Assessment of the State-of-the-Art", Recent Developments in Bridge Engineering. Proceedings of the Second New York City Bridge Conference. pp 269-284, 2003.

6 Wu, Z; Hossain, M "Pilot Instrumentation of a Superpave Test Section at the Kansas Accelerated Testing Laboratory", KTRAN: KSU-98-2,; Final Report Kansas State University, Manhattan, 2003.

7 Karr, Al "Test Smarties: New Accident Prevention Technology in Development Stage", Transportation management + engineering. Vol. 9, no. 1. 2004.

8 Akinci, B; Hendrickson, C; Karaesmen, I. "Exploiting Motor Vehicle Information and Communications Technology for Transportation Engineering", Journal of Transportation Engineering. pp 469-474, 2003.

9 SRF Consulting Group, Incorporated. "Bicycle and Pedestrian Detection", SRF Consulting Group, Incorporated. 2003.

10 Fontaine, MD. "Guidelines for Application of Portable Work Zone Intelligent Transportation Systems", Transportation Research Record 1824. pp 15-22, 2003.

11 Kim, Seongmoon. "Optimal Vehicle Routing and Scheduling with Real-Time Traffic Information", 2003.

12 Tuan, CY; Yehia, SA. "Implementation of Conductive Concrete Overlay for Bridge Deck Deicing at Roca, Nebraska", Sixth International Symposium on Snow Removal and Ice Control Technology. E-C063, SNOW04-002, 2004.

13 Swearingen, KC. "Odot Deploys Massive Wireless Environmental Sensing Station Technology in RWIS Expansion", APWA Reporter. Volume: 70 Issue: 9, 2003.

14 Casas, JR; Cruz, PJS. "Fiber Optic Sensors for Bridge Monitoring", Journal of Bridge Engineering. pp 362-373, 2003

15 Ross, R; Goldstein, M. "Monitor Warns of Bridge Corrosion",

Better Roads. Volume: 73 Issue: 8, pp 88-90, 2003.

16 Lin, MW; Thaduri, J; Gopu, V. “A Distributed Strain Sensor for Bridge Monitoring”, UTCA Report 02304,; Final Report. University of Alabama, Huntsville. 2003.

17 Watters, D. “Wireless Sensors Will Monitor Bridge Decks”, Better Roads Volume: 73 Issue: 2. pp 74-75, 2003.

18 Kim, Sung-Wook; Cho, Ilsoo; Lee, Joo-Hyung; Park, Jongyeon; Yi, Dong-Hoon; Cho, Dongil. “A new Method for Accurately Estimating the Weight of Moving Vehicles Using Piezoelectric Sensors and Adaptive-Footprint Tire Model”, Vehicle system dynamics. Vol. 39, no. 2, 2003.

19 Sawyer, T. “Threats Fray Nerves but Spawn Innovation: The Rush is on to Address Vulnerability with Surveillance Technology and Protections”, ENR Volume: 252 Issue: 2, pp 10-11, 2004.

20 Tyler, David. “Smart and Semi-Smart Containers Arrive to Counter Terrorism”, Professional mariner. No. 78, p. 4-7, 2004.

21 Bosco, CD. “Hand-Held Explosives Sensor System”, UTCA Report 03306,; Final Report. University of Alabama, Huntsville, 2003.

22 “Security Spurs Pace of AIS Implementation”, Marine Log, V. 108, No. 7 P. 13-16, July 2003.

23 Aloni, S. “Defending the Perimeter: Airports Perimeter Security is Often Overlooked”, Airports International Volume: 36 Issue: 2, pp 30-31, 2003.

24 Shenkiryk, M. “Automated Surveillance for Water Utilities”, New Pipeline Technologies, Security and Safety. Proceedings of the ASCE International Conference on Pipeline Engineering and Construction, Volume 1,pp 214-216, 2003.

INVESTIGATION OF THE DYNAMIC PROPERTIES OF THE BROOKLYN BRIDGE

Qi Ye[1], Guang-Nan Fanjiang[1], and Bojidar Yanev[2]
[1]*Weidlinger Associates, Inc;* [2]*Department of Transportation, New York City*

Abstract: The dynamic response of the Brooklyn Bridge in New York City to service and extreme event conditions is the subject of several investigations. Pedestrian type excitations were studied by ambient vibration monitoring and forced vibration tests. Mode shapes and frequencies, extracted from the collected data, compared well with the results of finite element analysis. Modal damping ratios were also estimated.

Key words: Acceleration, ambient, bridge, damping, excitations, forced, frequency.

1. THE BROOKLYN BRIDGE

The Brooklyn Bridge (Fig. 1) was first of the four East River crossings in New York City. Construction started in 1867 and was completed in 1883 at a total cost of USD 14 m. The land for the project had cost USD 25 m. The bridge was designed with two streetcar tracks, four carriage lanes and a pedestrian walkway. A 5 ct. toll was initially charged for crossings. The structure was later modified to accommodate 4 train track and, once again, to remove all tracks and restrict use to vehicular traffic and pedestrians, as shown on Fig. 2. The average number of daily users has fluctuated between 426,000 and 130,000.

At 1595 ft (487 m), the main span of the bridge almost doubled the existing record for length. Earlier attempts to span lesser distances with suspension structures had failed due to wind as in the case of Charles Ellet's (1810 – 1862) Wheeling bridge over the Ohio River (1854). John Roebling

Farhad Ansari (ed.), Sensing Issues in Civil Structural Health Monitoring, 65–72.

(1806 – 1869) stabilized his suspension bridges with a brilliant hybrid system of suspenders, diagonal fan-type stays and longitudinal stiffening trusses. The redundancy he sought is clearly expressed in his statement that removing the stays would cause the bridge to "sink in the centre", but not fail.

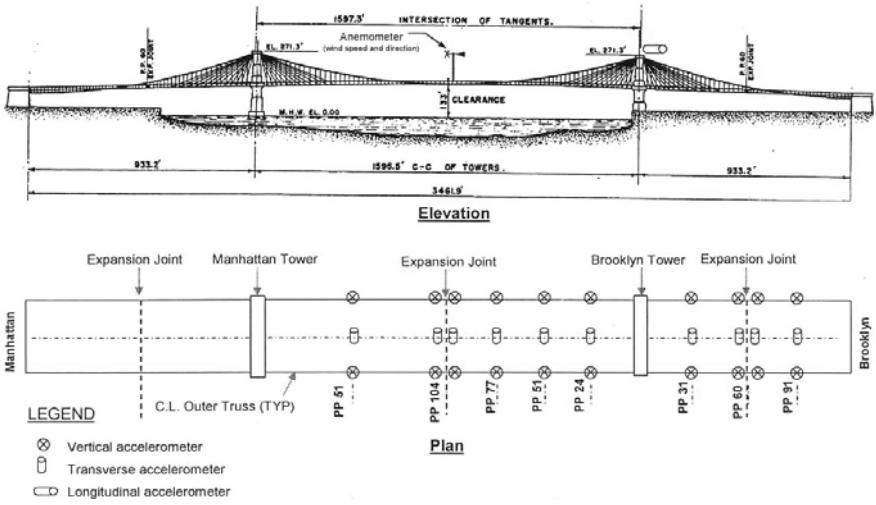

Figure 1. Brooklyn Bridge elevation and plan with sensor locations.

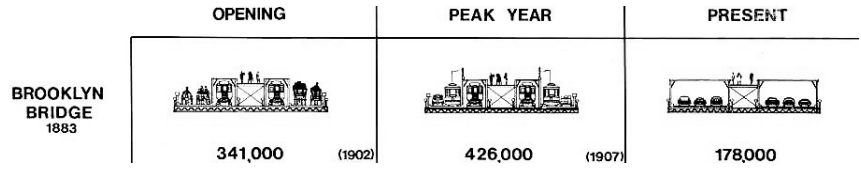

Figure 2. Cross-section modifications and corresponding number of daily users.

J. Roebling's model of stiffening against torsion was eventually abandoned, first by eliminating the stays and then by replacing the trusses with girders. After the Tacoma bridge was excited to a torsional mode failure by a moderate wind on November 7, 1940, various stiffening methods were rediscovered. In a 1988 tribute to the Brooklyn Bridge, J. Schleich and R. Walter proposed an award - winning hybrid stay and suspension structure for a replacement of the Williamsburg Bridge.

The redundant design saved the Brooklyn Bridge under circumstances Roebling might not have envisioned. In 1981 one of the diagonal stays, weighing an estimated 2 tons ruptured and fell on the footwalk, killing a

pedestrian. The subsequent investigation revealed advanced corrosion in the suspenders and stays. The structural redundancy allowed a full replacement to be conducted without traffic interruption at a cost of USD 53.57 m. (1991). Other work, beginning in 1981, and including deck and traveler replacement, rebuilding of approaches, painting, etc. has added up to USD 464.07 m. (NYC DOT 2003 Bridges and Tunnels Annual Condition Report).

After 121 years of service, professional confidence in the dynamic stability of the bridge remains unchallenged, however the general public has not always taken that on faith. On May 30, 1883, one week after the bridge opening, a rumored collapse caused the crowd, estimated at 20,000, to panic. 12 people were trampled to death in the ensuing stampede towards the bridge exits.

During the East Coast blackout of Aug. 14, 2003, the Manhattan-bound vehicular lanes of the bridge were opened to pedestrians, while the Brooklyn bound lanes remained under automobile traffic. In the following several hours a number of users reported large lateral motions on the bridge. None of the DOT engineers present at the site, including the author, could confirm the reports. Pedestrians are known for the following proclivities:

- to excite bridges laterally, as was recently demonstrated at the Millennium Bridge in London;
- to sense acutely small displacements.

Taking into account the management needs of the Brooklyn Bridge, NYC DOT undertook a dynamic analysis of the structure in 2003.

2. FINITE ELEMENT MODEL AND ANALYSIS

In order to study the dynamic behavior of the bridge, finite element models are essential. A 3-D finite element model (Fig. 3), including all the major elements of the bridge, was developed by Weidlinger Associates, Inc. using ANSYS 7.0 **[1]**.

Link (tension-only) elements were used for the cables, suspenders, over-floor stays, under-floor stays, truss diagonals/counters. Beam elements were used for floorbeams and truss chords, etc. The roadway decks were modeled by shell elements. Stays and suspenders were modeled with tension forces obtained from existing contract drawings. Longitudinal and rotational springs, whose properties were obtained by independent analysis, were used for modeling of the tower foundations. The towers were modeled by a combination of beam and shell elements. The below-floor stays near the towers were coupled with (slaved to) adjacent tower nodes. Cable ties, which connect the cables together to form their lateral curvature, were also modeled.

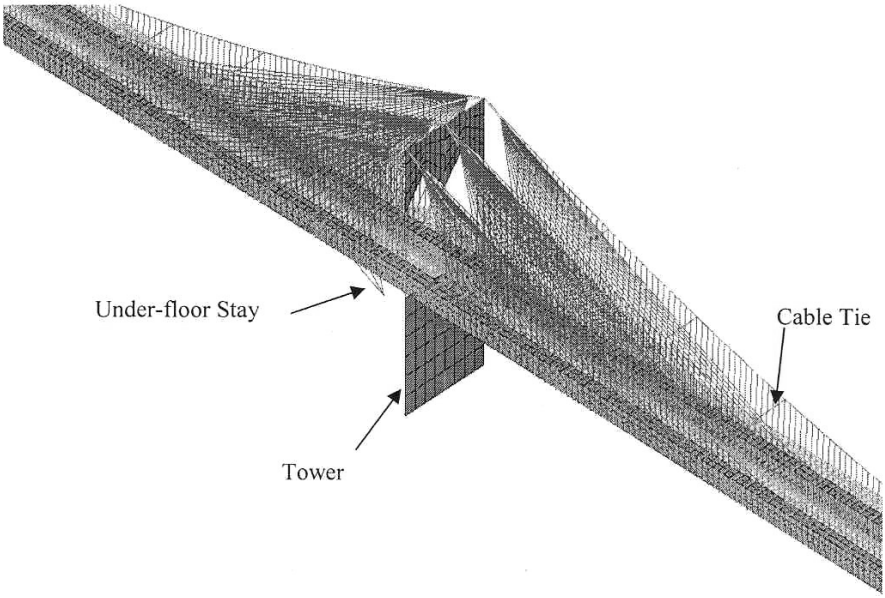

Figure 3. Finite element model for the analysis with ANSYS.

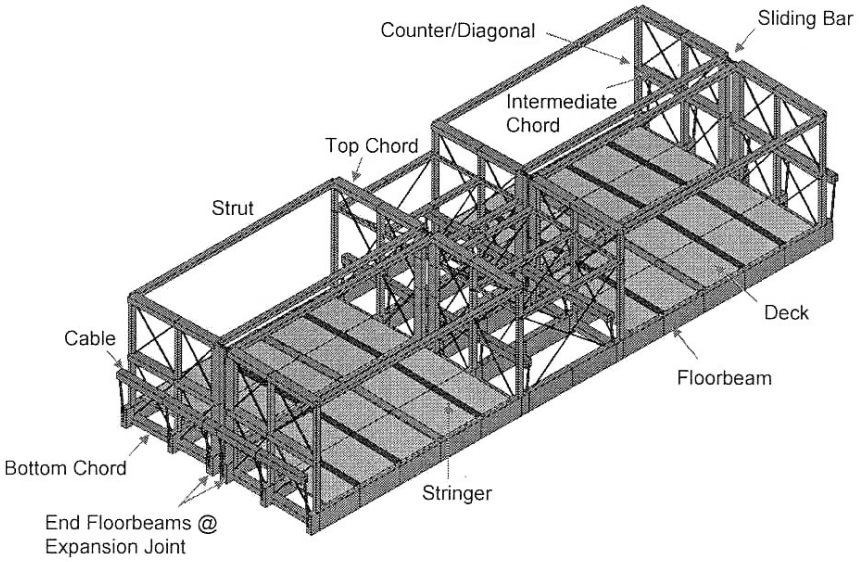

Figure 4. Details of the model.

Fig. 4 shows the details of the model. The 10 stringers in each roadway deck were modeled by 4 beam elements with equivalent properties. The decks were connected to the floorbeams by a set of linear springs in three directions at each node. Each deck relief joint was modeled by two sets of nodes, one per side. They were coupled together to restrict relatively translational movements, while allow relative rotations.

After the completion of the model, modal analysis was performed and the first lateral, vertical and torsion modes in the main span are shown in Fig. 5.

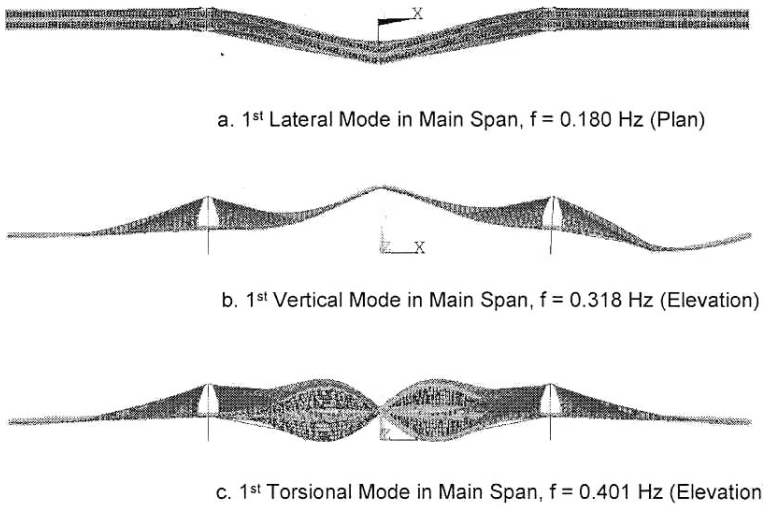

Figure 5. First modes obtained from analysis

3. AMBIENT VIBRATION MONITORING

Ambient vibration monitoring was performed on the bridge by ATLSS Research Engineering Center (ATLSS) of Lehigh University.

Fig. 1 shows the instrumentation plan for the ambient vibration monitoring. Accelerometers were installed at 10 cross-sectional locations along the bridge. At each location, there were 3 accelerometers – 1 in the transverse direction and 2 in the vertical direction. The only longitudinal accelerometer was installed at the top of Brooklyn Tower. Wind speeds and directions were measured by an anemometer at the middle of main span, 30 feet above the walkway. In total, 35 accelerometers were used for the monitoring.

Modes and damping ratios were determined from the collected data by ATLSS, Lehigh University. The field - measured modes were grouped into lateral, torsional and vertical. In each group, measured frequencies and mode shapes were matched with the analytical ones, obtained by Weidlinger Associates. 35 modes were observed from the field measurements between 0.0 Hz and 2.5 Hz. 34 of them were identified in the finite element model. The differences in frequencies were mostly small, except for a few of roughly 8%. The agreement between the measured and analytical results demonstrated that the finite element model was reliable and could be used for further analysis.

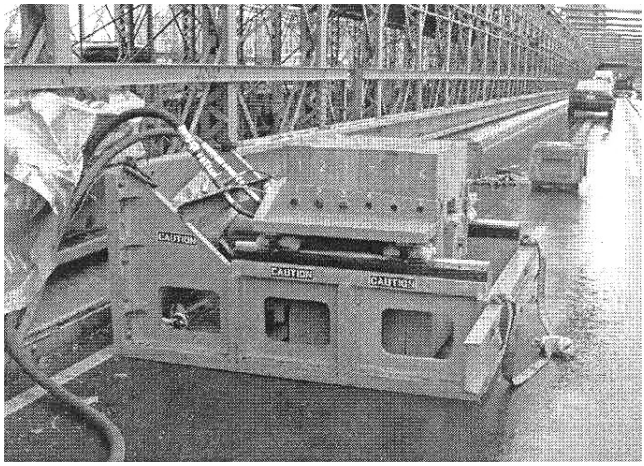

Figure 6. Electro-hydraulic actuator weighing 6.5 tons, with 2.5 ton capacity.

4. FORCED VIBRATION TESTS

Forced vibration tests in both the lateral and vertical directions were conducted on the bridge for the modes in the frequency ranges sensitive to pedestrian induced vibrations. These ranges were considered to be between 1.5 Hz and 2.5 Hz for the vertical direction and between 0.5 Hz and 1.5 Hz for the lateral direction. An electro - hydraulic shaker was provided by the US Army Corps of Engineers Engineering Research and Development Center (ERDC) for the tests. The shaker, shown in Fig. 6, weighs 6.5 ton and has a 2.5 ton capacity.

The tests, performed by ERDC, were conducted at the mid- and quarter-points of the main span and the mid-point of the side span. At each location, a variety of tests were performed in both the lateral and vertical directions. ATLSS analyzed the collected the data.

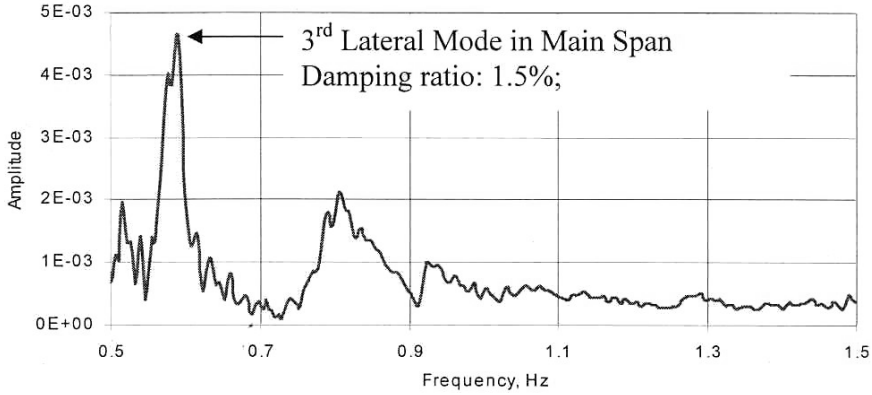

Figure 7. Figure FRF of a horizontal accelerometer near the Brooklyn tower, main span.

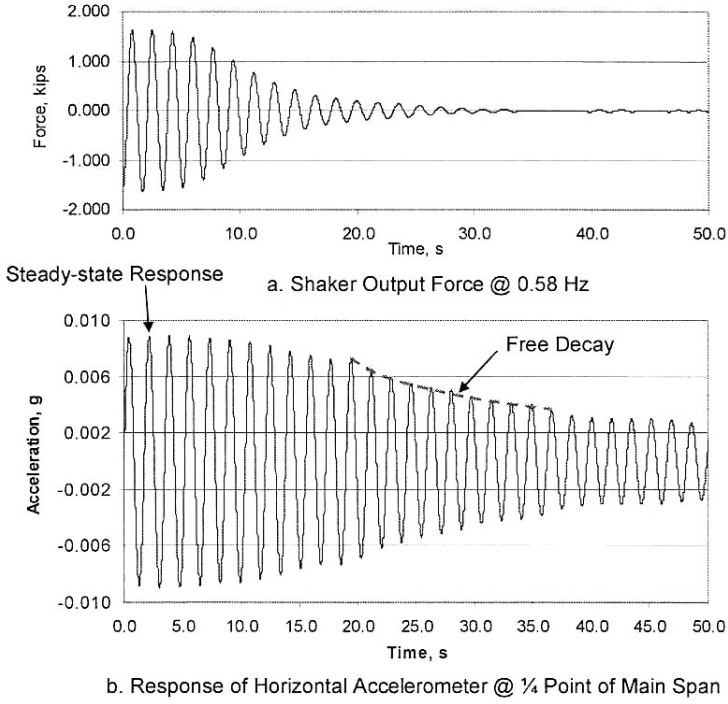

Figure 8. Resonant response of the 3rd lateral mode in the main span, f = 0.58 Hz.

First, slow sweep tests were performed. During these tests, the shaker frequency was modulated from the starting frequency to the final frequency

over 500 seconds. Since the shaker swept through the frequency range at a slow pace, at each resonant frequency, steady-state modal responses were achieved. Frequency response functions, as in Fig. 7, were generated for the collected data. Damping ratios were calculated by both the "circle fit" and the 'half power bandwidth" methods **[2]**.

The slow sweep tests were followed by resonant vibration tests. During these tests, the output frequency of the shaker was tuned to excite one modal frequency of the bridge until steady-state responses were achieved. Then, the shaker was turned off quickly to allow the bridge to vibrate "freely". Equivalent viscous damping ratios were calculated from the free vibrations decay. Fig. 8 shows the end of the resonant test for the 3rd lateral mode in the main span. The shaker was turned off quickly (Fig. 9-a) and the free decay of bridge vibrations was captured, as shown in Fig. 9-b. The damping ratio was estimated to be 0.85% for this mode. In total, 18 modes were tested by this method and their damping ratios vary from 0.7% to 3%.

5. CONCLUSION

In total, 35 modes were identified by the ambient vibration monitoring and their damping ratios were estimated.

The forced vibration tests excited 18 modes in the frequency ranges sensitive to pedestrian induced vibrations, and their damping ratios were also estimated.

The measured modes and frequencies compared well with the analytical results obtained by Weidlinger Associates and verified the finite element model.

The results of the investigation will serve in the long-term bridge maintenance and rehabilitation plans. They are already taken into account in the current seismic evaluation of the structure.

REFERENCES

1. ANSYS Program Version 7.0, ANSYS, Inc.
2. D. J. Ewins, 2000, "Modal Testing: theory, practice and application, Second Edition", Research Studies Press LTD.

Chapter II

Monitoring Issues in Ancient and Modern Structures

DISTRIBUTED SENSING TECHNOLOGIES FOR MONITORING FRP-STRENGTHENED STRUCTURES

Z.S. Wu and C.Q. Yang
Department of Urban & Civil Engineering, Ibaraki University, Japan

Abstract: In this paper, some research achievements on the damage detection of Fiber-Reinforced-Polymer (FRP) strengthened structures are briefly reviewed. Two primary methods are developed to make the FRP-strengthened structures with distributed damage detection functions. One method is to make full use of the inherent characteristics of materials to form smart structural systems. For HCFRP (Hybrid Carbon FRP)-strengthened structures, the HCFRP, used both as reinforcing and sensing materials, can provide the structures with smart structural health monitoring (SHM) function in virtues of the electrical conductivity. Another method, particularly for the electrically inert FRP-strengthened structures, is to embed distributed fiber optic sensors. It is revealed that these kinds of distributed sensing technologies are effective in monitoring the distributed damage, debonding behavior and the overall structural performance of FRP-strengthened structures, which can also be combined for the SHM and damage detection purposes.

Key words: SHM, FRP composites, damage detection, ER measurement, optic fiber sensing, Brillouin scattering, FRP-strengthened structures

1 INTRODUCTION

A number of existing civil engineering structures need being strengthened or monitored for the safety or realizing a long life span. FRP composites, in the forms of rod, cable, grid, sheet or plate etc., are widely accepted as attractive and innovative materials in rehabilitating and strengthening the existing

Farhad Ansari (ed.), Sensing Issues in Civil Structural Health Monitoring, 75–84.

infrastructures, due to their high strength, high stiffness and lightweight. In contrast to the traditional strengthening methods such as bonding steel plate and jacking, the bonding FRP represents a practical and effective method due to their excellent properties as well as high corrosion resistance, easy operation and so on. However, the FRP composite is a new kind of material in civil engineering, which results in a knowledge lack about the long-term properties, load transfer mode, failure mechanism and criteria. Moreover, the stress-strain behavior of FRP is linear-elastic up to the ultimate failure, and the energy release is mainly elastic and sudden. This kind of mechanical behavior can lead to a sudden rupture of the FRP. For the structures externally bonded with FRP sheets, the debonding of FRP sheets due to the limited ability along FRP-concrete interface is another critical failure mode.

Consequently, it is necessary to take some counter measures to lower or avoid the influence of such disadvantages. An effective and direct method is to resort to SHM technologies to inspect the FRP-strengthened concrete structures in a real time for signs of abnormality.

For the CFRP-strengthened structures, it is realized that they possess self-SHM capacity attributed to the electrical conductivity and piezoresistivity of carbon fibers. Both d.c. and a.c. ER measurements [1, 2] may be used as indicators about their structural health. However, for the CFRP with only single kind of carbon fibers, some issues limit its wide applicability. To upgrade the mechanical properties and obtain a more satisfactory self-sensing function, the authors developed the HCFRP in the forms of sheet or rod by hybridizing several types of carbon fibers and investigated their mechanical and electrical properties [3-5]. For the electrically inert FRP, such as Poly-p-phenylene benzobisoxazole (PBO) strengthened structures, the distributed fiber optic sensing technology, based on Brillouin Optical Time Domain Deflectometry (BOTDR), has been treated as an innovative monitoring strategy for the large-scaled civil engineering structures. The BOTDR sensing technology is based on the basic principle that Brillouin frequency shift in the Brillouin back-scattering spectrum is linearly dependent on the strain or temperature of the fiber[6-10].

The objective of this work is to investigate the sensing technologies for FRP-strengthened structures. For the HCFRP-strengthened structures, the ER method can be used to monitor the structural health, without discrete sensors and actuators. For the electrically inert FRP-strengthened structures, the structural health is monitored by means of optic sensing. Of course, the fiber optic sensing can be used to monitor the health of HCFRP-strengthened structures, and the HCFRP can also be used as sensors to monitor the electrically inert FRP-strengthened structures. The experimental program indicates that both sensing technologies are effective in monitoring the structural health and detect the damages of the FRP-strengthened structures.

2 DESCRIPTIONS OF SENSING PRINCIPLES

2.1 ER measurement principle of HCFRP composites

Due to the electrical conductivity of carbon fibers, the CFRP are expected to act as sensing material or both sensing and structural materials. As a result, a broad-based and distributed sensing function of HCFRP-strengthened structures can be realized. A simple ER measuring system can be schematically shown in Fig. 1, only consisting of simple electric equipments such as a DC generator and a digital multimeter. The main advantages are its directness, simplicity and low cost.

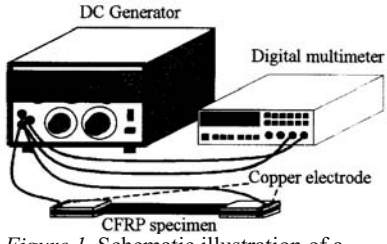

Figure 1. Schematic illustration of a simple ER measurement system

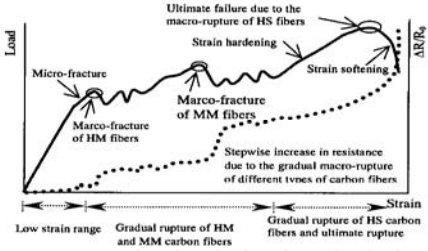

Figure 2. The electrical and mechanical models of hybrid CFRP composite

However, a number of issues limit the applicability of CFRP with only single type of carbon fibers to civil engineering structures [11]. To overcome the issues, the authors have brought out the concepts of a broad-based sensing with HCFRP, the electrical and mechanical models of which are illustrated in Fig. 2 [5,12]. In the model, three types of carbon fibers are involved, high modulus (HM), middle modulus (MM) and high strength (HS) carbon fibers. The HM carbon fibers are expected to fracture during a low strain range, and the fractures lead to a high rate at which the ER of HCFRP increases. HS carbon fibers are mainly used to improve the load carrying capacity and ensure the stability and safety of the HCFRP after the macro-fracture of HM and MM fibers. The hybridization can also result in a step-wise increasing manner for the ER. Consequently, it can be believed that the hybridization can enlarge the strain-sensing range and realize the self-health monitoring serviceability of HCFRP composites.

2.2 BOTDR measurement principle

The distributed sensors make use of optic fibers in which each element of the optic fiber is used for both measurement and data transmission purposes. The measurement purpose of optic fiber is to determine locations and values of desired parameters along the entire length of the fibers.

In the BOTDR, a short pulse of light is transmitted along the fiber and the backscattered energy due to Brillouin backscattering is measured at the sending end. The time interval between the sending and detection of the backscattering energy provides the spatial information, and the intensity of the backscattered energy provides a measure of the fiber attenuation.

The relationship between the Brillouin frequency shift and the tensile strain on the optic fiber can be described by the following equation,

$$v_B(\varepsilon) = v_B(0)(1 + C \cdot \varepsilon)$$

where $v_B(\varepsilon)$ is the Brillouin frequency shift with strain ε, $v_B(0)$ is the Brillouin frequency shift without any strain, C is the strain coefficient and ε is strain. Consequently, the strain distribution can be measured through detecting the frequency shift of Brillouin back-scattering.

3 EXPERIMENTAL DETAILS

To elucidate the self-SHM function, two specimens are referred to, which are a RC beam strengthened with HCFRP sheets and a full-scale PC girder externally strengthened with prestressed PBO sheets.

3.1 HCFRP strengthened RC beam specimen

The self-SHM functions of plain concrete structures and RC structures externally strengthened with HCFRP in the forms of sheet or rod was investigated, based on the mechanical and electrical characterization of HCFRP [1,2,13]. It was shown that the electrical behavior was very sensitive to the change of mechanical condition. However, for the plain concrete beam strengthened with HCFRP sheets, the electrical behavior was not stable enough due to the instability of the concrete structures especially after the macro-factures of HCFFRP sheets. In addition, it was shown that the values of $\Delta R/R_0$ of the structure strengthened with HCFRP rods were smaller than those of the one strengthened with HCFRP sheets at the same condition.

Herein, a RC beam strengthened with HCFRP sheets was referred to as an example to elucidate the self-SHM function of HCFRP-strengthened structures. The HCFRP sheet consists of two types of carbon fibers, HS type (C1) and HM type (C7) in a ratio of 1:1. The mechanical properties of the carbon fibers are listed in table 1 based on the manufacture's specification. After the surface treatment, the carbon fiber sheets were bonded on the bottom surface of the beam with epoxy resins. Then, the specimen was cured at room temperature for about one week. Four copper electrodes were assembled on both ends of the specimen, and silver paste was applied in order to ensure a good electrical contact between the specimen surfaces and

copper electrodes. A small direct current (DC) about 5mA was introduced into the specimens from the electrodes, and the voltage was measured by using a digital voltmeter. Fig. 3 shows the schematic illustration of the HCFRP-strengthened concrete beam and the ER measurement system.

Table 1 Properties of applied continuous carbon and PBO fiber sheets

Type of materials	Tensile strengthen (Gpa)	Young's Modulus (Gpa)	Thickness (mm)	Elongation (%)	Density (g/cm^3)
C1	3.40	230	0.111	1.478	1.80
C7	1.90	540	0.143	0.352	2.10
PBO	3.50	240	0.128	1.458	1.56
PC strand	1.86	200			
Steel bar	0.60	200			
Concrete	50Mpa	33.9			

* For concrete, the value of compressive strength is listed

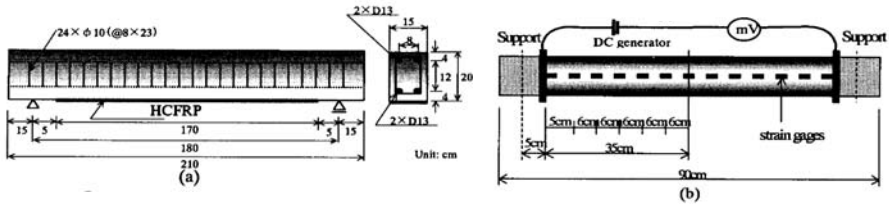

Figure 3. Dimension of RC concrete beam (a); schematic illustration of ER measurement and distribution of strain gauges on the surface of the HCFRP

The specimen was subjected to three-point bending. A hydraulic universal testing machine (UH-500KNI) was employed under a load control mode at a loading rate of 1kN/min. The strains were measured with conventional strain gauges, as shown in Fig. 3 (b).

3.2 PBO strengthened full-scale PC girder specimen

The authors had used distributed BOTDR fiber optic sensors, which are characterized with long gauge length, to measure the tensile and compressive strain distribution and crack width of concrete cylinders [10]. It was showed that the optic fiber bonding length had great influence on the measuring results. When the fiber optic bonding length was more than 1m, the measurements of BOTDR sensors agreed well with the results of strain gauges. However, when the optic fiber bonding length was less than 1m, such as a length of 0.3m, the maximum error between the measurements of BOTDR sensors and those of conventional strain gauges amounted to 46%.

In this study, the BOTDR fiber optic sensors are used to monitor the bonding/debonding behaviors of FRP-strengthened PC structures through measuring the strain distributions. To elucidate the sensing method and its

application in details, a PBO strengthened PC girder is referred to, as shown in Fig. 4. The tensile steel cables were prestressed up to 1512 kN. The material properties of concrete, steel strands, reinforcing bars, and PBO sheets are shown in Table 1. In this study, the prestress level for the PBO sheets with 3 layers was set to be 33% of the assumed effective strength of PBO sheets. The PFRP sheets were impregnated with epoxy resins before prestressed.

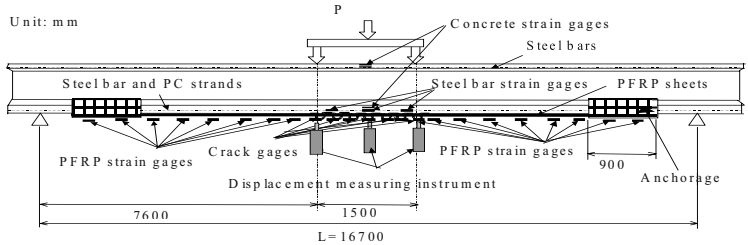

Figure 4. Test-set up for four point bending

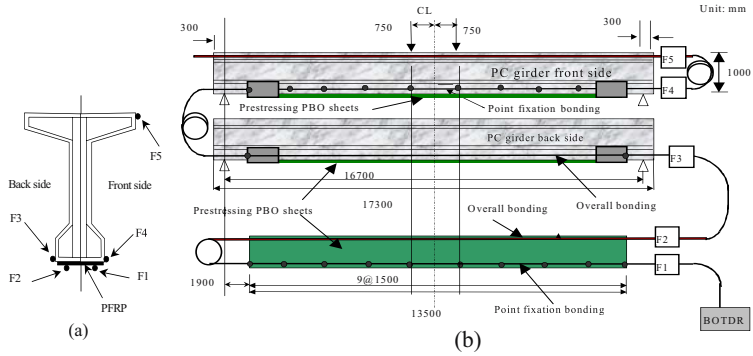

Figure 5. Position of fiber optic sensor on the cross section of PC girder (a); installation of fiber optic sensor (b)

Two methods are considered to bond the fiber optic sensors. One is called as overall bonding (OB) method, where the necessary measured length of optic fiber sensor is bonded on specimen with epoxy resin. The other is called as point fixation (PF) method, where two ends of the part are bonded to the specimen in order to form a uniform strain distribution within these two bonding points. The sensors were bonded after the release of the pretension of PBO sheets. In the following, all the strain distribution means the strain variation distribution. The installation of BOTDR optic sensors on the PC girder and PBO sheets is schematically shown in Fig. 5 (a) and (b).

The fiber optic sensor can be divided into five parts, named as F1, F2, F3, F4 and F5 successively, shown in Fig. 5 (b). The first two parts of F1 and F2 are bonded on the outer surface of the PBO sheets. Part F1 is bonded on the outer surface of PBO sheets with the PF method with an interval of fixation points of 1.5 meter. Part F2 is mounted with the OB method. Parts F3 and F4

are bonded on the surface of the concrete in tensile region. Part F3 and F4 are bonded with OB method and PF method, respectively. Part F5 is pasted on the compressive surface of the PC girder to monitor the compressive strain of concrete. A strain/loss analyzer AQ8603 (Ando Electric Co. Ltd.) based on the BOTDR technique is used for the continuous measurement of strain distribution with optic fiber sensors.

4 RESULTS AND DISCUSSION

4.1 Experimental results of HCFRP strengthened RC beam

Previous investigations indicated that for the HCFRP sheets strengthened plain concrete beams the electrical behavior was not very stable [1,13]. In this case, the HCFRP sheets were the only reinforcing materials, which act as both reinforcements and sensing materials. The gradual rupture of the HCFRP sheets results in a great instability of the whole structure. For this

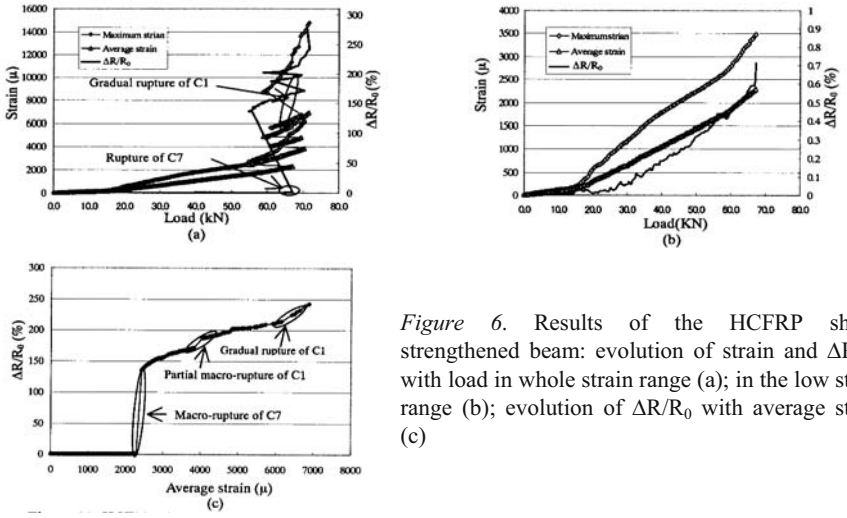

Figure 6. Results of the HCFRP sheets strengthened beam: evolution of strain and $\Delta R/R_0$ with load in whole strain range (a); in the low strain range (b); evolution of $\Delta R/R_0$ with average strain (c)

reason, herein, the SHM functions of HCFRP sheets strengthened RC structures are discussed. The experimental results of the specimen are shown in Fig. 6 (a)-(c). It is seen that during a low strain/load range, the ER changes slowly, and that in a high strain/load range the ER changes with the applied strain/load in a step-wise manner. The macro-fractures of one certain type of carbon sheets can result in a sudden jump in ER.

Fig. 6 (a) shows that the electrical behavior is correlated to the mechanical behavior. However, the values of $\Delta R/R_0$ are relatively small before a load of 69kN. The $\Delta R/R_0$ vs. average strain curve (Fig. 6(c)) of

HCFRP-strengthened RC beam is somewhat similar to that of HCFRP sheets [11]. The initial fracture strain (about 2300μ) at which the HM carbon fibers (C7) began to fracture is smaller than that (about 3000μ) of the HCFRP sheets. The reason is due to the different loading manners. For the 3-bending experiments, the average strain is smaller than the strain in the middle span but much larger than that of the beam-ends. However, the specimens of HCFRP sheets were subjected to unidirectional tension, and the strains of the specimen are relatively uniform. From Fig. 6 (a) and (b), one can obtain that after every macro-fracture of carbon fibers the load increases with strain at a lower rate, while the $\Delta R/R_0$ increases at a higher rate.

4.2 Experimental results of RC girder strengthened with prestressed PBO sheets

For the FRP strengthened concrete structures, the FRP bonding technique is critical to ensure good performance of the adhesive layer. The failure in this stress transfer zone may invalidate the composite action between concrete and FRP and lead to a brittle, catastrophic failure without foreboding prior to achieving the expected strengthening effects, which is often observed in the experiments of FRP-strengthened RC beams. In order to achieve effective strengthening by FRP, debonding needs to be monitored and avoided.

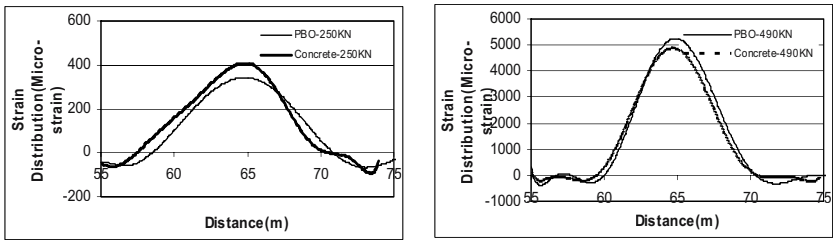

(a) (b)

Figure 7. Comparison of strain distribution on the surface of PBO sheets and it of concrete on the fringe

The strain distribution measurement of concrete and PBO sheets provides a useful indication for the purpose of deciding whether debonding occurs or not in the adhesive layer. Fig. 7(a) and (b) give the comparison of strains on the surface of PBO sheets and at the fringe of concrete at different load cases. It can be found that the strain distribution on the surface of the PBO sheet can agree well with that of the concrete. Only slight discrepancy can be observed from this figure. Fig. 8(a) and (b) give the comparison of the strain measurement of PBO sheets and concrete in the middle of the span under different load levels with OB method and PF method, respectively. It is clear that the strains of PBO sheets are close to that of the concrete at the fringe of PC girder. There is no obvious difference between the strain and the strain

distribution of PBO sheets and concrete when load is lower than 490kN, which means that the interface between PBO and concrete was perfect and no interfacial shift occurred prior to a load of 490kN. The strain monitoring results can agree with the experimental results.

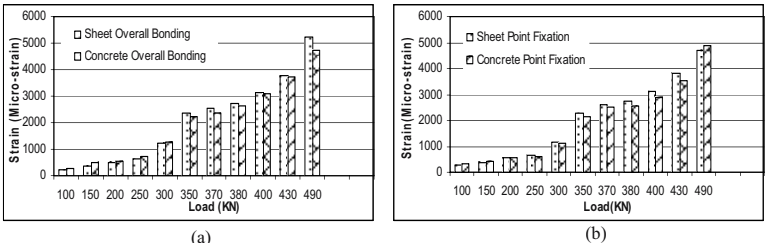

Figure 8. Comparison of strain of PBO sheets and concrete in tension under different load levels

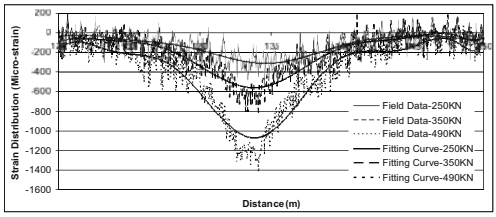

Figure 9. Strain measurement of concrete in compression.

The field strain measurement results of the concrete in compressive region of the upgraded PC girder and its fitting curve are shown in Fig. 9. It can be found that the compressive strain of concrete increased with the increase of load levels. It is clear shown that the BOTDR optic sensors can be used to monitor both tensile strain and compressive strain of concrete structure. OB and PF bonding method are both suitable for tensional strain measurement.

5 CONCLUSIONS

The SHM and damage detections of FRP-strengthened concrete structures are reviewed and discussed based on two kinds of sensing technologies—ER measurement and BOTDR techniques. For the ER sensing with HCFRP composites, in a low strain range the ER changes almost linearly but slowly with strain, while in a high strain the ER increases with strain quickly in a step-wise manner corresponding to the macro-fractures of different types of carbon fibers. Thus, an indicator on the mechanical state of the HCFRP strengthened structures is provided. As a distributed sensing technique, it is revealed that the BOTDR technique is a promising method in measuring the strain distribution, assessing the damage and performance and monitoring

the structural health and the bonding/debonding behaviors of the FRP sheets from the FRP strengthened structures.

REFERENCES

1. Wu, Z. S., Yang, C. Q. and Harada, T. Self-diagnosis of hybrid CFRP sheets-strengthened structures. Smart Materials and Structures. (in press)
2. Kupke, M., Schutle, K. and Schüler, R. "Non-destructive testing of FRP by d.c. and a.c. electrical methods", *Composites Science and Technology,* 61, pp.837-847, 2001.
3. Wu, Z. S., Yang, C. Q. and T. Takahashi, Y. H. "Self-Diagnosis of Concrete Beams Reinforced with Hybrid CFRP Rods", *Proc. of 4th International Workshop on Structural Health Monitoring*, Stanford, USA, 2003, pp.155-62.
4. Wu, Z.S., and Yang, C.Q. "Damage detection of hybrid CFRP reinforcements by DC measurement technique", *Proceeding of International Conference on Advanced Technology in Experimental Mechanics 2003*, Nagoya, Japan, 2003, CD.
5. Wu, Z. S., Yang, C. Q. and Tobe, Y. H. "Electrical and mechanical characterizations of hybrid CFRP sheets". Submitted for the possible publication of *Journal of Composite Materials*.
6. Bao, X., Webb, D.J., and Jackson, D.A. "32-km distributed temperature sensor based on Brillouin loss in an optical fiber", *Optics Letters*, 18, pp. 1561-1563, 1993.
7. Ishii,T., Wu,Z.S, and Horiuchi T. "Study on characteristics of strain measurement with optical fiber", *Transactions of the Japan Concrete Institute*, 23, pp. 133-140, 2002.
8. Wu, Z. S., Takahashi, T., Kino, H. and Hiramatsu, K. "Crack Measurement of Concrete Structures with Optic Fiber Sensing", *Proceedings of the Japan Concrete Institute*, 22(1), pp. 409-414, 2000.
9. Wu, Z.S., Takahashi, T. and Sudou, K. "An experimental investigation on continuous strain and crack monitoring with fiber optic sensors", *Concrete Research and Technology*, 13(2), pp.139-148, 2002.
10. Wu, Z.S. and Xu B. "Infrastructural health monitoring with BOTDR Fiber Optic Sensing technique", *Proceedings of the First International Workshop on Structural Health Monitoring of Innovative Civil Engineering Structures*, Manitoba, Canada, Sep. 22-23, 2002, pp. 217-226.
11. Wu, Z.S. and Yang, C.Q. "Structural Sensing and Diagnosis with Hybrid Carbon Fibers", *Proceeding of the Second International SHM ISIS Canada Workshop*, Manitoba, Canada, Sep. 22-23, 2004, 3-22.
12. Wu, Z.S. and Yang, C.Q. "Hybridization and characterization of smart CFRP composites", *Proc. of the 1st Smart Structures Technology workshop*, Hawaii, USA, Jan. 2004, 495-503.
13. Wu, Z. S., Yang, C. Q. and Tobe, Y. H.. "In-situ damage detection of concrete beams strengthened with hybrid CFRP sheets by DC ER", *Proc. of the 1st Inter. Conference on SHM and Intelligent Infrastructure*, Tokyo, Japan, Nov. 13-15, 2004, pp. 853-860.

MONITORING AND RESPONSE OF CFRP PRESTRESSED CONCRETE BRIDGE

A. De Stefano and R. Ceravolo
Politecnico di Torino, Dipartimento di Ingegneria Strutturale e Geotecnica

Abstract: In Europe, and specially in Italy, there is an impressive amount of historical architectural treasures. They need an effective maintenance strategy that cannot be achieved without a reliable real-time or quasi-real-time knowledge of the structural behaviour. Mechanical properties of ancient masonry are highly uncertain. This makes that every step of the mechanical characterization, from sensing system design and location to model updating, should be robust. Robustness against local property changes and large spatial scattering requires distributed sensing and appropriate data mining and data fusion techniques, allowing to reduce data redundancies and to save only the useful information. This goal is among the main targets of a proposal for an Italian national research project, coordinated by the Authors and involving 9 Italian Universities.

Key words: Structural health monitoring, Historical masonry, Distributed sensing, Stochastic Modeling.

1. INTRODUCTION

The historical architectural heritage, so widely present everywhere in Europe, is a resource and a fundamental part of the cultural European background, but also a problem, due to the huge investment needed to maintain it, or even to repair it after environmental injuries. Maintenance requires a strategy, that shall be rationally optimized to reduce and control the investment needing without loosing safety.

Knowledge is a fundamental aid towards such target. To a structural engineer, knowledge means to keep under control, in real-time or nearly

Farhad Ansari (ed.), Sensing Issues in Civil Structural Health Monitoring, 85–94.

real-time, all the parameters governing the stability, bearing capacity and safety of the existing structure.

The present trend is to realize on-line monitoring systems, making "smart" the traditional structures. On-line monitoring, in service conditions, without specific experimental tests on materials cannot provide an absolute evaluation of the structural safety but can catch the symptoms of a decay in the mechanical properties. Experimental analyses on a structure can be divided in two groups: a first one for monitoring local quantities, such as deformations, opening of cracks, local humidity and temperature conditions, etc., for which fiber optics have encountered a substantial development; the second are devoted to the characterization of the structure as a whole, like dynamic testing. On the other side, dynamic testing for control and diagnosis involves the solution of an "inverse problem", which is severely ill-conditioned; noise, from electrical, mechanical or environmental source, and low sensitivity make it even harder to extract reliable interpretations from experimental results.

2. SPECIFIC PROBLEMS OF ANCIENT MASONRY STRUCTURES: KNOWING THE STRUCTURE IN ITS ACTUAL CONDITIONS.

The most important aspect of the mechanical behavior of ancient masonry structures is the uncertainty of the mechanical properties. One can summarize the nature of such uncertainty in the following way:

1. local variability of the geometric properties and of the masonry internal organization, lack of material continuity, hidden empty volumes, loss of verticality of walls subject to lateral loads caused by vaults, arches or roofs;
2. local variability of the material strength and stiffness, due to original defects or electro-chemical degradation;
3. distribution of cracks, subject to thermal path (seasonal width oscillation with basic trend to increase continuously, due to cumulated debris inside the crack,);
4. effects of past, non documented, damages and repairs, architectural changes, local manipulations.

Inspections, by means of endoscopes, thermographs, radar, metal detectors; physical measures, via sonic tomography; or geometric measures by photogrammetry, or other available technologies, can be executed once only or periodically to improve the knowledge level and to reduce the

uncertainties. False color images and spectrometry can reveal the chemical degradation.

Unfortunately all those observations and measures, while increasing largely the knowledge level, supply only local information, generally not extendable to the whole structure. The complete inspection and measure process shell be repeated for every other location where a better information is required. Usually budget limitations reduce the number of locations where such controls can be done; the result is a spot knowledge, very useful but often arbitrarily assumed as representative of the whole construction body.

Reliable evaluations of the bearing capacity and ultimate strength shall come, fundamentally, from destructive testing, but very seldom the extraction of samples is allowed in case of important architectural heritage; even in case that some extractions are allowed, they are always few and statistically not relevant. Sometimes spare bricks or stones are collected from the real structure and assembled in the lab by means of a new-cast mortar. The bearing capacity of the structure is strongly dependent on the quality of mortar, so destructive testing on such reconstructed samples may prove insignificant.

Thus, so as in every case when each knowledge source is poor, it is necessary to use as many different sources as it is possible. local inspections should be integrated with global measures, supplied by dynamic testing. Dynamic tests supply information about the whole-body response; they make it less arbitrary and more reliable to extend to the whole body the outcomes of the local inspections and measures.

3. DYNAMIC TESTING

In civil engineering fields, the objects of monitoring are essentially flexible structures, as modern bridges, tall buildings, frames, etc.

Ancient masonry buildings, in general, are not flexible, except towers and large domes or vaults; therefore literature shows that dynamic testing is more often applied to such types of objects. Its applicability to other types of masonry structure shall be checked case by case, but, due to the stiffness and mass distribution properties, it happens often that more local and global modes concentrate in a narrow frequency band, making confused and hard to analyze the response. Moreover, non-linear behaviour, which observable in the ancient mansonry even at low strain levels, can introduce spurious spectral peaks, adding further disturbances to the analysis process.

One can first classify modal identification techniques by the domain in which they have been formulated

- frequency domain;
- time domain;

- joint time-frequency domain.

Techniques using known excitations generally build response functions intrinsically related to the own characters of the responding mechanical system.

In case of nearly linear response, one can process signals in frequency domain, where it is naturally possibile to reduce the size of the problem. A frequency Response Function (FRF) is approximated through a "curve fitting" procedure [10]. Frequency domain techniques, though affected by the disturbance due to the needing of a edge-smoothing time window on digital samples, are again made interesting by the powerful cleaning effect of SVD tool [8].

If the response is recognized as non-linear, frequency domain methods, although effective, are too much affected by ucertainties and reduce, generally, to mere non-linearity classifiers

The time-domain identification can save the causal nature of the dynamic problem [1,6,10]. It can take advantage from formulations based on recursive processes, as Autoregressive estimates, Kalman filters, Markov chains, Eigenrealization processes.

Time-domain approaches seem more flexible and adaptable to face moderately non-linear identification problems on large, uncertain MDOF systems, as ancient masonry buildings are, although they need the intermediation of specifically selected models.

Although time domain approaches proved to be more flexible and robust, they share with the frequency domain techniques the necessity of the hypotesis of a stationary and generally ergodic nature of the input.

Techniques in time-domain, accepting the assumption of stationary input, lead to auto-regressive models, with or without exogenous noise, or, more simply, to techniques based on free dacay analysis, where free decay is supplied by the Random Decrement signature [1]. More conveniently, auto and cross correlation functions can replace the Random Decrement signature, through or similar equations. The ERA method uses the free-decay attenuation functions and is based on a recursive Markov-like process described throughe a Hankel matrix [9]. The realization process is acted by a psudo-inverse, which is optimized through a SVD. The Random Subspace Realization can be seen as an extention of the ERA method, where RD signatures of each signal are replaced by auto-correlation and cross-correlation functions between each couple of simultaneous signals.

In applications to the historical heritage the frequency domain approach is generally prevailing. Very seldom the examined contribution explain the reasons for the methodological choice; in many cases those reasons seem rely more likely on the availability of software and tools than on comparative evaluations.

In the time-frequency representation (bi-linear, Cohen class) of the response signals, the energy is concentrated around the modal frequencies and modulated according to smoothing effect of the structure, acting as a

low-damped filter. Due to the fact that in the (*t,f*) plane the shape of the modulating waveform is maintained, it can be demonstrated that the amplitude ratio and phase difference between two measured signals $s_i(t)$ and $s_j(t)$ can be determined directly from their bilinear time-frequency auto and cross distributions $D_{s_i}(t,f), D_{s_j}(t,f), D_{s_i s_j}(t,f)$ in the following manner [3]:

$$PH_{i,j} = \frac{\mathrm{Im}(D_{s_i s_j}(t,f))}{\mathrm{Re}(D_{s_i s_j}(t,f))}; \qquad AR_{i,j}(t,f) = \sqrt{\frac{D_{s_i}(t,f)}{D_{s_j}(t,f)}} \tag{1}$$

or, better:

$$AR_{i,j}(t,f) = \frac{D_{s_i s_k}(t,f)}{D_{s_j s_k}(t,f)} \tag{2}$$

where $AR_{i,j}(t,f)$ is the time-frequency estimator for the modal amplitude, $PH_{i,j}(t,f)$ represents the time-frequency estimator for the modal phase difference and s_k is a pure sinusoidal signal tuned to the previously detected modal frequency *f*.

The phase difference estimator $PH_{i,j}(t,f)$ is a variable defined in the range 0-π. Given *f,* its SD_t (Standard Deviation along the *t* axis) is generally not far from the mean value π/2. This, however, is not true if *f* is a modal frequency; in that case, instead, the scattering of the phase difference between simultaneous records decreases suddenly and $SD_t[PH_{i,j}(t,f)]$ falls down to zero. On the $SD_t[PH_{i,j}(t,f)]$ versus frequency plot, therefore, modal frequencies are revealed by sharp downward peaks, as shown in Fig.1, related to an application to a real building.

If the unknown input is a random non-stationary process, then different modes can be excited in different time windows. A powerful property of Time-Frequency distributions, therefore, is its ability to separate closely coupled modes, that contributes to makes it a robust approach.

Given a time-frequency representation of a displacement signal, a few instantaneous parameters associated with the Frequency Response Function (FRF), *H*, can be estimated by minimising the following functional at each time *t* [2]:

$$D(\omega,t) - \left|H(\omega,t)\right|^2 \tag{3}$$

In this minimisation there is an explicit assumption that the instantaneous energy spectrum $D(t,\omega)$ associated to a general time-frequency transform, approaches a scaled version of the squared modulus of the FRF.

4. A SAMPLE APPLICATION: THE STRUCTURAL IDENTIFICATION OF MATILDE'S TOWER IN S. MINIATO

Recently, results from dynamic tests performed on a certain number of bell towers were processed at the Department of Structural Engineering of the Politecnico di Torino.

All the tower were tested under different types of excitation [5]: ambient vibration, bells tolling, vibration caused by core drilling.

Accelerometric signals were processed according to different techniques:

- identification in the time domain, through the ERA method, using as inputs the Random Decrement (RD) functions of ambient excitation [1,9];
- identification in the time domain, through the PRTD method, using as inputs the RD functions of ambient excitation [1,10];
- identification in the time domain, through auto-regressive methods (DSPI) [9];
- identification in the time-frequency domain (TFIE, "Time-Frequency Instantaneous Estimators"), using Choi-Williams transforms with different values of the kernel parameter, σ [3].

The need to consider the results obtained from different measuring methods can be met by means of charts such as those illustrated in Figures 1, which show the recurrent natural frequencies determined experimentally through applying two very different methodologies, i.e., the ERA method and the TFIE method, respectively.

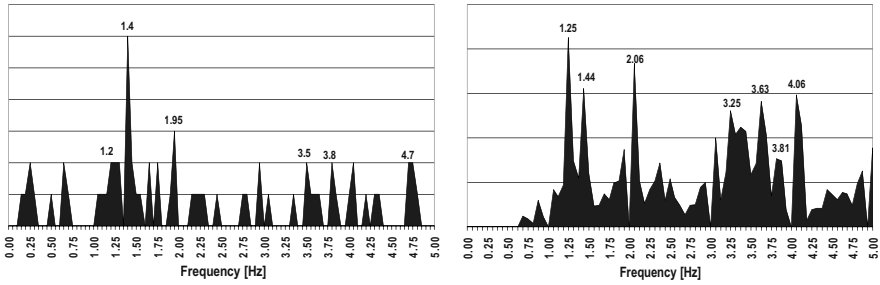

Figure 1. Recurrent natural frequencies evaluated by ERA(left) and TFIE (right) [5]

As an example it is shown here the preliminary analysis of the "Torre di Matilde" (Figure 3), erected in San Miniato (Pisa) in the 12th century. It is a rare example of the military architecture of the time: its construction dates back to when the Emperor Henry IV (1184-1194) visited the city. The structure, including the bell tower, was badly damaged by the bombings of 1944. The tower, rising about 35 m above the cathedral floor, is parallelepiped shaped, with crown and end shrines added in the 13th century.

Inside the tower, three wooden storeys prove too weak to ensure a valid connection between the four walls. At the top of the tower, a small masonry vault closes the structure by linking together the side walls. The cracking pattern of the building displays major lesions at the corners, extending over virtually the entire height.

An extensive measuring campaign was performed on the tower, within the framework of an inter-university scientific program (PRIN). The sensor location sets were redundant, to reduce the amount of arbitrary assumptions in the modal shape extraction. Tests were performed under instrumented hammer shots, low energy harmonic excitation and ambient vibrations, including the effects of oscillating bells

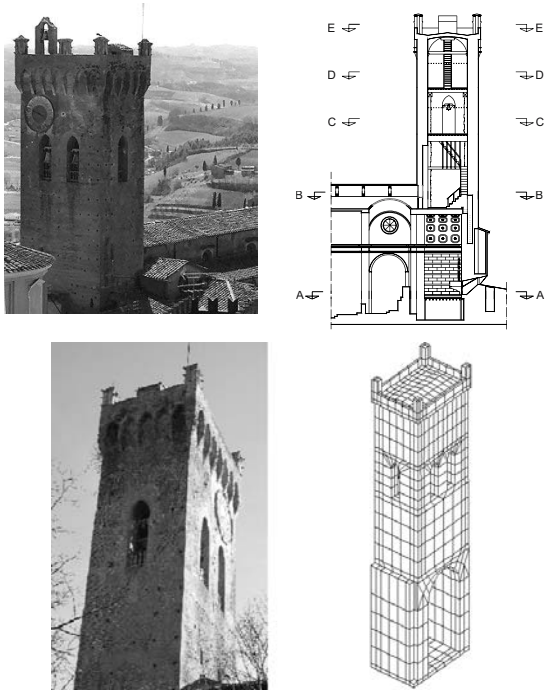

Figure 2. Views of the Torre di Matilde in S.Miniato (Pisa) and F.E. model

Figure 3 shows a sample diagrams of phase difference estimator (TFIE method), calculated on a signal measured along the X principal direction.

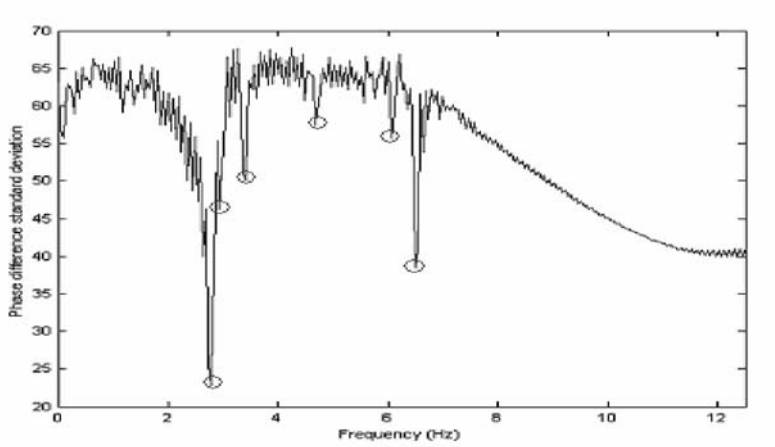

Figure 3. Phase difference estimator – Sensors arranged along the X axis [5]

Figure 4 shows the three modal shapes identified most reliably. Due to a lack of symmetry torsion and bending are always mixed.

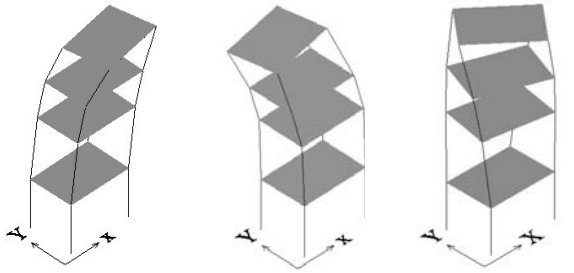

Mode 1 (2.7 Hz) Mode 3 (3.4 Hz) Mode 5 (6.4 Hz)

Figure 4. Three of the modes identified [5]

The main goal of the experimental modal analysis of the tower was the assessment of a predictive model to be used as a tool to evaluate in advance the effectiveness of retrofitting and reinforcing actions. The F.E. code in use was Visual Cast3m, produced by the French Commissariat pour l'Energie Atomique (CEA), adapted to the non-linear analysis of masonry structures at the EU Joint Research Centre in Ispra (Italy) and distributed in Italy by ENEA.

A numerical modal analysis of the tower allowed the extraction of the first seven modes.

The structural body of the tower has been divided into 18 macro-elements. The mechanical properties of the elements were assigned as stochastic values, described by a likely probabilistic distribution. Each-one among the 18 macroelements could have different elastic properties. Using

the FE model, a conveniently designed Monte Carlo process allowed to associate a distribution of outcomes, in terms of modal parameters, with each set of locally variant elastic properties of the 18 macroelements. A covariance matrix was built in this way, to play the role of sensitivity map and to help to estimate the conditional probabilities of the outcomes, given the input set. A Bayesian hierarchical (the most sensitive parameters are fixed first) and iterative process allowed the assessment of the inverse conditional probability and the definition of the set of elastic parameters of the 18 macroelements, most likely fitting the experimental modal parameters [11].

5. TOWARDS A PERMANENT ON-LINE MONITORING: PERSPECTIVES AND FINAL REMARKS

Optical measures of relative distances, by laser sensors, crack widths, foundation stability, verticality of bearing walls can be checked continuously in time, by a permanent monitoring process. Dynamic testing too can be performed permanently on-line, thanks to the ability to handle the ambient vibration responses. The Authors proposed a new national research project, involving 9 Italian Universities, in which their role is mainly focused on that subject and the general goal is a rational, effective strategy for maintenance and retrofit planning on the historical heritage.

The permanent monitoring application to ambient dynamic identification techniques is very critical in the case of ancient masonry. The redundancy of sensors distribution is made mandatory by the large scattering of mechanical properties from point to point; otherwise the reconstruction of the modal shapes shall fail. The analysis of a great number of data, the quality of which is not excellent due to the significant noise disturbance and non-linearities, can be done by means of the Complexity Science tools, through which it is possible to deal with the computational complexity issue that derives from the large amount of experimental data. Many complex systems are characterized by quite simple basic principles and fundamental equations, as simple as the principles, but they can contain dynamic instabilities, bifurcations, high level of uncertainties and space-time interactions among the involved variables.

It is also important to correlate the evolution in modal and local mechanical parameters with the modification in time of the temperature and humidity and of the path and width of the cracks which can be monitored by simple and cheap Plastic Optical Fibers, more easy and robust to place on site. A good monitoring system for monumental structures should have the following properties:

- a large number of sensors, which must be small and low-cost; the number and the placing have to be determined by optimization procedures;
- cables, which cannot be hidden in an easy way, have to be substituted by a wireless monitoring system sensor have to be locally charged and in an independent way (i.e. by a wind power generator);
- Fiber-optic systems should have multiplexing capability, to reduce the number of fibers and hide them easier;
- "ad hoc" mathematical methods are needed to manage the data in order to transmit only relevant data.

ACKNOWLEDGEMENTS

This research was supported by the Italian Scientific Research Ministry (PRIN project).

REFERENCES

1. Asmussen, J. C "Modal Analysis based on Random Decrement Technique." *Ph. D. – thesis Aalborg University, Denmark,* 1997.
2. Bonato, P., Ceravolo, R., De Stefano, A., Molinari, F., "Damping Evaluation in Structures Subjected to Unknown and Non-Stationary Excitation", *Proc. European COST F3 Conference on System Identification & Structural Health Monitoring*, Universidad Politecnica de Madrid, Spain, 6-9 June, 2000, pp. 255-264.
3. Bonato, P., Ceravolo, R., De Stefano, A., Molinari, F "Use of Cross-Time-Frequency Estimators for the Structural Identification in Non-Stationary Conditions and Under Unknown Excitation", *Journal of Sound and Vibration*, 237(5), pp. 775-791, 2000.
4. Brincker, R., De Stefano, A., Piombo, B., "Ambient Data to Analyze the Dynamic Behavior of Bridges: a first comparison between different techniques"; *Proc. 14th International Modal Analysis Conference, Dearborn, Michigan,* 1996, pp. 477-482.
5. Ceravolo, R., Demarie, G.V., De Stefano, A., Matta, E., "Bell-Towers Monitorino through Ambient Vibration Measurements", Proc. 3rd European Conference on Structural Control, 12-15 July 2004, Vienna University of Technology, Vienna.
6. De Stefano, A., Sabia, D., Sabia, L., "Structural identification using ARMAV models from noisy dynamic response under unknown random excitation" - DAMAS 97, International Workshop, Euromech 365, Sheffield (UK), 1997, pp. 419-428.
7. Ewins, D. J. *Modal testing*. Research Studies Press LTD, 2000.
8. Golub, G. H., Van Loan, C. F., *Matrix Computations*, The Johns Hopkins University Press, 1983.
9. Juang., J. N., and Pappa, R. S. "An eigensystem realisation algorithm (ERA) for modal parameter identification and modal reduction." *NASA/JPL Workshop on Identification and Control of Flexible Space Structures,* 1984.
10. Maia, N. M. M., Silva, J. M. M. *Theoretical and Experimental Modal Analysis*. Research Studies Press LTD, 1998.
11. Brondello, A. *Model Updating stocastico di struttura monumentale*. "Laurea" thesis (in Italian), Dipartimento di Ingegneria Strutturale e Geotecnica, Politecnico di Torino, 2003

MONITORING AND RESPONSE OF CFRP PRESTRESSED CONCRETE BRIDGE

Nabil F. Grace
Civil Engineering Department, Lawrence Technological University, Southfield, Michigan, USA

Abstract: This paper presents data obtained from automated monitoring of the Bridge Street Bridge-Structure-B, in the City of Southfield Michigan. This data was stored every two hours from vibrating-wire strain gages, thermistors, deflection transducers, and load cells installed within the bridge. Examples of the variation of strains, temperatures, and deflections along the three-spans of the bridge and strains and forces in longitudinal unbonded post-tensioned tendons, and forces in the transverse unbonded post-tensioned tendons are presented. In addition to the data collected from the automated data logging system, manually collected data are also presented on the same data plots for ease of correlation between manually read and automated collected data. The measured concrete strains, deflections, and forces in the longitudinal and transverse post-tensioned tendons over a period of one year indicate that the bridge is performing as expected. The monitored response of the bridge also demonstrates that the unbonded post-tensioned tendons and their anchorages are intact and effectively serving within the environmental conditions encountered at the bridge. Moreover, the results also demonstrate the integrity of the bridge in both longitudinal and transverse directions.

Key words: Carbon fiber, prestressed concrete, highway bridges, field instrumentation.

1. INTRODUCTION

The worldwide research [1] using innovative construction materials [2-17] such as carbon fiber reinforced polymers (CFRP) requires continuous monitoring of implemented innovative structures over a long period. Only data showing long-term predictable behavior can foster the confidence necessary to advance both research and implementation of design standards with respect to experimental materials, such as CFRP. The Structure B of the

Farhad Ansari (ed.), Sensing Issues in Civil Structural Health Monitoring, 95–105.

Bridge Street Bridge Deployment Project [4], is the first carbon fiber reinforced polymer (CFRP) prestressed concrete bridge to have been constructed in the USA, and is currently being monitored for a period of five years, beginning with the completion of its construction in November 2001. Details of construction and instrumentation can be found elsewhere [4]. The plan view of the instrumented DT-beams of structure B is shown in Fig. 1.

The primary objectives of this paper are to present and evaluate examples of the structural response data of the DT-beams collected during construction and the period from November 15, 2001 to early January 2003. The term "automated data" is used to indicate the data recorded through the automated data logging system as discussed below. The automated data presented include the concrete strains, deflections, strains, and forces in the external longitudinal unbonded post-tensioned tendons, and forces in the internal unbonded transverse post-tensioned tendons. In addition, temperature measurements of the bridge at selected locations are also presented. Conclusions regarding the performance of the bridge overall, and various critical components are drawn.

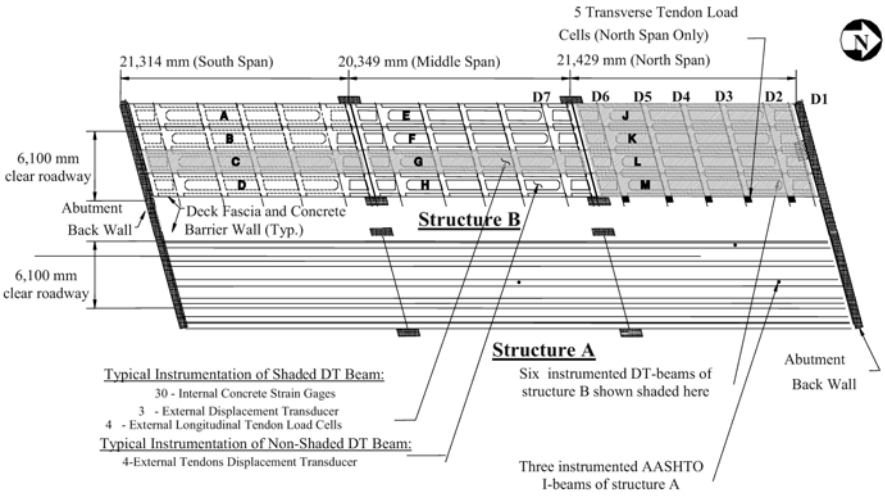

Figure 1. Instrumental and plan view of Bridge Street Bridge.

2. INSTRUMENTATION AND MONITORING

The automated monitoring system reads and reduces data every ten minutes with data being stored every two hours, to better determine the reliability of the sensors and system, as well as the integrity of the data. This system provides a continuous monitoring of responses of selected bridge elements, for use by the design team as relevant information to evaluate the serviceability of the bridge structure. Most of the instrumentation was

installed during the fabrication of the beams at the precast facility. All 12 DT beams were instrumented and monitored during fabrication to measure and document forces and stress levels during prestressing operations. Six DT-beams [C, G, J, K, L, and M] were instrumented with both internal and external sensors for long-term monitoring.

2.1 Measurement of concrete strains

Embedded vibrating-wire Geokon VCE – 4200 strain gages with an effective gage length of 152 mm (6 in.) were installed to measure the strain distributions across the depth of the beam cross-section. These gages were positioned at the midspan and quarter points of each of the six instrumented DT beams. A total of 30 strain gages per beam were installed in the composite beam section. Fig. 2 shows the location of vibrating-wire strain gages at midspan cross-section of DT-beam G.

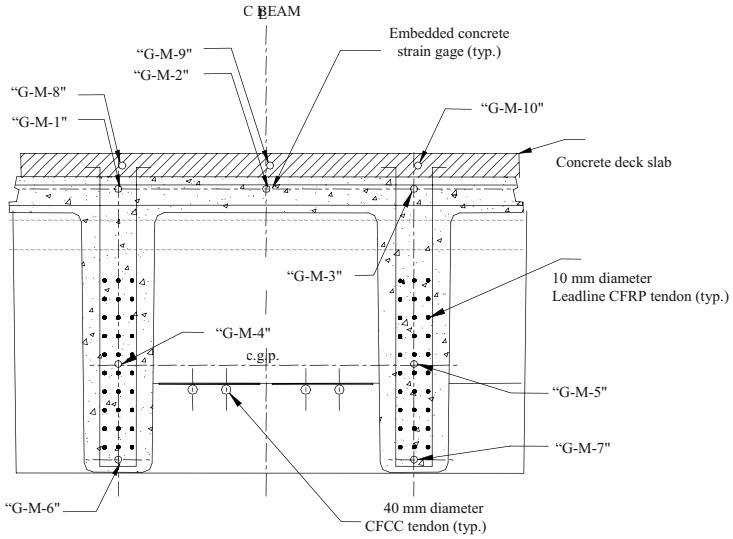

Figure 2. Location of vibrating wire strain gages at midspan cross-section of DT-beam G.

2.2 Measurement of temperatures

To measure the concrete temperature distribution in DT-beams, selected thermistors were used in the embedded vibrating wire strain gages. The selected locations of thermistors, where concrete temperature is measured, are shown in Fig. 3.

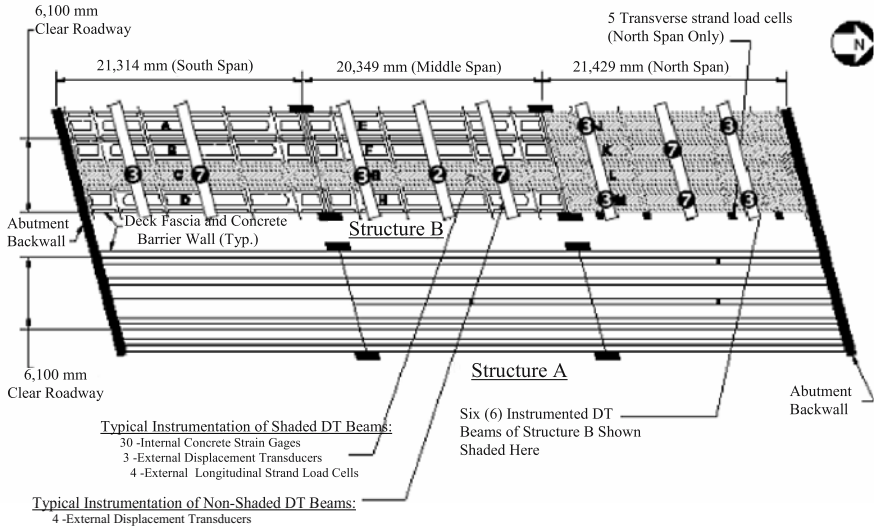

Figure 3. Embedded concrete temperature measurement locations.

2.3 Automated measurement of deflection

Automated deflection transducers were installed on the six instrumented beams after erection. A taut high-strength stainless steel wire was strung between two fixed anchorage points established near the ends of the beams to serve as a reference. Displacement transducers were then installed along one beam-stem at the north quarter point, midspan, and south quarter point.

2.4 Measurement of post-tensioned tendon forces

All four CFCC post-tensioned tendons of each of the six instrumented DT-beams were installed with load cells at one end of the beams. These load cells were installed between the anchorage nut on the tendon sleeve and the bearing plate embedded in the transverse diaphragm, near the north end of the DT-beam. Similar load cells were also installed on the transverse post-tensioned tendons provided through diaphragms D1 through D7, in the north span.

2.5 Monitoring the status and integrity of external CFCC tendons

To monitor the structural behavior and long-term status/integrity of external CFCC post-tensioned tendons of the six non-instrumented DT-beams, strain gages and displacement transducers were installed on the four longitudinal tendons of each beam. The purpose of these sensors is to determine potential failure or loss of anchorage in the external CFCC tendons. A total of 21 strain gages and three hybrid displacement sensors were installed on the 24 tendons.

2.6 Automated Data Acquisition System

The response of the Bridge Street Bridge is being monitored by an automated data acquisition system. A total of more than 400 sensors are scanned continuously and stored every two hours by the data acquisition system. During the scanning process, the data from selected sensors is compared against a previously established limit value for that sensor. If that limit value is exceeded, the system activates a dial-out alarm modem to alert appropriate personnel to the failure of that sensor or unexpected bridge behavior. Access to the system for downloading of data, real-time data review or software modification is performed remotely using hardwired telephone communication.

3. RESULTS AND DISCUSSION

3.1 Concrete strain

Fig. 4 shows typical measured concrete strains at midspan of DT-beam C. DT-beam C is located in the South span of the bridge. In the figure, the first letter of designated gages refers to the DT-beam, the middle letter refers to the location of the beam cross-section, and the number represents the gage identification number. For example, C-M-1 represents strain gage #1, located in DT-beam C at its midspan cross-section. The portion of the curves showing rapid fluctuation in the figures represents automated data collected after opening of the bridge to the traffic and is due to significant variation in temperature condition of the bridge. The concrete strains shown to have occurred before November 25, 2001, are the strains developed during beam fabrication and construction of the bridge [4] and were obtained by manual computer download.

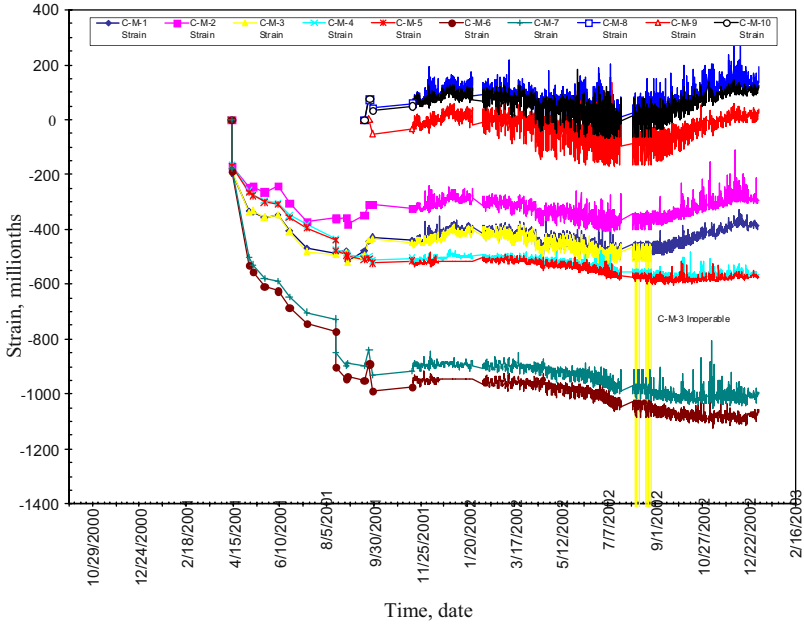

Figure 4. Measured concrete strains at the midspan of beam C.

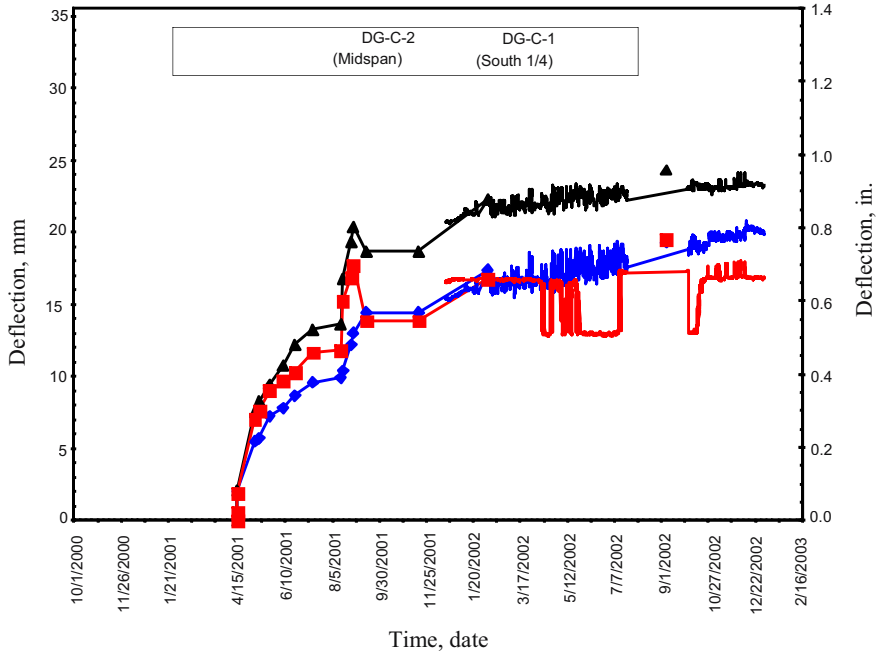

Figure 5. Measured deflection for beam C.

Compressive strains in the bottom of the DT-beam webs, shown in Fig. 4 range from 800 to 1100 microstrain. Corresponding strains in the concrete deck slab are generally tensile with values of up to about 200 microstrains. These measurements describe total accumulated strain, and include components due to fabrication, pretensioning, post-tensioning, shrinkage, creep, temperature and flexure. Daily temperature and live load fluctuations are not readily distinguishable from each other, but as a combination cause strain value differences of 30 to 60 microstrain in the bottoms of the webs and from 50 to as much as 130 microstrain in the concrete deck slab. Over the course of the first year in service, an increase in compressive strain in the bottoms of webs of between 110 and 190 microstrain was recorded amounting to as much as a 20% increase in total strain. This increase can be attributed to creep in the lower part of the section, which is subject to much greater compressive stress.

3.2 Beam deflection

Fig. 5 shows the measured deflections at quarter and midspan of DT-beams C. In the notations of Fig. 5, DG represents the deflection gage, middle letter represents the DT-beam, and the number represents the gage identification number. In this figure, data plots contain both manual and automated data. The readings from the automated system have been superimposed onto the manual readings obtained on February 6, 2002 and September 6, 2002. As shown in the figure, significant fluctuations in the measured deflections have been observed, including erratic behavior by some of the sensors.

3.3 Post-tensioned tendon forces

To monitor forces in the external longitudinal unbonded post-tensioned tendons, special purpose fabricated load cells were installed on each of the four tendons of the instrumented DT-beams. As shown in Fig. 6, the fluctuation in the forces of longitudinal unbonded post-tensioned tendons is negligible, except due to the effect of seasonal temperature change. In the figure, LC refers to a load cell, where the middle letter represents the DT-beam, and the number represents the load-cell number in the DT-beam. Forces in the transverse post-tensioned tendons (see Fig. 7) installed through diaphragms (D2 through D6) were measured. As shown in Fig. 8, again there

is no significant fluctuation in the forces in transverse post-tensioned tendons, except due to seasonal effects. Examination of the data from the load cells on the post-tensioned tendons indicates that there has been no appreciable loss of force during the first year of service. This demonstrates the integrity of the tendons and anchorages and suggests that creep and relaxation effects have been minimal.

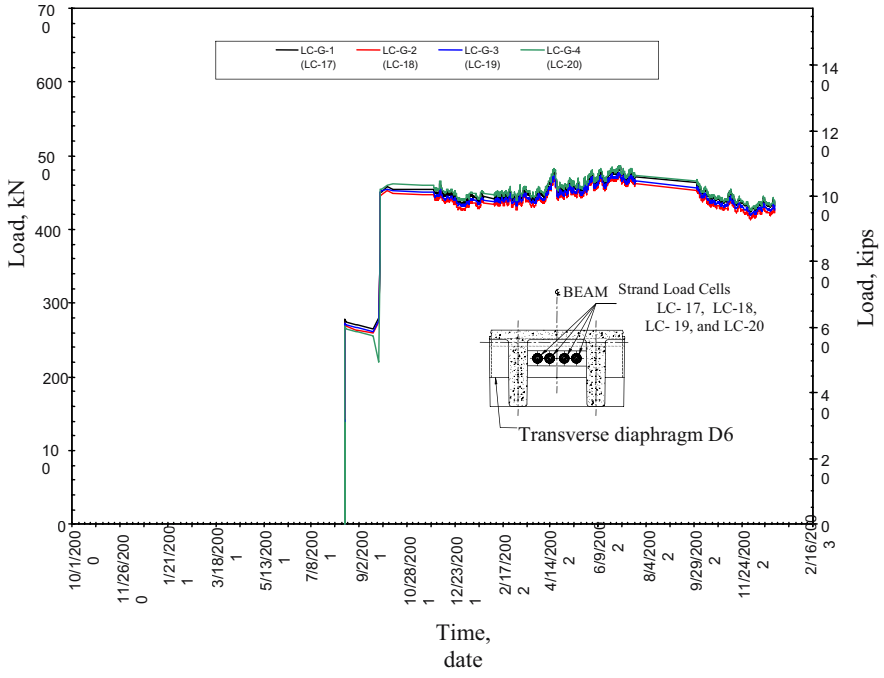

Figure 6. Force in longitudinal post-tensioning tendons for beam G.

3.3 Post-tensioned tendon forces

To monitor forces in the external longitudinal unbonded post-tensioned tendons, special purpose fabricated load cells were installed on each of the four tendons of the instrumented DT-beams. As shown in Fig. 6, the fluctuation in the forces of longitudinal unbonded post-tensioned tendons is negligible, except due to the effect of seasonal temperature change. In the figure, LC refers to a load cell, where the middle letter represents the DT-beam, and the number represents the load-cell number in the DT-beam. Forces in the transverse post-tensioned tendons (see Fig. 7) installed through diaphragms (D2 through D6) were measured. As shown in Fig. 8, again there is no significant fluctuation in the forces in transverse post-tensioned tendons, except due to seasonal effects. Examination of the data from the load cells on the post-tensioned tendons indicates that there has been no appreciable loss of force during the first year of service. This demonstrates

the integrity of the tendons and anchorages and suggests that creep and relaxation effects have been minimal.

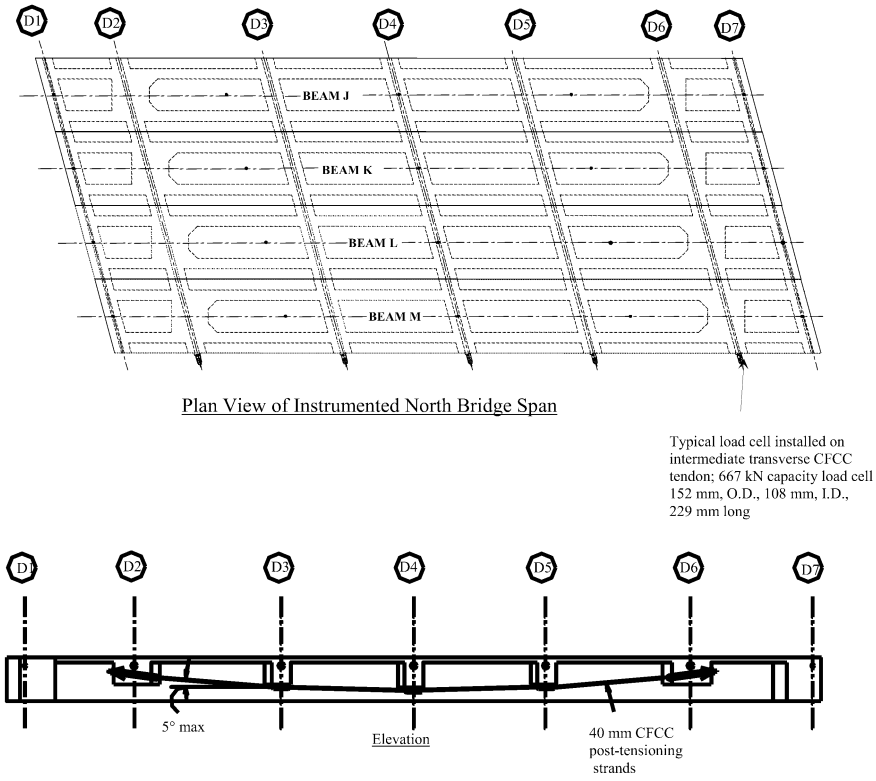

Figure 7. Locations and identification of transverse post-tensioned strand load cell.

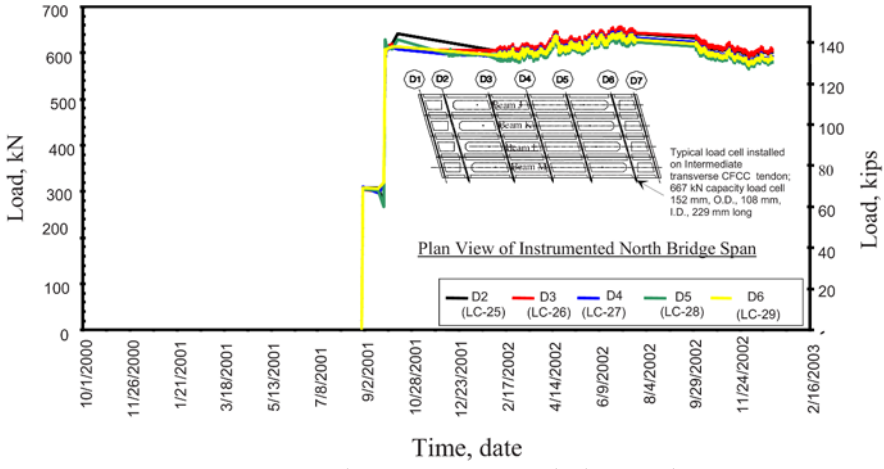

Figure 8. Force in transverse post-tensioning strands.

4. CONCLUSIONS

The measured concrete strains, deflections, and forces in the longitudinal and transverse post-tensioned tendons over a period of about one year indicate that the Bridge Street Bridge is performing at levels better than expected by the design team. No discernable deviations have yet to be noted beyond the variations due to seasonal temperature changes in the concrete strain and forces in the post-tensioned tendons over the first year of the scheduled monitoring period. The monitored response data also demonstrates that the unbonded tendons are intact and effectively carrying the traffic load imposed on the bridge. Furthermore, it shows satisfactory performance by the permanent anchorages provided at the ends of the unbonded longitudinal and transverse post-tensioned CFCC tendons. In addition, the uniformity of data from similar locations and components, serves to argue that the monitoring system is performing as expected and providing a reliable database from which the above conclusions can be made.

ACKNOWLEDGEMENT

The success of this project is due to the efforts of many people, including various researchers, designers, manufacturers, suppliers, and builders. The bridge monitoring program requirements were established by the Structural Testing Center at Lawrence Technological University, Construction Technology Laboratory (CTL) Inc., Skokie, Illinois, and Hubbell, Roth & Clark (HRC), Consulting Engineers, Bloomfield Hills, Michigan in conjunction with the Michigan Department of Transportation Testing and Research Section. The site construction was funded through the Federal Highway Administration (FHWA) as one of the TEA-21 High Priority Projects. Further funding for instrumentation and monitoring was provided under the Innovative Bridge Research and Construction Program of TEA-21. The Bridge Street Industrial Park Subdivision property owners and the Michigan Economic Development Corporation contributed to the funding of the project. Furthermore, the National Science Foundation funded the research upon which the project design and monitoring concept was based. The Project benefited from the congressional support of Michigan Representatives Joseph Knollenberg and Sander Levin. Finally, the Mayor of the City of Southfield, the City Council, and the City Administration are commended for their vision of the future and their courage to venture into this unconventional construction arena.

REFERENCES

1. ACI Committee 440. *State–of-the-Art Report on Fiber Reinforced Plastic Reinforcement for Concrete Structures*. Farmington Hills, American Concrete Institute, 1996.
2. Rizkalla, S. H. " A New Generation of Civil Engineering Structures and Bridges", *Proc. of the Third International Symposium on Non-metallic (FRPRC) Reinforcement for Concrete Structures*, Sapporo, Japan, October 1997, pp. 113-128.

3. Fam A. Z., Rizkalla S. H., Tadros G. "Behavior of CFRP Prestressing and Shear Reinforcements for Concrete Highway Bridges", *ACI Structural Journal*, **vol. 94**, **no. 1**, pp. 77-86, 1997.
4. Grace N. F., Navarre F. C., Nacey R. B., Bonus W., Collavino L. " Design-Construction of Bridge Street Bridge-First CFRP Bridge in the United States", *PCI Journal*, **vol. 47**, **no**. **5**, pp. 20-35, 2002.
5. Grace N. F., Abdel-Sayed G., Sakla S., Wahba J. "Finite Element Analysis of Bridge Street Bridge, City of Southfield, Michigan", Lawrence Technological University *Research Project # 36*, Report Submitted to Hubbell Roth & Clark Consulting Engineers, 1997, Bloomfield Hills, Michigan, USA.
6. Grace N. F., Abdel-Sayed, G. "Double Tee and CFRP/GFRP Bridge System", *ACI Concrete International*, **vol. 18**, **no. 2**, pp. 39-44, 1996.
7. Grace N. F., Abdel-Sayed G. "Ductility of Prestressed Concrete Bridges Using CFRP Strands", *ACI Concrete International*, **vol. 20**, **no. 6**, pp. 25-30, 1998.
8. Grace N. F., Abdel-Sayed G. "Behavior of Externally Draped CFRP Tendons in Prestressed Concrete Bridges", *PCI Journal*, **vol. 43**, **no. 5**, pp. 88-101, 1998.
9. Grace N. F. "Continuous CFRP Prestressed Concrete Bridges", *ACI Concrete International*, **vol. 21**, **no. 10**, pp. 42-47, 1999.
10. Grace N. F., Abdel-Sayed G., Wahba J., Sakla S. "Mathematical Solution for Carbon Fiber Reinforced Polymer Prestressed Concrete Skew Bridges", *ACI Structural Journal*, **vol. 96**, **no. 6**, pp. 981-987, 1999.
11. Grace N. F., Abdel-Sayed G. "Behavior of Carbon Fiber Reinforced Prestressed Concrete Skew Bridge", *ACI Structural Journal*, **vol. 97**, **no. 1**, pp. 26-34, 2000.
12. Grace N. F. "Response of Continuous CFRP Prestressed Concrete Bridges Under Static and Repeated Loadings", *PCI Journal*, **vol. 45**, **no. 6**, pp. 84-102, 2000.
13. Grace N. F. "Transfer Length of CFRP/CFCC Strands for Double-T Beams", *PCI Journal*, **vol. 45**, **no. 5**, pp. 110-126, 2000.
14. Grace N. F., Enomoto T., Yagi K. "Behavior of CFCC and CFRP Leadline Prestressing System in Bridge Construction", *PCI Journal*, **vol. 47**, **no. 3**, pp. 90-103, 2002.
15. Grace N. F, Singh S. B. "Design Approach for CFRP Prestressed Concrete Bridge Beams", *ACI Structural Journal*, **vol. 100**, **no. 3**, pp. 365-376, 2003.
16. Grace N. F., Abdel-Sayed G., Navarre F. C., Nacey R. B. Bonus, W., Collavino L. "Full-Scale Test of Prestressed Double-Tee Beam", *Concrete International*, **vol. 25**, **no. 4**, pp. 52-58, 2003.
17. Grace N. F., Enomoto T., Abdel-Sayed G., Yagi, K., Collavino L. "Evaluation of CFRP/CFCC Full-Scale DT-Beam: Experimental Study and Analysis", *PCI Journal*, **vol. 48**, **no. 4**, pp. 120-139, 2003.

DESIGN OF TEMPORARY AND PERMANENT ARRAYS TO ASSESS DYNAMIC PARAMETERS IN HISTORICAL AND MONUMENTAL BUILDINGS

Paolo Clemente and Dario Rinaldis
ENEA, Italian Agency for New technologies, Energy and the Environment, Italy

Abstract: In this paper some issues about the seismic monitoring of historical and monumental buildings are faced. The experimental analysis carried out on a earthquake damaged building is shown. On the basis of the experimental results obtained by means of temporary arrays, a permanent network was designed and installed, which recorded several seismic events.

Key words: Seismic monitoring, historical buildings, monuments, temporary arrays, permanent arrays.

1. INTRODUCTION

The distribution of sensors on a structure depends mainly on the scope of the experimental analysis and is influenced very much by the expected dynamic behaviour of the structure and the maximum number of sensors available. The numerical analysis by means of a finite element model can be very helpful to analyse the expected behaviour and to interpret the experimental results. This is possible when dealing with new constructions but is quite difficult in the case of old masonry buildings for the following reasons: i) the structural size of the various elements (walls, floors, etc.) cannot be evaluated with the needed accuracy; ii) the material characteristics, such as the tension-strain relationship, the strength, etc., are not known; iii) structure and materials often exhibit inelastic behaviour; iv) rigid floors are often missing and substituted by masonry vaults or by

Farhad Ansari (ed.), Sensing Issues in Civil Structural Health Monitoring, 107–116.

wooden floors, whose effectiveness in connecting walls is uncertain; v) the deep of the foundation is not known and so are their geometry and material properties; often the deep is variable as well as the soil characteristics; vi) buildings are often connected to other constructions, so that their behaviour is very complex.

For such kind of structures the experimental analysis is often the only way to improve our understanding about their dynamic behaviour, both to assess possible dynamic behaviour of structures during strong events and to gain experience on the general dynamic characteristics of structural systems such that the experience and data base can be used in future design and analyses. Data bases for dynamic characteristics of new building structures are sufficiently populated, so estimation of fundamental periods and critical damping percentages can be obtained. On the contrary, data on dynamic characteristics of historical and monumental structures are scarce. Some past efforts in determination of dynamic characteristics of monumental structures have been done [1].

The data bases are in general obtained from two sources: dynamic testing of structures (ambient and forced vibration) and analyses of data from instrumented structures. The second is based on strong-motion response data, which depends on a long duration project that is costly to implement and maintain. Therefore, whenever possible, low-amplitude tests are used to verify the results of analytical studies. On the other hand the seismic behaviour of structural systems can be better understood if arrays of seismic sensors can be deployed throughout the structures in order to record their responses during strong shaking events.

In more details, temporary arrays are generally used for dynamic characterisation of structures, which can be excited by means of ambient or forced vibrations. These latest can be obtained by means of a vibrodine, impulse loading, explosions, etc. In this case velocimeters are to be preferred for the following reasons: i) sensors must be just placed on an horizontal surface, so their deployment is often easier; ii) velocimeters are more sensitive than accelerometers, so also vibrations of very low amplitude, such as ambient vibrations, can be recorded. Accelerometric sensors, which have to be fixed at the structure, are to be preferred in the cases of: i) strong motion recording, due to their larger full scale value; ii) long term monitoring of structures. Obviously, for a fixed instrumentation the choice of the locations of sensors and the ways for the cables is influenced very much by: i) the interference of the instrumentation with the normal use of the building and the optimisation of the ways of the cables; ii) the accessibility of the locations, which must allow the safe installation of sensors. These problems can be often ignored for temporary arrays. The experimental study of a structure should be organised in two steps: i) the dynamic

characterisation should be first performed, in order to have a first glance at the dynamic properties of the structure, such as resonance frequencies, modal shapes and damping; sensors should be temporarily deployed in different configuration in order to define their optimum deployment; ii) then the permanent array is designed on the basis of the experimental results obtained from the temporary deployment.

The health monitoring of historical buildings and the structural interpretation of the recorded data are very hard and must be committed to knowledgeable technicians. They need multidisciplinary studies, including those involved with art, architecture, earth science and earthquake engineering. Such analyses must include clear identification of the structural systems, their dynamic characteristics and the knowledge of the mechanical properties of the materials used to construct the original buildings. Furthermore, the building under investigation may have been altered repeatedly over time. This can be a critical issue because, and the building may be founded on older buildings that got buried over.

When recording seismic events, it is essential to use integrated arrays, i.e., to deploy, in parallel to sensors in the building, instrumentation to assess the ground shaking level (free-field arrays) [2, 3]. It is worth to notice that during strong earthquakes, the structure may experience non-linear behaviour. Thus, if the parameters of linear behaviour are known beforehand, it may be easier to extrapolate the non-linear behaviour. This process is very difficult for old, slightly or severely damaged masonry buildings, because it is quite difficult to establish their elastic properties. For such cases, even for very small excitation, non-linear behaviour may be experienced by the structure. However, it is possible to approximate their behaviour with a pseudo-linear approach.

2. TESTED BUILDING

The building object of this study is the head office of the Centre for Anthropological Documentation and Research of Nerina Valley [CEDRAV]. It was built as a monastery in the 14th century on the top of a ridge of a "scaglia rossa" rock formation. The building is irregular both horizontally and vertically (Fig. 1). The vertical carrying structure of the building is made of stone masonry walls. The floors of the intermediate levels are made of masonry vaults, while the upper ones are in concrete. The lowest level is mostly founded directly on the rock and only partially embedded into the ground. The N-W part of the building is not well known. In that area, the second level is partially founded on rock. A small church was added at the East side of the construction.

The building was seriously damaged during the Umbria-Marche seismic events. By observation, it was determined that the building suffered some damage during the main shocks of September 26th although the epicentre of the earthquake was 30 km away from the building. Then, the October 14th event, the epicentre of which was approximately 8-10 km away from the building, caused most of the damage. Following these two earthquakes, the structure was evaluated to characterise its dynamic properties by using natural and man-made excitations, as shown in this paper.

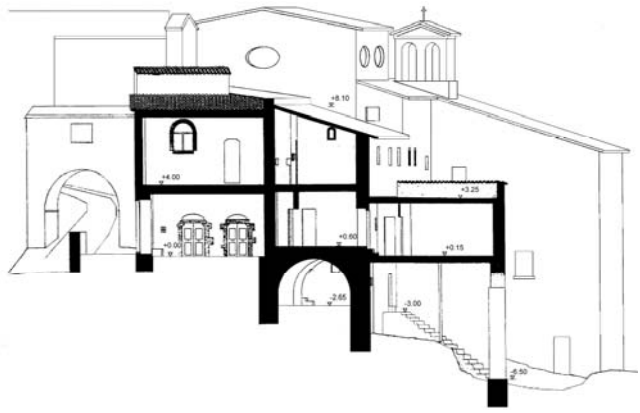

Figure 1. Vertical section of the building

As already said, the experimental dynamic analysis of the building was performed in two phases: the building was first tested by using a temporary array made of fifteen seismometers; then an accelerometric array of 36 sensors was installed, which recorded seismic events for about one year.

3. TEMPORARY ARRAYS

The temporary instrumentation consisted of fifteen seismometers, which were installed in several configurations. Configuration 1 (NS oriented sensors – solid arrows), Configuration 2 (EW oriented sensors – dashed arrows) and Configuration 9 (underlined sensors) are shown in Fig. 2. For each configuration different tests were performed using the following different kinds of excitation: ambient vibrations, man-induced vibrations by lifting a caterpillar tractor arm and dropping, seismic events. The analysis of all the records due to both ambient and forced vibrations is shown in [14]. Only the most interesting aspects of the structural behaviour are here discussed.

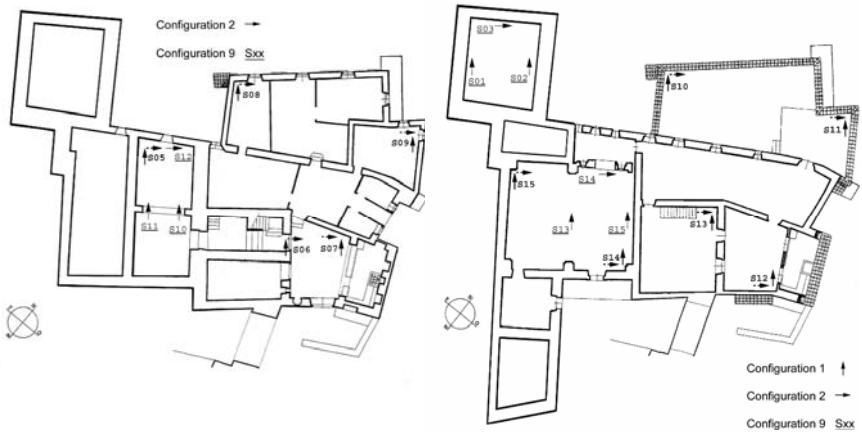

Figure 2. Temporary arrays (second and third level)

The temporary deployment was active for several hours in each configuration, especially during the nights. This allowed to record several sets of seismic events of low and medium amplitude. In Fig. 3 the velocity time-histories recorded at the 2nd (Ch9) and 3rd (Ch11) floors, respectively, are compared with that on the basement (Ch1). As you can see, Ch9 and Ch11, and so Ch12 and Ch13 not shown here, shows unusual long duration with particular low frequency content, not visible in the input record (Ch1), which is to be related to the closely-coupled torsional-translational mode that causes beating phenomenon. Normally, such beating occurs when the system has low damping in addition to closely-coupled translational-torsional modes.

Fig. 4 shows the PSDs of the most significant sensors. Peaks at very close frequencies, 8.80 Hz and 9.75 Hz, are apparent in the spectra of Ch09 and Ch11, which are along the same vertical alignment. The spectra of Ch08 and Ch10, which are along another vertical alignment, show an amplification only at 9.75 Hz. Because these do not show evidence of the 8.80 Hz peak, it is possible to assume that this frequency content should be linked to a physic phenomenon mainly connected to the wall instrumented by Ch09 and Ch11. In other words Ch8 and Ch10, which are connected to a more rigid wall that does not have this torsion (probably the rotation axis is positioned on a parallel plane and very close to the wall). Peaks at 8.80 and 9.75 Hz are relevant also for Ch12, while for Ch13 the first peak is more apparent. Peak at 8.8 Hz is apparent also at the input level.

Peaks in the PSD are very sharp indicating that, even thought the building was old and damaged at some locations, damping value is small. Thus, the damping for the mode at 8.8 Hz, calculated using the half-power band width method, is approximately 0.5% for Ch09, Ch11 and Ch12.

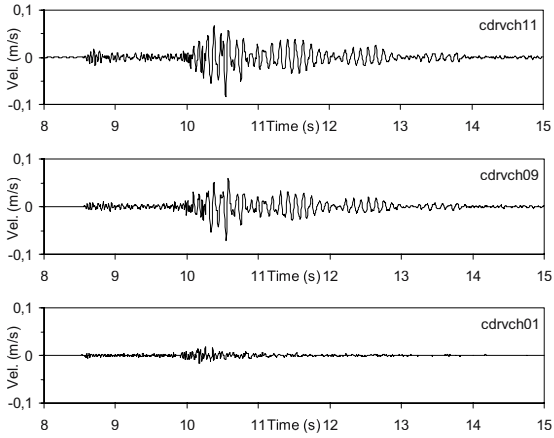

Figure 3. Velocity responses recorded at three different levels: Ch11 (3rd floor), Ch9 (2nd floor), Ch1 (Basement)

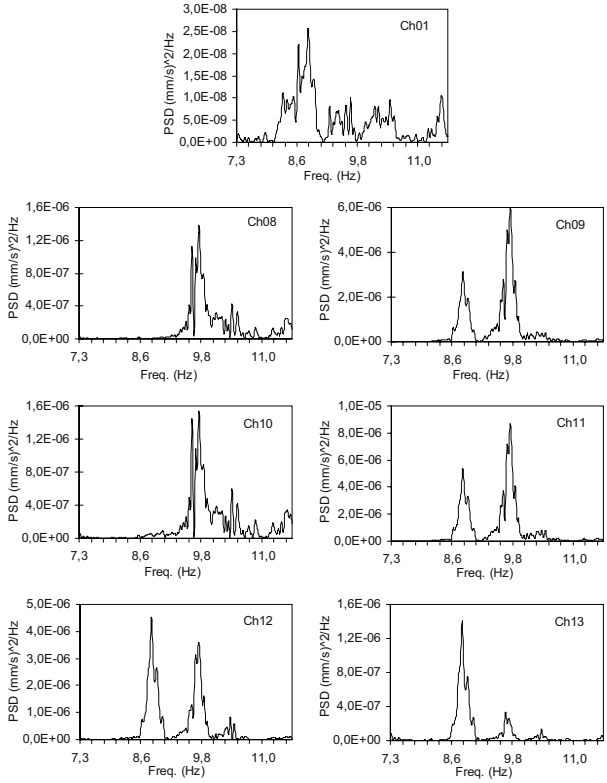

Figure 4. PSD sensors Ch01, Ch08, Ch09, Ch10, Ch11, Ch12 and Ch13

The CSDs plotted in Fig. 5 confirm what already said. In fact, the peak at 8.80 Hz appears only from the motion of the wall instrumented by Ch09 and

Ch11 (and by Ch12 and Ch13 as well). In fact the analysis of CSDs confirms that the mode at 9.75 Hz has more energy at the third floor (Ch10-Ch11) than at the second one (Ch08-Ch09) and they are 180 degrees out of phase with a significative value of the coherence, which is a clear indication of torsional mode. The cross-spectra CSD of Ch10-Ch8 and CSD of Ch9-Ch11 show as well a spectral peak at 9.75 Hz. A phase angle of zero degrees confirms that this frequency peak is associated to a translational movement of the walls in the NW-SE direction. The detected behaviour may be linked with the positions of the centre of mass and the centre of rigidity of the building. In fact, the response at 8.80 Hz is larger at the perimeter walls in the NW-SE direction due to the contribution of the torsional component of the motion. Besides, there are several peaks around the torsional frequency (9.75 Hz) in the frequency interval 9-10 Hz, that could be related to structural modes. The mode associated with this second peak seems to have, as for the peak at 8.8 Hz, a very small damping (very sharp frequency peak). On the other hand all spectral peaks at frequencies larger than 9.0 Hz seem to be associated only to torsional modes (see CSD phase of Ch10-Ch11 and Ch08-Ch09, respectively).

4. ACCELEROMETRIC PERMANENT NETWORK

The permanent instrumentation consisted of 36 accelerometers deployed in the locations shown in Fig. 6. These were fixed on the basis of the previous results from the temporary arrays, but it is worth to note that the number of sensors used is very high and that the building was in use in the period of the recordings. So deployment of sensors and cabling also had to take into account this requirement. Three triaxial accelerometers were located at different level of the building, all directly founded on the rock.

The accelerometers network has been working for several months. It recorded several seismic events, which were classified in terms of input energy. The analysis in time and frequency domain of all the records and the structural interpretation are the subject of another paper.

Three sample time-histories of the recorded response to a seismic event are plotted in Fig. 7, where the already pointed out beating effects are observable. The approximate beating period, computed for the plotted responses, is ($T_1 = 0.104$ s, and $T_2 = 0.096$ s) $T_b = 2.5$ s. From the corresponding amplitude spectra the translational frequency 9.7 Hz and the torsional frequency 10.4 Hz are apparent. Using system identification, very low damping percentages (< 1%) have been extracted. The comparison between the frequencies identified by the accelerometric recording and those from the seismometer arrays are summarized in Table 1.

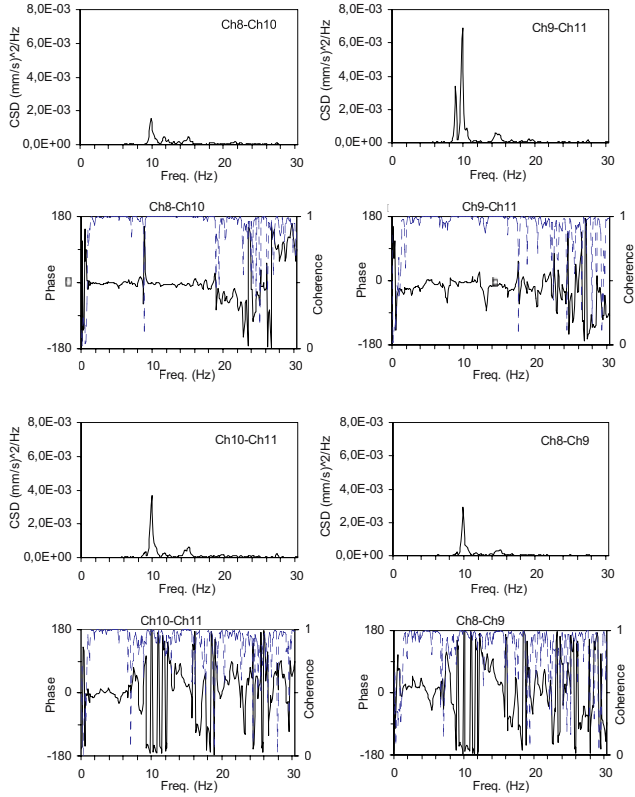

Figure 5. CSD of Ch8-Ch10, Ch9-Ch11, Ch10-Ch11 and Ch08-Ch09

Table 1. Dynamic Characteristics of CEDRAV Building

Excitation	Ambient	Man-induced	Earthquake (temp.)	Earthquake (perm.)
Translational Freq. (Hz)	8.88	9.08	8.80	9.70
Torsional Freq. (Hz)	10.05	10.15	9.75	10.40

The results obtained from the velocimetric recordings are very similar to those obtained by means of the accelerometric recordings. The differences in the resonance frequency values are to be related to the fact that higher energy events were recorded by the temporary arrays. Just the opposite happens usually. It is worth to note that new technology accelerometers with very high dynamic (19 bits) were used, so also seismic events of very low energy were recorded by the permanent network. Records on the ground gave very similar trends, both in time and frequency domain.

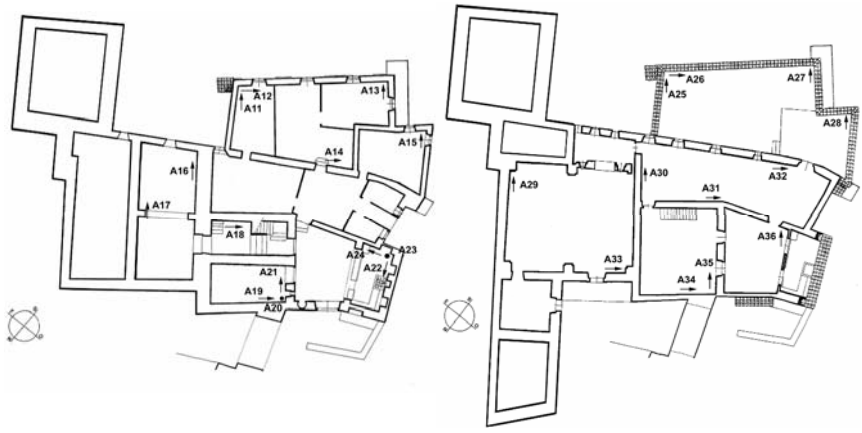

Figure 6. Location of accelerometers in the permanent array (second and third level).

5. CONCLUSIONS

The CEDRAV building, as most of the historical constructions, is very complex and rigid. Translational and torsional frequencies are close to one another. Coupling occurs and damping percentage is low; as a result beating effect is strong enough. These characteristics were already pointed out by means of the velocimetric recordings obtained by using temporary arrays and have been confirmed by the accelerometric recordings.

The number of sensors used in the temporary arrays was lower than that of the permanent one. Just the opposite happens in practice, when a large number of seismometers can be used for dynamic characterisation of a structure but only very few sensors can be provided for permanent monitoring networks. Actually, one of the objectives of the first phase, with temporary arrays, was to establish the optimum locations of sensors in order to minimise their number.

Vibrations of buildings under dynamic loads, such as earthquakes, winds, etc. should be studied by means of measurements of the actual motion. These measurements not only allow engineers to determine the dynamic characteristics of the building and those of the excitation, but also to estimate the complex interaction between them.

In most practical cases, it can be assumed that buildings vibrate horizontally and the floors are rigid in their own planes. Therefore, we need three sensors at each floor that satisfy the conditions given for “plane motion”.

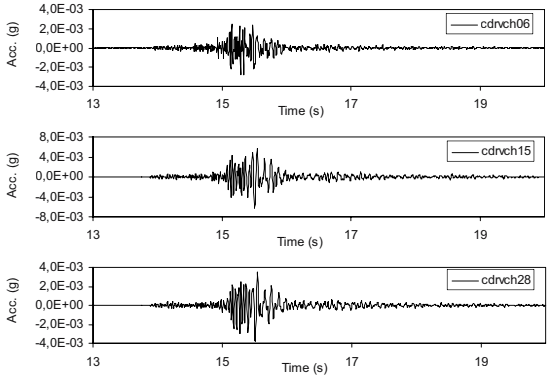

Figure 7. Recorded acceleration time-histories of Ch06 (Level 1), Ch15 (Level 2) and Ch28 (Level 3) exhibit the beating effect of the structural response at higher levels

A typical instrumentation plan for a floor includes then 3 sensors. In the case of CEDRAV the complexity of the structural system stimulate a much higher sensor density. In fact 15 velocimeters were deployed in 9 different temporary configurations. Some of them were installed at the same position and in the same direction depending on the configuration aims, others even if installed at different positions, but very close to the previous ones, do not show substantial differences in the time-domain and the frequency-domain analysis. Then the minimum number of sensors should be determined after a preliminary structure modelling and results from temporary array analysis.

REFERENCES

1. Clemente P. *L'analisi dinamica sperimentale nella salvaguardia dei beni culturali.* Rome, ENEA, 2002.
2. Clemente P., Bongiovanni G., Buffarini G., Rinaldis D. "Strategies for the seismic preservation of historical centres", *Proc., 7th International Symposium of the OWHC*, Rhodes, Sept. 23-26, 2003.
3. Clemente P., Margottini C. "Seismic Preservation of the Collective Memory", *Proc., International Conference "Choices and Strategies for Preservation of the Collective Memory"*, Dobbiaco, June 25-29, 2002 (Invited lecture).
4. Rinaldis D., Çelebi M., Buffarini G., Clemente P. "Dynamic response and seismic vulnerability of an historical building in Italy", *Proc., 12 World Conference on Earthquake Engineering*, Vancouver, Aug. 1-6, 2004, Paper No. 3211.

FRP-STRENGTHENED STRUCTURES: MONITORING ISSUES FROM QUÉBEC APPLICATIONS

Pierre Labossière, Pierre Rochette, Kenneth W. Neale, and Marc Demers
Université de Sherbrooke, Canada

Abstract Since 1996, our research group has been involved in the installation of fibre optic sensors in a number of structural rehabilitation projects with FRPs in Québec. Each project brought its share of technical problems, tested our capacity for innovation, and attained a different level of success. Fibre Bragg Gratings (FBG), Fabry-Perot sensors, or a combination of both, were used in each case. Following our first field tests on a multi-storey parkade and a highway overpass, which allowed us to gain familiarity with the installation of sensors in actual construction conditions, our first significant project making use of fibre optic sensors (FOS) was the rehabilitation of the Sainte-Émélie-de-l'Énergie Bridge. For this short-span bridge that was strengthened with FRPs in 1998, conventional instruments were also incorporated to the repairwork to corroborate the FOS measurements. The behaviour of the bridge has since been measured frequently. After more than six years of service following the installation of the FRP reinforcement and initiation of the monitoring procedure, it was submitted to a full series of load tests. Other FRP-reinforced structures that incorporated FOS include repairs to a nuclear reactor secondary containment structure and a new pedestrian bridge on the campus of the Université de Sherbrooke.

Key words: SHM, fibre-reinforced polymers, fibre optic sensors, structural applications.

1. INTRODUCTION

The extent of deterioration of the existing infrastructure in Canada has prompted many authorities to investigate the potential use of FRPs to extend the service life of their infrastructure [1]. Typical applications of FRPs in the province of Québec have included major rehabilitation schemes and numerous small-scale projects. However, because of uncertainties related to the fatigue behaviour and durability of these new materials, it was believed that structural health monitoring could significantly improve the safety level

Farhad Ansari (ed.), Sensing Issues in Civil Structural Health Monitoring, 117–126.

of FRP-strengthened structures. In addition, it was thought that the accumulation of data on actual FRP-reinforced structures under service loads would be useful for updating design codes and standards.

The objectives of structural health monitoring (SHM) are the assessment of a structure's performance under various service loads, the evaluation of its general condition and the detection of damage. Efficient SHM should provide the authorities with information useful to the management of their structural inventories. This efficiency depends on the capacity of this system to satisfy management requirements, such as short-term verification of innovative designs or early detection of structural problems. It should lead to an effective allocation of resources, reduced disruptions of service and lower maintenance costs. However, it appears that any SHM monitoring system will produce an enormous amount of data from which it will be necessary to select the appropriate information. This paper reports on practical applications of SHM on actual Québec structures rehabilitated with FRPs.

2. EARLY APPLICATIONS

We carried out our first structural health monitoring (SHM) experiments from 1996 to 1998 on a highway overpass, a multi-storey parkade and a short-span bridge. In all cases, FOS were installed on structures that were simultaneously reinforced with fibre-reinforced polymer materials (FRPs) to extend their service life.

At Saint-Étienne-de-Bolton, Québec, the objective of the rehabilitation of an overpass over Highway 10 (Figure 1) was to protect the columns against an increase of corrosion of their steel rebars and to demonstrate the durability of FRP rehabilitations in the severe climatic conditions of Canada. The deck is supported by 18 circular columns, 12 of which were in need of repair due to corrosion damage caused mainly by the close proximity of highway lanes. Nine columns were repaired with FRPs and three with conventional materials. Fibre optic sensors were installed on an experimental basis on four of the rehabilitated columns. With these instruments, we expected to measure the deformation of the columns caused by the variation of the temperature, the corrosion of rebars and the effects of loading. This first experience with fibre optic sensors vividly illustrated the difficulties of installing fragile instrumentation in civil engineering field conditions. In fact, almost half of the sensors were damaged during the installation or soon after. This led us to formulate some recommendations concerning the protection of the sensors. The surviving sensors were interrogated periodically during several months after being brought into service. However, the recorded data showed a high instability of the strain indicator unit. The unit was subsequently returned to the manufacturer, repaired and recalibrated. However, although this instrument was never satisfactorily restored and monitoring of this project had to be abandoned after a few

months, this real case was extremely useful in defining the requested properties of the monitoring devices for such a project.

Figure 1. Saint-Étienne-de-Bolton Overpass

The rehabilitation of the Webster parkade in Sherbrooke, our second project, took place in the following weeks. In this case, FRPs were used to increase the bending and shear capacity of concrete beams and to strengthen concrete columns, and integrated structural FOS were installed to monitor their behaviour under loading. Although the FOS installation was successfully installed, the monitoring remained plagued with the same problems as the Saint-Étienne overpass, and no critical information was ever obtained from the sensors. Although the acquisition of experience with the installation of various FOS was a positive outcome of these projects, it was expected that our third SHM application would provide us with a substantially significant long-term data acquisition.

3. STE-ÉMÉLIE-DE-L'ÉNERGIE BRIDGE

Our third project was undertaken in 1998, when the reinforced concrete beams of the Ste-Émélie-de-l'Énergie bridge were strengthened with FRPs (Figure 2). A complete description of the FRP–strengthening scheme was published by Labossière et al. [2]. For this bridge, conventional and innovative instrumentation was incorporated in the repairwork. Conventional instruments were used to corroborate the fibre optic sensor measurements, and controlled loading tests were performed in order to evaluate the behaviour of the bridge. The tests were conducted before and after the bridge strengthening, and they allowed the evaluation of the increase in flexural stiffness resulting from the external reinforcement. They also confirmed that the behaviour of the bridge was consistent with the design hypotheses for the FRP reinforcement. Long-term monitoring was then undertaken. The fibre optic sensors were interrogated on an intermittent but regular basis after the FRP strengthening was installed on the bridge. In addition, the

Figure 2. View of the Sainte-Émélie Bridge

measurements obtained from thermocouples on the same structure allowed the identification of the thermal effects in the data. Until now, measurements do not indicate any significant strain changes since the repair took place. More details on this project are provided hereafter.

3.1 Instrumentation of the Sainte-Émélie bridge

The Ste-Émélie bridge was instrumented with conventional resistive strain gauges and FOS. The mobile testing laboratory team of the Ministère des Transports du Québec (MTQ) installed eight gauges prior to the reinforcement. Concrete cover was removed around longitudinal rebars to allow installation of these strain gauges. All gauges are located at mid-span of the beams. Twenty additional resistive strain gauges were installed by the Université de Sherbrooke research group upon completion of the bridge strengthening, some of them at mid-span and others near the bridge supports. Mid-span gauges are located either on the longitudinal FRP strips, or on the side face of the section near the slab. Combining data from the various gauges at a given location then allows a comparison of its strain profile under load with the design hypotheses. Although it can be expected that the loads near the beam extremities will not be critical in bending, a number of strain gauges regularly spaced longitudinally in this area were expected to provide useful information on the shear transfer between FRP and concrete.

The integration of innovative technologies for continuous structural monitoring was an additional goal pursued by the research team. It was decided, at the planning stages of this project, to incorporate FOS in the FRP reinforcement. The characteristics and working principles of the two types of devices incorporated in this project, which are either Fabry-Perot or FBG sensors, are described in Tennyson et al. [3]. In order to compare strain measurements between conventional gauges and fibre optic sensors, the two types of instruments were systematically installed close to one another.

Fibre optic sensors were placed on steel rebars and on longitudinal composites. The values obtained from the FOS are not compensated for thermal effects. In order to evaluate thermal effects on strain sensors and gauges, 10 thermocouples were also installed permanently on the bridge. Four of them were embedded in concrete near the rebars while the remaining six were glued on the surface of the FRP reinforcement. The cables of all instruments were inserted into PVC pipes which all converge to a junction box, where instrument leads are easily reached. Other instruments used during the loading tests included load cells to measure strains at mid-span, and one displacement sensor under each beam. Accelerometers were also used for dynamic tests.

3.2 Continuous monitoring and periodic readings

A full, continuous monitoring of all gauges and FOS installed on the structure was not possible because of the cost of the readout units and technical difficulties of providing permanent electricity, communication and safety devices to the site. However, a multi-channel readout unit that allows for continuous monitoring of Fabry-Perot sensors was left installed for short periods of time, at regular intervals. From October 1999 to July 2001, extensive data were recorded over six periods of time, each varying between five to 14 days. These periods cover operation periods representative of the temperature ranges normally observed in the region where the bridge is located. For the present case, the temperature varied from –22 ºC to +32 ºC. The ambient temperature was measured with a Fabry-Perot temperature sensor placed in the junction box. The FOS strains and temperature measurements were recorded continuously on the basis of one reading of all instruments every 15 minutes. A clear correlation was established between the temperature and the measured deformations. While there is large dispersion in the FOS data, a coefficient of thermal expansion of 4.4×10^{-6} was determined for the structure. This coefficient is lower than the expected value of about 10×10^{-6} for reinforced concrete. The significant difference between the two values is due to the thermal inertia of the bridge, in which the temperature never reaches peaks as high as ambient. The data from the FOS are coherent with those of the thermocouples.

Other periodic strain readings were also performed at relatively regular intervals, for instance about every six weeks from the completion of the rehabilitation in 1998 until 2001, and on a three-month return period afterwards, until June 2004. For each period, one reading of every Fabry-Perot strain sensor and thermocouple was taken at a given time. Therefore, for each series of measurements, deformations can be associated to internal temperatures. From these data, a linear relation was established between the deformation and the temperature.

The measured residual strains oscillate slightly but, on an average basis and once the temperature effects removed, have remained constant for the

entire period of measurements. This is a good indication that the bridge did not sag during the period that followed rehabilitation. The calculation of the residual strains was also carried out for the other Fabry-Perot sensors, which were all installed on composites. The stability of the calculated deformations indicates that the bond between the composite materials and the concrete remained unaffected by climate or loading. These observations are consistent with the expected results. Given the initial condition of the bridge and the relatively low deformations observed under service loads, it was anticipated that no degradation would take place for many years. However, the results obtained demonstrated the accuracy and the reliability of the Fabry-Perot fibre optic system for long-term monitoring.

3.3 Long-term behaviour of the FOS

Major load tests were performed on the Ste-Émélie-de-l'Énergie bridge four times: prior to the repairwork in 1998, immediately afterwards, one year later, and in June 2004. The last loading program was an opportunity to verify extensively, six years after construction, the conditions of the Bragg grating and Fabry-Perot sensors. It also allowed testing of a new fibre Bragg grating sensor interrogation unit being jointly developed by ISIS Canada and IDERS Engineering Inc.

The loading tests were carried out using three four–axle trucks, each having an approximate mass of 30 metric tons. The trucks made multiple passes over the bridge and stopped at predetermined positions. Readings taken from the metal foil strain gauges validated the readings taken by the fibre optic interrogation units. Although the analysis of the collected data has only been partially completed so far, it must be pointed out that all FOS sensors installed six years ago were still in good working condition, thus demonstrating their durability in a relatively severe environment.

4. GENTILLY NUCLEAR REACTOR

The fourth structure that our team was involved with is the secondary containment structure of the Gentilly I nuclear reactor, shown in Figure 3. Since it had been brought into service, this structure had required repeated repair work, mostly located around the upper ring beam. In 1999, Atomic Energy of Canada Limited (AECL) needed a permanent solution to this costly problem. The degraded concrete was replaced by a high quality concrete and the ring was confined with FRP strips. The expected life of the repair being up to 75 years, AECL also requested that a reliable long-term monitoring system be installed. This provided an excellent opportunity to test several types of innovative instruments. Brillouin scattering sensors, long-gauge FOS, Fabry-Perot sensors and FBGs were integrated into the FRP rehabilitation, thus allowing simultaneous strain readings with various

instruments. In addition, the installation of thermocouples on the structure permitted the isolation of the thermal effects in the data. Strain and temperature readings of vibrating wires that were cast in the concrete by AECL provide additional information. The nature of this structure made it possible to install communication devices and to experiment with long-distance monitoring.

4.1 Instrumentation

Five types of instruments are used to monitor the structure, including two types of long-gauge sensors. The first one is based on the Brillouin scattering technology, which uses unique equipment to obtain strain and thermal measurements from common telecommunication optic fibres. The actual system consists of a set of instruments controlled by a dedicated computer. The computer can be programmed to the required time and frequency of acquisition. A complete description of the system is presented by Demerchant et al. [4]. Many loops of optic fibre have been installed on the ring beam. Four bare optic fibres were bonded directly on the FRP wrap and one of them is dedicated for strain measurements. One optic fibre placed in a sleeve will be used for temperature measurements. There is a second type of long-gauge instrument, called *long-gauge FOS*, are described by Tennyson et al. [3]. Twelve of these 27-m-long measuring devices were installed on the ring beam. Eight of them measure strain while four sensors are used for temperature measurements.

Contrary to long-gauge sensors, Fabry-Perot sensors and FBGs take localized measurements. Many of them must then be distributed on a structure to draw up a complete picture of its behaviour. However, due to the circular shape of the containment structure, installing such instruments at strategic positions around the perimeter can provide a global representation

Figure 3. Gentilly Nuclear Secondary Containment Structure

of its structural behaviour. Fabry-Perot and FBGs were concentrated at four locations around the ring beam, at different elevations on its side. Brillouin scattering sensors were all located at the same elevation, but placed around the entire perimeter.

4.2 Remote monitoring

The remote control of all the measuring devices except the Brillouin sensors and long-gauge FOS is achieved through a microcomputer installed on site. We get access to this computer from our Sherbrooke office, 120 km away, via a phone line and the software PCAnywhere. Data are downloaded on a weekly basis to a permanent database in our laboratory for analysis and evaluation. The maintenance of the data and their analysis are continuous challenges. Software tools were developed for data collection, storage and interpretation. The data collection task implies labelling and format conversion of the raw data coming from all acquisition systems. The storage task involves a database organized in order to facilitate data retrieval and selection. In addition to the above challenges, it has not yet been possible to obtain simultaneous data from the entire set of instruments since this project actually involves two other research teams operating from distant locations from Gentilly. The Brillouin scattering sensor device is a proprietary system of the University of Ottawa, while researchers from University of Toronto operate the long-gauge FOSs. We plan to gather all interested parties in the near future to proceed with a complete set of simultaneous data recording.

5. SHERBROOKE PEDESTRIAN BRIDGE

Our most recent project is a short pedestrian bridge built on the campus of the Université de Sherbrooke in 2002 (Figure 4). This bridge is made of two concrete girders and a slab reinforced with FRP rebars. The roof, supported by four square columns, is composed of a rigid frame, steel deck and concrete cover. Strain sensors, temperature probes, an accelerometer and a web cam were installed to monitor the bridge. Six Fabry-Perot strain sensors and four RTD elements, mounted on FRP bars, are located at mid-span on top and bottom girder reinforcements. The readout units and the computer are secured in a terminal box in the building. The thermal strains are picked up on continuous basis at a slow rate (one reading every 15 minutes). The accelerometer performs a real time analysis of the measured data and triggers fast rate acquisition when unusual events are detected. The recorded data are available on-line through a web site.

Figure 4. Université de Sherbrooke pedestrian bridge

A C++ program was developed to control and synchronize data acquisition from the various types of instruments and to record the data in a database. The software carries out a real time analysis of the data, in order to detect unusual events that could affect the structure. A Java Applet was programmed to show the data on a web page. We currently improve the software by using data filtering techniques to reduce data collection. The software and the database will be integrated into a knowledge-based system which will be designed to perform short term and long term evaluation of the available records of the structure. The data, which will have been filtered and sorted, will be correlated with a FEM model subjected to the same load conditions. The behaviour predicted by the model will be recorded and used for damage detection on the existing bridge. Then, we will implement decision-making algorithms that will produce text-based notifications when overloads occur or when any alarm threshold is exceeded.

6. CONCLUSION – CHALLENGES OF SHM

The first authors to consider SHM for civil engineering structures identified the three key components of smart structures as sensing, assessing data and reacting. The development of each component has to respond to its own challenges. The sensing issue is linked to the selection, installation, and maintenance of the sensing and communication devices used to implement SHM. Their efficient development requires the involvement of software, computer and communication specialists. A most pressing challenge appears to be the development of standardized protocols to read, store and transfer numerical data, independent of the source of the sensing devices.

The assessment and reacting issues have multiple components. A major

challenge in sensing the performance of most civil structures is that many physical parameters need to be measured to get a complete assessment of their behaviour. The need to collect significant data for a given structure may even extend for decades. Selecting data in a continuous flow of information and developing reliable alarm systems when critical events are detected is an extremely challenging situation. It may be advanced that solutions to this issue could be based on multidimensional analysis techniques already used in other fields such as geotechnical and dam engineering.

Extensive data collection can only be justified now for bridges or structures that play a critical role in a region. The integration of data collection systems on newly built structures can hardly be perceived as essential by public authorities, except when they incorporate advanced features, such as dynamic control, that need a critical assessment. One may argue that for conventional structures, the need for sensing only arises when critical elements already exhibit unsafe behaviour. Developing significant monitoring strategies for new and conventional structures that will be beneficial to public authorities still remains our most interesting challenge.

ACKNOWLEDGEMENTS

These projects were supported by the Natural Sciences and Engineering Research Council of Canada (NSERC) through the Network of Centres of Excellence (NCE) ISIS Canada. The technical assistance of Mr. Claude Aubé was essential during the installation of the instrumentation. The collaboration of the MTQ mobile laboratory team led by Dr. Marc Savard and Mr. Jean-François Laflamme for the loading tests and data acquisition at the Ste-Émélie-de-l'Énergie bridge is also gratefully acknowledged.

REFERENCES

1. Rizkalla, S.H. and Labossière, P., "FRP in Structural Engineering in Canada: Planning for a New Generation of Infrastructure," *ACI Concrete International*, **21** (10), 1999, pp. 25-28.
2. Labossière, P., Neale, K.W., Rochette, P., Demers, M., Lamothe, P., Lapierre, P., Desgagné, G., "Fibre Reinforced Polymer Strengthening of the Sainte-Émélie-de-l'Énergie Bridge: Design, Instrumentation and Field Testing", *Can.J.Civ.Eng.*, **27**(5), 2000, pp. 916-927.
3. Tennyson, R.C., Coroy, T., Duck, G., Mulvilhill, P., Cooper, D.J.F., Smith, P.W.E., Mufti, A.A. and Jalali, S.J., "Fibre Optic Sensors in Civil Engineering Structures," *Can.J.Civ.Eng.* **27**(5), 2000, pp.880-889.
4. Demerchant, M., Brown, A., Smith, J., Bao, X. and Bremner, T., "Distributed Strain Sensing for Structural Monitoring Applications," *Canadian Journal of Civil Engineering*, **27** (5), 2000, pp. 873-879.

STRUCTURAL AND MATERIAL HEALTH MONITORING OF HISTORICAL OBJECTS

Situation in the Czech Republic

Miloš Drdácký

Institute of Theoretical and Applied Mechanics of the Academy of Sciences of the Czech Republic – ARCCHIP Centre of Excellence, Czech Republic

Abstract: Paper presents basic data on monitoring of structural and material health of historical objects in the Czech Republic. It is based on recent experience attained during work on related national and European research grant projects. Some needs for further development and research in this field are summarized.

Key words: cultural heritage, monitoring activities, monitored parameter.

1. INTRODUCTION

All historical objects exhibit smaller or larger defects and failures. Cracks or material changes are their most typical manifestation. Determination of true causes of the origin of a failure and forecasting of its further development are usually not simple and unambiguous tasks. Especially, answering the latter question calls for a long term monitoring of the behaviour of a defect or damaged structure in response to exterior forces, environmental changes and excitations. The size or extent of any defect or failure does not give sufficient information for structural safety assessment. More over, the degradation processes develop with uneven rate and only long term continuous monitoring is capable to discover the reasons and/or a dangerous acceleration of defect development. Therefore, the Czech Ministry of Culture supported a five year research project (focused on monitoring methods and their application on important national or world heritage monuments, which has been coordinated by the author. Few other research projects focused on monitoring of subsoil conditions or rock

Farhad Ansari (ed.), Sensing Issues in Civil Structural Health Monitoring, 127–132.

movement under important historic buildings, e.g. St.Vitus Cathedral in Prague, or monitoring of the famous Charles Bridge in Prague have been supported from the Czech Grant Agency. This communication shortly informs about recent monitoring activities in the field of cultural heritage in the Czech Republic.

2. MONITORED PARAMETERS

In order to assess the state of a damaged historic object, we need to know, if its defect or failure (mostly a crack) is stable or if it changes in response to acting forces and/or environmental influences. The stability is evaluated on the basis of geometrical measurements of the shape and position of an objects, structures or structural elements and mutual spatial relations of structural parts separated by the defect. In most cases of masonry structures, we monitor movements in the vicinity of cracks. Further, it is important to measure leaning of towers or walls, vertical movement (downward movement of uplift) and expansion or shrinkage of objects or structural elements.

The movements mentioned above are always influenced by temperature changes which influence also measurement devices, therefore, the temperature of the monitored structure and its surrounding is another basic monitored parameter.

Many building materials are very sensitive to moisture changes, e.g. wood, sandstones, paper,..), which reflects in their volumetric changes or differential mechanical characteristics and a higher adherence to chemical or biological attacks. Moisture and humidity characteristics are also followed up as a rule. The exterior and interior relative humidity is measured together with moisture content in building materials.

From the family of climatic effects, the wind velocity, direction and fluctuations are monitored on special buildings and structures, usually together with vibration effects.

Air pollution is monitored in historic cities and in the vicinity of important historical monuments, together with measurements of corrosion damage on historical materials and with monitoring of soiling of monument surfaces. In special cases, also chemical or ion characteristics of historic materials has been checked. There are some places in the Czech Republic where the water pollution or rather aggressiveness is monitored, also the variations of water table in the vicinity of monuments in danger of additional settlement or wooden pile degradation are registered.

A substantial part of structural monitoring involve records of building history and events which might change or influence the building behaviour,

e.g. restoration interventions, building activities in the vicinity of the monitored object, namely digging, as well as of activities with a stronger impact on environmental conditions (transport, dust production, etc.).

3. DURATION OF MONITORING ACTIVITIES

The length of measurements depends on the type of the problem and its history. Some damages develop and propagate very quickly and they require an immediate intervention which prevents larger damages or even catastrophic failures. In such cases, the monitoring is recommended also during the remedial works and at least one-year-long climatic cycle after the works are terminated.

In other cases of a slow defect propagation or its relative stability, it is recommended to measure at least for five years, because a shorter period does not give enough data for a reliable approximation of the future development. Then, if an unstable defect propagates with a remarkably decreasing velocity, the measurement can be stopped. On the other hand, if there is a linear, accelerating or unremarkably decreasing velocity, we recommend to continue with measurements. In such a case, the monitoring becomes a warning system with lasting and continuous measurement, which is the ideal situation.

4. METHODS AND DEVICES

The main activities are connected with monitoring of cracks in historic buildings and monuments. Use of gypsum strips (or glued glass plates) are not recommended, even though, there were quite widely applied at short time monitoring of several objects affected by recent floods in the Czech Republic, Fig.1. In similar cases where a failure suddenly occurred after some disaster, such as an earthquake, flood or other subsoil movement, there is possible to check the stability using this very traditional method which is otherwise not very useful for monitoring.

Mechanical extensometers represent another traditional method which gives excellent results. It needs, however, personal operation which might be seen as an unpleasant disadvantage, similar to geodetic methods.

For long term monitoring of deformations, electrical sensors are widely used, e.g. LVDT sensors. Sensors with electrical outputs are also used for measurements of temperature and humidity. The acquired data are stored in data loggers and read by operators in periods lasting several months or they are sent automatically on the web server for further elaboration.

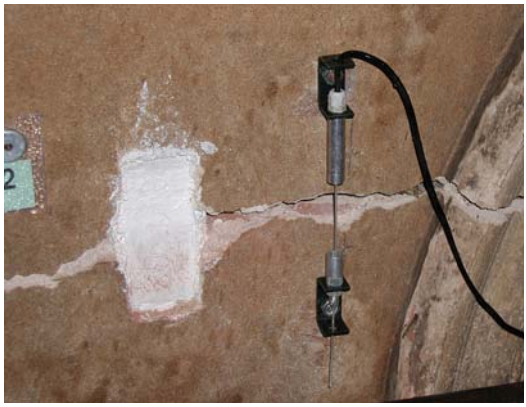

Figure 1. Traditional monitoring elements – geodetic target, gypsum strip, LVDT sensor – used for monitoring of Veltrusy Castle severely damaged by flood..

Environmental monitoring and measurement of damages on historic materials are materialized using special "stations" and sensors. This activity has been supported by several European grants and it involves also monitoring of wind effects. (For example EC 5th FP Grant projects REACH or MULTIASSESS, EC 6th FP Grant projects NOAH'S ARK or CULTSTRAT. A special optical system for surface quality assessment has been developed within EC 5th FP CRAFT Project HISTOCLEAN. Details can be seen on the relevant project websites and www.arcchip.cz.

Optical methods and systems are developed and used for assessment of surface degradation and deformation measurements, including crack movement.

5. EXAMPLES OF MONITORING ACTIVITIES ON IMPORTANT HISTORICAL OBJECTS

5.1 Telč Castle and Historic City

(World Heritage and National Cultural Monument). Several cracks in historic masonry have been monitored since 1996 together with temperature and humidity. A typical graph of a crack opening documents the necessity of long term monitoring for a reliable prediction of future behaviour, Fig.2. At the same time, it shows how human failures can influence the data acquisition process.

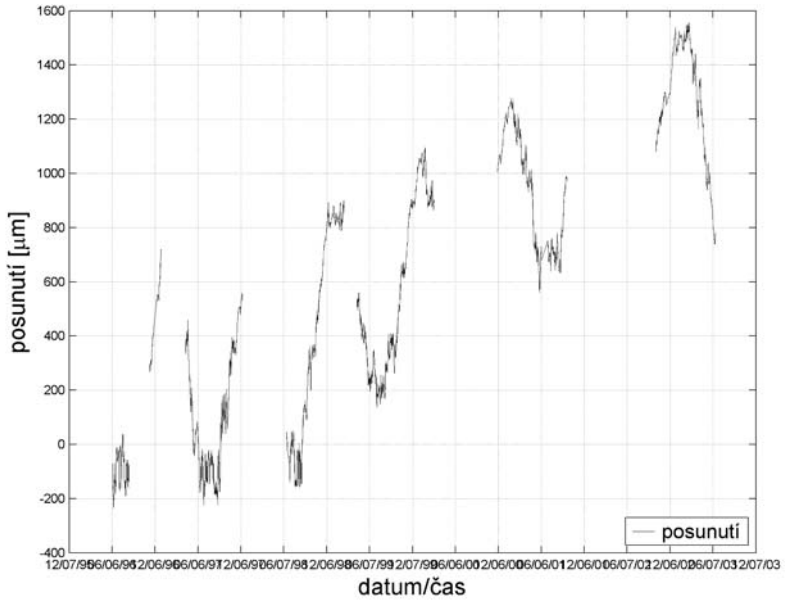

Figure 2. Telč Castle – crack opening tendency in the years 1996-2003.

5.2 Prague New Town Hall

(National Cultural Monument, further NCM). Several cracks in historic masonry walls and vaults have been monitored since 2000, again together with temperature and humidity variations. The measured data are automatically sent to the Institute server using GSM modems and a specialized software written in the Perl language, Fig.3. Monitoring is complemented by some other NDT investigations, e.g. georadar measurements, within another EC 5th FP Research Grant Project ONSITEFORMASONRY.

6. FUTURE NEEDS IN MONITORING OF CULTURAL HERITAGE

Let us try to briefly identify some needs for further research and development in the field of monitoring systems for cultural heritage:

From the examples presented above, it follows that monitoring systems for cultural heritage require small reliable sensors capable to measure temperature, humidity, moisture content in materials, time dependent

deformations and environmental situation around the monitored cultural monument. Especially inexpensive and reliable sensors for moisture content and humidity measurements are to be developed.

Figure 3. Data logger with transmitter in the New Town Hall in Prague.

In cultural heritage objects, the wireless systems are advantageous, which is also a challenge for further research. They should be, of course, automatically operated.

Many cultural heritage sites are not supplied with electricity and they are, unfortunately, easily accessible by public and therefore suffering from vandalism, which prevents installation of systems which can be damaged or stolen.

There is still a potential in development of acoustic sensors capable to distinguish changes in materials or changes of stress state in structures from acoustic response, similarly to what the human ear can do.

The same is valid for optical sensors and systems, including non-traditional applications. (For example, suitable sensors for soiling or deposits measurements are not available).

Relevant theories and methods for interpretation and evaluation of acquired data must be simultaneously developed for intelligent sensors.

ACKNOWLEDGEMENTS

Support of the Czech Ministry of Culture Grant. No.PK99-P04-OPP006 and the EC 5th FP Grant No. ICA1-CT-2000-70013 (Advanced Research Centre for Cultural Heritage Interdisciplinary Projects – ARCCHIP Centre of Excellence) and No. EVK4-CT-2001-00060 ONSITEFORMASONRY is acknowledged.

Chapter III

Sensing of Structural Parameters and Extreme Events

INTERNAL AND EXTERNAL SENSING FOR POST-EARTHQUAKE EVALUATION OF BRIDGES

M. Saiid Saiidi, Robert Nelson, and Patrick Laplace
University of Nevada, Reno, USA

Abstract: Internal and external sensors have been used extensively in research on the seismic response of bridges in the Large Scale Structures Laboratory at the University of Nevada, Reno. These sensors record how a structure responds to the dynamic loading conditions produced by seismic activity. When the data obtained from these sensors are combined, they can show what deterioration has occurred and to what extent. This paper demonstrates how the data were used to determine the failure sequence and the behavior of the models.

Key words: Sensors, Shake-table, Post-earthquake evaluation.

1. INTRODUCTION

Instrumenting structures can be a multipurpose undertaking: (1) the data under service loads can provide insight into the behavior of the structure and point out possible critical situations that were not foreseen in design, (2) following an extreme load the data can help assess the structure and determine its safety and the level of service it could provide, and (3) under moderate and extreme loads the post-yield response of the structure can be evaluated and the validity of analytical models can be examined. For all three objectives, it is essential to equip the structure with both internal and external sensors. Examples of internal sensors include strain gages, piezoelectric devices, optical fibers, and others. External sensors may include displacement transducers, accelerometers, titlmeters, and video recording equipment. The effectiveness of the sensors in accomplishing the

Farhad Ansari (ed.), Sensing Issues in Civil Structural Health Monitoring, 135–144.

second and third objectives can be generally judged only if sufficiently instrumented structures are subjected to frequent extreme loads. However, extreme loads are infrequent, thus making such evaluation difficult. In contrast laboratory testing of large-scale models can be used as a vehicle to assess the usefulness of the instruments towards the aforementioned goals. Combining measured strains and deflections with video recordings can be a very descriptive and accurate means of studying the behavior and performance of a test subject under extreme loads. Using results from three tests performed at the University of Nevada, Reno (UNR), this article briefly demonstrates the use of sensors to evaluate the behavior of a structure.

2. EXPERIMENTAL STUDIES

Experiments have been carried out at UNR to study the seismic retrofitting of deficient bridges, one retrofitted with fiber reinforced polymer (FRP) composite sheets (B2RC), one with an infill wall (B2RW), and the third with FRP bridge restrainers. These studies utilized various sensor types, both internally and externally.

2.1 Description of Test Specimens and Instrumentation

The study on the piers was on the seismic behavior of two-column bents with drop cap beams built in the 1970s and earlier. Identical ¼-scale models were used. The prototype for the models was based on typical properties of substandard bridges in California **[1]**.

The piers were instrumented to register the strains in the longitudinal and transverse reinforcement, column and beam curvature, and pier displacement. Camcorders were also used to provide visual data. The instrumentation varied slightly among specimens. More details about the specimens and tests are provided in Ref. **[1, 2]**.

Bridges in seismic areas require restraining devices against large longitudinal movements at expansion joints and supports to prevent unseating. Researchers at UNR have been developing and testing restrainers consisting of one or more types of FRP. The focus of this paper is on an FRP restrainer made with carbon fibers (CFRP).

2.1.1 Two-Column Pier with FRP Composite Retrofit (B2RC)

The pier retrofit was designed to provide adequate confinement in the lap-splice zone at the bottoms of the columns, improve flexural performance of the beam, and to improve shear performance of the columns, beam, and

joints **[1]**. The retrofit consisted of wraps embedded in resin and adhered to the columns and beam. Along with strain gages on select transverse and longitudinal reinforcement, stain gages were placed on key areas on FRP.

2.1.2 Two-Column Pier with Infill Wall Retrofit (B2RW)

Three representative infill walls from three bridges in California were studied to develop an infill wall model **[2]**. The prototype consisted of a wall of 1.5 ft (460 mm) thick with a 6-in (150-mm) gap between the top of the wall and the bottom of the pier cap. The gap is left for improved constructability. Horizontal and vertical dowels were used to connect the infill wall to the existing columns and footing.

In addition to strain gages, accelerometers, and displacement transducers, the instrumentation of the infill wall specimen consisted of displacement transducers around the perimeter and the diagonal direction of the infill wall.

2.1.3 Carbon Fiber-Reinforced Polymer Restrainer

The restrainers consisted of two CFRP plates with a bond area of 8 in (203 mm) by 14 in (356 mm) and a central segment with a length of 10.5 in (267 mm). The plates were comprised of two layers of carbon fiber fabric at 45 and 135 degrees. The central piece was a strip of carbon fiber fabric embedded in an elastomer with a height of 3 in (76 mm). Details of the restrainer studies are presented in Ref. **[3]**.

The restrainers were made by first cutting the fabric to the correct size. Then the ends of the center strip that were to overlap the plates were coated with epoxy. Next, elastomer was applied to non-epoxy coated section of the center strip using a vacuum box to ensure the fabric was fully saturated. Following this the plates were made by coating both layers of fabric with epoxy. Finally, the center strip was attached to the plates with epoxy.

The restrainer test made use of a machine vision camera as an external sensor. Along with the camera, displacement transducers and string displacement transducers were used to measure the block displacements and determine the elongations of the restrainer **[3]**.

2.2 Testing Program and Measured Response

The tests were conducted on the shake tables at UNR. For each run on the shake table the selected ground motion was incremented with a slightly higher multiplier than the previous run. This allows the detection of gradual deterioration, yielding, and failure of the specimen.

In the case of the two-column piers, the selected ground motion was the 1994 Northridge earthquake, as recorded in the Sylmar Hospital. A vertical load was applied corresponded to an axial load of 5% of the product of the concrete compressive strength and the gross area of the columns **[1]**. The lateral load was generated through an inertial mass system. Both B2RC and B2RW were subjected to the same loading protocol.

For the restrainer test, two concrete blocks separated by a gap similar to an expansion joint were placed on the table. The blocks rested on elastomeric bearings and were connected by one CFRP restrainer per side. The ground motion selected for the restrainer tests was a synthetic record that matched the soft soil spectra specified in the Applied Technology Council document 32 (ATC32E).

2.2.1 Two-Column Pier with Composite Retrofit

The CFRP fabrics covered most of the surface of B2RC, thus the damage was visible only on the CFRP surfaces and at the gaps at the ends of the column jackets. Under 2.0 x Sylmar, the vertical CFRP fibers from the left joint region that extended to the column began to debond. The crack in the composite at the top of the right column widened significantly and the jacket debonded from the concrete. The pier failed under 2.25 x Sylmar with a total separation between the pier and the footing by rupture of the column bars. The failure was abrupt, although the drop in the measured lateral load during the previous run had indicated that the failure was imminent.

2.2.2 Two-Column Pier with Infill Wall Retrofit

A shear crack was formed in the left column under 1.5xSylmar.. A vertical crack ran along the interface between the wall and the columns. The shear crack in the left column began where the vertical interface crack ended and extended to the bottom of the column. The column shear crack had an inclination of approximately 30^{o} relative to the column axis. The shear crack was formed as the specimen displaced from right to left, and the left column was pushed away from the wall. Model B2RW failed under 2.0xSylmar, with a PGA of 1.21g. During the last run, the columns partially separated from the wall at their mid-height to the top. Some of the anchorage dowels were pulled out and some ruptured.

2.2.3 Carbon Fiber-Reinforced Polymer Restrainer

The blocks were setup with unequal masses to produce a period ratio of 0.6 for the two segments. The period ratio of 0.6 was the worst case for out

of phase motion, while still represented field condition. Neither of the CFRP restrainers was damaged until 0.57xATC32E, which has a PGA of 0.2g. Under that motion there was fiber rupture in the elastomer coated section in the hinge area of the south restrainer and debonding between the inner and outer layers of FRP could be seen on the east block of the north restrainer.

3. POST-FAILURE EVALUATION

The data obtained from the strain gages and displacement transducers were combined with images obtained from video cameras to perform post-failure evaluation of the behavior of the pier models. For the restrainer model only the images obtained from the machine vision camera could be used to assess the failure.

3.1.1 Two-Column Pier with Composite Retrofit

The failure of B2RC occurred during 2.25 x Sylmar, when the columns were detached from the footing. During testing it was not clear as to which column detached first. This was important because the axial loads in the two columns were different due to the overturning moment. To determine which column base failed first the data from the displacement transducers that measured vertical displacement at column bases were used. It was decided that the maximum extension displacement reading should correspond to the column failures because one end of each transducer was attached to the column and the other rested against the footing. It should be noted that when the displacement reaches a maximum it is not necessarily the exact time of failure because the column may or may not have fully uplifted at this point. However, the time should be very close to the failure time and furthermore the relative times between the left column and right column separation can disclose the sequence of failure.

The displacement history is shown in Fig. 1. The figure shows that the right column failed first at 16.27 sec followed by the failure of the right column at 16.34 sec. The images captured during the test confirm this sequence (Fig.2 and 3). Figure 2 shows a larger separation at the base of the right column. In Fig. 3 the right column has separated from the footing while the left column is partially attached.

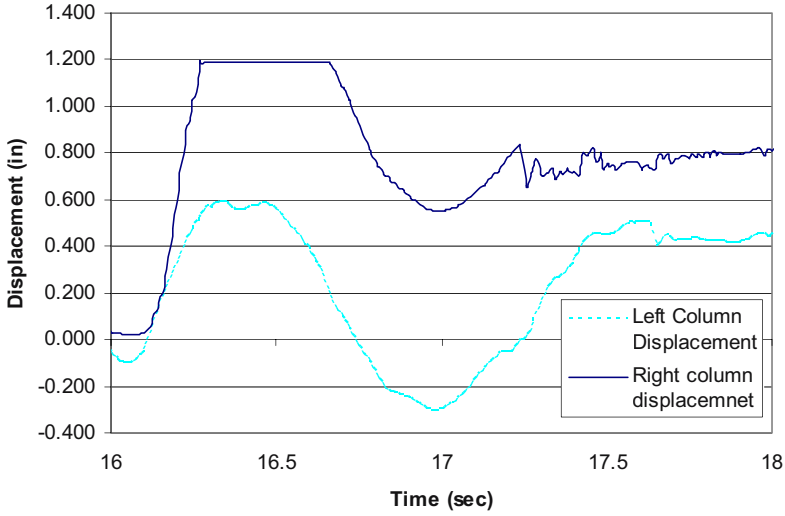

Figure 1. Displacement transducer data at column bases

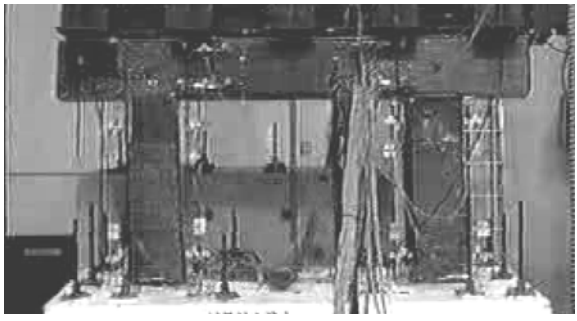

Figure 2. Columns begin uplift

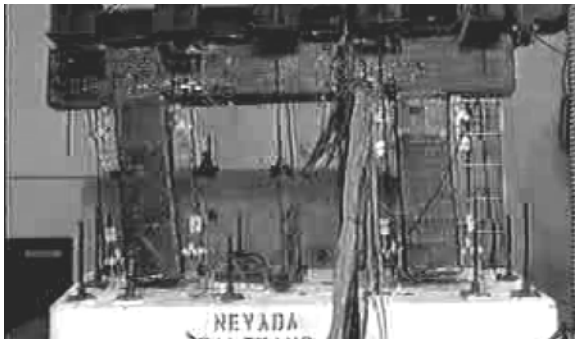

Figure 3. Right column leaves footing while left is still partially attached

It appears that the overturning effect led to tension on the left column and caused its separation from the footing. With the loss of connection at the base of the right column, the left column had to resist the entire lateral force and hence it failed in shear.

3.1.2 Two-Column Pier with Infill Wall Retrofit

Specimen B2RW failed under 2.0 x Sylmar. Previous to this run a large diagonal shear crack developed in the middle of the left column. During the failure run this crack opened and the column slid down the crack face. The right column failed in compression/sliding shear immediately below the beam. The failure of the two columns appeared to be simultaneous. Because the failure mode was different in the two columns, it was important to determine which failed first and why. The most descriptive data from internal transducers were from strains in the column bar gages.

Within the left column, strain gages located on a tie provided the best data. The tie was 8 in (203 mm) from the base of the column and was the closest instrumented tie to the shear crack. Because saturation of the two gages differed (one at 16.23s and one at 16.75s) by 0.52 second an average of the two was taken to determine the time of failure, 16.49s.

The closest useful gage within the right column consisted of a strain gage located on a longitudinal reinforcement bar. The gage was positioned 4 in (102 mm) down from the beam-column interface. The gage was saturated at 16.76s. These results can be seen in Fig. 4, along with the lateral force on the bent, which further confirms the time of failure.

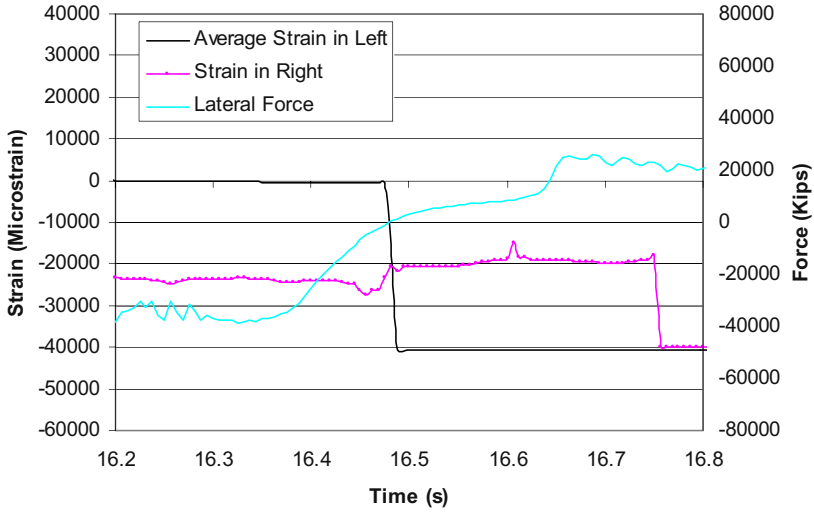

Figure 4. Lateral force and strain in column ties

The failure sequence can be seen in Fig. 5-7. Figure 5 shows the steep shear crack in the left column. Note that no damage is visible in the right column. In Fig. 6 the left column crack has opened and cracks are becoming visible at the top of the right column. Finally Fig. 7 shows that the left column has failed in shear, the left part of the beam has slid down, and the right column has failed in compression on its left side while being sheared off by the beam.

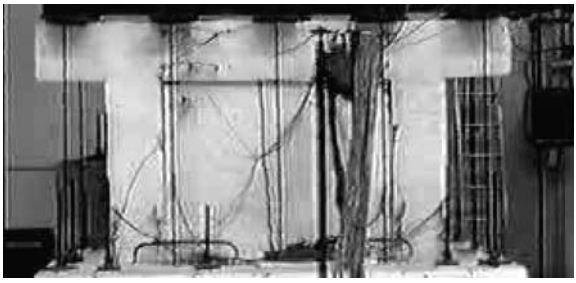

Figure 5. Steep shear crack in the left column

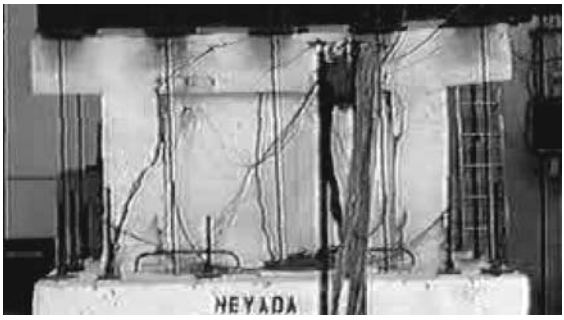

Figure 6. Opening of shear crack in the left column

Figure 7. Start of shear/compression failure in top of right column

3.1.3 Carbon Fiber-Reinforced Polymer Restrainers

The restrainers introduced an interesting problem. Most of the sensors could only tell the maximum elongation of the restrainers and the force at which a specimen failed. More information as to how the restrainer failed was desired. Previous FRP strip tensile tests had shown that there can be an edge effect, in which the fibers at the edge fail first because of possible shear lag and the lack of sufficient continuity in the transverse direction. The elastomer was intended to eliminate these problems. Question was raised during the test on whether the restrainer failure was due to the edge effect or was initiated within the restrainer itself. Figures 8-10 reveal that a crack developed in the top half (not just the edge) of the restrainer followed by complete fracture and that failure did not start as a localized effect. It was concluded that the elastomer was effective in eliminating the edge effect.

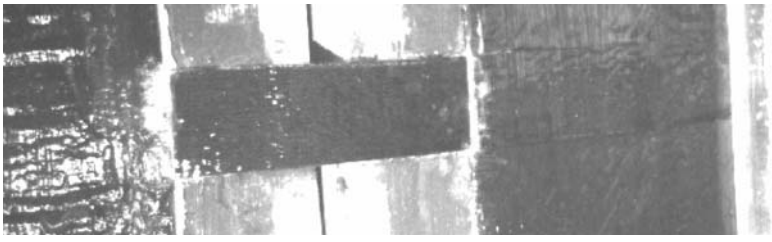

Figure 8. CFRP restrainer just prior to failure

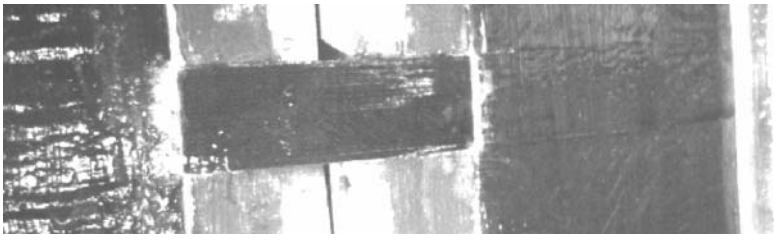

Figure 9. Crack forming in upper half of restrainer

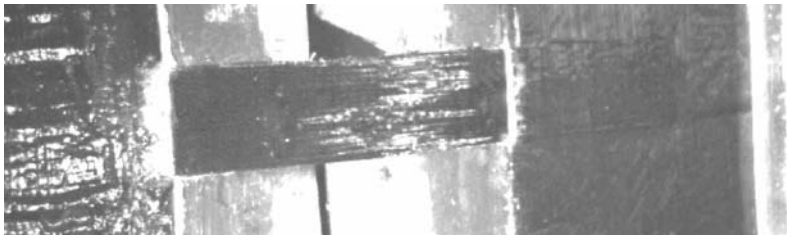

Figure 10. Rupture of restrainer

4. CONCLUDING REMARKS

This paper demonstrated the use of strain gages, displacement transducers, and camcorders to explain the ultimate performance of two bridge piers and an FRP restrainer. Instrumentation of similar types can provide useful information on the field performance of actual structures. Much research and development work needs to be conducted to maximize the usefulness of the sensors for structural health monitoring. Other essential consideration is the selection of sensor location and types to obtain the most revealing information. Due to the high cost of instrumenting large full-scale structures, it is advisable to conduct extensive analytical studies to optimize the sensor locations.

REFERENCES

1. Pulido, Claudia, M. Saiid Saiidi, David Sanders, Ahmad Itani, and Saad El-Azazy, "Seismic Performance of Two-Column Bents – Part I: Retrofit with Carbon Fiber-Reinforced Polymer Fabrics," ACI Structural Journal, 101 (4), 558-568 (2004)
2. Pulido, Claudia, M. Saiid Saiidi, David Sanders, Ahmad Itani, and Saad El-Azazy, "Seismic Performance of Two-Column Bents – Part II: Retrofit with Infill Wall," ACI Structural Journal, 101 (5), 642-649 (2004)
3. Johnson, Rita, M. Saiid Saiidi, and E. Manos Maragakis, "A Feasibility Study of FRP Seismic Restrainers," (in preparation), Report No. CCEER-04-x, University of Nevada, Reno 2004.

APPLICATION OF EM STRESS SENSORS IN LARGE STEEL CABLES

Ming L. Wang, G. Wang, and Y. Zhao
Department of Civil and Materials Engineering, The University of Illinois at Chicago, Chicago, IL 60607, USA

Abstract: The employment of elastomagnetic (EM) stress sensors on large steel cables of Qiangjiang No. 4 Bridge in China is discussed. As an engineering application in the field of ferromagnetic magnetoelasticity, the EM sensors make possible non-contact stress monitoring for steel cables and pre-stressed tendons on suspension bridges, cable-stayed bridges, and other ferromagnetic structures. The correlation of the relative permeability and tensile stress is derived from the calibration. Automatic maneuvering is fulfilled by formalizing the calibration function with the temperature-influencing factor. Calibration reveals that the magnetoelastical characteristics of multi-wire hangers are analogous while that of post-tensioned tendons are similar to single wires. In-situ measurements on Qiangjiang No.4 Bridge demonstrate the reliability of the EM stress sensors.

Key words: elastomagnetic stress sensor, magnetoelasticity, tension, temperature

1. INTRODUCTION

It has been long discovered and extensively studied that the magnetic properties of ferromagnetic materials can be changed by stress [1-5]. This discovery began with the conception of magnetostriction, which indicates the magnetization of a magnetic material leads to shape variation, as described below (Bozorth, 1951):

$$\frac{1}{l}\frac{\partial l}{\partial H} = \frac{1}{4\pi}\frac{\partial B}{\partial \sigma} \tag{1}$$

Farhad Ansari (ed.), Sensing Issues in Civil Structural Health Monitoring, 145–154.

l stands for length of the sample; H and B are respectively magnetic field and induction; σ is stress. The equation indicates that tension leads to the increase of induction, provided that the material concerned has positive magetostriction.

This phenomenon, called magnetoelasticity, can be inferred from the interaction between stress and magnetic domain orientations. The applied stress changes the energy of the imperfections and impurities, as well as residual stress, all of which can pin the domain walls [6]. More directly, it can be interpreted from the point of magnetic strain energy [2]. Many researchers and engineers have explored industrial utilities of magetoelasticity, especially in no-destructive tests [3, 7-13]. As a promising application in stress monitoring for cable-stayed or suspension bridges, the EM stress sensor discussed below is aimed to characterize the stress dependence of the magnetic properties, represented by the relative permeability.

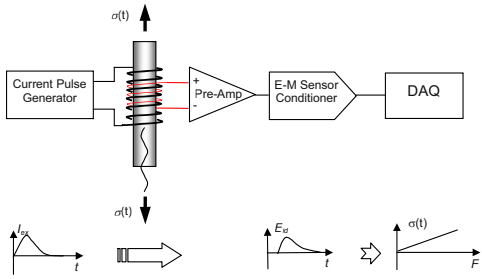

Fig. 1. Principle of PowerStress Magnetic Measurement System

An EM stress sensor consists of a primary coil and a secondary coil, which work cooperatively to measure the apparent relative permeability and formalize the magnetoelastic characterization of the material. As shown in Fig.1, when pulsed current passes the primary coil, the ferromagnetic material is being magnetized and a pulsed magnetic field is introduced along the steel rod. Initially a gentle upward trend of the B-H hysteresis curve is produced. Then, as H field reaches the maximal value and decreases, B field follows a gentle return too. The relative permeability

$$\mu_r = \mu_0 \Delta B / \Delta H \tag{2}$$

is measured in the descending section of the hysteresis curve, where ΔB and ΔH respectively signifies the variation in induction and magnetic field, and μ_0 is the permeability of the free space. However, the relative permeability of the EM stress sensor can not be derived directly from the hysteresis curve since several uncertain variables might be unexpectedly introduced. In present study, the relative permeability is measured via the sensing coil

following proper procedures [13]. Therefore the relative permeability of the steel rod could be rewritten as

$$\mu(\sigma,T)=1+\frac{A_0}{A_f}\left[\frac{V_{out}(\sigma,T)}{V_0}-1\right] \tag{3}$$

Where μ is permeability, σ tensile stress, T temperature, V_{out} the integrated voltage with the rod in the solenoid, and V_0 is the integrated voltage without the rod in the solenoid.

Through calibration, the temperature and stress dependence of the relative permeability are revealed. Such characterization is therefore used in stress monitoring of the steel rod. During in-situ monitoring, with temperature and relative permeability measured, the tensile stress can be calculated. Due to the specific advantages of the EM sensors, such as non-contact measurement, high repeatability, and low cost, they are drawing an increasing attention in load monitoring of the ferromagnetic cables.

2. QIANGJIANG NO. 4 BRIDGE

The QianJiang No.4 Bridge which is still under construction located in Hangzhou, China. It is the longest double-deck and multi-arch bridge in the country. The upper deck is a segment of a six-lane highway and the lower one is a railway with sidewalks for pedestrians, as seen in Fig. 1. To guarantee the reliability of its services, a state-of-the-art health monitoring system was built during the bridge construction, including EM stress sensors on the hangers and the post-tensioned tendons.

Fig. 2 Visual painting of Qianjiang No. 4 Bridge

3. EQUIPMENT AND MEASUREMENT SETUP

EM sensors can be used in stress monitoring either in single wire or large cable. For Qiangjiang No.4 Bridge, four kinds of cables/tendons need to be monitored: 109_7mm hangers, 85_7mm hangers, 55_7mm hangers and 37_15.5mm post-tensioned tendons. All are made from cold drawn, low relaxation cable or strand. The material is high strength piano steel. The hangers are pre-anchored in Liuzhou OVM Company and the 37_15.5mm tendons are to be erected on the bridges. The sensors are manufactured at the University of Illinois at Chicago (UIC), and then shipped to Liuzhou OVM Company and bridge construction field for mounting. The mounting pictures are given in Fig. 3.

I. II. III. IV.

Fig. 3 Pictures of Sensors, I. Sensor, II. Sensor mounted on hanger, III. Post-tensioned tendon with EM sensor, IV- Hanger with sensor on bridge.

The load monitoring is carried out in the PowerStress Measurement system (PSM) developed in UIC. The PSM system undertakes principal tasks such as providing a large pulsed current to magnetize the steel cable, picking up signals from the primary coil, the secondary coil, as well as the temperature sensor and conducting data processing. Each unit can sequentially manipulate dozens of EM stress sensors.

4. TEMPERATURE INFLUENCE

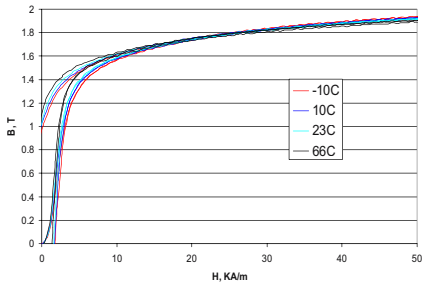

Saturation magnetization increases as temperature drops

Fig.4 Hysteresis curve of the 7mm piano steel wire tested at different temperatures

Temperature obviously affects the magnetic behaviors of the steel, as Fig. 4 indicates. As shown in Fig.5, EM sensor calibration curve shifts in a parallel manner due to temperature fluctuation, which is consistent with previous research at UIC [14]. Therefore, in order to eliminate this influence, it is necessary to find the temperature dependence of $\mu(0,T)$. Fig. 6 reveals that temperature effects for Chinese 15.5mm strands are the same as those for Chinese 7mm rods and for Japanese 37_7mm hangers since the these strands, rods, and cables have similar microstructure. Considering the working points, we have:

$$\mu(0,T) = A_T T + B_T = -0.018T + B_T . \tag{4}$$

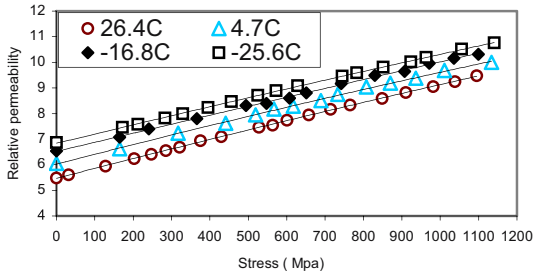

Fig.5. Temperature influence of stress-permeability correlation for 7mm piano wire

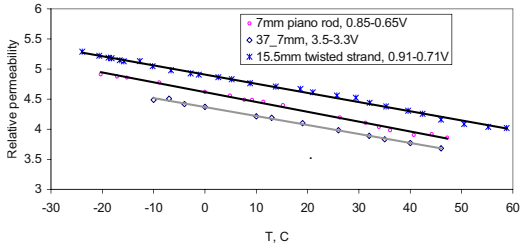

Fig.6 μ(0,T) of Chinese 7mm rod, 15.5mm strand and Japan 37_7mm hanger, slope is -0.018/°C

5. LOAD MONITORING CALIBRATION

The stress monitoring calibration for Florida strand was conducted in the lab, with the results given in Fig. 7. The calibrations for the three kinds of hangers used in QJ bridge are close to each other, as shown in Fig. 8 (a). The slope of the calibration curve is constant regardless of the working point

variation in a large range, as shown in Fig. 8(b). Therefore, a small shift in initial permeability does not change the slope of the calibration curve.

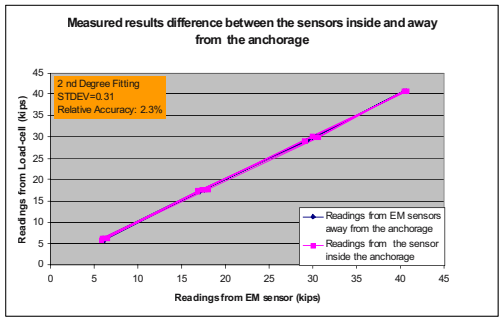

Fig.7. Calibration curve of the 0.6inch Florida wire

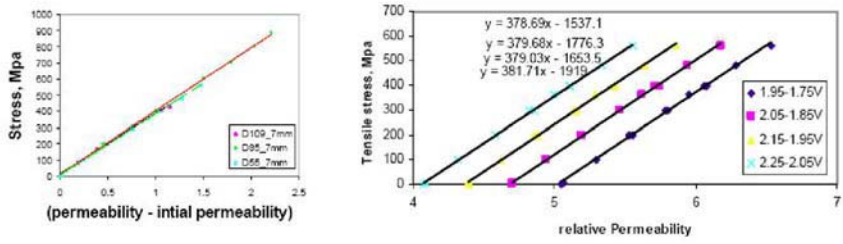

(a) *(b)*

Fig. 8 Calibration curves for the three types of hangers (a) and the post-tensioned cable (b) at different working points employed in the construction of Qianjiang No. 4 Bridge

In order to achieve a higher accuracy, a second degree stress function is derived for in-situ load monitoring through calibration. For 55_7 mm cable the function can be expressed as:

$$F = -19.854\left(\left(\mu(\sigma,T)-\mu(0,T)\right)^2 + 405.15\left(\mu(\sigma,T)-\mu(0,T)\right)\right) \quad MPa \quad (5)$$

The linear alternation of Eqn.(5) is:

$$F = 377.86\left(\mu(\sigma,T)-\mu(0,T)\right) \; MPa \quad (6)$$

where $\mu(0,T) = -0.018T + 4.97$.

In the monitoring process, the repeatability of zero point, $\mu(0,T)$, is extremely important. To achieve the stabilization of $\mu(0,T)$, it is necessary to magnetically saturate the cable section near the location of the EM sensor, via many trials prior to the final measurement. The repeatability of the single

wire and multi-rod cable are shown respectively in Fig. 9 and Fig. 10. The stress maintaining tests of all three kinds of cables are given in *Table I*. Temperature variations are taken into account in the stress calculation using Eqn.(6). It should be noted that load cell relaxation can not be avoided.

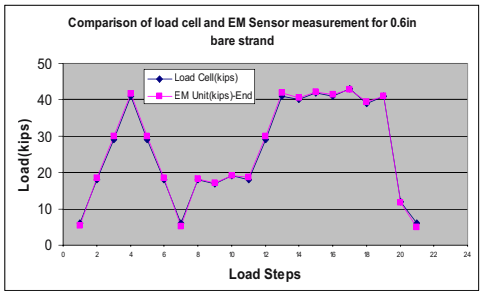

Fig. 9 Repeatability tests for the EM sensor on 0.6 inch Florida strand

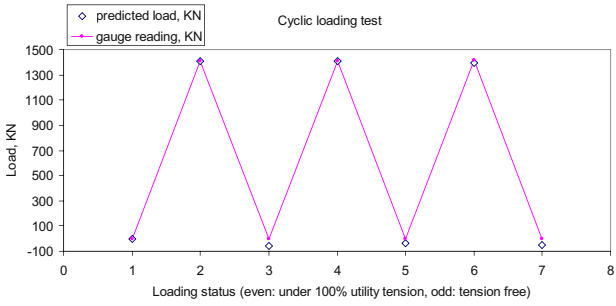

Fig.10 Repeatability tests for the EM sensor on 109_7mm hanger

Table I. Load maintaining tests for the hangers, including temperature influence

Cable	Time and date	Gauge reading, KN	Tem.(C)	Calculated load, KN
55_7mm	5PM,12/27/2003	843	18.5	832
	9AM,12/28/2003	826	13.5	803
85_7mm	6PM,11/22/2003	2630	23.7	2620.7
	9AM,11/23/2003	2583	17.9	2499
109_7mm	8:30PM, 09/03/2003	1407	32.3	1425
	9AM, 09/04/2003	1373	29.3	1411

6. IN-SITU STRESS CALIBRATION OF THE POST-TENSIONED TENDON

In order to load the post-tensioned tendon of 190meters long for QJ No. 4 Bridge, two hydraulic loading cells were mounted on both sides of cable, and pulled alternatively at a step of 20mm elongation toward both ends. The tendon was pulled to 45% of its yielding strength, accordingly the total elongation is 880mm. For the convenience of the sensor calibration, the total loading process was principally divided into four procedures. Measurements were taken during the intervals, after maintaining the hydraulic pressure at least three minutes for stress stabilization. The result was plotted in Fig. 11. The measurement results of both sensors were consistent with each other. Fig.12 indicates the relationship between the stress and the permeability of the post-tensioned tendon is similar to that of the single 7mm wire and 15.5mm strand.

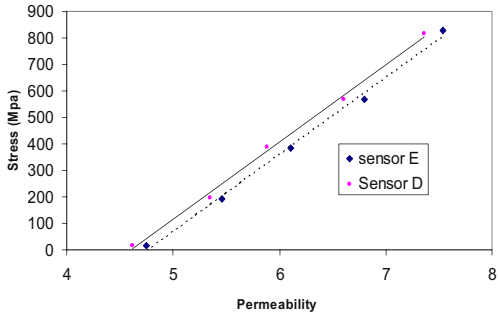

Fig.11 Stress measured by the two EM sensors for the 140mm tendons.

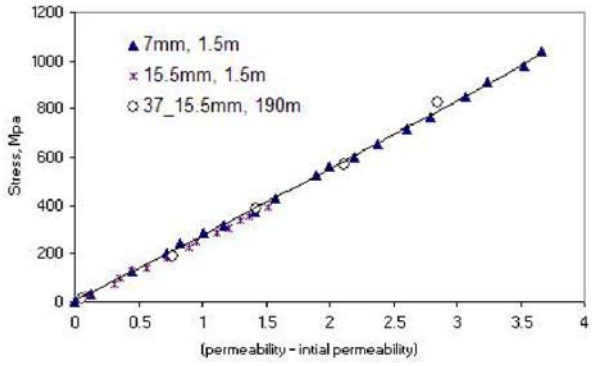

Fig.12 Stress vs. differential permeability of multi-strand tendon and single 7mm wire and 15.5mm strand

To sensor E, the stress-permeability relationship can be obtained through calibration:

$$F = 18.909\left(\mu - \left(-0.018T + 5.20\right)\right)^2 + 236.13\left(\mu - \left(-0.018T + 5.20\right)\right) MPa \quad (7)$$

In the respect of stress-permeability relationship, hangers (109_7mm, 85_7mm, and 55_7mm) deviate from single rods while the 140mm tendon coincides. It is mainly because their structures are different. The wires within the hanging cables contact each other and are galvanized with zinc while each wire in the tendon is covered with an anti-corrosion epoxy resin layer. Therefore, the eddy current in the former can introduce a greater radial magnetic field gradient than the latter. During stress monitoring, the integration and temperature are the only parameters that need to be measured. For example, for the 140mm tendons, the stress can be calculated through Eqn.7. *Table II* gives the stress measurement of the 140mm tendons two weeks later following the pulling of the tendons. V_{charge} =430V, working point: 2.8~2.6V,

Table II. Stress measurement for the 140mm tendons, sensor 1 and 4 are on both ends of one diagonal of the steel box, while 2 and 3 are on the other diagonal

sensor	$V_{inte}(\sigma, T)$	temp.	V_0	$\mu(\sigma, T)$	B_T	F(Mpa)
No.1	141.06	28	54.12	7.07	5.05	717
No.2	143.05	28	53.29	7.37	5.3	731
No.3	143.37	30	53.35	7.38	5.15	798
No.4	139.47	30	52.99	7.17	5	778

It can be seen that the measured tension is lower than designed (804Mpa). There are two reasons. First, there is a tension loss due to the load cell relaxation. Second, on the day of the measurement, the temperature was high, which can lead to a drop in tension. For example, a temperature variation of 10°C can introduce a stress change of $12.0\times10^{-6}\times(10\text{-}0)\times2\times10^{5}$=24Mpa.

7. CONCLUSIONS

Through the stress monitoring calibration of the sensors for three types of hangers, it can be asserted that the relationship between stress dependence and permeability is similar if the cable is composed of the same type of steel rods. While for the post-tensioned tendons, the relation is close to that of the single wires, as the tendon is composed of isolated 15.5mm strands. In engineering consideration, a small shift of $\mu(0,T)$ does not change the

correlation of permeability and stress. It is also found that temperature influences for all the cables are the same. Generally, to monitor the tension of the cables, the following values are required: V_0, a fixed value of each sensor; μ(0,T)and T before tension is applied; μ(0,T) and T when tension is applied.

REFERENCES

1. J. P. Joule, "On a new class of magnetic forces", Ann. Electr. Magn. Chem., Vol. 8, 1842, pp. 219-224.
2. R. M. Bozorth, Ferromagnetism, D. Van Nostrand Company, INC., Canada, 1951
3. P. E. Mix, Introduction to nondestructive testing, John Wiley & Sons, Inc., Hoboken, NJ, 1987.
4. B. D. Cullity, Introduction to Magnetic Materials, Adision-Welsley Publishing Company, Reading, MA., 1972.
5. M. J. Stablik and D. Jiles, "Coupled magnetoelastic theory magnetic and magnetostrictive hysteresis", IEEE Trans. Magn., Vol. 29, 1993, pp. 2113-2123.
6. D. C. Jiles, C. C. H. Lo, "The role of new materials in the development of magnetic sensors and actuators", Sensors and Actuators A, Vol. 106, 2003, pp. 3-7.
7. M. L. Wang, S. Koontz and A. Jarosevic, "Monitoring of cable forces using magneto-elastic sensors", 2nd U.S.-China Symposium workshop on Recent Developments and Future trends of computational mechanics in structural engineering, May 25-28, 1998, Dalian, PRC, pp. 337-349.
8. J. M. Daughton, "GMR applications", J. Magn. Magn. Mat., Vol. 192, 1999, pp. 334-342.
9. P. Tayalia, D. Heider, and J. W. Gillespie, Jr., "Characterization and theoretical modeling of magnetostricitve strain sensors", Sensors and actuators A, Vol. 111, 2000, pp. 267-274.
10. M. L. Wang, G. Lloyd and O. Hovorka, "Development of a remote coil magneto-elastic stress sensor for steel cables", SPIE 8th Annual International Symposium on Smart Structures and Material, Health Monitoring and Management of Civil Infrastructure Systems; Newport Beach CA, Vol. 4337, 2001, pp. 122-128.
11. R. Schaer, H. Boni, P. Fabo, P and A. Jarosevic, "Method of and Device for Determining a Time-Dependent Gradient of a Shock Wave in a Ferromagnetic Element Subjected to a Percussion Load", United State Patent, Patent No.: US 6,356,077 B1, 2002.
12. V. Singh, G. D. Lloyd and M., L. Wang, "Effects of Temperature and Corrosion Thickness and Composition on Magnetic Measurement of Structural Steel Wires", the 6th ASME-JSME of 2003.
13. M. L. Wang, Z. Chen, S. S. Koontz and G. D. Lloyd, "Magneto-elastic permeability measurement for stress monitoring", In Proceeding of the SPIE 7th Annual Symposium on Smart Structures and Materials, Health Monitoring of the Highway Transportation Infrastructure, 6-9 March, CA, Vol. 3995, 2000, pp. 492-500.
14. Z. Chen, Characterization and Constitutive Modeling of Ferromagnetic Materials for Measurement of Stress, PhD thesis, the Univ. of Ill. At Chicago, 2000.

ENHANCING DURABILITY OF STRUCTURES BY MONITORING STRAIN AND CRACKING BEHAVIOR

Bernd Hillemeier, Horst Scheel, and Wolfgang Habel
Technische Universität Berlin, Berlin, Germany

Abstract: Powerful testing methods are available for the diagnostics of engineered structures. Promising methods in the laboratories should be developed for application in practice. Responsible owners are capable of maintaining durability in their structures at low cost by a better planning during use.

Key words: Fiber optic sensing, safety, reliability, structural monitoring, self-compacting-concrete, non-destructive-testing (NDT), detection of steel fractures, prestressed concrete, swelling, shrinkage

1. INTRODUCTION

One cubic meter of concrete per person is built annually into civil engineering structures in developed countries. Concrete, this most famous construction material of the present century is getting reinforced by a considerable mass of reinforcing steel.

Both concrete and steel are the dominant materials that control safety, serviceability, durability and economy of our built infrastructure.

Both materials suffer from degradation by stress, induced deformation and chemical attack.

Sound materials show high resistance and excellent performance over a long period of time. The Romans built the town wall of Cologne with concrete that is now 2000 years old. More than 1600 years old is the Iron Pillar in the Quwwat-al-Islam-Mosque in Delhi, unprotected, uncoated under the monsoon weather conditions.

Farhad Ansari (ed.), Sensing Issues in Civil Structural Health Monitoring, 155–164.

Many of our recent existing structures show poor quality and behaviour. Why? The main two reasons are uncontrolled influence of water and visible and non-visible crack-formation in the mentioned construction materials. Both negative influences can be avoided by quality assurance measures supported by non-destructive testing methods and monitoring the deformation behaviour during hardening of the concrete and during use.

2. SELF-COMPACTING-CONCRETE (SCC) AND FALLING-BALL-RHEOMETER

The development of self-compacting concrete (SCC) has changed fresh concrete from needing vibration for compaction into a fluid. The market for SCC is growing rapidly. SCC offers many advantages in comparison with conventional concrete: It is a silent concrete: the noise is significantly reduced, it is a healthy concrete: the white fingers syndrome is avoided, it is a tolerant concrete: bad workmanship is considerably reduced. Vibration is not necessary anymore, concrete is opening for new design options.

SCC requires a careful control of its flow behavior. Therefore the quality-parameter “self compaction” should be monitored continuously. SCC behaves as a non-Newtonian fluid. Rheological measurements are essential to determine the flow behavior dependent on the shear rate and to keep the mixture in compliance with self-compacting properties.

In order to continuously verify the capability of self-compaction during a time consuming placing of SCC, we have developed a rheometer appropriate for steady control [1]. The principle of the measurement is comparable to the well-known falling-ball viscometer. Different from the viscometer the new method evaluates data from an accelerating sphere. The velocity function of the accelerating sphere gives the information to determine the flow curve. The advantages of the new so-called falling-ball-rheometer are the short measuring time, the easy handling and the objective documentation with a continuously actualized graph of the flow curve. The most important result is that the robust test method is applicable to determine rheological properties of a self-compacting concrete on site.

The concept of a falling-ball-rheometer is based on a modified Stokes law in which a sphere sinks under constant velocity. Herein, the viscosity of the Newtonian fluid is an absolute material property. For non-Newtonian fluids, the relative viscosity according to the measured sink velocity is used.

To allow characterization of non-Newtonian fluids, viscosity as a function of the sink-/shear-rate must be known. Utilizing the time-distance relationship of the accelerating sphere, a numerical method is applied after each measurement to compute the relative viscosity for various shear rates. From this the flow curve can be plotted.

DETERMINATION OF A FLOW CURVE

While descending through the SCC specimen, the steel ball is continuously monitored e.g. by means of electromagnetic induction. Data acquisition by a local computer is performed with a sampling rate of 1 kHz. The measuring instrument is situated below the measuring pot, as depicted in Figure 1. For measuring self-compacting mortars and concrete mixes, a sphere of 9 cm diameter was used.

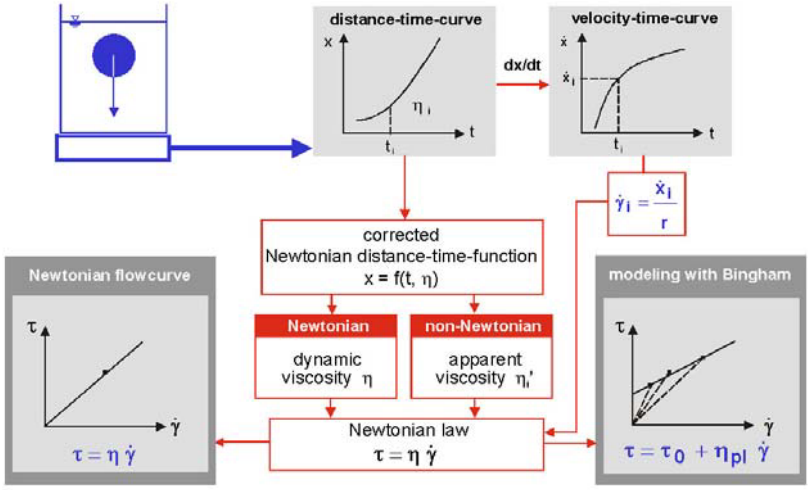

Figure 1: Method for evaluating the flow-curve of SCC from a Falling-Ball-Rheometer.

Within the measurement range of the falling-ball-rheometer, flow curves of mortars and concretes may be approximated by the Bingham model, which is applicable for cement-based media. Results are relative values of plastic viscosity and yield stress. They are thus referred to as relative viscosity and effective yield stress. The range of shear rate of the falling-ball-rheometer lies between 5 and 10 s^{-1}.

Good compaction of concrete is the precondition for durability.

3. SELF-COMPACTING-CONCRETE AND FABRY-PÉROT-SENSOR

SCC is characterized by a high powder content of about 600 kg/m^3 and a fairly high strength of 70-90 MPa. Fresh SCC is less robust than normal fresh concretes. It is more sensitive in regard to shrinkage. Shrinkage cracks are most unwelcome in durable concrete structures.

The risk of micro shrinkage cracks is focused on the first hours of a concrete during its transition phase from a fluid to a solid. Swelling, chemical shrinkage, poor compaction and insufficient curing can be the reasons for micro- and macro-cracks in concrete.

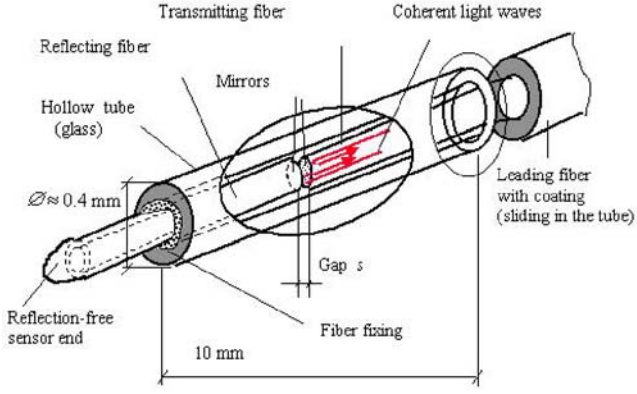

Figure 2: Fiber Fabry-Pérot interferometer sensor EFPI (principle structure).

Deformation measurements of fiber optic microstrain sensors (EFPI) in cement pastes with low w/c-ratios at early age deformations of cement pastes with a w/c ratio 0.3 were measured by EFPI sensors. The function of EFPI sensors has been described in detail by the authors in previous publications [2,3]. The tubular sensor element (length approximately 10 mm, outer diameter 0.5 mm), Figure 2, is connected with the leading optical fiber (diameter =1mm). This leading fiber links the sensor element to the measuring instrument. Inside the glass tube two smoothly broken fiber ends are positioned face to face, the distance between them varies between a few micrometer and 120 µm at maximum depending on the strain stage of the surrounding material. When a change in strain occurs, an axial displacement

of the fiber end-faces produces intensity variations due to interference of light. These signals are recorded.

In order to minimize the necessary force to shift the fiber in the tube, the connecting fiber is able to slide inside the tube. This flexible form of the classic EFPI sensor makes sure that these sensors work almost without reactions to the surrounding material. The optically active space inside the tube is protected against water ingress. The measuring range of the sensor is about -2000 με to +2500 με, the strain resolution in combination with the recording device is in the order of 10^{-7} to 10^{-8}.

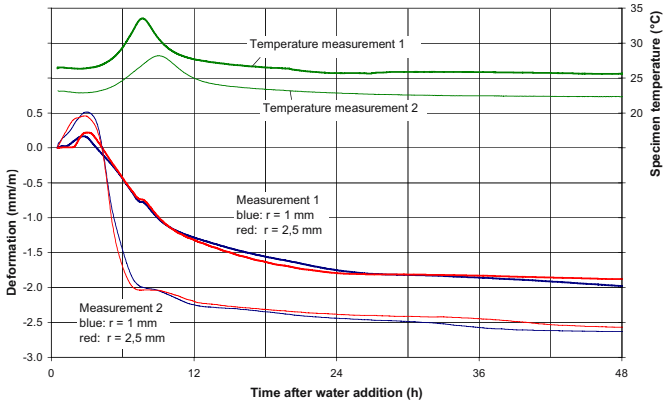

Figure 3: Fiber Fabry-Pérot interferometer sensor measuring the expansion in the very early hours of the setting of the lime.

Despite curing with a sealant coating, expansion of the fresh cement pastes was measured in the first 3 hours. When the specimen temperature started to increase, caused by the hydration-heat, the cement pastes showed shrinkage due to self-desiccation. These observations shortly after leaving the liquid phase of the lime are astonishing and obviously dependent on the cement-type, Figure 3.

To be sure that the measured phenomena are correct, EFPI sensors have been embedded in wax and their deformations during cyclic heating of the wax has been measured. The good reproducibility of the fibre-sensors could be demonstrated. The lime-phenomena quicken the interest for a thorough investigation.

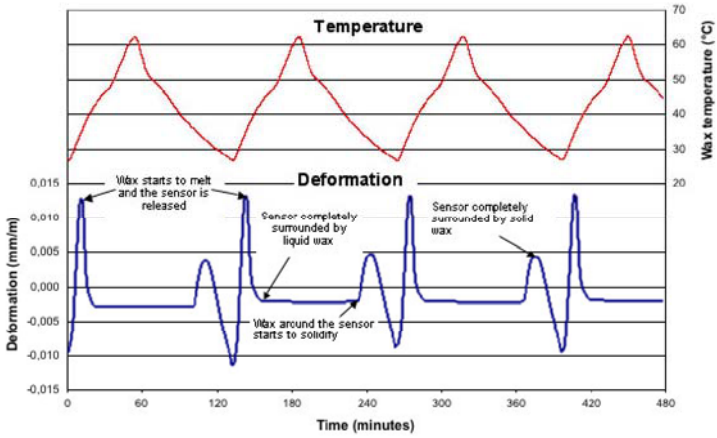

Figure 4: Deformation of the fiber optic microstrain sensor (EFPI) during cyclic heating of wax showing the good reproducibility of the sensor.

4. DETECTION OF CRACKS ORTHOGONAL TO THE CONCRETE SURFACE

Direct tensile stress often leads to cracks orthogonally oriented to the longitudinal extent of reinforced concrete elements and thus orthogonally oriented to the concrete surface. The detection of orthogonal cracks is much more difficult than the detection of parallel to the surface oriented delaminations. Orthogonally orientated defects are nevertheless detectable with ultrasound using the transmitting intensity. A crack between ultrasound-transmitter and receiver, as shown in figure 5 schematically, inhibits the nomally transmitted intensity to pass entirely to the receiver.

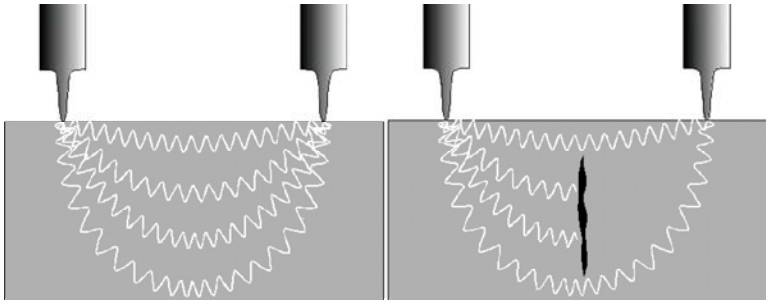

Figure 5: The transmission of ultrasound without (left) and with (right) defect between transmitter and receiver (schematically).

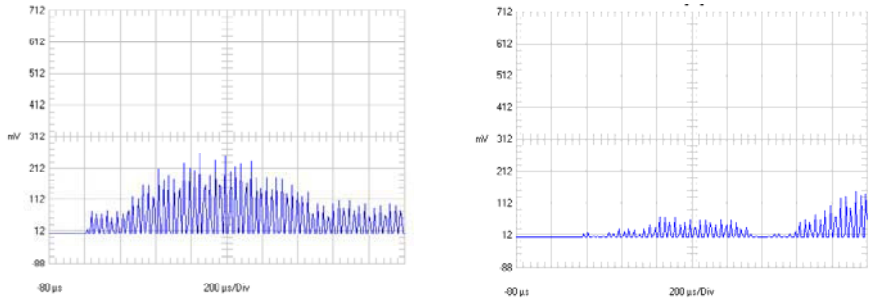

Figure 6: Representation of the transmitted intensity on an oscilloscope. Left: Sound concrete, right: concrete with a crack orthogonally to the surface.

This method has meanwhile been automized for the monitoring unit for continuous inspection of the Emscher sewage water collector in the Ruhr region in Germany, between Dortmund und Dinslaken. This sewage pipe is 58 km long and varies in diameter from 1500 mm to 3400 mm.
For high speed detection of cracks the infrared technique is applied: a powerful light generates a temperature difference between the wet concrete and a water bearing crack. The equipment is placed on a high-tech-boat which is drawn through the collector, subdivided into 600 m long sections of the sewage pipe [4], Figure 7.

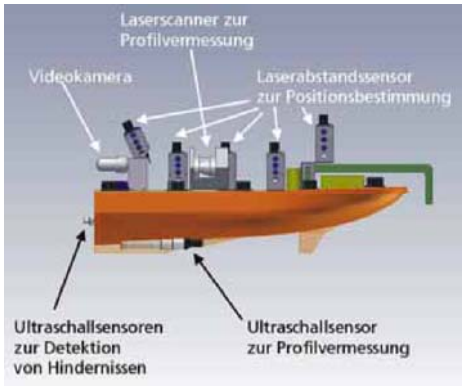

Figure 7: The swimming inspection system with video-camera, laser-scanner for profile verification, laser positioning system and ultrasound for profile verification and detection of obstacles. Photo: Emschergenossenschaft and Fraunhofer-Institut[4].

Great efforts have been attained to monitor the soundness of concrete structures. What about the reinforcing steel?

5. LOCATION OF FRACTURES IN PRESTRESSED STEEL WIRES

Some types of heat-treated prestressing steel are so sensitive to stress-induced corrosion that fractures have been found even if the wires were embedded in alkaline mortar inside a completely grouted, intact duct. Failure of prestressed concrete members often happens abruptly.

SoundPrint – an acoustic monitoring system

The failure of a prestressed steel wire is characterized by the sudden release of energy at the moment of fracture. This energy is dissipated through the structure in the form of sound waves, which can be detected by acoustic sensors. The different arrival times of the sound waves at several sensors allow the calculation of the location of the fracture. The system requires a permanent data acquisition with a sufficiently high sampling rate[5]. The technology cannot provide information on failures which occurred before its implementation. This information can be delivered by the Remanent-Magnetism-Method, Figure 8.

Figure 8: The SoundPrint System (left), the white boxes under the ceiling are covering the acoustic sensors. Application of RM-Method on a bridge deck (right).

The Remanent-Magnetism-Method (RM-Method)

The Remanent-Magnetism-Method (RM-Method)[6,7] allows for the identification of potentially unsafe conditions in pre-tensioned and post-tensioned concrete structures by locating fractures of single wires, even if they are bundled with intact wires. The tendons are magnetized with an electromagnet. The magnetic field of the tendons is measured from outside

the prestressed concrete member. Steel-fractures produce characteristic leakage fields, Figure 9, which can be measured with appropriate sensors from the concrete surface.

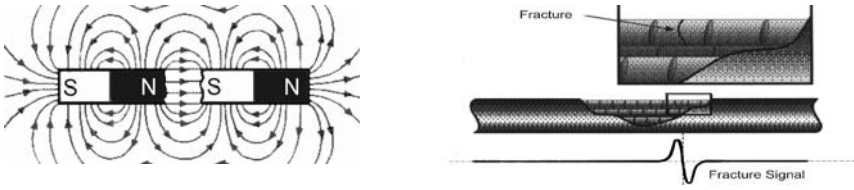

Figure 9: A magnetized prestressing steel wire has a magnetic field comparable with the field of a bar magnet, (left). The transverse component of the leakage field is shown on the right.

The measuring speed of the RM-Method can be enhanced significantly by replacing the time-consuming multi step magnetization [6,7] by a single-step-magnetization. Large yoke-shaped magnets have been constructed to magnetize complete transverse tendons in bridge decks in a single process, Figure 10. Measuring the magnetic flux density of an entire bridge deck simplifies the comparison of data from measurements at different times, which would be helpful for monitoring the long time behavior of the structure.

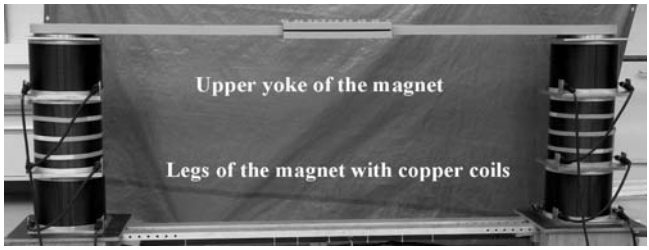

Figure 10: The electromagnetic yoke, for 3.5 m long strand-sections, 1.5 t, 16 kW .

The reproducibility of the magnetic measurement e.g. for bridge and park-decks allows the monitoring of the time dependent behavior of the structures. By subtraction of the measured values at different times, the deterioration process can be evaluated, because corrosion influences the magnetic field of the ferromagnetic reinforcement. Also damages by heavy impacts like earthquakes can be detected.

Powerful testing methods are available for the diagnostics of engineering structures. Promising methods in the laboratories should be developed for

application in practice. Responsible owners are capable of maintaining durability of their structures at low cost by a better planning during use.

6. REFERENCES

1. Buchenau, G. and Hillemeier, B., Quality –Test to prove the flow behaviour of SCC on site, Proceedings of the 3rd International RILEM Symposium, 2003, Reykjavik, Iceland, pp. 84-93
2. Habel, W., Hofmann, D., and Hillemeier, B., Deformation measurements of mortars at early ages and of large concrete components on site by means of embedded fibre optic microstrain sensors. J. of Cement and Concrete Composites (Special issue: Fiber Optic Sensors in Concrete), 19(1997)1, 81-101.
3. Habel, W., Hofmann, D., Buchenau, G. (TU Berlin), and Hillemeier, B. (TU Berlin), High-performance concrete - lime optimization with fiber-optic sensors. In: Proceedings 14th Engineerings Mechanics Conf. May 21-23, Austin, Texas/USA (2000) 4 S., CD-ROM.
4. http://www.emschergenossenschaft.de
5. Halsall, A.P., Welch, W.E., and Trépanier, S.M., (1996), Acoustic Monitoring Technology for Post-tensioned Structures, Symposium Papers ofthe FIP Symposium 1996 on Post-Tensioned Concrete Structures, p. 521-527.
6. Scheel, H. and Hillemeier B., Capacity of the remanent magnetism method to detect fractures of steel in tendons embedded in prestressed concrete, *NDT&E International*, Vol. 30, No. 4, pp. 211-216, Elsevier Science Ltd., 1997
7. Scheel, H. and Hillemeier, B., Location of Prestressing Steel Fractures in Concrete, Journal of Materials in Civil Engineering, Vol. 15, No. 3, pp. 228-234

DEVELOPMENT OF AN EARTHQUAKE DAMAGE DETECTION SYSTEM FOR BRIDGE STRUCTURES

Hiroshi Kobayashi and Shigeki Unjoh
Public Works Research Institute, Japan

Abstract: After a large scale earthquake, evaluation of damage of highway structures such as bridge structures has great importance to assure the emergency route for rescue and transport of urgent supplies. Currently, the damage evaluation is basically conducted by means of visual inspection by bridge experts, but generally it takes so long time to collect whole damage information in the affected area. Therefore, the authors are developing a new damage evaluation system using advanced sensors, which can detect the damage level of structures more correctly and quickly just after the earthquake. This paper presents the proposed "Seismic Damage Evaluation System for Bridge Structures" and the effectiveness of proposed damage evaluation method is demonstrated through a series of shaking table tests. Also, the integration of proposed system to the SATURN system, which is practically used in Japan as a seismic damage information system, is discussed.

Key words: Damage evaluation, Bridge structures, RC columns, Shaking table test, Natural period, Ductility factor, Intelligent sensor, SATURN system.

1. INTRODUCTION

The importance of the quick disaster response including emergency rescue and recovery immediately after an earthquake was recognized anew in the 1995 Great Kobe Earthquake. Especially, the evaluation of damage of highway networks such as bridge structures has great importance because they play key roles in the disaster rescue operations and transports of emergency materials. Currently, the damage evaluation of highway bridges,

Farhad Ansari (ed.), Sensing Issues in Civil Structural Health Monitoring, 165–174.

which are one of the important highway structures, is made based on visual inspection by bridge experts. If a large scale earthquake occurs and several damages are caused, it takes so long time to gather the reliable damage information of all bridge structures in the affected area. And generally it is difficult to evaluate the damage quantitatively by the visual inspection. Since the visual inspection is based on human observation, it is not effective to inspect the damage during night time and to inspect the damage of the structural parts under the ground or water.

Therefore, more detailed and systematic damage inspection system, which can evaluate the structural damage correctly and rapidly without any seasoned professional engineers, is required. The authors are developing the advanced sensors which can detect the damage of structures using new materials such as fibers and TRIP steel, and new damage evaluation method using data set from the sensors.

Figure 1 shows the illustration of the "Seismic Damage Evaluation System for Bridge Structures."

This paper proposes the damage evaluation method of bridge structures based on the natural period change. The relation between the ductility factor and elongation of the natural period is simply obtained and the effectiveness was demonstrated through the shaking table tests for a reinforced concrete column. And the Seismic Assessment Tool for Urgent Response and Notification (SATURN) system, which has been currently used at practical stage, is introduced and the integration plan of the Seismic Damage Evaluation System for Bridge Structures to the SATURN system is introduced.

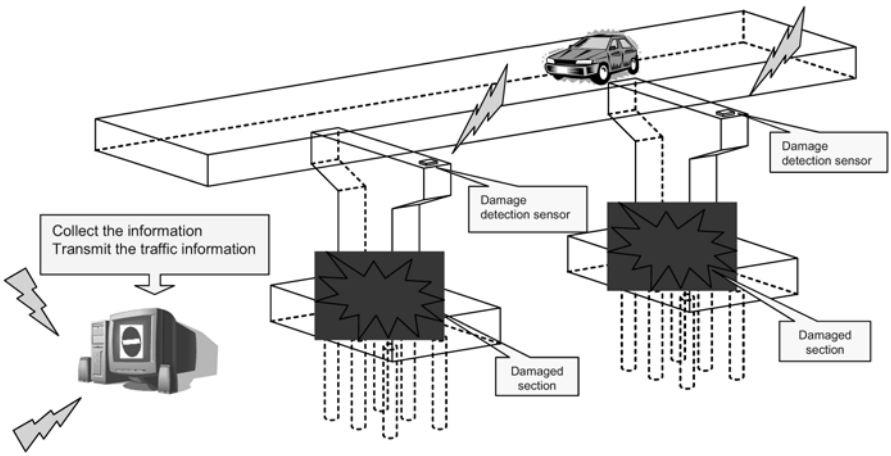

Figure 1. Seismic Damage Evaluation System for Bridge Structures

2. DAMAGE EVALUATION METHOD USING ACCELERATION RECORD

2.1 Damage sensing of reinforced concrete columns

To measure the displacement or strain properly, the sensors have to be placed at the most possible damage sections such as the bottom of columns. But the bottom of bridge columns is generally under the ground or water. It is generally hard to put the sensors at the appropriate sections. The authors are proposing a damage evaluation method using acceleration sensors which can be easily put on the existing bridges columns.

Assuming that the bridge system is supported by a reinforced concrete (RC) column as a single degree of freedom system, and assuming that the column has an elasto-plastic force-displacement relation, the natural period of the system is calculated by the Eqs. (1) and (2) as below.

$$T = 2\pi\sqrt{\frac{m}{K}} \tag{1}$$

$$T_0 = 2\pi\sqrt{\frac{m}{K_0}} \tag{2}$$

Where,

T_0: Natural period of elastic system without damage

T: Natural period of system after earthquake with certain damage

m: Mass

K_0: Elastic stiffness of system without damage

K: Equivalent Stiffness of system with some damage

The relationship between the change of natural period and ductility factor is simply obtained as follows:

$$T/T_0 = \sqrt{\frac{K_0}{K}} \tag{3}$$

$$K_0 = P_y/\delta_y \ , \ K = P_y/\delta \tag{4}$$

$$T/T_0 = \sqrt{\frac{\delta}{\delta_y}} = \sqrt{\mu} \tag{5}$$

Where,

P_y: Yield strength

δ_y: Yield displacement

δ: Maximum displacement response by earthquake

μ: Ductility factor

In the above equation, the equivalent stiffness after earthquake is assumed to be obtained by maximum displacement response and this assumption is generally acceptable for RC structures.

As shown in Eqs. (6), the change of natural period from the initial period without damage is equal to the square root of ductility factor. This means that the damage (ductility ratio) of columns can be evaluated by the data set from the acceleration sensors on the top of the columns.

2.2 Shaking table test

2.2.1 Test specimen and testing conditions

To verify the proposed damage evaluation method, the shaking table tests were carried out at PWRI. Figure 2 shows the RC column specimen with rectangular section of 45cm x 80cm. The geometric scale is assumed as about 1/4 of the real one. The reinforcement ratio is designed based on the typical highway bridge columns in the urban area of Japan. Steel weight was fixed at the top of the RC column as an auxiliary mass to apply the axial force and horizontal inertia force. Computed yield displacement and ultimate displacement at the centroid point of the weight were 18.9mm and 62.3mm, respectively.

The shaking table was excited in the direction of column weak axis and the north-south component of the records observed at JR Takatori Station in 1995 Kobe earthquake was used as an input earthquake ground motion to the shaking table. Since the geometric scale of the column model is about 1/4 of real one, so the time axis of the input acceleration was compressed to 50%. The amplitude of the input ground motion was increased stepwise from 15% to 80%.

Three axis accelerometers were put on the shake table, the footing of the column specimen and the centroid of the weight at the top of the column. The displacement response was also measured by contactless laser displacement sensor. Strain gauges were put on the re-bars around the bottom of column. Photo 1 shows the test set up.

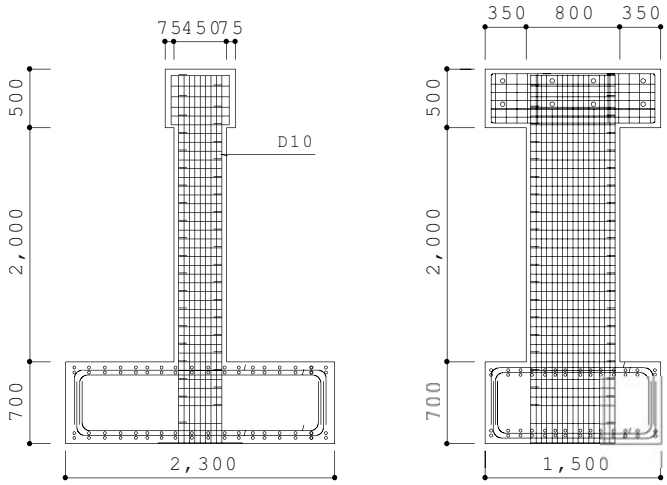

Figure 2. RC column specimen for shaking table test

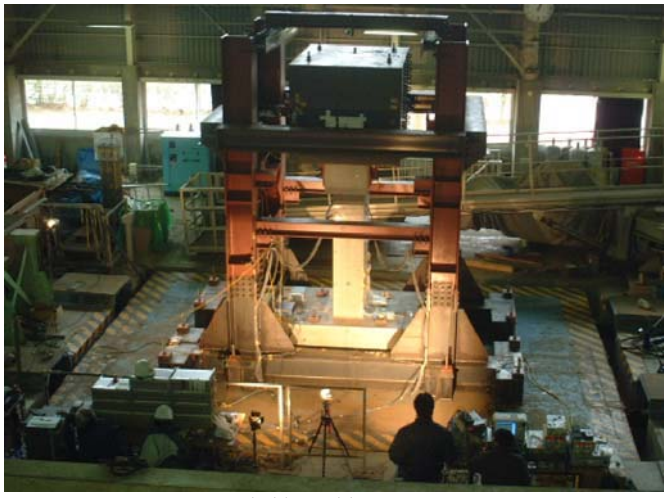

Photo 1. Shaking table test setup

2.2.2 Test results

Figure 3 shows the time history data when the column was subjected to the 50% amplitude of JR Takatori record. Time histories of acceleration of the shaking table, response acceleration at the centroid of the weight and response strain of re-bar at the bottom of the column were shown in the

figure. The figure shows that the response exceeding the yield point of the column was developed after around 10 seconds of the input motion.

Table 1 summarizes the tested data including the natural period, maximum accelerations, maximum displacement and ductility factors of each shaking step. Natural periods were computed using the Fourier transform of the acceleration data set of 10 seconds after the response became stable. According to the obtained results, the response was in the range of the elastic limit when 15% amplitude of JR Takatori record was input to the shake table. The natural period was increased significantly when 50% amplitude of JR Takatori record was applied.

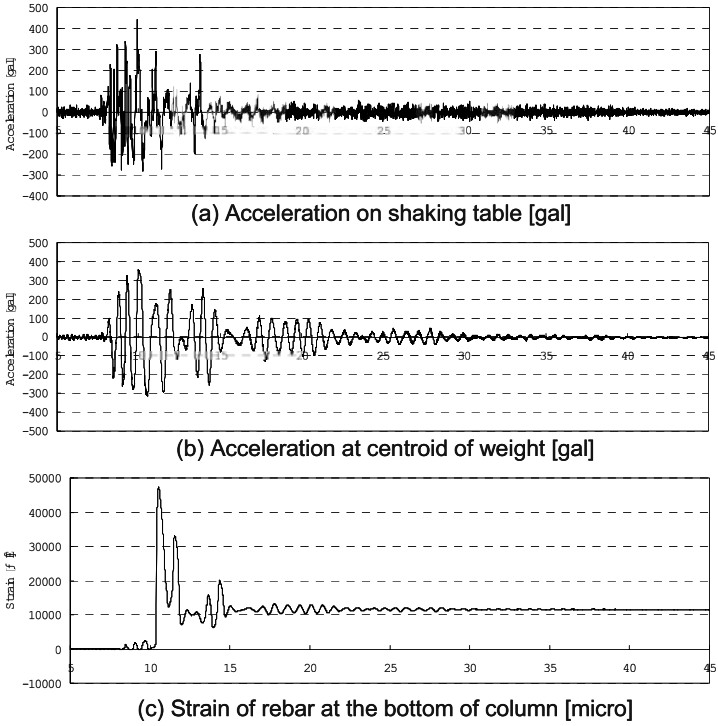

Figure 3. Time history of accelerations and strain (50% amplitude of Takatori record)

As shown in Figure 3, maximum strain of re-bar at the bottom of column exceeded far beyond the yield point and maximum displacement of the weight also reached to the computed ultimate displacement. After the shaking, the cracks were recognized at the bottom of column by visual observation but no peeling off of the cover concrete was found. Afterward, 60% amplitude and 80% amplitude of the JR Takatori record were applied for input excitation but no significant damage progress was found. The cover concrete was peeled-off when the second excitation of 80% amplitude of JR Tkakatori record was input.

Table 1. Results of the shaking table test

Stages of the test	Natural period (s)	Maximum acceleration on shaking table (gal)	Maximum acceleration on centroid of weight (gal)	Maximum strain of rebar at the bottom of column (micro)	Maximum displacement of weight (mm)	Yield displacement (mm)	Ductility factor calculated from displacement	Ductility factor calculated from natural period
Background shaking befor the test	0.29							
15% of Takatori record	0.34	111	213	894	6	18.9	0.33	1.36
50% of Takatori record	0.64	443	356	47,481	63	18.9	3.32	4.79
60% of Takatori record	0.68	481	339	40,339	96	18.9	5.07	5.44
80% of Takatori record (1)	0.79	722	352	47,490	136	18.9	7.2	7.25
80% of Takatori record (2)	0.93	707	346	46,643	148	18.9	7.84	10.12
80% of Takatori record (3)	0.93	693	308	20,912	137	18.9	7.27	10.12

2.2.3 Evaluation of damage based on natural period change

Figure 4 shows the Wavelet transforms of the acceleration response recorded at the centroid of weight at the top of the column. They show the change of the natural period of the column during the shaking. Figure 4(a) shows the case when 15% amplitude of JR Takatori record was input and no damage was found.

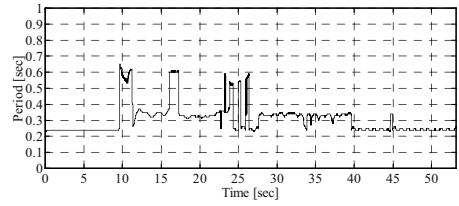

(a) Input: 15% of JR Takatori record

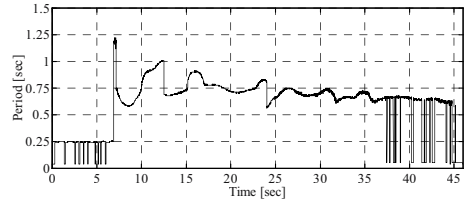

(b) Input: 50% of JR Takatori record

Figure 4. Shift of natural period

Figure 4(b) shows the case when 50% amplitude record was input and the nonlinear response exceeding yield displacement was developed. From Figure 4(b), it is found that the natural period was significantly elongated due to the damage occurrence in the column.

2.2.4 Evaluation of damage using ductility factor

Figure 5 shows the comarison between the ductility factors computed from the natural period by Eqs. (6) and calculated from the observed response displacement. The natural period, yield dispalecment and displacement response are summrized in Tabel 1. As shown in Figure 5, the good agreement was found between them. Therefore, it is possible to easily evaluate the maximum ductility response based on the natural period change usind the accerelation data observed at te top of column. Then the damage degree can be evaluated from te ductility response.

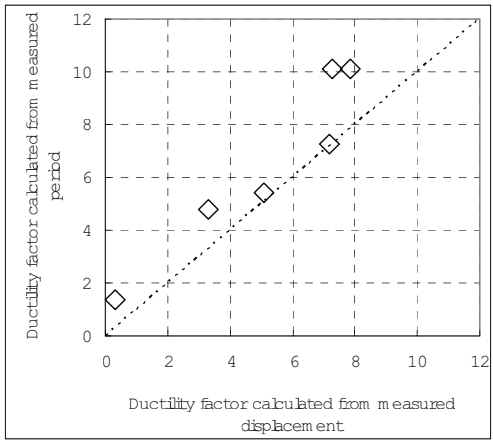

Figure 5. Comparison of ductility factor estimated by natural period change and observed displacement

2.3 Development of intelligent sensor

In the above, the damage evaluation method using the natural period change was proposed, and the effectiveness was demonstrated through the shaking table test of an RC column. Based on these results, the authors are developing the following advanced intelligent sensor system which can be easily put on the existing bridges columns.

1. MEMS (Micro Electro Mechanical System) sensor to be applied as an accelerometer. MEMS sensor is mass-produced at low cost recently.
2. The computer program in order to evaluate the damage and estimate the functionality of the bridge structures are being developed and installed in the microcomputer system.
3. Information transmission function is being installed using wireless LAN or ditto technology for notifying the evaluation results and accumulation of evaluation data.
4. Semi permanent power source system which consists of electric generating unit and storage unit is to be installed. The most promising system is the use of solar, wind and vibration generator units and double layer capacitor storage units.

Applying these developed systems, the evaluation of the damage and the judgment of functionality of the bridge structures can be made more reliably and quickly.

3. SATURN SYSTEM

3.1 Outline of SATURN

SATURN (Seismic Assessment Tool for Urgent Response and Notification) is a tool which gives urgent information to the sectors who are in charge of managing public infrastructures and supports their decision making immediately after an earthquake. This system provides rough estimation of damage on public infrastructures in the early stage when the sectors have insufficient information. This system is already being used in some regional development bureaus of MLIT (Ministry of Land, Infrastructure and Transportation).

MLIT has the seismograph network system to get earthquake ground motion characteristics such as maximum acceleration, spectrum intensity value and JMA (Japan Meteorological Agency) seismic intensity immediately after an earthquake. From the data collected in the network, SATURN provides ground motion distribution monitored at some 100 sites of each regional development bureau in a short time. SATURN also provides rough estimation of liquefaction risk and damage on river embankments as well as highway bridges in about 15 minutes. System functions of SATURN are display of the earthquake information and simulation of contingent earthquake.

Immediately after an earthquake, SATURN will display the information from seismograph and the estimated damage of public infrastructures on the screen. It also displays detailed damages and geological information and manages the damage investigation data.

3.2 Integration of intelligent sensor system into the SATURN system

Current SATURN system estimates damage of bridges empirically based on calculated ground vibration intensity levels, soil conditions and structural conditions. Accordingly the accuracy of the estimation results can be significantly improved while the information is obtained from the intelligent sensors.

4. CONCLUSIONS

- New damage evaluation method for bridge structures based on natural period change is proposed. The effectiveness of the method was demonstrated by shaking table test. It is shown that the response ductility factor can be estimated from the natural period change with reasonable accuracy.
- The concept of the new advanced intelligent sensor which contains of a sensor, a microcomputer, a self-generator and a wireless LAN or similar system was introduced.
- The new damage evaluation system using advanced intelligent sensors will be integrated to the SATURN system and it will be able to give urgent information more properly and promptly with the purpose of the time after an earthquake.

REFERENCES

1. Adachi Y, and Unjoh S. "Development of Shape Memory Alloy Damper for Intelligent Bridge Systems", *Proc. of the 6th smart structures and materials*, Newport beach, CA, March 1999
2. Adachi Y, Unjoh S. "Seismic damage sensing of bridge structures with TRIP reinforcement steel bars", *Proc. of the 7th smart structures and materials*, Newport beach, CA, March 2000
3. Kusakabe T, Sugita H, Ohtani Y,Kaneko M, Hamada T. "SATURN –Seismic Assessment Tool for Urgent Response and Notification", Technical note of NILIM No.71, Jan 2003 (In Japanese)

DETERMINATION OF REBAR FORCES BASED ON THE EXTERIOR CRACK OPENING DISPLACEMENT MEASUREMENT OF REINFORCED CONCRETE

Takashi Matsumoto and Mohammad Nazmul Islam
The University of Tokyo, Japan

Abstract: This paper presents the determination of rebar forces based on the exterior crack opening displacement measurement of a reinforced concrete beam. The problem formulation of the forward and inverse analysis of reinforced concrete fracture is briefly mentioned. The forward problem is to solve for the crack opening displacement profile with externally applied load and rebar forces given, while the inverse problem is to solve for rebar forces with the crack opening displacement measured and the externally applied load given. The inverse problem is ill posed; therefore it is regularized with Tikhonov regularization method. Numerical solution of the inverse estimated rebar forces is compared with experimental measurement. A four point flexural loading experiment of a reinforced concrete beam is conducted, and, with the usage of a digital microscope, the crack opening displacement profile is captured. The measured profile is input into the inverse analysis scheme, leading to the rebar forces as output. The comparison of the estimated rebar forces with the gauge measurements shows a reasonable agreement, and also the location of rebars is identified correctly. Finally, the error and the influencing factors are discussed.

.Key words: Inverse analysis, rebar force, crack opening displacement, reinforced concrete

1. INTRODUCTION

Infrastructure aging problem is becoming an important issue in a country that experienced a mass construction period in the past. In order to manage

Farhad Ansari (ed.), Sensing Issues in Civil Structural Health Monitoring, 175–183.

the coming mass maintenance period, it is necessary to have an efficient testing method, which is a key to the efficient maintenance management of structures and infrastructures.

In the case of reinforced concrete structures, it is crucial to have enough cross sectional area of steel rebars, especially under corrosive conditions. In order to check the rebar conditions, destructive testing methods, such as cover concrete removal, can be employed to directly observe the rebar cross sectional area, or non destructive testing methods, such as electrochemical methods, can be carried out to measure the corrosion susceptibility of rebars, thereby indirectly evaluating their cross sectional area.

This paper studies the estimation of rebar forces in a reinforced concrete beam based on exterior crack opening displacement measurement (COD). The relation between crack opening displacement and bridging stress transmitted across a crack is modeled based on fracture mechanics, and this problem is solved inversely to obtain the transmitted bridging stress distribution on the crack surface from the measured crack opening displacement profile.

Below, the problem formulation of the forward and inverse problem is described briefly. The loading experiment of a simple reinforced concrete beam under flexure is conducted for the purpose of comparison. The COD on the exterior surface under loading is measured with a digital microscope, and, based on the measured COD, the inverse analysis of bridging stress distribution is conducted. The estimated bridging stress distribution indicates the transmitted force and location of rebars, therefore the rebar forces are compared with the measurements of gauges attached on the rebars.

It is shown that the rebars' force and location can be obtained with the inverse analysis, and that the estimated force agrees reasonably well with the experimental measurement. This shows that the current method can be used as a non destructive testing method in order to evaluate the interior rebar forces based on the exterior crack opening displacement.

2. PROBLEM FORMULATION OF FORWARD AND INVERSE ANALYSIS

A reinforced concrete beam under flexure is modeled in the following manner. It is assumed that concrete and steel are a linear elastic material and that, under loading action, a single crack initiates and develops in the center on the tension face. This crack is assumed as a Mode I crack, where only normal bridging stresses are transmitted across the crack.

Bridging stresses are exerted by concrete aggregates and steel rebars. In the current study, the aggregate bridging is ignored, and only the bridging

exerted by rebars is taken into account, since the effect of aggregate bridging is negligible compared to the crack tip shielding effect of rebars. The current model is schematically shown in Figure 1.

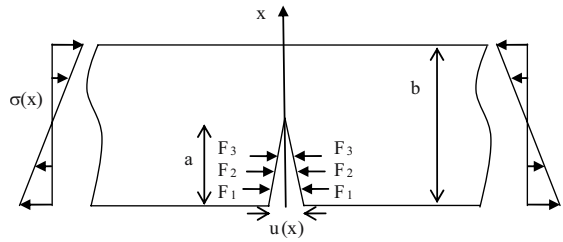

Figure 1. Reinforced concrete beam under flexure. Rebars are bridging the crack with forces F_i.

Crack opening displacement of a reinforced concrete beam, u', can be related to the bridging stress and the externally applied load through the following equation:

$$u'(x) = \frac{4}{E'}\int_{x}^{a}\int_{0}^{a'} G(x',a',b)\left[\sigma(x') - f(x')\right]dx' G(x,a',b)da' \tag{1}$$

where $E' = E_c$ for plane stress and $E' = E_c/(1-\nu^2)$ for plane strain respectively, E_c the Young's modulus of concrete, and ν the Poisson's ratio. $\sigma(x)$ is the stress from external flexural loading that would exist in the crack line if there was no crack (shown linear in Figure 1 at the edges), and G(x, a, b) is the weight function to determine stress intensity factors, where a is the crack length and b the beam height. Weight functions of various configurations including the current configuration can be found in the stress intensity factor handbook [1], and the weight function of the current configuration can be found elsewhere [2, 3]. f(x) is the bridging stress distribution of rebars, and is expressed with the use of a Heaviside step function:

$$f(x) = \sum_{i=1}^{r} f_i\left[H(x-h_i) - H(x-h_i-d_b)\right] \tag{2}$$

where $f_i = (F_i/d_b)$ is the uniform rebar stress within its diameter along the crack length, F_i the total force in i-th layer, r the total number of reinforcement layers, h_i the distance of a layer from the bottom face, d_b the bar diameter.

With the externally applied load given and Fi obtained via section analysis, the forward problem of Eq. (1) can be numerically approximated and solved [3, 4].

The inverse problem is to determine the distribution of f(x) along the crack length from the measured u(x). It is not necessary to know the function form of Eq. (2), but to know the crack opening displacement profile, u(x), at a prescribed load level. Such an inverse problem is ill-posed, therefore Tikhonov regularization method is applied to solve the problem with experimentally measured COD data.

The net crack opening displacement, u', is the sum of opening due to externally applied loading, $\bar{u}$, and closing due to rebars, u.

$$u(x)=\frac{4}{E'}\int_x^a\left[\int_0^{a'}G(x',a',b)f(x')dx'\right]G(x,a',b)da'=\bar{u}(x)-u'(x) \quad (3)$$

We consider Eq. (3) as a linear operator equation

$$Tf=u, \text{ with } f\in Z \text{ and } u\in U \quad (4)$$

with

$$T:Z\to U. \quad (5)$$

F and U are infinite dimensional real Hilbert spaces with corresponding inner products and norms.

We are interested in the approximate solution giving the extremals of the following Tikhonov functional

$$M^{\alpha}[f]=\|T_h f-u_{\delta}\|_U^2+\alpha\|f\|_Z^2 \quad (6)$$

where T_h is the numerical approximation of the transform, T, and $\alpha > 0$ the regularization parameter. We have $u_{\delta}\in U$, the available noisy data up to noise level δ. After finite difference approximation, we reach at the following normal equation:

$$\mathbf{B}f+\alpha\mathbf{C}f=\mathbf{v}. \quad (7)$$

Detail theoretical assumptions and numerical method for solving the inverse problem are available in [4].

3. RC BEAM EXPERIMENT

An experiment was conducted to compare the inverse estimated rebar forces with experimental measurement and to show the validity of the inverse analysis described in the previous section.

A model reinforced concrete (RC) beam with 40 cm length, 10 cm height, and 10 cm thickness was tested under four point flexural loading (Figure 2). The specimen was reinforced with deformed reinforcing bars diameter, where 3.5 cm clear cover and 2 cm side cover were given. The compressive strength of concrete at 28 days was 30 MPa, and the yield strength of steel rebars was 345 MPa. Strain gauges were attached on the surface of steel rebars at the locations 3 cm away from the center line, where a 1 cm notch is introduced on the bottom face to introduce a crack. The specimen was painted white to get adequate contrast between cracked and non-cracked zones, so that the COD measurement on digital pictures was facilitated. .

A digital microscope that was mounted on an X-Y stage system was used to capture and record the crack on the specimen side surface. A 4 cm by 10 cm rectangular area, which included the notch in the middle, was divided into 189 points (21 rows with 9 points each), and each point was scanned to cover the whole length of a crack. The capture was carried out while the load was paused; several captures were successfully completed.

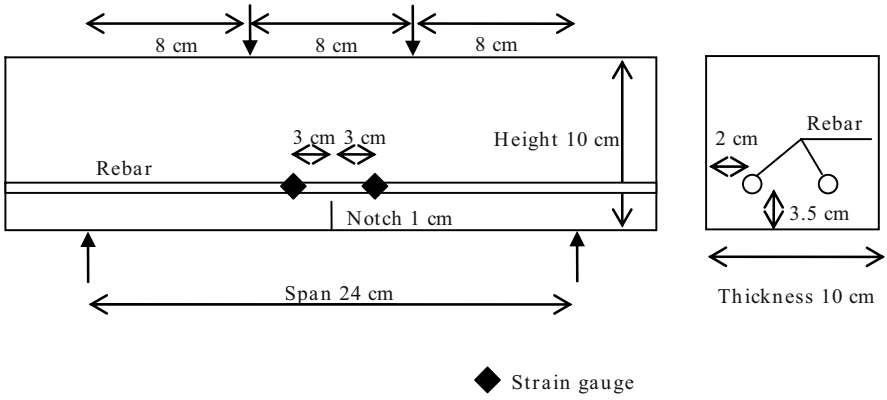

Figure 2. Specimen dimensions and strain gauge locations

Four point flexural loading was conducted under displacement control with a feed back controlled loading machine. Load and stroke displacement were recorded, and the strain development of the rebars was also recorded with strain gauges. When load was paused and kept constant at prescribed load levels, the microscope was employed to capture a continuous COD

profile on the RC beam surface. The rectangle area image was assembled with microscopic pictures at each scan point. An example crack image in the area is shown in Figure 3.

The crack image was expressed in terms of gray values in the current research. The color varied from white on the surface to black at the crack, and crack boundaries were gray. The determination of crack boundaries, which was necessary to measure the COD, was made in such a way that the boundaries were at the middle of the declining and ascending part of gray value variation. The COD was measured at a predetermined equal spacing along the crack from the crack mouth to the crack tip.

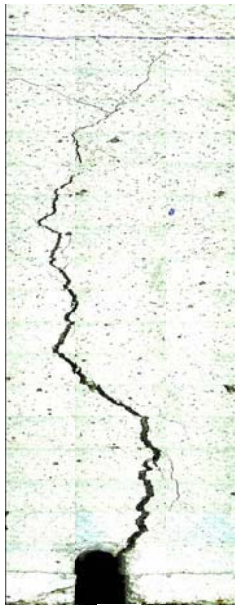

Figure 3. A combination of microscopic pictures. In this case, 60 pictures are combined in 20 rows (3 pictures in each row). Overlaps are adjusted.

Figure 4 shows the crack opening displacement of the RC specimen loaded at 25 kN. Although the measured COD profile is tortuous, it is observed that the COD is narrower around the probable rebar location, at the distance along the crack of 35 mm, and that the linear COD profile, which is the case of this flexural loading configuration, is captured. The short dashed and long dashed lines are the forward analytical and numerical analysis results respectively. The large difference is due to the problem simplifications such as neglecting the bond-slip behavior of rebars and simplifying a three dimensional RC beam to a two dimensional one. The former is taken into account, and the modified result is shown as a dotted

line. Although the dotted line is improved and close to the experimental line, there still remains some difference. This may be explained by the latter factor.

However, the transformation is an integral form, and it is sensitive to the gradient of COD profiles, not to the absolute COD values. Therefore, by assuming that the factors responsible for increasing the absolute COD values do not affect the gradient of COD profiles, the inverse analysis for the rebar force estimation is carried out in the next section.

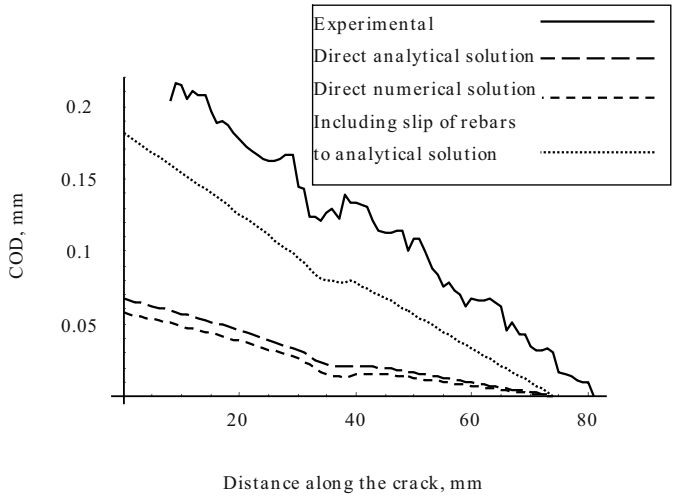

Figure 4. Comparison of experimentally measured COD profile and analytical COD profiles under total load = 25 kN.

4. INVERSE ANALYSIS OF REBAR FORCES

The inverse analysis is carried out with the experimentally measured COD as input, and the obtained result is presented in Figure 5 which shows the estimated bridging stress distribution along the crack. In reality, the bridging is exerted by rebars and should not be distributed. It is interpreted that the rebars are located around 35 mm where the peak bridging stress is observed. It is also seen that other minor peaks are obtained together. However, these are due to the errors of measurements and model simplifications, since the inverse analysis with the COD of the forward analysis as input yields only one peak around the location of rebars.

The rebar stress can be computed by integrating the area below the bridging stress distribution. The estimated rebar stress is 296 MPa for the specimen under the total load of 25 kN, and it can also be compared with the rebar stess by section analysis and fracture analysis. For this case they are 309 MPa and 328 MPa respectively. The inverse estimate is compared with the strain gauge measurement in terms of steel strain. The estimated strain is 1148 μ, and agrees well with the measured strain of 1113 μ. However, it should be noted that the error increases up to 31 % for other loading levels. The large variation of errors is due to the measurement error as well as the model simplifications. The latter includes neglecting factors such as the bond-slip behavior of rebars, the heterogeneity of concrete, and the three dimensional characteristics of a crack. With a more precise model, the inverse estimate could be improved and applied to a more complicated structure.

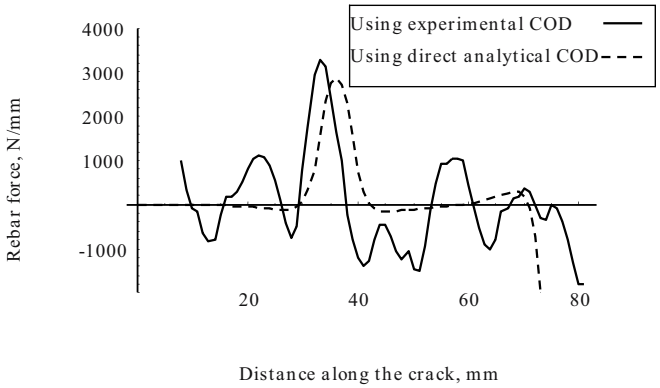

Figure 5. Inverse analysis estimate of crack bridging stress distribution using experimental COD and direct analytical COD.

5. CONCLUSIONS

This paper presented the problem formulation of the forward and inverse analysis of a reinforced concrete fracture, conducted an experiment for the comparison with the inverse estimate of rebar stress, and discussed the error and the influencing factors.

The forward problem of a reinforced concrete fracture was formulated, and it was to solve for the crack opening displacement with externally applied load and rebar forces given. On the other hand, the inverse problem was to solve for rebar forces with the crack opening displacement measured

and the externally applied load given. The inverse problem is ill posed due to the errors of experimentally measured crack opening displacement. Therefore, Tikhonov regularization was introduced to regularize the problem, and the problem was numerically solved.

A four point flexural loading experiment of a reinforced concrete beam was conducted for the purpose of comparison. With the usage of a digital microscope, the crack opening displacement profile was captured at the paused load levels. The measured profile was input into the inverse analysis scheme, leading to the distribution of the transmitted stress on the crack surface. The rebar force was compared with the gauge measurement in terms of strain.

The comparison showed a reasonable agreement; the error of rebar stress varied between 3 to 31 %. Also, the location of rebars was identified very well. The error was due to the simplified assumptions such as neglecting the bond-slip behavior of rebars, the heterogeneity of concrete, and the three dimensional effects of a crack. For further study, a more precise model should improve the inverse estimate and should be developed for a more complicated structure.

REFERENCES

1. Tada H, Paris PC, Irwin GR. *The stress analysis of cracks handbook,* St. Louis, Paris Productions Inc., 1985.
2. Cox BN and Marshall DB. “Stable and unstable solutions for bridged crack in various specimens”, *Acta Metallurgica et Materialia.,* vol. 39, no. 4, pp. 579-589, 1991.
3. Islam MN and Matsumoto T. “Determination of steel stresses in reinforced concrete structures from crack opening profile”, *Proc. of the First Int. Conf. on Structural Health Monitoring and Intelligent Infrastructure*, Tokyo, Japan, Nov. 13-15, 2003, pp. 739-746.
4. Islam MN, Matsumoto T. “Inverse Analysis to determine re-bars’ force from external crack widths measurement”, *Journal of Applied Mechanics*, JSCE, vol. 7, no. 2, pp. 1179-1186, 2004.

MONITORING SYSTEM BASED ON OPTICAL FIBER SENSING TECHNOLOGY FOR TUNNEL STRUCTURES AND OTHER INFRASTRUCTURE

Kazuhiko Fujihashi[1], Kazumi Kurihara[2], Kazuyuki Hirayama[2], and Shuji Toyoda[2]

[1]*NTT Infranet Corporation (Hamacho-Center, Building 15F, 2-31-1, Nihonbashi-hamacho, chuo-ku, Tokyo, 103-0007, Japan)*

[2] *NTT Infranet Corporation (NTT Koishikawa, Building 1-18-1, Koishikawa, Bukyo-ku, Tokyo, 112-0002, Japan)*

Abstract: Lifeline facilities, such as roads, railways, electric power, water supply and wastewater systems, natural gas, and telecommunications function because of the widespread presence of an enormous infrastructure which acts as a network. Unfortunately, these infrastructure elements are subject to degradation over time, reduced functionality, and loss of functionality as a result of factors such as a wide variety of installation environments, natural disasters, and nearby work. Therefore, it is necessary to perform appropriate inspections, repairs, and renovations to ensure safe and efficient maintenance and operation.

Optical fiber sensing (OFS) technology has gained attention in recent years as a key technology for lifeline inspections and diagnostics because of its many advantages, including corrosion resistance, the fact that the sensors do not require a power supply, and the ability to obtain measurements over long distances. This paper introduces a variety of OFS technology methods, and discusses an actual system for monitoring changes in existing tunnels (e.g., communication tunnels), as well as the development of related sensors.

Key Words: Optical fiber sensing, BOTDR, FBG, OTDR, tunnel, monitoring

1. INTRODUCTION

Nearly all sensors currently used in structure monitoring, such as strain gauges and clinometers, are electric. While these devices are able to capture point information, it is difficult for them to capture linear or planar continuous

Farhad Ansari (ed.), Sensing Issues in Civil Structural Health Monitoring, 185–195.

information. In addition, because sensors are installed in the field, measures to counteract lightning, induction, and corrosion must be incorporated. Furthermore, in cases where numerous points are measured over a wide area, many sensors require separate, individual cables for supplying power and transmitting measurement signals. This increases the system complexity and is also problematic in terms of construction costs as well as ongoing maintenance and operating costs.

By contrast, OFS technology has gained attention as a technology which overcomes such problems with electrical sensing technologies. It is excellent for sensor applications involving outdoor installation over a wide area. However, OFS technology includes a variety of methods, so it is necessary to select the appropriate method based on factors such as what is being measured, the measurement parameters, and the required precision.

This paper describes a variety of OFS technology methods, and discusses an actual system for monitoring tunnel changes as well as the development of related sensors. In addition, issues related to the future growth of OFS technology are considered.

2. A VARIETY OF OFS TECHNOLOGY METHODS

Optical fiber types used in sensing include types in which the optical fiber itself is used as a sensor, and types in which a processed part of the optical fiber is used as a sensor. BOTR, OTDR, and ROTDR are examples of the former. In general, these types require an external sheathing structure so that strain and other disturbances are not transmitted to the core. FBG, SOFO, OSMOS, and interferometry are examples of the latter.

2.1. BOTDR method

Brillouin Optical Time Domain Reflectometory (BOTDR) was originally an application of telecommunication optical fiber maintenance technology, and was developed to find locations with strain before an optical fiber was cut.[1)] Brillouin scattered light, which is part of the backward scattered light, is characterized by frequency shifting in proportion to the amount of strain on the optical fiber (Fig. 1). A strain amount of 1% results in a frequency shift of 500 MHz. By measuring changes in this Brillouin scattered light frequency, it is possible to measure the amount of strain and measure the time required for the light to return. As a result, the location where the strain is occurring can be determined. Advantageous features of this approach include the fact that the optical fiber material does not need to be processed in advance, and the ability to measure continuous strain distribution along the optical fiber. Brillouin scattered light is very weak in terms of power, so numerous measurements are averaged. For this reason, measurement takes several minutes and dynamic

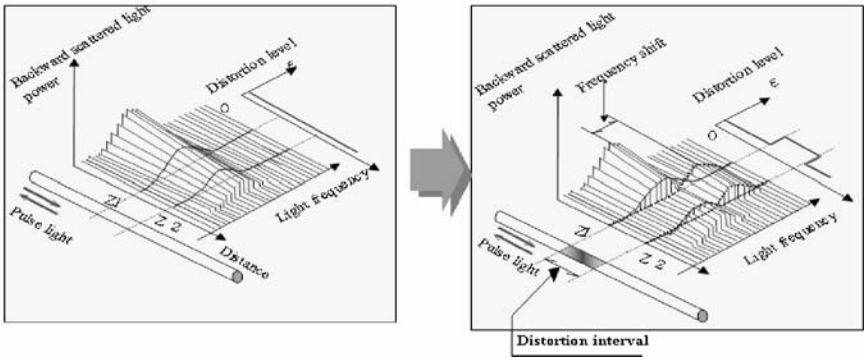

Fig. 1 BOTDR Operating Principles

measurement is not possible. The optical fiber used in strain sensors is single mode (SM) fiber, which is used in ordinary telecommunications. Typically, a fiber with an external sheath structure allowing strain to be easily transmitted to the core is used. The measurable strain range is approximately 2%, based on factors such as analyzer performance and optical fiber tensile strength.

2.2. FBG method

The Fiber Bragg Grating (FBG) method uses the optical fiber body as a measurement sensor. With this method, a single optical fiber simultaneously acts as a measurement sensor and transmits a signal. With the FBG method, gratings, which are parts with different refractive indexes, are arranged in a

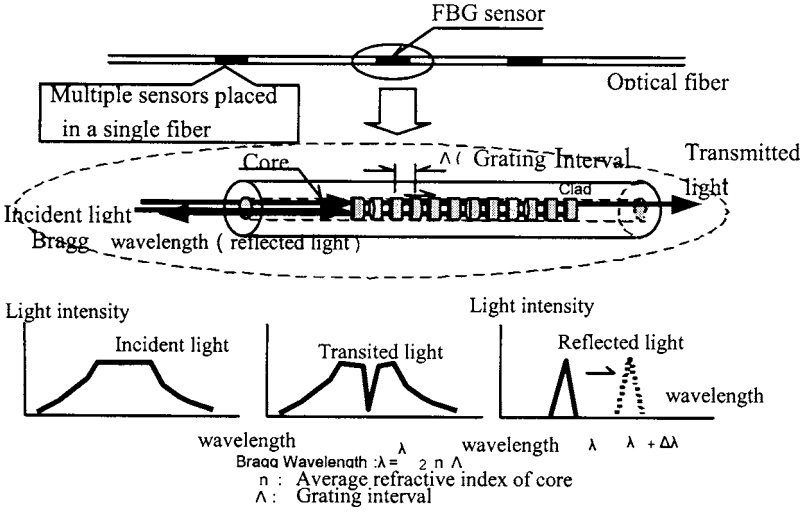

Fig. 2. FBG Operating Principles

grating pattern with pitch Λ in the core at specific parts along the optical fiber. These gratings are used as sensors (FBG). The gratings are created at a high density of 20,000 per 10 mm length (Fig. 2).

Light incident from one end passes through the fiber. When it reaches an FBG sensor, only a certain wavelength (the Bragg wavelength) is reflected and returned. If the FBG sensor grating pitch changes, the Bragg length also changes. If a strain change of 1μ strain occurs in the grating, the Bragg wavelength changes by 1.2 pm. The FBG method uses this principle to measure strain. The distance between the analyzer and the measurement point may be as great as approximately 30 km. Another feature of this method is the ability to determine compression strain. FBG is characterized by a short sampling time.

FBG was first introduced to Japan around 2000 for use in detecting falling rocks. Since then, work has continued on the development of a variety of measurement sensors. Currently, analyzers are made by European and American manufacturers and not by Japanese. 250 Hz analyzers are already available, and 1 kHz models may be available in the near future. Applications to vibration sensors are anticipated.

3. APPLICATION TO TUNNEL MONITORING

A telecommunication tunnel monitoring system has been developed and installed as a commercial system for NTT group companies.[2] NTT group companies own telecommunication tunnels with a length of 600 km centered in cities designated by ordinance. The system was installed to enable early detection of problems such as cracking due to aging, as well as rising or sinking due to nearby work such as subway projects. Once problems are detected, countermeasures can be implemented to minimize tunnel damage. A major example of an actual application is presented below.

3.1. Tunnel monitoring to measure the effects of nearby subway work

Construction of the Tokyo Metro Subway Line No. 13 approaches and crosses NTT's telecommunication shield tunnels in many areas (Fig. 3), and the tunnels will be affected by this work. In particular, in three station-building construction sections, the tunnels will be exposed, after which suspension and holding protective work will be performed. Therefore, it was necessary to manage measurements of the effects on the tunnels over an extended time period and wide spatial area. In order to do this, a continuous, wide-area

measurement and monitoring system based on fiber sensors (BOTDR method) was adopted for precise management of measurements of tunnel changes.

Fig.4 presents a summary of the optical fiber sensor installation and installation conditions. The optical fiber sensor installation involved installing

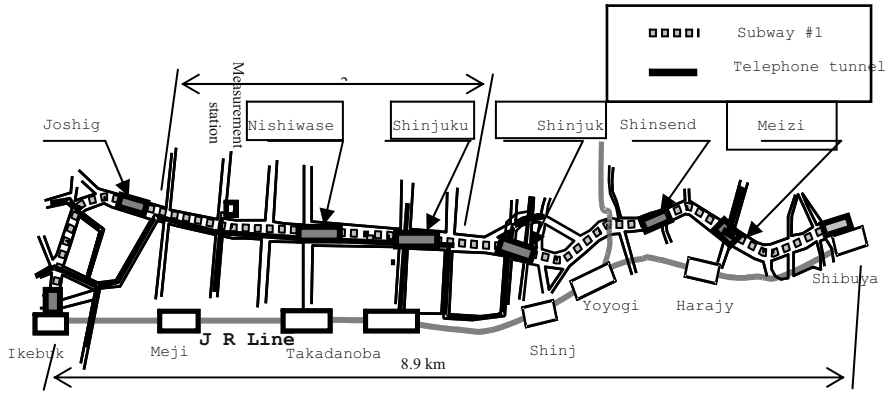

Fig. 3 Outline of Neighborhood Construction

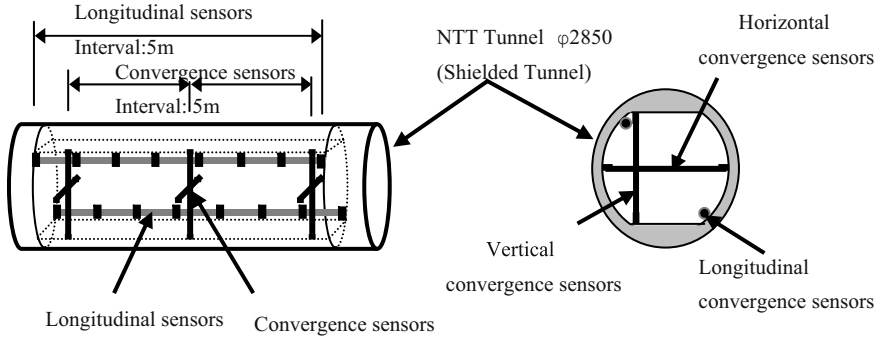

Fig. 4 Outline of optical fiber sensors and installation

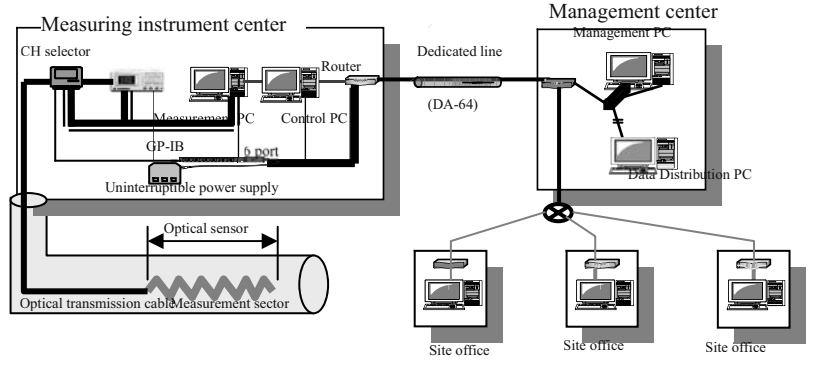

Fig. 5 Optical measurement system

longitudinal sensors at 5 m intervals in the tunnel axial direction, and convergence sensors were installed at 15m intervals on the top, bottom, left, and right sides of the tunnel cross section. This project is long-term, extending until 2006. Therefore, the measurement system shown in Fig. 5 was built. BOTDR measurement devices installed at field observation stations deliver data to a management office, and the management office delivers data to the individual field offices. All of these deliveries can be handled through automated transmission. In addition, the measurement management system is designed to be very robust, including features such as systematization so that an alarm is sent to measurement administrators if a measurement management threshold value is exceeded or a measurement system abnormality occurs.

3.2. Measurement results

The cross section in Fig. 6 shows progress in the excavation of tunnel measurement segment A. Excavation steps #1 through #5 in the figure show the excavation progress from month to month. Step #5 is partial excavation. In a 33 m interval near the center of the excavated area, the tunnel is exposed, and tunnel suspension protective work for the next excavation is performed.

1) Tunnel sectional displacement Fig. 7 illustrates changes over time in tunnel the amount of convergence in the center of the excavated area (measurement point IV) in measurement segment A. There is little amount of convergence due to excavation in steps #1 through #3, but there is a large amount of displacement from the excavation in step #4 (excavation of 2.4 m interval at tunnel top). The tunnel's shape changes so that it is elongated (maximum +0.9 mm vertical, -0.9 mm horizontal) due to the excavation in step #4. The tunnel then settles with the completion of step #4. From step #5, the decline in the side weight load in conjunction with excavation of the tunnel side area causes the tunnel shape to be nearly restored to its initial state.

2) Tunnel longitudinal strain Fig.6 shows the axial strain distribution every 5 m in the tunnel's longitudinal direction at the completion of each excavation step. The horizontal axis shows the tunnel's longitudinal distance. Longitudinal strain in the tunnel due to excavation in steps#1 through #4 can be seen in the form of slight pulling near the end areas, but there is little strain in the excavation area as a whole. The pulling strain near the ends is believed to have occurred due to the suppression of the tunnel's rebound displacement by the retaining wall. In step #5, there are new points of curvature due to pulling strain away from the ends. This strain occurred at the edges of partial excavation, and is believed to represent the effects ofeccentric weight load due to partial excavation, and support-point bending due to suspension protective work. The tunnel's strain distribution is all compression except for the ends and the edges of the partial excavation areas. Compression strain at

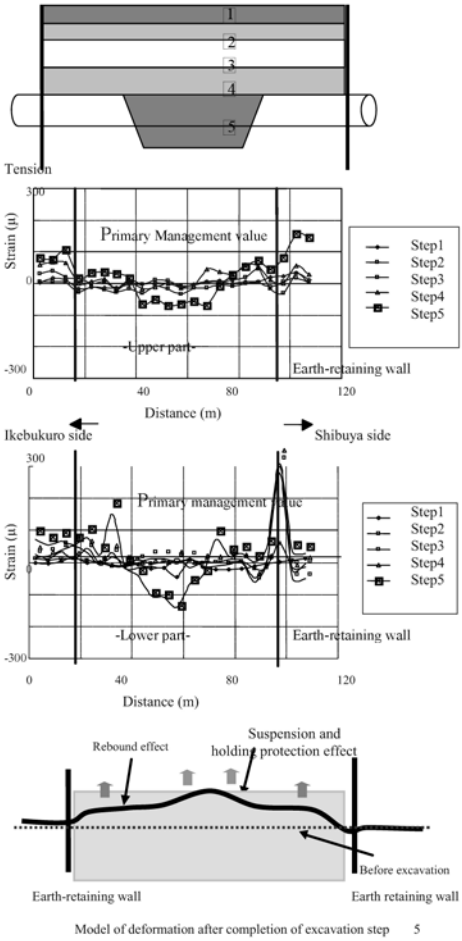

Fig. 6 Test result for longitudinal distortion measurement

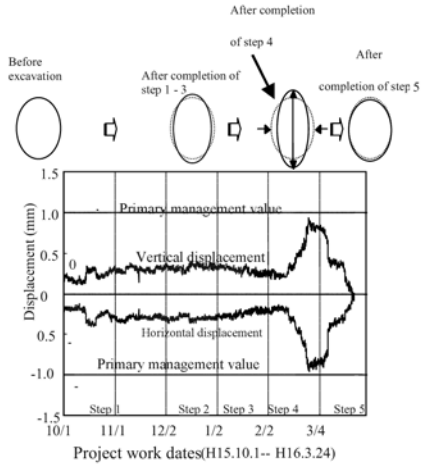

Fig. 7 Periodical change in tunnel convergence sensors

the bottom is greater than at the top (negative bending). Therefore, the tunnel's longitudinal displacement at the time of step #5 seems to be a displacement distribution like that shown in the deformation model of Fig. 6.

3) Summary The tunnel convergence after excavation steps #1 through #5 was in the range of the primary management value (maximum value: 0.9mm). The primary management value for longitudinal strain is exceeded at the ends as well as the edges of the partial excavation areas. Therefore, we have implemented countermeasures based on a protective network which predicts strain increases in advance, and are conducting periodic examinations for cracks.

4. DEVELOPMENT OF OFS DISPLACEMENT METERS

The strength of the optical fiber material is approximately 3 %. The measurable strain distribution range based on the BOTDR method is up to approximately 2 % for strain occurring in the fiber itself. Therefore, even within the fiber, it is not possible to measure large displacement values at certain points. In consideration of this, we developed a light displacement meters by fabricating mechanisms (sensor units) for converting strain to displacement, so that measurements ranging from minor displacements to large displacements could be handled. We developed three different displacement meters, using BOTDR, OTDR and FBG (Table 1).

Table.1 Various Optical Fiber Displacement Meters

Parameter	BOTDR displacement meter	FBG displacement meter	OTR-A displacement meter	OTDR-B displacement meter
Size (mm): L*H*D	715*100*54	341*160*55	150*100*80	150*116*60
Weight(kg)	3.8	2.2	0.9	1.1
Target Precision (mm)	±5.0	±0.5	±2.0	±2.0
Measurement range	200mm	200mm	Ultra-detection of points within 200mm	

4.1. Measurement principles of BOTDR displacement meter

Displacement between two points is generally determined by measuring the strain on an optical fiber sensor cable set between two points with a known distance. However, because of the limitations on the minimum spatial resolution of the BOTDR analyzer and the tensile strength of the optical fiber, this type of method requires a distance of at least 1 m between the two points, and can only handle a displacement range of several mm to several cm. In light of this, we developed a compact displacement meter capable of measuring displacement of up to 20 cm by arranging the parts of an optical fiber bundled in a loop and spring units in a series. The measured displacement δ is given by the equation below. The balance of forces P, k1,

and k2 acting on the displacement meter must be adjusted so that the displacement level occurring in the optical fiber is at least several hundred μ (δ value is per cm).

$$\delta=(1/K1+1/K2)P \quad (1)$$

Equation variables δ: Displacement, k1: Spring value of optical fiber (tensile), k2: Spring value of spring unit

4.2. Measurement principles of FBG displacement meter

We developed a compact displacement meter capable of measuring displacement of up to 20 cm by arranging an optical fiber and spring units in a series. The design utilizes the fact that the Bragg wavelength shift has a proportional relationship to the strain acting on the optical fiber (FBG unit). One feature of this FBG displacement meter is the ability to measure displacement with a high level of precision.

4.3. Results of indoor test on OFS displacement meters

A simple pulling displacement (measured with a dial gauge) was applied at fixed intervals to the optical fiber displacement meter, and measurements were made using each type of analyzer. After the maximum stroke was reached, measurements were taken while returning it to zero at fixed intervals.

1) BOTDR displacement meter

Fig.9 shows the relationship between the applied displacement and the strain occurring in the optical fiber. This shows that a high degree of linearity has been achieved. A strain/displacement conversion equation was derived from this figure. The maximum tolerance was -4.5 mm, so the targeted range of ±5.0 mm was achieved.

2) FBG displacement meter

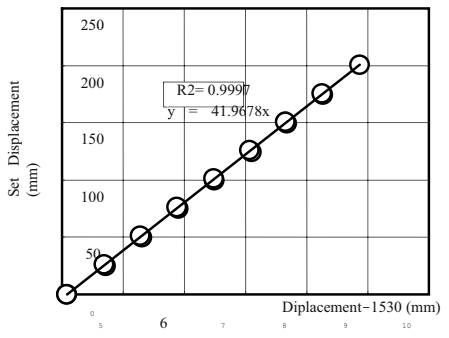

Fig. 8 Test result for FBG displacement meter

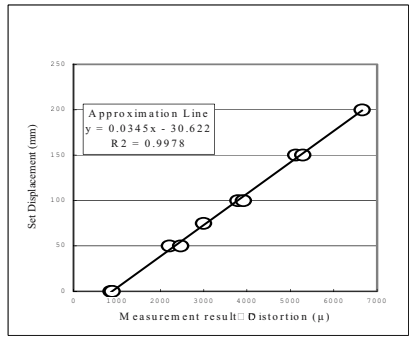

Fig. 9 Test result for BOTDR displacement meter

Fig.8 shows the relationship between the applied displacement and the FBG wavelength change. This shows that a very high degree of linearity has been achieved. A wavelength shift/displacement conversion equation was derived from this figure. The maximum tolerance was -1.7 mm, so the targeted range of ±0.5 mm was not achieved. Improvements such as temperature calibration are needed to improve precision.

5. ISSUES FOR EXPANDING APPLICATIONS OF OPTICAL FIBER SENSING TECHNOLOGY

OFS technology has many advantages over conventional technologies such as electrical systems. However, a number of challenges still remain before OFS technology can be fully commercialized. In terms of field sampling, an important issue is reducing costs. For example, light sensors incorporating FBG sensors currently cost twice as much as commonly used electrical sensors. In addition, the analyzer itself is also expensive. And BOTDR analyzers remain expensive, and cost reductions will be needed to expand their ranges of application. The second issue is that these new systems have little history at the commercial level, and there is little in the way of application menus or corroborative data. Therefore, users at present must be very careful in adopting OFS technology. Steady effort will be needed going forward, to collect basic data (data on temperature correction methods, etc.) and perform numerous demonstration tests to improve the reliability of measurement data. The third issue is that the wider the measurement area and the greater the number of measurement points, the more difficult it is for users to comprehend measurement results. This challenge can be addressed through software improvements, such as visual measurement result displays that can be easily understood by users. The fourth issue, which is common to all monitoring systems, is the establishment of system operating methods, such as how to interpret measurement results and link them to subsequent actions.

6. CONCLUSION

This paper has presented an overview of optical fiber sensing (OFS) technology, and described an actual applied system for monitoring tunnel changes as well as future challenges. OFS technology certainly holds much potential as a powerful technology in monitoring fields such as lifeline maintenance and disaster prevention[3)]. However, as mentioned above, OFS technology faces a variety of challenges to gaining widespread use. These challenges must be overcome through demonstration tests and the like in order to better establish the technology.

REFERENCES

1) H. Naruse, ”Development of Strain measurement system using fiber optic sensing technology”, The Japan Society of Mechanical Engineers Journal, 2003,Vol. 106

2) Takatsuka, Hashimoto, Fujihashi, ”Tunnel Structure monitoring system using fiber optic sensing technology”, annual meeting Oct. 2000, JSCE

3) S. Kato, N. Tsuneoka, ”Development of surface failure monitoring system using optical fiber sensor”, Ministry of Land, Infrastructure and Transport Government of Japan, The 4th conference of road new technology, 4, July, 2000

DEVELOPMENT OF FBG SENSORS FOR STRUCTURAL HEALTH MONITORING IN CIVIL INFRASTRUCTURES

Zhi Zhou and Jinping Ou
School of Civil Engineering, Harbin Institute of Technology, Harbin, 150090, P. R. China

Abstract: In recent years, FBG (Fiber Bragg Grating) has been accepted as a new kind of sensing element for structural health monitoring (SHM) in civil infrastructures. Cost of FBG fabrication, high-quality FBG demodulation system, practical encapsulation (package) techniques and indirect FBG-based sensors, and practical applications are the cores for FBG to be widely popularized in infrastructures. In this paper, firstly, the FBG fabrication and demodulation system are briefly introduced and the practical needs from infrastructure are pointed out; Secondly, the practical encapsulation (package) techniques and indirect FBG based sensors from Harbin Institute of Technology (HIT), have been conducted; Thirdly, some practical applications, taken as examples, are carried out; Finally, the future studies and problems are also set forth. Researches and practical applications show that FBG sensors have become one of the key sensors in SHM instead of some conventional electrical sensors.

Key words: FBG, sensor, structural health monitoring, civil infrastructure.

1. INTRODUCTION

After almost 10 years' development, SHM has currently become the highlight of researches and applications in civil infrastructures all over the world. And its core is damage detection and identification. As is known, it is a big challenge to perform accurate damage analysis, especially the damage location, via global information. Local damage monitoring seems paramount. Generally speaking, local damage behaves as crack, fatigue, slip, debonding, effective force-resistance area loss, and so on. Strain is an

Farhad Ansari (ed.), Sensing Issues in Civil Structural Health Monitoring, 197–206.

alternative parameter which can be used to describe deformation, study the crack opening and even detect the slip and bonding, so high-quality strain sensor has always been pursued by the structural researchers. However, infrastructures are generally large, long span and serve for a very long time, so the local durable and reliable sensors are the foundation of successful health monitoring systems. Optical fiber sensors, especially the sensors based on FBG, show distinguishing advantages: electro-magnetic resistance, small size, resistance to corrosion, multiplexing a large number of sensors along a single fiber, etc. FBG has more and more become the most prominent sensors for structural monitoring.

In this paper, aiming at the practical application of FBG sensors in infrastructures, the FBG fabrication and demodulation system are introduced briefly and the practical needs from infrastructure are pointed out. Then, the practical encapsulation (package) techniques and indirect FBG based sensors, especially from Harbin Institute of Technology (HIT), have been conducted. And some practical applications from HIT taken as examples are carried out. Finally, the future studies and problems are also set forth. By and large FBG sensor is predicated that have become one of the key sensors in SHM instead of some conventional electrical sensors.

2. FBG FABRICATION AND DEMODULATION

2.1 FBG fabrication

Due to the great potential of FBG's applications, more research was conducted on the fabrication methods of FBG. Currently, there are two major methods for fabricating Fiber Bragg Grating: holographic method and phase mask method (Hill, 1993). In 1989, Meltz used holographic interference setup to write FBG, and the grating was written from the side of fiber. Away from G. Meltz's two UV beams interference, other methods were given to improve the stability during the fabrication process, such as using a prism to split the UV beam and then interference. The advantage of the Holographic method: it is easy to adjust the angle between two beams to create different periods, therefore, to fabricate FBG with difference wavelengths. The disadvantage of this method is that a more stable setup is needed and a good coherence light source is also requested in the meantime.

In 1993, Hill et al gave another easy method to fabricate FBG by phase mask. Phase mask is a piece of diffractive grating with depth modulation on fused silica. The phase mask were designed to suppress 0^{th} order diffraction efficiency (<5%) and increase +/-1^{st} order efficiency (>35%). When a UV

beam incident on phase mask, the +/- 1st order beam will credit an interference pattern, this pattern will write the FBG on the fiber. The period on FBG is the half of phase mask. The advantage of Phase Mask method: it is simple with great repeatability as well as the disadvantage of Phase Mask: each mask can only generate one wavelength of FBG.

2.2 FBG demodulation

Currently, interrogators for multiple Bragg grating sensors fall into two main categories: time division multiplexing (TDM) and wavelength division multiplexing (WDM). TMD discriminates between many sensors on a single optical fiber by gauging the time required for a pulse of light to return to the detection system. TDM systems must be designed to balance the sensor-sampling rate with the distance of the sensor from the light source and detection system. Blue Road Inc. has successfully developed FBG interrogators based on such idea. The most popular approach is WDM. WDM systems discriminate individual sensors by wavelength. That is, several sensors may have nominal center wavelengths separated by a few nanometers. Each sensor is tracked simultaneously as its center wavelength changes due to environmental changes like strain, temperature or pressure. Most WDM systems are designed using the basic configurations: broadband source and swept detector (BSSD) or laser source and broadband detector (LSBD). BSSD systems generally use an ASE, LED or SLED source coupled with a tunable filter and broadband detector. Micron Optics Inc. has developed such kind of interrogators as FBG-IS and Sm220. Whereas LSBD overcomes the sensor limitation with much more optical power and laser-based interrogators can illuminate more than 100 sensors per channel, whose limiting factor is usually wavelength range. Micron Optics Inc. has developed high-quality interrogators based on its FFP-TF (fiber F-P tunable filter) technology like SI425.

2.3 Needs from civil infrastructures

General speaking, infrastructures are large, long span and serve for a very long time. Sometimes it is hard to judge the definite positions where the local damages will take place. So in order to assure the reliability of health monitoring system, we can do nothing but install local sensors as many as possible. Unfortunately, it conflicts much with the cost of FBG sensors and interrogators. In order to popularize of FBG sensors in infrastructures, high-quality and effective FBG fabrication techniques should be developed. And the best way is to produce FBG by batch, which can drop down the cost. 3 kinds of FBG interrogators should be developed urgently due to the needs of

quality control of construction, real-time and long- term heath monitoring system, and FBG-based sensors calibration and quality-control. The first kind of interrogator should be small size, high-precision, portable and battery based, which does not need high frequency and multi-channel. The second should be high frequency (> 100Hz), multi channels (>16 channels) and durability (> 10 years). The third should be high precision (< 2 *pm*) and revolution (< 0.5 *pm*). The 3 kinds of FBG interrogators are the base of FBG popularization in civil engineering.

3. SENSORS BASED ON FBG FOR INFRATRUCTURES

Bare FBG shows good compatibility with infrastructures, but due to its fragility, bare FBG without encapsulation (package) is not proper to be directly applied in practical infrastructures. Otherwise, we have to develop special in-situ installation and protection techniques for bare FBGs. Unfortunately, the "perfect" installation techniques often conflict with the in-situ construction, or it can not meet the demand of critical schedule of construction. Besides, in order to make full use of FBG, we should develop indirect sensors device based on FBG and combine the FBG and construction materials. Many sensors based on FBG have been developed. Under the support of several projects related to heath monitoring, Harbin Institute of Technology, China, has developed some practical packaged FBG sensors, indirect sensor devices and FRP-combined sensors, which are commercially available.

3.1 Encapsulated FBG strain sensor for embedment

In order to overcome the embedment of FBG strain sensor in concrete structures, HIT has developed the technique of mental tube encapsulated FBG strain sensor, depicted as figure 1.

Figure 1 Picture of mental tube encapsulated FBG strain sensor

3.2 Encapsulated FBG strain sensor for surface strain measurement

In order to overcome the installation of FBG strain sensor on surface of steel or concrete structures, HIT has developed the technique of mental slice encapsulated FBG strain sensor, depicted as figure 2.

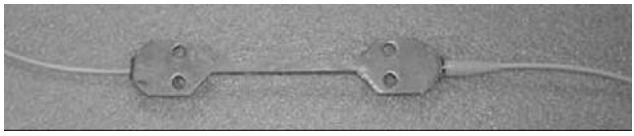

Figure 2 Picture of mental slice encapsulated FBG strain sensor

3.3 Encapsulated FBG temperature sensor

In order to overcome the installation of FBG temperature sensor on or inside structures, HIT has developed the technique of encapsulated FBG temperature sensor, depicted as figure 3.

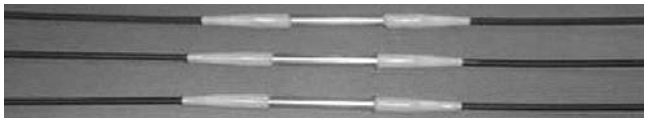

Figure 3 Sketch for steel capillary encapsulation for FBG temperature sensor

3.4 Smart rebar based on FBG sensors

FRP is now more and more accepted as a kind of important construction material. To make full use of FRP's strength properties and FBG's sensing properties, Prof. OU has developed the fabrication technique of FRP-OFBGs bars and gotten the products, shown as Figure 4.

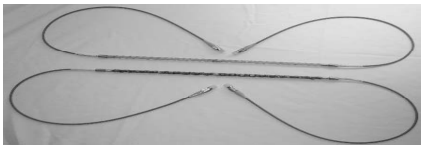

Figure 4 FRP-OFBG sensors

3.5 Indirect sensor devices based on FBG

1) Ice pressure sensing device based on FBG

Ice load is important force acting on offshore platforms in the high-latitude district. Conventional ice pressure meter is based on electrical strain gauge, whose durability is very bad. A novel ice pressure sensing device based on dual FBGs is developed by HIT. Its inside structure is shown as figure 5. The main idea for the ice pressure sensing device is based on cantilever with dual FBGs installed up and down the surface and the load transfer structure. When load acting the device, we can get it by the dual FBGs, which is self-temperature compensation and the measurement results is not relative to the acting position. Such kind of ice pressure sensing device is proper for practical application.

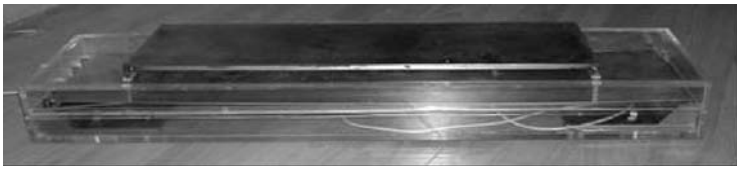

Figure 5 Structure of ice load sensing device based on dual FBG

2) Smart cable based on FBG

Figure 6 Smart cables based on FBGs

Cables are the key member of cable-stayed bridges, suspension bridges, hanging bridges and so on. The bridge cables in service are easily damaged due to the factors of environment corrosion, fatigue, materials aging, stress redistribution, etc. How to evaluate the damage or stress state of the cables in service has always still been a big challenge for civil engineers. HIT has developed a new kind of cables installed with FBGs during manufacture of the cables, shown as figure 6. The feasibility and advantages of smart bridge cable based on FBGs are test. This kind of cables has been applied in Luoguo Bridge in Panzhihua, and Binzhou Yellow River Bridge in Shangdong, China.

3) Smart weight in motion

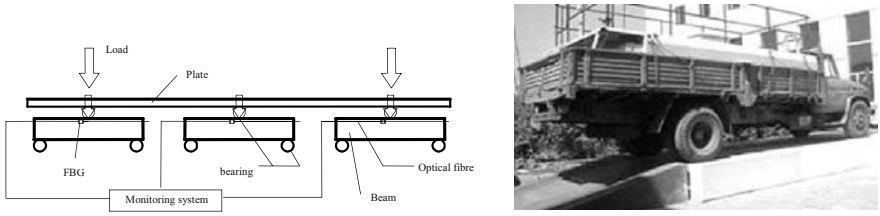

Figure 7 Weight in motion based on FBG

Based on the sensing properties of FBG, a new kind of smart weigh in motion, namely smart FBG weighbridge, has been developed, shown as figure 7. The smart FBG weighbridge is based on the principle that the traffic weight can be gotten from the deformation of the reinforced concrete beam with embedded FBG strain sensors which measure the deformation. This kind of weighbridge shows the features of simplicity, convenience, high precision, good durability, low cost and so on.

4. APPLICATIONS OF FBG SENORS

FBG sensors have been applied in many infrastructures. HIT have developed intelligent monitoring system based FBG and applied it in several projects as follows. And more than 2000 FBGs has been used

4.1 Intelligent monitoring systems based on FBG

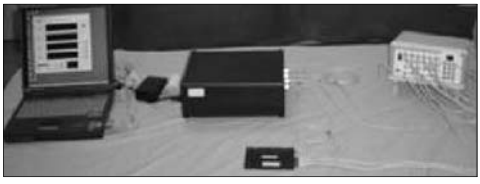

(a) Practical devices for monitoring system based on FBG sensors

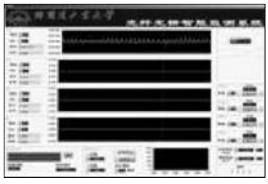

(b) Software of intelligent monitoring system based on FBG sensors

Figure 8 Intelligent monitoring system based on FBG sensors

The intelligent monitoring system based on FBG sensors include FBG sensors, optical coupler (optical switch), FBG interrogator, transmission cable, jumpers and relative software, which shown as figure 8 (a) and (b).

4.2 FBG sensors applied in Bridges

Due to that the bridges is the key part of transportation, lots of large-span bridges are under construction in developing countries as well as China. With the development of structural health monitoring, the bridge owners realize the importance of adding structural health monitoring system to the bridges under construction in order to avoid disastrous tragedy to happen. OU has developed several structural health monitoring systems based on FBG sensors to be applied in the several large-span bridges, shown as figure 9-12, to monitor the performance of the bridges under construction and in service.

Figure 9 Songhua River Bridge in Heilongjiang (2003, over 50 FBGs uses)

Figure 10 Dongying Yellow River Bridge in Shandong (2003, over1800 FBGs used)

Figure 11 Binzhou Yellow River Bridge in Shandong (2002, over 130 FBGs used)

Figure 12 Nanjing third Yangtze river Bridge (2003, over 300 FBGs used)

4.3 FBG sensors application on offshore platform

Offshore platform is the key infrastructures for oil exploitation, which serve in extremely bad environments with wind, wave, ice and ocean current, even corrosion, so the life of the offshore platform are very short, 20 years or so. It is in great need to real-time evaluate the safety and predict the remaining life of the platform.

Under the support of 863 High Tech. Research Program, OU and Duan (2002) have developed a large real time structural health monitoring system to monitor the global and local performances of the platform, such as acceleration, strain, temperature and crack and so on, and even the environment load mentioned above by the ocean weather observation station. According to the monitoring information and the designed model, the safety

state of the platform can be given real time. CB32A located in Bohai Bay is the application demonstration of the project achievement, shown as *Figure 13*, where the intelligent monitoring system based on FBG sensors is applied. And more than 350 FBGs has been used.

Figure 13 CB32A platform in Bahai bay (more than 350 FBG used)

5. CONCLUSIONS AND REMARKS

FBG (Fiber Bragg Grating) has been accepted as a new kind of sensing element for structural health monitoring (SHM) in civil infrastructures. FBG sensors' key research areas include FBG fabrication, FBG demodulation, FBG encapsulation, indirect sensing device based on FBG and practical applications. The core problems focus on reliable FBG standardized encapsulated sensors and the multi-channels, high frequency, and high precision low-cost demodulation devices. Researches and practical applications show that FBG sensors have become one of the key sensors in SHM and will take the place of some conventional electrical sensors.

As a new kind of sensor for structural health monitoring system, popularization of FBG is still a challenge for researchers. Following problems should be the directions of future studies on FBG: 1) Develop low-cost standard bare FBG with stable sensing coefficient; 2) Effective temperature compensation techniques for FBG strain sensors used in long-term monitoring systems; 3) How to develop standardized FBG encapsulated sensors; 4) How to develop smart devices based on FBG to detect special parameters of infrastructures, such as corrosions, slip, debonding, and so on; 5) How to avoid the damage of the FBG sensors and cables during constructions; 6) How to develop low-cost multi-channel interrogators when we have to face the embarrassment that we have no choice but to cut down the number of FBG sensors along one cable, even sometimes one sensor on one cable, which makes us not able to make full use of the advantages of FBG; 7) How to develop large integrated FBG monitoring system and make

it become the important part of the Structural Health Monitoring System and give useful information for damage identification.

ACKNOWLEDGEMENT

This paper is supported by the Chinese "863" High Tech. Research Project (Granted No.2001AA602023 and 2002AA313110), NFSC (Granted No.50308008) and Chinese Postal doctoral foundation.

REFERENCES

1. Aftab AM. *Proceeding of First International Workshop on Structural Health Monitoring of Innovative Civil Engineering Structures*, Winnipeg, Canada, 2002.
2. Wu ZS. *Proceeding of the first international conference on structural health monitoring and intelligent Infrastructures*, Tokyo, Japan, 2003.
3. Hill KO. "Photosensitivity in optical fiber waveguides application to reflection filter fabrication". *App. Phys. Lett.,* 32(10), pp. 647-653, 1978.
4. Meltz G., Morey W.W., Glenn W.H. "Formation of Bragg gratings in optical fibers by a transverse holographic method". *Optical letter*, 14 (15), pp.823-825, 1989.
5. Ou JP. "Some recent advance of intelligent monitoring system for civil infrastructures in mainland China". *Proceeding of the first international conference on structural health monitoring and intelligent Infrastructures,* Tokyo, Japan, 2003, pp. 131-144.
6. Ou JP. Zhou Z. "Encapsulation Techniques for FBG and Smart Monitoring for Bridges with FBG Sensors", *Proceeding of the 4th International Workshop on Structural Health Monitoring at Stanford University,* Stanford University, 2003, pp. 180-187.
7. Ou JP. Zhou Z., Wu ZJ. "The sensing properties and practical application in civil infrastructures of optical FBGs". *SPIE,* 5129, 2003, pp. 10-17.
8. Zhou Z. Thomas W. G., Luke H. and Ou JP. "Techniques of Advanced FBG sensors: fabrication, demodulation, encapsulation and their application in the structural health monitoring of bridges". *Pacific Science Review,* 5 (1), pp.116-121, 2003.
9. Zhou, Z., Wang, B., and Ou, J. P. "Local damage detection of RC structures with distributive FRP-OFBG sensors". *Proceedings of 2nd International Workshop on Structural Health Monitoring of Innovative Civil Engineering Structures*, Winnipeg, Manitoba, Canada, 2004.
10. Ansari F. "Fiber optic sensors and systems for structural health monitoring system", *Proceeding of First International Workshop on Structural Health Monitoring of Innovative Civil Engineering Structures*, Winnipeg, Canada, 2002, PP. 3-22.

Chapter IV

Smart Sensors, Imaging and NDT of Civil Structures

MONITORING OF A SMART CONCRETE BEAM

Qingbin Li [1], Lei Li [1], and Fan Zhang [2]

[1] Dept. of Hydraulic Engineering, Tsinghua Univ., Beijing 100084, P.R. China

[2] Dept. of Transportation of Henan Province

Abstract: Smart concrete beams with dimensions 1996cm × 99cm × 85cm were manufactured, six bounds of Shape Memory Alloy (SMA) were mounted in each beam as actuators. Experiment of the smart concrete beam was carried out, the temperature and the smart pre-stress of the SMA bundle, as the distortion of the beam, were monitored during the experiment. The results show that the smart concrete beam may change its performance as needed.

Key words: Monitoring, Smart, Concrete beam

1. INTRODUCTION

1.1 What is an Intelligent Structure?

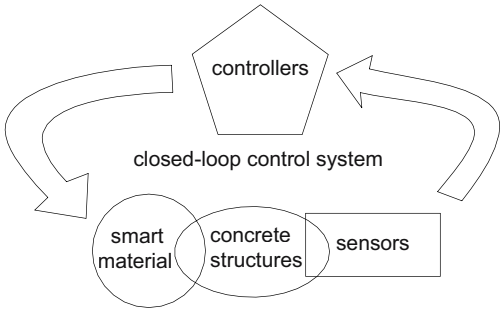

Figure 1. Frame diagram of intelligent structure

Farhad Ansari (ed.), Sensing Issues in Civil Structural Health Monitoring, 209–218.

Intelligent structure is an integrality that concludes matrix material, sensors, actuators and controllers, as shown in Fig. 1. This integrality is capable of altering its mechanical states according to the external loading.

1.2 Shape memory alloys (SMAs)

Shape memory alloys possess an interesting property that the metal "remembers" its original size or shape and reverts to it at a characteristic transformation temperature [1], as shown in Fig. 2.

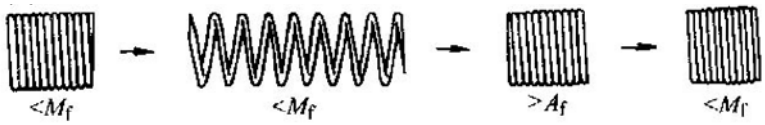

Figure 2. Schematic of SME

When shape memory alloy is free to deform, its constitutive behavior is as shown in Fig. 3 [2-3]. Whereas, in the case of constrained, large stresses should be induced inside it. This consequent behavior is depicted in Fig. 4, which is the principle of SMA used as actuators.

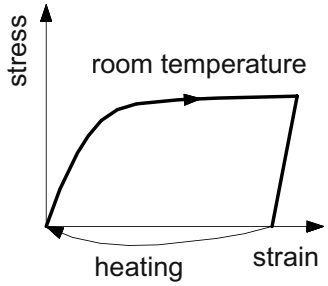

Figure 3. Schematic of strain-stress relationship of SMA on free state

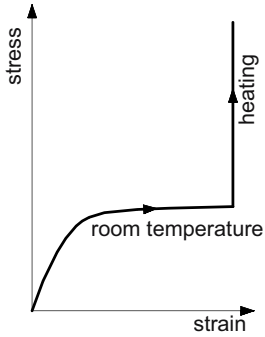

Figure 4. Schematic of strain-stress relationship of SMA on full-constrained state

2. DESCRIPTION OF THE SMART CONCRETE BEAM

The cross section of the smart concrete beam with dimensions 1996cm× 99cm×85cm is shown in Fig. 5, the layout of sensors and wires are depicted in Fig. 6.

Sixteen bounds of pre-stressed high-strength steel strands were mounted on the bottom of the beam to resist to the normal loads; six bounds of SMA were constructed upside the steel strands to create smart forces to resist to the over-loads when needed.

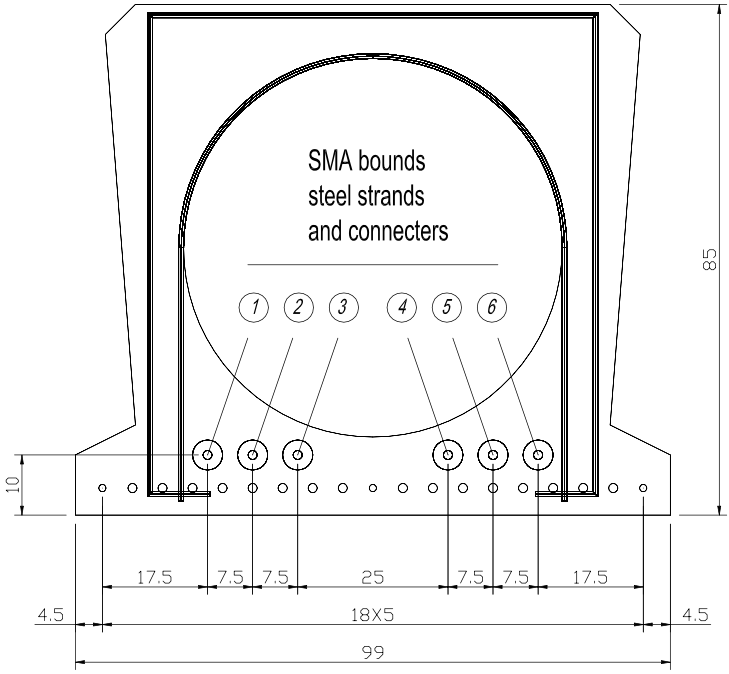

Figure 5. Schematic of cross-section of the smart concrete beam

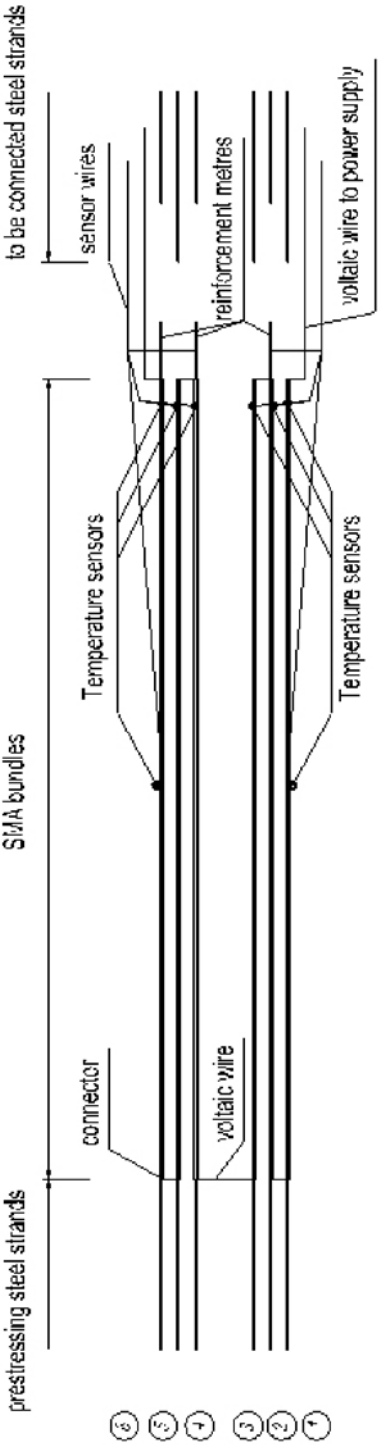

Figure 6. Schematic of layout of the sensors and wires

3. MANUFACTURING OF THE SMART CONCRETE BEAM

The manufacturing process of the smart concrete beam is shown in Fig. 7 through 11.

Figure 7. Connection of SMA bundle with pre-stressed steel strand

Figure 8. Photograph of SMA bundles in framework of steel reinforcement

Figure 9. Photograph of connection of voltaic wires

Figure 10. Photograph of framework of steel reinforcement with stretched SMA bundles

Figure 11. Photograph of depositing concrete

4. EXPERIMENTAL PHENOMENON OF THE SMART CONCRETE BEAM

The experimental results given in this section were carried out at 17 O'clock on July 20th, 2004. The experiment site is shown in Fig. 12.

Figure 12. Photograph of the experiment site

Displacement sensor was mounted at the middle span of the beam, as shown in Fig.13

*Figure 13. P*hotograph of layout of displacement sensor

The history of the displacement at the middle span of the beam is shown in Fig. 14.

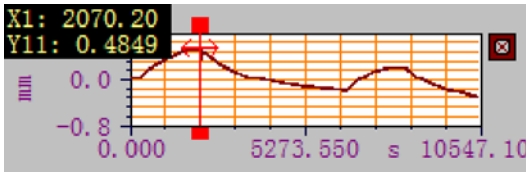

Figure14. Diagram of displacement history at the middle span of the beam

When the SMA bundles were actuated, the displacement of 0.4 mm generated, and if stopped, the beam came back to the original state. Environment temperature also affected the shape variety of the beam.

The time histories of temperature on SMA bundles and intelligent forces generated are depicted in Figs. 15 through 19.

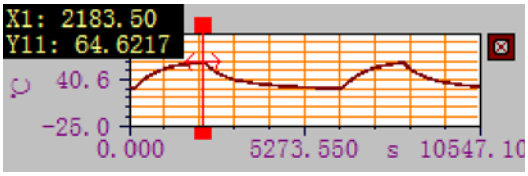

Figure 15. Diagram of temperature history on the side of NO.1 SMA bundle

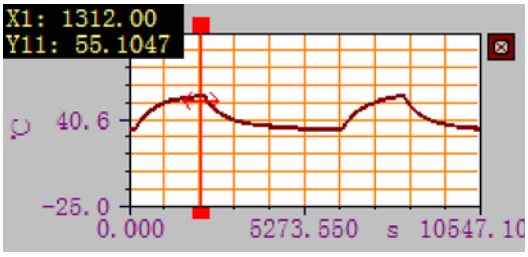

Figure 16. Diagram of temperature history on the middle of NO.4 SMA bundle

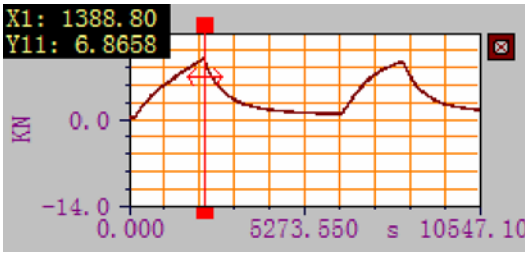

Figure 17. Diagram of intelligent force generated by NO.2 SMA bundle

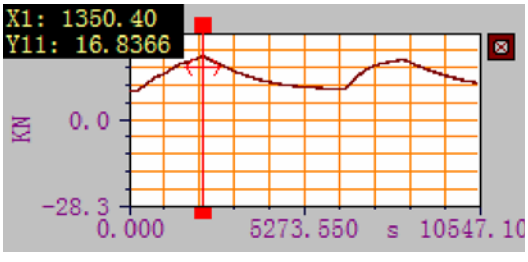

Figure 18. Diagram of intelligent force generated by NO.4 SMA bundle

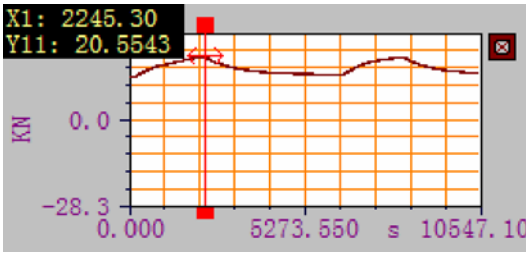

Figure 19. Diagram of intelligent force generated by NO.6 SMA bundle

5. SUMMARY

In this paper, smart concrete beams mounted with SMA bundles were manufactured. The main parameters, temperatures and smart force of SMA bundles and the distortion of the concrete beam, were monitored through an experimental program. According to the results, the smart concrete beam can alter its mechanical performance as needed. The monitoring of this smart bridge will be carried out in the near future.

REFERENCES

1. Srinivasan A.V., Mcfarland D. Michael. “Smart structures: analysis and design”, Cambridge University Press, 2001.
2. Sun Qing Ping, Hwang Keh Chin. “Micromechanics modeling for the constitutive behavior of polycrystalline shape memory alloy – I. Derivation of general relations”, J. Mech. Phys. Solids, Vol. 41, No. 1, pp. 1-17, 1993.
3. Birman, Victor. “Review of mechanics of shape memory alloy structures”. Appl. Mech. Rev Vol. 50, No 11, part 1, Nov., 1997.

FIBER OPTIC NERVE SYSTEMS WITH OPTICAL CORRELATION DOMAIN TECHNIQUE FOR SMART STRUCTURES AND SMART MATERIALS

Kazuo Hotate

Department of Electronic Engineering, School of Engineering, The University of Tokyo
7-3-1 Hongo, Bunkyo-ku, Tokyo 113-8656, Japan
E-mail: hotate@sagnac.t.u-tokyo.ac.jp, Phone/ Facsimile: +81-3-5841-6683/ 8562

Abstract: We have developed "fiber optic nerve systems" for "smart structures and smart materials," in which an optical fiber acts as sensor to measure distribution of strain and/or pressure along it. In our laboratory, an original technology to analyse the distributed optical parameters along the fiber by use of synthesis of correlation characteristics of continuous lightwave has been developed. Adopting this technology, "fiber optic nerve systems" with a high spatial resolution and a fast measurement speed have been established.

Key words: Smart materials, Smart structures, Optical fiber sensing, Distributed Sensing.

1. INTRODUCTION

Optical fiber acts as a sensor for strain, pressure, and so on, through its optical properties, such as, scattering and propagation-modes coupling, etc. By additionally applying a way to analyze these properties distributed along the fiber, the fiber provide us with nerve function for materials and structures, in which the fiber is embedded. The fiber nerve can sense damages appeared in the materials and structures. These having self diagnosis function are called "Smart Materials and Smart Structures."

Time domain techniques have been studied as the distributed sensing scheme. However, these have shown difficulties in realizing ultimate performances, such as a high spatial resolution and a high sampling rate. To

Farhad Ansari (ed.), Sensing Issues in Civil Structural Health Monitoring, 219–228.

overcome the difficulties, we have proposed optical correlation domain techniques with continuous lightwave [1,2]. By applying the technique, for example, to fiber Brillouin distributed strain sensing, we have demonstrated 1cm spatial resolution and 57Hz sampling rate, which are 100 times and 10^4 times higher than the time domain technologies, respectively .

2. PRINCIPLE OF OPTICAL CORRELATION DOMAIN TECHNIQUE

The visibility of the interference pattern in an interferometer changes as a function of the differential time delay between the two waves. The visibility as a function of the time delay is called the optical coherence function[1,2]. In general, the function is determined by the optical spectral characteristics of the light source. We have shown that the function can arbitrarily be synthesized by modulating both the frequency of a laser source and the phase in one arm[1,2]. By using the synthesized coherence function shapes, we have proposed and developed various distributed sensing systems.

3. FIBER BRILLOUIN OPTICAL CORRELATION DOMAIN ANALYSES FOR DISTRIBUTED STRAIN SENSING

3.1 Principle and Functions

Distributed strain sensing based on Brillouin scattering in an optical fiber is an promising technique[3,4] as the fiber optic nerve system. Brillouin scattering has a frequency of about 11GHz down-shifted from the input lightwave. The frequency shift is changed by longitudinal strain applied to the fiber. The techniques developed so far, however, have a spatial resolution limit of about 1 meter. Optical spectrum width of the lightwave for generating Brillouin scattering has to be narrower than that of the Brillouin gain spectrum (BGS). Since the typical BGS width is 30MHz, the practical limit of the spatial resolution in the pulse-based systems turns out to be 1m[3,4]. Additionally, the pulse-based systems require several minutes of measurement time, because the back scattered power in a single pulse is quite tiny.

To improve the resolution and the sampling rate, we have proposed and developed a technique, “Brillouin Optical Correlation Domain Analysis; B-OCDA”[5-7]. It is based on control of the correlation between the pump and

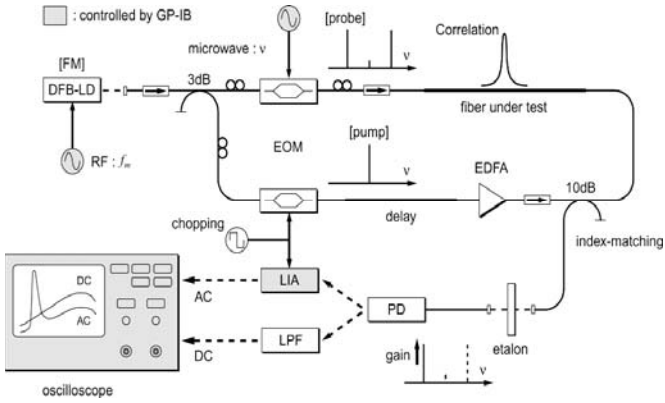

Figure 1. Brillouin optical correlation domain analysis [3,4].

probe continuous lightwaves, which excite the Stimulated Brillouin Scattering (SBS). Figure 1 shows the proposed system[5-7]. One output of the coupler, serving as the pump, is chopped by an electro-optic modulator (EOM) with a radio frequency, and launched into the fiber under test. The other output is modulated by another EOM with a microwave frequency ν, so that sidebands are generated around the incident lightwave of a frequency ν_0[4]. The first lower sideband at $\nu_0 - \nu$, serving as the probe, propagates against the pump in the fiber and reached the detector.

It is the point in our system that the pump and the probe are identically frequency-modulated at the LD. As a result, SBS occurs exclusively at the correlation peak position, where the two lightwaves are highly correlated. We can shift the correlation peak along the fiber by simply changing the FM frequency f_m. The increase in the probe power due to the Brillouin gain is detected by a lock-in amplifier. We obtain BGS by varying the frequency ν. Then the BGS distribution is obtained.

By using the BOCDA system, we have already demonstrated 1cm spatial resolution[5-8], and 57hz sampling rate[9-12].

3.2 Crack Detection in Concrete

Figure 2(a) shows the experimental setup for crack detection with a surface-bonded fiber, using the BOCDA system[13]. The 60-cm concrete specimen was loaded in the middle to generate cracks, at an interval of 10cm, along its 2 planes of weakness. The vertical displacement d of its midpoint was measured using displacement gauges. A UV resin coated SMF, that was surface-bonded to the underside of the 60-cm concrete specimen using an epoxy adhesive, was used as the sensing fiber in the experiment.

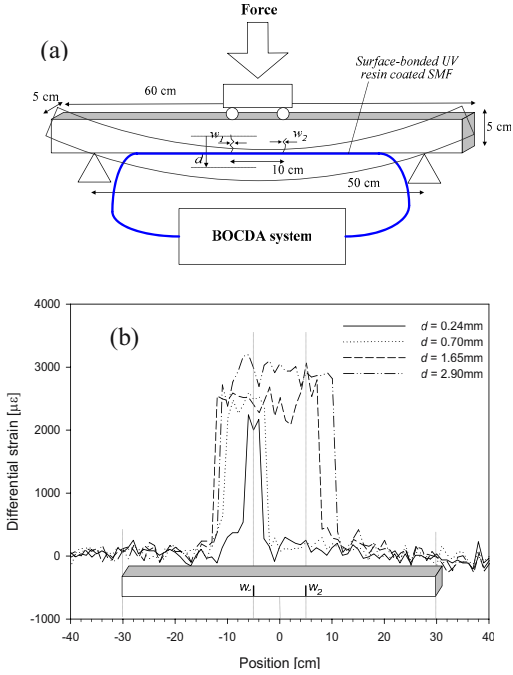

Figure 2. Experimental setup for crack detection with surface-bonded fiber using the BOCDA system (a), and distributed strain profiles measured along the 60-cm conc-rete specimen as a function of vertical displacement d (b) [13]. (with Shimizu Corp.)

Distributed strain profiles were measured along the concrete specimen using the BOCDA system with a 2-cm spatial resolution, as the concrete specimen was progressively loaded. The strain profiles along the concrete specimen are shown, corresponding to the crack widths, in Fig. 2(b)[13]. At small vertical displacements d of less than 0.5mm, a single crack at position -5cm from the midpoint was observed. Correspondingly, a well defined and sharp Brillouin frequency shift was observed at that position.

As the crack width increased to about 0.7mm, the strain distribution was observed to disperse over a range of about 10cm. When the vertical displacement d was further increased above 1mm, a second crack was observed at a position 5cm from the midpoint. Instead of observing two sharp peaks at about the ±5cm position, a uniform strain deviation was observed over a range of about 20cm [13].

3.3 Dynamic Strain Measurement of a Building Model

Figure 3(a) shows an illustration of the 2-storey building models used in the dynamic strain measurements[14]. A Kobe earthquake waveform was applied, and the dynamic strain response measured at the two positions are

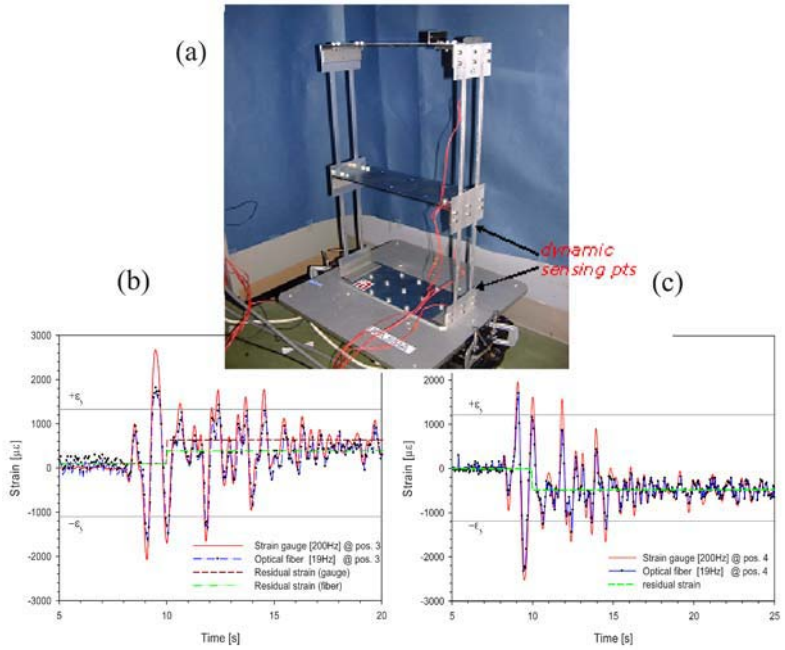

Figure 3. Experimental setup with a building model having two storey (a), and measured strain-time waveform at two positions when a Kobe earthquake waveform was applied to the model (b and c) [14]. (with Kajima Corp.)

shown in Figs. 3(b) and (c) [14]. Here, we can see that the instantaneous peak strain value greatly exceeds the yielding strain, resulting in the accumulation of residual strain.

We have also measured the distributed residual strain.

By the BOCDA system, both the distributed strain information with cm-order spatial resolution and the dynamic response of the structure can be obtained.

3.4 Simplified System with Time-Division Pump and Prove Generation

Fig. 4 shows the configuration of the simplified BOCDA system, where we use the direct frequency modulation of the LD to generate the pump and probe lightwaves in time domain[15]. We modulate the emission frequency of LD as shown in Fig. 4 (a), which is summation of the rectangular wave component (b) and the sinusoidal wave component (c). The rectangular wave component makes the pump and probe lightwaves alternatively. The frequency difference between the two is linearly swept by changing the modulation amplitude, so that the BGS profile is obtained. The sinusoidal

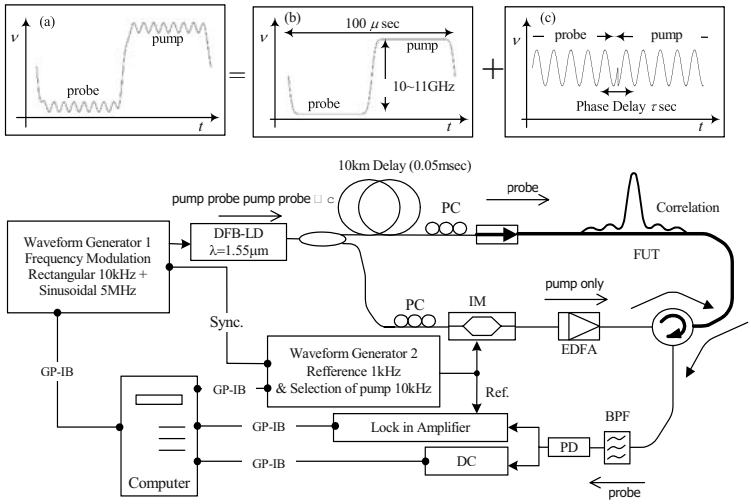

Figure 4. Experimental setup of the simplified BOCDA system [15]. (a)Total waveform for the LD frequency modulation, (b) rectangular waveform for the time division pump-probe generation, and (c) sinusoidal modulation for generating the correlation peak.

wave component modulates the pump and probe synchronously to generate the correlation peak, and a phase delay, at the point sifting from the probe to the pump, makes it possible to sweep the peak position (Fig. 4 (c)) [15].

We have estimated and compensated the RF transfer function of the LD (λ = 1.55μm) and the driver circuit for the rectangular modulation of the LD. We have successfully synthesized the waveform to generate ideal rectangular frequency modulation, and obtained a strain distribution with a spatial resolution higher than 10cm[15-17].

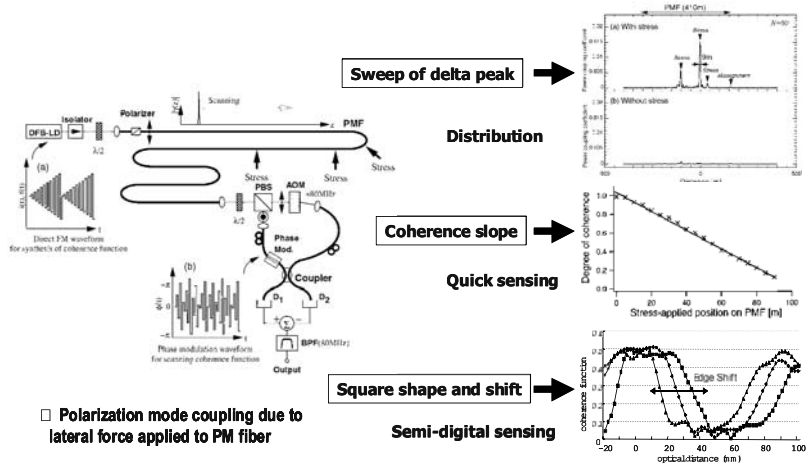

Figure 5. Distributed fiber-optic lateral force sensing by synthesis of optical coherence function [19-23].

3.5 Temporal Gating Scheme for Enlargement of Measurement Range

Measurement range is restricted to be about 10m in the basic BOCDA system, because of the periodical nature of the correlation peaks. We have developed methods to enlarge the measurement range of the BOCDA[6,10]. Recently, we have additionally developed a new way, in which a relatively wide pulse is used to select only one peak[18]. We have measured the Brillouin gain spectrum distribution along a 100-m long DSF with about 10cm resolution[18].

4. DISTRIBUTED FORCE SENSING FOR SMART STRUCTURES AND SECURITY SYSTEMS

Applying the SOCF technique to polarization mode coupling in a high birefringent optical fiber, a distributed fiber-optic lateral force sensing can be realized[19-23]. The basic setup is shown in Fig.5[19]. A continuous lightwave from a LD is linearly polarized, and excites one polarization mode of the PM fiber. When the stress is applied on the PM fiber, the orthogonal polarization mode is induced at the point. The two polarization modes are separated by the polarization beam splitter, and interfered with each other. The orthogonal polarization has a time delay linearly dependent on the stress-applied point.

By synthesizing and scanning the coherence peak, the distribution of the mode coupling coeffi-cient can be directly obtained. The lateral force distribution measured by this measurement mode is shown at the top of the right side in Fig.11 The resolution is im-proved by using lasers with wider

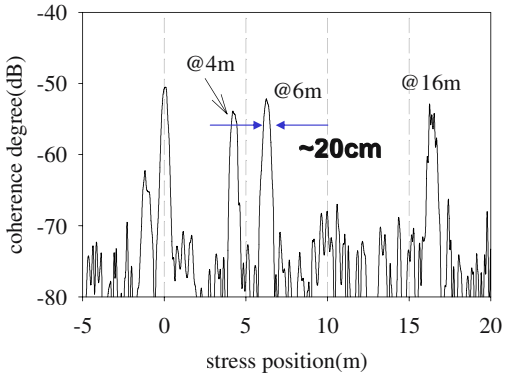

Figure 6. Demonstration of 20cm spatial resolution with a widely tunable SSG-DBR-DL light source [21].

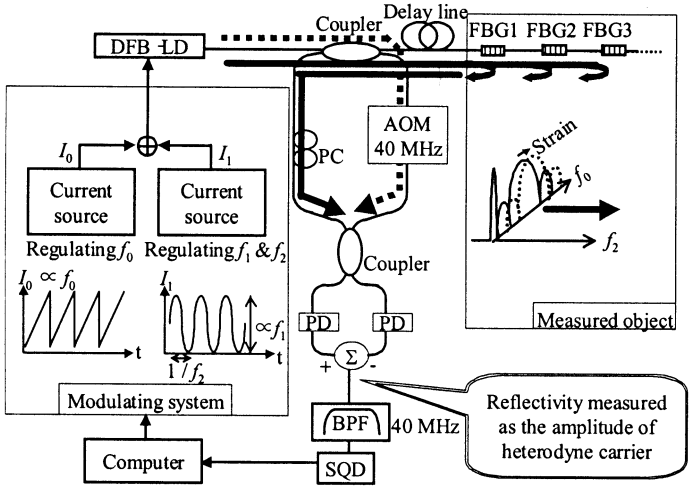

Figure 7. Setup for multi-point strain measurement by fiber gratings with the same Bragg wavelength by synthesis of optical coherence function [24,25].

tenability [20]. Recently, we adopted a super structure grating DBR laser diode (SSG-DBR LD), and obtained 20cm spatial resolution[21].

We have also proposed other measurement modes, as shown in Fig. 5.

5. MULTIPLEXING SCHEME OF FIBER BRAGG GRATING SENSORS WITH SAME BRAGG WAVELENGTH

Fiber Bragg grating multiplexed strain sensing has been widely studied. However, wavelength division multiplexing scheme, which have mainly been used, has a drawbacks. We need different kinds of FBGs. The number

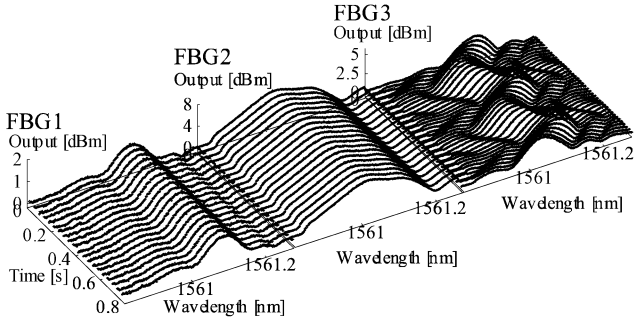

Figure 8. Simultaneous and dynamic FBG spectrum measurement with random access function [25].

of FBGs multiplexed is limited to be about 10, because of a finite band width of the source for the WDM measurement.

We have proposed a scheme, in which the FBGs with the same Bragg wavelength can be multiplexed by using SOCF scheme[24]. Fig.7 shows the setup. Location of the coherence peak, synthesized by a simple sinusoidal frequency modulation, is tuned so that one FBG is selected, and the center frequency f_0 of the LD is swept to measure the FBG reflection spectrum.

Recently, dynamic strain measurement has been demonstrated in this configuration with a function of random access to FBGs and with 100Hz sampling rate [25,26], as shown in Fig.8.

6. CONCLUSION

Without using any mechanical moving parts nor calculation, distributed sensing function can be provided by the optical correlation domain technique. We have, for example, developed a system to measure the strain distribution along an optical fiber through the Brillouin scattering, which has already achieved 1cm spatial resolution and 57Hz sampling rate.

REFERENCES

1. K. Hotate, “Fiber Sensor Technology Today,” Optical Fiber Technology (Academic Press), 356-402 (March 1998) <Invited>.
2. K. Hotate, “Application of synthesized coherence function to distributed optical sensing,” IOP Measurement Science and Technol., 13(11), 1746-1755 (2002).
3. T. Horiguchi, A. Rogers, W. C. Michie, G. Stewart, and B. Culshaw, a chapter in “Optical Fiber Sensors IV”, Ed. J.Dakin and B.Culshaw, Artech House, 309-368 (1997).
4. L. Thévenaz, a Chapter in “Trends in Optical Non- Destructive Testing and Inspection,” Ed. P. Rastogi and D. Inaudi, Elsevier, 447-458 (2000).
5. K. Hotate and T. Hasegawa, “Measurement of Brillouin gain spectrum distribution along an optical fiber using a correlation-based technique –Proposal, experiment and simulation-,” IEICE Trans. on Electronics, Vol.E83(3), 405-412 (2000).
6. K. Hotate and M. Tanaka, “Correlation-based continuous-wave technique for fiber optic distributed strain measurement using Brillouin scattering with cm-order spatial resolution □Applications to smart materials□,” IEICE Trans. on Electronics, E84-C(12), 1823-1828 (2001) <Invited>.
7. K. Hotate and M. Tanaka, “Distributed fiber Brillouin strain sensing with 1cm spatial resolution by correlation-based continuous-wave Technique,” IEEE Photon. Technol. Lett., 14(2), 179-181 (2002).
8. M. Tanaka and K. Hotate, “Application of correlation-based continuous-wave technique for fiber Brillouin sensing to measurement of strain distribution on a small size material,” IEEE Photon. Technol. Lett., 14(5), 675-677 (2002).
9. K. Hotate and S.S.L. Ong, “Distributed dynamic strain measurement using a correlation-based Brillouin sensing system,” IEEE Photon. Technol. Lett., 15(2), 272-274 (2003).

10. K. Hotate and S.S.L. Ong, “Dynamic strain measurement at 50Hz using a Brillouin optical correlation domain analysis based fiber optic sensor,” Proc. SPIE Photonics Asia, Shanghai, 4920-51, 299-310 (Dec. 2002) <Invited>.
11. S.S.L. Ong and K. Hotate, “Correlation-based Burillouin optical sensor for dynamic strain monitoring,” Proc. in CLEO/QELS 2003, Baltimore (June 2003).
12. S.S.L. Ong and K. Hotate, “Dynamic strain measurement at 50Hz using a Brillouin optical correlation domain analysis based fiber optic sensor,” Proc. in CLEO/Pacific Rim 2003, Shanghai (Dec. 2003).
13. S.S.L. Ong, H. Kumagai, H. Iwaki and K. Hotate, “Crack detection in concrete using a Brillouin optical correlation domain analysis based fiber optic distributed strain sensor,” Proc. in 16th Intern. Conf. on Optical Fiber Sensors (OFS-16), Nara, We3-3 (Oct. 2003).
14. S.S.L. Ong, M. Imai, Y. Sako, Y. Miyamoto, S. Miura and K. Hotate, “Dynamic strain measurement and damage assessment of a Building model using a Brillouin optical correlation domain analysis based distributed strain sensor,” Proc. in OFS-16, Nara, We3-2 (Oct. 2003).
15. K. Hotate and T. Yamauchi, “Simplified system of fiber Brillouin optical correlation domain analysis for distributed strain sensing,”Proc. in OFS-16, Nara We2-3 (Oct. 2003).
16. T. Yamauchi and K. Hotate, “Distributed and dynamic strain measurement by BOCDA with time-division pump-probe generation scheme,” Proc. in the 2004 CLEO/IQEC, CWA57, San Francisco (May 2004).
17. T. Yamauchi and K. Hotate, “BOTDA fiber strain sensing system with pump-probe time-division generation scheme,” Proc. in OECC/COIN 2004, Yokohama, 15D3-5 (July 2004).
18. M. Kannou, S.Adachi and K. Hotate, “Temporal gating scheme for enlargement of measurement range of Burillouin optical correlation domain analysis for optical fiber distributed strain measurement,” Proc. in OFS-16, Nara, We3-1 (Oct. 2003)
19. T. Saida and K. Hotate, “Distributed fiber optic stress sensor by synthesis of the optical coherence function,” IEEE Photon. Technol. Lett., 9(4), 484-486 (1997).
20. Z.-Y. He and K. Hotate, “Distributed fiber-optic stress-location measurement by arbitrary shaping of optical coherence function,” J. of Lightwave Technol., 20(9), 1715-1723 (2002).
21. K. Hotate and K. Makino, “High spatial resolution fiber optic distributed force sensing with synthesis of optical coherence function,” Proc. in SPIE Photonics East, Rhode Island, 5272-23 (Oct. 2003).
22. K. Hotate, X. Song and Z.-Y. He, “Stress-location measurement along an optical fiber by synthesis of triangle-shape optical coherence function,” IEEE Photon. Technol. Lett., 13(3), 233-235 (2001).
23. K. Hotate, A. Kuramoto and Z. He, “Optical fiber stress-location measurement by synthesis of binary optical coherence function,” IEEE Photon. Technol. Lett., 16(2), 578-580 (2004)
24. K. Hotate, M. Enyama, S. Yamashita, Y. Nasu, “A multiplexing technique of fiber Bragg grating sensors with the same reflection wavelength by the synthesis of optical coherence function,” Measurement Science and Technol., 15(1), 148-153, 2004.
25. K. Hotate and M. Enyama, “Dynamic strain measurement by FBG sensing system with synthesis of optical coherence function,” Proc. in 16th Intern. Conf. on Optical Fiber Sensors (OFS-16), Nara, Th1-2 (Oct. 2003).
26. M. Enyama, Z. He and K. Hotate: “Expansion of spatial measurement range by use of Vernier effect in fiber bragg grating strain sensing system with synthesis of optical coherence function,” Proc. in OECC/COIN2004, Yokohama, 15D3-4 (July 2004).

USE OF ACTIVE SENSORS FOR HEALTH MONITORING OF TRANSPORTATION INFRASTRUCTURE

Soheil Nazarian
The Universityof Texas at El Paso, El Paso, TX, USA 79968

Abstract: Even though the use of innovative passive sensors is very desirable for health monitoring of infrastructure, the use of active sensors is also desirable for use on older infrastructure. The theoretical background and recent advancements in real-time implementation of active sensors and methods for real time implementation of them are discussed here. A case study is included to demonstrate the usefulness of the methods.

Key words: Health Monitoring, Active Sensors, Ultrasonic Techniques.

1. INTRODUCTION

The use of active sensors for nondestructive tests based on wave propagation theory for diagnosis of infrastructure is increasing. One of the advantages of the wave propagation techniques is that fundamental material properties are measured. These methods are especially useful in determining the stiffness and thickness of the structural members as well as detecting and locating defects within them.

If used for material characterization, these methods typically rely on determining the stiffness (moduli) of different layers by either measuring the compression wave velocity, V_p, or the shear wave velocity, V_s, of each material. Young's modulus, E, is determined from

$$E = \rho (V_p)^2 \quad (1)$$

Farhad Ansari (ed.), Sensing Issues in Civil Structural Health Monitoring, 229–238.

Parameter ρ is the mass density of the material, which can be estimated or measured. Poisson's ratio, ν, can be determined from

$$\nu = [1 - 0.5 (V_s / V_p)^2] / (1 - (V_s / V_p)^2]. \quad (2)$$

Alternatively, the compression wave velocity can be determined from shear wave velocity if an estimated Poisson's ratio is input in Equation 2.

2. TESTING METHODOLOGIES

Two or three different methods are typically used in diagnostics of infrastructure. The methods include: 1. Impact Echo, 2. Ultrasonic Body Wave, and 3. Ultrasonic Surface Wave. Each method is briefly described here.

2.1 Impact-Echo (IE) Method

The impact-echo method can effectively locate defects, voids, cracks, and zones of deterioration within concrete [**1**]. In the Impact-Echo method, a high-frequency disturbance is imparted to the surface of the member, and the reflection of the disturbance from the bottom of the deck or a delamination is obtained.

The solution has been demonstrated to be simple in the frequency domain, where the depth-to-reflector, T, can be determined from:

$$T = V_p / 2f. \quad (3)$$

Parameter f is the resonant (return) frequency obtained by transforming the deformation record into the frequency domain. The compression wave velocity of concrete, Vp, has to be measured independently or has to be estimated.

A typical frequency-response spectrum is shown in Fig. 1. The major peak (at about 10 kHz) corresponds to the thickness of the layer and is called the return (resonant) frequency which is input in Equation 3.

2.2 Ultrasonic-Body-Wave (UBW) Measurement

The goal of this method is to independently measure the compression wave velocity of the infrastructure. Compression waves travel faster than any other type of seismic wave, and are detected first on seismic records.

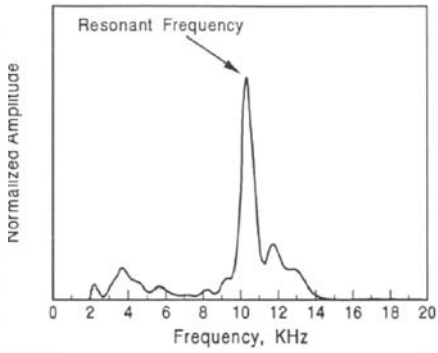

Figure 1. Typical Amplitude Spectrum from IE

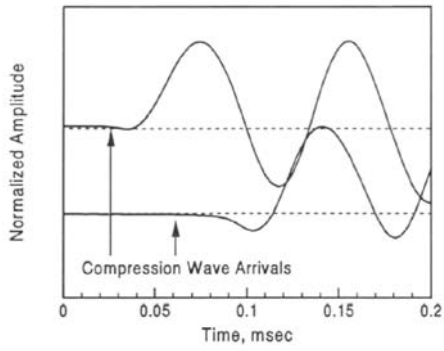

Figure 2. Typical Time Record

To perform the test a high frequency source and one or more receivers are used. Typical travel times, measured at two spacings from the source are shown in Fig. 2. The arrow in each record corresponds to the arrival of these waves.

An automated technique for determining the arrival of V_p have been developed based on triggering on an amplitude range within a time window [**2**].

2.3 Ultrasonic-Surface-Wave (USW) Method

With the ultrasonic-surface-wave method the properties of any material can be easily and directly determined without a complex inversion algorithm. To implement the method, a high-frequency source and two or more receivers are utilized. At wavelengths less than the thickness of the uppermost layer, the velocity of propagation is independent of wavelength. Therefore, if one simply generates high-frequency (short-wavelength) waves, the shear wave velocity, V_s of the top layer can be determined from

$$V_s = (1.13 - 0.16\nu)\,(360D / m) \qquad (4)$$

Parameter m (deg/Hz) is the least-squares fit slope of the phase of the transfer function in the high-frequency range.

A typical phase spectrum is shown in Fig. 3a. The shear wave velocity of the layer can be obtained using a complex-valued curve-fitting process with the coherence as the weighing function [**3**]. The actual and fitted curves compare quite favorably as shown in Fig. 3a. In the next step, the phase is "unwrapped"; that is, the appropriate number of cycles is added to each phase as shown in Fig. 3b. The slope of the line, which is basically constant with frequency, is used in Equation 4.

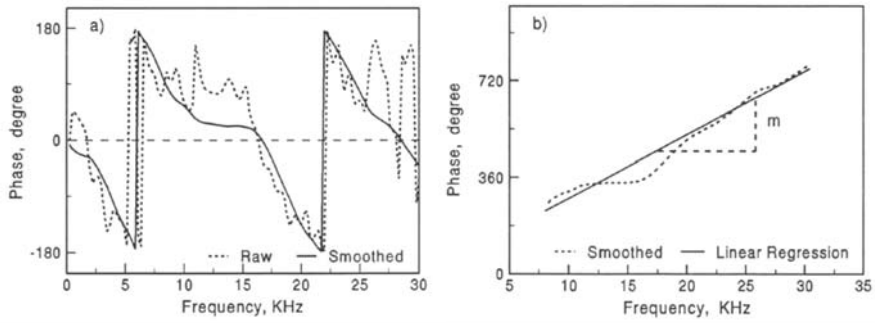

Figure 3. Typical Spectral Functions from USW Method
a) Wrapped Phase, b) Unwrapped Phase

3. EQUIPMENT

A typical device for conducting such tests consists of two transducers and a source. The sensors can be packaged into a hand portable system that can rapidly perform the Ultrasonic Body Wave, Ultrasonic Surface Wave and Impact Echo tests. One such device for conducting tests automatically is shown in Fig. 4. A computer is tethered to a hand-carried transducer unit through a cable that carries power to the accelerometers and hammer and returns the measured signals to the computer.

Several distinct advantages of the device: are the integration of the three independent methods in one system so that comprehensive diagnostics can be performed; capabilities for signal enhancement by averaging (stacking) signals for higher quality data; and real-time data reduction capabilities.

The collection, preliminary reduction and archiving of data take about 15 sec. Tests are typically carried out using a grid pattern. A 1-m square grid is typically used. Since these seismic methods can distinguish the onset of deterioration much earlier than chain dragging, such a test interval seems to be reasonable. However, depending upon the philosophy of the agency using the device, the grid pattern can be modified.

4. CASE STUDY

The results from tests on one bridge are described in this section. The bridge tested, as shown in Fig. 5, was about 64 m long and about 8.5 m wide. Tests were carried out on the southbound lane of the bridge, along four lines

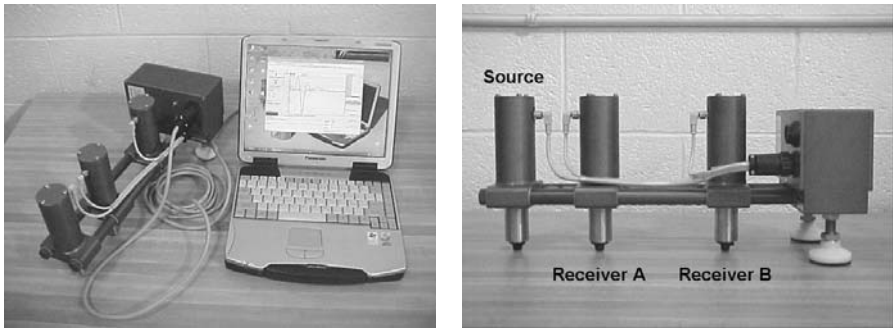

Figure 4. Automatic Device for Field Testing

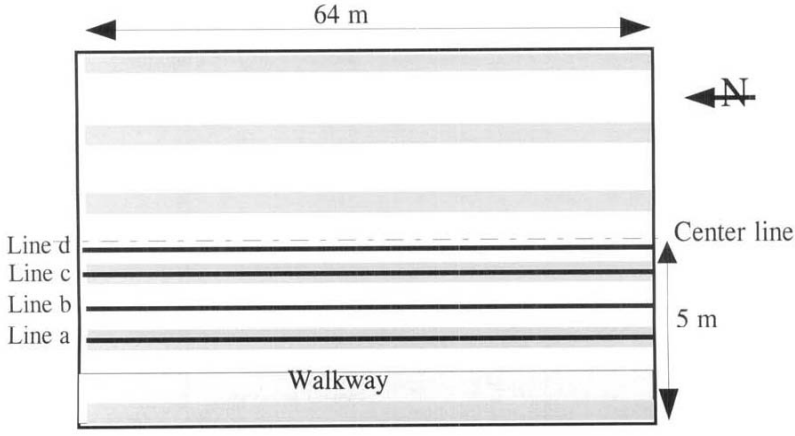

Figure 5. Schematic of Bridge Deck Tested

at 1-m intervals. One test line (Line d) was located about the center line of the bridge, while the other three lines were 1 m (Line c), 2 m (Line b), and 3 m (Line a) to the west of the centerline. Lines a and c were located on girders. The deck was not covered with asphalt; however, the methods should be applicable to asphalt-covered decks as long as an intimate contact between the asphalt and concrete exists.

The impact-echo method was the primary method used to identify delaminated areas. This can be easily done by observing the pattern of the distribution of energy in the amplitude spectrum of each record after it is transformed into the frequency domain. Four levels of delamination were qualified:

Very Bad: the separation between concrete has occurred and an air pocket exists

Bad: the delamination has most probably occurred, however grain-to-grain contact between the concrete exists

Marginal: the concrete is in contact but the signs of delamination as some depth are evident.

Intact: the concrete is well bonded.

Typical frequency-domain representations of the four scenarios are shown in Fig. 6. For a "Very Bad" location (see Fig. 6a), the energy is concentrated at low frequencies. This is representative of the bending (drum-like) mode of vibration of a shallow delaminated area. The drum-like vibration can be easily heard during chain dragging of the bridge decks; and as such can be readily identified. For a "Bad" location (see Fig. 6b), the energy is shifted towards lower frequencies; however, one can still detect a peak corresponding to the return frequency of the slab. In other words, the bending mode is not very dominant because some degree of contact still exists. These types of defects, depending on the ambient and traffic noise level and the level of contact, may or may not be detectable by the chain-dragging operation.

A "Marginal" location as shown in Fig. 6c, exhibits two distinct peaks in the amplitude spectrum, one corresponding to the thickness of the slab and one corresponding to a depth where the delamination is about to occur. These can typically not be determined by chain-dragging operation.

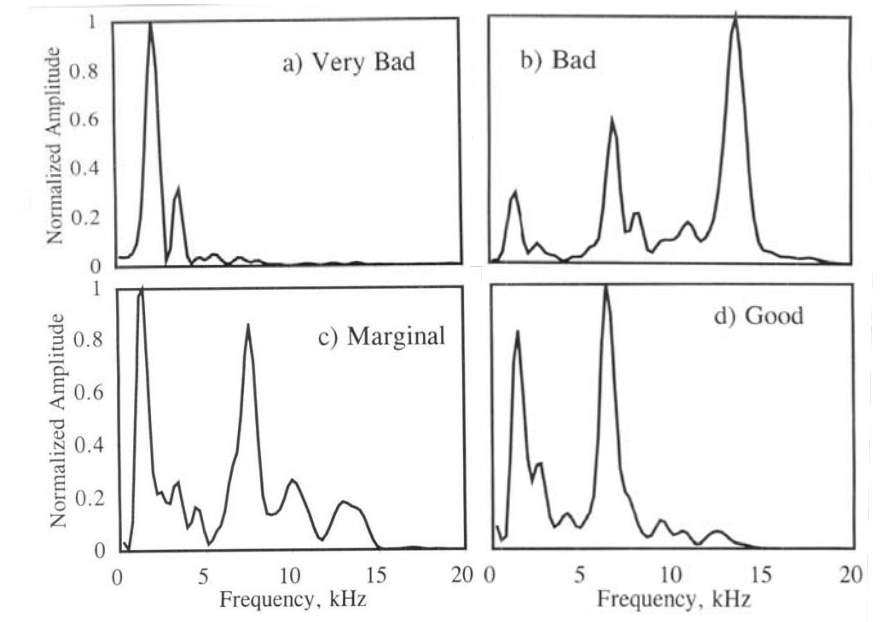

Figure 6. Typical Responses from IE Method

Finally, an intact point, exhibit only one distinct peak corresponding to the thickness of the slab (see Fig. 6d). One exception is when the intact point is located on top of the girder. In that case, depending on the shape of the girder and the bond between the slab and the girder, two peaks may be detected. One peak corresponds to the thickness of the slab and other to a reflection from the girder.

This rating scheme was used to determine the degree of delamination of the bridge. The delamination potential of the southbound lane of the bridge is mapped in Fig. 7a. The delamination is concentrated around the first 8 m, about 20 m and about 45 m and about 64 m (from the north edge of the bridge).

The quality of concrete can be assessed from compression wave velocities. Typically, the compression wave velocity of a concrete varies from 3000 m/sec to 4000 m/sec. Any value below this level is an indication of severe cracked concrete or severely deteriorated concrete. Occasionally, very large compression wave velocities are measured. This situation happens when a significant crack exists between the receiver 1 and the source and not between the receiver 2 and source. The crack causes a delay in the arrival of the compression wave to the first receiver, as such the difference in the traveltime will be unrealistically small, and hence the velocity unrealistically high. The assessment of the quality of the concrete at the bridge is summarized in Fig. 7b. On the average, the compression wave velocity of this bridge was estimated at about 3600 m/sec. The white area

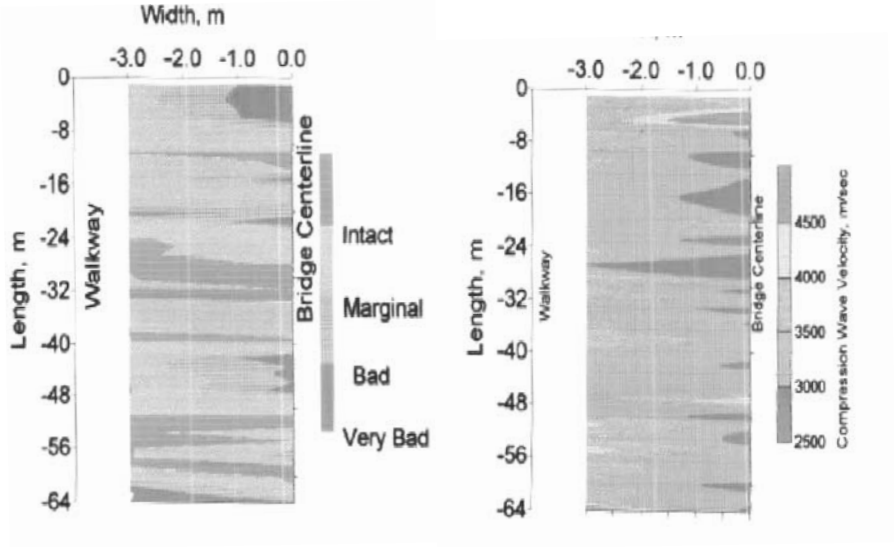

a) Delamination Assessment b) Velocity Variation

Figure 7. Condition Rating of Bridge Deck

around 5 m corresponds to the case where the velocity is exceptionally high. In general the concrete located near the walkway is in better condition than the areas closer to the centerline.

The major reflectors of seismic energy, which typically correspond to the thickness of the slab or depth of delamination, can also be identified. As reflected in Equation 2, the depth to reflector is inversely proportional to the return frequency. Therefore, if one identifies the return frequency(ies), the depth(s) of reflectors can be easily identified. Traditionally, the amplitude spectra from all measurements are individually used to determine the return frequency.

It would be significantly easier if one transform the frequency axis to depth using Equation 3. Such a contour map is shown in Fig. 8. The average velocity along the bridge was used to calculate the thickness.

Line a contains two reflectors. The reflector, which is about 180 mm deep, may be from the bottom of the slab. The other reflector from a depth of about 330 mm is probably from the girder which was located under the test line.

Line b contains a defective area in the first 4 m to 5 m of the section, after which the slab seems to be intact. Anomalous points can be detected in the areas located from 25 m to 35 m from the north edge. The slab seems to be about 180 mm to 190 mm thick.

The first 15 m of Line c (especially the first 8 m) seems to contain a delamination at a depth of about 140 mm. A deep reflection because of the presence of the girder under this line is again present.

For Line d, the areas contained by the first 8 m, around 20 m, and 40 m to 50 m are delaminated. The slab is about 180 mm to 200 mm thick. Onset of delamination at a depth of about 130 mm can be observed in a large area of this line.

In summary, the defect contours of Fig. 7 are quite useful in detecting the general areas that are defective. However, the depth contours similar to Fig. 8 can be used to get a detailed description of the slab along a certain line. Shortly after these tests, the bridge deck was destructively evaluated. The results from the seismic tests confirmed well with the in situ condition.

5. CONCLUSIONS

Active seismic methods, as methods for diagnosis of bridge decks are presented here. The seismic methods effectively estimate the modulus and thickness of the concrete, and locate positions that are delaminated. A rapid field device is commercially available that can perform appropriate field tests.

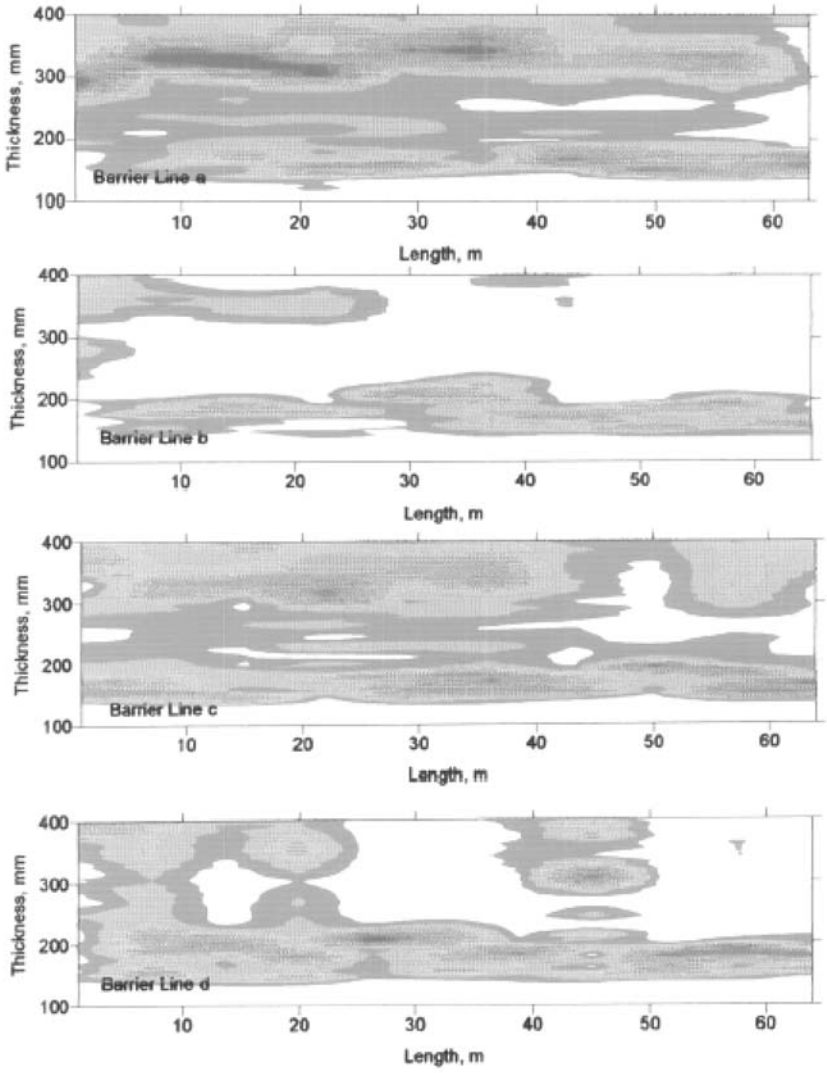

Figure 8. Thickness Contour for Bridge Deck

REFERENCES

1. Sansalone, M. and Carino N.J., " Detecting Delaminations in Concrete Slabs With And Without Overlays Using the Impact-Echo Method," ACI Materials Journal, vol. 86, no. 2, pp 175-184, 1989.
2. Nazarian, S., Baker, M., and Crain, K., "Assessing Quality of Concrete with Wave Propagation Techniques," ACI Materials Journal, vol. 94, no. 4, pp. 296-306, 1997.
3. Nazarian, S. and Desai, M.R., "Automated Surface Wave Method: Field Testing," ASCE Journal of Geotechnical Engineering, vol. 119 no. 7, pp 1094-11, 1993.

HEALTH MONITORING OF CONCRETE STRUCTURES USING SELF-DIAGNOSIS MATERIALS

Hiroshi Inada, Yoshiki Okuhara, and Hitoshi Kumagai
Ohsaki Research Institute, Japan Fine Ceramics Center, Shimizu Corporation, Japan

Abstract: The authors have been continuously conducting a series of research on the development of the fiber reinforced composites as self-diagnosis materials. The fiber reinforced composite, which is the glass fiber reinforced plastics containing carbon particles to give electrical conductivity, has been confirmed to possess excellent sensitivity as self-diagnosis material. With the aim of developing the technology for maintaining safety of civil infrastructures, several types of self-diagnosis materials have been developed for the monitoring sensor to detect damage to structures. Subsequently, the applicability of the self-diagnosis materials for the monitoring of the integrity of structures has been evaluated through experimental studies. In this paper, the performance of the proposed self-diagnosis materials to detect damage to concrete structures is discussed in detail.

Key words: health monitoring, sensor, carbon particle, concrete

1. INTRODUCTION

In recent years, structural health monitoring techniques to detect deterioration or damage to the structures using sensors are attracting wide attention. In Japan, particularly, deterioration of infrastructures such as bridges, tunnels and energy plants has become a social problem, and demands for sophisticated health monitoring systems are growing stronger. Especially, an urgent need for the development of effective monitoring techniques to detect damage to concrete structures has been pointed out. Therefore, several types of monitoring systems using high technology such as fiber optic sensors, piezoelectric transducers and MEMS sensor have been

Farhad Ansari (ed.), Sensing Issues in Civil Structural Health Monitoring, 239–248.

proposed and investigated by a number of researchers. Although some of those developed systems have been demonstrated to possess satisfactory performance as a structural monitoring sensor, difficulties have also been indicated in regards to their cost or practical applicability. In the meantime, the monitoring sensors using carbon materials have also been proposed and investigated by several researchers. Muto et al. have proposed carbon fiber glass fiber reinforced plastics (CFGFRP) as structural materials with the ability to monitor fatal fracture of the structures [1]. The sensor, known as intelligent materials or self-diagnosis materials, is based on the electrical conductivity of carbon materials, and has advantages of being easy to operate and being economical in the measurement. One of the authors has developed the monitoring techniques using carbon fiber, and demonstrated its practical applicability to the monitoring of concrete piles [2], [3]. On the other hand, another author has continuously carried out the experimental studies on the performance of the self-diagnosis materials using carbon particles [4].

Recently, the authors have conducted research project on the development of the self-diagnosis materials as a monitoring sensor and its application for monitoring civil infrastructures. The applicability of the materials for monitoring the integrity of structures has been evaluated through experimental studies [5], [6]. In this paper, characteristics and performance of the proposed self-diagnosis materials to detect damage to reinforced concrete (RC) structures are discussed in detail on the basis of the obtained experimental results.

2. SELF-DIAGNOSIS MATERIALS

In the previous studies, the electrically conductive fiber-reinforced composite has been shown to possess the property to diagnose its integrity by increasing its electrical resistance value against the applied strain [4]. The sensor, which is named rod type sensor after its shape, serves as a monitoring sensor attached into the structures prior to casting the concrete. The characteristics as a sensor is found to depend on the property and volume fraction of the carbon particles. Originally, the graphite particle were applied to give electrical conductivity, and the sensor possessing high sensitivity to increase its electrical resistance value against the applied slight strain has been developed. The sensor, named high sensitivity sensor, responds consistently corresponding to the deformation of the target structure. Based on the following studies, the application of the nano-sized carbon black enables the sensor to possess memory function. Because the percolation structure formed from spherical carbon black causes irreversible

resistance change, the sensor shows the residual variation in its electrical resistance value corresponding to the applied maximum strain after the load is off. Therefore, the sensor, which is named maximum strain memory sensor, possesses the ability to memorize the experienced load and damage of the structures.

In this study, three types of the self-diagnosis materials as shown in Table 1 are applied as the sensor to detect damage to the structures. As mentioned above, two types of the rod type sensors have been applied. Figure 1 shows the schematic drawings of the sensors. In the rod type sensors, carbon particles are dispersed in a thermoset epoxy resin diluted by MEK (methyl ethyl ketone). The glass fiber filaments are incorporated in the mixture as an insulating part, and formed by a pultrusion process. The carbon particles form a continuous link (percolation structure) with each other. Applying tensile strain on the composite increases the electrical resistance. The graphite particles (SEC, SGP-5), having a mean diameter of 5μm, are contained in the high sensitivity sensor, and the carbon black (MITSUBISHI Chemical, 3050B) with a mean diameter of 50nm is contained in the maximum strain memory sensor, respectively. The composite with graphite particles of 10% in volume is found to monitor applied strain continuously from small range of strain [7]. The residual electrical resistance value of the maximum strain memory sensor also depends on the volume fraction of carbon black; increasing the volume fraction enhanced the ability to memorize maximum applied strain [8].

Table 1. Types of the sensors.

Name	Type	Characteristics	Carbon particle
A	Rod	High sensitivity	Graphite
B	Rod	Maximum strain memory	Carbon black
C	Film	High sensitivity	Graphite

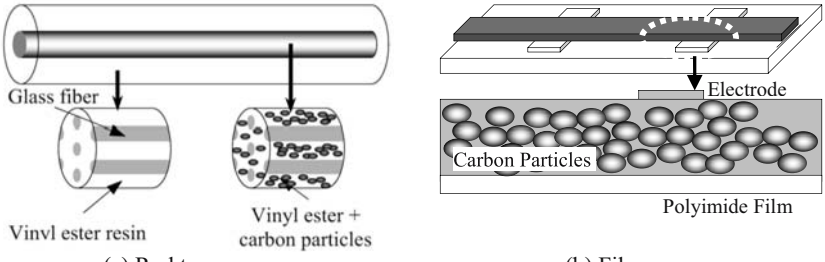

(a) Rod type sensor (b) Film sensor

Figure 1. Schematic Drawing of self-diagnosis materials.

The authors have also developed an electrically conductive film sensor bonded onto the concrete surface to detect cracks and measure crack width. Figure 1(b) shows the schematic drawing of the film sensor. The film sensor is manufactured by spraying carbon particles on the polyimide film using the screen printing technology. The volume fraction of carbon particles is 30% and the thickness of the conductive part is 10μm. The electrodes of silver foil placed at appropriate intervals enable the measurements of electrical resistance at arbitrary sections

3. BENDING TESTS OF RC COLUMN SPECIMEN

3.1 Specimen and Loading Condition

Extensive damage to the reinforced concrete (RC) pier columns of the highway viaduct was reported based on investigations following the 1995 Hyogoken-Nambu earthquake. The urgent need for the development of techniques to judge the integrity and the propriety of continued use of the damaged structure immediately after the occurrence of earthquakes has been pointed out. Then, in this study, the applicability of our developed self-diagnosis materials for monitoring damage to the RC pier columns is experimentally investigated. Figure 2(a) shows the general description of the specimen and arrangement of the sensors. The column has a height of 1.7m and a cross section of 300mm×300mm, which corresponds to the upper half part of the pier columns with nearly half size of general structures. As a result of material tests, the yielding strength of the main reinforcing bar was 369N/mm^2, and the compressive strength of the concrete was 24.5N/mm^2.

Four specimens of the same specifications were prepared. In each specimen, one high sensitivity sensor and six maximum strain memory sensors with various volume fraction of carbon particles were placed along the main reinforcing bars. The diameter of high sensitivity and the maximum strain memory sensors are 6mm and 3mm, and the lengths are 1m and 30cm, respectively. Having completed the casting and curing of concrete, a couple of film sensors with a length of 70cm were bonded onto both sides of the column using epoxy adhesive resin, as shown in the Figure 2(b). Because the electrodes have been planted at regular intervals of 20mm, the electrical resistance value in the section of arbitrary location and length can be evaluated. In this case, the electrical resistance values in 8 sections with lengths of 20, 100, 200mm have been measured. The vertical layout of the pi-shaped displacement meter corresponds to the location of high sensitivity sensors in the column.

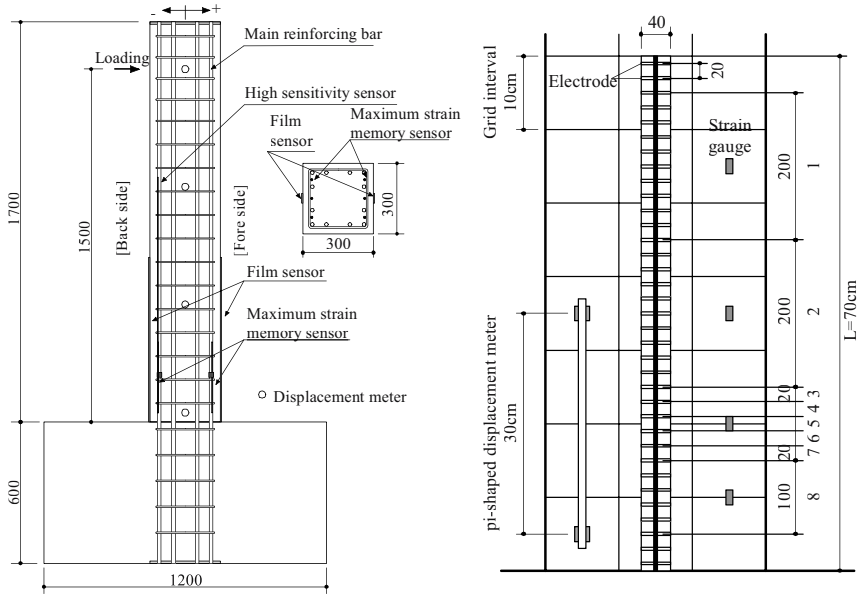

(a) Arrangement of rod type sensor (b) Layout of film sensor

Figure 2. Schematic Drawing of self-diagnosis materials.

All four specimens were subjected to quasi-static cyclic lateral loading of the same pattern. Loading and unloading were repeated while gradually increasing the maximum load symmetrically to 20, 30, and 40kN. After the reinforcing bar yielded at the load around 65kN, the load was increased until the horizontal displacement at the loading position reached 2, 3 and 4 times the displacement δ_y when the reinforcing bar yielded. In the last cycle, the load was increased up to a horizontal displacement $6\delta_y$ only in the positive direction.

3.2 Results and Discussions

The horizontal displacement at the loading position against the load for one specimen is shown in Figure 3(a). The deformation of the specimen to the positive and negative direction is almost the same, and the responses of the four specimens agree well. The initial crack appeared around 10kN, and the main reinforcing bars yielded at the load of 65kN.

Figure 3(b) shows the corresponding response of high sensitivity sensor. The variation in the electrical resistances of the sensor is illustrated as variation ratio $\Delta R/R_0$ from the initial value. The initial electrical resistances of the sensors are 38-58kΩ. The sensor is placed on the back side of the specimen in Figure 2(a), and the electrical resistance of the sensor increases

due to the tensile strain while the specimen is loaded in a positive direction. The variation in the electrical resistance during negative loading is much smaller, the sensor is found to function as tensile strain sensor. The characteristic of the variation during positive loading has a resemblance to the result of the horizontal displacement. Furthermore, the sensor responds sensitively to the deformation of the specimen even in a small range of loading. Figure 4 shows the variation ratio of electrical resistance against the maximum horizontal displacement in each cycle of loading for four specimens. The response of the sensors against the displacement agrees well, which represents the good repeatability of the sensor. And the sensor responds almost linearly against the deformation of the specimen during positive loading. The obtained results show that the high sensitivity sensor is capable of detecting consistently the deformation of the target structure in a wide range of loading.

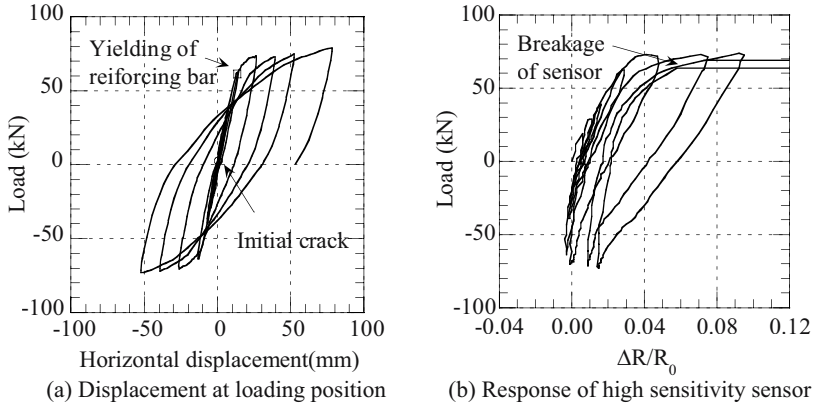

(a) Displacement at loading position (b) Response of high sensitivity sensor

Figure 3. Examples of the deformation of the specimen and response of the sensor.

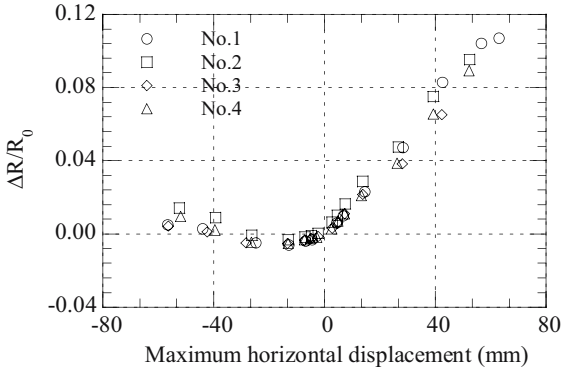

Figure 4. Relation between maximum displacement and variation ratio of electrical resistance.

Figures 5(a) and (b) show the corresponding response of the maximum strain memory sensors. The volume fractions of carbon particle are 100% and 80%, respectively. The initial electrical resistances of sensors are 800Ω and 500Ω. Both sensors are located on the back side of the specimen, and the increase in the electrical resistance during positive loading is observed. Comparing to the result of high sensitivity sensor, the decrease during the loading of negative direction is much smaller, and the residual values of electrical resistance when the load is off are considerably large. Furthermore, while the sensors suffer compressive stress during the negative loading, the electrical resistance values of the sensors do not make significant changes. The obtained results show an excellent ability of the sensor to memorize applied maximum load. Comparing the results of two sensors, the result of 100% volume fraction shows a larger variation of electrical resistance from smaller range of loading. The sensor with higher volume fraction is confirmed to possess superior ability to memorize the maximum load and damage to the structures.

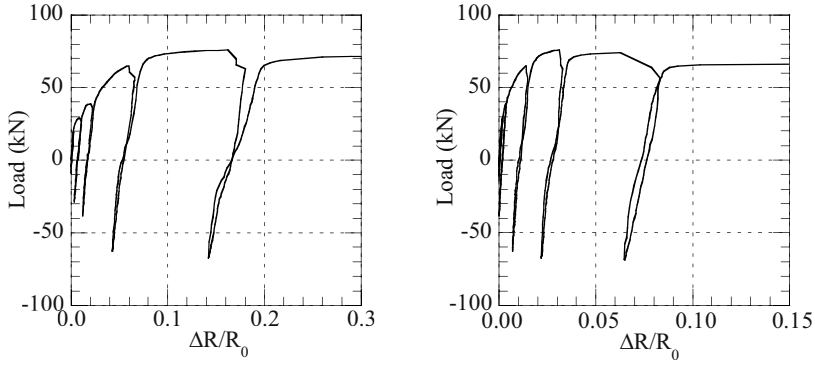

(a) Volume fraction 100% (b) Volume fraction 80%

Figure 5. Examples of the response of the maximum strain memory sensor.

Two pairs of sensors of volume fraction 100% were placed in two different specimens. As for the 4 sensors, the ability of the sensor to memorize applied deformation and damage of the structure is discussed. The relation between the maximum deformation of specimens developed during each cycle of loading and the residual variation ratio of electrical resistance of the sensor when the load is off are compared in Figure 6. Figure 6(a) shows the relation between the maximum horizontal displacement at the loading position and the residual variation ratio. Two sensors on the back side of the specimen retain the memory of positive horizontal displacement, and two on the fore side retain that of the negative displacement. The residual variation ratio can be found against slight displacement, and increases almost linearly against the applied horizontal displacement. Figure

6(b) shows the relation between the maximum vertical displacement measured by pi-shaped displacement meters and the residual variation ratio. The obtained vertical displacement corresponds to the total of the crack widths and deformation inside the gauge length of the pi-shaped displacement meter. The cracks appeared on the grid lines spaced 10cm apart, which corresponds to the location of the hoops shown in Figure 2(a). Therefore, the vertical displacement measured by the pi-shaped displacement meter represents the sum of the three crack widths. The results from the four sensors in two specimens agree well, and represent the good repeatability of the sensor. The rod type sensor of volume fraction 100% is confirmed to achieve the ability to memorize slight crack width caused to the structure.

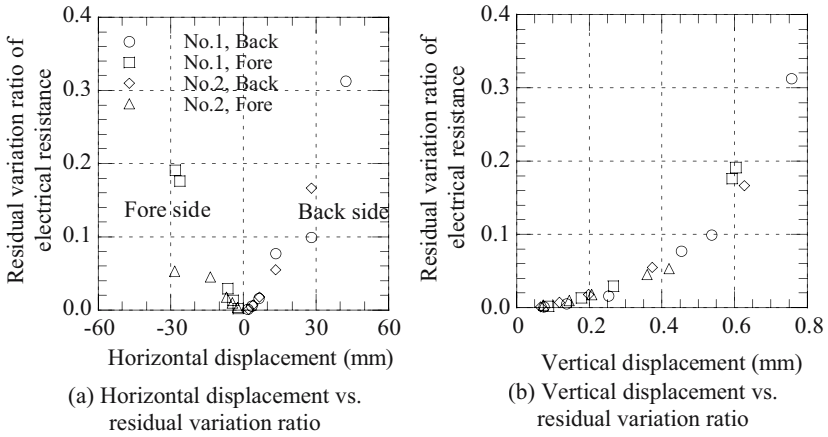

Figure 6. Relation between maximum deformation and residual variation ratio of the sensor.

As shown in Figure 2(b), the electrical resistance values in eight sections of each film sensor were measured. Here, the variations of electrical resistance in five narrow sections from section No.3 to section No.7 are evaluated. The length of each section is 2cm. The initial electrical resistance values in the reference section of 2cm, range from 125kΩ to 140kΩ. As an example of the results, the variation in electrical resistance from the initial value, ΔR, in the five sections for one side of a specimen is shown in Figure 7(a). In this case, only one crack through section No.6 has developed on the sensor. As shown in the figure, only the electrical resistance in section No.6 increases according to the progress of loading. The result illustrates that the sensor is capable of detecting the appearance of the crack and its location accurately. Moreover, the sensor was not peeled from the concrete surface until the breakage of the sensor itself. Therefore, the adhesive, which was developed for this study, is confirmed to possess the required performance.

At the maximum load in each loading cycle, the crack widths were measured by visual observation using a crack scale. Figure 7(b) shows the relation between the measured crack widths and the variations in the electrical resistance obtained in the section where the crack was located. As for the three specimens, the results in the five sections are compared. Accuracy of the measured crack width is not so high especially in the small range due to the limitation of the measurement. The obtained results of four sensors, however, show good agreement. The variation of electrical resistance increases almost linearly against the crack width.

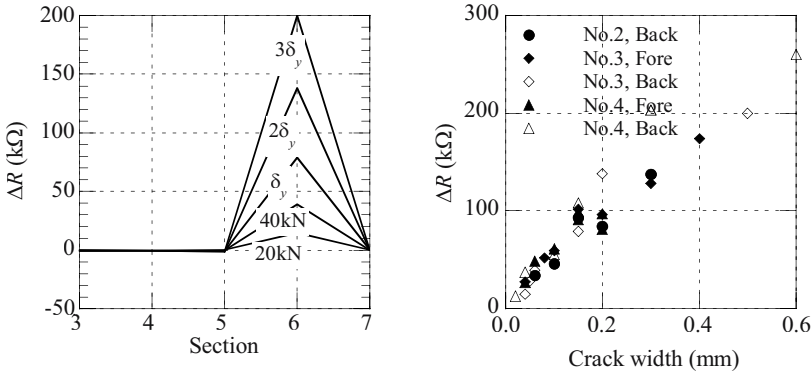

(a) Distribution ΔR in 5 section (b) ΔR vs. crack width

Figure 7. Variation in electrical resistance of film sensor.

4. CONCLUDING REMARKS

In this study, the applicability of self-diagnosis materials as a health monitoring sensor for concrete structures has been experimentally investigated. The three types of developed sensors, high sensitivity, maximum strain memory and film sensors, are demonstrated to possess excellent performance as monitoring sensor as follows:

1. The high sensitivity sensor responds almost linearly against the deformation of the specimen and shows good repeatability as a sensor.
2. The maximum strain memory sensor shows apparent irreversible electrical resistance change and possesses superior ability to memorize load and damage.
3. The film sensor can satisfactorily detect the appearance of the cracks, their location and the crack widths.

ACKNOWLEDGEMENTS

This research was conducted as a part of the “Advancement of Basic Technological Research” supported by NEDO (New Energy and Industrial Technology Development Organization), Japan.

REFERENCES

1. Muto N, Yanagida H, Nakatsuji T, Sugita M and Ohtsuka Y. "Preventing Fatal Fractures in Carbon fiber-glass fiber reinforced plastic composites by monitoring change in electrical resistance", *Journal of American Ceramics Society*, Vol.76, No.4, pp.875-879, 1993.
2. Inada H, Ishii K and Sugimura Y. "Carbon Fiber Sensor for Monitoring Integrity of Concrete Piles", *Proc. of SPIE's Smart Structures and Materials*, San Diego, CA, USA, Mar., 2003, pp.497-506.
3. Inada H, Ishii K and Sugimura Y. "Application of carbon fiber sensor for monitoring damage to concrete piles", *Proc. of 1st International Conference on Structural Health Monitoring and Intelligent Infrastructures*, Tokyo, Japan, Nov, 2003, pp.1287-1294.
4. Okuhara Y, Shin S G, Matsubara H Yanagida H and Takeda T. "Self-diagnosis Function of FRP Containing Electrically Conductive Phase", *Proc. of SPIE’s Sensory Phenomena and Measurement Instrumentation for Smart Structures and Materials*, pp.191-198, 2000.
5. Inada H, Kumagai H. and Okuhara Y. "Application of Self-Diagnosis Materials to Structural Health Monitoring for RC Slabs", *Proc. of 4th International Workshop on Structural Health Monitoring*, Stanford, CA, USA, Sept., 2003, pp.1134-1141.
6. Inada H., Kumagai H. and Okuhara Y. "Experimental Study on Structural Health Monitoring of RC Columns using Self-Diagnosis Materials", *Proc. of SPIE’s Smart Structures and Materials,* San Diego, CA, USA, Mar., 2004, pp.609-917.
7. Okuhara Y, Shin S G, Matsubara H, Yanagida H and Takeda N. "Development of Conductive FRP Containing Carbon Phase for Self-Diagnosis Structures", *Proc. of SPIE’s Smart Structures and Materials*, New Port Beach, CA, USA, Mar., 2001, pp.314-322.
8. Okuhara Y, Jang B K, Matsubara H and Sugita M. "Fiber Reinforced Composites as Self-Diagnosis Materials for Memorizing Damage Histories", *Proc. of SPIE’s Smart Structures and Materials*, San Diego, CA, USA, Mar., 2003, pp.314-322.

APPLICATION OF IMAGE ANALYSIS TO STEEL STRUCTURAL ENGINEERING

K. Tateishi and T. Hanji
Nagoya University, Japan

Abstract: We introduce three applications of the image analysis technique into steel structural engineering. The first is the surface shape measurement of corroded steel plates using digital stereography. The second and third are strain measurements by digital image analysis. In all cases, the image analysis technique works well and provides us with innovative information on mechanical behaviors of steel structures.

Key words: Image analysis, Fatigue, Corrosion, Strain measurement

1. INTRODUCTION

Recent remarkable progress in digital technology has provided great changes in research fields of steel structural engineering. Effectively using the newly developed digital techniques in measurements of steel structures in laboratory tests and field inspections, particularly the usage of digital image analysis to detect the shapes and strains of the steel structures, has become increasingly important. These measurements and analyses could provide us with substantial important information about the mechanical performances, such as durability and seismic resistance, of steel structures. In the current study, we introduce three applications of the image analysis technique to steel structural engineering. In all the cases, the digital image analysis was performed using low cost general-purpose digital cameras. The first is the surface shape measurement of corroded steel plates using digital stereography. The second and third ones are strain measurements by the digital image analysis.

Farhad Ansari (ed.), Sensing Issues in Civil Structural Health Monitoring, 249–258.

2. SURFACE MEASUREMENT OF CORRODED STEEL PLATE

We used the stereography method to measure the surface configurations of corroded steel plates[**1**]. This is a technique that can obtain the three-dimensional shape of an object by two digital images taken at different viewpoints. We applied this method to a sample specimen of corroded steel plate and compared the results with what obtained from laser displacement meter.

2.1 Measuring Method

Fig.1 illustrates the measurement system, which consists of a general-purpose digital camera and a macro lens. On the lens front, we mounted a stereo-adapter specially designed for taking a pair of images from two different viewpoints and then simultaneously recording them onto one film (CCD) on its right and left halves. The sample image taken by the system is shown in Fig.2. This system was selected because of its low cost and because it is easy to use, particularly in steel bridge inspections.

Figure 1. Camera system

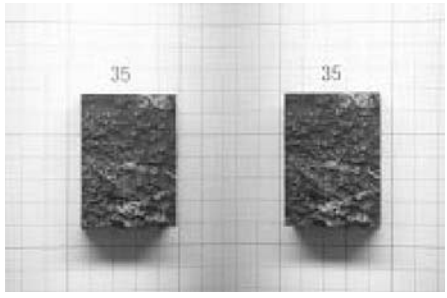

Figure 2. Example of stereo-image

A general-purpose camera has uncertainties in lens distortion and focal length. Therefore, we introduced several parameters, called orientation elements, to compensate these effects. On images taken from different positions, we can have two sets of picture coordinates for a point $P(X,Y,Z)$. The coordinates (x_L, y_L) are in the left-half of the image and (x_R, y_R) are in the right-half image. These three coordinates can be related as,

$$x_L \text{ or } x_R = -f\frac{a_{11}(X-X_0)+a_{12}(Y-Y_0)+a_{13}(Z-Z_0)}{a_{31}(X-X_0)+a_{32}(Y-Y_0)+a_{33}(Z-Z_0)} - x(k_1r^2+k_2r^4) \quad (1a)$$

$$y_L \text{ or } y_R = -f\frac{a_{21}(X-X_0)+a_{22}(Y-Y_0)+a_{23}(Z-Z_0)}{a_{31}(X-X_0)+a_{32}(Y-Y_0)+a_{33}(Z-Z_0)} - y(k_1r^2+k_2r^4) \quad (1b)$$

$$r^2 = x_L^{\ 2} + y_L^{\ 2} \quad \text{or} \quad x_R^{\ 2} + y_R^{\ 2} \tag{1c}$$

where (X_0, Y_0, Z_0) is the projection center; f is the focal length; a_{ij} is the transformation matrix due to rotations angles about the x, y, and z-axes; and k_1 and k_2 are coefficients of lens distortions[**2**].

The orientation elements in Eq.(1) should be determined through the camera calibration process. We prepared a calibration block on which some reference points were arranged. The positions (ground coordinates) of these reference points had been precisely determined by a precision coordinate measuring machine. Before measurements, we took a stereo-image of the calibration block and obtained the picture coordinates of each reference point. Substituting the ground coordinates and picture coordinates of each reference point into Eq.(1), the orientation elements for the left- and right-half images could be individually determined. We then replaced the block with the corroded steel plate specimen and made measurements.

2.2 Pattern Matching

In stereo-images, certain point in the real object is individually projected onto two images. For stereography, we have to find the corresponding points in both images that project the same point in the real object. The pattern matching technique is usually used to obtain the correspondence of the two images. As shown in Fig.3, first we set up a small imaginary region at a certain position in the left-half image and call it the base window. We then placed a window of the same size on the right image and moved it until finding one that was the most similar to the base window. We call this one the corresponding window. The similarity between the two windows was quantified with the correlation coefficient between the pixel color data in both windows. After setting the base window and finding the corresponding window, the position of the corresponding window was memorized in computer. We then repeatedly shifted the base window slightly until all of the target areas were covered. From the position of the corresponding

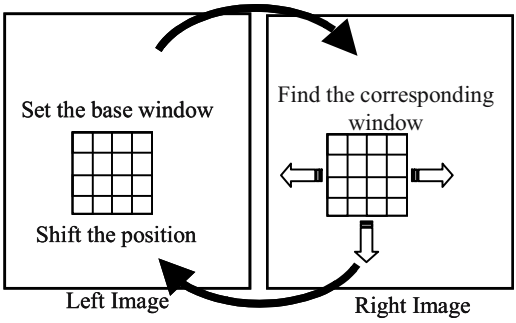

Figure 3. Method of pattern matching

window obtained for all of the base windows in the left image, the corresponding position of a pixel in the left image was calculated as the average of the positions of all of the windows with the pixel.

The size of the base window used in the pattern matching process is a key parameter. We used two-step matching processes with different base window sizes. In the first step, the rough correspondence was built with a larger window having 15 by 15 pixels to avoid one-to-many correspondence. The correspondence was then refined in the second matching process performed with a smaller window of 7 by 7 pixels to get a high spatial resolution.

2.3 Results

The specimen used in our experiment was about 55 mm high, 40 mm wide, and 20 mm thick. The camera distance (the distance between the lens and the specimen) varied from 250 mm to 500 mm.

Along a reference line settled in the specimen, the measured surface profiles were compared with the measured results obtained by a laser displacement meter in Fig.4. When the camera distance was large, the stereography could only provide us with the general surface shape of the specimen and overlooked any small unevenness. On the other hand, the

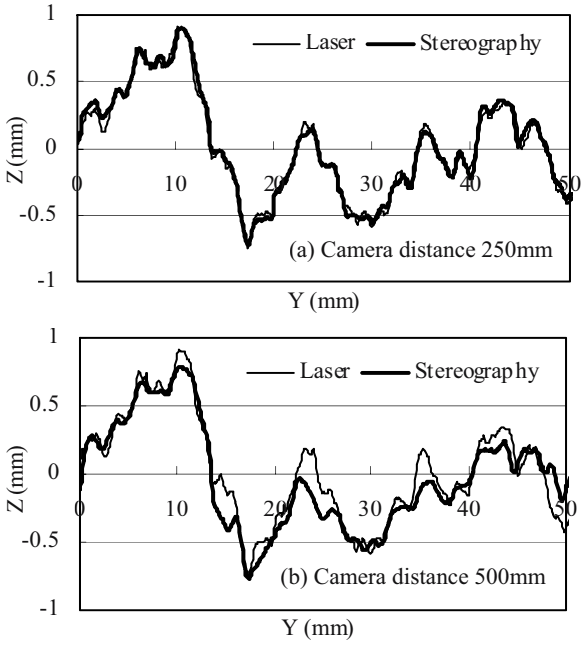

Figure 4. Comparisons of surface shape

stereography could measure the surface profiles much more accurately, when the distance was small, even though they had a notch-like unevenness.

The accuracy of the method depends on many factors such as the camera distance, image resolution, parallax of the viewpoints, patter matching method, etc. However, the result shown in Fig.4 demonstrates that the image analysis can be used as a simple measurement tool for corroded steel plate surfaces when suitable conditions are chosen.

3. NEW LOW CYCLE FATIGUE TESTING SYSTEM APPLYING IMAGE ANALYSIS

An hourglass shaped specimen has been used in low cycle fatigue tests. This is because its shape is suitable when trying to avoid local buckling and is easy to measure especially large strains in the specimen. However, this specimen shape is not suitable for testing the fatigue strength of non-uniform material. In this section, we introduce a new low cycle fatigue testing system using the digital image analysis[**3**]. In this system, the specimen was subjected to bending deformation, and the strain in the specimen was measured by the image analysis technique.

3.1 Specimen and Testing Method

This testing system is illustrated in Fig.5. It consists of a general-purpose digital camera, a personal computer, and a fatigue-testing machine. A typical shape of testable specimen is illustrated in Fig.6. Simple steel plate, even if it is welded, can be tested.

Before conducting the test, we painted small red dots on the side surface of the specimen that were 2 to 3 mm apart. During the loading test, pictures

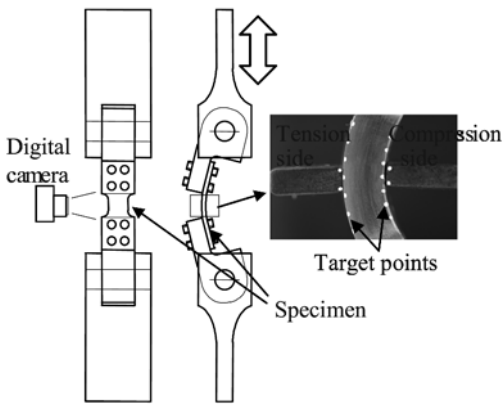

Figure 5. Testing system

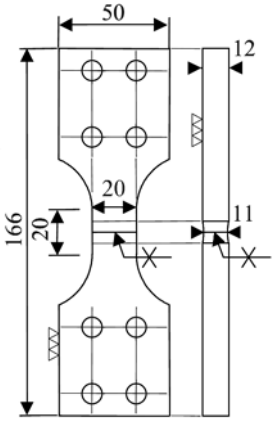

Figure 6. Example of specimen

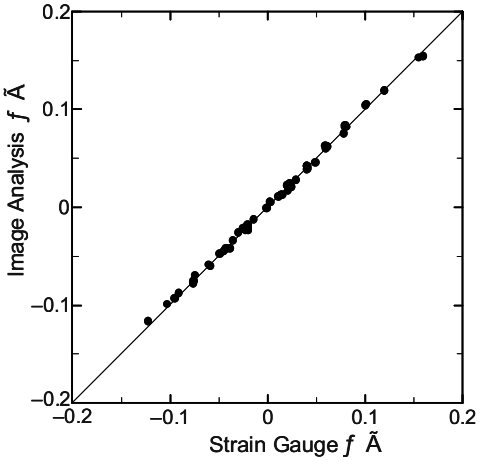

Figure 7. Comparison of strains

of the deformed specimen were captured in certain intervals, as shown in Fig. 5. The following processes were repeated to evaluate the strain: 1) picking out target points by image processing, 2) determining the position of each target point, 3) calculating the strain from the movement of each target point.

3.2 Comparison with Strain Gauge

In order to verify the strains measured by the image technique, we also measured the strains using a strain gauge. Fig.7 compares the results obtained by these two methods, and it can be seen that they are consistent. It was impossible to compare them in a larger strain range because of the performance limit of the strain gauge.

3.3 Fatigue Test Results

Fig.8 shows the crack initiation life of a plain steel material. The solid line represents the fatigue strength of the plain material given by Nishimura [**4**], which was obtained using the hourglass shaped specimens. The data obtained in our test are very close to this line. This indicates that the strain measurement and strain control method used in this testing system are sufficiently accurate, and that the system is a good low cycle fatigue testing system.

Fig.9 shows the crack initiation life of welded joints. The solid line is the fatigue strength of the base material. The crack initiation life of the weld deposit is only 50% of the base material. This result, the low cycle fatigue

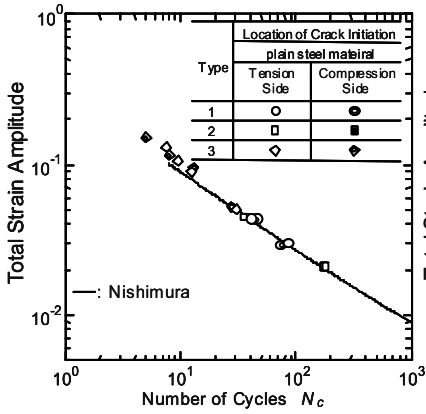

Figure 8. Low cycle fatigue strength of plain steel

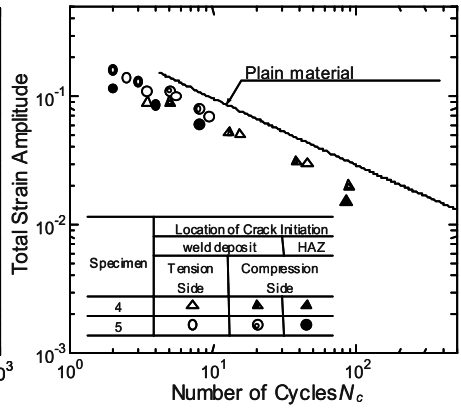

Figure 9. Low cycle fatigue strength of weld material

strength of the welded material in a large strain field, was difficult to obtain by any conventional method. This is the first time we have obtained it using our new testing system.

4. STRAIN MEASUREMENT IN LOCALLY BUCKLED STEEL MEMBERS

Steel tube or concrete filled steel tube (CFT) pier subjected to large cyclic loads loses its ductility mainly due to local buckling. It is reported that a crack sometimes occurs around the local buckling portion and triggers sudden fall of the load carrying capacity. Since the cracks can be low cycle fatigue cracks under large strain repetitions induced around the buckling portion, strain behavior around the buckling portion should be carefully investigated. In this section, a strain measurement method using digital stereography was used to check the strain field around the local buckling portion[**5**].

4.1 Testing Method

The system developed in this study consists of two sets of digital cameras and personal computers. The specimen used in this test is illustrated in Fig.10. Two specimens were connected by high-tension bolts and loaded, as shown in Fig.11. On the surface of the steel tube near the base, target points of 15 by 15 at 5mm intervals were painted as shown in Fig.11.

The strain was measured using a combination of the two methods introduced in the previous sections. Namely, during the loading test, we captured the stereo-pictures of deformed specimen in certain intervals, picked out target points by image processing, determined the three-

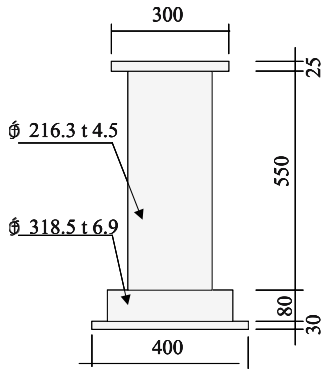

Figure 10. Specimen

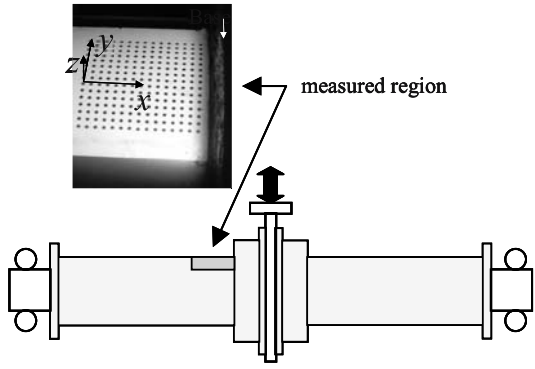

Figure 11. Loading method and target points

dimensional position of each target point by stereography, and then calculated the strain.

4.2 Verification of the System

Strains measured by the strain gauge and image analysis are compared in Fig.12. These two methods give almost the same results. At the displacement level of $6\delta_y$ (δ_y : yield displacement), small but obvious local buckling deformation was observed around the measuring point. Strains measured by these two methods are also coincidental. Therefore, it is confirmed that the proposed system can measure the strain even when the local buckling deformation occurs in the specimen.

4.3 Results

At the 25.2mm displacement ($7\delta_y$), a crack was detected at the location 5mm from the base. This crack propagated with loading cycles and caused

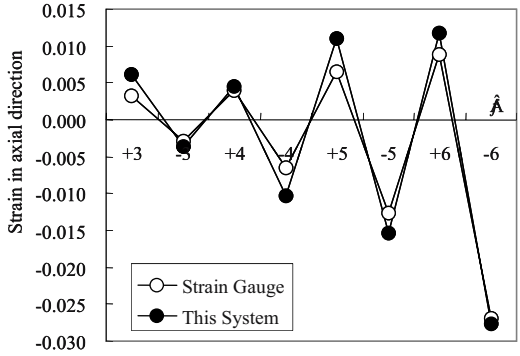

Figure 12. Comparison of strain

the sudden loss of load carrying capacity at the displacement of $10\,\delta_y$.

Fig.13(a) shows the distribution of the strain in *x* direction (see Fig.11) when the compressive loads were at the peaks. Strain distributions around the buckling portion were characterized by the tensile strain at the top of the buckling portion (point B) and the compressive strains at the foot (point A and C). Fig.13(b) shows the strain distributions at the tensile peak loads, which were relatively flat comparing to that under the compressive load.

Fig.14 demonstrates the strain histories at the three points where large

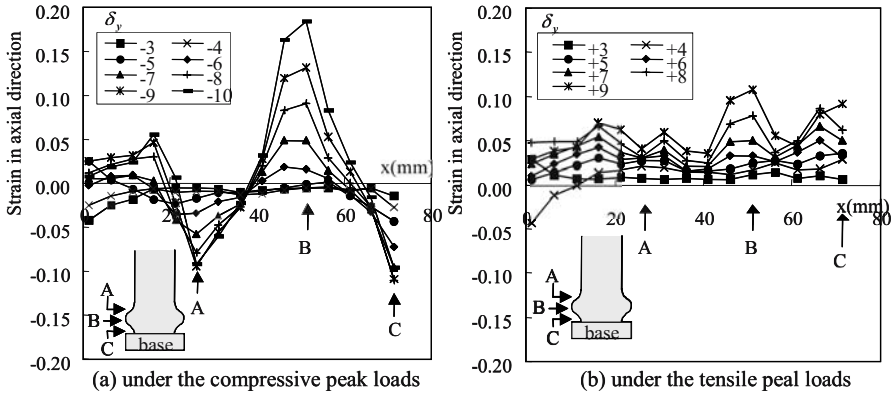

Figure 13. Strain distributions

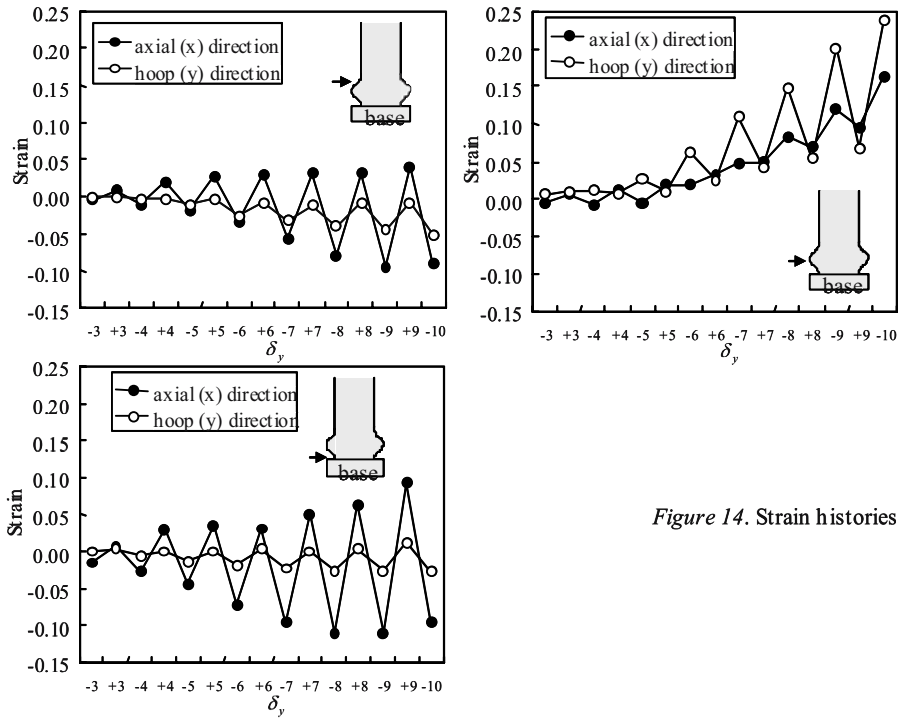

Figure 14. Strain histories

strains were observed in Fig.13. At the top of the buckling portion, the strain in the hoop direction (*y* direction, see Fig.11) fluctuated largely, and exceeded the strain in x direction. At the upper foot and lower foot of the buckling portion, the strain manners are almost similar. But the strain at the lower foot of the buckling portion was larger than that at the upper foot, which is consistent with the fact that the crack was formed at that position.

The digital image analysis makes the strain measurement possible even for the local buckling portion with three-dimensional deformation. This method makes the investigation of mechanical behaviors of steel structural members more easily and accurately.

5. SUMMARY

Three applications of digital image analysis to steel structural engineering were introduced. First, it was shown that the surface shape of corroded steel plate could be accurately measured by this method. In the second application, a new low cycle fatigue testing system using the digital image analysis, which can be applied even to simple steel plate, was presented. Finally, the strain measurement for the local bucking portion with three-dimensional deformation was performed using this technique. The digital image technique provides us with innovative information on mechanical behaviors of steel structural members, which used to be difficult or even impossible to obtain. This technique has proven to be inexpensive.

REFERENCES

1. Hanji,T. ,Tateishi,K., Kitagawa,K. “3-D Shape Measurement of Corroded Surface by using Digital Stereography” *Structural Health Monitoring and Intelligent Infrastructure*, pp.699-704, 2003.
2. Murai,S., Okuda,T. and Nakamura,H., "A Study on Analytical Photogrammetry by Non-metric Camera", *Report of the Institute of Industrial Science*, The University of Tokyo, **vol.29(6)**,pp.1-15, 1981.
3. Tateishi,K., Hanji, T. “A Study on Low Cycle Fatigue Strength of Butt Welded Joint by Means of Image Analysis Technique” *Proc. of JSCE*, **No.752/I-66**, pp.277-288, 2004 (in Japanese).
4. Nishimura,T., Miki,C., "Strain Controlled Low Cycle Fatigue Behavior of Structural Steels", *Proc. of JSCE*, **No.279**, pp.29-44, 1978 (in Japanese).
5. Tateishi,K., Murata, K. “Strain Measurement of Strain in CFT Members by Image Analysis”, Journal of Structural Engineering, JSCE, **vol.45A**, pp.1537-1544, 1999 (in Japanese)

SHAPE MEMORY ALLOY-BASED SMART CIVIL STRUCTURES WITH SELF-SENSING AND REPAIRING CAPABILITIES

Hui Li, Chenxi Mao, Zhiqiang Liu, and Jinping Ou
School of Civil Engineering, Harbin Institute of Technology, Harbin, 150090, P. R. China

Abstract: Self-sensing and actuating properties of shape memory alloys (SMAs), NiTi wires and NiTiCu wires, are experimentally studied. Strain rate dependent constitutive model of austenitic SMAs through phase transformation test is proposed. Self-sensing and repairing civil structures embedded with NiTi wires are proposed and the repairing effectiveness on cracks is verified through test of RC beams embedded with NiTi wires. Self-sensing passively controlled civil structures attached with SMA dampers are proposed. Two innovative SMA dampers with self-sensing, re-centering and energy dissipation capabilities are developed and shaking table tests of a five-story frame attached with SMA dampers at the first story are carried out.

Key words: Shape memory alloys, smart materials and structures, health monitoring, structural control.

1. INTRODUCTION

Recent years, many researchers have paid more attention on smart materials and structures. Shape memory alloys (SMAs) are multi-functional materials and various composite structures embedded or attached with SMA devices have been developed in aeronautic engineering. SMA material properties have been investigated by many researchers (Liang and Rogers, 1990; Brinson, 1993).

Several kinds of SMA-based smart civil structures have been developed (Li, et al, 2002). One of them is smart reinforced concrete structures embedded with pre-stretched SMA wires. The pre-stretched SMA wires can

Farhad Ansari (ed.), Sensing Issues in Civil Structural Health Monitoring, 259–268.

generate recovery force by heating them due to their shape memory effect, and thus repair the damage of the structures. Another is smart civil structures attached with SMA-based dampers. The distinguished feature of SMA dampers is that they simultaneously play a role of energy dissipation device and displacement transducer. Therefore, SMA dampers provide a potential to assess the post-earthquake safety of structures attached with SMA dampers. However, SMAs used in the smart civil structures behave different material properties as that in other areas.

In this paper, the SMA material properties under the circumstances of civil structures are firstly investigated. Self-sensing and repairing civil structures embedded with NiTi wires are proposed and the repairing effectiveness on cracks is verified through test of RC beams embedded with NiTi wires. Self-sensing passively controlled civil structures attached with SMA dampers are also proposed. Two innovative SMA dampers with self-sensing, re-centering and energy dissipation capabilities are developed and shaking table tests of a five-story frame attached with SMA dampers at the first story are carried out.

2. MATERIALS

Three SMA wires are employed in this study. One of them is TiNi wire made in China with a diameter of 1.2mm. TiNi wire is an approximate iso-atom alloy with 50.8%Ti and 49.2%Ni. These NiTi wires show pseudoelastic behavior at room temperature. Another two SMA materials are martensitic TiNi and TiNiCu wires also made in China with a diameter of 2mm. TiNi wire is an approximate iso-atom alloy with 49.2%Ti and 50.8%Ni. And TiNiCu wire is a three-element alloy with 49%Ti, 44%Ni and 7%Cu. The measured phase transition temperatures using DSC are summarized in Table 1.

Table 1 Phase transition temperature of martesitic TiNi and TiNiCu SMA

Phase transition temperature / SMAs type	M_f (˚C)	M_s (˚C)	R_f (˚C)	R_s (˚C)	A_s (˚C)	A_f (˚C)
TiNi SMA	0.08	34.7	37.7	58.2	53	70.9
TiNiCu SMA	8	27	—	—	32.8	47.6

3. STRAIN AND TEMPERATURE SENSING PROPERTIES

Tests are conducted in MTS-810 installed in Harbin Institute of Technology, as shown in Figure 1. The constant-current source supplies a constant current for the SMA specimens. When the SMA specimen is stretched by MTS, the voltage at the two ends of the specimen can be collected by the Data Acquisition Modules ADAM-4018 produced by Advantech Inc. in Taiwan together with the computer. The voltage of the standard resistance box can be also obtained by the Data Acquisition Modules and the computer. The specimens are stretched up to a certain strain and then unloaded to zero loads. The data of stress, strain and voltage variation are simultaneously collected by the testing system. The resistance of SMA specimen can be obtained.

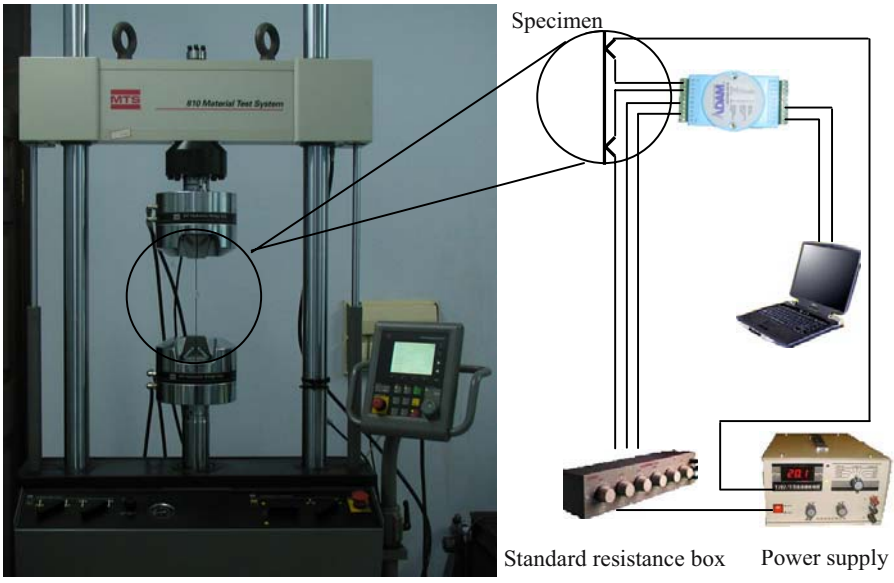

Figure 1. Setup of the testing apparatus

3.1 Strain sensing properties of martensitic NiTi wires

Figure 2 and Figure3 show the change rate of resistance-stress-strain of martensitic TiNi SMA wires subjected to two loading cycles. The Change rate of resistance is expressed as the resistance variation ΔR divided by the initial resistance R_0 of SMA wires, namely $\Delta R / R_0$. According to Figures 2

and 3, the change rate of resistance of martenitic TiNi SMA wires is approximately linear with applied strain, although the stability is required to be examined further.

3.2 Strain sensing properties of martensitic NiTiCu wires

With regard to TiNiCu SMA wires, the similar conclusions mentioned above are also drawn, as shown in Figure 3 and Figure 4. Therefore, TiNi and TiNiCu SMA wires in martensitic phase can be used as a sensing element to measure strains. And they can also monitor stress by measuring strain since stress-strain relation has been obtained in the tests.

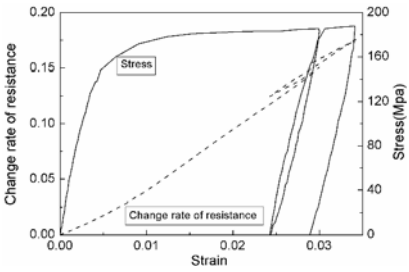

Figure 2 Resistance-stress-strain relation of TiNi SMAs within a strain of 3%

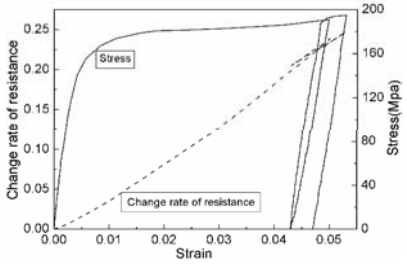

Figure 3 Resistance -stress-strain relation of TiNi SMAs within a strain of 5%

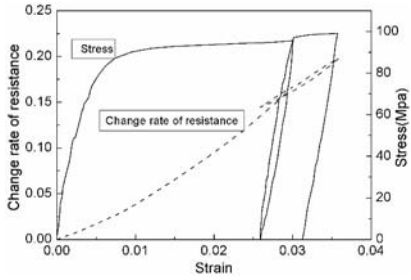

Figure 4 Resistance -stress-strain relation of TiNiCu SMAs within a strain of 3%

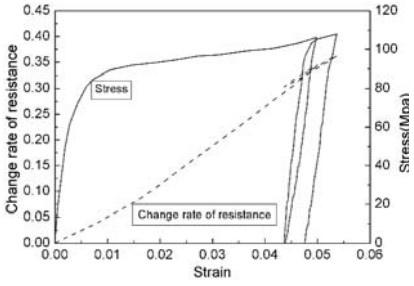

Figure 5 Resistance -stress-strain relation of TiNiCu SMAs within a strain of 5%

3.3 Strain sensing properties of austenitic NiTi wires

The relationship of the fractional change in electric resistance and applied strain is shown in Figure 6. The loading frequencies are 5×10^{-3}/sec, 5×10^{-2}/sec and 2×10^{-1}/sec, respectively, and the ambient temperature is room

temperature. It can be seen that the relationship between the fractional change in electric resistance and applied strain of this NiTi SMA wire under austenitic phase is nearly linear and independent on loading frequency. 2) The fitting lines of $\Delta R / R_0$ vs. applied strain are also shown in Figure 6 (the thick black line). The slope of these lines is defined as the strain sensitivity coefficient. The strain sensitivity coefficients of this NiTi SMA wire at loading frequencies 5×10^{-3}/sec, 5×10^{-2}/sec and 2×10^{-1}/sec are respectively identified as 6.062, 5.986 and 5.796, so the influence of loading frequency on the strain sensitivity coefficient can be ignored. The average strain sensitivity coefficient of the NiTi wire can be calculated as 5.948.

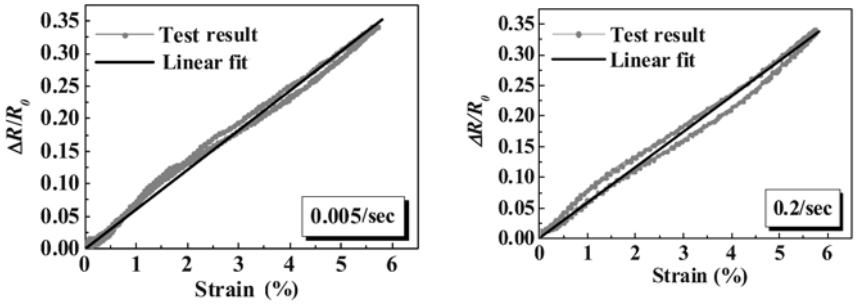

Figure 6 $\Delta R / R_0$ vs. ε relationship of the SMA wires at room temperature

3.4 Temperature sensing properties of martensitic NiTi wires and NiTiCu wires

Figure 7 shows the change rate of resistance-temperature of martensitic TiNi wires and NiTiCu wires constrained at two ends and subjected to heating load. The resistance firstly decreases with raising temperature and then increases. The decreasing branch is independent on the current intensity, however, the increasing branch is influenced by current intensity.

4. ACTUATING PROPERTIES

SMA wires can generate recovery force when heating the prestrain SMA wires due to their shape memory effect. The effect of different heating strategies on the recovery forces of martensitic NiTi wires and NiTiCu wires are tested and the results are shown in Figure 8. The recovery forces are strongly influenced by heating strategy; however, the maximum recovery force is independent on the heating strategies.

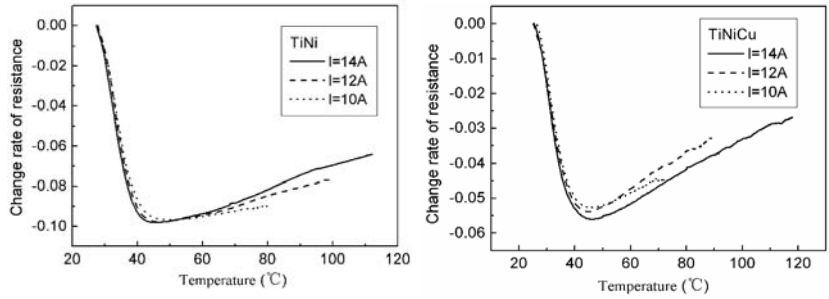

Figure 7 Temperature sensing properties of NiTi wires and NiTiCu wires

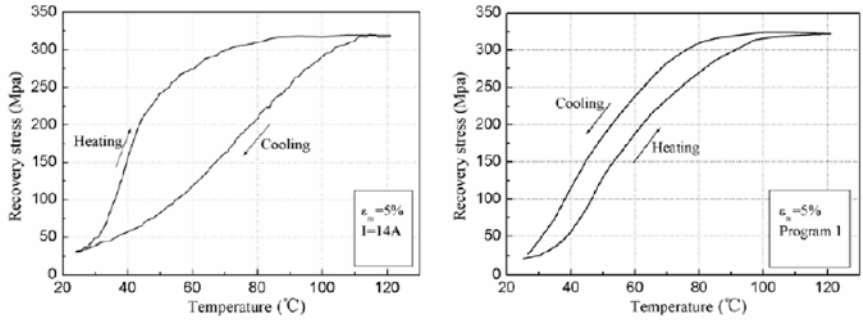

(a) NiTi wires pre-stretched to 5% using constant current

(b) NiTi wires pre-stretched to 5% using terrace current

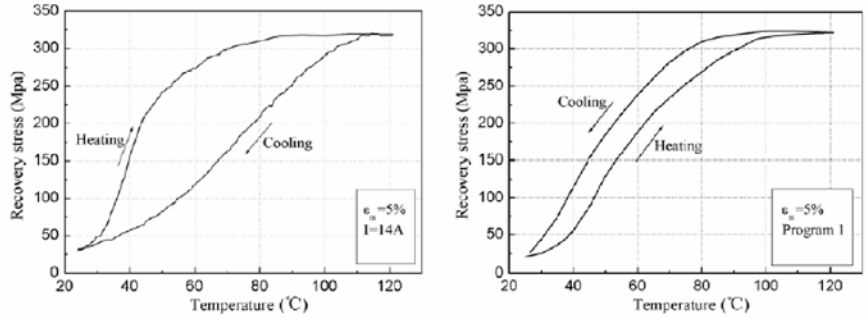

(c) NiTiCu pre-stretched to 5% using constant current

(d) TiNiCu pre-stretched to 5% using terrace current

Figure 8 Recovery force of SMA wires under different heating strategies

5. STRAIN RATE DEPENDENT CONSITUTIVE MODEL

Strain rate dependency of stress-strain relationship of SMAs is found by Dolce and Cardone (2001) and authors, as shown in Figure 9. Based on the test results and the constitutive model of SMA proposed by Liang and Rogers (1990), a strain rate-dependent constitutive model is proposed and the numerical results, shown in Figure 11, indicate the model can precisely predict the stress-strain relationship of SMA under static and dynamic loading conditions.

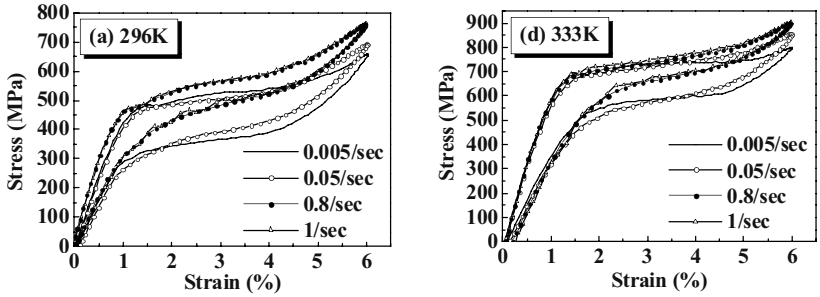

Figure 9 Influence of loading frequency on pseudoelasticity of the NiTi wires at various ambient temperatures

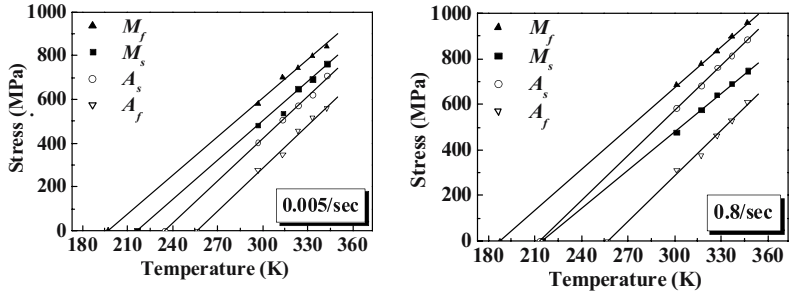

Figure 10 Phase transformation diagrams of the NiTi SMA wire under different frequencies

6. SELF-SENSING AND REPAIRING CIVIL STRUCTURES

Pre-stretched SMA wires embedded in reinforced concrete structures can monitor structural strain and repair cracks by recovery forces. The tests of reinforced concrete beams embedded with pre-stretched SMA wires in tensile zone near the bars are carried out. The results are shown in Figure 12.

It can be seen from Figure 12 that the recovery force of SMA wires can decrease the tensile strain and stress of rebar and concrete in tensile zone.

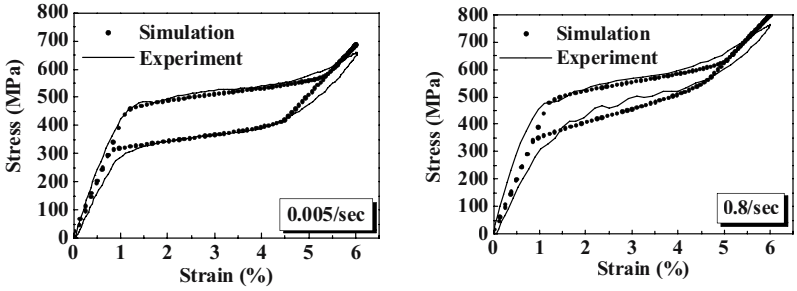

Figure 11 Comparison of the simulated hysteresis loops with the test results under different loading frequencies

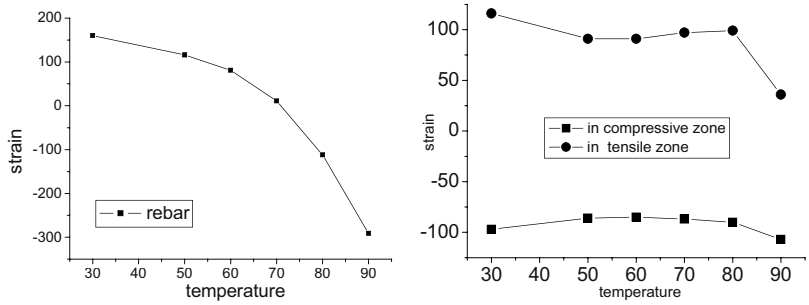

Figure 12(a) Repairing effect before crack

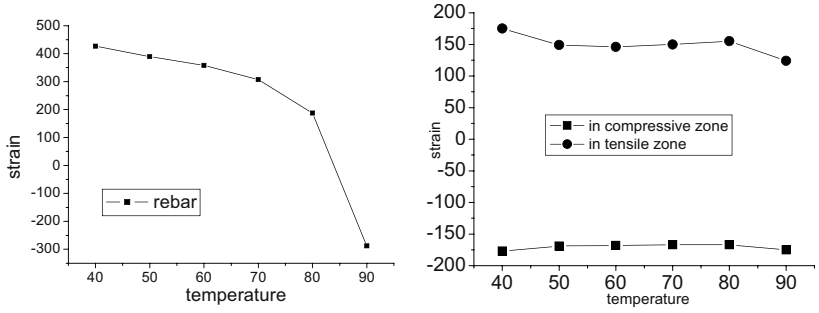

Figure 12(b) Repairing effect after crack

7. SELF-SENSING AND PASSIVELY CONTROLLED STRUCTURES

Two innovative dampers are developed in this paper, which have three characteristics: 1) SMA wires in the damper are always elongated during the entire excitation; 2) SMA wires dissipate energy with re-centering ability due to pseudoelasticity; 3) SMA dampers can simultaneously play the role of displacement transducer due to the strain self-sensing property of SMA wires in the damper. The smart SMA-based dampers incorporated into buildings and bridges provide a potential way to assess post-earthquake structural safety. They are called as SMA-based dampers/displacement transducers. The schematic diagram of the dampers is shown in Figure 13. The performance of the dampers is investigated through series of tests. And then a shaking table test of a five-story steel frame attached with the SMA dampers at the first story is conducted. The test results are shown in Figure 14. It can be seen that the SMA dampers can effectively reduce the first story displacement; however, it cannot always reduce displacement of other stories.

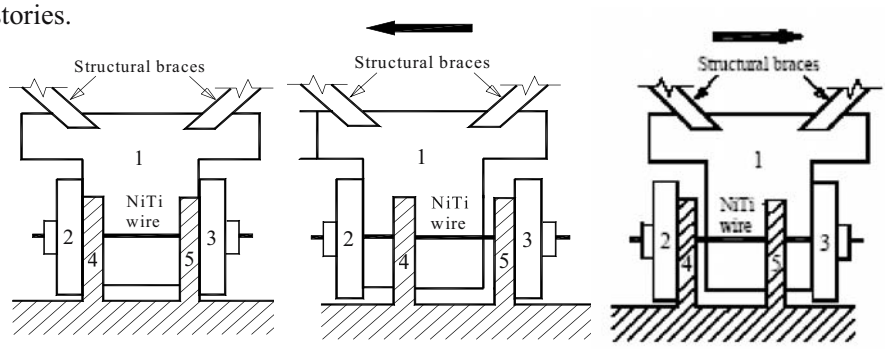

Figure 13 Schematic diagram of the SMA dampers

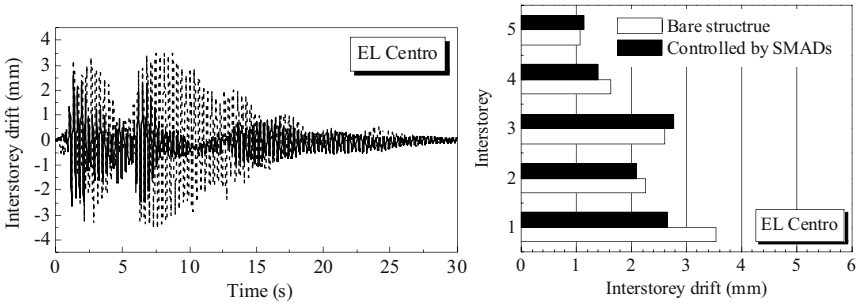

Figure 14 Time histories of the displacement at the 1st floor and interstory drift along the height of the model

8. CONCLUSIONS

This paper introduces some advances of material properties of SMA and SMA-based smart civil structures. Following conclusions can be drawn: 1) The relationship between electric resistance and applied strain is linear; 2) The recovery force of SMA wires is influenced by heating strategies; 3) The stress-strain relationship of SMAs is dependent on loading frequency; 4) SMAs can effectively decrease strain and stress in tensile zone of reinforced concrete beams; 5) SMAs-based dampers can sense their own displacement and reduce the response of the controlled buildings.

ACKNOWLEDGMENT

This research is financially supported by the National Natural Science Foundation of China under the grant number 50238040 and 50176025, and Ministry of Education under the grant number 20020213027and Heilongjiang Distinguished Youth Experts.

REFERENCES

1. Brinson, L. C. (1993). One-dimensional constitutive behavior of shape memory alloys: thermomechanical derivation with non-constantmaterial functions and redefined martensite internal variable. *J. Intell. Mater. Syst. Struct.*, 4, 229–42.
2. Dolce, M., and Cardone, D. (2001). Mechanical behavior of shape memory alloys for seismic applications 2. Austenite NiTi wires subjected to tension. *International Journal of Mechanical Sciences*, 43, 2657-2677
3. Liang, C., and Rogers, C. A. (1990). One-dimensional thermomechanical constitutive relations for shape memory materials. *J. Intell. Mater. Syst. Struct.*, 4, 207–34
4. Li H, Wang Z. Y., Mao C. X. Liu M. and Ou J. P. (2004). Study on Structural Vibration Control with Shape Memory Alloy. *Pacific Science Review*, 2002 (4):100-104

SMART SENSORS AND INTEGRATED SHM SYSTEM FOR OFFSHORE STRUCTURES

Zhongdong Duan, Jinping Ou, Zhi Zhou, and Xuefeng Zhao
School of Civil Engineering, Harbin Institute of Technology, China

Abstract: Structural Health Monitoring (SHM) technology, which is synthesis of advanced sensor technology, data processing, damage diagnosis and condition assessment techniques, is now shaping for the safety and cost-effective managements for infrastructures. Some advanced sensors and their integrated SHM system for monitoring CB32A offshore jacket platform structures is reported in this paper. Fiber Bragg Optic Sensors for strains, Polyvinylidene Fluoride (PVDF) sensors for cracks and fatigue life gauge for accumulative fatigue damage are adopted for monitoring structural local responses. The characteristics of these sensors, the encapsulation techniques, and placement of sensors in this structure are introduced. The integration of load monitoring subsystem and data management and process program into a SHM system for CB32A platform structure is discussed.

Key words: Optical fibre bragg grating sensor, Polyvinylidene fluoride sensor, Fatigue life gauge, Integrated structural health monitoring system, Offshore platform structure

1. SMART SENSOR TECHNOLOGY FOR MONITORING OFFSHORE PLATFORM STRUCTURES

For offshore jacket platform structure, which is usually a frame with welded tubular joints, the fatigue and cracks frequently develop at the joints. Enabling sensor technology that can sense the crack initiation, development, and fatigue damage accumulation is critical for monitoring performance of the structure. Three kinds of sensor and their encapsulation technology are developed for this purpose.

Farhad Ansari (ed.), Sensing Issues in Civil Structural Health Monitoring, 269–278.

1.1 Optical Fibre Bragg Grating (FBG) sensor and its encapsulation

Optical fibre sensor is most suitable for long-term monitoring of local strain of structures, and optical FBG sensor with high precision, quasi-distribution and compact sized characteristics, is of great interest for civil engineers.

Bare optical FBG sensor can not be planted into the monitored body because of its fragility. Encapsulation technique for the sensor while not sacrificing its sensibility is crucial for the practical implementation of the sensors. Two techniques are developed in this study to protect the sensor from damage in the process of construction and operation.

The first one is tube encapsulated FBG strain sensor. The optical FBGs are encapsulated in mental capillary by epoxy resin as shown in figure 1. The mental holder ring is used to keep the FBGs deformation consistent with the base, on which the sensor is attached, and the stretched optical fiber is ready for temperature compensation connector. Mental tube encapsulated FBG strain sensor can be used in concrete structures.

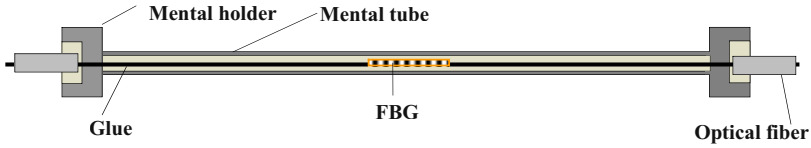

(a) Sketch of mental tube encapsulated FBG strain sensor

(b) Actual Mental tube encapsulated FBG strain sensor

Figure 1 Mental tube encapsulated FBG strain sensor

The second one is the slice encapsulated FBG sensor. The slice can be mental or glue. Figure 2 shows the glue slice encapsulated FBG sensor. The slice based sensor is flexible for different structural surface, and it can be used in both steel structure and concrete structures.

The effect of encapsulation on the sensing property of FBG sensor is be investigated before it is used in practical application. The sensing property of the encapsulated sensors is tested. The result shown in figure 3 demonstrates that the encapsulation keeps good linearity between wave length change and

strain.

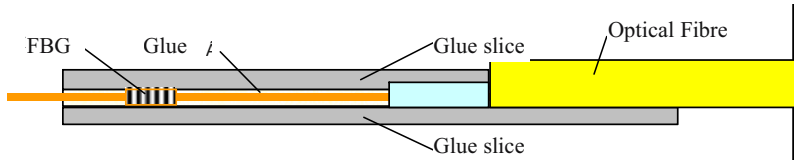

(a) Sketch of glue slice encapsulated FBG strain sensor

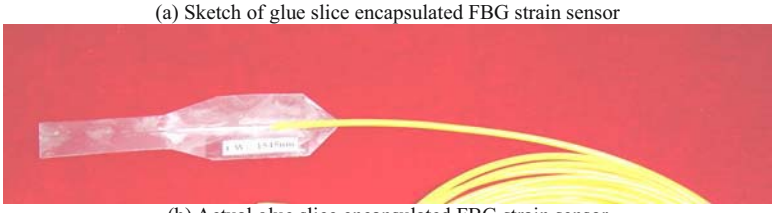

(b) Actual glue slice encapsulated FBG strain sensor

Figure 2 Glue slice encapsulated FBG strain sensor

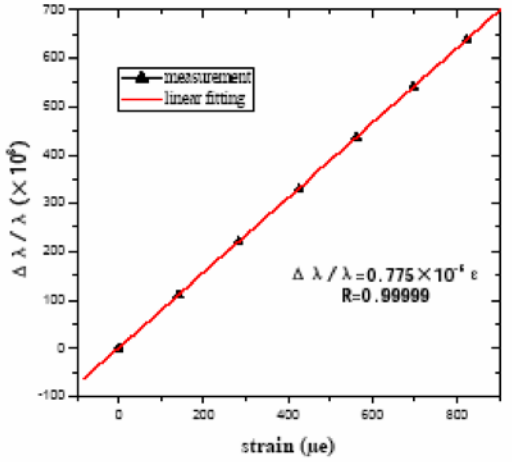

Figure 3 Linearity of wavelength increment and strain for encapsulated FBG

1.2 Polyvinylidene Fluoride (PVDF) sensor

Detecting the onset of crack in welded joint is very important for integrity evaluation of offshore platform structure. PVDF sensor is developed as a detector of crack.

PVDF sensor is made of a kind of piezoelectric polymer, which is easy to be tailored to different shape to monitor structure with geometrically complex members, and to be layed out on structure surface. The PVDF sensor and its strain sensibility are shown in figure 4. It shows that perfect linear relationship within strain and output voltage exists for PVDF sensors.

Because the PVDF membrane sensor can be tailored to different size to cover a certain area, it may be used as a crack detector if its output has a significant change when crack opens. This concept is tested on PVDF sensors to detect crack open in a cantilever is conducted. The output signal with a sharp spike in figure 5 indicates crack opens. So the PVDF sensor can be taken as a crack detector.

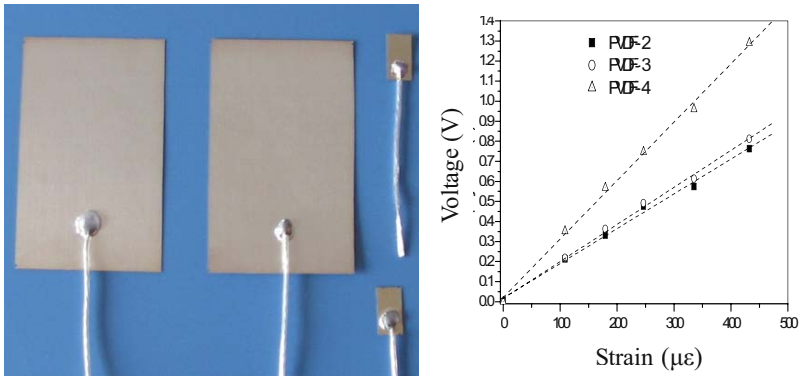

(a) PVDF sensor (b) Linearity between strain and voltage

Figure 4 PVDF sensor

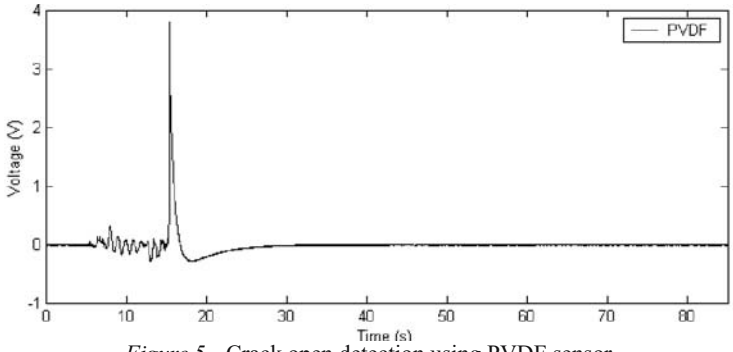

Figure 5 Crack open detection using PVDF sensor

1.3 Fatigue life gauge

Although the fatigue life gauge in the same appearance as the conventional strain gauge, it is made of a specially designed alloy with specified heat treatment techniques, which causes very different response to dynamic loading from strain gauge. The fatigue life gauge is made of material with 43% Cu, 55% Ni, 2% Mn and some quantity of C, S, Si and Co elements. The specially designed alloy has the unique characteristic that the electric resistance in the material monotonously increases as it experiences cycle loading, and the accumulated resistance doesn't discharge even the material is unloaded. Figure 6 shows the difference response between strain gauge and

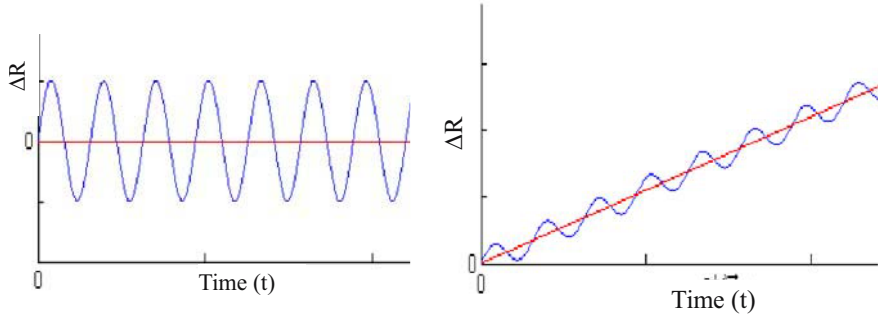

a) Resistance change of strain gauge b) Resistance change of fatigue life gauge

Figure 6. Difference response between strain gauge and fatigue life gauge

fatigue life gauge.

The accumulative resistance of fatigue life gauge as a function of strain amplitude and loading cycles can be represented by [7]

$$\Delta R/R \times 100\% = K(\varepsilon_a - \varepsilon_0)N^h \tag{1}$$

where R, ε_a, ε_0, N and are electric resistance, strain amplitude, strain threshold, load cycles, respectively. K and h are constants. The parameters of the material in Eq.(1) are determined by fatigue tests, as shown in Eq.(2).

$$\Delta R/R \times 100\% = 5.32 \times 10^{-6}(\varepsilon_a - 1146)N^{\left(0.163+3.24\times10^{-4}\varepsilon_a - 4.78\times10^{-8}\varepsilon_a^2\right)} \tag{2}$$

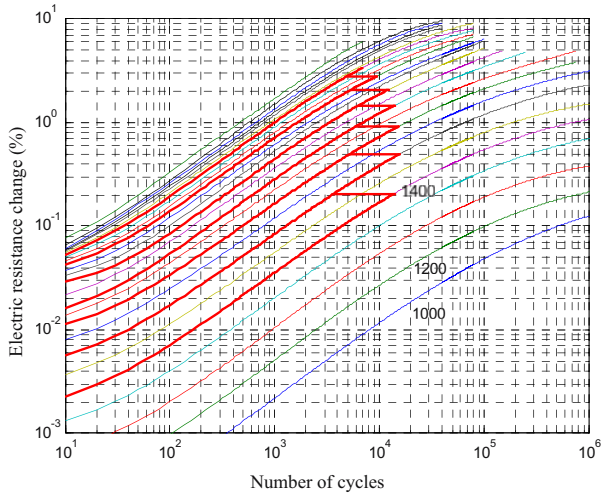

Figure 7 $\varepsilon - \Delta R - N$ curve

The resistance change in the sensor with cycle loading can also be characterized by figure 7.

2. INTEGRATED SENSOR SYSTEM FOR CB32A PLATFORM STRUCTURE

The CB32A platform structure is a four-leg jacked structure located in China Bohai Bay. The water depth of the location is about 18.2m.

CB32A platform is comprised of piles, jacket frame and upper modulars. The jacket frame is fabricated with steel tubes connected by welded joints, and it is the main part of offshore structure that supports the upper modular , and it deservers to be monitored. The profile of the jacket frame is shown in figure 8.

2.1 The placement of sensors

Finite element analysis of the CB32A platform is conducted using standard software SACS to determine the "hot" members with large internal forces. The analysis shows that the "X" braces, which mainly withstand lateral wave load, are the most loaded member for this structure. The four legs are also critical members because failure of any of the four legs will lead to immediate collapse of the structure. Therefore the "X" braces, legs and affiliated joints are the major monitored parts. For the braces and legs, only internal forces are monitored with strain sensors, but for welded joints, the very local strains are to be monitored. The PVDF for detecting crack open and the fatigue life gauge for fatigue damage accumulation are placed on the joints because the strain concentrations in complex joints likely lead to crack development. The placement of FBG sensors on one vertical profile of the structure is shown in figure 9. Together with FBG sensors, the other two kinds of sensors are mainly placed at joints. These sensors are placed perpendicularly to the intersection according to the finite element analysis results of joints.

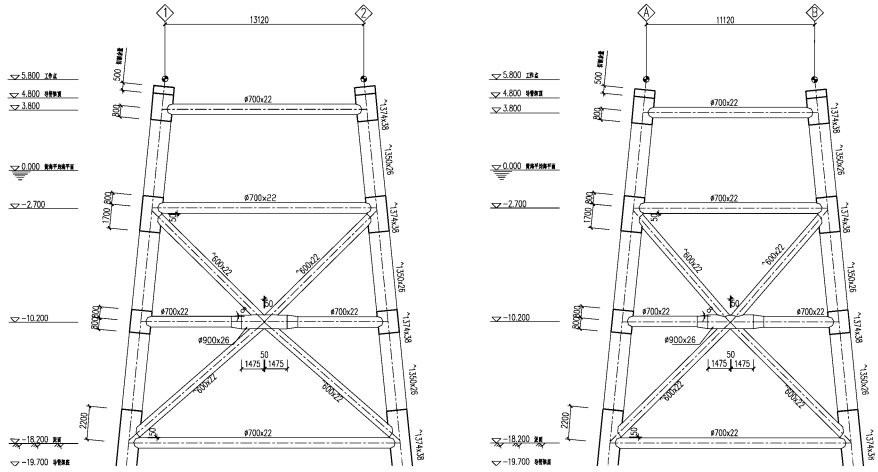

Figure 8 Vertical view of CB32A jacket frame

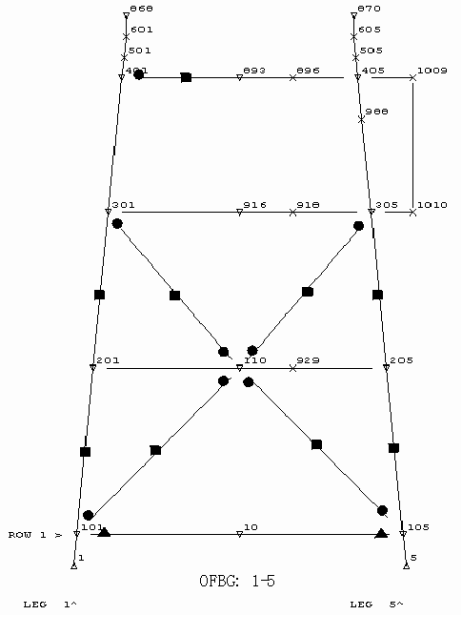

Figure 9 Placement of FBG sensors

Figure 10 Test of the protection techniques

2.2 Techniques for sensor attachment and protection in offshore environment

To make the sensors fully attached to the structure surface, and prevent coat debonding in the erection process of the platform structure in the sea, a strict procedure is designed and followed to attach the sensors on the structures. The procedure is as following

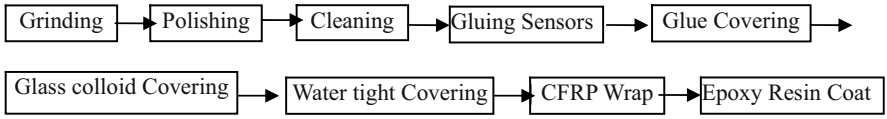

The technique proposed is tested in simulated sea water environment as shown in figure 10. After the procedure for planting and protecting the sensors, normal anti-corrosion procedure for offshore platform is done.

After the implement of sensor embedment, 259 optical FBG sensors, 178 PVDF sensors and 64 fatigue life gauges, with totally 27,000 meters of various wires are embedded into the jacket frame.28 accelerometers are instrumented, 8 in the jacket frame and 20 in the upper modular. Figure 11 shows the scenario of embedded sensors and wires, and the jacket frame instrumented with sensors.

Figure 11 Scenario of sensor placement for CB32A platform

3. THE INTEGRATED SHM SYSTEM FOR CB32A OFFSHORE PLATFORM STRUCTURE

In addition to the local and global responses measurement system by using optical FBG sensors, PVDF sensors, fatigue life gauges and accelerometers, a

load measurement system is designed to record the external environment loads such as wave, current and wind. An AWS 2700 weather station by Aanderaa Instrument, Norway, a SeaPac 2100 wave and tide station by Woods Hole Instrument System, USA is to be integrated to form the loads monitoring subsystem.

The data acquisition system is developed on the National Instrument PXI platform in the laboratory. A database is in developing to harbor the data from structural responses monitoring subsystem and the load monitoring subsystem. Data processing, parameter identification and damage detection, model updating, and safety evaluation program are to be integrated, and these software modules are in development in the laboratory.

4. CONCLUSION

The smart sensors and encapsulation techniques for monitoring offshore structure are developed. An effective technique to safely attach the sensors on the structure and protect the sensor from underwater corrosive environment is proposed and tested. More than 500 different sensors, along with 27,000 meter wires are successfully embedded into CB32A platform structure. This work shapes the first monitored offshore platform structure with densely instrumented smart sensors in China.

ACKNOWLEDGEMENTS

This research is supported by China High-tech Research and Development Program ("863" Program) under contract 2001AA602023 and 2003AA602230.

REFERENCES

1. Ou JP, "Some recent advances of intelligent health monitoring systems for civil infrastructures in mainland China", Structural Health Monitoring and Intelligent Infrastructure, Edited by Wu ZS and Abe M, Vol.1,pp.131-144,2003.
2. Mufti AA, "Integration of sensing in civil structures: development of new discipline of Civionics", Structural Health Monitoring and Intelligent Infrastructure, Edited by Wu ZS and Abe M, Vol.1,pp.119-129,2003.
3. Ko JM, "Health monitoring and intelligent control of cable-supported bridges", Structural Health Monitoring and Intelligent Infrastructure, Edited by Wu ZS and Abe M, Vol.1,pp.51-64,2003.
4. Koh HM, Choo JF, Kim SK and Kim CY, "Recent application and development of structural health monitoring systems and intelligent structures in Korea", Structural

Monitoring and Intelligent Infrastructure, Edited by Wu ZS and Abe M, Vol.1, pp.99-111,2003.
5. Wu ZS, "Structural health monitoring and intelligent infrastructures in Japan", Structural Health Monitoring and Intelligent Infrastructure, Edited by Wu ZS and Abe M, Vol.1, pp.153-167,2003.
6. ISIS, "Guidelines for Structural Health Monitoring", ISIS, Canada, Winnipeg, Canada, 2001.
7. Harting DR, "The S/N Fatigue Life gage: A Direction Means of Measuring Cumulative Fatigue Damag", Experimental Mechanics, Vol.6, No.2, pp:19-24,1996.

Chapter V

Sensor System Design, Data Quality, Processing, and Interpretation

DESIGN CONSIDERATIONS FOR SENSING SYSTEMS TO ENSURE DATA QUALITY

Ruifeng Zhang and Emin Aktan
Drexel University, The United States

Abstract: This paper discusses issues in designing sensing systems in order to control the various mechanisms of uncertainty that impair meaningful and reliable interpretation of data. Based on the analysis of possible errors of the sensory components, measurement setups and data acquisition elements, a paradigm of designing sensing systems is proposed, which centers at structural health monitoring and permeates the modeling, experiment, data collection, parameter estimation, model verification and correction, simulation and utilization procedures. The statistical data quality control process is further discussed focusing on the data processing and post-processing in the sensing system.

Key words: Sensing systems, data quality assurance

1. INTRODUCTION

A sensing system is meant to capture a physical phenomenon or the response of an object to that phenomenon. This task, however, is usually hindered by various errors caused by improper measurement setups and uncertainties of the environment. As a result, the low-quality measurement data do not lend to meaningful interpretations. To ensure the data quality, conceptualization and estimation of the bounds of the expected measurement should permeate the design of the sensing system and direct the calibration procedure.

A measurement made by any sensor is the result of an interaction between a transducer and the environment surrounding the transducer. The transducer is potentially a multi-input multi-output device, picking up many

Farhad Ansari (ed.), Sensing Issues in Civil Structural Health Monitoring, 281–290.

environmental inputs and outputting a compound response. Usually, only one of the inputs is the measurand and only one of many possible outputs is the desired signal (often just referred to as the signal) corresponding to the measurand. Moreover, not all environment influences are of equal magnitude and the measurand and the signal are not necessary the dominant one amongst. That means, measurement errors will be devastating unless it is accounted for properly.

The design of a sensing system should make the measurement error control a critical criterion. This should start with an identification of the types and sources of the errors. Then calibration of individual sensory component and the integrated sensors and data acquisition system should follow. Finally, the sensor operating status has to be verified for long-term performance after installation on the actual field structure by various in-situ calibration strategies.

In this paper, we focus on the system design issues of data quality assurance for sensing systems, trying to provide a paradigm for the modeling, experiment, data acquisition and interpretation, model verification, and etc. components in sensing system design.

2. SENSING ERRORS

2.1 Systematic Error

Of the two categories of errors, systematic errors often have much more serious consequences. Systematic errors are the same for each observation with a given measurement setup and method, or are some definite function of the value of the quantity being observed. These errors often are due to imperfect design of the measurement setup and the approximations made in characterizing the phenomena being measured, such as ignoring various components of a displacement vector. Systematic error is also referred to as *bias error*. A measurement setup may contain various sources of systematic error (incorrect alignment or positioning) causing a fixed percentage of error unless corrected or calibrated. It is also a fact that the measurement system rarely directly measures the quantity it is supposed to; it rather measures a variable, which is assumed to be related to the quantity in question by a known law of physics. Human errors are also a type of bias since each individual (or in the case of electronic components, different sets of data acquisition devices) will systematically obtain different results from the rest based on their reading or judgment or collection characteristics/perspectives.

These errors can easily be detected by having several observers (or different systems) making the same measurement set.

The careful investigation of the measurements in parallel with the known laws reduces the uncertainty often by identifying the causes of error and their impact on the measurements. The measurements are affected by large numbers of variables, and attempts should be made to control the critical ones that are due to assignable causes. Variables that are not controlled but still have important affects are called assignable causes, and if they are not accounted for or corrected, may interfere seriously with the accuracy and reliability of results. Typical systematic errors caused by the components and the design of the measurement setup that can be accounted for are: Errors due to

- Mechanical (kinetics, kinematics) mechanisms (including those related to geometry),
- Thermal mechanisms
- Electronics
- Mapping/referencing

The majority of the systematic error sources can be identified by careful and repeated tests and corrected by improving experimental design and calibration.

2.2 Random Error

Random errors are variations due to a number of uncontrolled variables, each of whose effects is individually small. Successive observations of the same quantity should form a random sequence when only random errors are occurring. Random errors are also referred to as *common errors*. Random errors are usually assumed to be distributed according to the normal law of errors, i.e., the error value as a random variable follows Gaussian distribution. The probability distribution for the Gaussian curve is simply expressed in terms of mean (μ) and standard deviation (σ). When these two parameters are established, the concept of confidence intervals for mean can be determined as a measure of reliability.

The theoretical argument for the normal law is based on the Central Limit Theorem. However, the theoretical justification is not applicable to all measurements since there are many situations in which it is not obvious that there are a number of independent sources of error or, if so, that they are of roughly equal importance. The process may be quite non-normal if there is only one major source of error such as due to bias (often, 500 or more data points are needed under constant conditions to verify this fact).

2.3 Error Components

A typical response measured by a sensor and its related data-acquisition system will include five distinct error components:

- Transducer assembly and installation errors (e.g., self-response of the installed transducer and assembly as a structure), resulting in systematic types of errors
- Additional systematic errors due to thermodynamic mechanisms (e.g., drift due to vibration or temperature effects)
- Instrument/data-acquisition variance errors (e.g., spurious readings or electrical noise)
- Apparent structural response (e.g., unrestrained temperature strains and rigid-body displacements as well as rigid-body or non-stress associated settlements, and temperature, creep or shrinkage strains)
- Actual structural response associated with stress and force

The total error that can be expected in a response from a system is a complex entanglement (far beyond linear combination) of the error components list above.

The logistics for monitoring include the careful decomposition of a sensor's reading into the above components. For this reason, the sensors should be individually calibrated, and their short-term accuracy evaluated by measurement-system scaling techniques in the laboratory. This should be followed by an evaluation of long-term reliability of sensor clusters and data acquisition hardware by conducting studies both in the laboratory and under field-similar environmental conditions. The reliable limits of the monitoring equipment must be determined and accounted for and the performance of each piece of equipment must be monitored in-situ to lend confidence to the results.

2.4 Static Characteristics and Error Definitions

An ideal or theoretical output/measurand relationship exists for every transducer. If a transducer were truly ideal, the transducer would only indicate the true value of the measurand. The output of an actual transducer, however, is affected by the non-ideal behavior of it, which causes the indicated measurand value to deviate from the true value. Thus, a systematic and reliable characterization of each sensor type is of utmost importance for reliable measurement. The relevant characteristics of the sensors to achieve the desired level of characterization are defined as follows.

Range: Two types of ranges were utilized for instrument verification and calibration:

Usable Range (Full Range): It defines the minimum and maximum values of a quantity that the instrument is designed to measure. The usable range is also a function of the range of the linear calibration jig (maximum range of 1").

Application Range: It defines the minimum and maximum expected values of a quantity that is expected for the actual measurement location in the field. The application range values were obtained from past case studies and experiences with similar research sensor readings.

Sensitivity: A measure of the change in instrument output which occurs when the quantity being measured changes by a given amount. It is defined by the slope of the straight line drawn over the full range, and the application range of the transducer. A linear curve fit analysis is useful to find the corresponding sensitivity value.

Hysteresis: The difference in a reading that depends upon whether the displacement or tilt was obtained through extension or retraction of the sensor (positive or negative displacement or tilt). In the reported calibration tests, the maximum hysteresis value was calculated by taking the largest difference from all of the differences in extension and retraction of the sensor in each cycle.

Repeatability: Repeatability is the ability of the device to output the same value for the same displacement or angle over a number of trials, under the same conditions, and in the same direction of application. It is expressed as the maximum difference between output readings for the same sensor position over several calibration cycles. This error is illustrated in Figure 1.

Linearity: Linearity is a measure of the deviation of the data (output signal) from a best-fit straight line for a given linear range of the sensor. In the tests performed the maximum linearity error is defined as the maximum deviation of any calibration point from the corresponding point on the best fit sensitivity line during any one calibration cycle. When more than one calibration cycle is made, the maximum deviation seen during any one calibration cycle is stated. Linearity error is not independent from the hysteresis and repeatability errors. In order to separate the effects of these other errors from the linearity error, the simple approximation shown below can be used:

$$\text{Independent linearity} = L - (h+r),$$

where L = Max. linearity error, 2h = Max. hysteresis error, 2r = Max. repeatability error.

Noise: Noise is the random fluctuation in the value of measurand or input that causes random fluctuation in the output value. Noise at the sensor output is due to either internal noise sources, such as resistors at finite temperatures, or externally generated mechanical and electromagnetic fluctuations. In

calibration tests, the baseline noise can be quantified by observing the maximum random fluctuations of a sensor output for a constant input.

Precision: Precision describes the reproducibility with which an unknown value is measured by a certain sensor. It has nothing to do with how accurately the measured value represents the unknown parameter.

Resolution: The smallest increment in the value of the measurand that results in a detectable increment in the output. It is expressed as a percentage of the measurand range (% MR). For example, if a displacement sensor yields an increment of DV output voltage in response to a DX change in the displacement, than the maximum resolution (Rmax) is the smallest DX (DXmin) that yields a detectable DV and is expressed as:

$$\text{Rmax}\ (\%) = \text{DXmin} / (\text{Xmax} - \text{Xmax}) \times 100$$

Accuracy: A measure of how closely the result of the experiment (Sensor output) approximates the true value. The value given must represent the combination of all errors, and must further represent a statistical confidence in the sensor output. In general, two basic methods can be employed in defining sensor accuracy:

Statistical methods: A more global yet practical approach on defining the accuracy is based on experimental calibration and statistical identification. Here, the statistical deviation from the expected or reference sensitivity curve, which defines the output/measurand relationship over the transducer's range, is directly determined from a sufficient set of trial experiments. This provides an overall or system definition of the experimental mean squared error or variance from the expected system I/O performance. However, this method cannot readily distinguish the more dominant error components except through trial-and-error.

Error budget method: An analysis of the typical monitoring system describes each functional component of the system and provides a tabular form for itemizing worst-case errors. The error budget presents all error sources and their bounds in a standard format to allow comparison and combination of all system errors.

Error terms may now be quantified and combined to provide an overall measure of performance or reliability for the sensor. The analysis and quantification of component errors allow the identification of critical errors and directs any further efforts at hardware optimization or data post-processing. In the error budget approach, each independent maximum error is considered for a given sensor by taking the Root-Sum-Square of these errors, an error band is calculated which represents the worst-case.

3. PARADIGM OF SENSING SYSTEM DESIGN

The systems to be sensed are usually highly complex, comprising intertwined engineering, natural and human elements. The design of the sensing system should be based on controlling the various mechanisms of uncertainty that impair reliable interpretation of data coming from this integrated system. This may be possible by formulating a multi-objective function to simultaneously: 1) account for uncertainty due to a lack of knowledge and insight governing the application problem; 2) capture data, which, when processed and fused, will have the greatest impact on decision-making and action; 3) minimize the impacts of experimental uncertainty affecting the data; and 4) maximize the benefit/cost of the sensing, networking, data processing and interpretation process. Reliable system identification of the integrated applications, sensing, networking, data processing, interpretation and decision-making becomes a key.

A common paradigm is centering on health monitoring and system identification and addresses various uncertainties in the modeling, experiment, data acquisition and processing, parameter estimation, model validation and correction, simulations and utilization procedures, irrespective of the form(s) of specific models. Following this paradigm, the design of a sensing system can be schematized in Figure. 1.

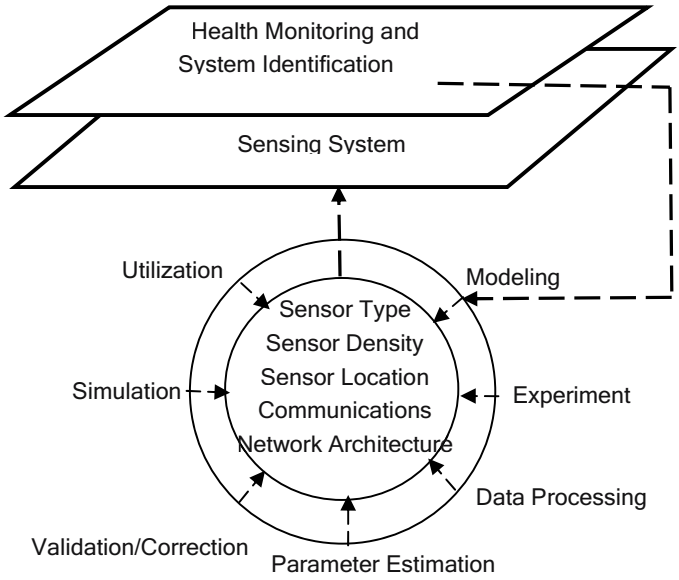

Figure 1: Paradigm of Sensing System Design

4. ERROR HANDLING IN DATA PROCESSING BY QUALITY ASSURANCE

It is critical to identify the type and the sources of variation in a measurement in terms of systematic/bias or common/random errors. The systematic sources of errors introduce relatively larger and sparser variations in measured values. Thus a critical investigation in identifying these sources will aid in improving the design of measurement procedures such that they are eliminated or accounted for. The common/random sources of variation occur on a regular basis with smaller magnitude, resulting in smaller variations in the measured values. The common causes are chance based and are in general expressed in statistical terms, and these can be named as a constant-cause-system if the outcome distribution is certain. Both causes of variation are often identified and handled using a Statistical Process Control (SPC) approach, based on measurements and analysis of these measurements.

Statistical quality control processes are a necessity when dealing with complex systems with numerous components and large amount of data points and observations. SPC provides tools and techniques for problem identification (Brain storming, cause and effect diagrams, Pareto charts, histograms and scatter diagrams) and process control charts for improving a design and increasing its efficiency. SPC benefits from basic statistical concepts such as mean of the selected subgroup. Measures are utilized to describe the central tendency and the dispersion-spread characteristics of the data. Typical central tendency measures include the mean, median and mode, where basic dispersion measures are range and standard deviation of the data. The normal distribution is a valuable tool for comparison purposes. However, checks for stability should initially be performed over time in terms of "control-charts." Control charts serve as a measurement tool for the ongoing measurement sequence. Plots of upper and lower control limits bound the data. Control charts for mean, range and proportion can be plotted. Control charts are instrumental in identifying the cause of variations in terms of common and assignable effects.

Stability checks over time point to the sources of variation (error). Stable variations, often called as constant cause systems, point to variability that is entirely due to common causes, which are due to natural and expected effects and can be managed. However, a system that is not stable indicates presence of assignable causes of variation, which are relatively large effects and occur in a rare or sporadic manner. The design and implementation of a successful SPC requires clear understanding of the system and heuristics involved. A detailed description of the measurement system and component characteristics and instrumentation design often accompany the preliminary

presentation of the measurement process. Engineered systems and measurement of their characteristics require knowledge of the heuristics to help design the SPC and identify the sources of variation and errors. A data flow chart is presented in Fig. 2 as an example of the data-flow-process of an actual health monitoring system of a major bridge. Various types of statistical measurements and control measures are listed for implementation at different levels.

The chart above indicates data flow channel for two purposes: 1) real-time presentation and 2) storage and archival. Real-time data presentation requires control-chart type validity checks on concurrent data and measurements where as the stored data can be used for different types of analysis and post-processing such as time-series modeling. In general, a statistical quality control process searches for various types of anomalies that can appear in forms of trends, jumps, periods, changes in precision, functional dependence and memory or serial correlation of various components. Statistical control charts can be used to test for jumps and other characteristics based on basic nonparametric tests such as: control limits, ranges, number of runs, length of runs, and etc.. Other tests for trends are in general based on analysis of variance and least square methods. Care must be taken in compounding different variation and error causes which are identified by different tests.

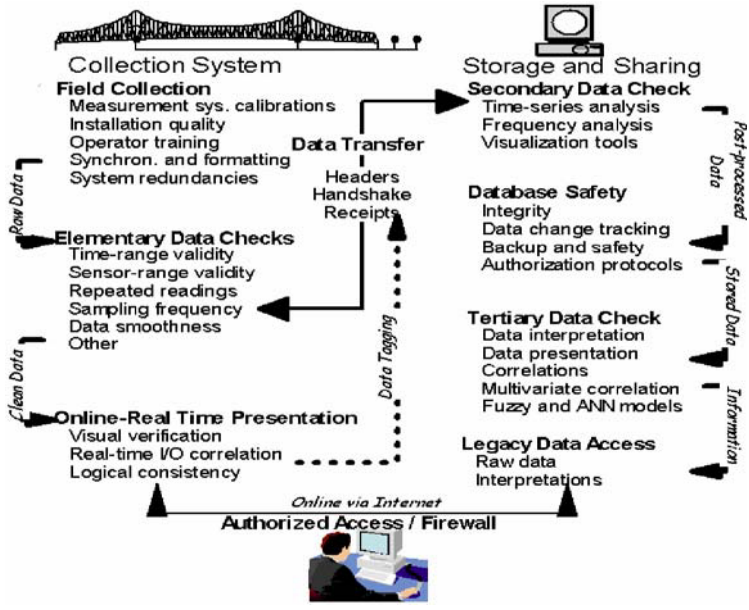

Figure 2 Data Flow Process Quality Assurance Chart

5. CONCLUSION

The objective of sensing is to provide meaningful and reliable image of a system. However, uncertainties of the physical phenomenon, imperfectness of the system model, ill calibration of the sensors, and improper design of the sensing scheme will impair the interpretation of the measurement data. Therefore, the design of a sensing system must consider the ability to identify those errors and extract the desired signal from interference; and this design consideration must permeate the he modeling, experiment, data collection, parameter estimation, model verification and correction, simulation and utilization procedures.

REFERENCE

1. Aktan AE, Frangopol DM, Ghasemi HM, Shinozuka M, Madanat S, and Shenton HW. “A Problem-Focused Agenda for the Highway Transportation Infrastructure: A Holistic Systems Identification and Integration Approach Using Field test Sites”, Final Report: NSF Grant CMS 0338817, March 2004.
2. Aktan, AE, Catbas FN, Grimmelsman KA and Pervizpour M. “ Development of a Model Health Monitoring Guide for Major Bridges”, Report developed for the FHWA Research and Development, 2002.
3. Devore JL. “Probability and Statistics”, 6 ed., Belmont, CA, Thomson Learning, 2004.
4. Zhang, R, Aktan AE, Wen J, Oh, P and Reddy A. “Unified Sensor Network Design for Infrastructure Systems”, Proposal to NSF, 2004.

PRACTICAL IMPLEMENTATIONS OF INTELLIGENT HEALTH MONITORING SYSTEMS IN HIT

Jinping Ou
School of Civil Engineering, Harbin Institute of Technology, Harbin, 150090, P. R. China

Abstract: The intelligent health monitoring systems more and more become a technique for ensuring the health and safety of civil infrastructures and also an important approach for research of the damage accumulation or even disaster evolving characteristics of civil infrastructures, and attracts prodigious research interests and active development interests of scientists and engineers since a great number of civil infrastructures are planning and building each year in mainland China. In this paper, some recent advances on research, development and implementation of intelligent health monitoring systems for civil infrastructures in mainland China, especially in Harbin Institute of Technology (HIT), P.R.China, are summarized. In this paper, integrated health monitoring systems and implementations in practical infrastructures such as offshore platform structures, hydraulic engineering structures, large span bridges and large space structures are introduced. The relative research projects supported by the national foundation agencies of China are briefly introduced and some issues to be further researched are pointed out.

Key words: Intelligent health monitoring, smart sensors, wireless sensor networks, full-scale implementation

1. INTRODUCTION

In mainland China, a great number of civil infrastructures are planning and building each year, e.g. the hydraulic engineering of the Three Gorges Project in Yangzhi river to have been finished, Sutong cable-staged bridge with a main span 1088m to have been building, a lot of offshore structures

Farhad Ansari (ed.), Sensing Issues in Civil Structural Health Monitoring, 291–300.

and seabed pipe line for Bohai Ocean oil field exploitation to have been planning and building, and many large space structures for 2008 Olympiad to have been planning and building etc. Chinese government, Chinese people and as well Chinese scientists and engineers have been paying much attention on their health, durability and safety in the following long term service periods. It is just the urgent and extensive needs of civil infrastructure construction and management in mainland China that the Chinese scientists and engineers work closely with others in the world together to promote the research and development of intelligent health monitoring systems for civil infrastructures.

In this paper, some recent advances on research, development and implementation of integrated health monitoring systems for civil infrastructures in mainland China P.R.China, are summarized. Finally, the relative research projects supported by the national foundation agencies of China are briefly introduced and some issues to be further researched are pointed out.

2. BASIC FRAME OF HEALTH MONITORING SYSTEMS

A health monitoring system of civil infrastructure at least includes the four functional modules as shown in Fig.1. There are three basic requirements for the system: long term, real-time and automatic monitoring.

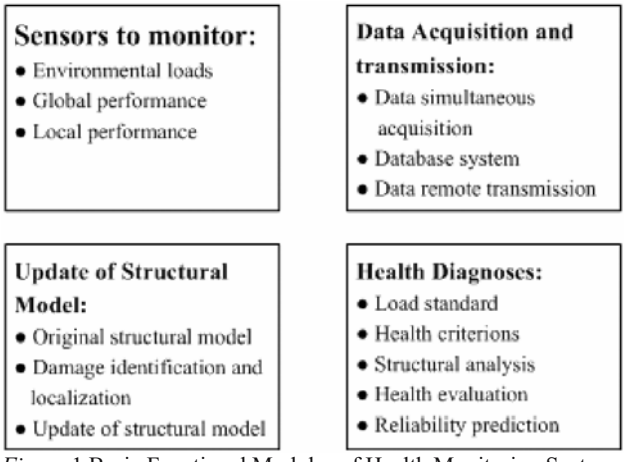

Figure 1 Basic Functional Modules of Health Monitoring Systems

In mainland China, the health monitoring systems of civil infrastructures more and more attract the attentions of government, scientists and

engineering. Both of the National Natural Science Foundation of China and the National Hi-tech Research and Development Program set up major and key projects for the fundamental research and hi-tech development of health monitoring systems. Besides, the health monitoring systems begin to be installed in some of civil infrastructures.

3. OFFSHORE PLATFORMS

Bohai Ocean Oil Field is one of main ocean oil fields in China, in which the ice force is very heavy in winter and becomes the main environmental force of offshore platforms. In 1960's and 1970's, there were respectively two platforms to be collapsed by heavy ice force action.

(a) Bohai JZ20-2MUQ platform to be monitored

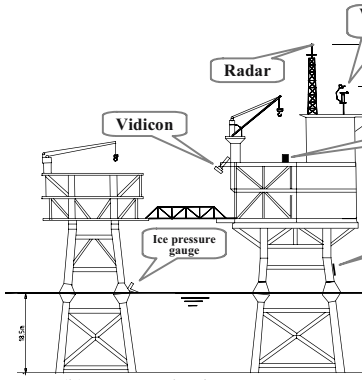

(b) Sensors in the system

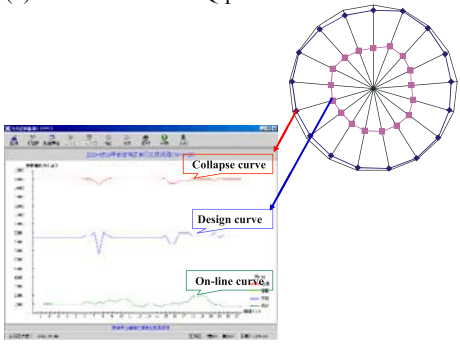

(c) Interface of safety evaluation subsystem

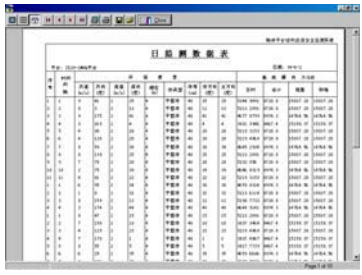

(d) Report form of database

Figure 2 Health monitoring system of Bohai JZ20-2MUQ Platform

Since 1980's, the ice conditions, ice pressure on and response of platforms in Baihai ocean have being monitored under support of China Ocean Oil Company. Based on these facilities and systems, Ou *et al* (2001)

developed an on-line health monitoring system for one of typical platform structures, JZ20-2MUQ steel jacket platform as shown in Fig.2a, which have been implemented in the platform since 1999. The platform with total height 55.4m was built in 1991 and located in the heavy ice region of Bohai ocean with design water depth 15.5m. The system includes the following three subsystems: environmental condition and structural response monitoring subsystem in which the sensors are shown in Fig.2b, safety evaluation subsystem in which the total base shear force under environmental loads compares in real time with the ultimate base shear force of structure in the same direction as shown as Fig.2c, and database subsystem which report form is shown in Fig.2d.

(a) Original Steel Jacket and Smart Sensors Installing

(b) Fabricated steel Jacket and the jacket built in the ocean

Figure 3 The Steel Jacket of CB32A Platform to be monitored

Another health monitoring system have being developed by Ou and his research group for CB32A steel jacket platform in Bohai ocean under the project supported by the National Hi-tech Research and Development Program of China. The Platform with jacket height 24.7m was built in 2003 and located in water depth 18.2m. The system includes 259 OFBG sensors, 178 PVDF sensors, 56 fatigue life meters, 16 acceleration sensors, a set of environmental condition monitoring system and also the transmission wire 27, 000m. Fig.3 shows the steel jacket and the scene that the sensors are installed on the jacket and Fig.3b shows the fabricated jacket and the jacket built in the ocean.

4. HIGH-RISE BUILDINGS

Based on the wireless sensors developed at Berkeley, Ou and Li (2003) developed a wireless sensor network system including a base station and 5 wireless sensor nodes and this system has been applied in the wind-induced vibration and acoustic noise monitoring of Diwang Commercial Building in Shenzhen city of China, as shown in Figure 4. The building is 68 stories, standing 324.95m above street level and the natural frequency is less than 0.2Hz.

(a) Wireless Sensor (Berkeley Mote)

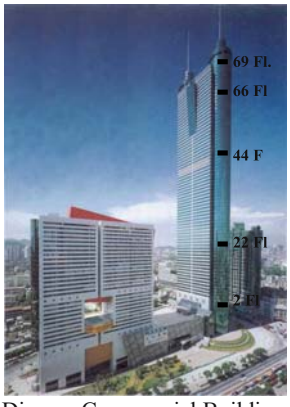

(b) Diwang Commercial Building and Wireless Sensor Placements

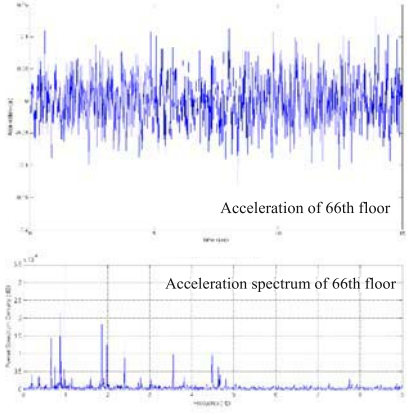

(c) Acceleration and its spectrum of 66th floor

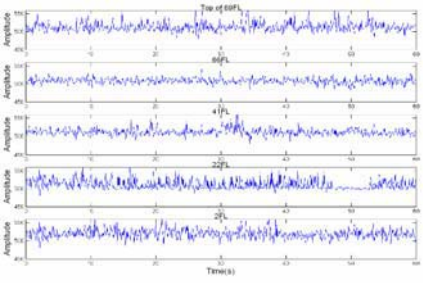

(d) Acoustic noise along the height of the building

Figure 4 Wireless sensor network and monitored results in Diwang Commercial Building

5. HYDRAULIC ENGINEERING STRUCTEURES

Since 1998, the health monitoring systems including optical fiber sensors began to be implemented in some hydraulic engineering structures of the Three Gorges Project. Cai (1998), when he was working in HIT developed the crack monitoring systems using optical fiber sensors and implemented them respectively in a temporary ship milldam and Gudongkou concrete face rockfill dam of the Three Gorges Project., as shown in Fig. 5. The dam is located in Xiangqi anabranch of Yangzhi river, Xingshan county of Hubei province, which control drainage area is 956km^2, height 120m and volume 1, 880, 000m^3. The cross distributed optic fiber and optical time domain reflection TES3031 was employed in the crack monitoring system for the field detection, as shown in Fig.5.

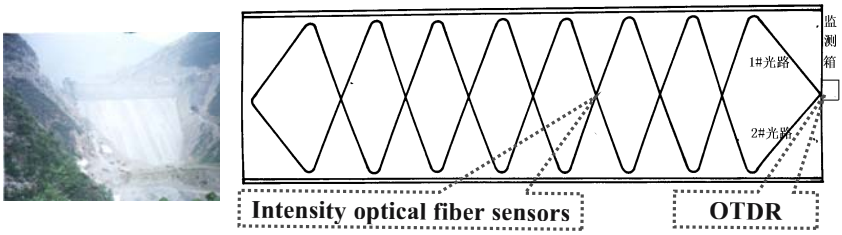

Figure 5 Gudongkou Concrete Face Rockfill Dam and optical fiber monitoring system for the crack of Gudongkou Concrete Face Rockfill Dam

In June 16 and July 30, 1998, the two monitored results shown a crack with length 0.2mm on the concrete face of dam 71.m far from OTDR along with optical fiber line 2, which was verified by a person checking in the field.

6. LONG SPAN BRIDGES

In mainland China, a lot of large bridges have been built or will be built with fast development of economics and transportation engineering, especially from Shanghai Nanpu cable-stayed bridge to be built and finished in 1991. According to the Chinese specifications for the construction of large span bridges, a bridge should be monitored when constructed and it will be tested by simulating design loads after finished. For these purposes, a temporary monitoring and testing system should be set up and then can be employed to monitor the performance of the bridge in service for a short term. For instances, Guangdong Humen cable-suspended bridge with a main span 880m, Shanghai Xupu cable-stayed bridge with a main span 590m and Jiangsu Jiangyin cable-suspended bridge with a main span 1358m on

Yangzhi river were monitored by employing the temporary systems for short term.

From 2001, Ou and his group have implemented intelligent health monitoring systems on some bridges in mainland China. One of them is the intelligent health monitoring system for Shandong Binzhou Yellow River Bridge has being developed and constructed by Ou and his research group. The bridge is a cable-stayed bridge with three towers and 84+300+300+84m span distribution and located in Binzhou city, Shandong of China. The system includes 96 optic fiber sensors embedded in the girders, deck and towers, measuring the strain and temperature of the members, 39 accelerometers attached on the deck, cables and towers, 2 anemoscopes installed respectively on the middle-span between the middle-tower and the side-tower and top of the middle-tower, 1+3 GPS receivers installed on the top of the middle-tower (1 receiver) and the middle-span between the middle-tower and the side-tower (2 receivers), and the outside of the bridge (1 base-receiver), respectively, measuring the displacement of the tower and middle-span of bridge. The system has been integrated with damage detection, model updating and safety evaluation and a database. The data are transmitted by wireless communication system and the system is running for 4 months. The website of this system is www.hitbzbridge.8866.org.cn. Fig.6 shows the bridge and the health monitoring system.

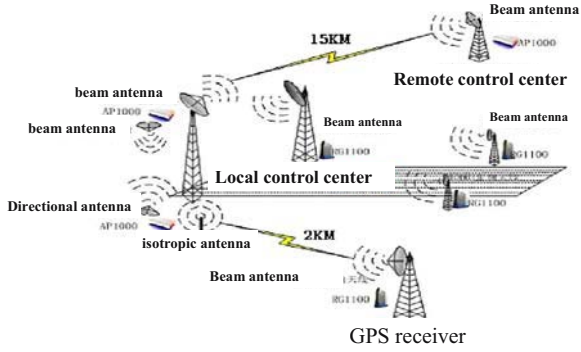

Figure 6 The wireless communication system for SHM of Binzhou Yellow River Bridge

In mainland China, there are about 10 large span bridges to have been planned or to have being planned to develop and implement the intelligent health monitoring systems. For examples, the third Nanjing Yangtse River cable-stayed bridge with a main span 648m, Jiangsu Runyang Yangtse River cable-suspended bridge with 1490m and Zhejiang Sutong Yangtse River cable-stayed bridge with a main span 1088m have being planned to develop and implement the intelligent health monitoring systems.

7. LARGE SPACE STRUCTURES

In mainland China, a lot of large space structures for 2008 Olympiad have been planning and building.

In 2002, Qu *et al* (2002) finished the health monitoring system for the large-space truss roof of Shenzhen Government Office Building. The building roof is 486m length and 156m width, in which the branch truss braced on the towers in the middle span and some other members of the truss maybe buckle when subjected to strong wind, as shown in Fig.7. The monitoring system consists of sensors measuring the response of the roof-system, analysis program calculating the response and evaluating the safety of the roof-system. The signals are saved in a database and the signals in the database can be transmitted to the local network and internet by remote severs. The sensors include optic fiber sensors, electric strain gauges, accelerometers, anemoscopes and wind-pressure meters. The strain of the members can be measured by electric strain gauges and optic fiber sensors. The acceleration and displacement of the roof can be measured by accelerometers. The wind pressure distribution can be measured by anemoscopes and wind-pressure meters. The program can detect the damage of the roof, update the analysis model and evaluate the safety based on the measured response and the wind loads.

(a)The middle span of roof under constructed

(b) The building after constructed

*Figur*e 7 Shenzhen Government Office Building to be monitored

8. RELATIVE RESEARCH PROJECTS

The research projects about the health monitoring systems of civil infrastructures mainly comes from the government research foundation agencies such as the National Natural Science Foundation of China (NSFC), the Ministry of Science and Technology, especially the National Hi-Tech Research and Development Program, and practical engineering projects.

NSFC supported or will support the following projects:

1) In 2003, NSFC supported an international cooperative major project—China-USA-Japan Project: Intelligent Health Monitoring Systems of Civil Infrastructures.

The National Hi-Tech Research and Development Program, from 2001-2005, supported the following projects in the area of Technology for Ocean Resource Development:

1) Inspective and Monitoring Technique of Oil Pipe Line on Seabed.

2) Inspective and Monitoring Technique of Offshore Platform Structures.

3) Inspective and Monitoring Technique of Geotechnical Conditions of Ocean Engineering.

The Ministry of Transportation and many local governments of China have been supporting the research and development projects for the health monitoring systems of various large span bridges.

9. CONCLUSIONS

The following areas may be the future main areas need to pay more attention on:

1) The durability of sensors themselves is one of key problems.

2) A heath monitoring system of civil infrastructure often includes several hundreds or even several thousands of sensors, so, the wireless sensor network is no doubt an important research area.

3) The integration and implementation of heath monitoring systems in practical infrastructures are the symbol that the systems show their advantages and vitality, and also are the main research area.

4) Benchmarks of health monitoring systems are very necessary for the development of systems or other branches. But, these Benchmarks should be physical or practical systems, which can be shared by remote researchers.

5) The design guideline of SHM and standard SHM systems are key issues for the development and implementation of SHM systems in practical infrastructures.

ACKNOWLEDGMENT

This research is financially supported by the National Natural Science Foundation of China under the grant number 50238040 and the National Hi-Tech Research and Development of China under the grant numbers 2001AA602023, 2002AA3131110, 2002AA335010.

REFERENCES

1. B. Wang, Z. He, X. Y Zhang. and J. P. Ou (2003), "Fiber reinforced polymer bars applied to civil engineering", *Architecture Technology*, 34 (2): 134-136. (in Chinese)
2. D. S. Cai (1998), "Monitoring technical researches of crack in dam using optical fiber and stability analysis of dam foundation", *Postdoctoral Research Report*, Harbin Institute of Technology, P. R. China, (In Chinese)
3. H. W. Li, Z. Zhou, and J. P. Ou (2003), "Offshore platform health monitoring applications of wireless sensor", *Proceedings of the 21th International Modal Analysis Conference* (IMAC XXI), Florida, USA
4. J. L. Li, Z. Zhou and J. P. Ou (2004), "Interface transferring mechanism and error modification of embedded FBG strain sensor", *SPIE 11th Annual International Symposium on Smart Structures and Materials*, San Diego, California, USA.
5. J. P. Ou & Z. Zhou (2003), "Encapsulation techniques for FBG and smart monitoring for bridges with FBG sensors", *Proceedings of 4th International Workshop on Structural Health Monitoring*, Stanford, CA, USA.
6. J. P. Ou and H. W. Li (2003), "Wireless sensor information fusion for structural health monitoring", SPIE, Vol. 5099: 356-362.
7. J. P. Ou, B. Wang, Z. He and X. Y. Zhang (2003), "Self-sensing properties of CFRP and OFBG-GFRP bars for concrete structures", *Proceeding of 4th International Workshop on Structural Health Monitoring*, Stanford, CA, USA.
8. J. P. Ou, B. Wang, Z. He, X. Y. Zhang and M. Z. Qian (2002), "Mechanical and sensing properties of FRP bars for concrete structures", *Pacific Science Review*, 4: 93-99.
9. J. P. Ou, H. W. Li, Y. Yu (2004), "Development and performance of wireless sensor network for structural health monitoring", *SPIE 11th Annual International Symposium on Smart Structures and Materials*, San Diego, California USA.
10. J. P. Ou, Y. Q. Xiao, H. J. Huang, and Z. D. Duan et al (2001). "A real-time safety monitoring system of offshore platform structures", *Ocean Engineering*, 21(2): 1-6. (In Chinese)
11. J. P. Ou, Z. Zhou, Z. J. Wu (2002), "The sensing properties and practical application in civil infrastructures of optical FBGs", . SPIE., Vol. 5129.
12. Z. Zhou, B. Wang, and J. P. Ou (2004), "Local damage detection of RC structures with distributive FRP-OFBG sensors", *Proceedings of 2nd International Workshop on Structural Health Monitoring of Innovative Civil Engineering Structures*, Winnipeg, Manitoba, Canada
13. Z. Zhou, J. P. Ou, and B. Wang (2003), "Smart FRP-OFGB bars and their application in reinforced concrete beams", *Proceedings of 1st International Conference on Structural Health Monitoring and Intelligent Infrastructure*, 13-15, Nov, Tokyo, Japan: 861-866
14. Z. Zhou, Z. D. Duan, Z. H. Jia and J. P. Ou (2004), "New kind of structural fatigue life prediction smart sensor", *SPIE 11th Annual International Symposium on Smart Structures and Materials*, San Diego, California, USA.

HEALTH MONITORING, DAMAGE PROGNOSIS AND SERVICE-LIFE PREDICTION – ISSUES RELATED TO IMPLEMENTATION

Vistasp M. Karbhari
Department of Structural Engineering, University of California San Diego, USA

Abstract: This paper discusses the primary challenges to the implementation of a structural health monitoring system, while emphasizing the importance of assessing characteristics such as capacity and remaining life. A field test bed is presented to illuminate specific aspects and to identify key needs for the future.

Key words: Bridge, capacity, remaining life, damage, durability.

1. INTRODUCTION

Although the term Structural Health Monitoring (SHM) has gained prominence recently, its basis and motivation can be traced to the very earliest endeavors of mankind to conceptualize, construct, worry about deterioration, and then attempt to repair (or otherwise prolong the life) of a structure. Thus it represents an attempt at deriving knowledge about the actual condition of a structure, or system, with the aim of not just knowing that its performance may have deteriorated, but rather to be able to assess remaining performance levels and life. In its various forms, over the years, it has been represented as the process of conventional inspection, inspection through a combination of data acquisition and damage assessment, and more recently as the embodiment of an approach enabling a combination of non-destructive testing and structural characterization to detect changes in structural response. In recent years it has often been considered as a complementary technology to systems identification and non-destructive

Farhad Ansari (ed.), Sensing Issues in Civil Structural Health Monitoring, 301–310.

damage detection methods. In 1997, Housner et al defined it as "the use of in-situ, non-destructive sensing and analysis of structural characteristics, including the structural response, for detecting changes that may indicate damage or degradation" [**1**]. While this definition provides a basis for a data management system it falls short of the goal of considering the effect of deterioration on performance and thence on the estimation of remaining service life. These management systems thus focus on processing collected data, but are unable to measure or evaluate the rate of structural deterioration. In essence a true system should be capable of determining and evaluating the serviceability of the structure, the reliability of the structure, and the remaining functionality of the structure in terms of durability. This functionality has an analogy to the health management system used for humans wherein the patient undergoes a sequence of periodic physical examination, preventive intervention, surgery, and recovery [**2**].

Thus, what is needed is an efficient method to collect data from a structure in-service and process the data to evaluate key performance measures, needed by the owner, such as serviceability, reliability and durability. For the current work, the definition by Housner et al [**1**] is modified and structural health monitoring is defined as *the use of in-situ, nondestructive sensing and analysis of structural characteristics, including the structural response, for the purpose of estimating the severity of damage/deterioration and evaluating the consequences thereof on the structure in terms of response, capacity, and service-life.* Essentially, a SHM system then must have the ability to collect, validate, and make accessible, operational data on the basis of which decisions related to service-life management can be made.

It must be noted that a critical feature of such systems is embedded in the concepts of durability and damage tolerance as developed in the aerospace world, and as shown schematically in Fig. 1.

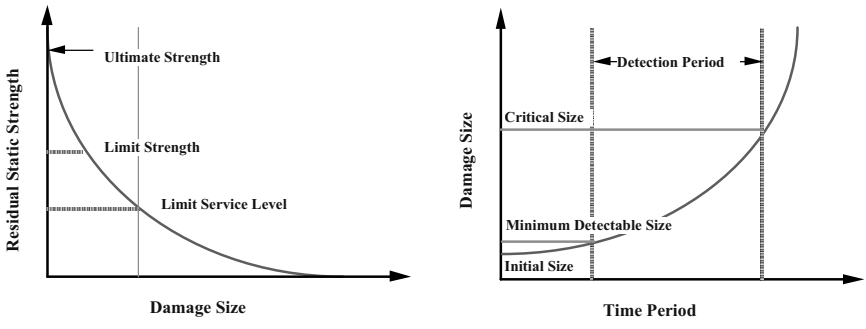

Figure 1. Application of Concepts of Durability and Damage Tolerance to Design

It should be noted that while the concept is depicted in terms of residual static strength and damage size, it could just as easily be expressed in terms of another residual performance characteristic, or even remaining life, and deterioration as measured through characteristics other than physical damage size.

Despite the tremendous advances in each of the critical areas needed for the implementation of efficient SHM systems, the full benefits of these are rarely realized. This paper presents a brief discussion of some of the reasons for this, while pointing out some of the principal challenges to be overcome, and then describing a simple system that incorporates parts of the solution, but is still incomplete in terms of overall effectiveness as a true SHM system.

2. CHALLENGES

SHM intrinsically includes the four operations of acquisition, validation, analysis, and management. Also, the concept of monitoring prescribes that it be an ongoing process rather than one that is used at preset intervals of time. Thus SHM is essentially the basis for condition-based, rather than time-based, monitoring and the system should be capable of integrating real time data on ageing and degradation into the assessment of structural integrity and reliability. Unfortunately, typical systems do not use an integrated approach to the design, implementation, and operation, of the SHM system, resulting in the benefits of the system not being realized. Too often, a disproportionate emphasis is placed on the collection of data rather than on the management of this data and the use of decision-making tools that would support the ultimate aim of using the collected data to effect better management of the infrastructure system. Typically, systems collect data on a continuous or periodic basis and transmit the data to a common point. The data is then compared with results from a numerical model. The weakness is that most systems do not attempt to update the model to reflect ageing and deterioration, or changes made through routine maintenance or even rehabilitation. While some systems incorporate a systems identification or non-destructive damage evaluation algorithm to rapidly process the data, these are the exception, not the rule. Even here, there is a gap between the management of this data, and its use towards the ultimate goals of estimating capacity and service life [**3**].

Through a review of a large number of SHM projects the following primary aspects can be identified as concerns and challenges:

- Lack of clearly defined goals for the system
- Problems with instrument selection and operation

- Lack of high rates of useable (i.e. valid) data
- Lack of real-time analysis of the validated data
- Lack of tools for appropriate data interpretation, and result implementation.

It is important to emphasize here that in most cases it is not the lack of solutions that is the challenge, but rather the selection and integration of the tools appropriate to the system under consideration. A brief discussion of each of the 5 aspects is given below.

SHM systems are often used based on technology push rather than applications pull based on a clearly defined objective. While the enhancement of systems safety (through use of the SHM as a mechanism of warning of failure) is desirable, SHM systems by themselves cannot ensure a higher level of safety, or even a better method of maintenance. SHM systems by themselves also cannot ensure a decrease in the level of maintenance, or even an increase in the periods between maintenance. If appropriately designed, however, they can reduce the amount of unnecessary inspections and ensure that deterioration/degradation is tracked such that the owner/operator has consistent and updated estimates of deterioration (quantity and general location), capacity, and remaining service life.

While a large number of sensors are now available ranging in size, sensitivity, method of measurement, and ability to work in a hard-wired and/or wireless mode, the intrinsic challenge still remains the same – appropriate selection (based on actual need, operational environment, and expected service life) and placement, and appropriate design of the system. All too often the small size, relative cost, or just the inability of the users to design a system, results in the overuse of sensors. The mere capability of placing a million sensors on a structure does not automatically ensure a better SHM system. Rather, it almost always ensures failure since attention has not been paid to design, nor of how to access and interpret data. Just as materials deteriorate under environmental exposure and through use, sensors can also degrade, and this fact is often completely forgotten, resulting in expensive and highly complicated systems either delivering invalid, or no data, in very short periods of time. When used in a civil engineering environment special care has to be taken to ensure compatibility with the changing environment and the vagaries of nature. This is of special importance when sensors are bonded or otherwise placed on surfaces, which may be subject to extremes of temperatures, large temperature variations (both daily and over seasons), moisture (ranging from humidity and precipitation to actual immersion such as when flash floods cause overtopping of bridges), and UV radiation. Compensation for temperature variation is well established for bonded resistance strain gauges and accelerometers. Yet false alarms are often seen due to fast transient

temperature changes especially in low frequency accelerometers and this must be kept in mind during sensor selection and deployment. In cases where the sensors are bonded onto the concrete or steel substrates, care needs to be taken to ensure that the bond itself does not deteriorate with exposure and time, and further that deterioration and/or changes at the level of the substrate do not cause recording of erroneous measurements. While these aspects may appear to be trivial, they are of extreme importance in ensuring the long-term reliability of data. There are special concerns related to use of SHM in cold regions beyond those associated with increasing brittleness of the materials used in the sensors, leads and connections. Rime (a form of ice which forms when super-cooled droplets, such as those in fog) freezes on contact with surfaces already below freezing and causes sensors to literally freeze. This can cause brittle rupture of components themselves, or stretching, fracture, or even pull-out of the connectors and leads. In addition the overall design of the system must take into account effect of accidental impact such as that from floating debris (Fig. 2) which can effectively cause severe damage due to repeated impact.

Figure 2. Floating Debris in the Form of a Tree Trunk and Roots

It is critical that sensor and system selection is based not just on considerations of sensitivity and durability, but also on robustness and reliability, especially if the SHM system is expected to be in operation over an extended period of time. In this vein it should be noted that although fiber optic systems have good sensitivity and fairly good short-term durability, the drift can be significant if intended to be used continuously over long periods of time at very high levels of sensitivity. In addition, even though these systems have been seen to show very good performance in extremely harsh environments (such as when mounted in automotive cylinders subject to instantaneous gas temperatures as high as 1500 C and continuous temperatures upto 300 C with pressures upto 300 bar), their

reliability to date rarely exceeds 10 years. It must be emphasized that this is only a fraction of the expected service-life of a bridge, thus pointing out the need for monitoring of the SHM system itself to ensure that parts are replaced prior to the end of their service lives.

It must be emphasized that even in times when sensor costs can be reasonably expected to decrease substantially there is a fallacy in the argument that "More is better." In fact it can easily be shown that the opposite is true – the increase of data channels not only complicates the issue of data transmission and synchronization, but also increases the complexity of data validation. Further, just having data by itself of points in the structure that are unimportant and do not provide any characterization of response, is in itself a waste. Thus there is a major challenge in minimizing (i.e. optimizing) the number of sensors based on actual need and ability to characterize pertinent aspects of response.

Similar to the challenge of selection of the sensor and its placement, is the challenge of assessing the validity of data. While large data streams may seem impressive to the routine observer (and unfortunately all too often even seem to be the ultimate goal of experienced engineers and scientists, without concern regarding the usefulness of the data) what is important is the ability to validate the data in real time, and thereby separate signals due to non-responsive sensors from those providing actual measurement of response. All too often a structure or system has been declared severely damaged, or conversely totally undamaged, after an extreme event, because the validity of data streams was not checked. There are two generic approaches to validation – analytical redundancy and hardware redundancy. In the first approach a mathematical model has to be implemented that allows for comparison of static and dynamic responses of the sensor to determine the anticipated value. Unfortunately this requires addition of sensors, and increases time and complexity. In the case of hardware redundancy validation is done through selection of data that is common to a majority of sensors. Again, for reliability the number of sensors has to be increased, but depending on the structure even this may not ensure validation of the data stream. Further, this results in overall loss in sensitivity since the result is necessarily a statistical approximation. The obvious solution, albeit with significant implementation challenges, is the development of a knowledge based system that applies reason through genetic algorithms, fuzzy logic, or other such tools to infer the right solution. This would enable validation in real-time (unlike the two previously described approaches) through use of reasoning under uncertainty. However, again the major challenge is to find the right compromise between performance and precision [**4, 5**].

While it is useful to be able to both see data streams in real-time and to archive them for future use, the real purpose of the data is to allow

interpretation and analysis. If the system is setup such that there are large streams of data, but none of it can be accessed in real-time the system must be considered a failure. Obviously data pertaining to damage done due to seismic excitation is largely useless if it is only accessible after visual inspection shows that the bridge has collapsed! If one assumes that a large percentage of available data is valid, then the benefits are still substantially curtailed if a preliminary assessment and characterization of response cannot be completed almost in real-time.

Unfortunately, the greatest challenge is that most SHM systems are designed merely to collect data, rather than to provide a means for its efficient management and interpretation. It is critical that the system provide a means not just of recording (and displaying) response, but also (and more importantly) of characterizing the response and comparing it to an appropriately updated model to enable assessment of the critical aspects of capacity and service-life.

Thus overall, the major challenges initiate with the development of an appropriate plan for SHM, and continue through the selection and placement of the sensors, collection and transmission of data, checking of its validity, and finally to the actual use of the data in a manner required by the owner/operator of the structure. In reality the major challenge is in moving past the mere attractiveness of a sensor network to the actual development and implementation of a system capable of serving as a true tool for health monitoring – i.e. not just being able to state that the "patient" is sick, but rather of being able to pinpoint the location and reason, as well as the effect of the incapacity.

3. IMPLEMENTATION ON A FRP BRIDGE

The Kings Stormwater Channel Bridge represents a class of hybrid fiber-reinforced polymer (FRP) composite bridges incorporating stay-in-place FRP structural formwork shells for girders (filled with concrete) with a FRP deck connected on top [**6**]. Given the fact that the bridge was the first of its kind in California, and was located on a major highway with significant truck traffic, there was concern related to the maintenance of structural integrity over time. A need thus existed for the development and implementation of a monitoring system that could not only measure bridge response, but also evaluate aspects related to structural safety.

Based on careful analysis of component and systems response, a sensor network consisting of 63 accelerometers, 20 strain gages, 4 linear potentiometers, 1 temperature sensor, and a pan-tilt-zoom (PTZ) camera., was designed and installed. A Campbell Scientific CR9000 modular high-

speed data-logger capable of making measurements at an aggregate sampling rate of 100K hertz for up to 200 channels was used as the core of the data acquisition system. collected data was conditioned and digitized, then stored into the cache memory of the CR9000 and simultaneously was transmitted using a 900 MHz wireless antenna to a network node on a mountaintop (Toro Peak) along the line of sight and from there along the main backbone of a wireless network to a central node at the University of California, San Diego (UCSD) at a rate of 45 Mbps. Data is then analyzed to (a) extract modal parameters, (b) determine changes, usually based on changes in mass or stiffness, (c) enable damage localization and estimation of damage severity, and (d) assess changes in capacity. The overall approach, as well as the details of damage detection and severity estimation algorithms, are provided in [**7**] and hence are not repeated herein. An overall schematic of data flow is given in Fig. 3 and an example of damage indicators are shown in Fig. 4. The system incorporates the use of a finite element model of the bridge that is constantly updated to provide in-service estimates of response deterioration. This provides the user with the capability of not only comparing modes, frequencies and severity indexes, but also of reviewing data against pre-determined thresholds that signify levels of acceptable response.

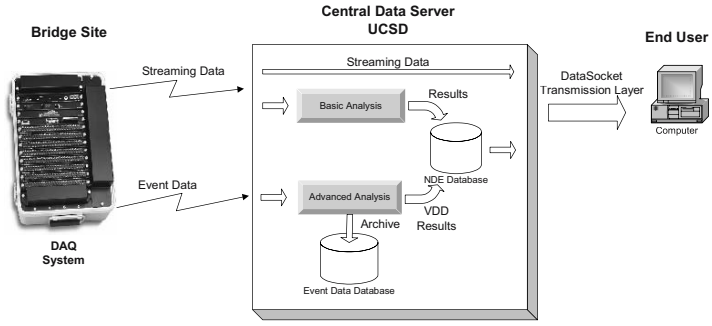

Figure 3. Schematic Showing Data Flow

Figure 4 shows a comparison of damage indicator estimates from two different data sets. As can be seen the region with the highest damage indicator magnitude is concentrated around an area about 3.3m (10 ft) on either side of the capbeam which correlates with visual observation of damage through deterioration of the construction joint between deck panels. It is of interest to note that the increase in damage indicators in these regions was noticed ahead of visual identification of the distress emphasizing the value of such a health monitoring system in not just monitoring response but also in providing advance warning of deterioration.

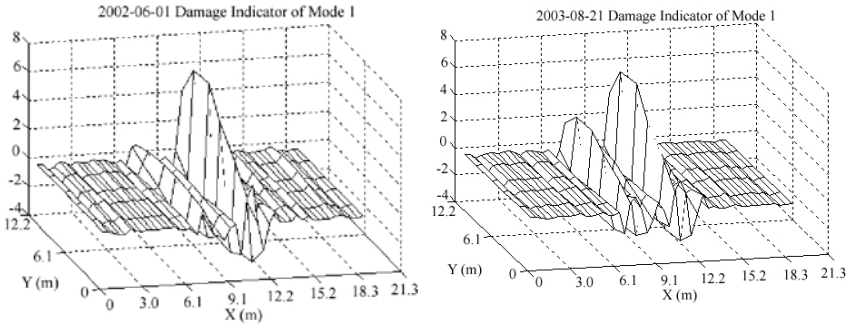

Figure 4. Progression in damage indicator of the first modal vector with time (the Z axis provides the amplitude of the damage indicator, the X axis is in bridge longitudinal direction and the Y axis is in bridge transverse direction)

While this system provides a reasonable example of data collection, transmission, validation and use, it falls short of fulfilling all the objectives of a true SHM system in that it does not provide direct estimates of capacity and remaining service-life – both of which are critical to an owner/operator. Further, the damage identification and severity estimation technique, while extremely efficient, only provides relative comparisons, making the characterization of absolute levels difficult. Continuous use of the system over a number of years has also brought to light another often neglected challenge – reliability of the data transmission system, and the need for ensuring backups right at site. Further it is clear that modifications need to be made both to the sensor network and the algorithms to enable determination of absolute levels of damage, rather than relative ones, as well as the real-time transfer of the results to a system capable of determining capacity and remaining service-life – both of which are currently done off-line using isolated data sets.

4. SUMMARY AND CONCLUSIONS

It is expected that the further developments of SHM systems will result in the establishment of a comprehensive methodology for autonomous health monitoring of structural systems to the point where true condition based physical inspection and monitoring would become a reality. The major sensing challenges lie in the appropriate design of the sensor network emphasizing optimal choice of type, number and location, as well as aspects of robustness and reliability. At the level of data management, beyond the challenges of cost-efficient band width, are the challenges associated with development of robust and effective tools for real-time data interpretation and use in developing measures of performance (such as capacity) and

remaining service life. The integration of damage identification and finite element based tools would then conceivably further provide assistance to the engineer in assessing health immediately rather than having to resort to expensive closures while assessments are made off-line.

ACKNOWLEDGEMENTS

The support of the California Department of Transportation for the research reported in this paper is gratefully acknowledged. The author acknowledges the efforts of his graduate students Mr. Luke Lee and Mr. Hong Guan in conducting the research. He would also like to acknowledge the discussions and insights provided by Prof. Dick Wilkins (University of Delaware), Dr. Charles Sikorsky (California Department of Transportation), Prof. Norris Stubbs (Texas A&M University), Prof. Masanobu Shinozuka (University of California Irvine) and Prof. Aftab Mufti (ISIS Canada and University of Manitoba) which have helped to develop his concepts on SHM and damage tolerant design.

REFERENCES

1. Housner, G.W., Bergman, L.A., Caughey, T.K., Chassiakos, A.G., Claus, R.O., Masri, S.F., Skelton, R.E., Soong, T.T., Spencer, B.F. and Yao, J.T.P. "Structural Control: Past, Present, and Future" *ASCE Journal of Engineering Mechanics*, 123[9], pp. 897-971, 1997.
2. Aktan, A.E., Catbas, F.N., Grimmelsman, K.A. and Tsikos, C.J. "Issues in Infrastructure Health Monitoring for Management," *ASCE Journal of Engineering Mechanics*, 126[7], pp. 711-724, 2000.
3. Sikorsky, C. and Karbhari, V.M. "An Assessment of Structural Health Monitoring capabilities to Load Rate Bridges" *Proceedings of the First International Conference on Structural Health Monitoring and Intelligent Infrastructure*, A.A. Balkema Publishers, pp. 977-985, 2003.
4. Ibarguengoytia, P.H., Sucar, L.E. and Vadera, S. "Real Time Intelligent Sensor Validation", *IEEE Transactions of Power Systems*, 16[4], 2001, pp. 770-775.
5. Andrew, J.F. "Integrity-Based Self-Validation Test Scheduling," *IEEE Transactions on Reliability*, 52[2], 2003, pp. 162-167.
6. Seible, F., Karbhari, V.M. and Burgueno, R. "Kings Stormwater Channel and I-5/Gilman Bridges, USA" *Structural Engineering Internationa*l, 9[4], pp. 250-253, 1999.
7. Karbhari, V.M., Guan, H. and Sikorsky, C. "Web-Based Structural Health Monitoring of a FRP Composite Bridge," *Proceedings of the First International Conference on Structural Health Monitoring and Intelligent Infrastructure*, A.A. Balkema Publishers, pp. 217-226, 2003.

ADAPTIVE EVENT DETECTION FOR SHM SYSTEM MONITORING

Dean K. McNeill and Loren Card
Electrical and Computer Engineering, University of Manitoba, Winnipeg, MB, R3T 5V6, Canada

Abstract: One of the greatest challenges affecting the use of structural health monitoring is the establishment of effective and reliable techniques for processing and management of the accumulated measurement data. This article presents results achieved in the use of an artificial neural computing approach applied to this problem. The unsupervised neural learning algorithm known as frequency sensitive competitive learning is employed in the processing of sensor data from three civil engineering structures. It is shown that the algorithm is capable of learning the normal response of the structure and provides effective means of identifying novel features in the sensor record thereafter. This permits further detailed study of these specific noteworthy events. Events are identified using a relative novelty index computed by the neural network architecture. Examples demonstrate the identification of vehicle traffic on one bridge, seismic activity on a second and the response to wind loading on a feature statue.

Key words: Novelty detection, artificial neural networks, unsupervised learning.

1. INTRODUCTION

Structural health monitoring (SHM) has, at its root, the goal of continuous evaluation and assessment of civil engineering structures in order to quickly and accurately focus expert attention on performance variations of potential concern. Unlike current practice, where structures are manually inspected and/or tested on a periodic basis, SHM systems rely upon the permanent installation of sensors and measurement equipment at the

Farhad Ansari (ed.), Sensing Issues in Civil Structural Health Monitoring, 311–319.

structure site to facilitate continuous monitoring. These sensors commonly consist of metal-foil strain gauges, accelerometers, thermocouples, displacement transducers and most recently, innovations in fibre-optic strain gauges.

Deployment of any SHM system brings with it many challenges, not the least of which is the problem of effective data analysis. As a consequence of the continuous nature of the structural monitoring, SHM systems generate vast quantities of sensor measurements which must be processed in order to extract some measure of the structure's current state of health. While from an electronic perspective, the rate of sensor interrogation is modest (typically less than 100Hz) the very number of sensors and the fact that they are being monitored on a continual basis results in extremely large collections of data being accumulated in a relatively short period of time. To illustrate the extent of this problem, consider that a single sensor channel sampled at 100Hz will generate 17MB of raw data each day or 6.3GB of raw data in a year. Given that a typical structure will employ tens or upwards of a hundred such sensors, the problem of data storage and information management quickly becomes apparent.

Clearly, any manual endeavor to analyze these measurements is untenable. As such, the ultimate success of a health monitoring approach depends upon the development of automated techniques for the analysis of the sensor record. On the surface, automating the signal processing task seems relatively straightforward, given that similar procedures have been developed for other industries and applications [1-3]. Civil engineering structures are, however, unique in that each structure is custom designed for the location in which it is deployed and is subject to the unique environmental conditions present at that site. This effectively makes each installation a one-of-kind system. If one is forced to custom design the data analysis process for every structure in addition to its physical design, the result will clearly be a substantial increase in project cost. This problem is exacerbated by the fact that infrastructure owners already have a large inventory of structures in service which could benefit from SHM technologies if an economical generic, rather than custom designed, signal analysis approach can be developed to retrofit selected structures.

Thus, in the ideal situation, it is desirable to look instead to data analysis techniques which are capable of adapting themselves in an automated and well defined way to the unique properties of an individual installation. At the same time it is required that the techniques employed be reliable, computationally efficient, and easy to deploy. Such is the objective which motivates the results presented in the balance of this article.

2. NOVELTY DETECTION

To address the need for the data analysis to adapt itself to each structure, this work has made use of an artificial neural computing approach known as frequency sensitive competitive learning (FSCL) [2,3]. Artificial neural networks (ANNs) [3] are essentially statistical signal processing techniques originally inspired by the learning capabilities of biological systems. They are highly abstracted from their biological counterparts, but do share a basic capability to learn through experience, rather than through explicit rules or procedures. This learning may be performed in a supervised or unsupervised manner, but in either case results in the system developing an internal model of the characteristic properties of a collection of data. In the case of SHM systems, the data being modeled represents the physical response of a structure to excitations it receives from its environment. This response takes the form of strain, acceleration and temperature measurements acquired under regular operating conditions.

The specific nature of the learned model is dependent upon the algorithm used to train the network and the quality of the data made available to it. If the network training data contains sample inputs which are pre-labeled by an expert, then the model will itself be capable, in general, of differentiating between similar varieties of such inputs in the future. In the absence of labeled data, identifiable classes may still be incorporated into the learned model in cases where clearly distinguishable types of phenomena exist within the input data. In either case, the learned model will provide a reference against which to compare future inputs. As such, it may be used to determine a measure of novelty for a given new input relative to the learned model [1]. Measurements which are consistent with the model will display low levels of novelty, while those which differ substantially from the model will produce a high novelty value.

In the case of SHM systems, obtaining labeled training data is rare. However, as has already been pointed out, there is no shortage of unlabelled SHM data upon which an (unsupervised) algorithm may be trained. The FSCL algorithm used is this study is such an approach and provides a natural novelty measure as a consequence of it normal operation. To facilitate training, FSCL computes the Euclidean distance between the current system input $\mathbf{x}$ and the network model stored in the weight vector $\mathbf{w}_i$.

$$h_i = \left\| \mathbf{x} - \mathbf{w}_i \right\| \tag{1}$$

During the training process the network units (neurons) adjust the system model encoded in the weight vector based on this distance measure. At any instant in time, the unit which most closely represents the input is adjusted

by a small amount in order to further reduce the distance h_i between the input and its weights. As training progresses the weights in the system take-on values consistent with the training data, encoding the overall statistical properties of that data.

At the conclusion of the training process the weights are then fixed allowing new inputs to be compared against the learned model by evaluating Eqn. 1 with the current system input. The result of this process is then interpreted as a novelty index (*NI*). By plotting the novelty index over time, it is possible to identify periods in the measured response of an SHM system which warrant further scrutiny.

3. EXPERIMENTAL RESULTS

The FSCL based approach to novelty detection was tested using data from three in-service structures in Canada. These include two bridges, the Taylor Bridge in Headingley, Manitoba and the Portage Creek Bridge in Victoria, British Columbia. The third structure is a statue, named "The Golden Boy," located at the pinnacle of the main regional government building in Winnipeg, Manitoba.

The Taylor Bridge is a traditional vehicle bridge made up of five simply supported spans. One approach span is monitored with metal-foil strain gauges which serve as the primary inputs to the network, along with two thermocouples. The strain gauges are located both mid-span (6) and at the end supports (6). The individual strain measurements are low-pass filtered with a cutoff of 10Hz, sampled at a rate of 32Hz, and transformed into the frequency domain before presenting them as inputs to the network. The input thus consists of 14 channels of frequency information, with a resolution of 0.5Hz over the range 0–16Hz, resulting in a 448 dimensional training vector.

Figure 1 shows the three most active strain channels in the time domain, along with the novelty value over a typical window of time. The sensor channels, in the upper portion of the figure, correspond to three of the six mid-span sensors. The novelty index, shown in the lower portion of the figure, clearly identifies periods in the sensor record which deviate substantially from the learned system response. The given figure represents just over one hour of measurements. The events corresponding to the large novelty readings shown here are the result of large vehicle traffic on what is normally a sparsely traveled structure. Based upon the information contained in the novelty plot, it is a simple matter to select the specific novel events out of the main sensor record. In this case the pertinent information is reduced from 256kB of raw measurements to little more than 1kB for the novel measurements. This translates into a substantial savings in data storage costs.

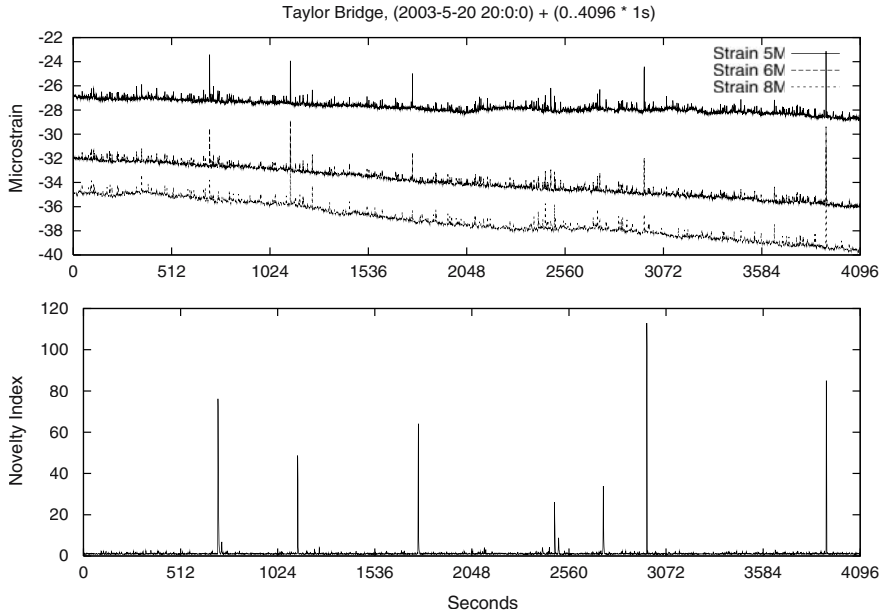

Figure 1. Typical strain gauge output and novelty plot for the Taylor Bridge.

This same process was applied to the Portage Creek Bridge. The SHM system deployed on that structure consists of 30 strain gauges, two three-axis accelerometers, and a single thermocouple. The strain and acceleration information are again sampled at 32Hz and converted into the frequency domain prior to their presentation to the neural network. The resulting total input from 37 sensor channels constitutes a 1184 dimensional training vector.

Unlike the previous example, however, the sensors are place on the supporting columns of the bridge, rather than on the spans themselves. As a result, the measurement data will not reflect vehicle traffic, but will instead record more substantial phenomena. In this particular case, we have investigated the correlation between sensor response and seismic activity in the area of the bridge. Preliminary results demonstrate a correlation between the novel events identified by the network and those recorded by seismic monitoring equipment in the region. While there was a lack of precise synchronization of clocks between the two sites, specific seismic activity in the general timeframe of the novelty spikes is apparent. Figure 3 shows the novelty index for one of these isolated events and the corresponding data on the most active strain gauge channel in Figure 4.

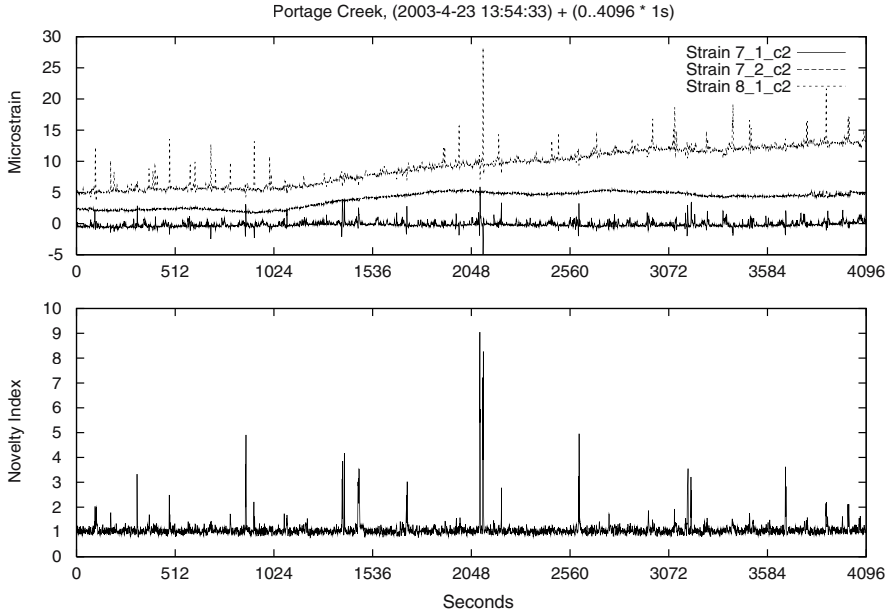

Figure 2. Typical strain gauge output and novelty plot for the Portage Creek Bridge.

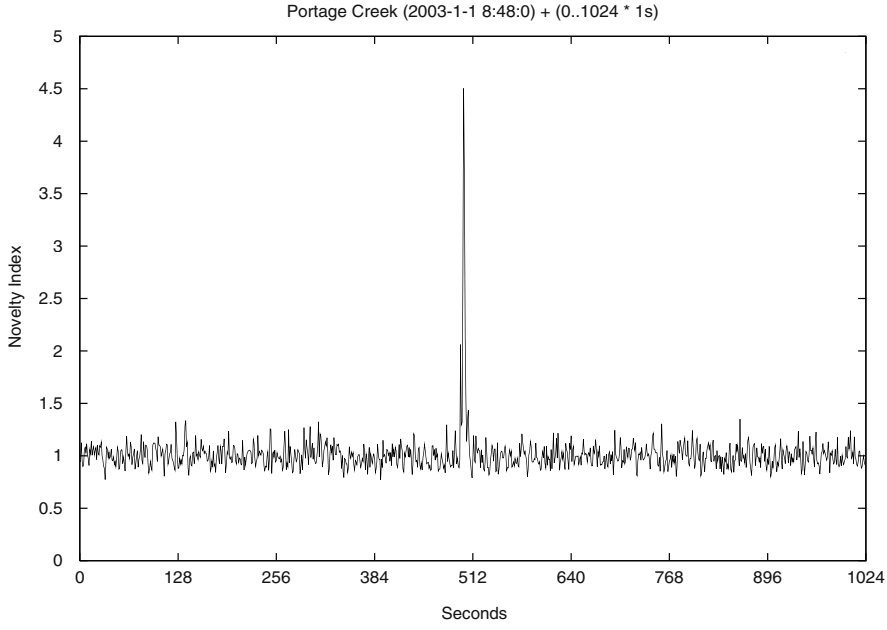

Figure 3. Localized novelty event identified in the Portage Creek Bridge sensor record.

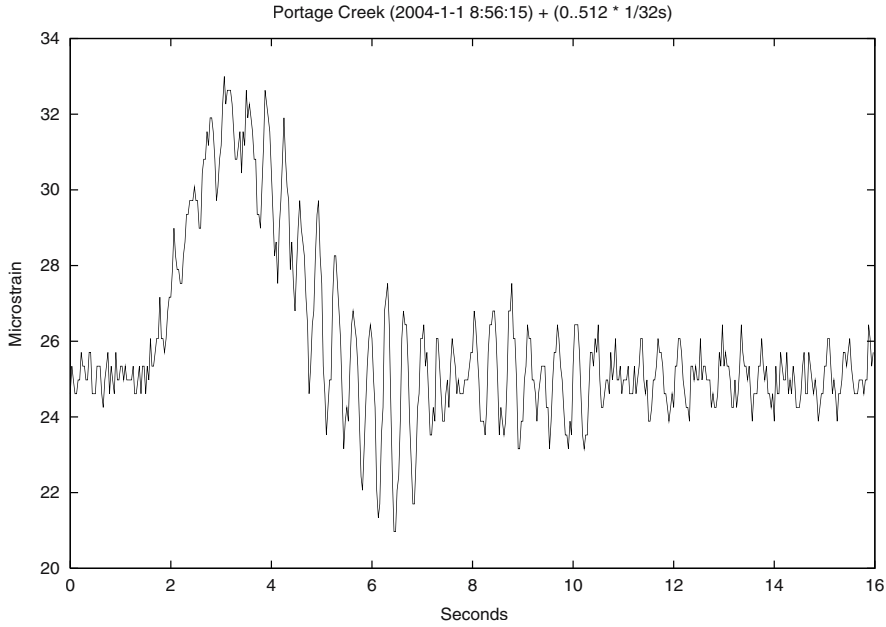

Figure 4. Most active gauge corresponding to seismic event at the Portage Creek Bridge.

The final structure on which the neural computing approach was tested is the Golden Boy statue. Its SHM system is comprised of five metal-foil strain gauges, two three-axis accelerometers and a thermocouple. Again, the strain and acceleration measurements are sampled at 32Hz and presented to the neural network as frequency domain information. The total training vector thus consists of a 416 dimensional input.

The source of excitation for the statue is primarily wind loading. As a result, the strain and acceleration channels show much more activity than those experienced by the bridges. The dynamic nature of the wind also translates into a more unpredictable excitation and therefore produces a more active novelty plot than those presented previously. Figure 5 provides an example of the response from three of the strain gauges together with the corresponding novelty plot of the same period of time (approximately one hour). The gusty nature of the wind can clearly be observed in the novelty and strain information.

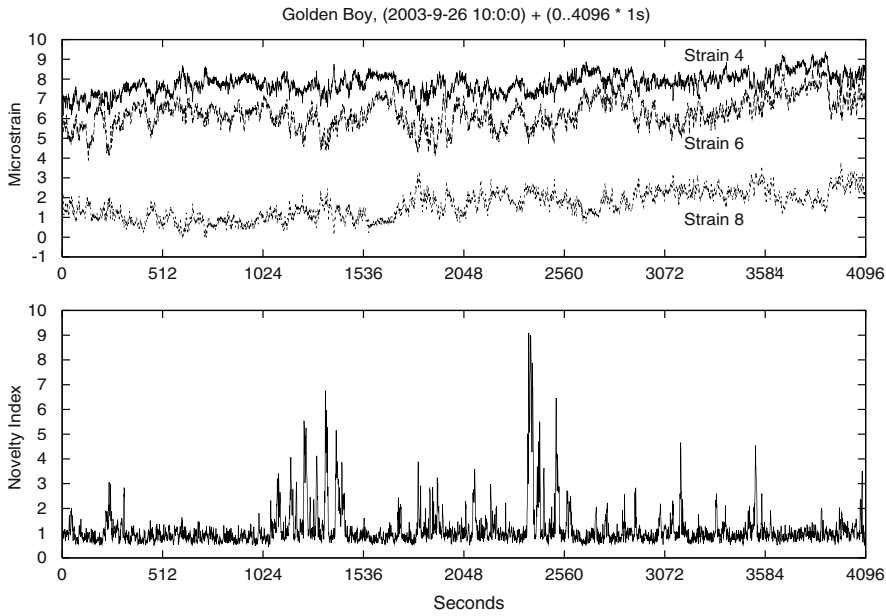

Figure 5. Typical strain gauge output and novelty plot for the Golden Boy.

The primary purpose of the Golden Boy's SHM system is to monitor the health of the statue by tracking changes in its natural frequency over an extended time period. The statue has recently been repaired to correct for corrosion in the single steel support shaft running through its centre. The goal is to detect any possible future corrosion in its early stages, before serious structural weakness develops. Should corrosion take place, the result will be a shift in the statue's natural frequency away from its present 3Hz and result in a corresponding increase in the computed novelty index.

To illustrate the sensitivity of the novelty index to changes in the measured strain values, small sinusoidal excitations of 3Hz and 10Hz were artificially introduced into the sensor record and the combined data was presented to the trained network for analysis. The results show that variations of 1.25 microstrain on a single input channel, or simultaneous variations of 0.5 microstrain on all strain channels produce a detectable increase in the novelty index. Variations of 1 microstrain on all strain channels or 2.5 microstrain on a single channel produce a five-fold increase in the computed novelty. Thus changes in either the peak amplitude of the strain measurements or the introduction of frequency values not present in the normal response give rise to significant increases in the level of novelty.

CONCLUSIONS

This article has examined the application of artificial neural computing techniques to the task of data analysis for structural health monitoring. The frequency sensitive competitive learning algorithm employed in this study was shown to be capable of modeling the normal response of a structure and subsequently provides a means to assess the novelty of the structure's response to new excitations. Experimental results for two bridges and one statue were presented to illustrate the practical application of the technology. It was demonstrated that the approach is capable of locating events resulting from vehicular traffic, seismic activity, or wind loading. The specific phenomena being modeled depends upon the placement of sensors on the structure of interest and the nature of the structure itself.

ACKNOWLEDGEMENTS

The authors gratefully acknowledge the financial support of Intelligent Sensing for Innovative Structures (ISIS) Canada, a Network of Centres of Excellence, and the Natural Sciences and Engineering Research Council of Canada (NSERC).

REFERENCES

1. S. King, D. King, P. Anuzis, K. Astley, L. Tarassenko, P. Hayton, and S. Utete, "The use of Novelty Detection Techniques for monitoring High-Integrity Plant," *Proceedings of the IEEE International Conference on Control Applications*, Glasgow, UK, 2002, pp. 221–226.
2. A. Krishnamurthy, S. Ahalt, D. Melton, and P. Chen, "Neural Networks for Vector Quantization of Speech and Images," *IEEE Journal on Selected Areas in Communications*, vol. 8, no. 8, October, 1990, pp. 1449–1457.
3. D. K. McNeill, H. C. Card, and A. F. Murray, "An Investigation of Competitive Learning for Autonomous Cluster Identification in Embedded Systems," *International Journal of Neural Systems*, vol. 11, no. 4, 2001, pp. 389–398.
4. C. Bishop, *Neural Networks for Pattern Recognition*, Oxford University Press, 1995.

A NOTE ON INTERPRETATION OF SHM DATA FOR BRIDGES

Baidar Bakht
JMBT Structures Research Inc., Toronto, Canada

Abstract: Notwithstanding the current advances in the development of sensors for SHM of civil structures, the interpretation of the collected data remains the Achilles heel for SHM. With the help of a few examples, drawn from the personal experience of the author, it has been shown that the interpretation of SHM data is not a straightforward exercise. Factors such as boundary conditions and temperature effects require careful and thoughtful investigation. Although it has not always been possible to do so for every type of structure, every effort should be made to explain the observed behaviour of the monitored structures. In predicting the failure loads of structures from responses collected under 'service' loads, allowance should also be made of the fact that the actual failure load of the structure might be different than that assumed.

Key words: Bearing restraint, bridge testing, boundary condition, failure test, interpretation, structural health monitoring, temperature effect.

1. INTRODUCTION

Sensors to determine the health of a structure have indeed been available for a long time. However, it is only recently that efforts are being undertaken to formalize the art and science of structural health monitoring (SHM) of civil structures in the same way as it has been done for aerospace structures. For civil structures, the aerospace term 'avionics' has been replaced with 'civionics'. While the use of the most appropriate sensors to identify the deficiency of a structure is irrefutable, it is also of paramount importance that the data collected from the sensors are interpreted correctly. As shown with the help of examples drawn mostly from personal

Farhad Ansari (ed.), Sensing Issues in Civil Structural Health Monitoring, 321–328.

experiences of the author, the interpretation of SHM data for bridges is not always straightforward.

2. BOUNDARY CONDITIONS

There are some bridges in which the boundary conditions, governing the load carrying capacity of a bridge cannot be determined directly from observed responses; instead, they are determined through back-calculations by comparing the observed responses with those obtained by rigorous analyses. One such type of bridge is the short-span concrete plank bridge, in which the planks are connected through a number of shear keys. A shear-connected concrete plank bridge on the forestry roads of British Columbia (BC) can be seen in Fig. 1 (a) carrying a fully-loaded logging truck. The simple support of this bridge can be seen in Fig. 1 (b). As noted e.g. in [**1**], a shear-connected bridge is analyzed as an articulated plate, a special case of the orthotropic plate in which the transverse flexural rigidity, D_y, is

(a) (b)

Figure 1. A short-span shear-connected bridge: (a) carrying a logging truck, (b) simple support.

The transverse load distribution characteristics of an articulated plate are governed by two of its stiffness parameters: (a) D_x, the longitudinal flexural rigidity per unit width, and (b) D_{xy}, the longitudinal torsional rigidity per unit width. When measured mid-span deflections of a shear-connected concrete plank bridge were compared with articulated plate analysis through the computer program PLATO [**2**], it was found that the actual pattern of transverse load distribution was poorer than that predicted by the articulated plate analysis. A search for the reason for the discrepancy revealed that while the deck is simply supported against vertical deflections (Fig. 1 b), the concrete planks at their supports are not restrained against rotation, as is assumed in the articulated plate analysis. By trial and error, it was found that the analytical distribution pattern becomes fairly close to the observed pattern if D_{xy} is assumed to have half its usual value. Were the actual boundary condition not identified, all shear-connected bridges on BC's forestry road would continue to be analyzed by an unsafe method.

Boundary conditions in some bridges are supposed to be so axiomatic that it is not considered necessary to even determine them during a test. One example for such a case was a single-span simply supported slab-on-girder bridge that was tested to failure under a ballast load; this bridge is shown in Fig. 2 (a) during the failure test along with timber framework below its mid-span, installed to avoid a catastrophic failure. The ballast load was placed on a rectangular pattern on the bridge with zero angle of skew. In such a bridge with true simple supports, the total moment at any transverse section is statically determinate. However, when the girder moments were back calculated from measured strains in the steel girders, it was found that the total calculated moments were about 30% smaller than the applied moments (Fig. 2 b) even for low levels of loads.

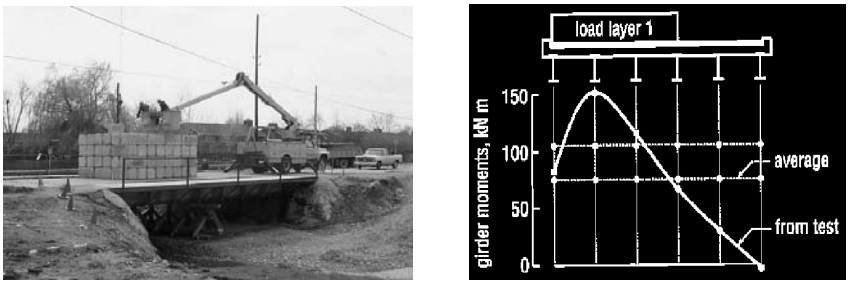

(a) (b)

Figure 2. A slab-on-girder bridge: (a) being tested to failure, (b) comparison of calculated girder moments with applied moments.

Years after the test, it was discovered that the reason for the apparent discrepancy was the bearing restraint between the steel girders and the concrete abutment [**3**]. The horizontal forces generated at the interface of the girders and abutment are large in older structures, such as the one under discussion. Even in new structures with apparently functioning neoprene bearings, these forces are not negligible, as discussed below.

The North Muskoka Bridge in Northern Ontario, a relatively new bridge with a simply supported span of 45.72 m, has five steel plate girders supported at each of their ends on a laminated neoprene bearing measuring 560×355 mm in plan and 64 mm in thickness; it was tested in June 1986. During the test, longitudinal strains in all girders were monitored at the mid-span and at sections 229 mm from the centreline of each bearing. Typical longitudinal strain distribution in one girder near the 'simple' support is reproduced from [**4**] in Fig. 3 (a), in which tensile strains are shown as +ve and compressive strains as –ve.

(a) (b) (c)

Figure 3. Longitudinal strain distribution over girder depth near a 'simple' support: (a) observed; (b) bending strains; (c) strains due to bearing restraint force.

It can be seen in Fig. 3 (c) that near the apparently simple support, the compressive strain in the bottom flange of the girder due to the bearing restraint force is very high as compared to the theoretical flexural strain at the same location. It was concluded in [**4**] that at the time of the test on a hot day in June, the bearing restraint forces generated in the laminated neoprene bearings reduced the mid-span deflections by about 12%. It was hypothesized in the same reference that the 20% reduction reported in [**5**] during a test on a cool day in October could have been the result of the bearing becoming stiffer in colder temperatures. A change in the shear stiffness of bearings due to change in ambient temperature clearly indicates that the bearing restraint is transitory in nature for the type of bridge under consideration.

3. TEMPERATURE-INDUCED STRAINS

Considers two bars, one of which, Bar A, is held against axial deformations at only one end, and Bar B is held rigidly at both ends. Subject both bars to a rise in temperature. Bar A will extend freely and experience no stress from the change in temperature. On the other hand, Bar B will not change in length but will experience a compressive stress. If each of these bars was installed with a strain gauge, the gross readings from the gauges will lead to false conclusions about the state of stress in the bars.

The most effective way to determine the 'net' strain in a component is to use a 'dummy' gauge, which is installed on an unrestrained piece of the same material as that of the instrumented component. Both the dummy and active gauges are used to form adjacent arms of the Wheatstone circuit, so that the net strain in the component is the difference between readings from the active and dummy gauges. It can be seen that by using a dummy gauge, the net strain in Bar A discussed above would be zero, indicating no stress. Similarly, the net compressive strain in Bar B will have the same magnitude as that of the tensile gross strain in Bar A. Unfortunately, the above simple and well proven method is not always used to correct the measured strain readings, thus leading to erroneous conclusions about the behaviour of the instrumented structure.

Even when the strain readings are corrected for effects of temperature, the presence of stresses due to thermal forces is not always detrimental. One example is given in the following to illustrate this point.

In a statically determinate structure, all components are free to expand and contract, thus experiencing no stress due to uniform changes in temperature. The same is not the case in statically indeterminate structures. Consider the trusses of a bridge, with X-chord members in the middle panel; these trusses can be considered to be statically indeterminate. However, a close scrutiny of the X-chord members will readily show that they are very slender, and thus incapable of carrying substantial compressive forces. When a vehicle traverses the bridge, the X-chord members share tensile forces alternately. The member in compression bows out, so that for all practical purposes the truss becomes statically determinate. For such trusses, the net strains in X-chord members induced by thermal loading should be interpreted by keeping in mind that the compressive members bow out carrying only bending moments. It is emphasized that the temperature-induced forces in the trusses under consideration are so small that they have practically no effect on the failure load of the structure.

4. MYSTERIES OF STRUCTURAL BEHAVIOUR

Despite the significant advances made over the last few decades in the field of structural engineering, not all mysteries of structural behaviour have been solved. One structure whose structural behaviour is still not fully understood is the reinforced concrete rigid frame bridge. This bridge is on the Trans Canada Highway in Ontario. It was proof tested in 1975 and given a clean bill of health despite its apparently deteriorated condition. The reason for the very high load carrying capacity of the bridge could not be identified. In order to unlock some of the mysteries of the rigid frame bridge, the McIntyre Bridge in Thunder Bay, Ontario, was instrumented before construction. A number of strain gauges were placed strategically on the reinforcing steel. The bridge was tested soon after construction. The measured strains in both the concrete and the reinforcing steel, however, were considerably smaller than expected. The only conclusion that could be drawn from the test was: “The standard rigid frame design method has yielded highly conservative and often unrealistic results.” [**6**].

5. UNEXPECTED OBSERVATIONS

It has been observed several time that the floor system of a through truss bridge acts with the bottom chords of the trusses, so that even when the bottom chord has either buckled or been severed, the bridge can continue to carry traffic. Ceased bearings also contribute to such apparent strange behaviour.

Reference [7] cites a number of 'surprises' encountered in bridge tests. Unless identified and accounted for, these surprises have a significant influence on the interpretation of SHM data. A surprise was encountered in the bottom chord strains of a through truss bridge under a truck load. As shown in Fig. 8, the tensile strain in the bottom chord panel closest to the right-hand support of the truss was about 15 times larger than the tensile strain in the adjacent panel. Since the two panels are divided by only a vertical chord member, their strains should theoretically be the same. This unexpected behaviour is accounted for by the presence of a small approach span on the right side of the truss (Fig. 4). This approach span is formed by extending the stringers of the floor system due to which the floor system could not be connected effectively to the end nodes of the trusses. Thus the floor system participates with the truss bottom chords in all their panels except the extreme right ones. It is obvious that even small changes in details of a structure can make it behave in an unexpected manner.

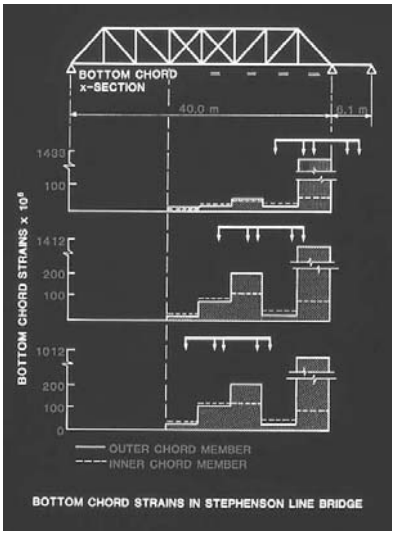

Figure 4. Bottom chord strains of a truss due to various truck positions.

It is indeed important to keep the number of sensors to a minimum so that the interpretation of data is not encumbered by their volume. However, it is also important to make sure that there are enough sensors to catch "surprises" such as the one mentioned above.

6. ULTIMATE RESPONSE vs. OBSERVED RESPONSE

The evaluation of the load carrying capacity of a bridge by the Canadian Highway Bridge Design Code [8] requires the determination of the capacity at the ultimate limit state (ULS). It is important, therefore, to extrapolate the capacity at the ULS beyond the observed SHM data, which necessarily corresponds to loads smaller than the ULS loads. As shown below, there could be a large difference between calculated and actual failure loads.

Figure 5. Truss bridge being tested to failure

A steel through truss in fairly good condition (Fig. 5) was tested to failure in late 1970's [9] to validate a rigorous method of predicting the in-plane buckling failure of steel trusses [10]. The trusses of the bridge were pulled down at nodes close to the ends of the trusses. To ensure that they do not fail in tension, the bottom chords of the trusses were strengthened. During the test, the bridge failed 'prematurely' due to the local failure of the inclined chord close to the point of load application. The local failure, caused by a ripple in the cover plate of the built-up section due to accumulation of rust, was so noiseless that it was discovered only after the hydraulic jacks pulling the trusses from rock anchors refused to pick up further load. Even a thorough condition survey failed to identify the potential source of weakness in the bridge.

It can be appreciated that extrapolation of SHM data to predict the ULS capacity of a bridge is not without its problems.

7. CONCLUSIONS

The end product of an SHM exercise for a bridge should be information that could be used by the bridge owners to make decisions about the management of the structure. Such information can be obtained only from a thoughtful and expert interpretation of the collected data. While a lot of effort is being expended on the development of new sensors and on the formulation of philosophy for field

application of SHM, little has been done on the interpretation of data. With the help of several specific examples, it has been suggested that the interpretation of data to determine the current behaviour of instrumented structures, and also its ultimate load carrying capacity, is the last, and perhaps the most important, knowledge gap to be bridged for the general acceptance of SHM by bridge owners.

REFERENCES

1. Bakht, B. and Mufti, A.A., "Testing of Two Shear-connected Concrete Plank Bridges", Technical Report of JMB Structures Research Inc., submitted to BC Ministry of Forests, 1999.
2. Bakht, B., Mufti, A.A., and Desai, Y.M., "PLATO User Manual", ISIS Canada, University of Manitoba, Canada, 2002.
3. Bakht, B. and Jaeger, L.G., "Ultimate Load Test on a Slab-on-girder Bridge', *ASCE Journal of Structural Engineering*, Vol. 118, No. 6, pp. 1608-1624, 1992.
4. Bakht, B. and Jaeger, L.G., "Observed Behaviour of a New Medium Span Slab-on-Girder Bridge", *Journal of the Institution of Engineers (India)*, Vol. 70, January, pp. 164-170, 1990.
5. Billing, J.R. 'Dynamic Loading and Testing of Bridges in Ontario', Proceedings, International Conference on Short and Medium Span Bridges, Toronto, Canada, Vol. I, pp. 125-139, 1982.
6. Kryzevicius, S., "Testing and evaluation of the McIntyre River Bridge Widening", Structures Research Report SRR-84-07, Ministry of Transportation of Downsview, Ontario, Canada, 1984.
7. Bakht, B. and Jaeger, L.G., "Bridge Testing - a Surprise Every Time", *ASCE Journal of Structural Engineering*, Vol. 116, No. 5, pp. 1370-1383, 1990.
8. CHBDC, Canadian Highway Bridge Design Code, CAN/CSA-S6-00, CSA International, Toronto, Canada, 2000.
9. Bakht, B. and Csagoly, P.F., "Bridge Testing", Structures Research Report 79-SRR-10, Ministry of Transportation of Ontario, Downsview, Ontario, Canada, 1979.
10. Csagoly, P.F. and Bakht, B., "In-plane Buckling of Steel Trusses", *Canadian Journal of Civil Engineering*, Vol.5, No.4, pp. 533-541, 1978.

Chapter VI

Sensor and Instrumentation Performance and Reliability

INSTRUMENTATION PERFORMANCE DURING LONG-TERM BRIDGE MONITORING

Ian N. Robertson, Gaur P. Johnson, and Shujun Wang
University of Hawaii, Dept. of Civil and Environmental Engineering, Honolulu, Hawaii, USA

Abstract: This paper reviews the performance of a variety of instruments installed in the North Halawa Valley Viaduct for a 10-year monitoring program. Over 200 electrical strain, displacement, temperature and load sensors were installed during construction of the long-span box-girder viaduct on the island of Oahu in 1994. These instruments have been monitored continuously since installation. Comparisons are presented where two types of sensor were used to monitor the same response. Each of the instrumentation systems is evaluated for its performance in monitoring short-term and long-term response. Advantages and disadvantages are presented for each type of sensor used in this project.

Key words: Instrumentation, long-term monitoring, sensor performance.

1. INTRODUCTION

The North Halawa Valley Viaduct (NHVV) is a 1.5 km box-girder viaduct with span lengths up to 110 m. It is part of the new H-3 freeway on the island of Oahu in Hawaii. The twin inbound and outbound viaducts were built by means of post-tensioned in-situ balanced cantilever construction as described by Banchik & Khaled [1]. Four spans of Unit 2 of the inbound viaduct (70 to 110 m span lengths) were selected for instrumentation to provide an adequate representation of the viaduct long-term behavior (Fig. 1). The instrumentation program was developed in conjunction with T.Y. Lin International, structural engineers for the viaduct. During construction, all instruments were installed by personnel from the University of Hawaii (UH) and Construction Technology Laboratories (CTL) in Skokie, Illinois.

Farhad Ansari (ed.), Sensing Issues in Civil Structural Health Monitoring, 331–340.

The instrumentation used in this project was designed to provide long-term monitoring of the structural performance of the viaduct. The measurements required to achieve the project objectives include concrete strains, concrete and ambient temperatures, concrete creep and shrinkage strains, span shortening, tendon forces, span deflections, and support rotations. The following instrumentation was selected and installed to perform these measurements: vibrating wire strain gages, electrical resistance strain gages, thermocouples, extensometers, tendon load cells, base-line deflection systems, tiltmeters, and automated datalogger recording systems. This paper presents results from the strain gages, span longitudinal and vertical deflection measurements, and temperature sensors.

2. DESCRIPTION OF INSTRUMENTATION

A detailed description of all instrumentation and the installation procedures used in this project is given by Lee and Robertson [2]. The following is a brief description of the strain, deflection, temperature and prestress force measurement systems pertaining to the results presented in this paper.

Seven sections were selected for instrumentation in order to provide an adequate representation of the viaduct behavior. Sections A, D, E and G are at, or close to midspan, while B, C and F are close to the ends of the instrumented spans as shown in Fig. 1.

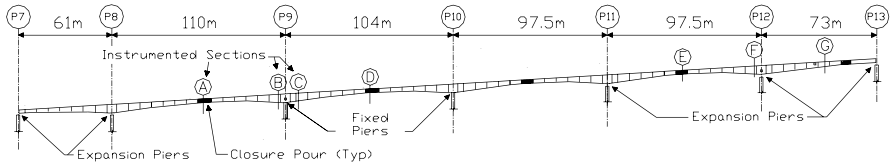

Figure 1. Viaduct elevation showing instrumented sections, A to G

2.1 Concrete Strains

Concrete strains were monitored using Electrical Resistance (ER) strain gages bonded to reinforcing steel coupons, and Vibrating Wire (VW) strain gages. These gages were embedded in the concrete to measure longitudinal strain. Ten VW strain gages were placed around the box-girder cross-section at each end span instrumented section as shown in Fig. 2. Eight VW gages were placed around the midspan sections in the same locations as shown in Fig. 2, but without gages 5 and 9. ER strain gages were installed at various locations in sections E and F for comparison with the VW gages.

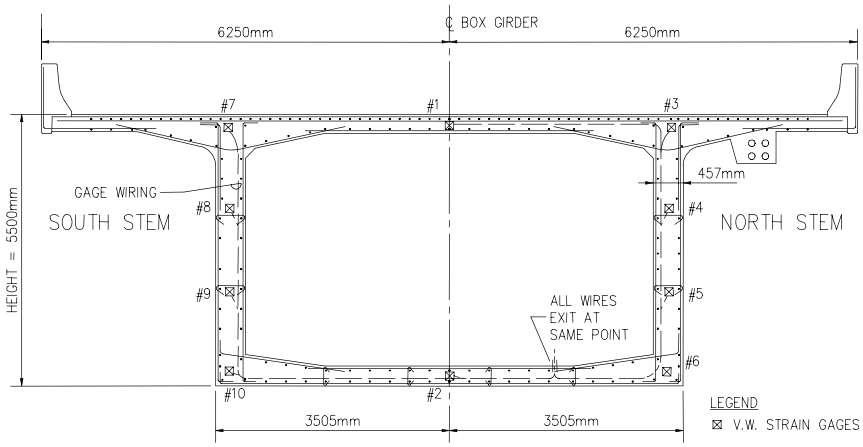

Figure 2. Vibrating wire strain gage locations at section B

2.2 Span Longitudinal Deflections

Extensometers were installed in the four instrumented spans to monitor the overall shortening of the box-girder. Each extensometer consists of a series of graphite rods (6mm diameter by 6m long) spliced together to span from pier to pier inside the box girder. One end of the rod is fixed to the top slab soffit at one end of the span, while the other end is coupled to a Linear Variable Displacement Transducer (LVDT) at the other end of the span. The relative displacement of the concrete at the two ends of the extensometer is measured by the LVDT, providing a measurement of the span shortening.

2.3 Span Vertical Deflections

A taut-wire base-line system was installed in each of the four instrumented spans to monitor vertical deflection of the box-girders. This system consists of a high-strength piano wire strung at constant tension from one pier to the next, inside the box girder, to act as a reference line as shown in Fig. 3. A precision digital caliper was used to measure the distance between the base-line and plates attached to the underside of the top slab. Changes in the caliper readings indicate the vertical deflection of the box girder relative to the ends of the span. The base-line system measurements are compared with optical surveys of the roadway surface, tiltmeter readings at the supports, and with analytical predictions by SAP2000 [3] for short-term events, and SFRAME [4], a time-dependent step-wise finite element analysis program written specifically for analysis of incrementally constructed bridges, for long-term monitoring.

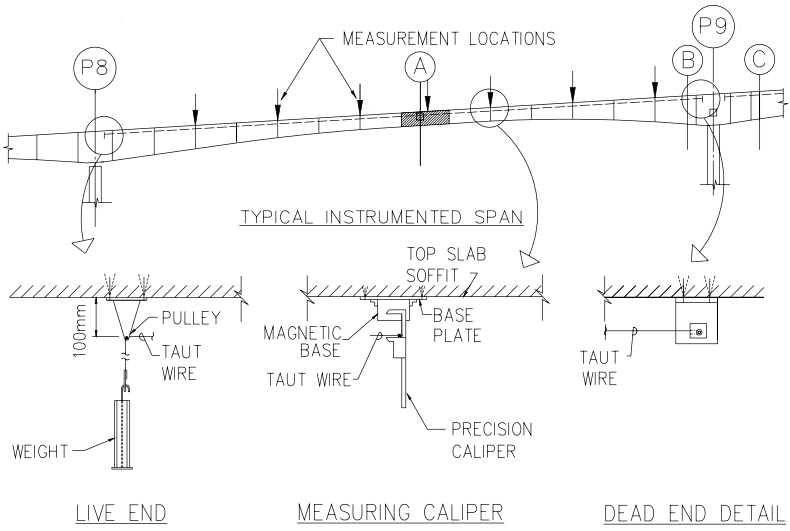

Figure 3: Base-line Deflection System

2.4 Concrete Temperature

Each VW strain gage contained a thermistor to monitor the temperature in the concrete at the gage location. In addition, Copper-constantan Type T thermocouples were located throughout the cross-section at sections E and F. Ambient temperature and relative humidity were also recorded inside and outside the box girder.

3. SHORT-TERM RESULTS

3.1 Strains during prestressing

During stressing of tendons crossing an instrumented section, the strain gages recorded the change in strain distribution through the depth of the section. Fig. 4 shows the strain gradient at section E for one particular prestressing event. Both VW and ER strain gages provided the same straight-line strain gradient through the depth of the section with very little scatter around this line. Analysis of this stressing event using SFRAME yields slightly different results. This is attributed in part to the lack of precision in the field measurement of the applied prestress force.

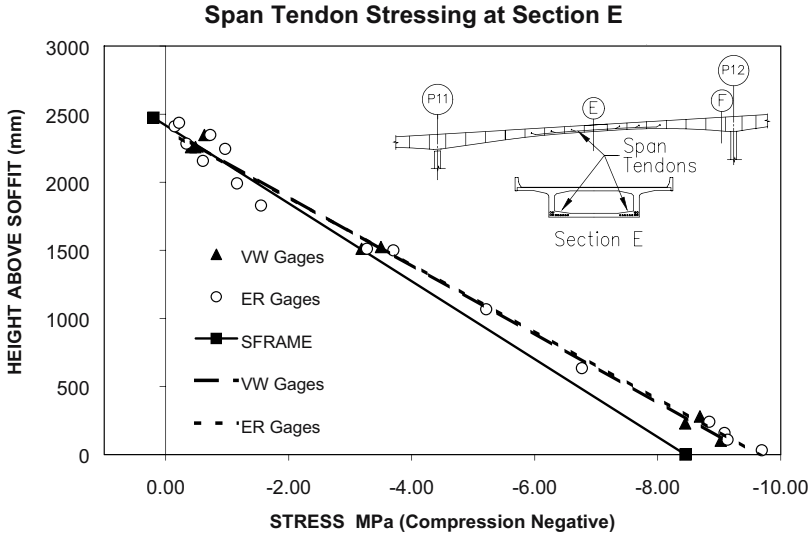

Figure 4: Section E Stresses during Span Tendon Prestressing

3.2 Deflections during load test

In August 1997, a load test was performed on the instrumented spans of the viaduct using four loaded trucks, each approximating an HS-20 design vehicle. Deflections were monitored using the base-line system, the support tiltmeters, and optical surveys of the top surface of the viaduct. For truck loading at midspan between pier 8 and 9, the deflections of this and the adjacent instrumented span are shown in Fig. 4, along with the SAP2000 analytical prediction of the deflected shape. The base-line system agreed well with the optical survey except for obvious survey errors as seen near pier 10. The tiltmeters at the supports confirm the base-line deflected shape at these locations. SAP2000 provided good predictions of the loaded span deflections but tended to overestimate the backspan deflections.

3.3 Strains during load test

The VW and ER strain gage readings were taken every 5 minutes during the load test as shown in Fig. 6 for the VW gages. The trucks were located at four different positions on Span P8-P9, indicated by locations L1 through L4. The distinct steps in the strain readings indicate the movement of the trucks to the next loading location. Fig. 7 shows the stress distribution through the depth of Section A (at midspan) for each of the truck locations. Note the excellent linearity of the stress gradients, and the consistent location of the neutral axis. Even at relatively small strain readings, the VW

strain gages were extremely accurate and consistent. Similar results were obtained for the ER gages, though there was slightly more scatter in the readings. The stress distributions obtained from SAP2000 analyses are added for comparison.

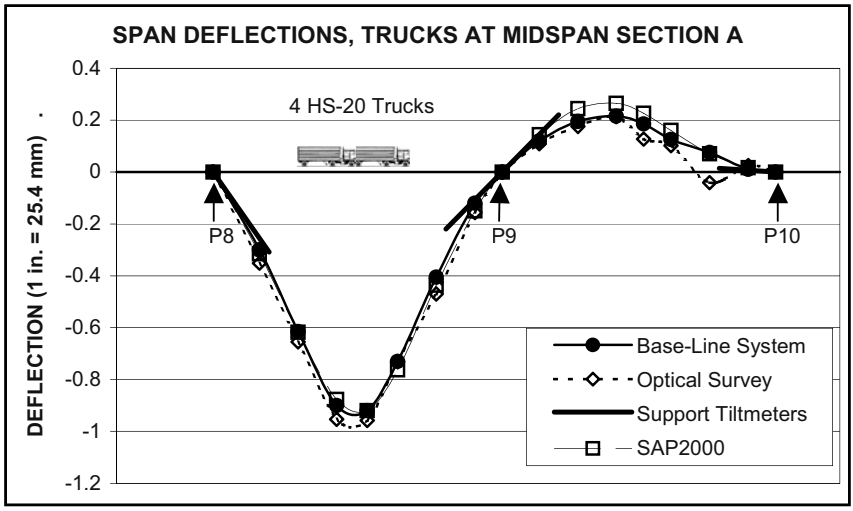

Figure 5: Comparison of Load Test Deflections (magnified).

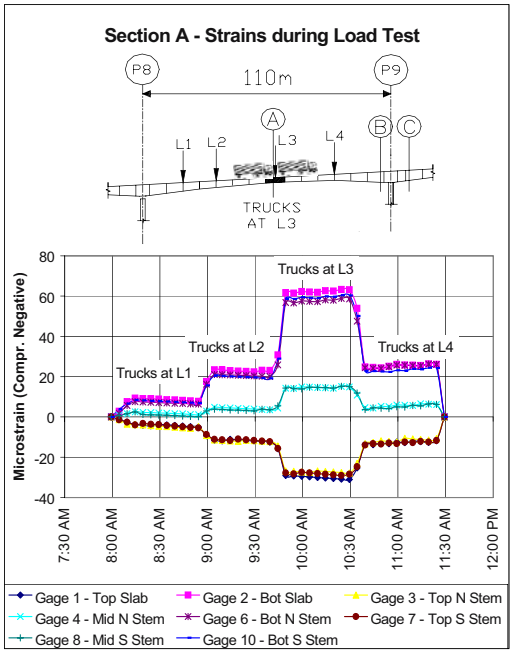

Figure 6: VW strain gage readings during load test on Span P8-9

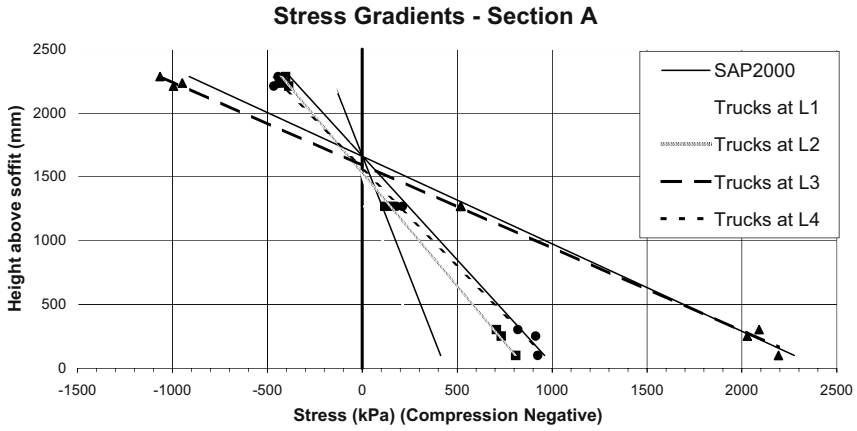

Figure 7: Stress gradients at section A during load test

3.4 Thermal Measurements

Thermistors and thermocouples placed at the same location provided identical temperature records as shown in Fig. 8. Low cost, simplicity of fabrication and ease of installation make the Copper-constantan Type T thermocouples ideal for both short and long-term thermal monitoring.

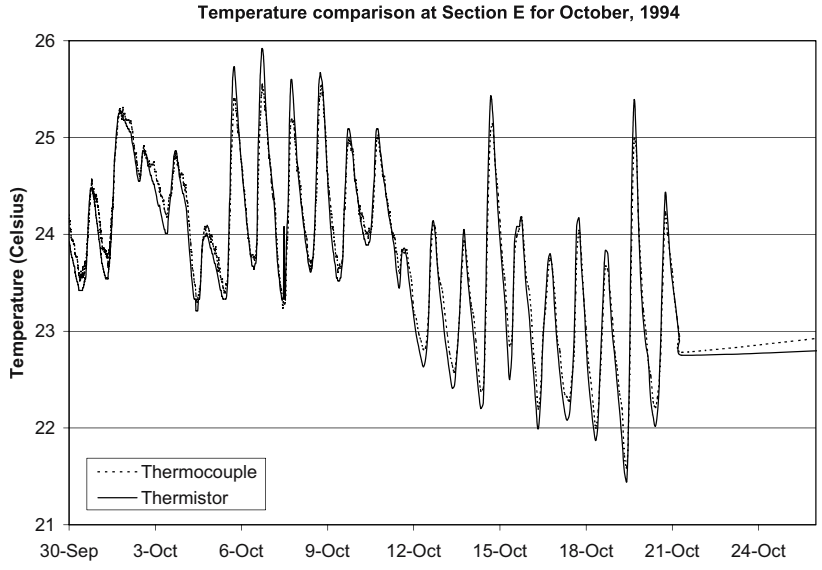

Figure 8: Temperature measurement comparisons

4. LONG-TERM RESULTS

4.1 Span vertical deflections

The long-term vertical deflections for Unit 2 of the Inbound viaduct from both the base-line and optical surveys are shown in Fig. 9. Apart from apparent errors in the optical survey, there is good agreement for the four spans with base-line systems, confirming the long-term performance of this relatively simple deflection measurement system. These measured deflections are compared with the theoretical prediction from SFRAME utilizing a concrete constitutive model based on short-term creep and shrinkage tests performed on the concrete used in the viaduct.

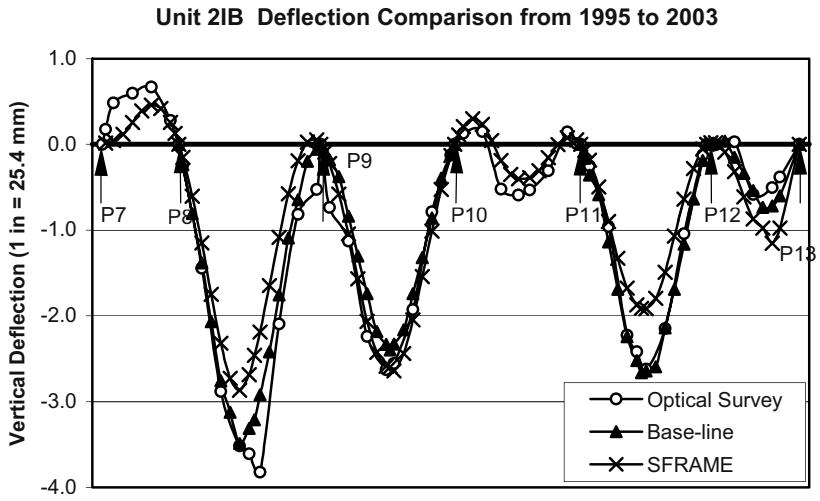

Figure 9: Vertical Deflections for Unit 2-IB, 1995-2003 (magnified).

4.2 Span axial shortening

Figure 10 shows good agreement between the span shortening from Pier 11 to 12 as measured by the extensometer, compared with the average strains measured by the VW gages at midspan and endspan sections (E and F). The extensometer readings also compared well with bearing movement measurements made at the slide bearings at the top of each pier. The extensometers provided a reliable record of overall span shortening due to elastic, creep, shrinkage and thermal effects.

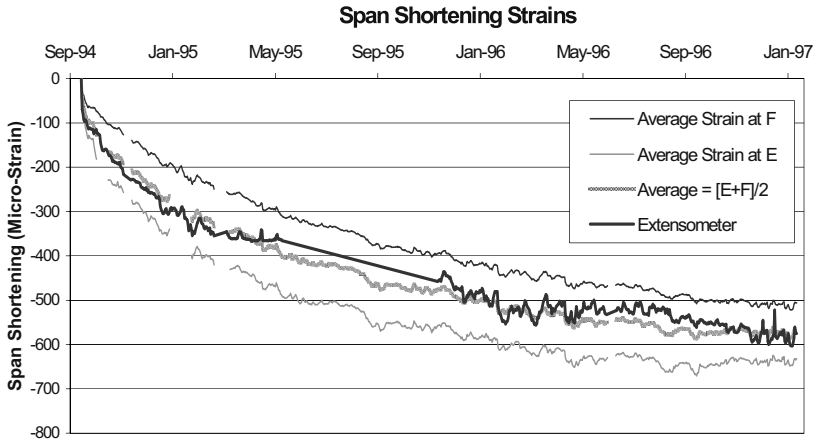

Figure 10: Span Shortening from Pier 11 to 12.

4.3 Long-term concrete strains

Figure 11 shows the long-term strains measured by the vibrating wire strain gages at the top and bottom of midspan section A compared with the SFRAME predictions. Similar comparisons were obtained for the other instrumented sections. In general, the SFRAME Final Model appeared to over-predict the long-term strains, however the shape of the strain-time relationships are very similar to those observed in the structure.

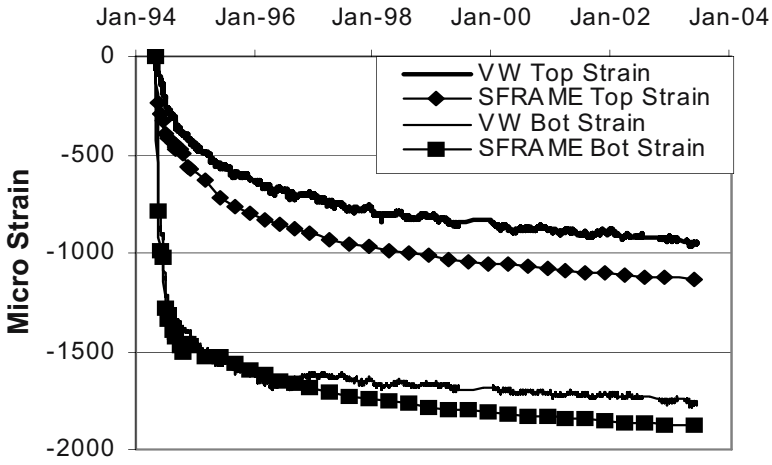

Figure 11: Top and Bottom Strains at Section A.

5. SUMMARY AND CONCLUSIONS

This paper describes the performance of various instruments installed in the North Halawa Valley Viaduct after 10 years of long-term monitoring. Of the 207 instruments installed in the viaduct, 190 were still operational after the 10-year monitoring period. Based on the measured long-term effects of creep and shrinkage on this long-span structure, an improved constitutive model was developed using short-term creep and shrinkage test data for use in future long-term bridge response predictions.

Vibrating wire strain gages proved accurate and reliable for both short and long-term monitoring of concrete strains in the prestressed box-girder. Electrical resistance gages were effective for short-term monitoring, but changes in the lead wire and data logger connections resulted in loss of reading continuity, making them ineffective for long-term strain monitoring.

A simple taut-wire base-line system proved extremely effective for both short-term and long-term measurement of vertical deflections of the box girder. Work is underway to develop automated monitoring for this system using LVDTs so as to avoid the need for manual caliper readings.

Graphite rod extensometers provided reliable monitoring of the overall shortening of bridge spans, while both thermistors and thermocouples were effective at monitoring internal concrete temperatures.

ACKNOWLEDGEMENTS

The authors wish to acknowledge the considerable assistance received during this instrumentation program. The input of Scott Hunter and Jose Sanchez of T. Y. Lin International and Henry Russell and Tom Weinmann of Construction Technology Laboratories was crucial to the successful implementation of this program. The assistance of a number of graduate students at the University of Hawaii is also greatly appreciated. In particular, Andre Lee's tireless efforts during instrument installation, and Michael Durbin's attention to detail during data processing. This project is supported by funds from the U. S. Federal Highway Administration and the Hawaii Department of Transportation. This support is gratefully acknowledged.

REFERENCES

1. Banchik, Carlos, and Khaled, Nahlawi, North Halawa Valley Viaduct Design and Construction. *Concrete International*, 1994, 16(3), 39-43.
2. Lee, Andre, and Robertson, Ian N. (1995), *Instrumentation and Long-Term Monitoring of the North Halawa Valley Viaduct*, *Report UHM/CE/95-08*, University of Hawaii, Honolulu, Hawaii.
3. SAP2000 (1996), *Integrated Finite Element Analysis and Design of Structures,* Computers and Structures, Inc., Berkeley, California.
4. Ketchum, M. A. (1986), *Redistribution of Stresses in Segmentally Erected Prestressed Concrete Bridges (SFRAME), Report UCB/SESM-86/07,* University of California, Berkeley, California.

STABILITY AND RELIABILITY OF FIBER-OPTIC MEASUREMENT SYSTEMS – BASIC CONDITIONS FOR SUCCESSFUL LONG-TERM STRUCTURAL HEALTH MONITORING

Wolfgang R. Habel
Federal Institute for Materials Research and Testing (BAM) Berlin, Germany

Abstract: Creation and development of long-term stable and reliable monitoring systems for large structures require the separate consideration of the relevant system components. The principle contributors: sensing element, cables/couplers, and sources/demodulation systems require very different reflection in regard to reliability and stability. Additionally, those aspects influence considerably the method of sensor application and its quality. The paper discusses the basic requirements on long-term monitoring systems, considers reliability aspects for different sensor application methods and provides important reliability aspects when fiber optic sensors are integrated into materials and structures. Emphasis is given on validation of measurement systems as a very important step for potential users and the use of a clear vocabulary when describing quality parameters of system components or entire monitoring systems.

Key words: Fiber optic sensor, reliability, long-term stability, structural monitoring, materials investigation, measurement uncertainty, validation.

1. INTRODUCTION

Fiber optic sensor (FOS) technique has gained worldwide recognition into diverse fields of application due to their specific characteristics. Fiber optic strain sensors are used to monitor plants and large structure components with high level risks or with high safety requirements. Very tiny sensor fibers are integrated into new materials, into adaptive and high-performance materials to characterize the materials behavior and to detect

Farhad Ansari (ed.), Sensing Issues in Civil Structural Health Monitoring, 341–351.

damage at early ages. In general, high demands are made both on operational safety of the sensor system (stability of sensor characteristics and components behavior, clear definition of drift effects) and on reliability of all components including data acquisition and editing.

In the discussion with users was getting obvious that everyone interprets the terms stability and safety differently. Indeed, there are no specific definitions for these terms in FOS technology, however, one can adapt the definitions from engineering community: *Reliability* is the ability of a system or a component to perform its required functions under stated conditions for a specified period of time [1]. Rather from a scientific view is *reliability* of a product (component, device, system or a chain of network components and devices) defined as the probability that the product will meet a set of specified properties for a given period of time in service [2]. *Stability* is the invariability of a specified property of a substance, device, or apparatus with time, or under the influence of typically extrinsic factors [3].

The end user is always interested in getting reliable and stable monitoring system. In order to obtain such a system, all components of the system have to fulfill the requirements separately. In the following considerations, some of essential reliability and stability aspects will therefore be considered separately.

2. BASIS REQUIREMENTS ON LONG-TERM MONITORING SYSTEMS

Measurement systems created for long-term measurements have to fulfill a number of basic requirements. On the one hand; they have to work stable for a long period of time under very different environmental conditions, such as temperature variations, moisture influences, chemical attacks to components of the sensor system, chemical interactions between sensing components and measurand if the sensing element must be transparent to the environment, and finally aging of materials in the vicinity of the zone to be evaluated. In a number of cases, especially when the sensor system is already operating during construction work, and when the measured object is modified within the period of measurement, the sensor system is subject to changes, which could lead to distortions or errors:

- Influence on the measurement signal when cabling conditions change during construction work.
- Loss of the bias value (initial value as zero-point reference) when leading fibers were cut and reconnected, or the power supply was disconnected or switched off.

- Influence on the measurement signal when the temperature distribution along the sensing element or along the optical fiber frequently changes (e.g. one part of the fiber is installed indoor; another part is installed outdoor under all the climatic conditions over a year).

On the other hand, the recorded data have to reproduce reliably the reaction of a structure. In order to ensure this, the measurement system has to be composed appropriately, and all system components - not only source, cabling and detector - have to be understood in its particular function.

These issues which can distort the measurement result are critical in fiber optic systems if the fiber sensor principle does not deliver absolute measurement values as e.g. intensiometric sensor types do not do.

3. PERFORMANCE-DEFINING COMPONENTS OF THE MONITORING SYSTEM

There are three principal contributors to monitoring system performance which require attention:

- The *sensing element* itself. This is the basic element in a measurement system because it has to reproduce reliably the interaction between the measurand and the sensing element and to transfer the physical sensor parameter of interest to the data processing unit. No matter whether the sensor is an integral component of a measurement system or if it is inserted as a separate element into a measurement configuration, it must always be designed carefully for the specific application.
- *Cables* with coatings and jackets, *connectors*, *couplers or branching elements*. Especially, in fiber sensor systems, coatings can work themselves as an intrinsic part of the sensor and influence the measurement signal. In another case, the cable link including passive components between the sensing region and the detector can also influence the propagating optical signal, and must be designed to avoid interference with them.
- *Sources*, *detectors* and *data processing unit*. They must be designed, tested and evaluated for stability in the context of the modulation process utilized by the sensor.

Not to forget the *quality of application* of the sensor and the system components. A well-designed monitoring system is always as reliable and stable as its last part in the chain: the quality of application.

4. RELIABILITY ASPECTS FOR DIFFERENT SENSOR APPLICATION METHODS

Reliability-related issues concerning sensors applied for long-term use strongly depend on the method of application. A reliable operation of surface-applied sensors seems to be easier to handle than those of embedded or integrated sensors. Indeed, structure integration of fiber optic sensors is the most difficult application type. Therefore, reliability aspects will be outlined.

4.1 Sensor assembling at/in structure components

Sensor fibers, which shall measure integral strain (comparable to classical extensometers), are often surface-mounted on structure components or fixed inside of components, e.g. fixed at reinforcing steels of concrete components. This installation process is rather simple; however, special attention must be put onto long-term stable fastening. Furthermore, the fixing components may not creep or change in any mechanical way during concreting because as the distance of defines the gage length. An uncertain gage length leads to an uncertainty in measurement result.

4.2 Sensor attachment (gluing) onto surfaces

Single fiber sensor elements (fiber Bragg gratings (FBG), fiber Fabry-Pérot sensors, short strain-sensitive fibers) can be glued to metallic, plastic or mineral surfaces to measure strain or vibrations. Such sensors are widely used, e.g. in chemical engineering plants, inside of load cells or measuring heads to record strain waves or acoustic emissions. The long-term performance of the sensor does not only depend on the long-term stable attachment of the sensing element to the particular material but also on the elastic behavior of the adhesive and the design of the gluing zone.

4.3 Integration into monolithic or complex materials

Single strain sensors (FBG sensors) and sensor fibers that are divided into several measuring sections (e.g. quasi-distributed strain sensors) can - because of their tiny dimensions - intimately be embedded into monolithic or complex materials. Two cases have to be distinguished: Each measuring section is separately fixed on its ends and the strain in the measuring section of the embedded sensor element varies when the distance between the fixing points changes. Experience shows that it is quite difficult to define the exact gage length of embedded measurement sections. Either the fixation area is

not really so small that the gage length can sharply be defined by two "points", or there is no opportunity to measure the actual gage length after having finished the embedment procedure. The only way would be a calibration of the embedded sensor, however, large components to be monitored such as bridges, towers, tanks, do not enable anymore a separate calibration of the sensor. Thus, a very critical problem gets obvious: reliable long-term measurements would actually require calibration from time to time. Without opportunity of an exact calibration, the long-term reliability of a measurement system cannot really be proven. This is most essential when the fiber sensor is fully material-integrated. Then it has to bond reliably to the measuring object along a certain fiber section or the length of the sensing element (e.g. FBG). In this case, the strain transfer, from which arises the strain value at the measurement device, essentially depends on the quality and durability of bonding between the sensing section and the measuring object, and, on the other hand, on the bond limit (ultimate bonding shear strength). This kind of fiber optic strain sensor application is far from a simple fiber sensor installation at the surface of a component. Such applications hold a number of uncertainties. Before material-integrated irretrievable fiber sensors can be considered as a standard tool in structural health monitoring systems, methods have to be developed to become able to prove their reliability. Another complicated issue is the simulation of the service environment for which the sensor reliability should be proven, especially under the aspect of accelerated investigations in laboratory environment.

5. CHOICE OF THE APPROPRIATE MEASUREMENT SYSTEM

The selection of a measurement system is usually done with regard to the measurand to be evaluated and to an acceptable price. If long-term use is intended, the expected lifetime - in other words the stability and reliability of the system components - is certainly discussed. However, the available measurement principles for the particular measurement task can strongly differ with regard to reliability issues. Table 1 shows some differences of usually used fiber sensor principles in case of long-term use. Reliability problems can arise when a data recording over months or years require an exchange of components of the sensor system such as cables or connectors. Not only the characteristic curve of the sensing element can be influenced, but also the first values at the beginning of the measurement cycle (zero-point reference) can be lost, and an irretrievably applied sensor cannot be recalibrated after its installation. Only in a very limited number of cases, the

sensor can be demounted or removed together with a part of the structure, and then recalibrated in the laboratory. It is worthy to note, that the mentioned recalibration problem cannot be overcome by calibration of the reading unit. Sometimes, a combination of two measurement principles helps to achieve long-term stable and reliable measurements; another way could be that the sensor is equipped with an integrated zero-point reference [4]. This method overcomes problems, when the power supply is switched off between two measurement events, when the recording device has been disconnected, or when components of the measurement system have to be exchanged. A zero-point stability information is then available.

Table 1. Characteristics of fiber optic sensor principles with regard to long-term practical use

	Gage length [cm]	Long-term stable sensor characteristics	Zero-point stability	Temperature influence on sensor is controllable	Line-neutrality	Data loss due to break in power supply	Reliable definition of the gage length is difficult	Sensitive to lateral mechanical influences
Intensity modulation [1)]	5-1000	+	--[2)]	+	-	+[2)]	-	0
White light interferometry	50-1000	++	++	++	+	-	-	-
White light Interferometry	0.5-10	+	0	+	+	-	-	-
Fabry-Pérot interferometry	0.5-5	0	--[2)]	++	+	0	+[3)]	-
FBG technique	0.5-5	++	++	0	+	-	++[3)]	++
OTDR (back reflection techn.)	>10	+	++	-	+	-	+[3)]	0

[1)] Intrinsic type; ++ means: yes; -- means: no; 0 means: under certain conditions yes.
[2)] if there is no additional evaluation of the bias (zero-point reference); [3)] if embedded

6. SELECTED RELIABILITY AND STABILITY ASPECTS FOR FIBER OPTIC SENSORS INTEGRATED INTO MATERIALS

6.1 Reliable strain transfer into structurally integrated fiber sensors

Intrinsic fiber optic deformation sensors such as fiber Bragg grating sensors, distributed crack sensors or Brillouin strain sensors use the coating for interaction between the measurand and the propagating light. Changes in the structure or in material behavior are transferred from the host material

via the coating to the sensing area. Therefore, the strain transfer has to work reliably and long-term stable when e.g. fiber Bragg gratings are integrated into a carbon or glass fiber reinforced composite. There are some important questions to be clarified:

- Bond behavior (shear strength distribution along the sensing area) and bond strength of the sensor coating to the material to be evaluated.
- Bond strength of coating/glass fiber in the sensing zone.
- Long-term stability of coating under long-term mechanical, thermal and environmental influences.
- Influence of irregularities in sensor coating (e.g. for recoated FBG or for FBG written through the coating)
- Influence of deviations or irregularities in the matrix microstructure, which could reduce the bond strength.

In order to get the required knowledge to evaluate and create a reliable and long-term stable strain transfer, the single fiber push-in test method can be used. A thin slice is carefully cut out from the material with the embedded fiber sensor to be investigated and, by using an indenter needdle, the fiber will slowly be pushed through the material. This fiber piece represents the macroscopic feature of an embedded fiber optic sensing element. This method is described in more detail [5]. Results of differently coated optical fibers, usually used in fiber Bragg grating sensors, are shown in Figure 1.

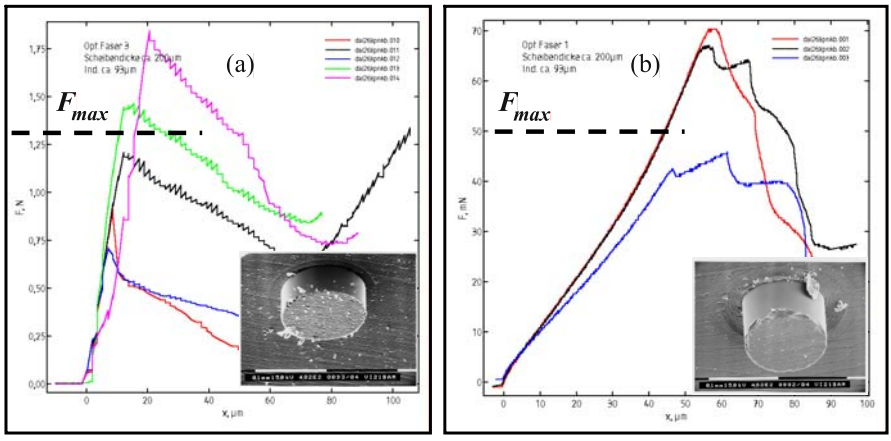

Figure 1. Comparison between the bonding behavior of a polyimide-coated (Fig. 1a) and an acrylate-coated (Fig. 1b) optical sensor fiber embedded in the epoxy resin matrix of a composite. The linear range in the relation force in axial fiber direction and contraction of the compound fiber/matrix was experimentally determined by using the push-in test method. (The single curves represent several test specimens.)

The difference in the bond strength of the used coatings can clearly be seen. Whereas the bonding of a polyimide-coated fiber is failing at a push-in

force of about 1.3 N (average); the acrylate-coated fiber already fails at 0.05 N (average). Another very important detail is becoming evident in these tests. The fiber, which contains the sensing element, is slipping within the coating - the strain transducer - shortly after reaching the bond strength. In particular under long-term dynamic loading conditions and under to slip. Reliable measurements are not any more possible.

6.2 Stability of strained and/or embedded fiber optic sensors

Fiber optic strain sensors are intrinsically under a permanent tension of a few thousand μm/m. This means that the coating is always under tension. Polyimide coatings are particularly appropriate for mechanical sensors. They are thin (typically a few microns), stiff (and therefore give effective strain transfer) and should adhere, in general, sufficiently to both external epoxy based adhesive joints and to the surface of the fiber. However, these coatings, like all polymers, can become brittle with exposure to ultraviolet light and/or high temperatures, or can change the strain their strain transfer properties under the influence of moisture. Then, even little tension can expose micro cracks and induce moisture penetration. Other coatings can tend to creep. In order to guarantee long-term stable function of coating, metal coatings can be used in some cases, particularly at higher temperatures. Concerning aging and mechanical strength behavior, there is a very large number of investigations and presentations worldwide, to elaborate the lifetime of sensor fibers when exposed to specific environmental or loading conditions; however, mostly of them are made for standard telecommunication fibers.

Another critical issue concerns the signal stability of embedded FBG sensors, when they are embedded into interface zones of textile reinforcements used in slender concrete members or in composite liners for strengthening reinforced concrete components. The sensors are then exposed to the influence of the surrounding inhomogeneous material. Single textile fibers (filaments) or multi filament yarns (rovings) might affect the FBG sensor, when they cross the fiber surface exactly at the position where the grating is, or when local stress zones arise along the grating. Depending on the amount of the inhomogeneity of the textile structure as well as on the grating and coating type, embedded FBG sensors suffer more or less from transverse and point-wise deformations with the result that the measurement signal (spectral behavior of the Bragg pulse) can be heavily disturbed. Such disturbances were observed, for example, in sensor-tipped composites after being cooled down to -20 °C and more [7]. Equally, transverse pressure to the grating, for example in high-pressure applications (down hole for oil

exploration), influences the reflected pulse of the grating considerably the measurement system. Another effect could also be observed: the sensitivity of embedded FBG sensors shows non-linear dependence with temperature. Therefore, each sensor should be calibrated in the final structure before its use. This enables to estimate experimentally the threshold beyond which interferences (reliability problems) can be neglected.

6.3 Stability of sources, detectors and data processing units

The influence of sources, detectors and demodulation systems on performance of the monitoring system is not less important. Not only in intensity-based systems stable source intensity and detector responsivity is fundamental. Changes in optical coupling to fibers lead to an instable measurement system, for example some sources change their spatial mode spectrum with ageing and/or drive current. Interferometers are another category of sensors. Here the wavelength of the source and the stability of the reference arm and/or the reference element are fundamental to the reliability of the measured result. In FBG sensor systems, the emphasis is put on the long-term stability and repeatability of the wavelength measuring system, e. g. precise wavelength measurement. There are huge differences in price for spectral units for FBG sensors. If long-term monitoring is intended, the device must be designed to calibrate itself by using an internal reference. Such a drift control and/or reference control is essential if the measurement values are to be used as driving signals in adaptronic systems. Investigations in NIST in Boulder/Colorado have revealed that it is problematic to obtain strain information from Brag grating sensors with a measurement uncertainty better than 10 pm (corresponds to 10 μm/m) over a long period of time if the read-out unit is not accurately calibrated to a known wavelength reference [7].

7. VALIDATION - THE METHOD TO ENSURE RELIABLE LONG-TERM MEASUREMENTS

Users of long-term monitoring systems want to be definitely sure that a chosen measurement system is suitable and reliable for the specific intended use. They need airtight results and they have to be able to draw feasible conclusions. A very useful method is the validation of a measurement system or of components of it because they get then assured information about the performance and limitations of a sensor system. Validation is explained in the international standard ISO/IEC 17025/2000 of the

International Standardization Organization (ISO) [8]. According to this standard, validation is the confirmation by examination and the provision of objective evidence that the particular requirements for a specific intended use are fulfilled. Following to this standard, the user gets the confirmation that the sensor or the measurement system works as reliable as demanded.

On the other hand, manufacturers and sales agencies also benefit from validation. Damage or weak points, which would reduce the reliability or stability, can be prevented already during manufacturing if validation aspects are kept in mind. In case of damage or if measurement results are not accepted by the user, the supplier is able to prove that he has complied with his obligation to exercise due care (product liability!). Thus, the supplier attains a competitive advantage at competent, unbiased validation. And finally, performance gaps in the measurement system can be displayed and removed by systematic optimization.

8. SOME GENERAL OBSERVATIONS AND CONCLUDING REMARKS

Every measurement system provides measurement results. Reliable data, however, are based on an appropriately chosen measurement principle, long-term stable system components as well as on a careful up to standard application.

In order to define technical requirements on a measurement task as well as on quality parameters for a sensor system which fulfills the request, the available set of definitions of quality-describing terms should strictly observed. Their correct use according to the international vocabulary [9] is the only way to compare specifications of similar monitoring systems. Definitions for the most important terms are, for example, called into memory in [10].

In order to come to a reliable monitoring system, each of its components must be treated individually and a careful system analysis is absolutely essential to determine errors in perceived measurements. Special effort deserves the sensing element(s), which means, the transducing part and packaging. Much relies also upon ingenious design of the sensor architecture and the careful implementation of the optoelectronic source and demodulation system.

Another important fact which should not be forgotten, when long-term monitoring systems are designed, concerns the re-calibration of installed sensors. If the sensor can be removed from the structure and re-calibrated in laboratory, there is an opportunity to compensate for unstable characteristic curves, drifts, and aging effects or signal perturbations. If there is no

possibility to calibrate the sensing part of the system from time to time, the measurement uncertainty increases over the time and the whole system gets unreliable. In only very few cases, irretrievably installed sensors for long-term measurement tasks can be forced to traverse the characteristic curve and be compared with a stable reference function. When creating a long-term stable and reliable sensor system, the optimal way would be to design a sensing element which enables an access to the characteristic data and provides a definite zero-point position (zero-point reference) to which all following measurements can be related. Drifts or environmental influences to the sensing part can then be evaluated.

ACKNOWLEDGEMENTS

The author would like to acknowledge Prof. B. Culshaw (Univ. of Strathlclyde/GB), Dr. P. M. Nellen (EMPA/CH) and Dr. F. Berghmans (SCK CEN/Belgium) for their thoughts and discussion, partly within the EU-COST 270 action. They have given valuable inputs.

REFERENCES

1. *IEEE Standard Computer Dictionary.* New York, NY: 1990.
2. Reliability of Optical Fibres and Components (ed. by T. Volotinen et al.). *Final Report of COST 246,* Springer-Verlag, London Berlin Heidelberg, 1999, p. 15.
3. *Federal Standard (FED-STD) 1037C.* Glossary of Telecommunication Terms, 2000.
4. Hofmann, D., et al.: Lightning-safe diaphragm pressure gauge for geotechnical applications using a long-term reliable absolute EFPI sensor. *Proc. of the 2nd Europ. Workshop on Optical Fibre Sensors*, Santander, Spain, June 9-11, **SPIE-vol. 5502**, pp. 128-131.
5. Habel, W.: Fiber optic sensors for deformation measurements: criteria and method to put them to the best possible use (Invited paper). *Proc. of the Conf. on Smart Structures and Materials 2004*, San Diego, California, USA, March 15-17, **SPIE-vol. 5384**, 2004, pp. 158-168.
6. Lebid, S: *Perturbations in behaviour of fibre Bragg grating sensors introduced by local thermal and mechanical influences.* Dissertation at Dresden Univ. of Technology 2003. BAM Dissertationsreihe vol. 2, ISBN 3-86509-136-9.
7. Dyer, S. D. et al.: Key metrology considerations for fiber Bragg grating sensors. *Proc. of the Conf. on Smart Structures and Materials 2004*, San Diego, California, USA, March 15-17, **SPIE-vol. 5384**, 2004, pp. 181-189.
8. Standard EN ISO/IEC 17025:2000 (trilingual version): *General requirements for the competence of testing and calibration laboratories* (ISO/IEC 17025:1999).
9. *International Vocabulary of Basic and General Terms in Metrology*. Beuth Verlag GmbH Berlin-Wien-Zürich. 1994.
10. Culshaw, B.; Habel, W.R.: Fibre sensing: Specifying components and systems (Invited Paper). *Symposium on Optical Fiber Measurements SOFM 2004, Session X: Fiber Bragg gratings and fiber sensors.* Boulder, Colorado, USA, September 28-30, 2004.

INSTRUMENTATION OF THE INDOOR CABLE STAYED BRIDGE AT EMPA

Masoud Motavalli, Glauco Feltrin, Daniel Gsell, and Jonas Meyer
Structural Engineering Research Laboratory, EMPA, Switzerland

Abstract: A cable stayed footbridge with a glass fiber reinforced polymer girder has been erected in the Swiss Federal Laboratories for Materials Testing and Research (Empa). The main purpose of this project is to close the gap between complex real-world applications in civil engineering and simplified laboratory experiments. The bridge is a research platform in the fields of active, semi-active and passive vibration mitigation, structural health monitoring, integrated distributed smart sensing and advanced structural materials. The bridge will be equipped with several interconnected sensors and actuators. This paper discusses different aspects of such instrumentation and communication techniques.

Key words: Smart cable stayed bridge, structural health monitoring, sensor networks, communication, wireless, multi-hop.

1. INTRODUCTION

In today's bridge design, a trend towards bigger spans and more slender structures and structural elements is observed. This structural development is based on an increased use of high performance building materials. Additionally more sophisticated models of material behavior and more advanced mechanical simulation tools enable the designers to stress the materials closer to their strength limit. As a consequence modern bridges are becoming increasingly prone to vibrations. The same external dynamic excitation energy causes larger vibration amplitudes since the inertial mass of the structures is reduced. Therefore, the structural components are

Farhad Ansari (ed.), Sensing Issues in Civil Structural Health Monitoring, 353–361.

subjected to an increased fatigue loading and lifetime decrease. An additional reason which causes more and more dynamic drawbacks in structures made of conventional construction materials is the stiffness reduction of components due to slender design. Since the reduction in stiffness is larger than in mass, lower resonance frequencies result. The maximal energy content of external dynamic loading, e.g. traffic, wind or earthquake, is located at low frequencies. Therefore the eigenfrequencies of the structure are shifted towards excitation frequencies containing higher mechanical energy. Again, the constructions are subjected to higher vibrational loading. Beside the increased fatigue of the material, visible and noticeable structural vibrations may force the bridge users to feel unsafe and uncomfortable. This has a negative influence to the road safety and to the acceptance of the structure by its users.

2. CABLE STAYED BRIDGE PROJECT AT EMPA

2.1 Motivation and Goals of the Project

In order to avoid the above mentioned dynamical drawbacks, the development of appropriate vibration mitigation set-up's and health monitoring systems become essential. Typically, such systems are developed and tested by means of simplified laboratory experiments. Usually, an elementary mechanical system with well-defined boundary and environmental conditions is used as test set-up. The gap between these simplified configurations and the much more complex real world applications, with partly unknown boundary and varying environmental conditions, is often quiet large. Therefore at the Empa-laboratory, a large scale model of a cable stayed footbridge has been built. The main objective of this project is to create a link between simplified laboratory experiments and more complex real-world applications. Different subprojects of our research group and of external partners will be integrated into this bridge project. The bridge becomes a research platform covering following topics:

- Passive, semi-active and active vibration mitigation
- Structural health monitoring
- Distributed, integrated and smart sensing
- Advanced materials in construction.

2.2 Bridge Design

Since the maximum dimension of this laboratory bridge is limited (20.0 x 2.5 x 7.5 m^3), a footbridge was designed. In order to get a realistic structure, the bridge was designed according to the European Union standards. Since this bridge is used as a testing platform for the development and investigation of new vibration mitigation systems, the structure was designed to show vibration problems. Therefore, the above-mentioned trends in civil engineering to lightweighted and slender structures are adhered consequently. The bridge girder is made of standard pultruded GFRP structural profiles. The total weight amounts to 1.5 tons. Compared to the 15 tons ultimate loading, an extremely light longitudinal girder resulted. Furthermore, as global static system a cable stayed structure is chosen. Despite the use of the soft GFRP profiles, suspending the bridge deck by cables in relatively short spans enables the design of a slender girder. To realize one long free span, an asymmetric bridge with one pylon close to one abutment is chosen.

Figure 1. Cable stayed footbridge in the Empa-laboratory.

3. INSTRUMENTATION OF THE BRIDGE

In parallel to the bridge project, several subprojects have been initiated. All these projects concern the instrumentation of the bridge in order to

monitor and control the dynamic behavior of the structure. They will be integrated step by step into the laboratory bridge in the near future.

3.1 Fault detection by curvature estimation with fiber optic sensors

Today, structural assessment of bridges is often done by modal analysis. Therefore translational degrees of freedom, typically acceleration amplitudes, are measured. From these measurements the eigenfrequencies and the mode shapes are determined. Since structural damages can be interpreted as stiffness reductions of the constructional elements they have an influence on the modal parameters. Therefore, changes in these parameters are used as damage indicators. This approach is applied to real structures with rather moderate success since the influence of local stiffness reductions on the modal parameters is small, whereas environmental temperature changes have a strong influence on the estimated frequencies and mode forms. In this project the structural assessment is based on directly measured curvatures. This approach is based on the fact that structural curvatures are much more sensitive to damages than displacements. The measurement of the curvatures will be done by fiber optic sensors. Sensors with moderately long gage length will be used to measure averaged strains.

3.2 Adaptive Tuned Mass Damper

TMD's are commonly used as efficient damping systems. TMD's are built of an inertial mass connected to the structure by an elastic spring and a damper. The stiffness of the spring and the parameters of the dashpot have to be chosen that the resonance frequency of the subsystems is close to the eigenfrequency of the whole structure. Tuned Mass Dampers operate only in an efficient way, if their frequency is well tuned. However, the resonance frequencies of lightweight structures are strongly dependent on their actual loading. In order to mitigate such a construction, an adaptive TMD will be developed within this project. The frequency of this damping system will be adapted permanently to the actual frequency of the structure.

3.3 Cable vibration mitigation using controlled magnetorheological fluid dampers

Wind, rain-wind and parametric induced vibrations of stayed cables lead to fatigue damages particularly in the anchorage area. Different types of damping elements can help attenuate the vibrations. Esthetical as well as practical considerations require mounting these elements in the area near the

lower anchor point of such a cable. In this project, magnetorheological fluid dampers, arranged perpendicular to the cable, are used to mitigate the vibrations of an inclined cable. The characteristics of such a damper, viscosity and coulomb friction, are controlled by an external magnetic field. According to the current vibration status of the cable, being instrumented with several accelerometers, an optimal damper force is calculated and realized by such an adaptive damping device. Since the eigenfrequencies of cables are strongly dependent on the load status of the bridge, the feedback control strategy has to be adjusted permanently to the actual loading state of the bridge.

3.4 High sensitive acceleration measurement

Using accelerometers is a common technique to measure structural vibrations. The frequencies of vibrations of civil engineering structures are typically quite low and the amplitude range is quite large, since ambient, traffic and earthquake induced vibrations have to be measured. Therefore high sensitive accelerometers with high dynamic ranges are needed. EMPA, in collaboration with EPFL in Lausanne, Switzerland, is developing a capacitive accelerometer based on passive magnetic bearing principles. Part of this project is the implementation of a wired network, connecting multiple sensors in order to acquire acceleration data in a distributed way.

4. COMMUNICATION OF MEASUREMENT AND MONITORING DATA

Dynamic investigations of large structures require many measurement points and sensors with high dynamic ranges. Since each sensor has to be connected individually to a data logger unit, the installation of such investigation systems is time and cost intensive. Within this project different communication strategies are evaluated and implemented on the bridge.

4.1 Wired communication

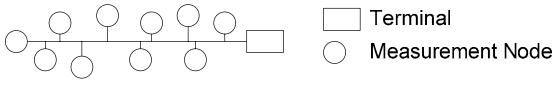

Figure 2. Measurement nodes communicating over a bus with data logger.

Generally measurements on civil engineering structures are realized by applying some sensors to the structure and connect them star like to a central data logger, which digitizes and stores the measurement signals. An expensive installation of large analog cable length is inevitable.

An improvement is achieved if a digital data bus, also called fieldbus, is used to interconnect the measurement nodes. To enable a digital communication the digitalization of the measured signals has to be moved to the nodes. In this subproject a commercial fieldbus solution is used and a general measurement node, which allows to connect different types of sensors, is developed and implemented. To reduce the demands on communication bandwidth, data compression algorithms are implemented in the node itself.

Due to the geometrical shape of bridges the bus topology is an adequate solution for communicating measurement data to a terminal or logger. Ideally a single cable can be installed along the bridge. The measurement nodes distributed over the entire structure are connected to the bus with drop lines. Furthermore it is possible to power the nodes over the bus cable, so additional power wiring can be omitted.

4.2 Wireless communication

The installation effort of a distributed measurement system can be minimized if no cables have to be connected to the sensors. In principle the topologies of the wired networks could be adopted to wireless technologies by simply replacing the cables with wireless links. For example the omnipresent WLAN shows a star topology and could be used for measurement and monitoring applications with the base station acting as data terminal. A drawback of most commercially available systems is their power consumption. The advantages of a wireless communication system vanish, if the remote nodes are not able to work for a long time using a battery and power wiring has to be installed.

In this subproject a low power wireless communication system is developed and implemented, consisting of a data logging unit, representing the data sink in the network, and several remote measurement nodes representing the data sources. Each node is equipped with a sensor, an electrical power supply, a digital signal processing unit and a radio transceiver.

In a first phase of the project the network topology is star-shaped. A central master node organizes the communication, synchronizes the measurement nodes and collects, stores and processes the acquired data.

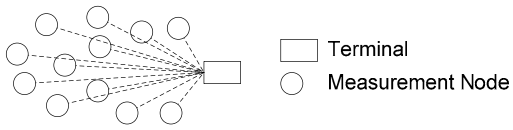

Figure 3. Star-shaped network consisting of several remote measurement nodes and a master node organizing the network.

In a second phase a multi-hop network is developed and implemented on the bridge. The main advantage of a multi-hop network is the ability to reduce power consumption. The transmission power needed to send data to a destination increases more than linearly with its distance (The power needed to transmit data over a distance d is approximately proportional to d^2 outdoors and d^4 indoors). In order to minimize power consumption it is preferable to send data over several short hops to the target instead of transmitting directly over the entire distance.

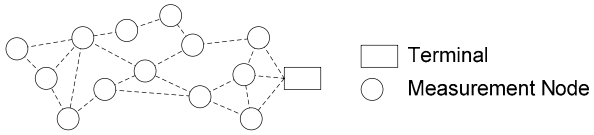

Figure 4.Multi-hop mesh topology. Each measurement node can operate as relaying station for its adjacent nodes.

Each measurement node figures as data source and relaying station, forwarding data of other nodes. Obviously multiple paths from each node to the terminal exist. The routing of the data is organized in a way to maximize network lifetime, i.e. energy consumption is distributed evenly among the nodes. Another feature of the network is its capability of self-organisation. If a single node or parts of the network fail, new routes to the destination are established.

4.3 Compression

Independent if using wired or wireless communication technologies, bandwidth is limited. In a wired system limitation occur due to physical constraints of the cable. In a wireless the available power resources of the remote nodes predominantly limit the achievable communication throughput. This limitation becomes more evident if multiple nodes are sharing the available bandwidth. For example when monitoring the vibrations of a civil structure, the upper bound of the interesting frequency range is about 50 Hz. If the signal is sampled with a resolution of 16 bits, the

resulting baud rate amounts to 2 kBaud. If some administration and configuration overhead is added, the rate increases to about 3 kBaud. This represents the raw data rate per channel. If multiple channels are required this rate increases linearly with each added channel. Even more bandwidth is needed if signals have to be sampled at a higher rate (for example acoustic emission measurements) or with a higher resolution (for example high precision acceleration measurement to detect seismic activities). Such applications impose high demands on communication throughput.

The space needed to store the data is another problem which arises when many sensor signals are recorded. Monitoring application running for years would fill several hard drives if the raw data streams would be stored.

To avoid these problems, the measurement nodes described above perform compression algorithms. At EMPA different data reduction algorithms and techniques are evaluated and tested on the indoor bridge. The aim is that each measurement node pre-processes its acquired data items, in order to compress and extract the relevant information in an intelligent way. Afterwards only the significant events and signal characteristics are transmitted to the logger or an alarm message is raised if some dangerous condition is detected.

If using battery powered wireless communication systems, data compression becomes even more important. Measurement nodes operating for several years from batteries have to perform compression algorithms in order to communicate as few data as possible. This increase the node lifetime since compressing data needs less energy than communicating.

Preferably each node can compute its local algorithms in order to compress the data or extract the relevant information out of the measurement stream. Also conceivable are algorithms which need to communicate with its immediate neighbours to determine if an event occurred has to be reported to the terminal or some supervisor device.

As a rule of thumb the compression rate should be at a level that the communication time can be kept around 1% of the desired network lifetime of several years. If more time is spent in the communication mode, energy resources degrade too fast.

4.4 Hardware

As prototype and experimentation platform Smart-Its particle computers from TecO (Uni Karlsruhe, Germany) are used. A particle consists of a low power short range wireless transceiver, a microprocessor and different, exchangeable sensor modules. They offer an open architecture and source code is freely available.

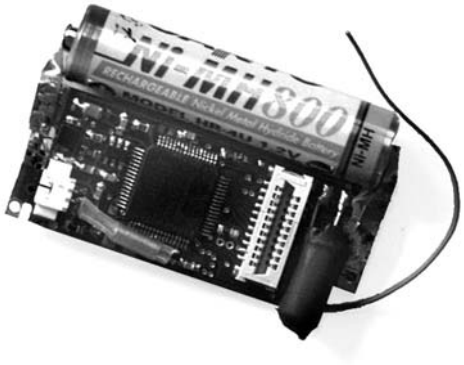

Figure 5. Smart-Its particle computer wireless transceiver with battery.

ACKNOWLEDGEMENTS

This project is financially supported by the Gebert Rüf Stiftung and the ETH council. The companies Fiberline S/A in Denmark and Maagtechnic AG in Switzerland are supporting the project with structural GFRP profiles. Additionally the project is integrated into the 6th European Union Framework Programme (Sustainable Bridge).

STRUCTURAL HEALTH MONITORING SYSTEMS FOR BRIDGE DECKS AND REHABILITATED PRECAST PRESTRESS CONCRETE BEAMS

Mohsen A. Issa, Hameed I. Shabila, and Mohammad Alhassan
University of Illinois at Chicago, Chicago, IL 60607, USA

Abstract: Bridges are an integral part of a highway network and represent a multi-billion dollar investment. It is imperative that they are always open to traffic, resistant to natural disaster, and undaunted by millions of loading cycles per year. However, bridges are expensive to maintain and do occasionally fail. Early signs of deterioration are often not seen because concrete, some type of deck overlay, paint, protective wrap or other bridge components mask them.

During service of bridge construction materials are subjected to degradation by aging; concrete cracks and creeps, steel oxides and may crack due to fatigue loading. The degradation of materials is caused by mechanical (loads higher then theoretically assumed) and physico-chemical factors (corrosion of steel, penetration of salts and chlorides in concrete, freezing of concrete etc.). As a consequence of material degradation, the capacity, durability and safety of structure decrease.

Structural health monitoring is the diagnostic monitoring of the integrity or condition of a structure. The intent is to detect and locate damage or degradation in structural components and to provide this information quickly and in a form easily understood by the operators or occupants of the structure.

In this study, a long-term structural health monitoring program was developed to identify any changes in the condition of the rehabilitated precast prestressed beams with CFRP over time due to sustained loads, traffic loads, and environmental exposure and to examine the performance of full-scale precast bridge deck under static and fatigue loading.

Key words: structural health monitoring system, bridge decks, fiber reinforced polymers, rehabilitation, and precast prestress beams.

Farhad Ansari (ed.), Sensing Issues in Civil Structural Health Monitoring, 363–372.

1. INTRODUCTION

The need for rapid assessment of the performance and safety of civil structures such as bridges, control centers, airports and hospitals, among many, has been amply demonstrated during recent natural disasters. In addition, continuous loading and extreme environmental conditions have caused extensive deterioration in our infrastructures. The ability to monitor the structural health of these systems is becoming increasingly important.

The health of bridge structures and their components has historically been determined using periodic inspections (visual and/or NDE/NDT-based) and/or reaction to structures or components that are rendered inadequate or unsafe before their anticipated service life has been expended. Past experimentation with monitoring structures involved expensive, elaborate systems requiring installation of strain gages and data collection systems for evaluation. These systems were not always reliable and were easily damaged by the elements. To overcome these problems, there are several technologies that have emerged and created the opportunity to develop a structural health monitoring system that has new configurations and characteristics. In particular, three technologies can potentially contribute significantly toward the possibility of new monitoring systems for civil structures: wireless communication, embedded systems, and miniaturized sensors [1, 2]. A new type of sensor has been developed to overcome the difficulties associated with hardwiring sensors along main cables. Remote monitoring and data acquisition systems have given the opportunity for fast and massive data collection. The collected information should be provided and interpreted in the form quickly and easily understood by the engineers.

2. RESEARCH SIGNIFICANCE

The main objective of this study is to evaluate the serviceability, reliability, applicability, and feasibility of the health monitoring systems currently installed on the repaired precast prestress beams with CFRP and the full-scale precast bridge deck. The other objective of the study is to understand the real-time behavior of the bridge deck and the repaired region of the precast prestress beams and to examine the accuracy of the data collected through the wireless transmission through the Internet. In addition to recommend a long-term bridge monitoring systems that will be cost-effective and reliably measure and monitor structure health.

3. BACKGROUND

Traditionally, engineers have relied on visual investigations to identify the problems and to evaluate the performance of bridge structures. The current and anticipated future costs of repair and rehabilitation of the nation's infrastructure due to deterioration are substantial. Despite its enormous importance and effectiveness, the conventional visual inspection regime for bridges cannot find many of the hidden and emerging deterioration problems in sufficiently advance time to make a meaningful difference.

Due to recent developments in new sensor systems, advanced wired and wireless communication systems, internet-based data sharing and monitoring, and data interpretation algorithms and software, we can now envision implementation of these sensors and health monitoring systems for bridges. In order for new system sensors to be effective and meaningful to bridge owners, inspectors and engineers, it must contain three important components [3]:

1. The first component involves development of cost-effective sensor systems that measure the most prominent factors influencing deterioration. For example, for years, the only effective way of measuring chloride content in concrete bridges was to take powder samples using hammer drills for chemical testing in the laboratory. This process is time consuming and provides only limited localized data on one of the most important predictors of durability in concrete structures. Now with the advent of embedded fiber optic chloride sensors, this parameter can be measured over time at a large number of points and depths within a structure.

2. The second component relates to ability to retrieve, transmit and view accurate data in real time (or near real time) from a large number of sensors on a bridge. The information from each sensor can be transmitted to a centralized control system located at the bridge through wired or wireless transmissions. From there, data can be relayed to the office through telephone lines, cell phones or other wireless transmissions for distribution and access via the Internet. Electric power for the sensing and monitoring systems can be provided by solar panels at locations where electricity is not available.

3. The third component involves the improved ability to make sense of the enormous amounts of data that would be typically collected. In the 1980’s and 1990’s, a number of testing companies tried to convince many bridge owners of the need to instrument structures. However, one of the major reasons for the lack of progress in instrument large numbers of structures has been the inability to interpret the data obtained from hundreds of sensors in a timely manner.

4. AVAILABLE SENSING TECHNOLOGIES

There exist a number of technologies that may enhance the monitoring of bridge structures. The following are the summary of the technologies developed and applied to evaluate the health monitoring systems of the bridges:

4.1 Microelectrochemical Systems

Known as MEMS, are micro sized devices that contain hundreds of sensors that may be embedded in a transportation system. Because of their small scale, microsystems can offer major advantages in cost versus functionality. Another application of Magnetostrictive sensor is to evaluate the corrosion in a strand or rebars. The propagation of guided waves traveling in a strand or rebars is dependent on the condition of the boundary between the steel and the concrete. Corrosion is a process that affects the boundary condition and hence can be detected and evaluated from properties of a guided waveform [4].

4.2 Nanotechnology

It has applications in virtually every field. Sensors embedded into highways could allow engineers to monitor the processes that contribute to deterioration and cracking without physical intervention. Sensors in bridges could monitor vibrations and loads and enable researches to assess weaknesses and fix them long before they are apparent to human inspectors. When the power of these technologies comes of age, bridge owners may have the tools to know, in real time, the condition of the complete bridge system.

4.3 Fiber Optic Sensors

The micromechanical resonator acts as a sensitive element, have been developed for measurement of many physical parameters. These sensors, capable of measuring acceleration and vibration, pressure, force and stress, temperature, and magnetic field, are electrically passive, lightweight, exhibit low mechanical hysteresis, and have shown to have high shock survivability. These are attractive for embedded applications in the structural integrity monitoring such as the bridges.

Optical fiber sensors have shown a potential to serve real time health monitoring of the structures. They can be easily embedded or attached to the structures and are not affected by the electro-magnetic field. It has its

unique advantages over conventional sensors and most of fiber optic sensors because it is reusable [5-7].

4.4 Piezoceramic (PZT)

The use of a piezoceramic (PZT) as an actuator–sensor shows great capability to detect damage of structures. The electro-mechanical coupling property has a direct and a converse effect. The direct effect is that the material will generate an electric charge when subjected to a mechanical stress. The converse effect is that the material will generate a mechanical strain in response to an applied electric field. When the structure is vibrated, the PZT patch also vibrates. The vibrating deformation will cause the PZT patch to generate an electric current. Since the response of the structure is influenced by structural properties such as stiffness and damping, a change in these properties due to damage will result in a change in the structural response and also the electrical impedance. Therefore, by observation of the electrical impedance, information about the damage of the structure can be obtained [8,9].

4.5 Acoustic

The acoustic monitoring system is a feasible health monitoring system to monitor the main cables of a suspension bridge, suspension, segmental concrete box girder, tied arch, and truss bridges. Acoustic monitoring continuously monitors the cable(s) to detect a wire break event as it occurs. Acoustic monitoring detects the release of strain energy associated with a wire break. The sensors are usually installed on a permanent basis to continually monitor the main cables for wire breaks related to corrosion, fatigue, or other deterioration mechanisms [10].

4.6 Magnetoelastic

Magnetoelastic sensors can be remotely interrogated by magnetic, acoustic, or optical means. The remotely detected resonant frequency of a Magnetoelastic sensor shifts in response to different physical parameters including stress, pressure, temperature, flow velocity, liquid viscosity, magnetic field, and mass loading. Compared to other physical effects, the magnetoelastic sensors have several important advantages: 1) Exclusive sensibility, considerably higher than that of strain gauges; 2) High output voltage; 3) Extremely high reliability; 4) Wide bandwidth and possibility to

measure fast changes of force and torque; 5) Long life time; 6) Small dimensions; 7) Simple construction; 8) Low cost.

5. CRITERIA FOR SELECTING HEALTH MONITORING SYSTEM

The process for evaluating the applicability, capability, and viability of continuous health monitoring sensors and techniques for bridges are based on the functionality of the system, initial and maintenance costs, durability and service life, portability and ease of use, history of use in other states or countries. The primary goal is to change the practice of using extensive cabling and high cost labor as is typical of the traditional monitoring systems to a system of inexpensive wireless embedded systems that can be installed, maintained, operated with ease, and without ever visiting the physical site. In selecting the health monitoring systems the following issues should be taken into consideration:

5.1 Installation Time and Cost

Among the key problems inherent in the structural monitoring systems are the installation time and cost. From experience, the installation time of a complete measurement system for bridges can potentially consume over 75% of the total testing time. Installation labor costs can approach well over 25% of the total system cost.

5.2 Maintenance

As for any monitoring system, maintenance is an expensive part of the structural monitoring system. For a structural monitoring system to make economic sense, the maintenance cycles should be long, generally years. It is safe to assume that regular power supply is available throughout the structure to support existing infrastructure requirements like lighting etc. In a wired monitoring system, wiring has to be done at a great expense and power is the least of the problems. But in a wireless monitoring system, the sensor units will have to depend on batteries for their power.

5.3 Real Time Monitoring System

Multiple sensors are comprised by a complete real time monitoring system with a digital network to acquire, process and store the measured data. In periodical intervals, the network returns the data to a central control

room by cellular phone, satellite, or conventional telephone circuit. From there, the data is distributed confidentially via Internet, therefore, one whose secret password can immediately asses the structure's condition from anywhere in the world without actually visiting structure's site. Such real-time, quantitative information greatly improves structural safety inspections and provides valuable information for directing timely maintenance relief to those areas of the structure most in need of repair; so structural lives of bridge structure can be extended [11,12].

5.4 Data Acquisition and Cleansing

The data acquisition portion of the structural health monitoring process involves selecting the types of sensors to be used, selecting the location where the sensors should be placed, determining the number of sensors to be used, and defining the data acquisition, storage, transmittal hardware. Economic considerations play a major role in these decisions. In some cases it is adequate to collect data immediately before and at periodic intervals after a severe event. However, if fatigue crack growth is the failure mode of concern, it is necessary to collect data almost continuously at relatively short time intervals.

One of the most common procedures is to normalize the measured responses by the measured inputs. Data cleansing is the process of selectively choosing data to accept for, or reject from, the feature selection process. The data cleansing process is usually based on knowledge gained by individuals directly involved with the data acquisition [13].

5.5 Feature Selection

The study of data features used to distinguish the damaged structures from undamaged ones receives considerable attention in the technical literature. The operational implementation and diagnostic measurement technologies needed to perform structural health monitoring typically produce a large amount of data. Condensation of the data is advantageous and necessary, particularly if comparisons of many data sets over the lifetime of the structure are envisioned.

6. FIELD APPLICATION

The damaged prestressed concrete beams on I90 were rehabilitated with carbon fiber reinforced polymer (CFRP) sheets to bring them back to their

design strength capacity and to their original shape [14-15]. The CFRP sheet was applied to the prepared surface according to manufacture specification.

To assess the structural performance of the bridge, the rehabilitated precast prestressed beams were instrumented at the rehabilitated locations. The instrumentation of the system included the installation of six vibrating wire strain gages at the outer surface (bottom) of the center of the damaged zone of the beams. Since electricity in not available, the electric power for the sensing and monitoring systems were provided by a solar panel. The strain gages and solar panel were connected to the collecting data logger box. Figure 1 shows the instrumentation of repaired beams.

The developed structural health monitoring plan consists of a non-destructive, long-term, monitoring program to evaluate and identify any changes in the condition of the rehabilitated precast prestress beams over time due to sustained loads, traffic loads, and environmental exposure. The rehabilitated precast prestress beams were monitored after repair to examine their behavior in terms of strength and durability on the long term.

Accurate data was transmitted, through this system, in real time from the six sensors on the structure. The information from each sensor was transmitted to a centralized control system located on the bridge. From there the data was relayed to the office through the wireless transmission through the Internet.

Figure 1 Instrumentation of precast prestressed girders

The strain variations for damaged beams and undamaged beam due to moving traffic and temperature effect were collected for a period of more than two years. The collected data from the structural health monitoring system and the visual inspection showed that the rehabilitated precast prestress beams are in a good condition and no cracks or signs of debonding of CFRP sheets from concrete was observed.

The full-scale precast bridge deck was monitored during the static service loads, overloads, and ultimate loads before and after applying the low cycle fatigues loading. The bridge was subjected to a low cycle fatigue test to

evaluate the structural performance of the segments of the bridge. The instrumentation of the bridge deck consisted of three strain gages and two vibrating-wire strain gages that were placed on the top surface of the bridge in addition to five vibrating-wire strain gages that were embedded in the concrete overlay during the casting stage. Figure 2 shows the monitoring of the crack opening and closing during the cyclic loading in the bridge deck. Overall, the health monitoring system performed well under all loading conditions and the collected data reflected the actual observation during the test.

Figure 2. Crack opening and closing during the cyclic loading in the bridge deck

7. CONCLUSION

The installed bridge health monitoring system on the bridge of I90 and on the full-scale precast bridge deck can be considered an intelligent monitoring system. The systems were supported by sensors that fulfilled the following characteristics: 1) accuracy: sensors had a reliable accuracy; 2) benefit: commercial price of the sensors are reasonable; 3) compact: sensor's shape were small enough; 4) durability: serviceability of the sensors were durable and long-lived; and 5) express: sensors were easy to operate and time consumed for measurement was close to real time measurement.

The collected data through a remote structural health monitoring system and the visual inspection showed that the rehabilitated precast prestress beams are in a good condition and no cracks or signs of debonding of CFRP sheets from concrete were observed.

REFERENCES

1. Chang, F.K. (ed.), Structural Health Monitoring 2000, Stanford University, Stanford, CA, 1999.
2. Kiremidjian, A.S., Straser, E., Law, K.H., Sohn, H., Meng, T., Redlefsen, L. and Cruz, R., "Structural damage detection", International Workshop on Structural Health Monitoring, pp.371-382, Stanford, CA, 1997.
3. Health Monitoring of Bridge Structures and Components Using Smart-Structure Technology, Wisconsin Highway Research Program.
4. V. Giurgiutiu and C. A. Rogers, "Recent Advancements in the Electro-Mechanical (E/M) Impedance Method for Structural Health Monitoring and NDE," Paper # 3329-53 at the SPIE's 5th Annual International Symposium on Smart Structures and Materials, 1-5 March 1998.
5. D. Inaudi, N. Casanova, S. Vurpillot, B. Glisic, P. Kronenberg, S. LLoret, "Lessons Learned in the Use of Fiber Optic Sensor for Civil Structural Monitoring," The present and the future in Health Monitoring, 3-6.09.2000, Weimar, Germany.
6. W. Lienhart, F. K. Brunner, "Monitoring of Bridge Deformations Using Embedded Fiber Optical Sensors," 11th FIG Symposium on Deformation Measurements, Santorini, Greece, 2003.Wu E, Smith FG. *Title of the Book*, City, Publisher, 1995.
7. Jianjun Ma and Anand Asundi, "On-line Structural Health Monitoring using Fiber Optic Sensor," School of Mechanical & Production Engineering Nanyang Technological University.
8. Z. Chaudhry, F. Lalande, A. Ganino, C. A. Rogers and J. Chung, "Monitoring the Integrity of Composite Patch Structural Repair via Piezoelectric Actuators/Sensors," Proceedings of the 36th AIAA/ASME/ASCE/AHS/ASC Structures, Structural Dynamics and Materials Conference, Adaptive Structures Forum, New Orleans, LA, Part 4, pp. 2243-2248, 1995.
9. F. P. Sun, Z. Chaudhry, C. Liang and C. A. Rogers, "Truss Structure Integrity Identification Using PZT Sensor-Actuator," Journal of Intelligent Material Systems and Structures, vol. 6, no. 1, pp. 134-139, 1995.
10. Michael S. Higgins, P.E., "Acoustic Health Monitoring of Suspension Bridge Main Cables- Case Studies," Regional Manager, Pure Technologies, 10015 Old Columbia Road, Suite B- 215, Columbia, MD, U.S.A.
11. F. P. Sun, Z. Chaudhry, C. A. Rogers and M. Majmundar, "Automated Real-Time Structure Health Monitoring via Signature Pattern Recognition," Proceedings of SPIE Smart Structures and Materials 1995, San Diego, CA, vol. 2443, pp. 236-247, 1995.
12. Ansari, F. Y. Bao, S. McNeil, A. Tennant, M. Wang, "Evaluation of Bridge inspection and Assessment in Illinois," Final Report Evaluation of Bridge Inspection and Assessment In Illinois, Project Ivd-H1, Fy 00/01, Report No. ITRC Fr 00/01-3. Illinois Transportation Research Center, December 2003.
13. Charles R. Farrar, Thomas A. Duffey, Scott W. Doebling, David A. Nix "A Statistical Pattern Recognition Paradigm for Vibration-Based Structural" 2nd International Workshop on Structural Health Monitoring, Stanford, CA Sept 8-10, 1999
14. Mohsen A. Issa, Hameed Shabila, and Moussa A. Issa, "Monitoring of Bridge Girders Retrofitted with CFRP Sheets," Concrete Solutions, Proceedings of the 1st International Conference on Concrete Repair, St-Malo, France, July, 2003.
15. Mohsen A. Issa, M. El-Metwally, and G. Monroy, "Evaluation of CFRP Composites for Seismic Retrofit of Beam-Column Joints," *International Congress, Challenges of Concrete Construction, Composite Materials in Concrete Construction*, pp. 277-287, Dundee, Scotland, UK.

CFRP STRENGTHENING AND MONITORING OF A BOX GIRDER BRIDGE

B. Täljsten[1,2]

[1]*Department of Civil and Environmental Engineering, Luleå University of Technology, SE-971 87 Luleå, Sweden, bjorn.taljsten@skanska.se*

[2]*Skanska Teknik AB, R&D, Råsundavägen 2, SE-169-83 Solna, Sweden, bjorn.taljsten@skanska.se*

Abstract: The Gröndal Bridge, is a large freivorbau bridge (pre-stressed concrete box bridge), approximately 400 meters in length with a free span of 120 m. It was opened to tram traffic in 2000. Just after opening cracks were noticed in the webs, these cracks have then increased, the size of the largest cracks exceeded 0.5 mm, and at the end of 2001 the bridge was temporarily strengthened. This was carried out with externally placed prestressed steel stays. The reason for cracking is still debated and will be further discussed in this paper. Nevertheless, it was clear that the bridge needed to be strengthened. The strengthening methods used were CFRP laminates in the Service Limit State (SLS) and prestressed dywidag stays in the Ultimate Limit State (ULS). The strengthening was carried out during 2002. At the same time monitoring of the bridge commenced, using LVDT crack gauges as well as optical fibre sensors.

To date, a large amount of data has been collected and the data is still under evaluation. Primary results show that the largest stress can be referred to the temperature load and that the contribution from the live load is minor. The results from the monitoring show that the CFRP laminates work as intended and that the cracks are not propagating

Key words: Monitoring, Fiber Optics, strengthening, CFRP, Box Bridge

Farhad Ansari (ed.), Sensing Issues in Civil Structural Health Monitoring, 373–382.

1. INTRODUCTION

The motivation for research and development into repairing, strengthening and restoration of existing structures, particularly concrete systems, is increasing. If consideration is given to the capital that has been invested in the existing infrastructure, it is not always economically viable to demolish and rebuild a deficient structure. In need of repair or strengthening epoxy bonded CFRP (Carbon Fiber reinforced Polymer) laminates could be one solution to overcome structure deficiencies. This technique proven to be very efficient and there is clearly a great potential for, and considerable economic advantages in FRP strengthening. At Luleå University of Technology, Sweden, research has been carried out in the area of plate bonding. The research work started in 1988 with steel plate bonding and is now continuing with FRP materials. Both comprehensive experimental work and theoretical work have been carried out. In Sweden the FRP strengthening methods have been used in the field for almost 10 years now, and both laminates and wrap systems are used. Sweden is also one of the first countries in the world where a national code exists for FRP strengthening [1]. This paper describes briefly the strengthening of concrete box girder bridge. The bridge was monitored after strengthening with FOS-seniors, this is also discussed in the paper.

2. THE GRÖNDAL BRIDGE

The main span of the Gröndals Bridge is 120 meters with two adjacent spans each of 70 meters (see Figure 1). The bridge carries two railway tracks which are placed symmetrically about the cross-section of the bridge. The bridge has no footpath. Bridge inspection carried out on the newly built, 2000, Gröndals Bridge revealed extensive cracking in the webs of its concrete hollow box-girder section. The bridge is a part if a light-rail commuter line which is located in the south of Stockholm. The cause of cracking is still under investigation and has resulted in several articles in Swedish construction industry magazines, [2] and [3]. The cracks first appeared after only a few years of service and subsequent inspections showed that the number and size of the cracks were increasing, [4]. The cracks widths were between 0,1 - 0,3 mm and in a few isolated cases between 0,4 - 0,5 mm in the most cracked sections. Preliminary investigations as to the cause of the cracking suggested that they were due to inadequate shear reinforcement in the webs. The webs are slender with a thickness of 350 mm and a total height of the box girder close to the main span supports of approximately 7,5 m.

In addition to that the flanges are quite thick, the bottom flange at most is about 1300 mm. The reasons for cracking can be summarized as follows: Due to the slender webs high tensile stresses are developed; the principal stresses, due to high permanent loads, are the main cause for cracking; the location of the cracks is in accordance with the highest principal stresses and the cross-sections are under-reinforced due to shear reinforcement. To increase the safety level of the bridge strengthening was decided.

3. STRENGTHENING

The bridge required strengthening in several sections, strengthening was needed both in the ultimate limit state (ULS) and in the service limit state (SLS), but in different sections. Strengthening in the ultimate limit state was carried out by pre-stressed dywidag-stays and in the service limit state by CFRP laminates. Strengthening in the SLS was in this case particularly complicated since for this type of structure the portion of the dead load is considerable, approximately 85 % of the total load. It was decided to use high modulus carbon fibre laminates to strengthen the bridge. The purpose of strengthening in the SLS was to inhibit existing cracks and prevent new cracks from developing.

Table 1 Material data for CFRP Strengthening

	Characteristic value		Design value	
Concrete	E_{ck}	*33.0 GPa*	E_c	*22.9 GPa*
	f_{cck}	*32.0 MPa*	f_{cc}	*17.8 MPa*
	f_{ctk}	*2.10 MPa*	f_{ct}	*1.17 MPa*
	ε_{cu}	*3.5 ‰*		
Steel	E_{sk}	*200.0 GPa*	E_s	*173 GPa*
	f_{yk}	*490.0 MPa*	f_{st}	*371 MPa*
			A_s	*2010 mm²/m*
BPE® Laminates	E_{fk}	*250 GPa*	E_f	*189 GPa*
(1.4 x 120 mm)	ε_{fk}	*11.0 ‰*	ε_{fd}	*5.0 ‰*
Dimensions	*b*	*1.0 m*	*d*	*3.8 m*

Therefore the existing crack widths would be reduced to no more than 0.3 mm (maximum allowed crack width in the Swedish code in the SLS). The design of the CFRP strengthening in the SLS is not covered by existing codes and a fracture mechanics approach was here applied where considerations to the total energy to open up new cracks over a unit distance was taken. The design, due to limited space, is not presented in this paper but the design philosophy is discussed.

The sections strengthened with CFRP laminates had no or only very small cracks, < 0,05 mm, at time of strengthening. In this particular case strengthening performed in the SLS state will also contribute in the ULS state. Carbon fibre strengthening was chosen to prevent and minimise future cracks in areas where minor or no cracking had developed. In the calculations the strain in the existing steel stirrups has been calculated due to sectional forces. In the calculation the following assumptions have been made: calculation in Stadium I, non-cracked concrete, the crack widths are the limited factor, the cracks are not allowed to become larger than 0.3 mm after strengthening; the effect of pre-stressing has in the crack calculation been neglected but is accounted for when calculating the internal forces. The concrete is only exposed to tensile stresses perpendicular to the crack plane. Only vertical reinforcement in the webs has been considered. The concrete starts to crack at approximately 100 μs. The first visible crack arises at approximately 0.05 - 0.10 mm. Characteristic material data has been used in the calculations. The material data for concrete, steel and CFRP laminates is given in Table 1. In the design it has been assumed that the steel reinforcement may yield in the crack tip for a crack width of 0.3 mm. However, bonding CFRP laminates to the surface of the concrete at development of cracks gives a stress (and strain) distribution between the steel and composite. The bridges are very important for the commuters going from the south parts of Stockholm into the center of the town. For that reason it was undesirable that the bridges were closed during strengthening. However, it has been shown that strengthening with CFRP laminates can be carried out during traffic [5]; therefore it was decided to permit traffic during strengthening. Before the strengthening work started the concrete surfaces were sandblasted and holes were drilled in the upper and lower flanges for anchorage of the laminates. Laminates were only placed on the inside of the bridge. The surfaces were thoroughly cleaned with pressurised air and vacuum cleaners. The surfaces to be bonded were treated with a primer for the system to enhance the bond. The laminates were bonded to the surface, the webs of the structure with a high quality epoxy adhesive, BPE® Lim 567, specific for the strengthening system used. The Young's modulus of the adhesive is approximately 6.5 GPa at 20 °C. The average thickness of the adhesive was 2 mm. A total of 2 500 meters of CFRP laminates was used for the bridge. The placement of the CFRP laminates in the Gröndal Bridge in section A, the east side is shown in Figure 1. It can also be noticed in Figure 1 that the CFRP laminates have been bonded at an angle of 70° to the horizontal plane. This was in order that for the laminates to be bonded perpendicular to the direction of the cracks. In Figure 2a) the anchorage system, steel plates with welded steel bars drilled into the concrete, is shown.

The anchor length was approximately 250 mm. The final result after strengthening is shown in Figure 2b.

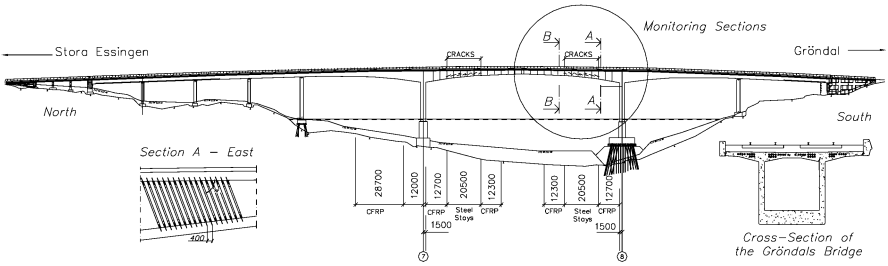

Figure 1 The Gröndals Bridge , CFRP strengthening and monitoring area

Figure 2 a) Anchor system for the CFRP laminates. The anchorages are bonded with an epoxy adhesive in pre-drilled holes in the flanges, b) Final result after strengthening

To follow up the behaviour of the bridge over time a monitoring system was installed. The system and some results from the monitoring are explained in the next section.

4. MONITORING THE BRIDGE

When the first crack in the webs of the bridge was found it would have been preferable if measurements had been undertaken immediately. A visual inspection has been carried out regularly, but unfortunately no real measurements have been carried out. In spite of this it has been decided to measure the behavior of the bridges after strengthening, and in particular the future crack developments. Consequently a monitoring program has been put together. In this program measurements have been suggested to be taken at specific locations to measure crack development and strain on the CFRP laminates. To obtain the most out of a measurement program it is important to carry out SHD (Structural Health Diagnostics) in a structured way and that a well-planned procedure is followed. Luleå University of Technology

has worked out a method termed Structural Health Diagnostics (SHD), which in short implies that a rough diagnosis is made on the structure; this can be simple calculations, on site visual inspections or minor measurements. Next it is decided what is to be measured and the purpose with the measurement. In this phase the acquisition system is also decided. Sensors and communications systems are established as well as hard- and software. On top of this, an evaluation system is connected which connects the data from the measurement to a model of the structure. From this action plans are then suggested. Two monitoring systems have been installed on the Gröndals Bridge, one traditional monitoring system using LVDTs (Linear Vertical Displacement Transducers), and one with Fibre Optic Sensors (FOS). The first is used for continuously monitoring and the second for periodic monitoring.

The traditional system is installed for monitoring the long term effect of the crack development. The FOS system was installed for two purposes; first to monitor crack development and strain changes due to temperature and tram traffic, second to increase the practical experience by using FOS in field. In addition to this a comparison between the two systems have been made. The traditional system has been installed and followed up by the Royal Institute of Technology (KTH) in Stockholm, [4] and the FOS system has been installed and followed up by Luleå University of Technology in collaboration with City University in London, UK. [6]. There are a total if six LVDT´s mounted on the Gröndals Bridge, one of which is a dummy used to verify the accuracy of the traditional monitoring system. With exception of the dummy and a sensor, which is positioned between the top flange and the web of the box girder, all the LVDT´s are positioned across and perpendicular to a crack so as to measure the opening and closing of a crack. The placement of the gauges can be seen in Figure 5. Four of the LVDT´s are mounted on the inside on the west web of the box girder, one of which is the dummy. One of the LVDT´s is mounted on the inside of the east web. The last of the LVDT´s is mounted between the top flange and the web of the box-girder and measures the relative displacement of the bridge deck to the web. In addition two temperature sensors, thermocouples, have been installed on the bridge and they are both positioned on the east web of the box girder, one on the inside and one on the outside, both belonging to the traditional system. In total 32 FOS gauges have been installed on the Gröndals Bridge, they are all installed in section A and section B, see Figure 1 and Figure 3. In section A, 12 sensors have been installed on the west side where three were used to compensate for the temperature. Two of these sensors (including temperature compensation) are positioned on a section of CFRP laminates, the others on different locations of concrete cracks. On the east wall in the same section seven sensors are installed, five on the concrete

(including temperature compensation) and two on a CFRP laminate also here including temperature compensation. In section B, west side, four sensors have been positioned on the concrete, one of which is for temperature compensation and two have been positioned on a CFRP laminate, where one is for temperature compensation. On the east side in the same section six sensors have been positioned on the concrete, one for temperature compensation and two on a CFRP laminate, of which one is for temperature compensation. The placement of all the gauges is shown in Figure 3.

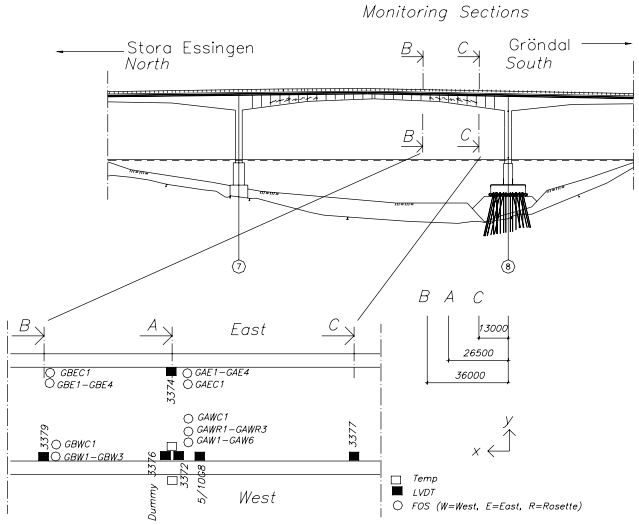

Figure 3 Position of gauges on the Gröndals Bridge

As can be noticed in Figure 3 many gauges have been placed on the bridge. The filled rectangular blocks represent the LVDT´s and the open rectangular blocks represent the thermocouples for the traditional system. The FOS are represented by open circles. In table 2 the sensors are presented systematically. For the FOS system the previously mentioned sensors for temperature compensation shall also be included, however, this is not recorded in Table 2.

Table 2 Sensors for monitoring

Section A (and C)				**Section B**	
Sensor	*Measure*	*Sensor*	*Measure*	*Sensor*	*Measure*
3372	Crack opening	GAW1-6	Crack opening	3379	Crack opening
3374	Crack opening	GWR1-3	Strain Concrete	GBW1-3	Crack opening
3376	Dummy	GAWC1	Strain CFRP	GBWC1	Strain CFRP
5/10G8	Displacement	GAE1-4	Crack opening	GBE1-4	Crack opening
				GBEC1	Strain CFRP

5. RESULT FROM MONITORING

It is not possible to present all the results from the measurements and therefore only the most interesting values are presented, however all data from the monitoring up to March 2004 may be found in [4] and [6]. The results from the monitoring are presented for the traditional and FOS systems respectively. The result from the entire year 2003 for the Gröndals Bridge is shown in Figure 4, [4]. It is not easy to extract a single value of the crack behaviour. However, from the figure it is possible to see that the cracks in the webs (indicated by sensors 3374, 3372, 3379 and 3377) do not appear to be of a progressive nature but rather that the cracks open and close depending on daily and seasonal temperature changes.

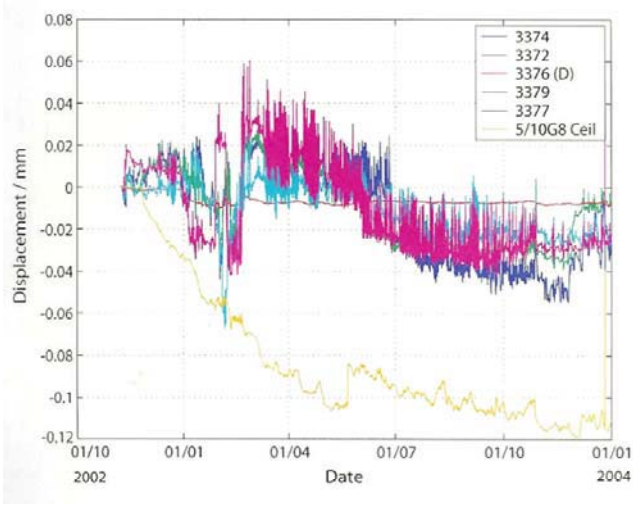

Figure 4 Result from crack-displacement with traditional monitoring system, from [4].

The crack widths of these gauges are not significantly different at the start of 2004 than at the start of 2003, with the variation in the order of 0.02-0.03 mm. The LVDT sensor (5/10G8) mounted between the underside of the top flange and the inside of the west web measures the longitudinal displacement in the top flange in relation to the web. The displacement appears from these results to be progressive even if the growth rate has decreased over the later half of the year.

Before we discuss the result from the FOS system, a brief discussion about the installation procedure and the SHD system used will be presented. Before installation calculation of stresses in the chosen sections had been carried out [3], however, these calculations also considered the dead load of the bridge. The monitoring systems installed can only follow the relative changes with regard to temperature and live load.

The FOS system used has been developed at City University in London and the University also took part in the installation work, calibration and monitoring of data. The FOS sensors are of type Bragg grating and at most 7 sensors were written on one fibre, the length of each senor was approximately 20 mm. The total time for installing and calibrating all the FOS sensors was approximately 10 days, this corresponds with the time it took to grind the concrete and CFRP laminate and bond and protect the fibres. Monitoring was carried out during May 2003 and over a time period of 3 days (periodic monitoring). It was not possible at that time to carry out a continuous monitoring due to the high cost of the system. Nevertheless, to store the data a portable hard disk was used, which was then transported from the bridge to the office for further evaluation of the data. Not all data has been evaluated up to date and has been planned to repeat the monitoring sequence during the next winter. However, it was found that using this FOS system was convenient and the installation procedure was quite simple.

This paper will not present results from all sensors however, in figure 5 crack displacement from sensors GAW1 to GAW6 is shown. From Figure 5 it can be seen that crack displacement for GAW3 is considerably larger than for the others, here the FOS sensor is placed in the same crack as the LVDT gauge 3372, however during this time the crack displacement for the LVDT is approximately 0,035 mm (this can not be seen in Figure 3 due to the scale). The large variation over time is due to daily variation in temperature. In Figure 5 small jumps may also be noticed, approximately 0,001 mm wide. This is due to the tram traffic, it seems that the effect of the temperature on opening and closing of the cracks is tenfold to the traffic load. Over the same crack as in Figure 6 a CFRP laminate has been bonded, in Figure 6 the strain is recorded in this laminate in the same position as the crack. A calculation of stress gives a level of approximately 30 MPa in the laminate.

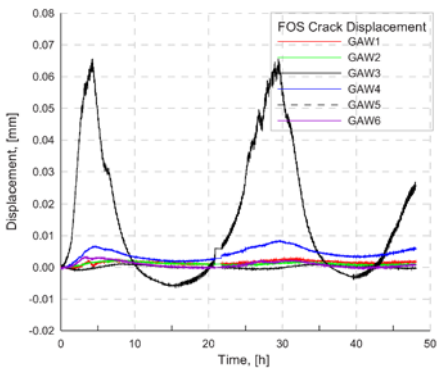

Figure 5 Result from crack-displacement with FOS system, [6]. Start date for monitoring 21-05-04

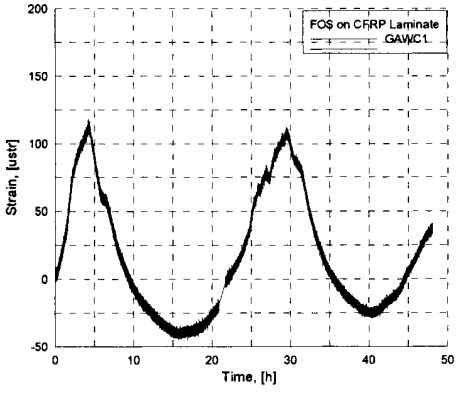

Figure 6 Result from crack-displacement with FOS system, [6]

6. SUMMARY AND CONCLUSIONS

In this particular project the most innovating part was not to use CFRP laminates for strengthening, it was the way the design of strengthening was carried out. By using fracture mechanics in design and in combination with CFRP laminates it was possible to (theoretically) use the energy needed to open a crack to a certain size and transfer that energy to the CFRP laminate, which then redistributes the cracks and the distance between the cracks over the length of the laminate. Therefore a cost effective solution for strengthening in the SLS (also contributing to the ULS) could be chosen and finally carried out. Both monitoring systems installed on the bridge showed that the cracks were not propagating and that the opening for the cracks was more or less negligible The largest crack opening measured was approximately 0,06 mm. Furthermore, the temperature effect was approximately 10 times larger than the effect from the tram traffic. Monitoring will continue and it will be interesting to follow the bridge over time.

ACKNOWLEDGEMENT

The research presented in this paper has been funded by several organisations. Here the Swedish National Road Administration, the Development fund of the Swedish Construction Industry, Stockholm Transport (SL) and Skanska Sverige AB should be acknowledged.

REFERENCES

1. Täljsten, B. 2003: FRP Strengthening of Existing Concrete Structures. Design Guideline Division of Structural Engineering, Luleå University of Technology, Luleå 2003, Second edition, 228 pp, ISBN 91-89580-03-6.
2. Sundquist H., 2002, Hur mår våra Frevorbau broar egentligen? Betong No. 1, 2002, pp 4-5 (In Swedish).
3. Hallbjörn L, 2002, Sprickor I Gröndalsbron och Alviksbron I Stockholm, Betong No. 2, 2002, pp 8-12. (In Swedish).
4. James G., 2004, Long term monitoring of the Alvik and Gröndal Bridges, TRITA-BKN Rapport 76, Byggkonstruktion, 2004, www.byv.kth.se, p 48.
5. Hejll, A Norling, 2002, O "Betongbalkar förstärkta med kolfiberkomposit: Dynamisk belasting under limmets härdningsförlopp" Luleå University of Technology, Division of structural engineering, ISSN:1402-1617
6. Täljsten B. and Hejll A., 2004, "Evaluation of the monitoring of the Gröndal and Alvik bridges", Report to be published.

SENSORS AND CONDITION EVALUATION FOR BRIDGE HEALTH MONITORING USING OPERATING VEHICLE LOADING

K. Yokoyama and A.K.M. Rafiquzzaman
Department of Civil Engineering, Ibaraki University, Ibaraki, Japan

Abstract: In case of short- and mid-span highway bridges, a large number of heavy vehicles introduce severe damages to bridge decks and girders. For health monitoring purpose, operating vehicle could be utilized because it avoids the application of artificial loading and interruption of any traffic flow. Furthermore, it may be possible to develop new monitoring method replacing a large scale and multi-channel measurement system. First this paper presents the results of field measurements and improvement of damage detection method. Next, basic idea of static damage detection algorithm using operating vehicle load is explained. Finally the paper presents an approach of using this technique to field application.

Key words: Bridge, Health Monitoring, Static Damage Detection, Operating Vehicle Load.

1. INTRODUCTION

The ability to continuously monitor the integrity of structures in real-time can provide for increased safety to the public, particularly for the aging structures in widespread use today. The ability to detect damage at an early stage can reduce the costs and downtime associated with repair of critical damage. Recently many non-destructive smart technologies [1] are being used to monitor and inspect bridges for damages that are either in its inception or small enough to be detected by human eye. Some of these

Farhad Ansari (ed.), Sensing Issues in Civil Structural Health Monitoring, 383–392.

technologies can be built directly into the bridge making it an intelligent structure.

In Japan, long-term observation system consisting of a large number of sensors and recorders are usually installed at long-span bridge in order to mainly validate the design against strong winds and earthquakes. Field static and dynamic loading tests are also conducted to confirm the structural features after completion of the structure. The test results can provide the reference data for damage detection at maintenance stage. Long-term observation systems, however, tend to deteriorate earlier than the structures.

Damages in the structures are associated with the changes in some structural parameters, which can be utilized for structural identification, namely stiffness [2-3], flexibility [4], damping, mass, eigen frequency [5] etc. Based on these structural changes many damage detection methods [6] have been developed which include but are not limited to, Damage Index Method, Mode Shape Curvature method (Curvature Method), Change in Flexibility Method, Change in Uniform Flexibility Curvature Method, Change in Stiffness Method, MAC, COMAC etc.

For bridges, a large scale and multi-channel measurement system is usually required to grasp the whole structural behavior. However it may cause cost, labor and maintenance problems. In case of ordinary short- and mid-span highway bridges, moving vehicle could be utilized for health monitoring of bridge superstructure [7]. The influence line of the rotational angle and reaction forces at the support for the damaged and undamaged structure can be constructed from the moving vehicle load [8]. It has been found that maximum changes of rotational angle and reaction forces for pre and post-damaged structures occur at the damaged location. This concept has been used to localize damages of the structures. However, dynamic noise with the data and the effect of multi-axle vehicle loading pose the major barrier towards its applicability to real field structures. These problems can be overcome by converting the wavy data to static format by filtering and by correcting the designated multi-axle load to reduced load.

2. BRIDGE RESPONSE AND DAMAGES DUE TO VEHICLE LOADING

Fig. 1 shows the deflection of the main girder measured at the mid-span of single span plate-girder bridge induced by moving 19.6kN[20ton] vehicles. The deflection curve includes both static and dynamic responses.

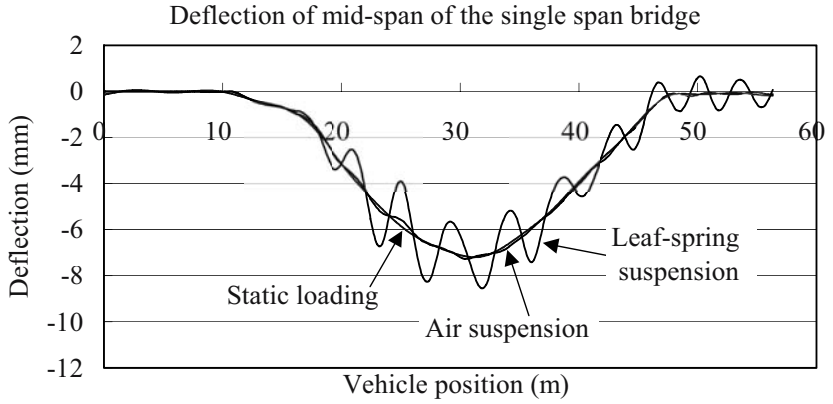

Figure. 1 Bridge response due to vehicle loading

Fig.2 shows the distribution of vehicle loading at four main girders. Distribution patterns are different depending on traffic lane.

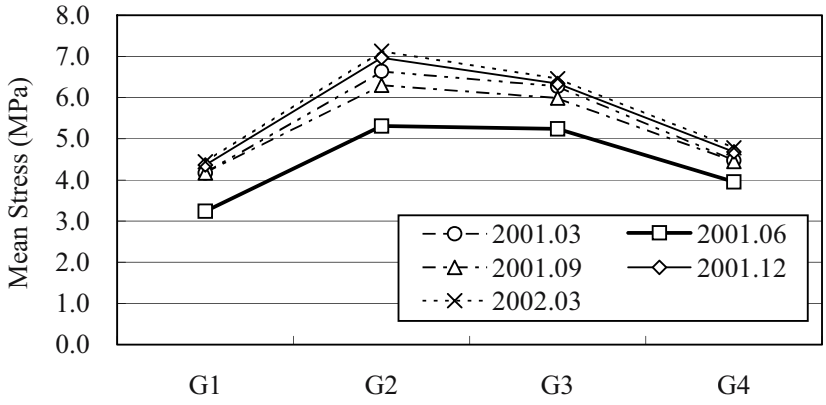

Figure 2. Distribution of loading at girders

Dynamic vehicle loading has a close relationship with damages induced in superstructure of highway bridges. Most of the damages at bridge superstructure are cracks at RC and steel deck, and steel members and joints due to fatigue. It is quite important to instrument observation system corresponding to the actual damage conditions. Hence observation of dynamic responses induced by vehicles can be utilized for health monitoring and damage detection of superstructure of highway bridges.

3. LONG-TERM OBSERVATION SYSTEM AT A SHORT-SPAN BRIDGE

Japan Highway Public Corporation, in charge of construction and maintenance of national expressway network, has monitored the behavior of the bridges over the years. Fig.3 shows the typical example of instrumentation of a short span bridge. A total number of 30 strain gauges and 2 temperature sensors have been installed. In addition, a loop type WIM system has also been embedded at approach road for monitoring the vehicle load. Dynamic strain data due to the moving vehicle is being measured in every 0.05 second (20 Hz).

This bridge was constructed in 1968 as a part of trunk road in Tokyo Metropolitan area. Daily traffic volume is about 66,000 and this bridge suffered severe cracks at steel girders and RC deck. Before instrumentation of health monitoring, the bridge has been retrofitted and strengthened in three phases beginning from the end of year 1994 to mid of 1995 by adding additional girder No 4, cover plate under girders No.1-3 and thickening the deck respectively. It is clear that maximum stress has been reduced due to strengthening the bridge by adding additional girder, cover plate and by thickening the deck.

After the full repair, health-monitoring system was installed in order to clarify the effectiveness of strengthening and monitoring the response of the bridge, as it grows old. The monitoring data of this bridge has been used to show the applicability of operating vehicle load data to structural health monitoring of bridges.

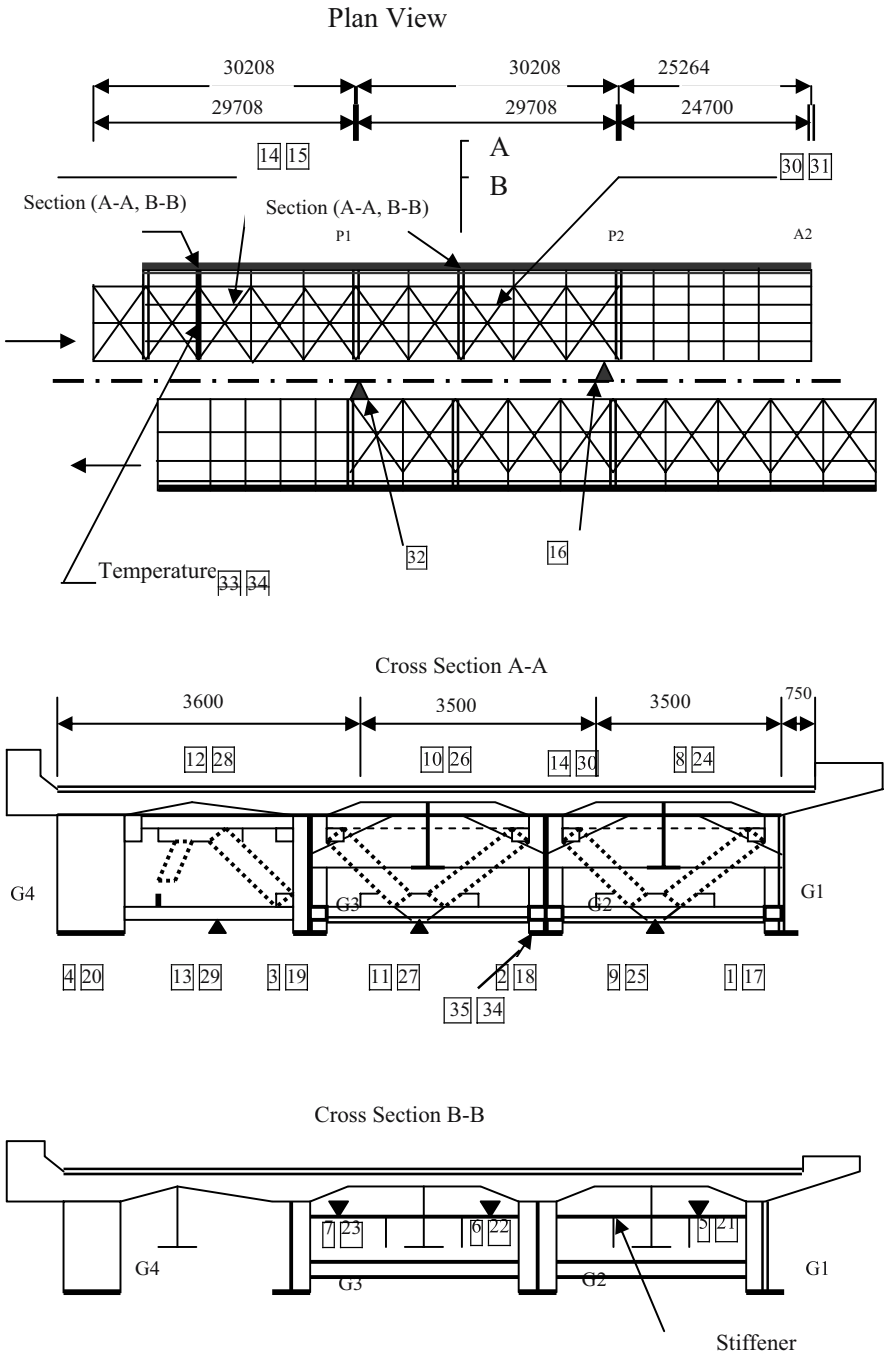

Figure3. Instrumentation of a short span bridge

4. CONDITION EVALUATION USING DYNAMIC RESPONSE BY MOVING VEHECHLE

Japan Highway Public Corporation proposed three kinds of condition evaluation methods using the measured strain data.

(1) Peak valley method
(2) Distribution pattern of stress at the main girders
(3) Daily maximum stress level

Though these methods can provide the signal, which shows the extraordinary condition of the bridge, they do not make use of vehicle characteristics. Each vehicle has different kind of characteristics (total weight, axle weights, axle arrangement, suspension system, speed etc) and provides different kind of dynamic loading effects on the bridge. Then, condition evaluation method using vehicle-induced dynamic response should include the loading condition.

However, generally we face two major barriers with data obtained from dynamic loadings while applying to damage detection algorithm. One of the two main problems of using this data is its dynamic noise component. The other problem is the multi axle loading effects. So to apply the damage detection algorithm to field application, we need to find out an approach of solving these two major problems associated with the dynamic data.

The following method proposes condition evaluation method using moving vehicle loads and bridge responses. In this method, dynamic effects of loading are eliminated and multi-axle effects are corrected. Due to various dynamic effects and inclusion of noises, the measured data is wavy in nature as compared to static strain data as shown in Fig.1. The strain data including dynamic component can be transferred to usable data by applying filtering method. In this paper smoothing in time domain has been used as an appropriate method for converting the dynamic data to static data.

The second problem lies with the compliance of the multi axle load of the vehicle and corresponding strain. It is clear that due to the arrangement of the axles, the effects of practically applied vehicle load is usually smaller than that of the total weight of the vehicle. So to make matching with the static strain the vehicle load has been corrected based on influence line.

Among numerous data, the strain data measured at girder No 2 with corresponding vehicle data has been used in this case as shown in Fig 4. Using the corrected effective vehicle load a high correlation coefficient (0.9009) has been found with converted static strain as shown in calibration graph in Fig. 5. Similar high correlation coefficients greater than 0.90 have been found with the data measured at other locations in other girders. This

calibration graph can be used to monitor the abnormal strain of the girder due to the moving vehicle load. In other way, from this converted static strain corresponding displacement and stress of the component can be calculated and thus can be used as a tool for health monitoring purposes. By using the reciprocal theorem displacement at one location for a running vehicle can be used to find the displacement of the entire structure. This can

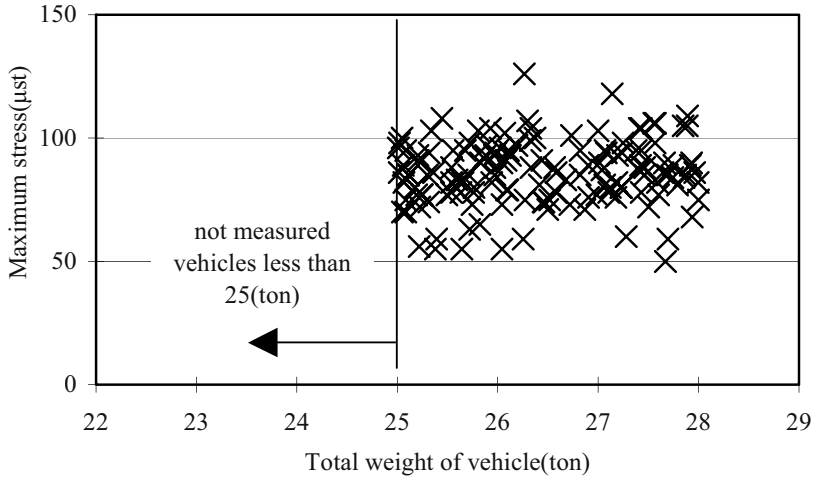

Figure 4. Measured strain of the vehicles over 25 ton

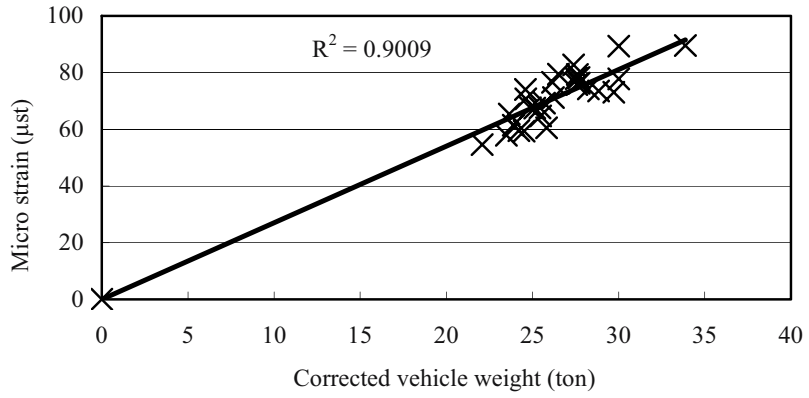

Figure 5. Strain Vs. corrected weight of the vehicle

be used to localize the damage with comparing to the data of the intact structure. Thus the applicability of data obtained from the monitoring bridge shows the suitability of operating vehicle load data to structural health monitoring of bridge structures.

5. ITEMS TO BE MONITORED AND CRITERION FOR CONDITION EVALUATION

Usually for structural health monitoring a large scale and multi channel measurement system is employed in highway bridges. Japan Highway Public Corporation installed 32channels of sensors at the monitoring bridge as mentioned above, but they usually use up to four channels for daily maintenance operation. It is very important what are to be monitored and how to grasp damage state of the whole bridge.

Operating vehicle loading can be utilized for the loading without any special arrangement for health monitoring. The following is the basic idea for bridge health monitoring using moving vehicle load.

The structure of interest here has been modeled as a beam. Consider a moving load 'P' is applied on a simply supported beam of length 'L' at a distance 'a' from the support A. The angle of rotation at that support is θA. Next, suppose the moment M_A is applied at support A of the same beam. Deflection at distance 'a' is δa2. Using reciprocal theorem,

$$P.\delta_{a2} = \theta_{A1}.M_A \tag{1}$$

If numerical value of applied moment 'M_A' is equal to moving load 'L', then

$$\delta_{a2} = \theta_{A1} \tag{2}$$

Hence by measuring rotational angle at the support due to a moving load we can get the deflection curve of that structure. These values of deflection can in turn be used to find the structural property, EI. The instantaneous curvature v'' at location 'a' along the length of the beam will be:

$$V'' = \frac{M_a}{EI} \tag{3}$$

where M_a is section moment at that section of beam.

Curvature method can be applied to detect damage. To realize the above-mentioned idea at bridge, rotational angle and reaction at bearings are observed for health monitoring.

Bridge bearing with sensor function (A smart bearing) may detect and diagnose the distribution of live and dead loads to the bearings through structural system of the bridges. If there is a significant change in the stiffness of a structural member through fracture, impact, or some other causes, it is likely that the distribution of the loads as well as the rotational angles of the bearing will change. Thus a smart bearing can be used to feel the damage in the bridge. This concept is simple, and once designed it is easy to operate.

Roller bearings consist of one or more steel cylinders between parallel upper and lower steel plate. Load distribution of the bearing can be measured by installing load cell. Rotational angle can be measured directly by inclinometer or calculated by deflection of the bearing measured by deflectometers or laser sensor at the masonry plate.

Now elastomeric bearings are generally used in most construction. It accommodates both translational and rotational movements through the deformation of the elastomer. The intelligence for the bearing can be provided by composite load cell using multiaxis fiber optic strain sensors that can be able to measure both vertical and shear strains and load distribution. These sensors are to be integrated into or bottom of the bearing pads as shown in Fig. 6.

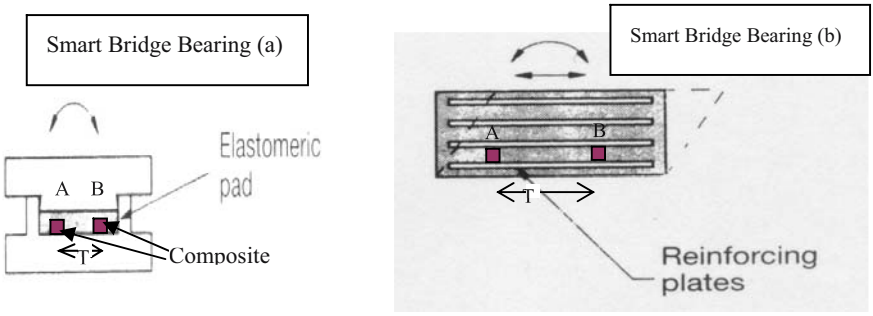

Figure 6. Elastomeric Bearing (a) and (b)

A prototype of smart bearing was developed by Non-destructive Evaluation Validation Center, TFHRC, USA. Here multi-axis fiber optic strain sensors, capable of measuring both vertical and shear strains, have been integrated into a composite panel. The panel can be laminated between the neoprene bearing pads commonly used on highway bridges and will measure the vertical and lateral forces transmitted from/to the bridge.

6. CONCLUSION

The proposed health monitoring approach developed in this research uses the static local damage detection algorithm using operating vehicle load. The basic theory of the method has been validated by numerical simulations with various types of structures with different levels of noises. Small-scale laboratory test also shows the applicability of the technique. To show the extension of the technique to field application, WIM data measured at the monitoring Bridge has been used. Here the approach has been found out to overcome the barriers associated with the applicability of the noisy data and multi-axle vehicle-loading problem. Noisy dynamic WIM data can be transferred to static data to be usable to local damage detection algorithm and to assess the health of the structure.

This damage detection technique can minimizes the number of required sensors and measurement difficulties, which gives an upper hand to other sophisticated global damage detection methods. Thus operating vehicle load could be utilized for structural health monitoring.

ACKNOWLEDGEMENTS

The authors are indebted to Japan Highway Public Corporation for providing the data of the monitoring Bridge.

REFERENCES

1. Steven B. Chase “High –tech Inspection”, Civil Engineering September. 2001.
2. A.K.Pandey, M.Biswas,M.M. Samman “Damage detection from changes in curvature mode shapes”, Journal of sound and vibration, 145(2), pp. 321-332, 1991.
3. Zimmerman, D.C., M. Kaouk “Structural Damage Detection using a Minimum Rank Update Theory”, J. of Vibration and Acoustics, 116, pp. 222-231, 1994.
4. A.K.Pandey, M.Biswas “Damage detection in structures using changes in flexibility”, Journal of sound and vibration 169(1) , pp. 3-17, 1994.
5. Sophia Hassiotis, Garret D. Jeong “Identification of Stiffness Reductions Using Natural Frequencies”, Journal of Engineering Mechanics, pp. 1106-1113, 1995.
6. Zongfen Zhang, A.E. Aktan “The Damage Indices for the Constructed Facilities”, Proceedings of the 13th International Modal Analysis Conf., 2, pp. 1520-1529, 1995.
7. K. Yokoyama, Rafiquzzaman A.K.M. “Bridge damage detection from operating vehicle Load”, Proc. of First International Conference on Structural Health Monitoring and Intelligent Infrastructure, Tokyo, Japan, November 13-15, 2003.
8. K. Yokoyama, Z.S. Wu, Rafiquzzaman A.K.M. “Damage Identification Method Using Moving Vehicle Load And Health Monitoring”, Proc. of the 18th US-Japan Bridge Engineering Workshop, St. Louis, Missouri, USA, October 22-24, 2002.

MEASURING INSTRUMENTS FOR OPTICAL FIBER SENSING

M. Horikawa, M. Komiyama, K. Hirata, and H. Uchiyama
Communications & Measurement Business Headquarters, Yokogawa Electric Corporation

Abstract: In this paper we introduced measuring instruments, BOTDR and ROTDR which are useful for the system using optical fiber sensor. Then we discussed how to separate the strain data from the temperature data to improve the accuracy. Also we introduced the FBG monitor with high reliability.

Key words: measuring instruments, BOTDR, ROTDR, optical fiber sensor, FBG, strain, temperature

1. INTRODUCTION

Recently optical fiber sensing technology is drawing attention in its application to the monitoring of structural damage in civil infrastructures. This is thanks to the practical advantages the optical fiber has, non-inductiveness, non-explosive and compatibility with fiber-optic communication.

We have succeeded in the production of three measuring instruments which are useful for optical fiber sensing. In this paper, we introduce BOTDR, ROTDR and how to separate the strain measurement from the temperature measurement. Then we introduce the FBG monitor with high reliability.

BOTDR;Brillouin Optical Time Domain Reflectometer

ROTDR;Ramman Optical Time Domain Reflectometer

FBG;Fiber Bragg Grating

Farhad Ansari (ed.), Sensing Issues in Civil Structural Health Monitoring, 393–402.

2. DISTRIBUTED SENSING MEASUREMENT

2.1 Principle of Measurement

2.1.1 Time domain technique (OTDR technique)

In order to measure the strain or the temperature distributing of an optical fiber, a pulse light is launched into the optical fiber, and the power of the Brillouin or Ramman backscattered light that is returned to the incident edge is sampled at a designated time.

If we assumed that the backscattered light measured when time T has elapsed after the pulse light was launched has been generated at distance Z from the incident edge, the following relationship can be established

Z=C*T/(2*N) C; the velocity of light in a vacuum
N; refractive index of the optical fiber

2.1.2 Block diagram of the BOTDR

This instrument detects Brillouin scattered light (back scattered light) being generated in the target optical fiber of measured when pulse light is conducted to one end of the fiber. The coherent detection is used for the measurement. Frequency of Brillouin scattered light is $\nu_0 \pm \nu_B$ because it is shifted from frequency ν_0 of incident pulse light by Brillouin frequency shift ν_B. Beat-processing it with local light ν_0 enables to detect Brillouin scattered light ν_B alone. Fig. 2.1.1 shows the basic configuration and signal waveform.

The system converts Brillouin scattered signal to electric signal at the photo detector and then switches its target frequency of processing on the frequency converter so that the system may measure spectrum distribution of Brillouin scattered signal.

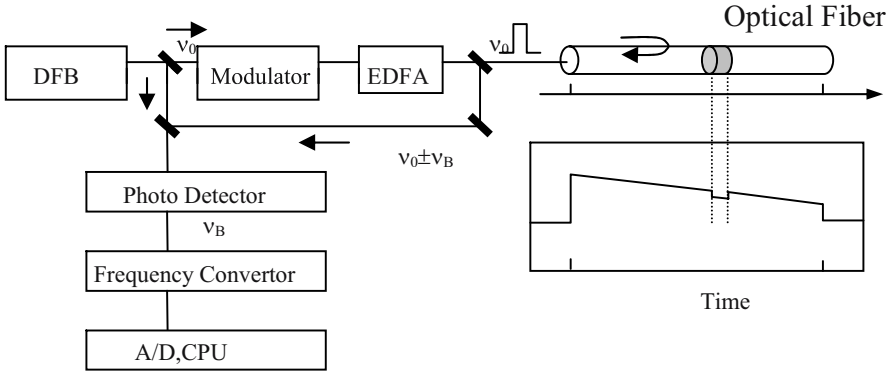

Figure 2.1.1 Basic configuration and signal waveform

Also, Brillouin frequency shift changes according to the temperature. For example, Table 2.1.1 is reported for standard single mode optical fibers to which an ultraviolet coating has been applied

Table 2.1.1 Coefficient of temperature and strain

ITEM	1300nm band	1550nm band
TEMPERATURE	1.22MHz/°C	1 MHz/°C
STRAIN	581MHz/%	493MHz/%

Thus, we can obtain distribution of the strain in the longitudinal direction by combining the spectroscopy that selectively measures the backscattered light power of a specific frequency usin a heterodyne detection or similar method with time domain technique.

Figure 2.1.2 shows AQ8603 BOTDR (made by YOKOGAWA).

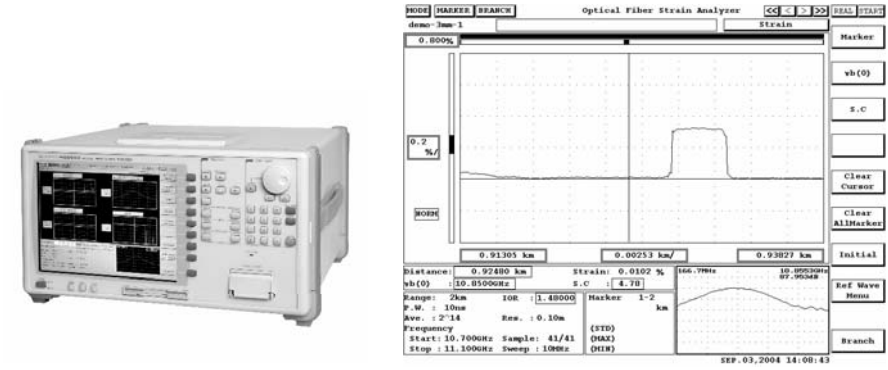

Figure 2.1.2 AQ8603 BOTDR

2.1.3 Block diagram of the ROTDR

Raman Scattering is generated inside the optical fiber when a pulse light is launched into an optical fiber. By measuring the Raman scattered light, it becomes possible to measure the temperature as a distribution in the longitudinal direction of an optical fiber.

Figure 2.1.3 is a block diagram showing how the main unit of the ROTDR unit is configured. The light reflected from the optical fiber is divided into strokes light and anti-strokes light by coupler/filter. They are introduced to each photodiode. Individual photodiode outputs are transferred through the A/D convertor and are successively A/D-converted into 12-bits data. The data are averaged by an adder.

Figure 2.1.4 shows a picture of AQ8920 ROTDR (made by YOKOGAWA).

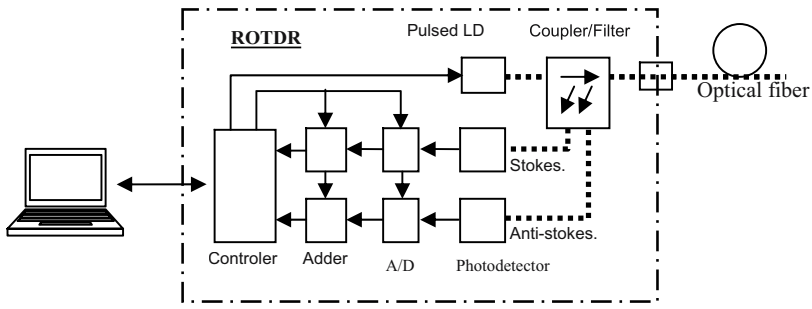

Figure 2.1.3 Blockdiagram of ROTDR

Figure 2.1.4 AQ8920 ROTDR

2.2 Separate the strain from the temperature

The data measured by BOTDR contains both temperature and strain information along the length of the optical fiber. We made a system using both BOTDR and ROTDR to extract the temperature information from the Brillouin signal. Figure 2.2.1 shows the block diagram of the system.

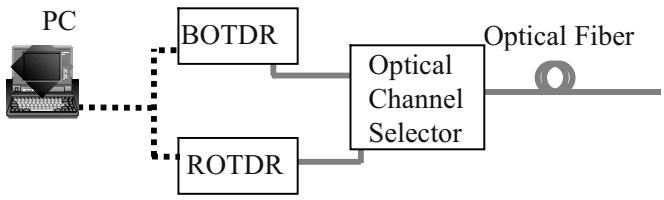

Figure 2.2.1 Block diagram of the system

Figure 2.2.2 shows an experimental diagram of fiber.

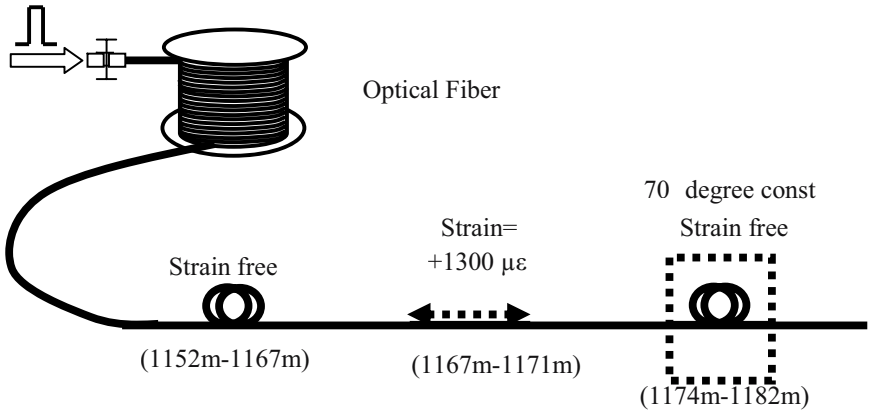

Figure 2.2.2 Experimental diagram

Solid line of Figure 2.2.3 shows the strain measured by BOTDR. It contains both strain information and temperature information. Broken line of Figure 2.2.3 shows the temperature measured by ROTDR. We can get only the strain information by deducting the temperature information converted into the strain. Figure 2.2.4 shows the strain after deduction. In this experiment the accuracy of strain measurements was less than ±0.005%.

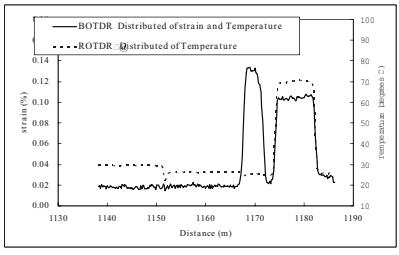

Figure 2.2.3 Data measured by BOTDR and ROTDR

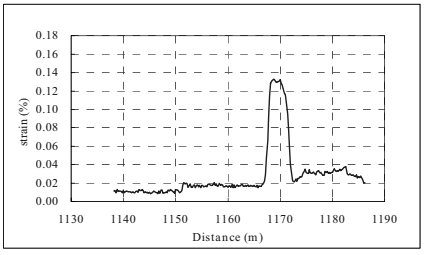

Figure 2.2.4 Strain after deduction

3. FBG MONITOR WITH HIGH RELIABILITY

3.1 Principle of Operation

A FBG is a fiber-type optical device in which the core of a fiber is given periodic refraction index change. This device selectively reflects a particular wavelength (Bragg wavelength). FB200 FBG monitor measures the change in the Bragg wavelength when the FBG undergoes strain and temperature change is given by. Figure 3.2.1 shows FB200 FBG monitor.

FB200

FB200
with power supply
Unit

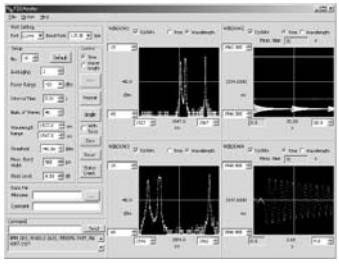

GUI Example (3 FBG)

Figure 3.2.2 FB200 FBG Monitor

3.2 Block diagram

The main unit of the FBG sensor monitor has no human machine interfaces, such as displays or keys. Everything, including monitor control, display operation, and output of measurement results, is performed through a serially connected (RS232C) external PC or other alternative means. Figure 3.2.2 is a block diagram showing how the main unit of the FBG sensor monitor is configured. The light reflected from the FBG is spectrally divided and introduced to the PDA. Individual photodiode outputs are transferred through the multiplexer and are successively I/V-converted and A/D-converted into 16-bits data. The data of the 640 photodiode pixels are subjected to corrective calculation, then used to identify the reflection spectrum and calculate the center wavelength and optical power for the detected spectrum. In order to expedite these calculations, a DSP is employed in the computing section, where some of the calculations are processed concurrently. Since the time required for the measurement results to be serially output in ASCII-format numeric data should also be shortened,

the monitor supports high transmission rates, including 921.6 and 460.8 kbps. Accordingly, it is now possible to measure and output 10 channels of reflection wavelengths and the optical power of FBG sensors at 10 ms sampling intervals with a wavelength resolution of 1 pm.

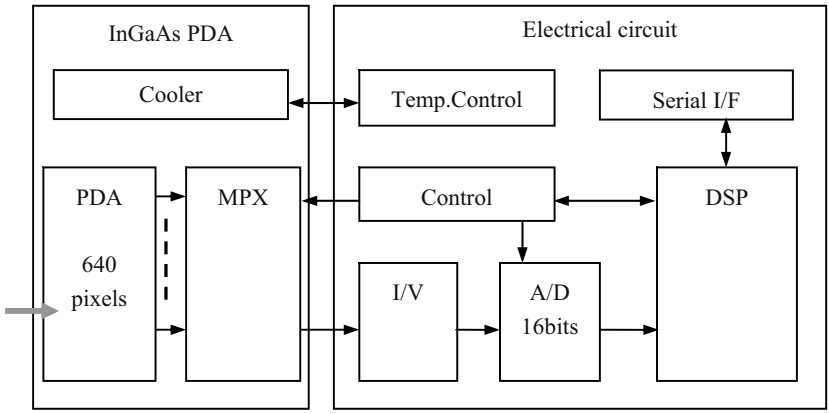

Figure 3.2.1 Overall Block Diagram of the FB200

3.3 Polychrometer

Figure 3.3.1 schematically illustrates the configuration of the polychromator, used for FBG sensor monitors. The spectrometry section has no moving parts, offering the advantage that it is immune to failures due to mechanical wear, is highly reliable, and can be reduced in both size and weight. The dispersion devices is a blazed holographic grating with a ruling density of 1200 grooves/mm. Lenses are used for both the collimating system and the focusing system.

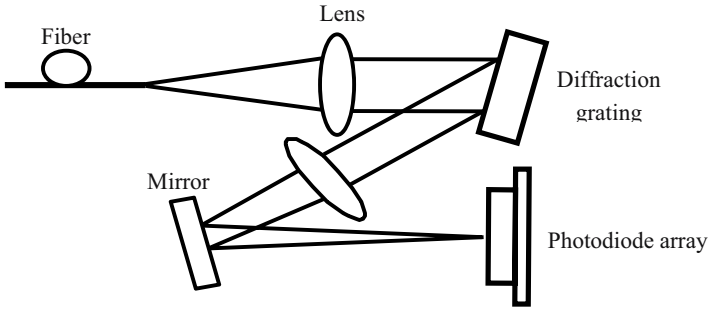

Figure 3.3.1 Polychromator-type Spectrometer Configuration

The photodiode array (PDA) is an InGaAs photodiode array comprising 640 photodiode pixels arranged at 20 micrometer pitches. The PDA package also contains a multiplexer for successively reading individual photodiode outputs and a thermoelectric cooler for temperature-controlling the photodiodes. Use of such an array-type photodetector makes the spectrometer advantageous in that it has no moving parts and can operate at high speeds. On the other hand, the spectrometer has a trade-off relationship between the range of wavelengths that can be measured and the wavelength resolution of each photodiode pixel.

Table 3.3.1 Reliability Test and Results

Item	Test Condition	Result
(1) Temperature Cycling	-20degreeC to +80deg.C 6H/cycle 300times	Good
(2) High Temperature Operating	+65degreeC 3500H	Good
(3) Damp Heat Operation	+60degreeC 90% 1000H	Good
(4) Vibration	XYZ3direction 2H/each direction 1min/sweep 5to9Hz amplitude 3mm, 9to150Hz 1G	Good
(5) Mechanical Shock	+-XYZ6directions 50G 5to11msec 5times/axis	Good
(6) Power ON/OFF cycling	ON:3min./OFF:3min. 2000times	Good

4. CONCLUSION

In this paper, the principles of both Raman and Brillouin OTDR have been described. We demonstrated the performance of the strain and temperature sensing system using both BOTDR and ROTDR and measured the strain distribution without influence of temperature variation along the fiber.

We also introduced FBG monitor with high quality and high speed.

In order for optical fiber sensing systems to be practically applied, there are still some obstacles to be overcome, such as the optimization of optical fiber sensor, installation technique, analysis technique of the data, a practical maintenance system.

It is necessary for us, as a measuring instrument manufacturer, to make an effort to resolve these issues, to reduce cost of the measuring instruments.

REFERENCES

1. Y.Sakairi, Y.Koyamada, Distributed Strain Measurement of GI Fiber by Using BOTDR, Technical report of IEICE, 2004
2. H.Uchiyama, Y.Sakairi, T.Nozaki, An Optical Fiber Strain Distribution Measurement Instrument Using the New Detection Method, Ando Technical Bulletin,October 2002
3. M.Komiyama, N.Tanaka, Y.Sanpei, Development of a Monitor for FBG Sensors, January 2004.

IMPLEMENTATION OF LONG GAUGE FIBER OPTIC SENSOR ARRAYS IN CIVIL STRUCTURES

Yujin Liang, Adam Tennant, Hongqiang Jia, Xiaoxu Xiong, and Farhad Ansari
Smart Sensors & NDT Laboratory, Department of Civil & Materials Engineering , University of Illinois at Chicago, Chicago, IL 60607, USA

Abstract: Civil structures have large dimensions, composed of diverse materials, and the construction environment is generally hostile. These issues, in turn, pose challenges to design and deployment of sensors for structural health monitoring. While optical fiber sensors provide superior sensing capabilities, their attributes remain ineffective if they are not properly designed considering the civil engineering applications. Design of proper sensors require considerations to measurements of interest, i.e. cracks, strains, displacements, coverage of all critical sensing locations, survivability during installation, and reliability of measurements. To address some of these issues, this article focuses on the applications of long gauge interferometric sensors, multiplexing strategies, and installation issues during construction of civil structures.

Key words: Structural Health Monitoring; Distributed Sensing; Fiber Optic Sensors; Long Gauge Sensors; Sensor Installation; Construction; Civil Structures; Reliability

1. INTRODUCTION

The primary component of every successful structural health-monitoring (SHM) program is selection and placement of sensors suitable for measurement of key parameters that influence the performance and health of the structural system. In addition to the structural considerations, sensors need to be chosen based on compatibility with the materials and the range

Farhad Ansari (ed.), Sensing Issues in Civil Structural Health Monitoring, 403–412.

and scope of measurements. Conventional sensors and strain gauges perform well in many applications. Fiber optic sensors provide flexibility and practicality in some other situations, where the conventional sensors are either not capable or feasible to make the appropriate measurements. This is especially the case in distributed and remote monitoring applications. They are small and embeddable within the structure, there is no need for insitu electrical cabling, they are immune to electric and electromagnetic fields, and moreover transmission and acquisition of optical signals can be accomplished kilometers away from the site. Furthermore, distributed measurements reduce the number of leads running through structures.

A number of distributed sensors have been developed such as those based on Brillouin scattering (Zou, et al, 2004, and Murayama et al, 2003), optical time domain reflectometry (Gu, et al, 2000), Brillouin Optical Time Domain Reflectometry (Wu et al 2002), long gauge sensors (Zhao et al 2002), and serially multiplexed fiber optic acoustic emission sensors (Sun et al, 2004). Since optical fibers are geometrically adaptable, distributed sensors can be configured to structural shapes for multitudes of measurements, including cracks, deformations, and strains.

Civil structures are inherently large in dimension, geometrically complex with different elements and joints, and composed of different materials. For this reason, localized sensing is only effective if the problematic areas are known in advance. Multiplexing of long gauge sensors will provide effective solution for civil structures. For very large structures serial multiplexing of long gauge sensors will provide advantages in terms of coverage, and reducing the number of leads in and out of the structure. The true application of fiber optic sensors is realized in distributed sensing where every segment of the optical fiber senses the location of anomaly and monitors the intensity of structural perturbations, i.e. cracks (Figure 1). The following sections of this article will include brief description for long gauge interferometric sensors and their adaptation for embedment within concrete bridge decks as well as in applications pertaining to monitoring of composites in civil structures.

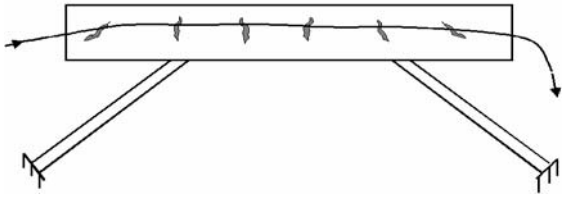

Figure 1 Optical fiber sensors in civil structures

2. SHM WITH LONG GAUGE SENSORS

The term long gauge and white light interferometric sensors have been commonly interchanged. This is primarily due to the fact that they are easily configured into gauge lengths of choice, and in civil engineering applications, longer gauge lengths anywhere from fraction of a meter to tens of meters have been employed. Since these sensors use the principles of interferometry, they are highly sensitive and with deformation resolving capability in the micron regime. Despite their long gauge sensing capability, since various segments of a large structural system go through myriads of different perturbations, clearly a single sensor will not be able to differentiate all. In practice health monitoring of the entire structure requires integration of several sensors. The number of required sensors increases depending on the size and the geometric complexity of the structure. Issues that need to be addressed in parallel multiplexing of sensors include real time multi channel data acquisition, tagging of sensor locations, analysis, and number of sensor leads from the system into the structure. The preferred approach is serial multiplexing where several sensors are connected along a single line providing quasi-distributed sensing capability. Development of the quasi-distributed long gauge sensor has been detailed elsewhere (Zhao and Ansari 2001). A brief description of the system is given here for completeness.

A serially multiplexed long gauge sensor consisting of *m*-segments in series is shown in Figure 2. The system consists of two parts: sensing interferometer module, and the receiving interferometer. The sensor is comprised of a number of individual single mode fibers coated on both ends and of desired gauge lengths. The individual fibers are mechanically connected through ferrules and a portion of the beam is reflected when the light wave passes through them. The interrogation section of the module is a Michelson interferometer with a scanning translation stage, signal processing and the system control unit that matches the optical path of the individual segments of the optical fiber to the reference path. The resolution of the system is partially dependant on the resolution of the translating mirror that is generally in the micron or sub micron level. Individual sensor segments starting from sensor 1 immediately following the coupler, all the way to the last sensor in the series, act as reference arms for the adjacent sensors. Since every sensor shares common pathway through the coupler and other fiber segments, possible errors due to disturbances caused by the lead fiber phase variations is automatically compensated for.

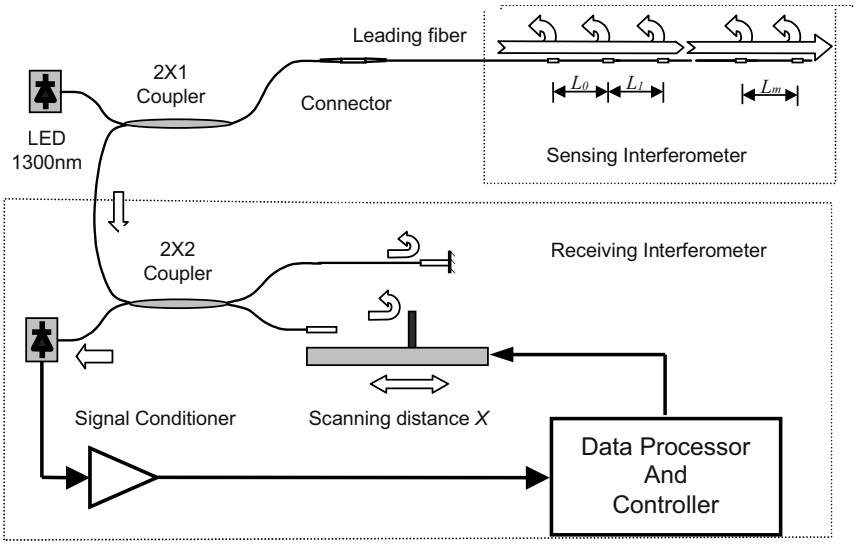

Figure 2 Serially multiplexed Long gauge sensor system

This system has been used in many applications and has matured for field use simply due to the simplistic nature of the interrogation unit that is generally configured in a portable small box and potential for very large structural applications with several sensors in parallel and series configuration. Example of a mobile unit with eight parallel sensors each with distributed sensing capability over four gauge lengths (32 channels) on a bridge site is shown in Figure 3. These sensors can be routed out of the structure into a junction box (Figure 4) during construction and then permanently installed in appropriate location for periodic or continuous access by a mobile or onsite monitoring system.

In applications that involve monitoring of interfaces for debonding or monitoring of strains, bare optical fibers can be directly adhered to the surface or embedded at the interface and the epoxy serves as a protective coating for the sensor (Zhao et al, 2002). One such application is in monitoring of debonding or peeling of the FRP fabrics from concrete elements i.e. beams. Figure 5 shows the schematic of a reinforced concrete beam with laminated FRP on the tension face and two sets of four-gauge distributed sensors. Three 3-ft x 2 inch FRP strips were glued to the tension face of the reinforced concrete beam in such a manner to form a continuous strip of 9-ft in length spliced at three locations. Two sets of distributed long gauge optical fibers were glued to the surface of the FRP as shown in the figure. Each set consisted of four sensors in one line, each sensor 30 cm (0.98-ft) in gauge length. The sensor system designated FOS1-1 through

FOS1-4 was adhered to the beam from left support to the mid span, and FOS2 was adhered from the opposite end.

Figure 3 Example of a mobile long gauge sensor interrogation unit during monitoring of the cracks in a bridge deck

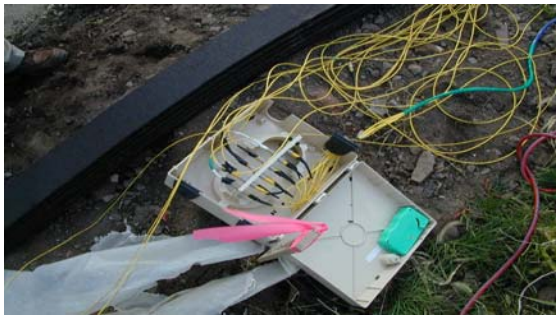

Figure 4 Temporary routing of the lead outs from the bridge deck to the junction box

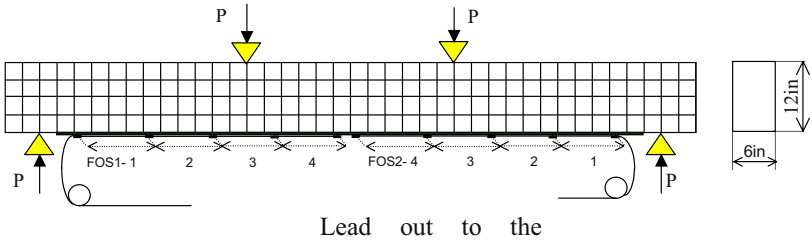

Figure 5 Sensor lay out on the beam

During the incremental loading of the beam to failure, the sensor system was able to predict the initiation of hairline cracks through deviation from linearity of the load strain relationship in the affected sensor areas as shown

in Figures 6 and 7. Sensors FOS1-3 and FOS2-3 exhibited the most level of strains due to their spanning over the splice points and appearance of the major cracks in those sections. Sensor FOS1-4 also indicates peeling of the FRP from the concrete substrate by unloading (Figure 6). Eventually upon further growth of the major cracks, these sensors were damaged by peeling of the FRP at those locations. The rest of the sensors kept on monitoring the fabric until failure of the beam.

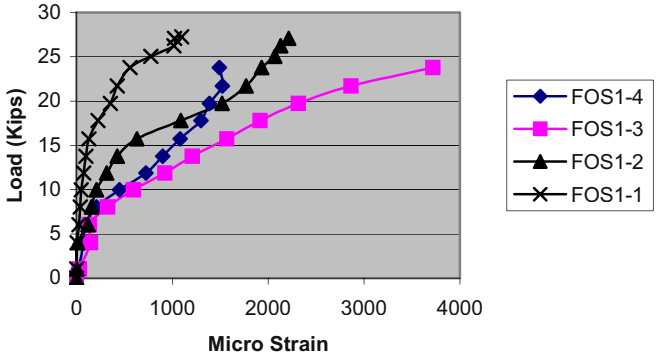

Figure 6 Fabric strains measured by FOS1

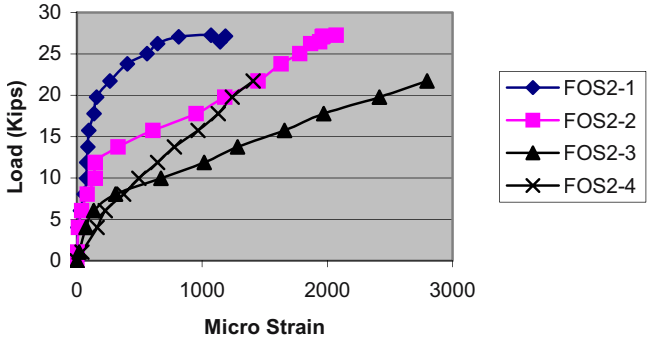

Figure 7 Fabric strains measured by FOS2

Other applications include monitoring of FRP tendon strains during the post tensioning process and their service lives. Figure 8 depicts the tendon strains as monitored by the embedded fiber during the post tensioning process. Figure 9 corresponds to the tendon strains after the post tensioning process and during destructive loading of the post-tensioned beam to failure.

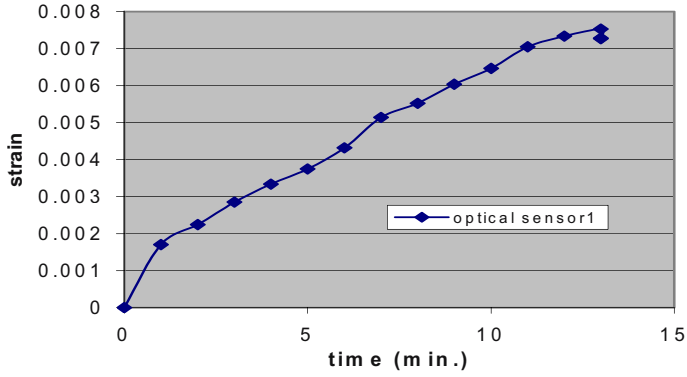

Figure 8 Monitoring of strain by the long gauge sensor during a typical post tensioning process

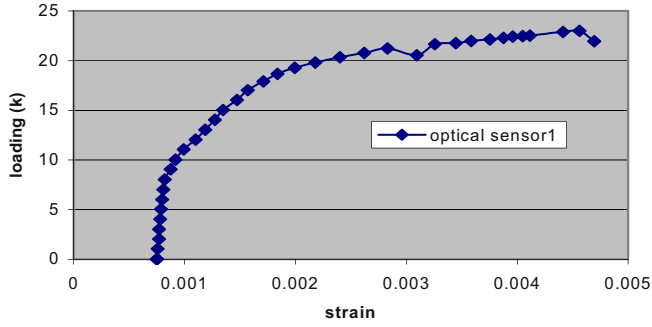

Figure 9 Tendon strains during the destructive test of the post tensioned beam

3. CONSTRUCTION SITE ISSUES

One of the major features of optical fibers is geometric conformity and capability for embedment within materials during their production such as in concrete and fiber reinforced polymer composites (FRP). Fragility of optical fibers however has been a hindrance to rapid employment of the technology in infrastructure projects. Issues involved include design of relevant protective gear for the optical fiber without jeopardizing sensing capability, durability within the concrete, and surviving the harsh construction

environment. An example of a long gauge sensor specifically designed for monitoring the deformations and cracks in a reinforced concrete bridge deck is shown in Figure 10. The sensor consists of a 3 mm diameter threaded rod and a shear key at each end. The threaded rod is made of stainless steel and a groove that runs along the one-meter gauge length of the rod to a depth of 1.5 mm. The optical fiber is inserted within the groove and sealed in place with a water resistant epoxy. The reflective ends of the optical fiber are extended through the shear keys and are protected in the brass tubes adjacent to the shear keys. Optical fibers from the adjacent sensors run through the brass tube and link through ferrules. The fiber optic lead outs need to be protected against shrinkage strains of mass concrete, especially during the first 24 hours after placement. The lead outs are protected by flexible metallic jackets, and then routed to conduits especially designed for merging of the fiber optic leads from all of the sensors. The conduit is then routed out of the structure and the fiber optic leads are accessed through a junction box from out side of the structure.

These particular sensors are designed to detect cracking in concrete and therefore are not adhered to the reinforcement. Depending on the desired location, the sensors are either positioned in place by the seats used for positioning of the reinforcement within the depth of the slab or they are tied across the rebars. Figures 11 and 12 illustrate the embedded sensors and close up view of sensor heads during placement of concrete. As shown, the sensors are designed to survive the construction process involving vibration and construction crew. Figure 13 shows the routing of sensor lead cables through especially designed Brass conduits.

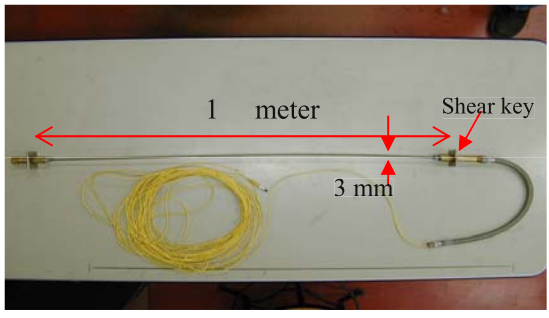

Figure 10 Ruggedized long gauge sensor for embedment in reinforced concrete structures

Figure 11 Embedded sensors during concrete placement

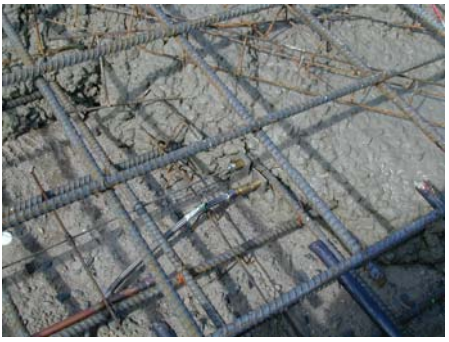

Figure 12 Close up view of sensor heads during concrete placement

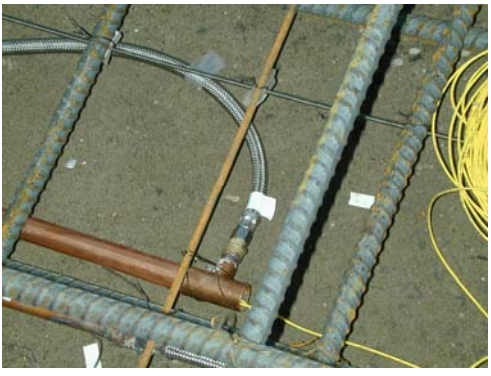

Figure 13 Details of sensor lead out route through specially designed Brass conduits

4. CONCLUSIONS

The true potential of optical fiber sensors in civil infrastructure applications can be realized through a combination of distributed serial and parallel multiplexing configurations. A short review of recent developments in multiplexed and distributed long gauge sensors were presented in this article. Measurement capabilities as well as concrete embedment and construction site issues were also discussed. There is however lack of sufficient information pertaining to the reliability, long term effects, especially in terms of survivability of the fiber optic sensors in structures. This is an important issue with practical ramifications in structural health monitoring. More research is needed to address the long term behavior of the sensors in structures

REFERENCES

Gu, X., Chen,Z., and Ansari, F., " Embedded Fiber Optic Crack Sensor for Reinforced Concrete Structures," ACI Structural Journal, V. 97, May-June 2000, pp. 468-476.

Murayama H, Kageyama K, Naruse H, Shimada A, Uzawa K, (2003),"Application of fiber-optic distributed sensors to health monitoring for full-scale composite structures," J. of Intelligent Materials Systems and Structures 14 (1): 3-13

Sun,C., Liang, Y., and Ansari, F., 2004," Serially Multiplexed Dual Point Fiber Optic Acoustic Emission Sensor," IEEE, Journal of Lightwave Technology, Vol. 22, No.2

Wu Z, and Xu B., (2002), "Infrastructural Health Monitoring with BOTDR Fiber Optic Sensing Technique," In proceedings of the 1st Int. Workshop on SHM of Innovative Civil Engineering Structures, A. Mufti, Ed., Winnipeg, Canada, PP.217 – 226

Zhao, Y., and Ansari, F., (2001), "Quasi-Distributed Fiber-Optic Strain Sensor: Principle and Experiment," Applied Optics, Vol. 40, No. 19, July 1, PP. 3176 – 3181.

Zhao, Y., and Ansari, F., (2002), "Embedded fiber optic sensor for characterization of interface strains in FRP composite," Sensors and Actuators A: Physical, 100(2):247-251

Zou, L., Ravet, F., Bao, X., Chen, L., Huang, R., and Khoo,H., " In-Line Inspection of Pipeline Buckling by Distributed Brillouin Scattering Sensor, in Proceedings of 2nd Int. Workshop on SHM of Innovative Civil Engineering Structures, Winnipeg, Canada, September 2004, A. Mufti, F. Ansari, Editors, pp. 183-192.

Chapter VII

Fiber Optic Sensors Principles

ABSOLUTE DEFORMATION MEASUREMENT USING FIBER-OPTIC WHITE LIGHT INTERFEROMETER WITH TWO BROAD-BAND SOURCES

Changsen Sun, Longcheng Yu, Qi Wang, and Qingxu Yu
Department of Physics, Dalian University of Technology, Dalian 116023, China

Abstract: Reading of the central fringe in absolute deformation measurement using white light fiber-optic interferometer (WLFOI) is proposed through introducing the second broadband source and a zero sensing arm. The zero sensing arm is a reminder about the initial position that have to be lost during the deformation. The second source is used to form a synthesized equivalent wideband source that, in general, is not available commercially. This combined source could simplify the central fringe identification. The design can carry out a good balance between the reading speed and precision in the absolute deformation measurement by WLFOI. A preliminary experiment confirms its efficiency.

Key words: Absolute deformation measurement, white light interferometer, precision measurement

1. INTRODUCTION

Deformation measurement systems based on white light fiber-optic interferometry (WLFOI) have been intensively investigated and micrometer accuracy has been achieved at unambiguous resolution [**1-2**]. When fully developed all-fiber-optic WLFOI will be a powerful technique for precise, remote deformation measurements with passive sensors heads. For a typical WLFOI that uses a scanning device in the local receiving interferometer, the overall measurement accuracy is determined by both the accuracy with

Farhad Ansari (ed.), Sensing Issues in Civil Structural Health Monitoring, 415–422.

which the central position of the interferometric signal pattern can be identified and the precision of the scanning device. Combining these two factors to obtain sub-micrometer accuracy was carried out in a vernier way [**3**]. The vernier principle was implemented by combining interference fringes itself and a virtual fringe that is generated by software-tracing the scanning mirror. When two rulers are read with respect to each other, the virtual fringes will provide a 1.0 micrometer spatial resolution and the sub-micro sensitivity can be calculated by combining the interference fringes in a vernier scalar way. Although the accuracy with $0.2\mu m$ was achieved the reading speed is very low. On the other hand, the autocorrelation function of the light source and the signal-to-noise ratio (SNR) of the interferometric output signal determine the resolution required to identify the central fringe position. The shorter the coherence length of the source, the lower the requirement is for the system SNR. From the point of view of the coherence length, only sources such as incandescent filament lamps or superluminescent diodes are ideally suited for the WLFOI. However, incandescent lamps have poor reliability, large size that makes it difficult to be coupled into optical fibers, etc. Superluminescent laser diodes are expensive, and their use would tend to make WLFOI uncompetitive. Based on the Fourier Optics we know that the autocorrelation function and the spectrum of light source is a couple of Fourier transform. Several synthesized source designs were proposed, such as: two sources [**4-5**], three sources [**6**]. This could enlarge the spectrum of the effective light source and sharp the interferogram to make the central peak clear. The disadvantage of this scheme is the choice of light sources both in central wavelength and in bandwidth. Another design used a novel signal processing method [**7**], which modified forward-backward least-mean-square algorithm and a threshold equal to 0.37 of the maximum power was used to switch the algorithms “on” and “off”. This threshold is an intensity-dependent and makes the system unstable. A breakthrough fine reading scheme was phase quadrature technique [**8**] with which the measurement can reach 10nm resolution. However, its complex optical adjustment and the limited reading speed made it difficult to implement a practical deformation measurement.

Here we report an absolute deformation measurement using the WLFOI with two broadband sources as proposed in Ref.4. The zero sensing arm can make the system robust to the error from the step-motor. The environmental factors, such as temperature fluctuation etc, that affect the sensing arm can also be compensated by measuring this zero sensing arm in each fulfill.

2. THE PRINCIPLE OF SCHEMATIC

The schematic of the design is shown in Fig.1. The system is specified by introduce a zero sensing arm in a published configuration like Ref. 4. The single-mode light emitted diodes used in this system are a LED 1310 operating wavelength at $\lambda = 1310 \pm 30nm$ and a LED 1550 operating wavelength at $\lambda = 1550 \pm 30nm$. The best theoretical coherence length of LED 1310 is $\phi = \lambda^2 / \Delta\lambda = 28.6\mu m$; that of LED 1550 is $\phi = \lambda^2 / \Delta\lambda = 40.0\mu m$. Both of their working currents are 60 mA. The LEDs are coupled into the two of the three input arms of the 3×3 coupler. The coupler could divide the input light into three outputs. Each of the output has equal intensity as the 1/3 of the total input intensity. The configuration of the system consisting of a Michelson white light interferometer that consist of one sensing arm, one zero sensing arm, and one reference arm as shown in Figure. 1. The sensing arm is composed of individual single-mode fiber in the desired gauge lengths; the zero sensing arm is with a corresponding length and will put in a most co-path with sensing arm in order to compensate the fluctuation; the reference arm is with a grade index self-focus len (GISL) at end of it. The GISL turns the light into parallel propagation beam and this beam is reflected from the scanning mirror that mounted on the step motor. The configuration of the system is quite like two Michelson interferometer working side by side. The sensing arm is circled on a piezoelectric (PZT) cylinder with the size as $51 \times 45 \times 50mm$ in outside diameter, inner diameter, and height respectively. The two LED sources work simultaneously. The step- motor is controlled by RS-232 port. Because the zero sensing arm is not sensitive to the deformation it could always indicate where the zero position is. After photodetector an current amplifier is connected to convert the photo-current into voltage that could be both monitored by oscilloscope and acquired by the data acquisition card that has been setup in the computer.

When sensor S interferences with two reference arms we can write:

$$I_0 = (1/2)\{\exp[-(2x/L_{c1})^2]\cos(2\pi x/\lambda_1) + \exp[-(2x/L_{c2})^2]\cos(2\pi x/\lambda_2)\} \quad (1)$$

Where λ_1, λ_2 and L_{c1}, L_{c2} are the central wavelength and the coherence lengths of the two LEDs respectively; I_0 is the intensity output between the interference of S *and* R, S_0 and R, respectively.

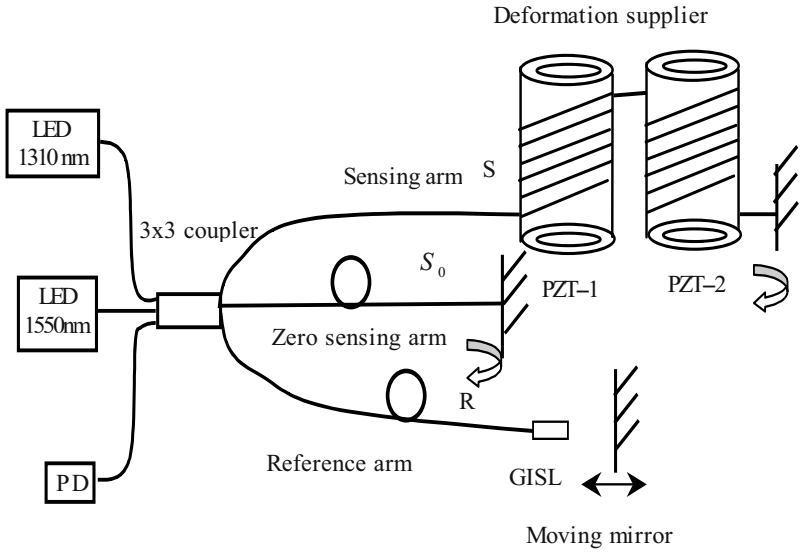

Figure 1. The schematic of the absolute deformation measurement with two broadband sources. (LED-Light emitted diode; PD-Photo detector; PZT-Piezoelectric; GISL-Grade index self-focus lens.)

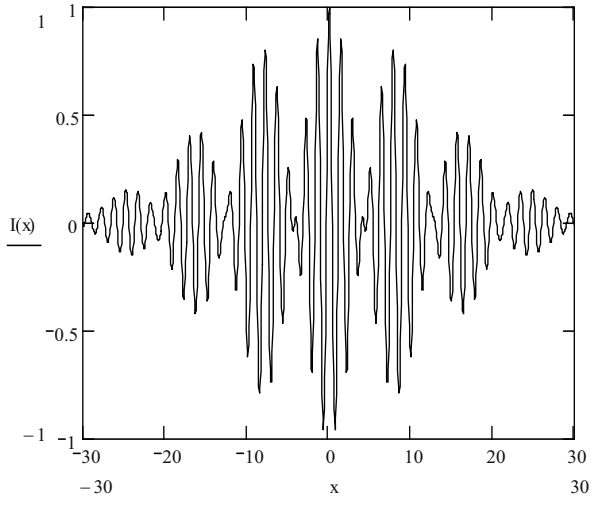

Figure 2. The computer simulation result of the interference with two sources. Parameters λ_1, λ_2, L_{c1}, and L_{c2} is 1310nm, 1550nm, 32 μm, and 40 μm respectively.

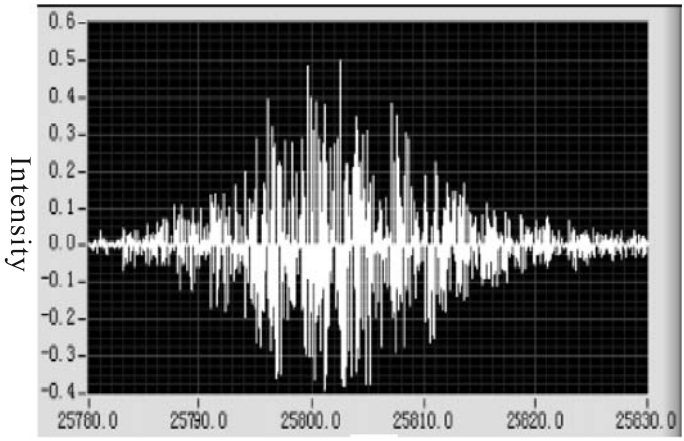

Figure 3 An interference fringe of the WLFOI with two broadband sources

A computer simulation is implemented with λ_1 , λ_2 , L_{c1} , and L_{c2} is 1310nm, 1550nm, 32 μm , and 40 μm respectively and the result is shown in Figure. 2. Based on this we found the central peak fringe is more obvious and easy to identify then either of the single source.

An experimental interference fringe of the WLFOI with two broadband sources is shown in Figure 3. The curve is not smooth enough because of the limitation of the response bandwidth of the home-made converter circuit, but the profile is OK for the central fringe identification. The data acquired by TDS 3052 (Tektronix Digital Phosphor Oscilloscope 500MHz) and save to the disk directly.

3. THE EXPERIMENTAL RESULTS

The measurement is able to implement in a normal WLFOI way. As the step motor scanning the reference arm will hit the equal optic path position with zero sensing arm and sensing arm respectively. We can get two interference fringes, which are the interference between zero sensing arm S_0 and the reference arm R ; sensing arm S and the reference arm R , and both are the function as the position of the scanning mirror, motor steps. The result is shown in the top of Figure 4 when PZT1 introduced a deformation.

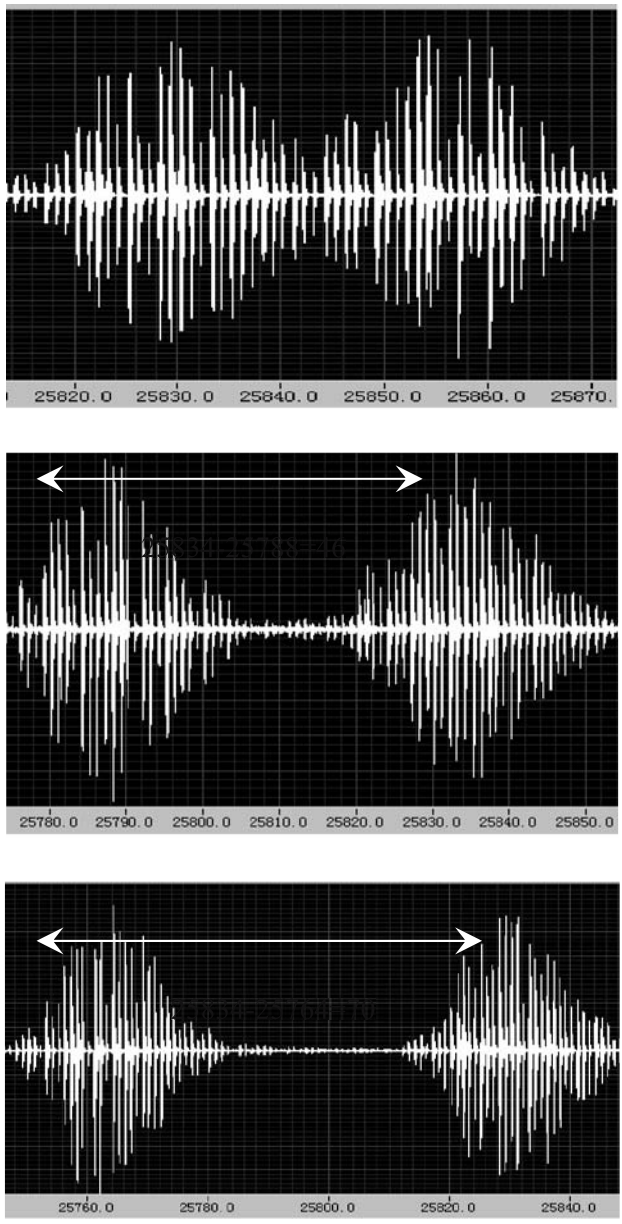

Figure 4 The results with different absolute deformation

The top one is with a small absolute deformation comparing with the initial position caused by PZT1; the middle one and the bottom one are with the increased deformation caused by PZT2 at 80V and 100V, respectively, with PZT1 standing constant. The central peak span is the absolute deformation changed from 46 steps to 70 steps doesn't matter with the value of motor position.

By identification the position of the mirror we can measure the deformation. With the deformation caused by PZT1 standing we stretch PZT2 and keep it constant when the measurement is done. We get the middle and bottom fringes with the driving voltage of PZT2 at 80 V and 100 V respectively. Even if we lost the initial position at the beginning of the measurement the absolute deformation still could be obtained by reading the span of the two interference fringes.

On the other hand, when the step-motor moving in the opposite direction it will introduce an error named as round-error. This error is a variable one based on the different moving length. But in our system just because the zero sensing arm, read as 35834steps, could provide us the free-deformation point, we found that the result is very robust to these factors.

4. DISCUSSION

The WLFOI has been used in the deformation measurement successfully. Its accuracy is improved step by step, but a convenient central fringe reading method is still under requirement. This research has obtained a kind of balance between the central fringe identification fast and precision. But further improvement is needed such as to reduce cost of the system etc. This also is the future work.

ACKNOWLEDGMENTS

The first author Dr. Changsen Sun greatly thanks to Prof. F. Ansari for the encouragement and financial support for my possibility to attend this workshop. Thanks for the project funding support from Dalian science and technology foundation.

NOTES

All the instruments are put on a vibration-isolation table. PZT cylinders are driven by the direct power supply.

REFERENCES

1. K. T. V. Grattan ad B. T. Meggitt, *Optical Fiber Sensor Technology*, London: Champman and Hall, 1995.
2. J. Tapia-Mercado, A. V. Khomenko, and A.Garcia-Weidner, Precision and Sensitivity Optimization for White-light Interferometric Fiber-Optic Sensors, *J. of Lightwave Technol.*, Vol. 19, No. 1, pp: 70-74, 2001.

3. Changsen Sun, Yang Zhao, Adam Tennant, and Farhad Ansari, Spatial resloution enhancement of optical fiber scanning white-light interferometer by using a vernier principle, *Applied Optics*, vol. 42, no.22, pp: 4431-4435, August, 2003. 4. Y. J. Rao, Y. N. Ning, and D. A. Jackson, Synthesized source for white-light sensing systems, *Optics Letters*, vol.18, no. 6, P:462-464, 1993.
5. D. N. Wang, Y. N. Ning, K. T. V. Grattan, A. W. Palmer, and K. Weir, The optimized wavelength combinations of two broadband sources for white light interferometry, *J. Lightwave Technol.*, vol. 12, no. 5, P:909-916, 1994.
6. D. N. Wang, Y. N. Ning, K. T. V. Grattan, A. W. Palmer, and K. Weir, Three-wavelength combination source for white light interferometry, *IEEE Photonics Technol. Lett.*, vol. 5, no. 11, P:1350-1352, 1993.
7. D. N. Wang, Y. N. Ning, K. T. V. Grattan, A. W. Palmer, Siganl processing scheme for cetral position identification in a white light interferometri system with a dual wavelangth source, *Optics & Laser Technology*, vol. 29, no. 7, p:377-382, 1997.
8. Ju-Yi Lee and Der-Chin Su, Central fringe identification by phase quadrature interferometric technique and tunable laser-diode, *Optics Communication*, vol. 198, p:333-337, 2001.

INTERACTION MODEL BETWEEN FIBER OPTIC ULTRASONIC SENSOR AND MATRIX MATERIALS

Libo Yuan, Guanyong Zhang, and Qingbin Li
[a]*Department of Physics, Harbin Engineering University, Harbin 150001, China*
[b]*Department of Bridge Engineering, Tongji University, Shanghai 200092, China* [c]*Department of Hydraulic Engineering, Tsinghua University, Beijing 100084, China*

Abstract: A dynamic model of a fiber segment with polymer coating, which was embedded in the concrete materials, is proposed to evaluating the response of the ultrasonic stress wave in matrix material. The photo-elastic response of optical fiber and the birefringence induced phase change are analyzed. The relationship between fiber optic sensor phase change and the ultrasonic wave in the matrix is established.

Key words: fiber optic sensor, ultrasonic detection, interaction, phase change, concrete structure, health monitoring.

1. INTRODUCTION

Fiber optic ultrasonic sensors have been intensively studied during the past twenty years [1-8]. The fiber sensors are simply used to detect the ultrasonic energy after it has interrogated the structure. There have been some publications on the detection of acoustic waves in solids using fiber optic sensors [9-12] that are embedded in the solid materials. The interaction between fiber optic sensor and the matrix materials has been developed [13] and the issue of the effect of fiber polymer coating has been recently addressed [14,15]. An ultrasonic beam impinging on the optical fiber causes a relative phase shift between the two modes because they encounter different refractive indices as they propagate down the fiber. In this paper, the interaction between the fiber with polymer coating and the concrete

Farhad Ansari (ed.), Sensing Issues in Civil Structural Health Monitoring, 423–431.

matrix materials are developed for the developed fiber optic Fizeau and Sagnac-like interferometric ultrasonic sensors.

2. BIREFRINGENCE INDUCED PHASE CHANGE

The birefringence in the single mode fiber comes from different sources. From the manufacturing process of the fiber, the modal birefringence is unavoidable. Bending of the fiber can cause elliptically induced birefringence. Moreover, the strain (as a result of external perturbation) in the fiber introduces strain-induced birefringence.

In fact, the dynamic phase change, mainly, corresponding to the ultrasonic stress wave induced phase change, i.e. [16]

$$\Delta\beta = \left(\beta_{\mathrm{x}} - \beta_{y}\right) \tag{1}$$

If the total length of fiber is l_0, the birefringence phase shift is

$$\Delta\phi = \Delta\beta l_0 = \left(\beta_{\mathrm{x}} - \beta_{y}\right)l_0 \tag{2}$$

The change of propagation constants of two orthogonal modes [17,18]

$$\Delta\beta_x = k_0\Delta n_x = k_0(C_1 - C_2/3)\sigma_{fx} \tag{3}$$

$$\Delta\beta_y = k_0\Delta n_y = k_0(C_2 - C_1/3)\sigma_{fy} \tag{4}$$

where $k_0 = \dfrac{2\pi}{\lambda}$, corresponding the propagation constant.

Therefore, the ultrasonic stress wave induced birefringence can be expressed as

$$\begin{aligned}\Delta\beta &= \Delta\beta_x - \Delta\beta_y \\ &= \frac{4}{3}k_0(C_1 - C_2)\sigma_{fx} \\ &= \frac{4}{3}k_0 C\sigma_{fx}\end{aligned} \tag{5}$$

Then the phase different between the two orthogonal polarization states can be expressed as

$$\Delta\varphi = \frac{4}{3}k_0 l_0 C\sigma_{fx} \tag{6}$$

Here, l_0 is the effective length of the optical fiber (i.e. the total gauge length) under the ultrasonic wave interacting zone. The photo-elastic constant is measured to be $C = 3.34 \times 10^{-5}$ mm^2/kg at $\lambda = 0.6328$ μ m, $C = 3.17 \times 10^{-5}$ mm^2/kg at $\lambda = 1.3$ μ m, $C = 3.0810^{-5}$ mm^2/kg at $\lambda = 1.5$ μ m, respectively [13].

3. EFFECT OF FIBER POLYMER COATING

For the case of the optical fiber with a soft coating (silicone or polypropylene) and embedded within a rigid host materials such as concrete matrix as shown in Fig.1, the fiber acoustic response is determined primarily by radial strains and the inertial effects do not permit the external excitation fully and directly act on the optical fiber due to the soft coating layer.

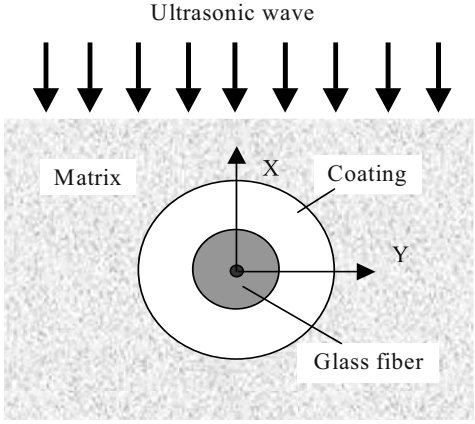

Figure 1 *The coordinate system showing the direction of ultrasonic wave applied to an optical fiber with coating that is embedded within a concrete matrix.*

The response of the sensing fiber will then be damped or desensitized. A simplified explanation for the desensitization is given as follows: an acoustic pressure wave applied to the matrix (e.g., concrete) material produces strain on the soft coating. However, because of the low Young's modulus of the coating material, a smaller stress is communicated to the glass fiber. The use of soft coating not only reduces the strain applied to the glass fiber, but also damps the higher frequency response. The effect of coating on the response of the embedded fiber sensor may be studied by a simplified model as shown in Fig. 2. In Fig.2, E_c and D_c represents respectively the Young's modulus (equivalent stiffness) and the equivalent damping coefficient of the coating

material and ρ is the mass density (equivalent mass of per unit length) of the glass fiber.

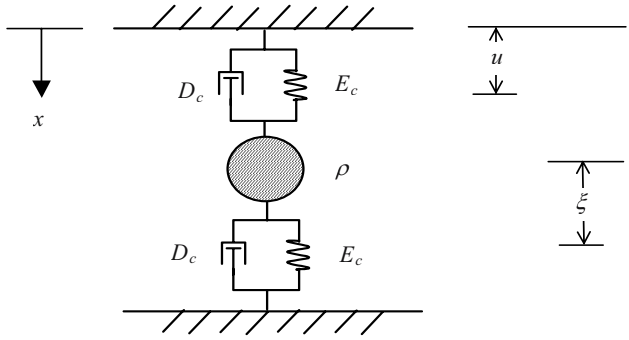

Figure 2 *A simple model for the study of dynamic response of embedded sensing fiber with soft coating.*

Assume a harmonic ultrasonic wave propagating perpendicular to the fiber axis along the *x*-direction and the medium displacement is given by:

$$\vec{u}(x,t) = A\hat{x}\cos(\Omega t - kx) \tag{7}$$

where *A,* Ω, *k* are respectively the amplitude, the angular frequency, and the propagation constant of the displacement wave. $\hat{x}$ is a unit vector.

The displacement in the sensing fiber $\vec{\xi}(x,t)$ satisfying the following equation of motion [19]

$$\rho\frac{\partial^2\vec{\xi}}{\partial t^2} + 2D_c\left(\frac{\partial\vec{\xi}}{\partial t} - \frac{\partial\vec{u}}{\partial t}\right) + 2E_c\left(\vec{\xi} - \vec{u}\right) = 0 \tag{8}$$

Substitute Eq.(7) into Eq. (8), we obtain

$$\rho\frac{\partial^2\vec{\xi}}{\partial t^2} + 2D_c\frac{\partial\vec{\xi}}{\partial t} + 2E_c\vec{\xi} = P_0\cos(\Omega t - kx + \delta) \tag{9}$$

with

$$\begin{cases} P_0 = 2A\sqrt{E_c^{\,2} + (\Omega D_c)^2} \\ \delta = -\tan^{-1}\left(\dfrac{\Omega D_c}{E_c}\right) \end{cases} \tag{10}$$

For initial conditions

$$\vec{\xi}(x,t)\Big|_{t=0} = 0\,,\ \frac{\partial\vec{\xi}(x,t)}{\partial t}\bigg|_{t=0} = 0 \tag{11}$$

The solution of Eq.(9) is

$$\bar{\xi}(x,t) = \frac{P_0}{2E_c} \frac{\cos[\Omega t - kx - (\alpha - \delta)]}{\left[\left(1-\eta^2\right)^2 + (2\varsigma\eta)^2\right]^{1/2}} \tag{12}$$

where we have defined a damping ratio $\varsigma = \frac{D_c}{\rho\omega}$, with $\omega = \sqrt{\frac{2E_c}{\rho}}$ represents the equivalent circular frequency of the sensor system; $\eta = \frac{\Omega}{\omega}$ represents the ratio of the applied external ultrasound frequency over the equivalent frequency of the system and the angle α is given by

$$\alpha = \tan^{-1}\left(\frac{2\eta\varsigma}{1-\varsigma^2}\right) \tag{13}$$

4. TRANSFER FUNCTION OF STRESS WAVE FROM MATRIX MATERIAL TO SENSING FIBER

As can be seen from Fig. 3, an externally applied ultrasonic stress wave caused stress in the sensing fiber after travelling through the elastic matrix material (concrete) and the soft fiber coating. The stress wave in the matrix materal can be obtained by using Eq.(7) as

$$\begin{aligned} \sigma_{mx}(x,t) &= E_m \varepsilon_{mx}(x,t) \\ &= E_m \frac{\partial \bar{u}(x,t)}{\partial x} \\ &= E_m kA \sin(\Omega t - kx) \end{aligned} \tag{14}$$

where E_m represents the Young's modulus of the matrix material. Similarly, by using Eq.(12), the stress wave in the sensing fiber is obtained as

$$\begin{aligned} \sigma_{fx}(x,t) &= E_f \varepsilon_{fx}(x,t) \\ &= E_f \frac{\partial \bar{\xi}(x,t)}{\partial x} \\ &= \left\{\frac{1+(2\varsigma\eta)^2}{(1-\eta^2)^2 + (2\varsigma\eta)^2}\right\}^{1/2} E_f kA \sin[\Omega t - kx - (\alpha - \delta)] \end{aligned} \tag{15}$$

where E_f represents the Young's modulus of the glass fiber. The magnitue of the stress transfer function from the matrix material to the glass fiber is the amplitude ratio of the stress waves as given by Eqs.(15) and (14), i.e.,

$$\frac{\sigma_{fx}(x,t)\big|_{\max}}{\sigma_{mx}(x,t)\big|_{\max}} = \frac{E_f}{E_m}\left\{\frac{1+(2\varsigma\eta)^2}{(1-\eta^2)^2+(2\varsigma\eta)^2}\right\}^{1/2} = \frac{E_f}{E_m}\Im(\varsigma,\eta) \tag{16}$$

Here $\Im(\varsigma,\eta)$ represents a dynamic magnification transfer function, defined as

$$\Im(\varsigma,\eta) = \left\{\frac{1+(2\varsigma\eta)^2}{(1-\eta^2)^2+(2\varsigma\eta)^2}\right\}^{1/2} \tag{17}$$

The phase angle $(\alpha-\delta)$ of the stress transfer function is

$$(\alpha-\delta) = \tan^{-1}\left(\frac{2\eta\varsigma}{1-\varsigma^2}\right) + \tan^{-1}(2\eta\varsigma) \tag{18}$$

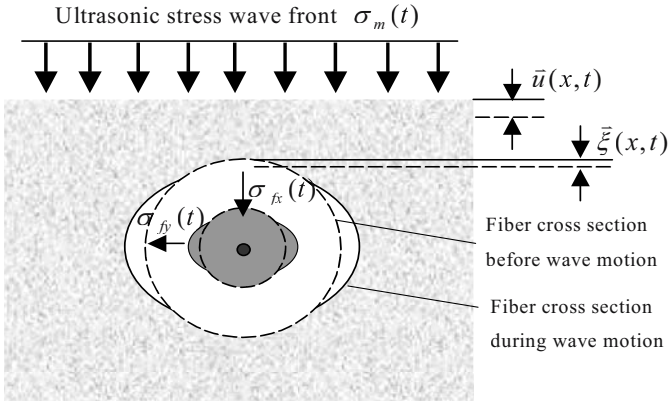

Figure 3 *A illustration showing the displacements in the matrix and the fiber materials for an applied stress wave.*

Fig. 4 shows the dynamic magnification factor plotted against the frequency ratio η for various values of the damping ratio ς. A number of interesting points may be observed from this figure. There are limiting values of unity and zero for the dynamic magnification factor, which correspond, respectively, to the low and high values of the frequency ratio for every value of the damping ratio. The response characteristic strongly depends on the coating material Young's modulus and damping coefficient. It is obviously that the higher frequency component is decayed due to the smaller dynamic magnification factor. Figure 5 shows how the phase angle varies with the frequency ratio and the damping ratio.

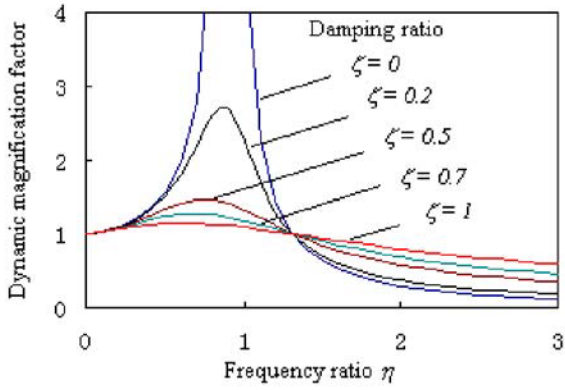

Figure 4 *Variation of dynamic magnification factor with damping and frequency.*

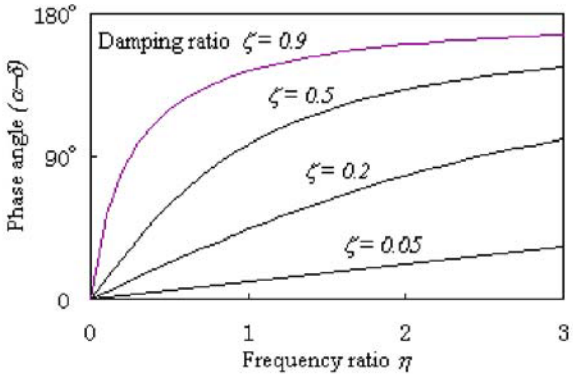

Figure 5 *Variation of phase angle with damping and frequency.*

5. CONCLUSIONS

Fiber sensors are simply used to detect the ultrasonic energy after it has interrogated the structure. The interaction between fiber optic sensor and the matrix materials are developed and the issue of the fiber soft coating factor has been discussed. The results indicated that the dynamic response characteristic strongly depends on the coating material Young's modulus and damping coefficient. It is obviously that the higher frequency component is decayed due to the smaller dynamic magnification factor of the fiber polymer coating. It is provide a bridge between the real ultrasonic in the matrix materials and the output signals of the developed fiber optic Fizeau and Sagnac-like interferometric sensors [20].

ACKNOWLEDGMENTS

This work was supported by the National Nature Science Foundation of China, under grant number 50179007, and the Teaching and Research Award Program for Outstanding Young Professors in Higher Education Institute, MOE, P.R.C., to Harbin Engineering University.

REFERENCES

1. R. O. Claus and J. H. Cantrell, Detection of ultrasonic wave in solid by an optical fiber interferometer, *IEEE Ultrason. Symp*., pp. 719-721, 1980
2. P. Cielo and J. Lapierre, Fiber-optic ultrasound sensing for the evaluation of materials, *Appl. Opt*., **21**(4), 572-575, 1982.
3. R. P. De Paula, J. H. Cole and J A. Bucaro, Broad-band ultrasonic sensor based on induced optical phase-shifts in single-mode fibers, *IEEE J. Lightwave Technol*. **LT-1**(2), 390-393, 1983
4. K. D. Bennett, R. O. Claus and M. J. Pindera, Internal monitoring of acoustic emission in graphite epoxy composites using imbedded optical fiber sesnors, In *Review of Progress in Nondestructive Evaluation* (D. O. Thompson and D. E. Chimenti, eds.), **6**, 331-335, Plenum, New York, 1986.
5. G. Meltz and J. R. Dunphy, Optical fiber stress wave sensor, *Proc. SPIE- Int. Soc. Opt. Eng.*, **838**, 69-77, 1987
6. S. G. Pierce, W. R. Philp, A. McNab, G. Hayward and B. Culshaw, Surface-bonded and embedded optical fibers as ultrasonic sensors, **35**(25), 5191-5197, 1996
7. J. Dorighi, S. Krishnaswamy, and J. Achenbach, A fiber optic ultrasonic system to monitor the cure of epoxy, Res. Nondestr. Eval. **9**, 13-24, 1997
8. Sun C, Ansari F, Design of the fiber optic distributed acoustic sensor based on Michelson interferometer and its location application, *Optical Engineering,* **42** (10): 2987-2993, 2003
9. K. Liu, S. M. Ferguson and R. M. Measures, Damage detection in composite materials using embedded fiber optic interferometric sensors, *Proc. SPIE- Int. Soc. Opt. Eng.*, **1107**, 205-210, 1990
10. J. J. Alcoz, C. E. Lee and H. F. Taylor, Embedded fiber-optic Fabry-Perot ultrasound sensor*, IEEE Trans. Ultrason. Ferroelectr., Freq. Control* **UFFC-37**(4), 302-306, 1990
11. K. Liu, Ultrasonic NDE for composite materials using embedded fiber-optic interferometric sensors, *In CAN-AM Eastern'90 Rochester,* NY. USA, Oct4-5, 1990, Vol. **1398**. Bellingham, WA, USA Publ. by Int. Soc. For Optical Engineering, 1991
12. N. Nadarajah, C. Zhou. L. Stephen, S. Arun, Fiber-optic acoustic sensor for nondestructive evaluation, *Optics and Lasers in Engineering*, **22**, 137-148, 1995
13. Y. Namihira, Opto-elastic constant in single mode optical fibers, *Journal of Lightwave Technology,* **LT-3**, 1078-1083, 1985
14. Libo Yuan, Limin Zhou, Wei Jin, K. T. Lau, Long gauge length fiber optic ultrasonic sensor for large scale concrete structures, *Optics and Lasers Technology*, **36(**1), 11-17, 2004
15. Libo Yuan, Limin Zhou and Wei Jin, Detection of acoustic emission in structure using Sagnac-like fiber-loop interferometer, Sensors and Actuators A, 2004 (in press)
16. L. M. Lyamshev and Yu. Yu. Smirnov, Fiber-optic sound level meter, *Sov. Phys. Acoust.*, **35**(6), 832-835, 1989

17. Y. Namihira, M. Kudo, and Y. Mushiake, Effect of mechanical stress on the transmission characteristics of optical fibers, *Trans. Inst. Electron. Commun. Eng. Japan,* **60-C**, 391-398, 1977
18. S. Timoshenko and J. N. Goodier, *Theory of Elasticity*, 3rd ed. New York: McGraw-Hill, 1970
19. L. F. Boswell and C. D'Mello, *Dynamics of Structural Systems*, Oxford: Blackwell Scientific Publications, 1993

BIREFRINGENCE AND TRANSVERSE STRAIN SENSITIVITY IN BRAGG GRATING SENSORS

Mohanraj Prabhugoud and Kara Peters
Department of Mechanical and Aerospace Engineering, North Carolina State University, USA

Abstract: This article presents the derivation of a finite element formulation for the calculation of the spectral response of a fiber Bragg grating sensor embedded in a host material system. The formulation is based on a 3D/2D element for which the local fiber propagation constants are calculated from the optical and geometric properties in the plane perpendicular to light propagation. Afterwards, a modified transfer matrix can be applied to calculate the Bragg wavelength shifts in each of the principle optical axes for the grating. The effects of axial strain, transverse strain, and fiber curvature can be implemented into the formulation. This novel approach permits the prediction of the sensor response when the sensor is embedded in a complicated material system for which analytical or approximate solutions do not accurately predict the strain state in the sensor. A numerical example demonstrating the response of the senor to diametrical compression is presented to verify the formulation.

Key words: Fiber Bragg grating, birefringence, finite element method

1. INTRODUCTION

Optical fiber Bragg grating sensors (FBG) have been widely embedded in material systems for the measurement of curing stresses, interlamina stresses, delamination, crack growth, and other phenomena [1]. A clear understanding of the spectral response of the Bragg grating in such environments is essential to their performance. A variety of models have been developed for the stress transfer to optical fibers materials embedded in various material systems [2-6]. Each of these models considers the stress or strain transfer from the host material system to the sensing fiber. The

Farhad Ansari (ed.), Sensing Issues in Civil Structural Health Monitoring, 433–442.

resulting strain fields on the sensor are generally combined together to define an “effective" axial strain of the grating, from which its spectral response is calculated.

Later works considered the effect of transverse strain components (i.e. normal strain not in the fiber axial direction) on the FBG and determined that significant transverse strain induces a birefringence in the optical fiber, creating two distinct Bragg wavelengths corresponding to each of the principle optical axes [7-12]. In general each of the theoretical work calculates the in-plane normal strain components at the center of the optical fiber due to the strain applied at the boundary of the optical fiber, typically through a finite element model of the fiber [7] and [9-10]. Next, the local change in index of refraction due to each of these two strain components is calculated, from which the change in Bragg wavelengths can be determined. Bosia *et al*. applied a slight modification to the formulation, using the principle strains at the center of the fiber, rather than the strains in the original coordinate frame [8]. As demonstrated by several of the experimental studies, however, satisfactory predictions have not been obtained, in particular for polarization maintaining fiber geometries [8] and [11-12]. This article proposes that the assumption that the local strain components at the center of the fiber does not sufficiently account for the effect of the non-uniform change in index of refraction throughout the region of the cross-section over which the propagated mode is distributed. In particular, the use of the strain values at the center of the fiber cannot correctly predict the non-linear shift as a function of applied load apparent when polarization maintaining fibers are loaded in diametrical compression at an arbitrary angle to their principle optical axes.

Therefore, a “FBG sensor element" is derived in this paper to accurately predict the sensitivity of the FBG to transverse strain, for integration into a structural analysis finite element code. The formulation is based on a 3D element for which the propagation constant is calculated from the optical and geometric properties in the plane perpendicular to light propagation, after which the optical transfer matrix is calculated. The effects of axial strain, transverse strain, fiber curvature and shear loading can be implemented into the formulation. This novel approach permits the prediction of the sensor spectral response when the sensor is embedded in a complicated material system for which analytical or approximate solutions do not accurately predict the strain state in the sensor.

2. FINITE ELEMENT FORMULATION

The propagation of a given mode through an optical fiber, can generally be characterized through the mode distribution in the cross-section of the

optical fiber and the propagation constant (i.e. speed of propagation), β. Exact solutions for the propagation characteristics of optical fibers are limited to relatively simple geometries (e.g. circular or elliptical cross-sections) with axisymmetric index of refraction profiles. To calculate the propagation characteristics of an optical fiber with an arbitrary cross-sectional shape or non-axisymmetric variation of refractive index one needs to adopt to a numerical method such as the finite element method.

Current finite element approaches can be classified into vector methods and scalar methods [13]. Vector finite element methods are applicable to all values of refractive index difference between the core and the cladding. The main disadvantages of this approach are the large computational effort required and the appearance of spurious modes. However, the spurious modes can be eliminated using a penalty approach [13]. Scalar finite element methods, on the other hand, are only applicable to weakly guiding fibers, i.e. the variation of the refractive index is negligible over a distance of one wavelength [14]. However, such an assumption is reasonable for an FBG within its elastic strain limit. The advantages of a scalar method are that no spurious solutions appear (i.e. only linearly polarized modes are captured) and only one component of the electric, $\vec{E}$, or magnetic, $\vec{H}$, field is considered, reducing the size of the matrix to solve for the propagation constant. For this reason, we derive a sensor element based on a scalar formulation without applying the assumption of axisymmetry.

2.1 Overview

Although the details of all calculations are not presented here, the prediction of the embedded FBG spectral response would be performed through the following series of steps (see Fig. 1):

- The surrounding host composite material and optical fiber sensor are meshed using conventional algorithms. The sensor mesh is shown in Fig. 2, where the fiber is divided into segments in the axial direction and then each cross-section is meshed into triangular elements.
- Using an existing finite element code, the stress and strain components in each element are calculated due to external applied loads and / or temperature. For each sensor element, the average strain components, the curvature about the x_1-axis, and the nodal displacements are stored.
- For the 2D front face of each element (as shown in Fig. 2), the index of refraction change and birefringence due to the applied strain field in calculated.

- The propagation constant for the optical fiber is calculated for each cross-section, discretized using the updated index of refraction distribution and the nodal displacements.
- The sensor spectral response is calculated from the local axial strain, effective index of refraction, and curvature of each segment using a modified transfer matrix formulation [15].

Using the above strategy as a motivation for the discretization used, in this article we present the calculation of the propagation constant for a given fiber segment due to the applied axial and transverse strain fields.

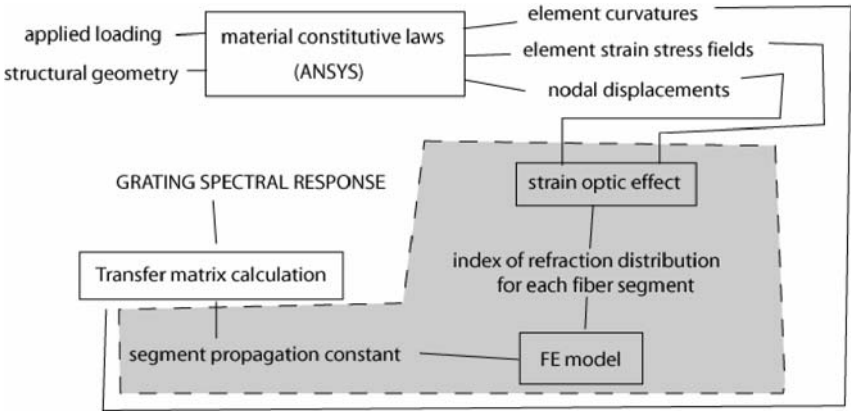

Figure 1. Schematic of the procedure for calculation of FBG spectral response for a sensor embedded in a host material system. The work presented in this paper is included in the shaded region.

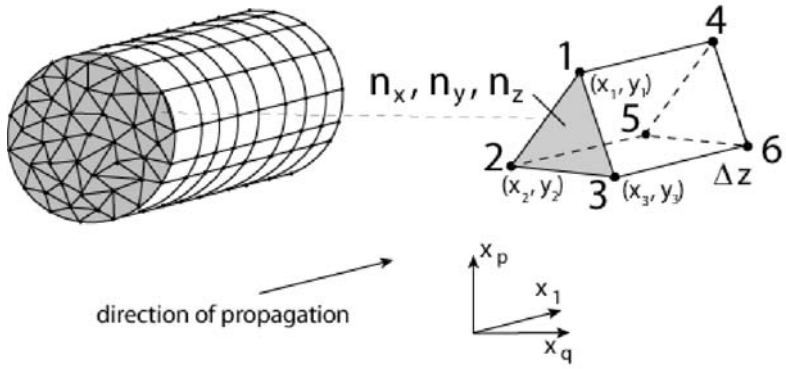

Figure 2. Discretization of optical fiber including definition of sensor element coordinates and 2D triangular element with nodal coordinates.

2.2 Calculation of n_e for an element

Each element is assumed to be optically isotropic with an index of refraction in the unstressed state of n_e^0. As stress is applied to the element, n_e changes due to two effects: the strain-optic effect and the area change of the element in the 2-3 plane. The area change is already included in the formulation through the nodal displacements, therefore we only calculate the former effect here. We can write the wave equation for the displacement field vector {D} as [9],

$$\{s\}\times(\{s\}\times[B]\{D\})+\frac{1}{(n_e)^2}\{D\}=0 \tag{1}$$

where $\{s\}$ is the unit vector in the direction of propagation, and

$$[B]=\begin{bmatrix} B_1 & B_6 & B_5 \\ B_6 & B_2 & B_4 \\ B_5 & B_4 & B_3 \end{bmatrix}. \tag{2}$$

For each solution $n_e = n_e^p$ or n_e^q where n_e^p and n_e^q are the element effective index of refractions about the principle optical axes (not necessarily the principle strain axes due to the applied loading). Writing *{D}* in terms of its components *{D} = (0,D2,D3)* and *{s} = (1,0,0)*, and evaluating (1) yields a matrix equation whose non-trivial solutions n_e^p and n_e^q are,

$$\frac{1}{(n_e^{p,q})^2}=\frac{(B_2+B_3)\pm\sqrt{(B_2-B_3)^2+4B_4^2}}{2} \tag{3}$$

For an optically isotropic material,

$$[B]=\begin{bmatrix} 1/(n_e^0)^2 & 0 & 0 \\ 0 & 1/(n_e^0)^2 & 0 \\ 0 & 0 & 1/(n_e^0)^2 \end{bmatrix}. \tag{4}$$

Therefore, $n_e^p = n_e^q = n_e^o$. Once strain is applied to the element, in the absence of thermal loading, the dielectric impermeability tensor change is defined by the strain-optic equation,

$$\Delta B_i = \sum_{j=1}^{6} p_{ij} \varepsilon_j \tag{5}$$

where the compact notation is used for the strain components ($\varepsilon_1 = \varepsilon_{11}$, $\varepsilon_2 = \varepsilon_{22}$, $\varepsilon_3 = \varepsilon_{33}$, $\varepsilon_4 = \gamma_{23}$, $\varepsilon_5 = \gamma_{31}$, $\varepsilon_6 = \gamma_{12}$) [9]. For an optically isotropic material, the strain-optic tensor reduces to, $p_{11} = p_{22} = p_{33}$, $p_{12} = p_{21} = p_{13} = p_{31} = p_{32} = p_{23}$, $p_{44} = p_{55} = p_{66} = (p_{11} - p_{12})/2$, and all other $p_{ij} = 0$. Writing $B_i \equiv B_i^0 + \Delta B_i$, substituting [$p$] into (5) into (3) and expanding yields the two principle indices of refraction after strain has been applied,

$$n_{eff}^{p,q} = \frac{1}{\sqrt{1/\left(n_e^o\right)^2 + p_{12}\varepsilon_1 + \frac{\left(p_{11}+p_{12}\right)}{2}\left(\varepsilon_2+\varepsilon_3\right) \pm \left(p_{11}-p_{12}\right)\sqrt{\left(\varepsilon_2-\varepsilon_3\right)^2+\varepsilon_4^2}}} \tag{6}$$

where the isotropic material properties have been applied.

Since most of the equations presented in this section are similar to those of Kim et al. [9], it is important to differentiate between the current formulation and the formulation of [9]. Whereas, Kim et al. treated the sensor as a single entity with isotropic or transversely isotropic optical properties, the current formulation defines the material properties for each element within the sensor. Therefore, when transverse strain is applied to the optical fiber, the previous formulation given in [9] calculates the change in propagation constant due to the average principle strains in the optical fiber. It does not however take into account the fact that the strain varies throughout the fiber cross-section. This variation is included in the current formulation.

2.3 Calculation of β for a sensor segment

The propagation characteristics for linearly polarized (LP) modes propagating through a waveguide of arbitrary cross-section and arbitrary variation of refractive index are determined by solving the following Helmholz wave equation in the region Ω [13]

$$p_x \frac{\partial^2 \Phi(x,y)}{\partial x^2} + p_y \frac{\partial^2 \Phi(x,y)}{\partial y^2} + q k_o^2 \Phi(x,y) - \beta^2 \Phi(x,y) = 0 \tag{7}$$

where the field $\Phi(x,y)$ and coefficients p_x, p_y, q are defined as follows:

- LP_x modes: $\Phi = e^{i\beta z}E_x$, $p_x = n_x^2 / n_z^2$, $p_y = 1$, $q = n_x^2$;
- LP_y modes: $\Phi = e^{i\beta z}E_y$, $p_x = 1$, $p_y = n_y^2 / n_z^2$, $q = n_y^2$.

In (7), $n_x(x,y)$, $n_y(x,y)$, and $n_z(x,y)$ are the refractive indices in the x, y, and z directions respectively, $k_o^2 = 2\pi/\lambda$, and β is the unknown propagation constant for the cross-section. The functional for (7) is given by,

$$F = \iint_{\Omega}\left[p_x(x,y)\frac{\partial^2\Phi}{\partial x^2} + p_y(x,y)\frac{\partial^2\Phi}{\partial y^2} + \left(q(x,y)k_o^2 - \beta^2\right)\Phi \right] dxdy \quad (8)$$

Taking the first variation of (8), reducing, and discretizing the region into triangular elements as shown in Fig. 2 with constant optical properties, n_x^e, n_y^e, n_z^e, the functional in (8) reduces to,

$$\sum_e \iint_e \left[p_x^e \frac{\partial\Phi}{\partial x}\frac{\partial\Phi^*}{\partial x} + p_y^e \frac{\partial\Phi}{\partial y}\frac{\partial\Phi^*}{\partial y} + \left(\beta^2 - q_e k_o^2\right)\Phi\Phi^* \right] dxdy - \int_{\Gamma}\left[\Phi^*\left(p_x^e \frac{\partial\Phi}{\partial x} + p_y^e \frac{\partial\Phi}{\partial y}\right)\right] d\Gamma = 0 \quad (9)$$

where Γ is the boundary of the region Ω. We expand Φ in each element,

$$\Phi_e = \begin{bmatrix} N_1 & N_2 & N_3 \end{bmatrix}\begin{bmatrix} \Phi_1 \\ \Phi_2 \\ \Phi_3 \end{bmatrix} = \{N\}^T\{\Phi\} \quad (10)$$

where N_1, N_2, and N_3 are shape functions and Φ_1, Φ_2, and Φ_3 are nodal values of Φ. Since we are only concerned with propagated modes, i.e. modes that are fully contained in the region Ω, we apply the boundary condition Φ = 0 on Γ. Substituting (10) into (9) we obtain the global matrix equation:

$$[K]\{\Phi\} - \beta^2[M]\{\Phi\} = 0 \quad (11)$$

$$[K] = \sum_e \iint_e \left[q_e k_o^2 \{N\}\{N\}^T - p_x^e \{N_x\}\{N_x\}^T - p_y^e \{N_y\}\{N_y\}^T \right] dxdy$$
$$[M] = \sum_e \iint_e \left[\{N\}\{N\}^T \right] dxdy \quad (12)$$

The required derivatives of the shape function for the triangular element defined in Fig. 2 can be derived from the element geometry [16]. Once the matrices [*K*] and [*M*] have been calculated separately for the LP_x and LP_y modes, (11) is solved for the eigenvalues, β, for each case. For uniform axial in the x_1 direction, the two resulting propagation constants can then be used to calculate the Bragg wavelength shift of the FBG in each of the two principle optical directions, $\Delta\lambda_p$ and $\Delta\lambda_q$. For non-uniform strain in the x_1 direction, a modified transfer matrix method can be applied in which the propagation constants are calculated for each grating segment using the above formulation and then the total response of the grating calculated from the multiplication of the optical transfer matrix for each segment [16].

3. NUMERICAL EXAMPLE

To demonstrate the application of the above method to a classic FBG sensor problem, we consider the case of a FBG written into a step-index circular fiber loaded in diametrical compression. This problem has been studied experimentally as well as theoretically in [8] and [11-12]. The specific parameters used for this simulation were: E = 72Gpa, ν = 0.17, core radius = 4μm, cladding radius = 62.5μm, n_1 (core) = 1.46, n_2 (cladding) = 1.44, p_{11} = 0.113, p_{12} = 0.252. The finite element model consisted of 270 core elements and 452 cladding elements. The element numbers, nodal coordinates, and boundary nodes required to calculate the propagation characteristics were generated from ANSYS.

During the solution process, the calculated index of refraction for the fiber, $n_{\text{eff}} = \beta/k_0$, was calculated and plotted as a function of the normalized frequency,

$$V = (2\pi/\lambda) r_1 \sqrt{n_1^2 - n_2^2} \tag{13}$$

for a fixed value of the applied load per unit fiber. Similar plots were generated for a series of applied loads and the change in indices of refraction recorded for V = 2.0. The resulting index of refraction vs. applied load for both the LP_x and LP_y modes is plotted in Fig. 3. For comparison, the index of refraction change calculated from the linear elasticity solution to the strains at the center of the fiber for the diametrical compression problem is also plotted in Fig. 3. The two results match well, validating the finite element solution for this problem in which the principle strains are aligned with the principle optical axes. Future studies will concentrate on problems such as diametrical compression of a FBG written into a polarizing maintaining optical fiber, for which the index of refraction

varies rapidly near the core of the fiber and the principle optical axes do not necessarily align with the principle strain axes. Therefore, the calculation based on center strain values and the calculation presented in this work are expected to differ considerably.

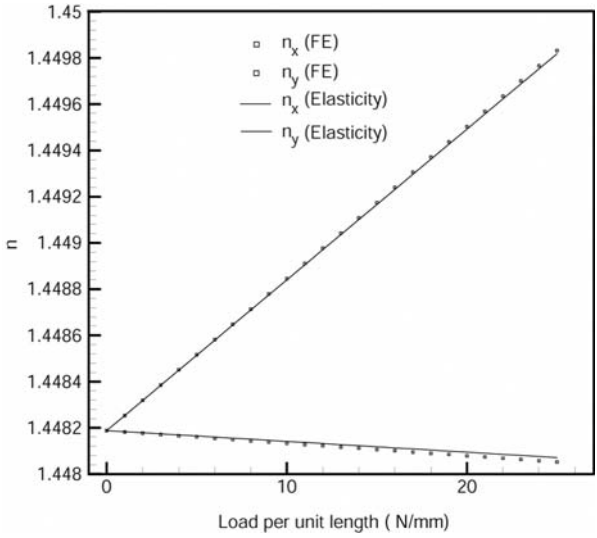

Figure 3. Index of refraction change for LP_x and LP_y modes as a function of applied load per unit length of fiber.

4. CONCLUSIONS

This paper presents a finite element formulation for the calculation of the change in propagation properties of a FBG including birefringence due to transverse strain. Coupled with a transfer matrix formulation for the calculation of the FBG spectral response, this model accurately includes the effect of transverse strain on the propagation characteristics, could incorporate power losses due to fiber curvature, and can be easily implemented into a structural finite element code for the calculation of the sensor response when embedded in a complex material system. Finally, the modeling approach could also be applied to FBGs in polarization maintaining fibers or non-fiber waveguide geometries, e.g. slab waveguides.

ACKNOWLEDGEMENTS

The authors would like to acknowledge the National Science Foundation for their financial support of this work through grant # CMS 0219690.

REFERENCES

1. Zhou G, Sim, LM. "Damage Detection and Assessment in Fibre-Reinforced Composite Structures with Embedded Fibre Optic Sensors - Review," *Smart Materials and Structures,* **vol. 11**, pp. 925-939, 2002.
2. Pak YE. "Longitudinal Shear Transfer in Fiber Optic Sensors," *Smart Materials and Structures*, **vol. 1**, pp. 57-62, 1992.
3. Yang HY, Wang ML. "Optical Fiber Sensor System Embedded in a Member Subjected to Relatively Arbitrary Loads," *Smart Materials and Structures*, **vol. 4**, pp. 50-58, 1994.
4. Libo Y, Ansari F, Qasim M. "Stress Analysis of Bond for Integrated Optical Fiber Sensors," *Intelligent Civil Engineering Materials and Structures*, ed F. Ansari *et al*, New York, ASCE, 1997.
5. Kollàr LP, Van Steenkiste RJ. "Calculation of the Stresses and Strains in Embedded Fiber Optic Sensors," *Journal of Composite Materials*, **vol. 32**, pp. 1647-1679, 1998.
6. Prabhugoud M, Peters K. "Efficient Simulation of Bragg Gratings Sensors for Implementation to Damage Identification in Composites," *Smart Materials and Structures*, **vol. 12**, pp. 914-924, 2003.
7. Haslach HW, Sirkis JS. "Surface-Mounted Optical Fiber Strain Sensor Design," *Applied Optics*, **vol. 30**, pp. 4069-4080, 1991.
8. Wagreich RB, Atia WA, Singh H, Sirkis JS. "Effects of Diametric Load on Fibre Bragg Gratings Fabricated in Low Birefringent Fibre," *Electronics Letters*, **vol. 32**, pp. 1223-1224, 1996.
9. Kim KS, Kollàr L, Springer GS. "A Model of Embedded Fiber Optic Fabry-Perot Temperature and Strain Sensors," *Journal of Composite Materials*, **vol. 27**, pp. 1618-1662, 1993.
10. Lawrence CM, Nelson DV, Udd E, Bennett T. "A Fiber Optic Sensor for Transverse Strain Measurement," *Experimental Mechanics*, **vol. 39**, pp. 202-209, 1999.
11. Bosia F, Giaccari P, Botsis J, Facchini M, Limberger HG, Salathé RP. "Characterization of the Response of Fibre Bragg Grating Sensors Subjected to a Two-Dimensional Strain Field," *Smart Materials and Structures*, **vol. 12**, pp. 925-934, 2003.
12. Zhang AP, Guan BO, Tao XM, Tam HY. "Experimental and Theoretical Analysis of Fiber Bragg Gratings under Lateral Compression," *Optics Communications*, **vol. 206**, pp. 81-87, 2002.
13. Koshiba M. *Optical Waveguide Theory by the Finite Element Method*, Boston, Kluwer Academic Publishers, 1992.
14. Bèlanger PA. *Optical Fiber Theory - a Supplement to Applied Electromagnetism*, River Edge, NJ, World Scientific, 1993.
15. Prabhugoud M, Peters K. "Modified Transfer Matrix Formulation for Bragg Grating Strain Sensors," to appear in *Journal of Lightwave Technology*, 2004.
16. Prabhugoud M, Peters K. "Modeling of Fiber Bragg Grating Sensor Response due to Combined Effects," *Proceedings of the ASME International Mechanical Engineering Congress and Exposition*, Anaheim, CA, USA, Nov. 15-19, 2004.

A NEW FIBER-OPTIC ACOUSTIC/VIBRATION SENSOR – CHARACTERISTICS AND APPLICATION TO CIVIL STRUCTURAL HEALTH MONITORING

Kazuro Kageyama, Hideaki Murayama, and Kiyoshi Uzawa
Department of Environmental and Ocean Engineering, School of Engineering, The University of Tokyo, Japan

Abstract: A new fiber-optic acoustic/vibration sensor has been developed and applied to structural health monitoring. The sensor is based on a new theory "Doppler effect in flexible and expandable light-waveguide." A very high sensitivity is achieved in the extremely wide frequency range. Principle, sensor configuration and sensitivity, measurement system and damage detection in the reinforced concrete structural models were described in the present paper. A new nondestructive evaluation (NDE) method for civil structural health monitoring and diagnostics has been proposed.

Key words: fiber-optic sensor, vibration, acoustic emission, Doppler effect, light-waveguide, health monitoring, railway girder, reinforced concrete.

1. INTRODUCTION

Fiber-optic sensors, such as Fiber Bragg Grating (FBG) [1], Fabry-Perot Interferometer (FPI) [2, 3], Brillouin Optical Time Domain Refrectometer (BOTDR) [4] and Brillouin Optical Correlation Domain Analysis (BOCDA) [5], have been applied to structural monitoring of civil infrastructures in order to assess the structural integrity. Most of the previous works were demonstrated under the static or quasi-static loading conditions. Non-destructive techniques based on ultrasonic and acoustic emission (AE) monitoring are very effective tools for structural health monitoring. Mach-Zender interferometer [6], FPI [7] and FBG [8] sensors have been applied to vibration/acoustic measurements, but these sensors have some limitations to sensitivity and frequency range.

Farhad Ansari (ed.), Sensing Issues in Civil Structural Health Monitoring, 443–452.

The authors have developed a new fiber-optic acoustic/vibration sensor [9]. The sensor is based on a new finding that the frequency of lightwave transmitted through a bended optical fiber is shifted by vibration at the bended region. A very high sensitivity has been achieved in the extremely wide frequency range. Principle, sensor configuration and sensitivity, measurement system, some applications to health monitoring of civil infrastructures are described in the present paper.

2. DOPPLER EFFECT IN FLEXIBLE AND EXPANDABLE LIGHT-WAVEGUIDE

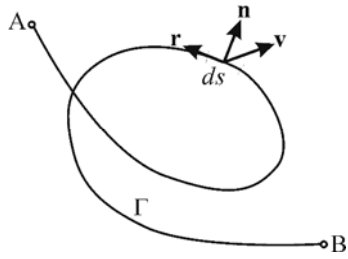

Fig. 1 Flexible and expandable light-wavequide.

Consider the light wave transmission in an arbitrary light-waveguide, Γ, as shown in Fig. 1. The path is flexible and expandable. It has finite overall length, L, and two ends, denoted as points A and B, respectively. An incident light from the one end A (light source) is transmitted through the waveguide and detected at the other end B (observer). When the waveguide moves or vibrates, Doppler frequency shift f_D is observed at B by the observer.

$$f_D = -\frac{n_{eq}}{\lambda_0} \cdot \frac{dL}{dt} \tag{1}$$

, where n_{eq} is the equivalent refractive index of the waveguide and λ_0 / n_{eq} is the equivalent length of light wave in the waveguide. From a geometrical consideration, dL/dt is given by Eq. (2),

$$\frac{dL}{dt} = \left[\mathbf{v} \bullet \mathbf{t}\right]_A^B + \int_\Gamma k \cdot \mathbf{v} \bullet \mathbf{n} ds \tag{2}$$

, where κ, $\mathbf{v}$ and $\mathbf{n}$ are the curvature, the velocity vector and the unit normal vector of the infinitesimal segment, ds, respectively, and $\mathbf{t}$ is the unit direction vector defined at the end points A and B. The operation $\bullet$ indicates inner product of two vectors. From Eqs. (1) and (2), we obtain the following equation;

$$f_D = -\frac{n_{eq}}{\lambda_0}\left[\mathbf{v}\bullet\mathbf{t}\right]_A^B - \frac{n_{eq}}{\lambda_0}\int_\Gamma k\cdot\mathbf{v}\bullet\mathbf{n}ds \tag{3}$$

3. SENSOR CONFIGURATIONS AND THEORETICAL SENSITIVITY

3.1 Circular Loop

In the case of a circular loop sensor, the sensitivity of strain rate can be evaluated by integrating Eq. (3) on the strain rate field. For simplicity, the uniform strain rate field, $\dot{\varepsilon}_{xy}$, $\dot{\varepsilon}_y$ and $\dot{\gamma}_{xy}$ is assumed on the integration path.

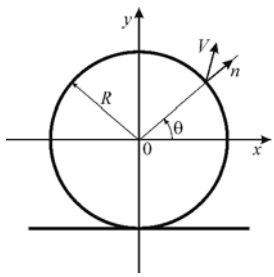

Fig. 2 Circular loop sensor and polar coordinate system.

The theoretical frequency shift, f_D^{th}, is obtained as follows;

$$f_D^{th} = -\frac{\pi R n_{eq}}{\lambda_0}\left(\dot{\varepsilon}_x + \dot{\varepsilon}_y\right) = -\frac{\pi R n_{eq}}{\lambda_0}\left(\dot{\varepsilon}_1 + \dot{\varepsilon}_2\right) \tag{4}$$

The sum of the axial strain rates or the sum of the principal strain rates is converted into the Doppler frequency shift by applying circular loop sensor. Shear strain has no effect on the frequency shift. In the case of N turns of loop, as shown in Fig. 3, the frequency shift becomes N times larger,

$$f_D^{th} = -\frac{N\pi R_{av} n_{eq}}{\lambda_0}\left(\dot{\varepsilon}_x + \dot{\varepsilon}_y\right) = -\frac{N\pi R_{av} n_{eq}}{\lambda_0}\left(\dot{\varepsilon}_1 + \dot{\varepsilon}_2\right) \tag{5}$$

, where R_{av} = (R_{max}+R_{min})/2 is the average radius of the loop. The circular loop sensor has no directional sensitivity.

We can control the sensitivity of the sensor by changing the radius and number of turns. The size of the loop is equivalent to a gauge length of the sensor, and it is recommended that the gauge length should be sufficiently smaller than the wavelength of the elastic wave measured.

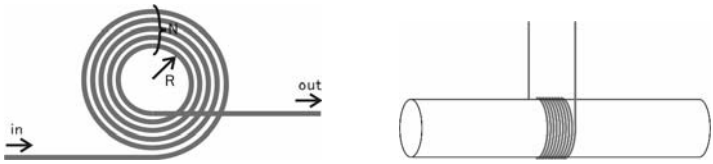

Fig. 3 Examples of circular loop sensors.

3.2 U-Shaped

Frequency change between points A and B along the U-shaped path, as schematically shown in Fig. 4, is considered.

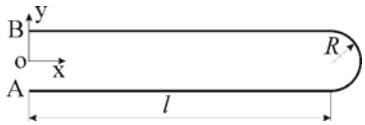

Fig. 4 U-shaped sensor

The theoretical frequency shift, f_D^{th}, is obtained by integration of Eq. (3).

$$f_D^{th} = -\frac{n_{eq}}{\lambda_0}\left\{\left(\frac{\pi}{2}R + 2l\right)\dot{\varepsilon}_x + \frac{\pi}{2}R\dot{\varepsilon}_y\right\} \tag{6}$$

This shape of the senor has directional sensitivity as a function of l/R. Sensitivity ratio, S_{xy}, of $\dot{\varepsilon}_x$ to $\dot{\varepsilon}_y$ is given by Eq. (7)

$$S_{xy} = 1 + \frac{4}{\pi}\cdot\frac{l}{R} \tag{7}$$

3.3 Elongated Circular Loop

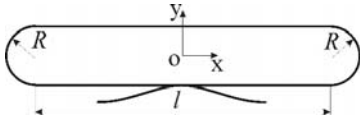

Fig. 5 Elongated circular loop sensor

In the case of an elongated circular loop as shown Fig. 5, the previous manner of calculation can be applied, and the Eq. (8) is obtained.

$$f_D^{th} = -\frac{n_{eq}}{\lambda_0}\left\{(\pi R + 2l)\dot{\varepsilon}_x + \pi R\dot{\varepsilon}_y\right\} \tag{8}$$

This shape of the sensor has also directional sensitivity, S_{xy}.

$$S_{xy} = 1 + \frac{2}{\pi} \cdot \frac{l}{R} \tag{9}$$

In the case of N turns of loop, the frequency shift becomes N times larger, but the ratio of directional sensitivity is unchanged.

$$f_D^{th} = -\frac{Nn_{eq}}{\lambda_0}\left[\left(\pi R_{av} + 2l\right)\dot{\varepsilon}_x + \pi R_{av}\dot{\varepsilon}_y\right] \tag{10}$$

4. SETUP OF MEASUREMENT SYSTEM

A Laser Doppler velocimeter (LDV) is used to detect the frequency shift. Light source is He-Ne laser (output power; 1mW, wavelength. λ_0: 632.8 nm), and heterodyne interference technique as shown in Fig. 6 is applied to the measurement in the present paper. An acousto-optical modulator (AOM) changes the frequency of the reference light source from f_0 to f_0+f_M (f_M = 80 MHz) in order to produce beating signals with frequency of f_D+f_M.

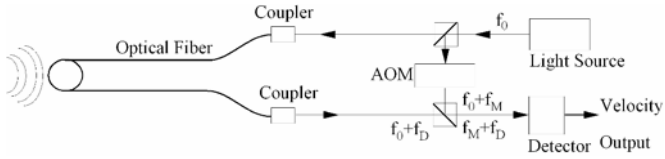

Fig. 6 Setup of measurement system.

The sensitivity of the optical circular fiber sensor (average diameter: 20 mm, number of turn: 10) is calculated theoretically. By applying commercially available performance data of the LDV (Melectro, V1002) [10], the resolution and dynamic range were obtained and listed in Table 1. Extremely high resolution less than nano-strain (10^{-10}) is expected in the very wide frequency range from 1 kHz to 1 MHz. Low frequency vibration of 0.1 Hz is detectable with sufficient sensitivity, which covers the measurement range from conventional strain gauge to AE sensor. The resolution of the newly developed sensor is extremely superior to the other fiber optic sensors, such as FBG, whose resolution is around 1 με (10^{-6}).

Table 1 Specification of optical loop fiber sensor (diameter: 20 mm, number of turns: 10)

Frequency Range	0.1 Hz - 3 MHz				
Resolution (at Ranges (4))	10 Hz	1 kHz	10 kHz	100 kHz	1 MHz
Strain Rate (με/s)		0.44		4.4	44
Strain (με)	0.01	0.0001	0.00001	0.00001	0.00001
Total Dynamic Range (dB)		160		140	120

5. STRAIN MONITORING OF REINFORCED CONCRETE BRIDGE PIER

The fiber-optic elongated circular loop sensor and conventional strain gauge were bonded on the surface of the structural model of reinforced concrete bridge pier, as shown in Fig. 7. The pier was shaken by electro hydraulic mechanical test frame. The output of the fiber-optic sensor was integrated and converted to the strain value. The detected strain histories are shown in Fig. 8. The fiber-optic sensor shows lower noise than the conventional strain gauge at low frequency of around 4 Hz.

Fig. 7 Structural model of reinforced concrete bride pier

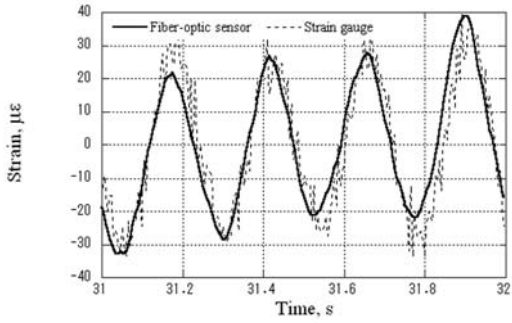

Fig. 8 Strain versus time history

6. STRUCTURAL TEST OF REINFORCED CONCRETE GIRDER

6.1 Preparation of Specimen and Measurement System

Test specimen was a full-sized model of a railway girder made of reinforced concrete. Vertical supports were fixed at the flange end and

subjected to horizontal force as shown in Fig. 9. Maximum bending stress was introduced into the root of the flange member. Six fiber-optic sensor arrays were arranged upper and lower surfaces of the specimen as illustrated in Fig. 9, and single sensor was bonded on the side surface of the flange. Total 25 fiber-optic sensors along about 30 meter optical fiber cable were bonded on the specimen.

The sensor arrays were covered with epoxy resin with phenolic micro balloon and woven GFRP wrap. The reinforced wrap can protect the sensors and optical fibers from the loads of sandbags heaped on and trampling force by workers.

Load carrying capacity of the specimen was tested by applying the cyclic loads in order to simulate the aging degradation. Test was continued for six days and finally complete fracture of the structure was occurred.

AE wave forms and AE event parameters were recorded and analyzed with Yokogawa DL750 data recorder and PAC MISTRAS-2001 system, respectively.

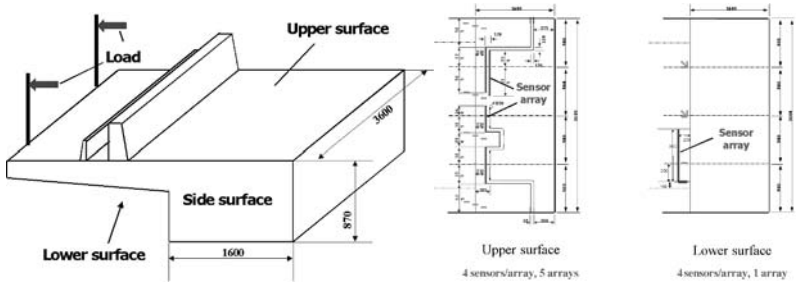

Fig. 9 Specimen configuration and sensor arrangement

6.2 AE Waves Detected by Fiber-Optic Sensors

AE waves can be detected simultaneously by the upper and lower surface sensor arrays. Examples of the wave forms are shown in Figs. 10 (a) and (b). Arriving time difference between the P and S waves in Fig. 10 (b) indicates the location of the AE source 200 mm away from the downside sensor array. Time to fly of the S waves from the upside and downside arrays were around 0.1 ms difference. It means that distance from the upside sensor array was around 200 mm larger than that from downside sensor array. Location of the observed crack front was well agreed with the results.

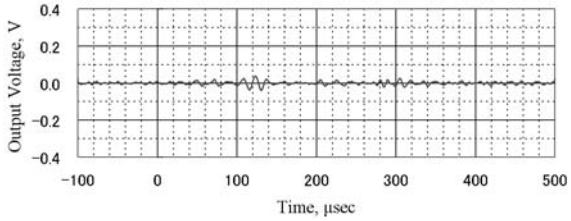

(a) AE wave detected by upper surface sensor array

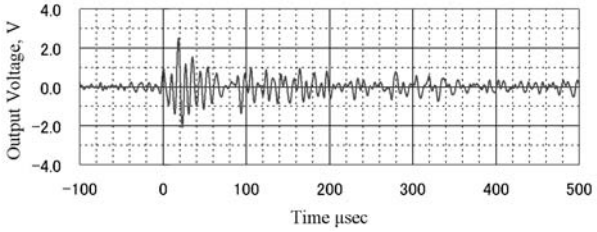

(b) AE wave detected by lower surface sensor array

Fig. 10 AE waves detected by sensor arrays

AE waves detected by side single sensor are shown in Fig. 11 (a) and (b). The AE waves have the wide frequency components from 10 kHz to 200 kHz. AE event close to the sensor gives the measured AE waves with higher frequency range as shown in Fig. 11 (a). AE wave in Fig. 11 (b) detected away from the sensor has the lower frequency components.

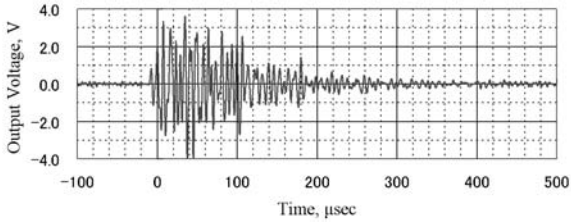

(a) AE event close to the sensor (estimated distance of 50 mm)

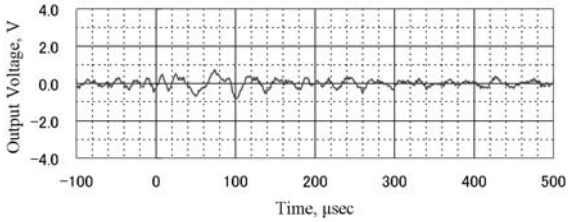

(b) AE event away from the sensor (estimated distance of 300 mm)

Fig. 11 AE waves detected by side single sensor

6.3 AE Event Histories

Load sequence and AE event histories are shown in Fig. 12, in which the result of the fiber-optic sensor is compared with the PZT sensor. Kaiser effect was observed in the AE history. The newly developed fiber-optic sensor shows almost equivalent results to the conventional AE sensor.

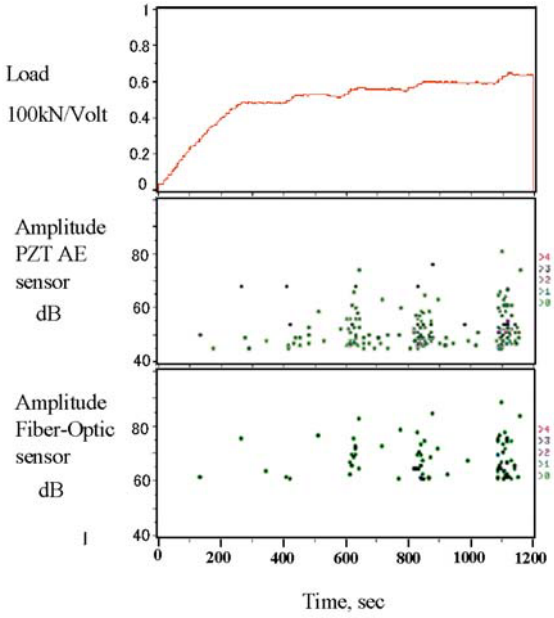

Fig. 12 AE event history and loading sequence

7. CONCLUSIONS

A new fiber-optic acoustic/vibration sensor has been developed by the authors. The principle of the sensor can be understood as Doppler's effect in flexible and expandable light-waveguide. Theoretical strain rate sensitivity of circular loop, U-shaped, elongated circular loop and meandering shaped sensors have been theoretically obtained.

The new optical-fiber sensors have successfully detected vibration and AE signals 4Hz-200 kHz of reinforced concrete structures. The new fiber-optic sensing system is applicable to the failure monitoring of the structures.

The trial tests of the new fiber-optic sensors for reinforced concrete have shown excellent results and have opened a new sight of wide-area

monitoring method from an AE perspective. Reinforced concrete has been used among most of aging infrastructure, such as bridges, tunnels, dams, mounted-railways, buildings, mounted-roads, etc. Man-saving, accurate, less-human-errors, and real-time on-line sensing technology could be established. This concept will be a new nondestructive evaluation (NDE) method for structural health monitoring and diagnostics.

ACKNOWLEDGMENT

The authors thank Mr. Y. Machijima, Mr. F. Matsumura and Mr. S. Takahashi, LAZOC, Inc., and Dr. I. Ohsawa, Mr. M. Kanai, Dr. Y. Akematsu, Mr. K. Nagata and Mr. T. Matsuo, The University of Tokyo, for technical supports to the new fiber-optic sensing technology.

REFERENCES

1. Kersey A. D., Davis M. A., Patrick H. J., LeBlanc M., Koo K. P., Askins C. G., Putman M. A., and Friebele E. J., "Fiber Grating Sensors", Journal of Lightwave Technology, Vol. **15**, No. 8, pp.1442-1463, 1997.
2. Lee C. E. and Taylor H. F., "Interferometric optical fibre sensors using internal mirrors", Electronics Letters, Vol. **24**, No. **4**, pp.193-194, 1988.
3. Murphy K. A., Kobb C. E., Plante A. J., Desu S. and Claus R. O., "High Temperature Sensing Applications of Silica and Sapphire Optical Fibers" Proc. of SPIE, Vol. **1370**, pp.169-178, 1991.
4. Horiguchi T., Shimizu K., Kurashima T., Tateda M., and Koyamada Y., "Development of a Distributed Sensing Technique Using Brillouin Scattering", Journal of Lightwave Technology, Vol. **13**, No. **7**, pp.1296-1302, 1995.
5. Hotate K. and Hasegawa T., Correlation-based continuous-wave technique for measuring Brillouin gain spectrum distribution along an optical fiber with centimeter-order spatial resolution", Proc. of SPIE, Vol. **4185**, pp.651-661, 2000.
6. Pierce S. G., Philp W. R., Gachagan A., McNab A., Hayward G., and Culshaw B., "Surface-bonded and embedded optical fibers as ultrasonic sensors", Applied Optics, Vol. **35**, No. **25**, pp.5191-5197, 1996.
7. Read I., Foote P., and Murray S., "Optical fibre acoustic emission sensor for damage detection in carbon fibre composite structures", Measurement Science and Technology, Vol. **13**, No. **1**, pp.N5-N9, 2002.
8. Perez I., Cui H.-L., and Udd E., "Acoustic Emission Detection Using Fiber Bragg Gratings", Proc. of SPIE, Vol. **4328**, pp.209-215, 2001.
9. Kageyama K., Murayama H., Ohsawa I., Kanai M., Motegi T., Nagata K., Machijima Y. and Matsumura F., "Development of a New Fiber-Optic Accoustic/Vibration Sensor: Principle, Sensor Performance, Applicability to Health Monitoring and Characteristics at Elevated Temperature", Structural Health Monitoring 2003, DEStech Publibations, PA, pp.1150-1157, 2003.
10. Technical report of *VIBRODUCER V1002*, Denshigiken Co. Ltd., 2002.

EMBEDDED CRACK TIP OPENING DISPLACEMENT SENSOR FOR CONCRETE

Zhijun Zhang and Farhad Ansari
Department of Civil and Materials Engineering, University of Illinois at Chicago, 842 West Taylor Street, Chicago, IL 60607-7023, USA

Abstract: Development of a fiber optic sensor (FOS) for embedment in concrete is described. The sensor transduction mechanism is based on the measurement of the normalized intensity variation of the speckle pattern (SIV) generated at the output end of the optical fiber. The fiber optic sensors with different gauge lengths were calibrated with the cantilever beam test to determine the optimal combination of sensitivity and dynamic range of the sensing system. Fiber optic sensors were employed for measurement of the crack tip opening displacements (CTOD) in notched three-point bend concrete beams, and results are compared with the analytical prediction based on effective-elastic crack approach.

Key words: Fiber Optic Sensors, CTOD, CMOD, Concrete.

1. INTRODUCTION

One parameter of significant importance in determining fracture properties of concrete is crack tip opening displacement (CTOD). CTOD is significant in many ways and for instance, crack extension or fracture may be assumed to occur when the crack-opening displacement exceeds a critical value. Moreover, CTOD embodies the constitutive properties of the micro cracked zone. A direct measurement of CTOD is so far impossible or very difficult. Current practice is to measure the crack mouth opening displacement (CMOD) by a clip gauge extensometers or a Linear Variable Differential Transformers (LVDT), and the CTOD will be related to the measured CMOD based on linear elastic fracture mechanics. However, the

Farhad Ansari (ed.), Sensing Issues in Civil Structural Health Monitoring, 453–462.

interrelationship between CMOD and CTOD is very complicated due to the considerable extent of the micro cracked zone in front of the crack tip.

Direct measurements of CTOD include using high resolution photography [1, 2] and fiber optic sensors [3, 4]. The former has limited applications and currently only suited for measurement of CTOD in thin metallic sheets. Optical fibers are small in diameter and can be embedded in concrete and therefore are good candidates for use as CTOD transducers. Ansari et al [3] and Lee et al [4] employed intensity and polarimetric type sensors for measurement of CTOD in concrete. The resolution of the intensity based sensor was too low for experiments involving monotonic tests. Interferometric techniques provide high-resolution measurements and they are perhaps the preferred method for measurement of CTOD [5]. However, these techniques require sophisticated instrumentation, such as an interferometer for the measurements.

The objective for the work presented here was to establish a simplified but high resolution speckle based fiber optic sensor embedded in concrete for the determination of CTOD. While detailed description of the optical method is beyond the scope of this article, a brief description of the sensor is provided for completeness.

2. FIBER OPTIC SENSING METHODOLOGY

The transduction mechanism for the sensor is based on correlation between the applied strain to the optical fiber and the light intensity variation of speckle patterns due to mode redistribution within a multimode fiber.

The variation in the propagating modes within the speckle pattern is described by the normalized speckle intensity variations, (*SIV*) over the whole speckle field

$$\Psi_n = \frac{\iint_S |\Delta I| dxdy}{\iint_S I dxdy} \propto \delta(\Delta\beta_{ml} L) \tag{1}$$

Where Ψ_n is the normalized *SIV*, $\iint_S I dxdy$ is a constant and it is the integrated intensity of the speckle field within the cross section of the optical fiber in the *x-y* coordinate system, ΔI is the change in the spatial intensity, $\Delta\beta_{ml}$ is the difference in the propagation constants between the *m* th and *l* th modes, and L is the gauge length of the optical fiber. ΔI is proportional to

$\delta(\Delta\beta_{ml}L)$ which is the phase variation due to the external perturbation change, i.e. strain. The variation from one state to another is given by

$$\delta(\Delta\beta_{ml}L) = C_{ml}Ln_{eff}\varepsilon \tag{2}$$

Where

$$n_{eff} = n\{1 - \frac{1}{2}n^2[p_{12}(1-\nu) - p_{11}\nu]\} \tag{3}$$

n is the refractive index of the glass core of the optical fiber, $\varepsilon = \frac{\delta L}{L}$ is the applied strain which alters both the fiber length and the local index of refraction (photo elastic effect), p_{11}, and p_{12} are the Pockel's constants related to the photo elastic effects in the optical fiber. C_{ml} is a proportionality constant corresponding to the m th and l th modes. Proportionality between the change in the propagation modes and the strain is only valid over a very small range of $L\varepsilon$. i.e. the dynamic range of the sensor is small. A video camera attached to an image capture board is employed for acquisition of speckle patterns from the output end of the fiber. Image data is then numerically evaluated for the computation of *SIV* according to Eqn. (1). Exhaustive description of the method including the numerical computations is given elsewhere by Spillman et al [6] and Pan et al [7].

3. EXPERIMENTAL PROGRAMS

The experimental program included calibration and experimentation with concrete beams. The purpose for calibration was to develop a relationship between *SIV* and the induced deformations. The calibration procedure was designed to measure the strain over the three different gauge lengths of 25, 50, and 75 mm. This procedure allowed for assessment of the sensitivity and dynamic range of the sensing system with the individual gauge length. The sensor with optimal combination of sensitivity and dynamic range were later employed in the three-point bending tests and the results were analyzed and compared with the estimated CTOD from the measured CMOD.

3.1 Calibration

Calibration tests involved point loading of the plexi glass cantilever beam shown in Fig.1. The beam had a cross section of 24mm x 6 mm and a span length of 320 mm. A He-Ne laser with a wavelength of 630 nm was used as

the light source. The signal was delivered to the multimode fiber by a lead-in single mode optical fiber. The multimode fiber was adhered to the surface of the beam according to the selected gauge lengths discussed earlier. A strain gage was affixed to the opposing surface of the beam. The video camera was used for capturing the speckle patterns at the output end of the optical fiber. The speckled images were then digitized by an image capture board for subsequent numerical processing by the computer. This setup could be replaced by direct use of a digitizing camera. Fig. 2 corresponds to the calibration test results in terms of *SIV* as a function of strain. The calibration results were repeatable and linear with coefficients of correlation varying between 0.97 and 0.99. Other parameters of importance including sensitivity in terms of displacements and the dynamic range for the three calibrated gauge lengths are given in table 1.

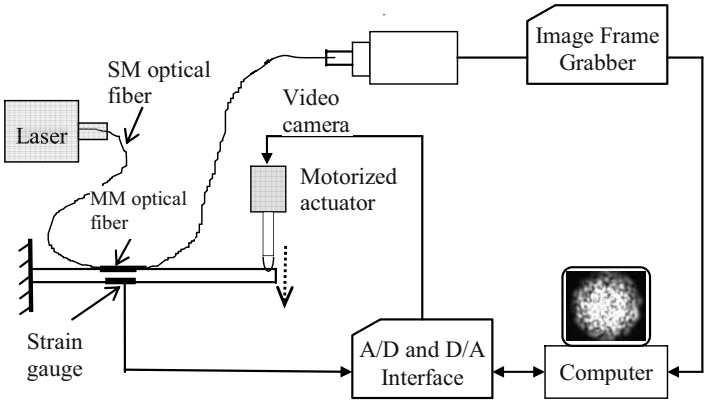

Figure 1 cantilever beam calibration test

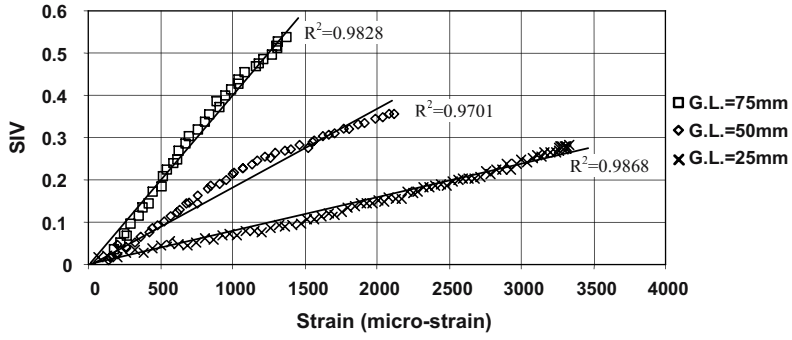

Figure 2 Cantilever beam calibration test results

Table 1 Characteristics of optical fiber sensors

Gauge Length (mm)	25	50	75
Sensitivity (SIV/Micron)	$3.26X10^{-3}$	$3.53X10^{-3}$	$6.02X10^{-3}$
Dynamic Range (in micro-strain)	3200	2000	1200

3.2 CTOD Measurements in Concrete

The main attributes of optical fibers in conjunction with embedment in concrete are their geometric conformity and the very small size. Therefore, optical fibers can be configured to appropriate shapes for embedment without disturbing the material properties. In this case however, the embedment process required some consideration in order to assure that the optical fiber measures only the displacements in front of the crack. Since the multimode optical fiber generates speckles, measures need to be taken to assure that the speckles are only generated within the 25 mm gauge length in front of the crack. A number of techniques are available for accomplishing this: (1) to use a single mode optical fiber for delivery of the signal to the 25 mm gauge multimode sensor; (2) shield the multimode fiber from vibrations by damping the movement of the multimode fiber outside of the gauge length region. A combination of the two methods was employed here, where a single mode fiber was spliced to the multimode fiber in front of the crack tip. In this arrangement, a 25 mm segment of the multimode fiber was embedded 3 mm ahead of the notch tip, and the lead out section of the multimode fiber was bent out of the plane of loading to exit the beam. The lead out section of the multimode fiber was then shielded with petroleum jelly, which is a simple effective damper for this purpose.

The schematic diagram for the experimental setup is shown in Fig.3. The center edge notched concrete beams had dimensions of 10cm×10cm×86cm and a notch depth of 5 cm. Optical fiber CTOD sensors were embedded in six beams. The specimen designations are given in table 2. The beams were tested under three-point bending in a closed-loop testing machine under constant rate of Crack Mouth Opening Displacement, CMOD, which was measured by an attached LVDT.

Table 2 measured and computed crack opening displacement

Specimen	Peak load (N)	Effective crack length at peak load a_c (mm)	Measured $CTOD_c$ (micron)	Calculated $CTOD_c$ (micron)	Measured $CMOD_c$ (micron)
S1	644.59	72.72	31.14	29.60	76.35
S2	542.58	76.40	36.45	36.47	89.70
S3	551.64		36.11		
S4	448.57	79.18	33.31	40.40	96.40
S5	444.13	76.86	36.90	39.52	94.37
S6	461.83		37.53		

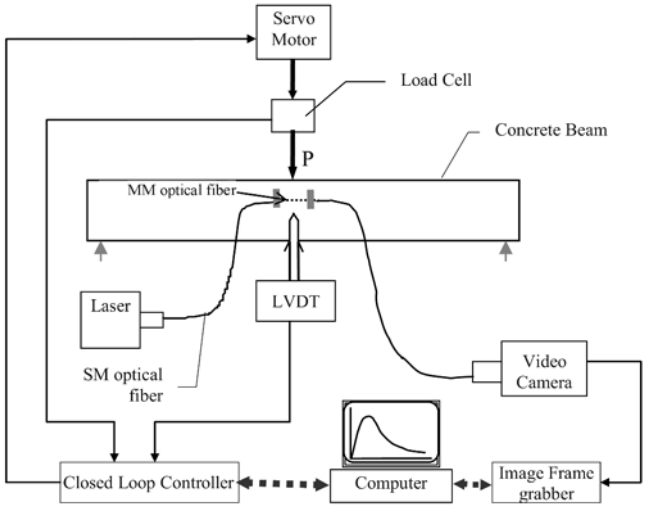

Figure 3 Three-point bead beam test setup

4. EXPERIMENTAL RESULTS

Typical load versus measured CTOD and CMOD results are shown in Fig.4. Critical CTOD and CMOD results for all of the specimens are given in table 2. However, conditioner unit for the LVDT malfunctioned during tests for specimens S3 and S6, and for this reason only CTOD data are reported for these beams in table 2.

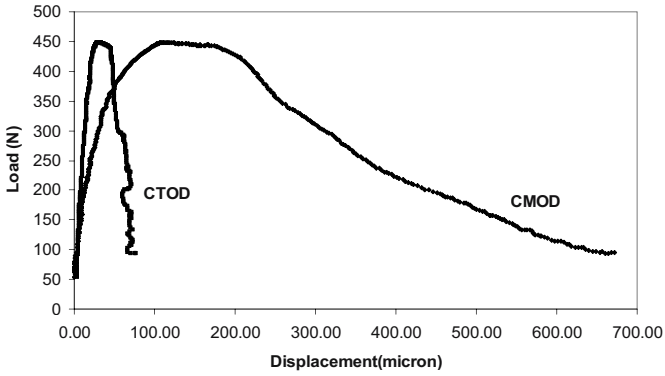

Figure 4 Comparison of typical measured CMOD and CTOD responses of the concrete beam

5. ANALYTICAL INVESTIGATION

To evaluate the validity of such methods, an effective-elastic crack approach is employed for computation of CTOD, effective crack length, and comparison of the computed values with the experimental results. The effective-elastic crack approach uses the Griffith-Irwin fracture energy dissipation mechanism and models the fracture process zone by employing an equivalent, traction-free elastic crack. The CTOD could be calculated with the combination of the following equations [8]:

$$CMOD = \frac{4\sigma a}{E} g_1\left(\frac{a}{b}\right) \tag{4}$$

$$CTOD = CMOD g_2\left(\frac{a}{b}, \frac{a_0}{a}\right) \tag{5}$$

$$\sigma = \frac{3PS}{2b^2 t} \tag{6}$$

Where, σ is tensile stress at the crack tip, P is the load, S is the span length, b is the width, and t is the depth of the beam, a_0 is the initial notch length, and a is the effective elastic crack length. The functions g_1 and g_2 are

related to geometric dimensions of the beams and for the beams studied here (S/b=6.2), they were estimated by interpolation with those for S/b = 4 and pure bending [8]. The modulus of elasticity E can be determined through the method proposed by RILEM [9]:

$$E = \frac{6Sa_0 g_1\left(\frac{a_0}{b}\right)}{C_i b^2 t} \tag{7}$$

Where C_i is the initial compliance determined from Load-CMOD curve.

The computed critical CTOD and effective crack lengths are included in Table 2, the crack opening displacements are compared with the experimentally determined values. As shown in this table, there is a close agreement between the computed and the measured values of critical CTODs. The computed and measured crack opening displacements for two extreme cases are further compared in Fig.5. As shown in the load–CTOD responses, while one of the beams exhibited an almost perfect match between the computed and measured crack opening displacements, the other did not, except for the peak value. The match between the computed and measured pre peak load-CTOD response for other specimens fall somewhere in between the two extreme cases and are shown in Fig. 6.

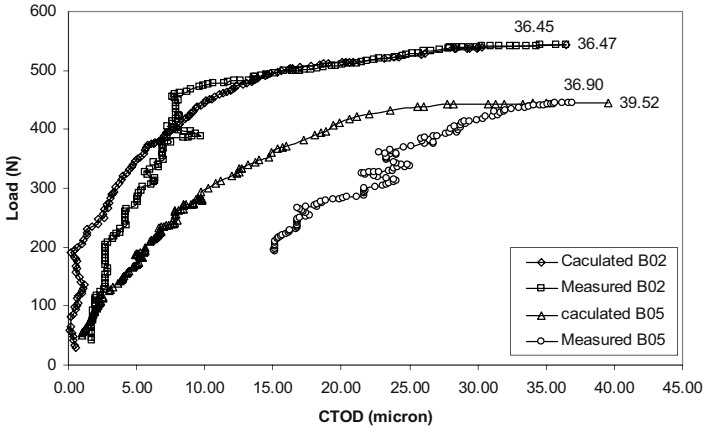

Figure 5 Comparison of measured and calculated CTOD for beams S2 and S5

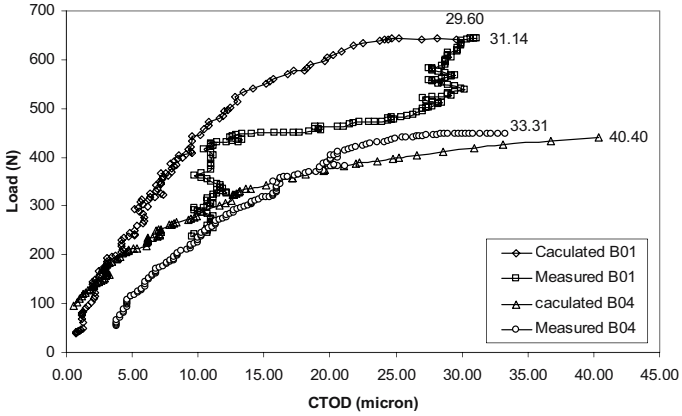

Figure 6 Comparison of measured and calculated CTOD for beams S1 and S4

6. CONCLUSIONS

Development and testing of a speckle intensity-based fiber optic CTOD sensor for embedment in concrete has been described. The sensor principle is based on propagation mode intensity modulations in the speckle patterns generated in multi mode optical fibers. Although, the theoretical formulations leading to the sensor characteristics seem complicated, the application and instrumentation is simplistic. The instrumentation includes a communication grade multi mode optical fiber, a laser with a wavelength in the visible range of the spectrum, and a digital video camera. The sensor has a high signal to noise ratio and is very sensitive with displacement measurement capability in the micron level.

The experimental program involved calibration of the sensor as well as embedment in concrete beams. The measured crack tip opening displacements were compared with analytical results and in general the measured and computed values of critical CTOD were in agreement. The proposed sensing technique promises a direct CTOD measurement.

REFERENCES

1. Dawicke DS, Sutton MA. CTOA and crack tunneling measurements in thin sheet 0240T3 aluminum alloy. Exp Mech. 34(4):357; 1994.
2. Dawicke DS, Newman Jr JC, Bigelow CA. Three dimensional CTOA and constraint effects during stable tearing in a thin-sheet material. ASTM STP. 1256:223-242; 1995.

3. Ansari F, Navalurkar R. Kinetics of crack formation in cementitious composites by fiber optics. ASCE, J. of Engineering Mechanics. 119(5):1048-1061; 1993.
4. Lee I, Libo Y, Ansari F, Ding H. Fiber optics crack tip opening displacement sensor for concrete. Cement and Concrete Composites. 19(1):59-68; 1997.
5. Yuan L., Ansari F. Embedded white light interferometer Fibre optic strain sensor for monitoring crack-tip opening in concrete beams. Meas. Sci. Technol. (9):261-266; 1998.
6. Spillman WB, Kline BR. Statistical-mode sensor for fiber optic vibration sensing uses. Applied Optics. 28(15):3166-3176; 1989.
7. Pan K, Uang C, Cheng F, Yu F. Multimode fiber sensing by using mean-absolute speckle-intensity variation. Applied Optics. 33(10):2095-2098; 1994.
8. Tada H, Paris PC, Irwin GR. The stress analysis of crack handbook. 3rd ed.; ASME Press, New York, NY, 2000.
9. RILEM Technical Committee 89-FMT (1990). Determination of fracture parameters (K^s_{IC} and $CTOD_c$) of plain concrete using three-point bend tests, proposed RILEM draft recommendations. RILEM, Materials and Structures. 23(138): 457-460.

LOOP TOPOLOGY BASED WHITE LIGHT INTERFEROMETRIC FIBER OPTIC SENSORS NETWORK

Libo Yuan and Jun Yang
Department of Physics, Harbin Engineering University, Harbin 150001, China

Abstract: Based on the one loop network technology, a coupled dual-loop network bi-direction interrogating technique has been developed and demonstrated. A practical implementation of theses coupled dual-loop schemes is configured by use of a popular ASE light source and standard single mode fiber, which are commonly used in communication industry. The sensor dual-loop topology is completely passive and absolute length measurements can be obtained for each sensing fiber segments so that it can be used to measure quasi-distribution strain or temperature. For the large-scale smart structures, this technique not only extends the multiplexing potential, but also provides a redundancy for the sensing system. It is mean that the coupled dual-loop sensors network permit two points breakdown, because the sensing system will still work whenever the embedded dual-looped sensors has been destroyed in somewhere. The robustness of the 9-sensor coupled dual-loop sensing network are discussed and demonstrated in our experiments. The intensity characteristic of the output signal of the interferometer is analyzed and verified by the experimental results.

Key words: multiplexing, white-light interferometer, sensing network, coupled dual-loop topology.

1. INTRODUCTION

Based on the one loop bi-directional white light interferometric sensing technique [1,2], the object of this paper is to further propose and discuss the coupled dual-loop schemes of the low-coherence interferometers array sensing system. This is advantageous since it not only extends the

Farhad Ansari (ed.), Sensing Issues in Civil Structural Health Monitoring, 463–472.

multiplexing capacity, but also provides a redundancy and satisfies the needs of indemnificatory and reliability for the sensing system and avoids the whole system failure in case of the embedded sensors chain damaged in somewhere. Therefore, this kind sensor dual-loop network is suitable for the use of large-scale smart structures condition monitoring.

2. COUPLED DUAL-LOOP FIBER OPTICS SENSORS NETWORK TOPOLOGIES

The idea of coupled dual-loop fiber optic sensor network is based on the one-loop schemes, in which a series fiber segments connected each other and linked forming a fiber loop sensor array. The basic configurations of the coupled dual-loop topology are the combination of fiber Sagnac loop and ring-resonator. The combination of the dual loop topologies is classified two types according to the connection in series or in parallel. Totally six kind dual-loop topologies can be configured, four kinds in series and two kinds in parallel, as shown in Fig.1 and Fig.2, respectively. One of the advantages of the dual-loop configuration is the enhanced multiplexing capacity. It is provides more redundancy for the sensing system.

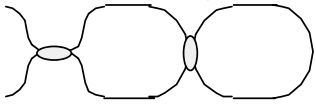

(a) Dual Sagnac-Resonator loop in series

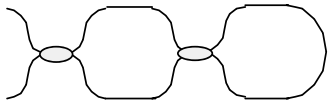

(b) Dual Sagnac-Sagnac loop in series

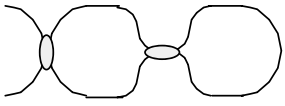

(c) Dual Resonator-Sagnac loop in series

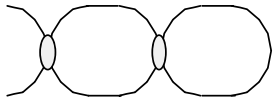

(d) Dual Resonator-Resonator loop in series

Figure 1 *Dual-loop in series topologies.*

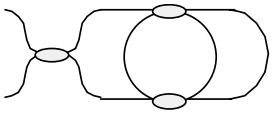

(a) Dual Sagnac-resonator loop in parallel

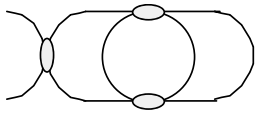

(b) Dual resonator-resonator loop in parallel

Figure 2 *Dual-loop in parallel topologies.*

The sensor array arranged in the dual loop are completely passive and absolute length measurements for each fiber-sensing gauge. The proposed sensing scheme can be used to measure quasi-distribution strain or

temperature. For the large-scale smart structure, this technique not only extended the sensors number, but also provides a redundancy for the sensing system. It is mean that the sensor loops permit one or two point breakdown, because the sensing system will still working whenever the embedded sensor array break in somewhere.

3. COUPLED DUAL-LOOP MULTIPLEXING PRINCIPLE

The fundamental operating of the dual-loop approach is based on optical fiber white light Michelson interferometer. As examples of coupled dual-loop schemes, the configuration of the Sagnac-resonator coupled dual-loop in series (Fig.1 (a)) and in parallel (Fig.2 (a)) of the sensing networks are shown in Fig.3 and Fig.4, respectively.

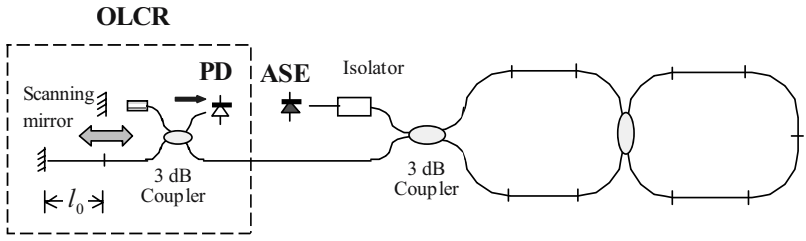

Figure 3 Dual Sagnac-resonator loop in series fiber optic sensor network schemes.

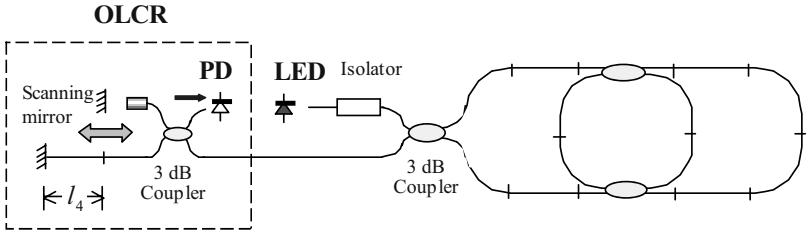

Figure 4 *Dual Sagnac-resonator loop in parallel fiber optic sensor network schemes.*

In the system, the light source is an erbium-doped fiber amplifier that provided up to 10mW of amplified spontaneous emission with a spectral width of 30 nm at wavelength of 1.55 μm. The low coherence light via a fiber optic isolator is launched into the dual fiber loop by a fused 3dB coupler. In the fiber dual-loop sensing part, it is a series fiber segments connected each other forming a sensor array coupled dual loop network. Reflected light from the fiber dual-loop is then coupled onto the optical low coherence reflectometer (OLCR). Inside the OCLR, the light signals split by a second 3 dB coupler. The lower (reference) path is reflected directly by the mirrored fiber end and then leads to the detector. The upper path leads to the

fiber optic collimator and reflected by a moving scanning mirror. While, the downer path directly reflected by the fiber end. Then the two reflective signals guided to the PIN photodiode detector.

The reflectivity of the sensor connection in-line reflectors are very small, it is nearly equal 1% or less of the input optical power. The fiber sensor gauge lengths l_i between adjacent reflectors can be of any value as long as the differences in their lengths are not larger than the scan range of the OLCR. In our experiments, l_i has been chosen about 500-millimeter long and the effective optical path difference l_0 of the OLCR is nearly same as the sensor gauge length. All the differences of the fiber optic sensor lengths are within 270mm corresponding to the 400mm scan range of the OLCR in air space. As the OLCR is scanned, the white light interference patterns occur whenever the path difference matches the distance between adjacent reflectors in the dual-loop.

The multiplexed sensing system is working same as the tandem of a Michelson demodulator interferometer and a series Fieazu interferometers (same as each fiber segment or sensor in the dual-loop). The optical-path difference (OPD) of the Michelson interferometer can be varied through the use of a scanning mirror. The scanning mirror is used to adjust the OPD of the Michelson interferometer to match and trace the change of the fiber length in each sensing segment. We make the OPD of the Michelson interferometer nearly equal to the fiber sensor gauge length, so that the two reflected light waves from the two-end surfaces of each sensing gauge can matched with each other. When the OPD of the Michelson interferometer is equal to the gauge length of a particular sensor, a white light fringe pattern is produced. The central fringe, which is located in the center of the fringe pattern and has the highest amplitude peak, corresponds to the exact match of OPD for that sensor. The optical path matching condition is given by

$$n_0 l_0 + X_k = n_0 l_k \tag{1}$$

Where X_k is the distance between reflective mirror and the fiber collimator, n_0 is the fiber mode refractive index. l_0 is the optical difference of Michelson demodulation interferometer. Therefore, the deformation of sensor *k* can be measured by tracing the change of the mirror moved displacement ΔX_k

$$\Delta X_k = \Delta(n_0 l_k) \tag{2}$$

As the optical path of the fiber sensor is modulated by the ambient perturbation, for instance strain or temperature, then the perturbation parameters related with the optical path change will be measured and

recorded by the shift of the interference signal peak. For the multiplexed fiber optic sensors in the dual-loop, in order to avoid the signals overlap, the gauge lengths of the fiber sensors should be satisfied the following conditions:

$$\begin{cases} l_i \neq l_j \\ \left| l_i - l_j \right| \geq L_c \\ \left| l_i - l_j \right| \leq D_s \end{cases} \tag{3}$$

Where L_c is the coherence length of the ASE light source. D_s is the maximum scanning distance of the reflective mirror.

4. EVALUATION OF MULTIPLEXING CAPACITY

In the fiber optic sensors dual-loop network, the fraction of optical source power coupled into the fiber and distributed it over the sensor array in each sensing branch. Each sensor elements absorbs or diverts a certain amount of power (insertion loss), typically between 0.1 dB and 0.5 dB. If the minimum-detecting limit of the photodiode is $I_{\min}$, then, the maximum number of the total fiber optic sensors can be evaluated by the condition

$$I_D(i) \geq I_{\min} \tag{4}$$

For our experiment sensing system, the minimum detecting intensity is about 2 nW (or –57dBm). The trend line of the maximum vs. the light source power are plotted in Fig. 5 and 6 for different arrangement of the fiber optic sensor in the dual-loop.

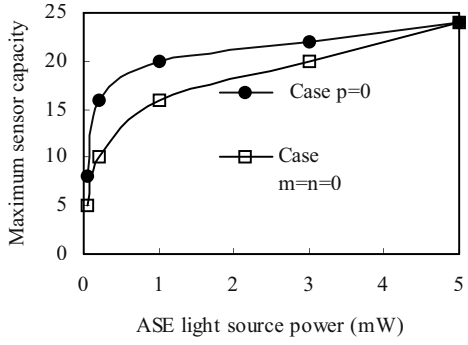

Figure 5 *The ASE light source power vs. the capacity of the maximum fiber sensors in the dual-loop network for case of one of the dual loop without any sensor.*

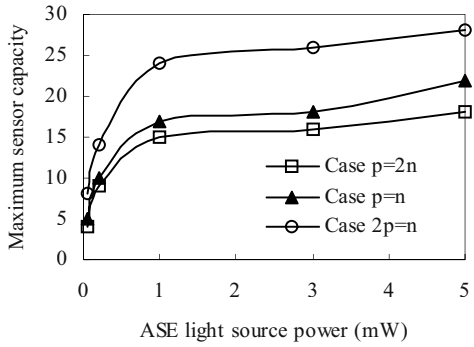

Figure 6 *The ASE light source power vs. the capacity of the maximum fiber sensors in the dual-loop network for case of different size in each sensing branch.*

5. EXPERIMENTAL RESULTS

The experiment setup is shown in Fig.3. The light source power is $1mW$ at wavelength 1550 *nm* with 35 *nm* bandwidth. The scanning range is 400 mm in air and the average insertion losses is about 5 dB with the fluctuation less than 0.2 dB. The totally 9 fiber sensors have been linked in the dual-loop network by butt-connectors and the gauge length of each sensor is about 500 *mm* and the difference in length is nearly equal to 1 mm which corresponding to the 1.5 mm scanning displacement in air. For the 400 mm scanning distance of the translation stage, if makes 1.5 mm fiber sensor gauge length difference include 1 mm dynamic range of each sensor to avoided the signals overlap, the multiplexing capability can estimated over 180 sensors. The sensors arrangement in each sensing branch is depicted in Fig.7. The 9 sensors gauge length and the positions distributed on the scanning translation stage, which is described by equation (1). The output signals characteristic of the 9 fiber sensors are plotted in Fig.8.

A series destroyed simulation experiments have been made to investigate the robustness characteristic of the dual-loop sensors network. The 5 classical breakpoints have been chosen as marked in Fig.7. For the case of only one point has been broken in the dual-loop, Fig. 9,10 and 11 gives the variations of the intensities output characteristics results corresponding to breakpoint P_1, P_2 and P_3 in Fig.7. It can be seen that the 9-sensors of the dual-loop sensing system are still working and each sensor's signal peak is still be there whatever break in point P_1, P_2 or P_3 except that some of sensor's signals amplitude lower then that before.

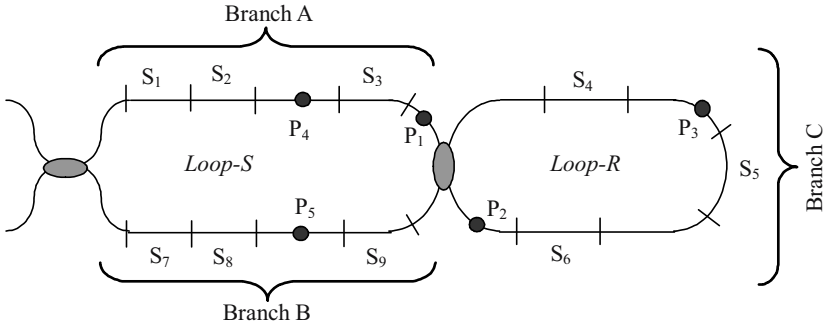

Figure7 *Schematic of 9 fiber optic sensors and 5 experimental break points arrangement in the dual-loop.*

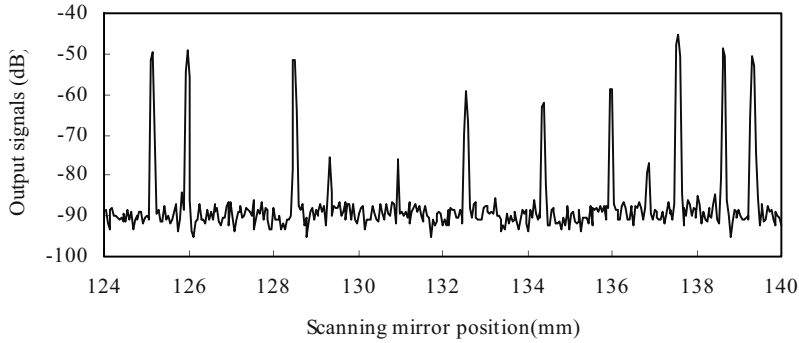

Figure 8 *Output signals characteristic of the 9 fiber sensors distributed in the dual-loop network.*

For the case of two points have been broken, the test results are plotted in Fig. 12, 13 and 14, respectively.

(1) If the broke points are P_1 and P_2, though the dual-loop has been destroyed, the 9-sensors sensing system are still working as shown in Fig. 12. Obviously, the signals intensity of sensor S_4, S_5 and S_6 is greatly reduced;
(2) If the broke points are P_3 and P_4, it can be seen from figure 13 that the output signals of the sensor S_5 and S_6 are vanished except the sensor S_4 signals amplitude has been reduced;
(3) If the broke points are P_3 and P_5, not only the signals amplitude of sensor S_5 and S_6 have been reduced, but also sensor S_3 except the sensor S_4 is invalid, as shown in Fig.14.

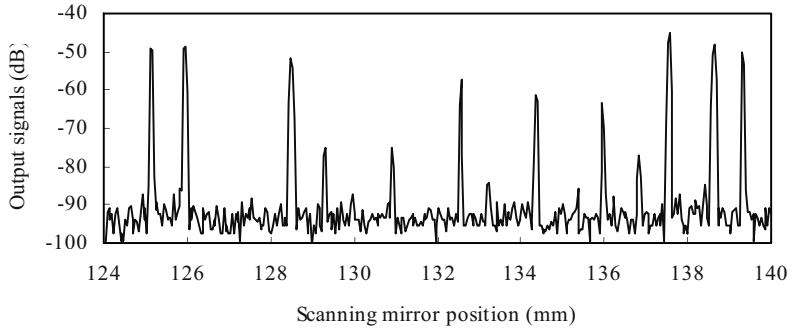

Figure 9 *Output signals variation after the dual-loop breaks only in point* P_1.

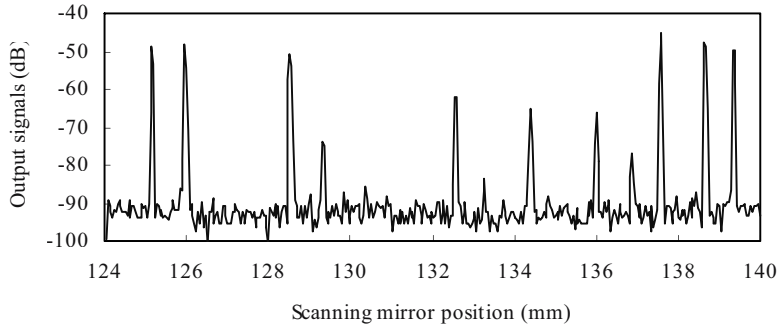

Figure 10 *Output signals variation after the dual-loop breaks only in point* P_2.

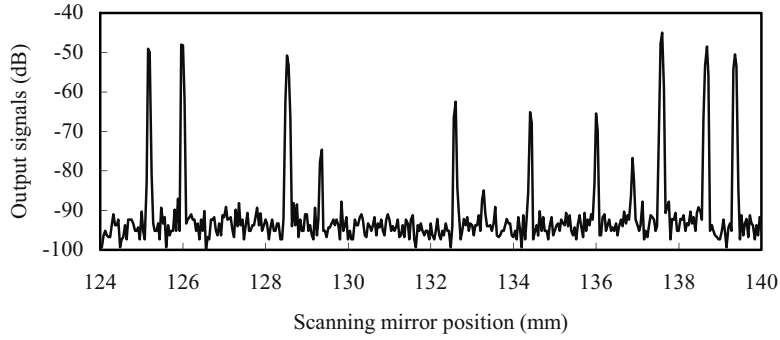

Figure 11 *Output signals variation after the dual-loop breaks only in point* P_3.

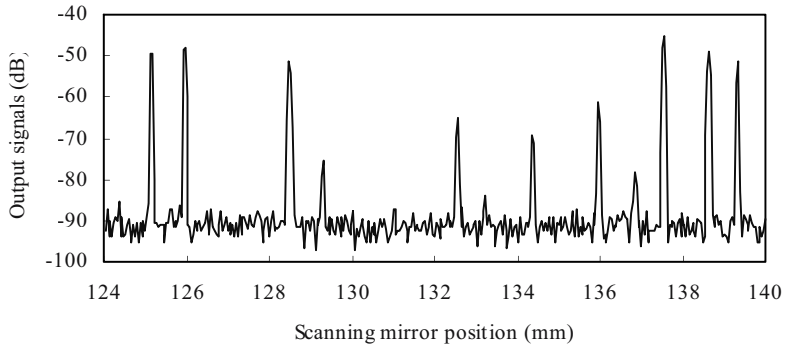

Figure 12 *Output signals variation after the dual-loop breaks in points* P_1 and P_2.

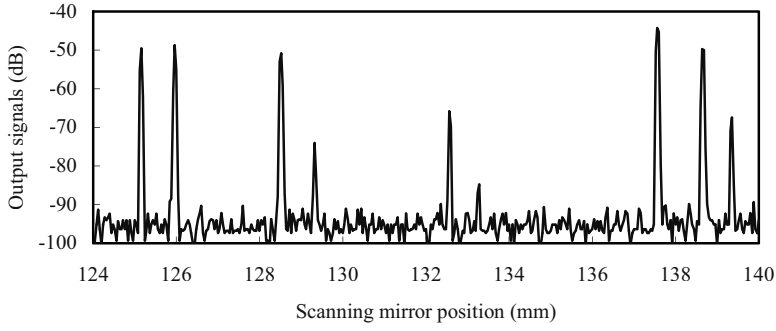

Figure 13 *Output signals variation after the dual-loop breaks in points* P_3 and P_4.

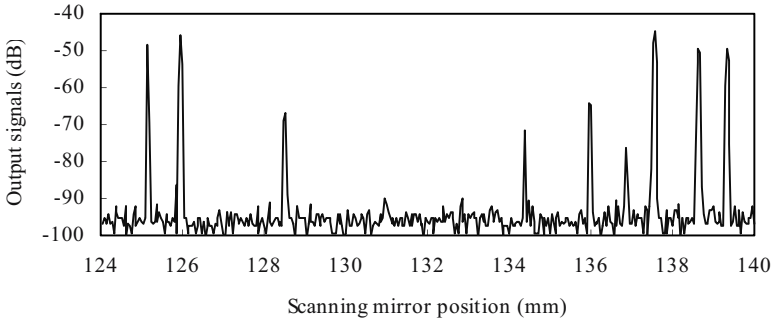

Figure 14 *Output signals variation after the dual-loop breaks in points* P_3 and P_5.

6. CONCLUSIONS

In conclusion, a multiplexed fiber optic deformation sensors based on loop topology network suitable for smart structure applications has been designed and demonstrated. The sensor system is based on white light Michelson or Mach-Zehnder interferometer as optical path demodulator. Such a loop topology is useful to construct sensor network for distributed strain or temperature measurement in smart structures. From the view of the scanning range of the translation stage, the multiplexing system permits to demodulate over 180 fiber sensors. However, it is clear that the multiplexed sensors in the single or dual-loop network suffering from relatively large fiber segments-induced optical reflective and excess insertion losses that generally limit the total number of sensors that can be accommodated in this configuration. It has been predicted that only 27 sensors can be operated on the single loop topology when using a 3*mW* light source [3], while 28 sensors can be operated on the dual-loop topology with ASE light source power 5 *mW*. In addition, this dual-loop network architecture greatly improvement the reliability of the system and provides a redundancy due to the dual-loop topology. It means that even somewhere breakdown of the sensors dual-loop network, the system will still work. Comparing with the case of fiber optic sensors single loop topology, the reliability of the dual-loop system has been further improved. That is the dual-loop sensors network system permitting two point have been broken at same time on the fiber sensors chain, and keep the mainly part of the sensors still work. It avoids the whole sensing system failure due to local damage of the sensors intergraded structure.

ACKNOWLEDGMENTS

This work was supported by the Teaching and Research Award Program for Outstanding Young Professors in Higher Education Institute, MOE, P.R.C., and the National Natural Science Foundation of China, grant number 50179007, to the Harbin Engineering University.

REFERENCES

1. Libo Yuan, Limin Zhou, Wei Jin and Jun Yang, *Optics Letters*, 27(11), 894-896, 2002
2. Libo Yuan, Wei Jin, Limin Zhou,Y.H.hoo and S. M. Demokan, *IEEE Photonics Technology Letters,* **14**(8) , 1157-1159, 2002
3. Libo Yuan, Limin Zhou, Wei Jin, Design of a fiber-optic quasi-distributed strain sensors ring network based on a white-light interferometric multiplexing technique, *Applied Optics*, 41(34), 7205-7211, 2002

Chapter VIII

Long Term Health Monitoring of Civil Structures

MONITORING RESULTS OF A SELF-ANCHORED SUSPENSION BRIDGE

Sungkon Kim 1, Chul Young Kim 2, and Jungwhee Lee 3
1 Department of Structural Engineering, Seoul National University of Technology,Korea
2 Department of Civil Engineering, Myungji Univserity, Korea
3 Korea Earthquake Engineering Research Center(KEERC), Seoul National Univerity, Korea

Abstract: Automatic measurement of instrumented civil engineering structures is now widely applied for behavior monitoring during construction in field as well as long-term monitoring for lifetime assessment of bridge structures.
This paper presents schematically the monitoring system installed in Yeongjong Bridge, a self-anchored suspension bridge located in the expressway linking Seoul and Incheon International Airport. Since (1) appropriate instrumentation, (2) reliable signal processing and (3) intelligent information processing constitute the major features to be considered for deploying proper monitoring system, corresponding general guidelines and suggestions are also proposed.
In addition, a representative example of results that can be acquired through structural health monitoring system is presented by means of data measured during 2 years after the opening of the bridge.

Key words: Monitoring system, bridge condition, assessment, health monitoring, sensor

1. INTRODUCTION

Automatic measurement of instrumented civil engineering structures is becoming more common for both diagnostic system identification purpose and in-field behavior monitoring during construction. In order to deploy a successful monitoring system, the required considerations are: proper instrumentation, reliable signal processing and knowledgeable information processing. Since instrumentation, which includes sensory device and data acquisition system (DAQs), obtains raw data from the real structure, sensor

Farhad Ansari (ed.), Sensing Issues in Civil Structural Health Monitoring, 475–484.

technology is of critical importance in the development of a monitoring system.

A number of sensor and sensing techniques have been developed in recent years which bear the potential for meeting the eventual need of an automatic monitoring system. These fall into the domain of remote sensing and nondestructive testing. Selection and installation of proper sensors constitute key considerations. Beyond the sensory system itself, some additional facilities need to be located in the field as well as in the control space. These facilities consist of DAQs, temporal data storage device, telecommunication facilities, and other auxiliary devices.

Sensor signal must be processed and interpreted. Immense volume of often noisy signals generated by a multiple-channel sensory should be manipulated concurrently and interpreted intelligently in both hardware and software. The signal processing procedure consists of numerous operations beginning from signal acquisition, generation, to interpretation. In order to assess the current condition of the structure based on signals, called as information processing, it is necessary to devise appropriate computational abstractions and support environments. To develop comprehensive computational environments for these purposes, a model of the information describing the system is required. This model must support a meaningful and computable representation of the components and their complex interrelationships that are characteristic of engineering system, such as physical configurations, sensors, signal processing, and diagnostic knowledge **[1]**.

2. BRIDGE DESCRIPTION

Yeongjong Bridge, completed in November, 2000, is a part of the Incheon International Airport Highway which connects Seoul and Incheon International Airport. Being the first bridge foreign visitors meet when arriving in Korea, particular attention has been paid on its design with unique features such as three-dimensionally profiled suspension cables, self-anchoring, and double decks for both automobile and train traffic.

The last design draft established in 1993 has been reviewed and completed in 1998 to fulfill the revised specifications and improve the structural safety and efficiency of construction. Yeongjong Bridge, shown in Figures 1, is a three-span continuous double deck self-anchored suspension bridge with a center span of 300 m long and side spans of 125 m long. Table 1 summarizes the principal characteristics and dimensions of the bridge.

Figure 1. Overview of Yeongjong Bridge

Table 1. Features of Yeongjong Bridge

Length	550 m (125+300+125 m)
Type of superstructure	Double deck Warren truss (height 12 m, width 35 m) - Upper deck: 6 roadway lanes - Lower deck: 4 roadway + 2 train lanes
Type of pylon	Diamond shaped steel pylon
Type of pylon foundation	Pneumatic caisson foundation
Suspension cable	3D cable (φ467.4 mm @ 14 strands) with dehumidification system - Vertical sag: 60 m - Lateral sag: 13.57 m

3. HEALTH MONITORING SYSTEM OF YEONGJONG BRIDGE

Health monitoring systems in Korea at the very beginning were installed in existing bridges in order to collect field data by full scale load capacity tests for design verification and, subsequently, evaluate the health of the structure. Immediately after the collapse of Seongsu Bridge, this first generation of monitoring systems has been applied in existing bridges, such as Namhae Bridge and Jindo Bridge.

Unlike earlier applications of health monitoring system, where conventional sensors, loggers and transmission methods were used and individual system served each bridge independently, recent systems that are usually adopted in newly built bridges, including Yeongjong Bridge, employ many modern technologies from sensing to processing. And also, an attempt to integrate health monitoring systems of several bridges together has been

made in order to reduce the total cost and to increase efficiency of management. This integrated system includes Bridge Management System (BMS) for inspection, evaluation, estimation and rehabilitation **[2]**.

A total of 393 sensors, including static and dynamic strain gauges, and 23 data loggers are distributed over the bridge. The hardware system was designed to remote collect data, and the software system was developed to process data and to display the results in a custom-designed format. The sensors installed in the bridge are categorized based on their locations and physical parameters measuring as listed in Table 2.

Table 2. Description of the sensors installed in Yeongjong Bridge

Category	Measurand	Sensor	Quantity	Location
Load	Temperature	Thermometer	21 ea.	Cable & Deck
			12 ea.	Tower
	Wind Speed/ Dir.	Anemometer	5 ea.	Tower, Cable, Deck
	Earthquake	Accelerometer	3 ea.	Tower foundation
Response	Geometry	Laser Disp. Sensor	5 ea.	Girder
		Potentiometer	4 ea.	Expansion joint
		Tiltmeter	10 ea.	Tower
	Hanger Tension	Accelerometer	12 ea.	Hanger
	Strain	Static Strain Gauge	32 ea.	Anchor bolt
			42 ea.	Deck cross section
			40 ea.	Anchor plate
			8 ea.	Link shoe
		Dyn. Strain Gauge	76 ea.	Deck cross section
			99 ea.	Etc.
	Acceleration	Accelerometer	4 ea.	Tower
			10 ea.	Deck

4. HEALTH MONITORING RESULTS

The monitoring system has been completed in 2001 and a huge volume of signals has been collected up to date. These signals were carefully analyzed for verifying the system performance and implementing further use for bridge health assessment. During the system stabilization period, signals showed regular pattern of fluctuation along with the daily and seasonal temperature changes. Some typical signal patterns are described here.

4.1 Hanger Tension Force

Hanger tension forces are obtained using the ideal vibrating chord theory **[3-4]**. As listed in Table 2, accelerometers were mounted on 12 representative hangers to evaluate tension forces. Frequencies computed

from responses measured under ambient vibration by these accelerometers were used to obtain tension forces.

No particular trend was observed from the analysis of the tensile force in each of the 12 hangers separately. However, the average of tension force for the whole set of hangers presented similar shape to the fluctuation of ambient temperature, as shown in Figure 2. This average ranged between 789 kN and 800 kN, which corresponds to a variation of ±1.4% compared to the overall mean value.

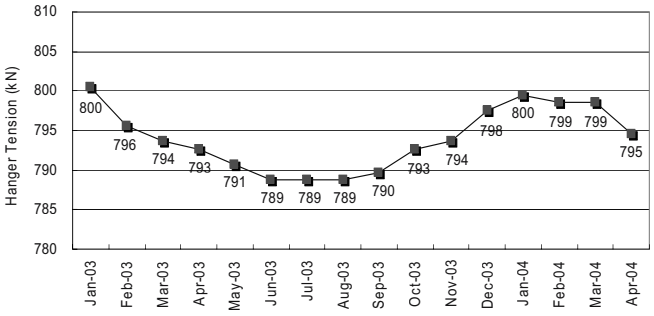

(a) Averaged hanger tension

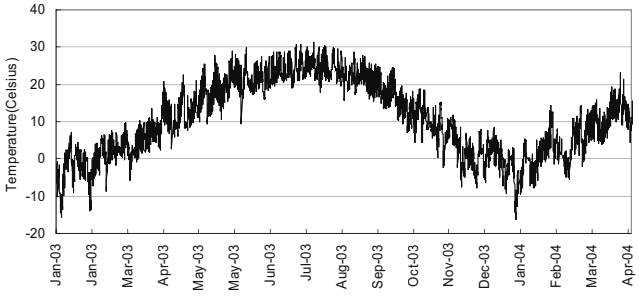

(b) Ambient temperature

Figure 2. Averaged hanger tension and ambient temperature observed during 15 months

4.2 Displacement of Expansion Joints

Joint displacements of both ends were seen to be essentially affected by temperature changes. Figure 4 plots the quasi-linear relationship observed between joint displacement and temperature. Displacement of the expansion joints averages 46 mm for a thermal variation of 10°C in ambient temperature.

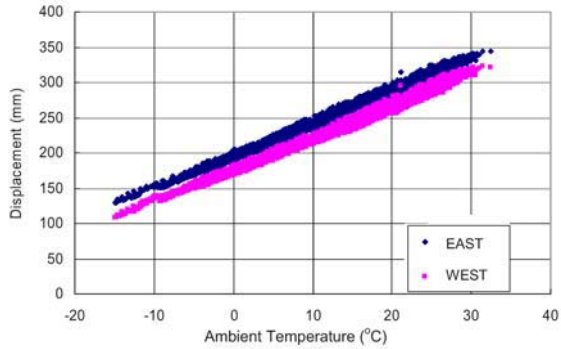

Figure 4. Joint displacement and ambient temperature measured in Yeongjong Bridge

4.3 Vertical and Lateral Displacement of Stiffening Girder

Vertical and lateral displacements at mid span measured by laser displacement sensor presented also the same seasonal pattern according to temperature changes. Vertical bars in the figures represent monthly fluctuation. Fluctuations of the vertical and lateral displacements ranged from –4 to 47 mm and from 2 to 43 mm, respectively.

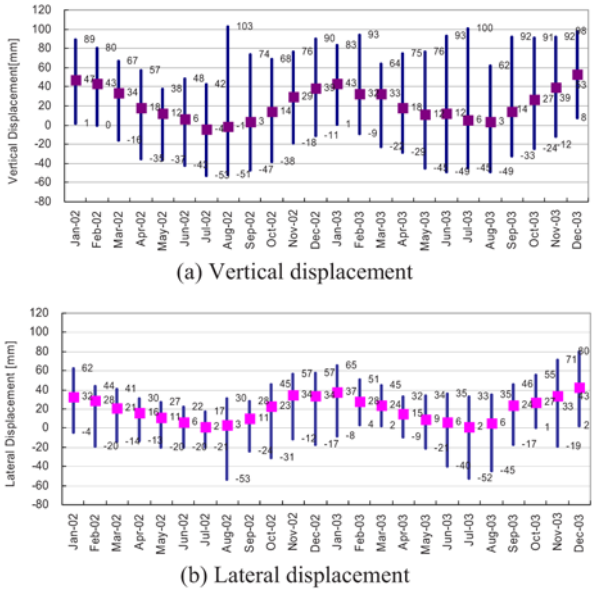

Figure 3. Displacements at mid span observed during 2 years

4.4 Acceleration and Frequencies

Dynamic properties have been analyzed using acceleration data under ambient vibration as shown in Figure 5. Measured frequencies of the 1st and 2nd modes are 0.494 and 0.831 Hz, which show almost no difference compared to the field vibration test results, 0.487 Hz and 0.810 Hz. Since temperature changes have direct influence on the dynamic properties of bridge structure **[5]**, temperature effects on the dynamic properties will be investigated in the future.

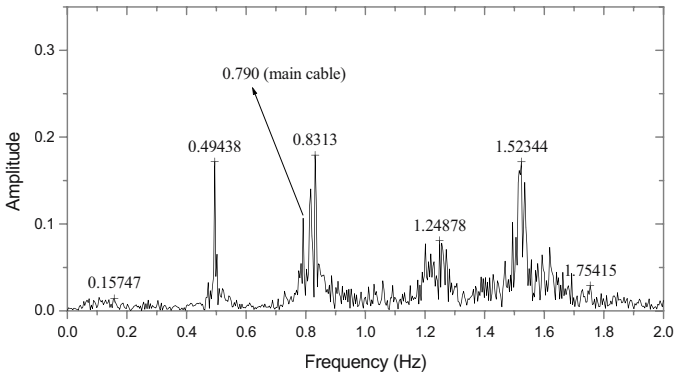

Figure 5. FFT spectrum of ambient acceleration signals measured in Yeongjong Bridge

5. DATA ANALYSIS: CONSIDERATION OF TEMPERATURE EFFECT

In Chapter 4, long-term responses of Yeongjong Bridge were seen to be governed by daily and yearly variations of temperature. Following, researchers aimed the assessment of the actual state of the bridge through the analysis of structural responses regard to temperature.

For this purpose, functional relations between temperature and structural response are defined before analyzing currently measured signals. Structural change or damage is found to occur when measured signals do not agree with the so-predefined temperature-response relationships **[5-6]**. Various kinds of system identification methods including neural networks, statistical method, and optimization method can be employed to construct a mathematical function. Among them, the ARX model, a statistical time series analysis method, is used for Yeongjong Bridge's data analysis.

Figure 6 plots the vertical displacements measured at center span during 30 months from July 2001 until December 2003. It is observed that vertical

displacements show a recurrence period of 1 year. Similarly, vertical displacements also show a daily periodicity as seen in Figure 7. Since Figure 6 as well as Figure 7 presents similar patterns to the temperature data shown in Figure 2(b), a strong correlation between temperature and displacement can be expected.

Temperature data measured during 18 months from July 2001 at 18 locations (12 at both pylons, 6 at cables) have been utilized together with the vertical displacement data measured during the same period to construct the ARX model. Then, the constructed ARX model was used to analyze data measured during the remaining 12 months.

The ARX model appeared to simulate closely the new displacement responses as shown in Figure 7. The slight differences between measured and simulated responses, plotted in Figure 8, may be explained by the effects of other loadings like vehicle load that were not considered when constructing the model. Assuming that these differences are normally distributed, evaluation of the health of the structure can be done through threshold values expressed by a mean, standard deviation, and appropriate confidence level. An example of threshold values for 99% confidence ($\mu \pm 2.58\sigma$) is shown in Figure 8. In case measured data exceed the threshold values or biased responses are continuously acquired, investigation should be performed to determine if such errors are caused by dysfunction of sensor, increase of traffic volume or, in worst case, structural change or damage.

When data fall within the confidence range, as shown in Figure 8, it can be assumed that the structure is healthy and that no structural change or damage occurred.

In addition, deflection that does not consider thermal effects (Figure 9) is seen to be produced essentially by traffic loads. Following, comparison of such deflection with the one induced by design loads makes it possible to evaluate the margin or excess of the actual traffic regard to design values.

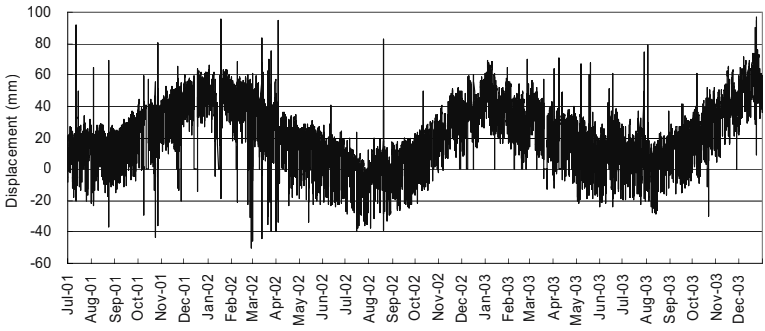

Figure 6. Vertical displacements of center span in Yeongjong Bridge

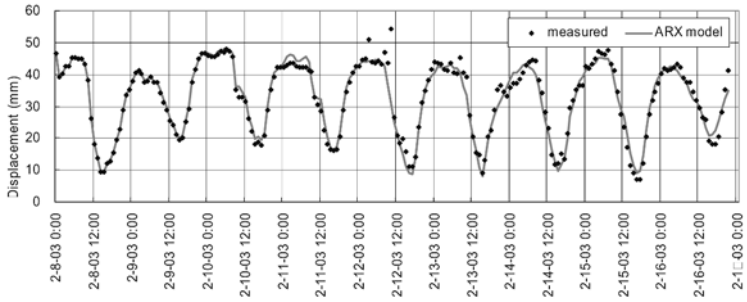

Figure 7. Comparison of displacements computed and measured during 10 days

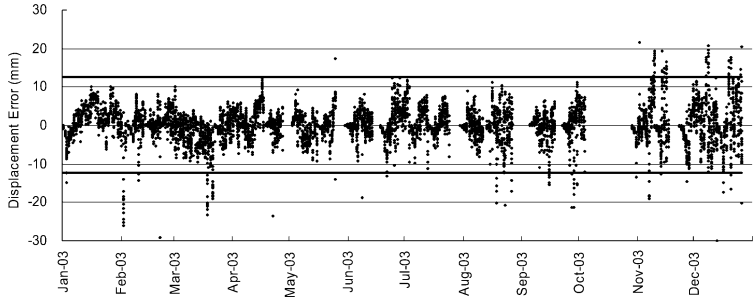

Figure 8. Difference between displacements computed and measured during 1 year

6. CONCLUSIONS

The monitoring system installed in Yeongjong Bridge is an integrated structural health monitoring system which is composed of sensors, data acquisition systems, signal transmission devices, signal control systems, and computer networks. This system has been successfully installed based on a proper development strategy. After its complete installation, test operation was performed on the system during one year, making it possible to stabilize the system and bring several rearrangements and minor changes in its configuration. The stabilized system produced valuable data to be used for health assessment of the bridge. The analysis of measured data verified that the behavior of the bridge is essentially governed by yearly and daily fluctuations of the temperature. Detailed analysis results of current signal data reveal that the bridge behaves as expected. Other research directions

have also been addressed to improve future performance of the monitoring system.

ACKNOWLEDGEMENTS

The authors would like to acknowledge the support of the New Airport Highway Co., Seoul National University, and Seoul National University of Technology.

REFERENCES

1. Chen SS & Kim S. "Automated signal monitoring using neural networks in a smart structural system", *J. Intelligent Material Systems and Struct*., **Vol.6,** pp.508-515, 1995.
2. Koh HM, Choo JF, Kim SK, and Kim CY. "Recent application and development of structural health monitoring systems and intelligent structures in Korea", *Structural health monitoring and intelligent infrastructures*, Wu & Abe (eds): pp. 99-111, 2003.
3. Yoon JG, Sohn J, Chang SP. "A study on tension measurement for cable-supported bridge", *Proceedings of the Annual Symposium of Korean Society of Civil Engineers,* **Vol.1**, pp.117-120, 1999 (in Korean)
4. Zui H, Shinke T, and Namita Y. "Practical Formulas for Estimation of Cable Tension by Vibration Method", *Journal of Structural Engineering*, **Vol.122**, **No.6**, pp.651-656, 1996.
5. Sohn H, Dzwonczyk M, Straser EG, Kiremidjian AS, Law KH and Meng T. "An experimental study of temperature effect on modal parameters of the Alamosa Canyon Bridge", *Earthquake Engineering and Structural Dynamics*, **Vol.28**, pp.879-897, 1999.
6. Hwang S. Temperature Effect on Structural Health Monitoring of Cable Supported Bridges, M.S. Thesis, Seoul National University, Korea, 2003.

LONG-TERM MONITORING OF A HYBRID CABLE-STAYED BRIDGE

Guanyong Zhang
Department of Bridge Engineering, Tongji University, Shanghai, China

Abstract: Various methods have been employed for health monitoring of cable-stayed bridges. It is of great interest and importance to choose the appropriate methods and instruments in terms of reliability, durability and long-term costs. This paper provides a case study of the in-service monitoring of a recently-built long span hybrid cable-stayed bridge, Queshi bridge, in southern China. Three parameters, namely the cable force, main structure deformation and vibration, were monitored with different methods at regular intervals in a span of a few years. The results are very satisfactory and encouraging, and provide vital healh information of the bridge to the transportation authority.

Key words: Cable-stayed bridge, health monitoring, cable force, deformation monitoring, vibrational characteristics

1. INTRODUCTION

The bridge management is very much interested to know that if some of the parameters of the structure in service, such as bridge axis and elevation, inner force status and vibrational characteristics under heavy dead and living load, change in linear and predictable manner. The bridge engineers, on another hand, are more interested to identify the mechanism of deterioration of the structure and how to maintain the good health of the structure. It is more and more required for the management of a modern bridge to develop some methodologies and technical capacities to establish and sustain a database for the bridge health monitoring.

Farhad Ansari (ed.), Sensing Issues in Civil Structural Health Monitoring, 485–494.

As part of synchronized effort in the bridge management, it has being carried out a systematic in-service monitoring of bridges since 2001. The key parameters of the monitoring include:

(1) Cable force under dead load
(2) Deformation of main girder and tylon, settlement of the foundation
(3) Vibrational characteristic of the structure

The cable force and deformation of the structure are measured once per year, and the vibration characteristics are however measured every five years according to the monitoring program. The program is being implemented as the following.

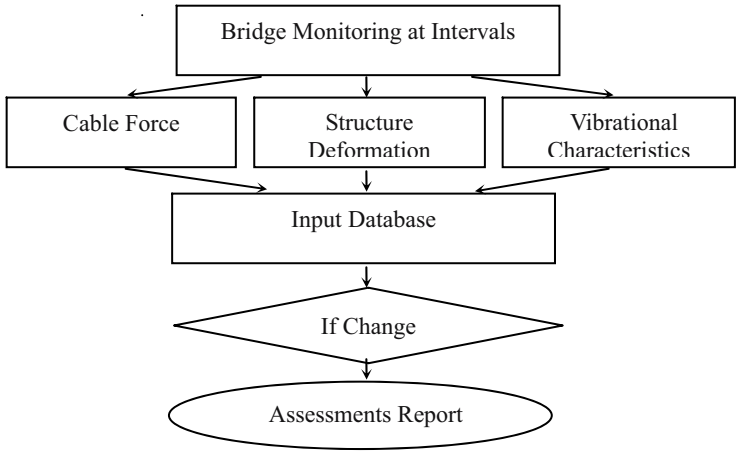

Fig.1 Bridge monitoring program

The methods and instruments used in the health monitoring program for the Queshi bridge will be described along with some practical implementation issues [1].

2. DESCRIPTION OF THE BRIDGE

Queshi Bridge at Shantou of Guangdong province in China was built in 1998 and is a first hybrid cable-stayed bridge with double pylon, double cable planes, and both steel and concrete composite box-girder of 30.35m wide. The bridge has six lanes with a total length of 2402m and a main span of 518m. The A-formed pylon of 148m height is adopted. The steel box girders are used for the 518m middle span and two 100m side spans while the prestressed concrete girder are applied everywhere else. The steel and

concrete boxes are of the same size and they are all flat structures with separated boxes and lateral beams. The rational design of the bridge assures great performance of seismic and strong wind resistance of the structure. The whole bridge has 160 parallel spiral-wire-strands cables cover by PE (polyethylene material) with high viscous sheared dampers installed outside. Fig. 2 shows the structure of the Queshi bridge.

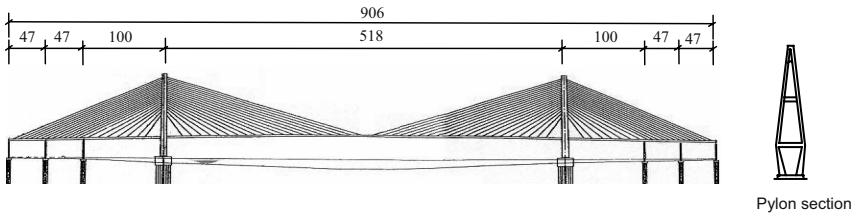

Elevation(m)

Fig.2 Queshi bridge structure figure

3. CABLE FORCE MEASUREMENT

The cables subjected external force is one of the most important structure members in the cable-stayed bridge. The variation of cable forces is a measure showing whether a bridge maintains the normal structural status or not, since the internal force of the bridge really depends on these cables force under the dead load to a great extent. By monitoring the cable forces of a long span cable-stayed bridge under the dead load at a regular intervals, not only the change of those cable forces can be understood so that a basis might be provided to rate the status of whole bridge, but the status of anchor system of the cable can also be determined to a certain extent.

3.1 Methodology

Ambient random vibration method is adopted to measure the lateral vibration. The measuring system, with very good low frequency signal response, has four channels and includes piezoelectric accelerators, filters, amplifiers, and dynamical signal acquisition and processing units. The calibration is carried out in the field prior to each test. The individual cable force is calculated by analyzing the acquired power spectrum in conjunction with such parameters as cable length, mass, stiffness, cline and boundary

condition of the cable. The tests are carried out in deep night and the traffic with few trucks are not interrupted.

3.2 Results and discussions

Fig. 3 shows an example of monitored cable forces (c1 to c20, 20 per 1/8 cable plane) from 2001 to 2004. The relative errors of the measured cable force for the critical center span between 2001 and 2002 year are also showed in Fig. 4. S and N denote southern and northern pylon, and Up and Down denote two side of the cable plan on the deck as showed in Fig. 6. All data were stored in a database for the bridge.

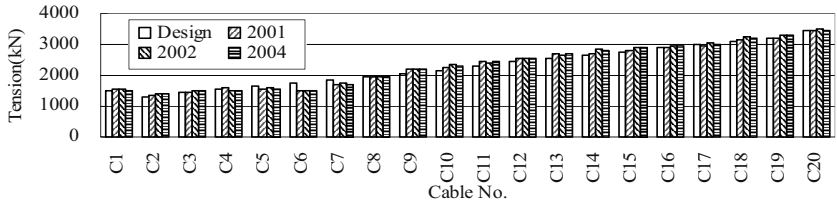

Fig.3 The comparison of the cable forces over the years (1/8 cable plane)

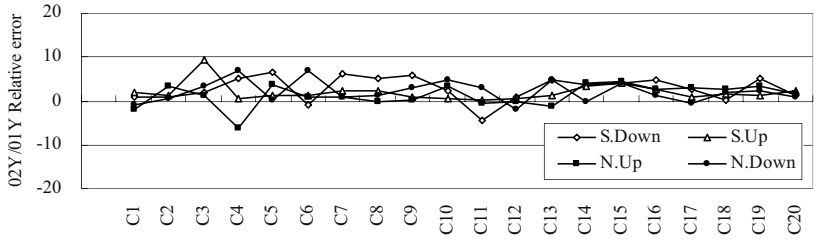

Fig.4 Relative errors of the cable forces between 2001 and 2002 (1/2 cable)

The database for the cable force has helped the bridge management to understand and monitor the health of the structure in case of potential damage happened. For instance, in 2003, there was an accident that a truck was droved out of the lane, and the c14 cable of the side span was severely impacted and the damper was almost broken. However, by checking the cable forces close to the damaged cable in the field and comparing it with pre-incidence data, the inspection engineer was able to make a sound judgment of the health condition of the bridge.

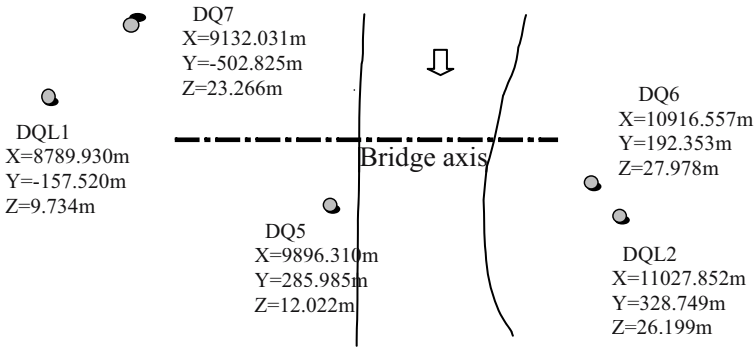

Fig.5 Control stations and net near the bridge

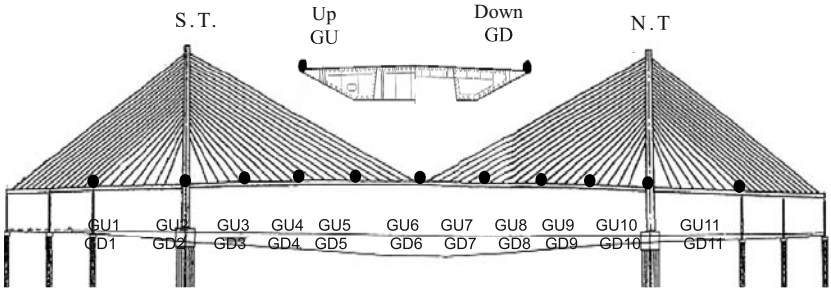

Fig.6 Deformation monitoring points on bridge deck

It must be pointed out that the method for measuring the cable force is a correct chose for the measurement of a amount of cables in the field where the efficiency be required and the time be limited. It takes only of 2 nights to finish the measurement of 160 cables in general.

4. DEFORMATION MONITORING OF GIRDER AND PYLON

The deformation of the bridge is an important control parameter. The pylons and girders might be overly deformed under external load in service. The engineers need to make sure that the deformation of the structure is within the tolerance of the design and there is no deviated axis, because any deformation deviated from the original design may cause additional bending

moment in pylon or girders, and therefore makes the axis of bridge deviate away from the normal position.

The foundation of bridge is also subjected to deformation under the superstructure dead load and heavy truckload. It will certainly change the elevation and space position of the pylons and girders, and will also likely cause addition changes of internal force of the structure if the settlement of foundation is too large or not uniform. Therefore it is necessary to monitor the settlements of the foundation and assure these settlements change in a regular way [2].

Deformation monitoring is actually to measure the three dimension coordinates of the control sections of the bridge when total station apparatus are applied. They include

- Three dimension coordinate of the girders
- Three dimension coordinate of the top and bottom of the pylons
- The subsidence and deformation of the piers of six anchor spans
- The torsion deformation of box girder

4.1 Monitoring method and instruments

It is essential to set up a control stations net for long term monitoring. A net with five permanent stations around the bridge used in the bridge construction will be utilized for the current monitoring task, so that all data is unified and continuous. Fig.5 shows the locations of these control stations of around the bridge. There are total 48 monitoring points (MP), 22 in two sides of the deck, 14 on the Pylon, and the rest of those on the 6 piers respectively. Fig.6 shows the locations of the measuring points on the deck. Some steel pieces were welded on the deck at all measuring points where all prisms can be conveniently installed and measured.

Two sets of Leica TCA2003 total stations, advanced apparatus that are able to measure angle with a resolution of 0.5 second and distance with an accuracy of ±1mm+1ppm to the range of 3500m, were used in the field. With automatic target recognition technology, each prism can be located and its geometric center can be identified to provide precise target pointing. The two sets of total stations are used to measure two sides (up and down of the river) of the girders and the pylons. The traffic was suspended and the tests were carried out at night at the time of measurement for the deformation of the girders and pylons. However, the traffic interruption was not required for the deformational measurement for the foundations.

4.2 GPS method

Global positioned system (GPS) technology was also employed to measure the static three-dimension coordinates and the dynamic vertical displacement of the deck as an alternative to monitor the deformation of the long-span bridge in 2002. Static measurement involved four sets of S530 GPS receivers in the field. The three of them were installed in the three sections with equal spacing (1/4 section of the center span) on the axis of the deck, another was put on DQL1 (see Fig. 5) as the reference station. The data was acquired over twenty minutes during the measurement with total stations after the traffic was shut down. For the dynamic measurement, there are seven measuring sections (1/8 section of the center span) on the axis of the deck for generating real time kinematics (RTK) during rush hour. The DQL1 (see Fig. 5) was again taken as the reference station, where one set of GPS receiver was placed. Another set portable GPS receiver was moved from one point to another and each measuring point took five minutes.

4.3 Results and discussion

Fig. 7 shows an example of the measured elevations of eleven monitoring sections by Leica TCA2003 total stations. The temperatures at the time of measurement and other conditions are the same. The new data each year be listed out and compared with old data last year, so any change MP coordinate in the structure will be checked out and provided to the management engineers.

Unit : m

Sections	G1	G2	G3	G4	G5	G6	G7	G8	G9	G10	G11
2002 ①	35.365	38.814	40.997	42.507	43.451	43.557	43.269	42.461	40.976	38.722	35.512
2001 ②	35.368	38.814	41.004	42.519	43.470	43.581	43.282	42.471	40.982	38.727	35.509
① - ②	-0.003	0.000	-0.006	-0.013	-0.019	-0.024	-0.013	-0.011	-0.007	-0.006	0.003

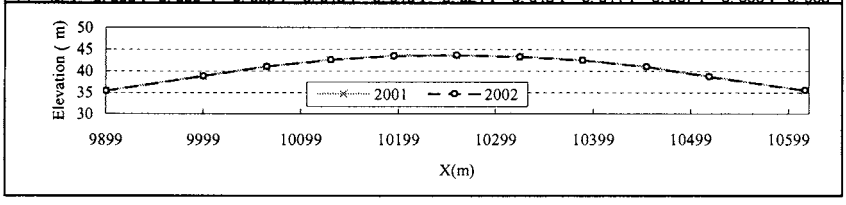

Fig.7 An example of the elevations curves of 11 monitoring sections on the axis of the bridge deck

Since all the control stations net near the bridge and monitoring points on the structure comprise of a deformation measuring system ready for use anytime, obviously this monitoring system is a relative appropriate and reliable method to monitor the long-term deformation of long span bridges.

The results of GPS static measurement is basically in consistant with the results of the total stations, and the absolute error of the measurement in the longitudinal and lateral directions of the deck is about 10mm and the elevation is over 50mm. The results of RTK, however, seems to be not better than the static data. Application of GPS, particularlly the RTK, for monotoring the long-span bridges is a ongoing work.

5. VIBRATION CHARACTERISTICS

Vibration characteristics is believed to be the finger data of the veins of the bridge structures, and it reveals not only the total stiffness, mass and their distribution as a initial status of the structure, it also accounts for part of the problems of structure to a great extent. In this study, the main parameters of vibration characteristics of the structure, which includes modes, frequencies and damping ratio, will be part of the established database for the health monitoring of the bridge.

An ambient method was used to measure vibrating signal through appropriately set points in the field, and a special data processing method by modal analysis was employed to obtain three basic vibrating parameters relating to the vertical, lateral and torsion modes of the bridge. Fig. 8 shows the location of measuring points on the deck; there are totally 58 points at 28 the sections.

The measuring instruments were similar to those used for measuring cable force, but the piezoelectric accelerator with a big of mass was of higher sensitivity and better stability. The vibration response of the bridge deck was characterized with no traffic, normal traffic and rush hour traffic respectively in order to obtain and explain why and what dynamic responses can be expected under live load. This is an ongoing work starting from the year of 2004. Table 1 lists the vibration parameters of first 10 measuring points.

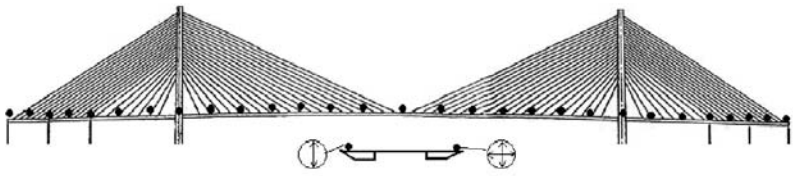

Fig.8 Measuring points on the deck

Table 1. Vibration parameters of first 10 measuring points

No.	Frequencies (Hz)	Modes	Damping Ratio	
			Range	Average
1	0.3027	Ver. bending s.*	0.0098~0.0119	0.0112
2	0.3174	Lat. bending s.	0.0153~0.0189	0.0176
3	0.3955	Ver. bending as.**	0.0104~0.0130	0.0122
4	0.5762	Ver. bending s.	0.0094~0.0120	0.0108
5	0.6885	Torsion s.	0.0079~0.0116	0.0091
6	0.7666	Ver. bending as.	0.0093~0.0110	0.0103
7	0.7910	Lat. bending as.	0.0090~0.0154	0.0121
8	0.8691	Ver. bending s.	0.0057~0.0085	0.0075
9	1.0205	Torsion as.	0.0049~0.0075	0.0056
10	1.1133	Ver. bending as.	0.0079~0.0096	0.0089

***: symmetry; **:ansymmetry**

6. CONCLUSIONS

The bridge monitoring should be started during the early age after completion of the construction in order to observe infrastructure settlement and superstructure deformation and promptly to detect structural deficiencies and damage trend. It is unfortunate that the chance to build basic data was missed when the Queshi bridge had been completed in 1998.

It is of great importance to choose the appropriate methods and instruments for long-term structure monitoring in terms of reliability, durability and long-term cost. The measurement of cable force using vibrating principal is not only an efficient method than others, but also very reliable. Based on current case study, there are no much differences in terms of the portability or the efficacy between the wire and wireless sensors. The total station with high accuracy is adequate to measure the deformation of the long-span bridge and provides crucial information of the global structural health status as well. It is also very convenient since it is able to be put into measurement at anytime after the completion of construction. The technique of the modal test and analysis of the bridge structure also seems to be working well although the complete evaluation is still to be finished. However, the challenge remains, which is how to make use of the established database to assess the structural variation or disaster. The monitored structural parameters must be rational and useful for rating the structure health status during the life time. "*If you don't do something, it's no use to monitor*" [3].

ACKNOWLEDGEMENTS

The financial support of this project was provided by Queshi Bridge Lt. Co. in Guangdong province in China. The engineers from Leica have being provided many help in this long-term monitoring project.

REFERENCES

1. Dept. of Tongji University, "The report of monitoring for Queshi bridge on service-term" (Chinese) , Tongji University, Shanghai, China. 2001, 2002 and 2004.
2. Craig D.Hill, Karl D.Sippel, "Modern Deformation Monitoring: A Multi Sensor Approach", Switzerland, FIG XXII International Congress, Washgton, D.C. USA, April 19-26, 2002.
3. Fu-Kuo Chang "A summary Report of the 2nd Workshop Structural Health Monitoring", Stanford University, Stanford, CA. 1999

STRUCTURAL HEALTH MONITORING SYSTEM APPLICATIONS IN JAPAN

Sunaryo Sumitro
Keisoku Research Consultant Co. Ltd., Japan

Ming L. Wang
University of Illionis at Chicago, USA

Abstract: Maintenance management of infrastructures has been one of the particular concerns of the engineering community and responsibility of the citizens in Japan to deliver their heritages in a sustainable performance to their next generation. In this paper, Structural Health Monitoring Based Maintenance (SHMBM) aimed to reduce structures' Life Cycle Cost (LCC) is reviewed. Structural Health Monitoring (SHM) system equipped with Elasto-Magnetic (EM) sensory technology to retrieve the actual stress structural information is discussed. Finally, some examples of in-site applications are provided to illustrate the utility-reliability of the SHM system.

Key words: Sustainability, LCC, SHMBM, Elasto-magnetic, SHM system.

1. INTRODUCTION

About one and a half centuries ago, construction materials have been enriched by steel and concrete. The distinguishing characteristics these two materials, such as 'easy form', 'high strength', have grown up and speedup the construction of infrastructures significantly. Even the combination of steel and concrete was believed to be one of the innovative composite to provide 'maintenance-free' construction material.

However, contradiction to the 'initial wish' as maintenance-free materials, significant deteriorations spread out everywhere. Especially in the last decades, fatigue and corrosion of steel structures and frost damage, alkaline silica response (ASR), carbonation of concrete structures, become serious issues. These phenomena occurred in the time when the 'true life' of

Farhad Ansari (ed.), Sensing Issues in Civil Structural Health Monitoring, 495–504.

steel and concrete have not been verified yet. Therefore, it gives 'critical feel' to us since we wish their health life at least to be 150 to 200 years.

If the deterioration propagates as the current speed, in a near future, preservation of the accumulated infrastructures' inventory need a huge amount of reinvestment and it will shake the national financial cores from the root at most countries all over the world. Therefore, the only one choice of the possible solution which can be expressed as: identify the current degraded condition; stop the structural deterioration process; choose a suitable repair/retrofit strategy to a certain service level; perform health monitoring systematically; and reduce LCC to provide the possibility to sustain the structural performance of those currently 'still-health' existing infrastructures.

As a serious social problem, Japan is facing the increasing of aging people and lacking of younger people. Actually as another most serious problem besides the increasing of aging people is the increasing of aging infrastructures. Fig.1 shows the estimation of the amount of investment to the public facility published by Ministry of Land, Infrastructure and Transport Japan. The amount of investment for maintenance and renew will be 70% compared to 20% for new structures in near future. Furthermore, it is also reported that in the year 2036 the 50 years old deteriorated civil infrastructures will become more than 100,000 (one hundred thousands) bridges.

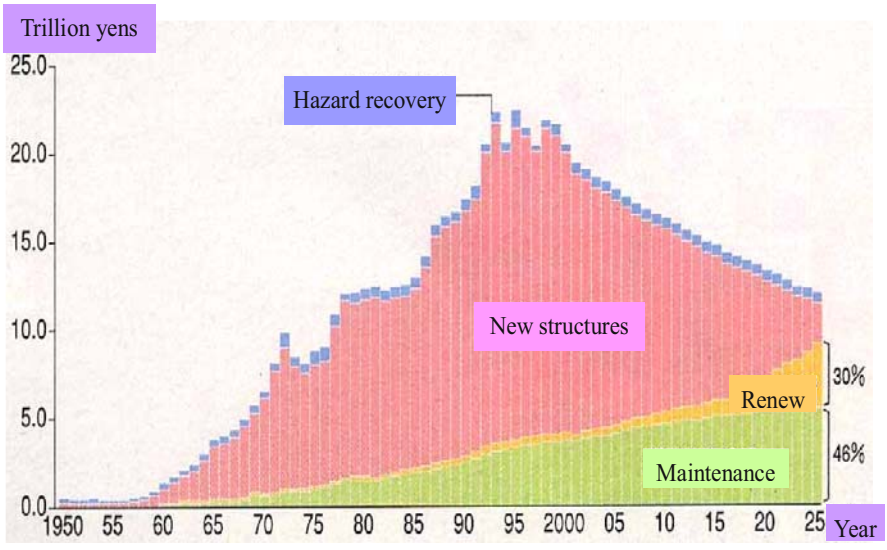

Figure 1. The estimated investment on the infrastructures in Japan (Ministry of LIT).

2. SHMBM ENGINEERING

Due to aging effect, the life of civil engineering structures is limited by its functional, beneficial and safety factors [**2**]. How to extend the structures' life is the wish of civil engineers. In the case to prolong human life, it is possible to train the body at the youth time, to maintain the health of the body by providing periodical medical checkup and suitable medical treatment. Similarly, in the case of civil infrastructures, it is possible to prolong the structural-life by utilizing Structural Health Monitoring Based Maintenance (SHMBM) Engineering i.e., a Universal Construction & Maintenance Management Paradigm based on the field structural information in order to optimize Life Cycle Cost (LCC) [**3**].

The objectives of this engineering are: (1) to manage the life cycle of structures in the stages of plan, execute, monitor, maintain, and rebuild in a most reasonable way to provide safety and healthy performance systematically; and (2) to keep in a minimum level of lost due to earthquake, typhoon and other unanticipated loads. SHMBM is the basic technology to collect maintenance information, forming a database system to open to the public or citizens for making decision on a suitable solution strategy to extend structure's life. In practicing this concept, citizens are not just as users but also as the owners of infrastructures.

2.1 Utilization

By considering theoretical background of SHMBM, efficient monitoring technique and related effective technologies in the areas of condition and health assessment, deterioration science and renewal engineering are carried out and can be summarized as listed in Table 1.

Table 1. Task flow in SHMBM

Task 1 Documentation	Prepare data base of the infrastructures
Task 2 Investigation and Assessment	Utilize high performance sensor to inspect, evaluate and assess current safety and health condition of the structures
Task 3 Prediction and Simulation	- Utilize LCC management - Predict future degradation condition - Analyze financing scheme - Examine suitable extend life strategy
Task 4 Publication	Open the identified current information of structural health condition to public as the owner of those infrastructures (it may be accessed through internet)
Task 5 LCC reduction	Reduce LCC by modifying design, revising design code, application of newly developed innovative material and developing new technology in construction method

2.2 Structural health monitoring

The essence of structural health monitoring can be considered to involve measurement, inspection, and assessment of in-service structures on a continuous basis with minimum labor requirement [**1**]. The ideal scenario is considered to carry out real time inspection and damage detection through "intelligent" sensors.

Multiple sensors are comprised by a complete real time monitoring system with a digital network to acquire, process and store the measured data. In a periodical interval, the network returns the data to a central control room by cellular phone, satellite, or conventional telephone circuit. From there, the data is distributed confidentially via intranet or internet, therefore, one whose secret password can immediately asses the structure's condition from anywhere in the world without actually visiting structure's site as shown in Fig. 2. Such real-time, quantitative information greatly improves structural safety inspections and provides valuable information for directing timely maintenance relief to those areas of the structure most in need of repair, so structural life of structures can be extended and the current structural performance can be grasped.

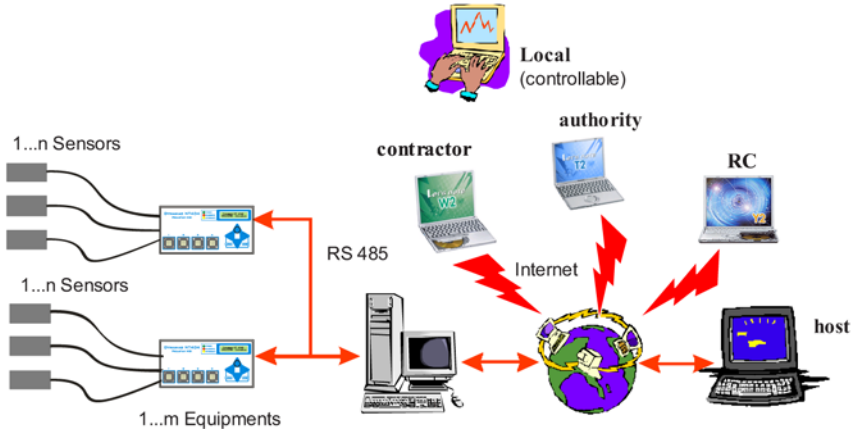

Figure 2. Health Monitoring system network.

2.3 EM sensory technology

The Elasto-Magnetic (EM) sensory technology is a simple nondestructive evaluation (NDE) technique for monitoring actual stress in steel cables based on observation in magnetic permeability respect to stress change. The

magnetization phenomenon is performed by two solenoids, i.e., a primary coil and a secondary coil. Pre-fabricated EM sensor (see Fig. 3) takes the form of a hollow cylinder in the middle of which the measured object (wire, strand, tendon, bar) passes through. It should be slipped onto the measured object beforehand.

In case of existing structure, the sensor is wound on the tendon or reinforcement in-situ by fixing two halves cylindrical bobbins as shown in Fig. 4 [**4**]. This type of EM sensor enables to measure actual stress of external tendons in outer tendon PC bridge, steel cables in cable stayed bridge and suspension bridge, and steel embedded in concrete without the necessity to install the sensor during the construction period [**5**]. This cylindrical EM sensor has no mechanical contact with the measured element so it will not be over-loaded, it is resistant to water and mechanical injury, its characteristics does not change with time and its lifetime is predicted to be at least 50 years.

EM Sensory technology application procedure is ease in operation, user-friendly, and time consumed for measurement is close to real time measurement. The EM sensory system principle (see Fig. 5) is designed as a compact system and user-friendly basic unit with the innovative features such as, remote/local mode, battery powered, automatic sensor identification, local back-up memory for 100 measurements, precise auto-calibrated integrators and fast multipoint measuring system.

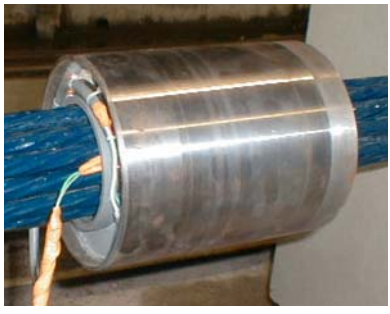

Figure 3. Pre-fabricated sensor.

Figure 4. Site-fabricated sensor.

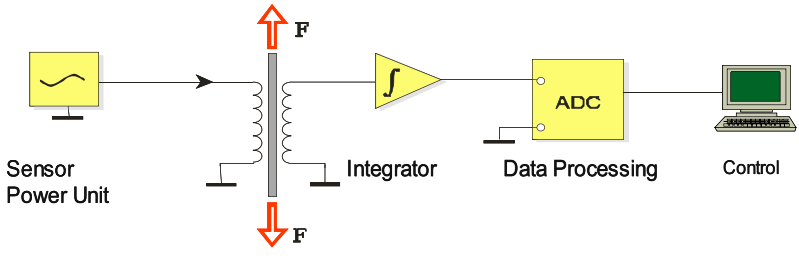

Figure 5. EM sensory system principle.

3. APPLICATIONS OF SHM SYSTEM

Some application examples of structural health monitoring system in civil engineering infrastructures will be introduced such as, intelligent ground anchorage, actual stress monitoring on space structure, PC-box-girder bridge, and cable-stayed bridge.

3.1 Ground anchor

Since an accident of ground anchorage failed, the tendon flew over distance of 200m, It is insisted to perform structural evaluation for existing ground-anchorages and directed to conduct Structural Health Monitoring System in at least 5% of newly constructed ground-anchorages.

A field-verification project for new EM sensory technology to monitor the actual stress of existing ground anchor was conducted in Kyushu prefecture. In order to make it possible for EM sensor installation, an anchorage shoe was constructed as illustrated in Fig. 6. The EM sensory results were compared with FBG fiber optic sensory results and hydraulic-jack-pressure results. Since another SHM method had some trouble and retired on the way, it is confirmed that EM sensory technology, as shown in Fig. 7, enable to provide reliable long-term monitoring system.

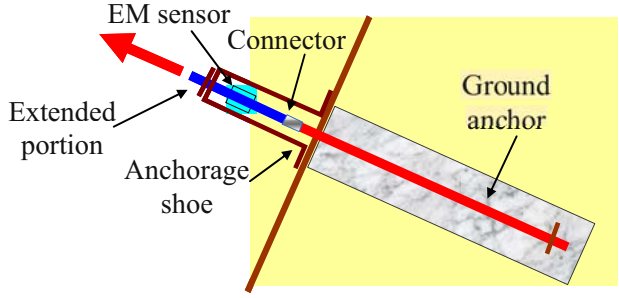

Figure 6. Proposed SHM for existing ground anchor.

Figure 7. Intelligent ground anchor.

3.2 Space structure

Kumagaya dome is a huge elliptical space structure with major axis length of 250m, minor axis length of 150m and height of 45m. The roof is supported by a dome structure with 1200 bracing cables in a 3D wire frame model. Up to now, current strain gauge and/or torque method are commonly applied to control the displacement during construction stage. However, those measurement methods cannot provide structural deformational information during service life of the structure. Therefore, EM sensory technology was introduced and installed in the middle as shown in Fig. 8 to monitor the actual stress of bracing cable.

EM sensors were installed at half of the 1200 bracing cables to enable to monitor global structural movement of the space structure together with an actual-stress monitoring system. It can be considered as 'a breakthrough in space structure construction method' from short-term strain-monitored construction method to long-term actual-stress-monitored construction method.

Besides actual stress controlling during 'jack-up and jack-down' construction stage, this monitoring system enables to figure-out any desired sectional stress distribution at every loading stage. For the sake of convenience in controlling the actual stress of each cable bracing, the capability in expressing the history of wire stressing and summary of wire stresses were also implemented in the intelligent space structure monitoring system.

Figure 8. Intelligent space structure.

3.3 PC- box-girder-bridge

Kamikazue viaduct is a double box girder PC bridge which is formed by connecting two single box-girder pre-cast segments. This bridge consists of 1040 segments in 17 span continuous box-girders, has a length of 630 m and width of 16 m. The segments are erected by span-by-span method using movable false-work. Pre-fabricated sensors and site-fabricated sensors were placed as shown in Fig. 9, to control pre-stressing during construction and to monitor the long-term stress change due to steel relaxation, concrete creep and shrinkage, and concrete elastic deformation effect.

The field-measurement items are summarized as (i)measuring friction coefficient between external PC tendon and deviator; (ii)pre-stressing control during construction; and (iii)long-term structural health monitoring on external tendon PC bridge. Fig. 10 illustrates the actual-stress measurement results by EM1 and EM2 compared to pressure gage measurement results at different pre-stressing levels. By investigating those field-verified results, it is confirmed that EM sensor is the most reliable, stable and practical method to monitor cables' actual stress for long-term structural health monitoring and enables to provide reliable information for repair and/or re-strengthen strategy.

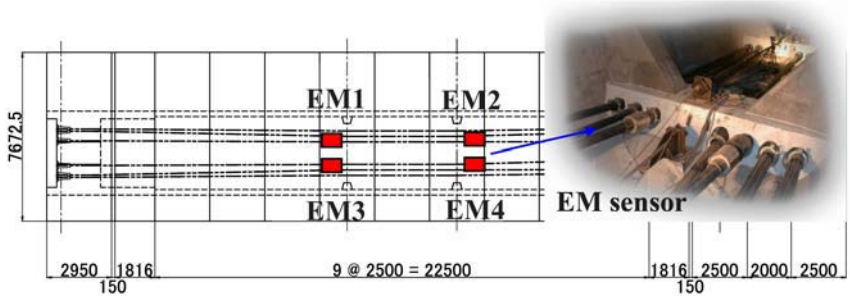

Figure 9. Sensor configuration.

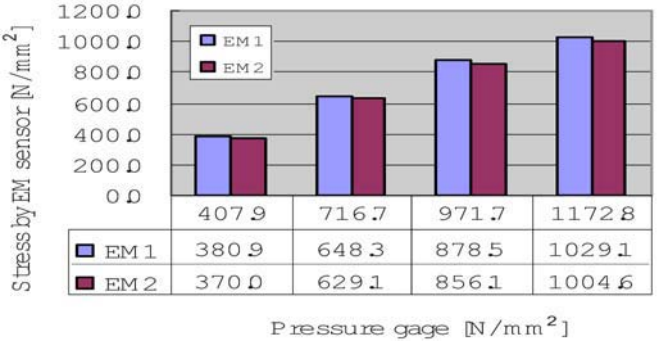

Figure10. EM measurement results.

3.4 Cable-stayed bridge

Ashidagawa bridge is a cable-stayed bridge with length of 491m located at Fukuyama City, Hiroshima prefecture Japan. The objective to utilize EM sensor is to control tensile stress during construction and monitor the actual stress performance during the service life of the bridge. The stresses of the stayed cables are also compared with forced vibration method.

The stayed cables are formed by parallel steel wires with diameter of 7mm. Five different diameters of stayed cables were used, i.e., 135mm, 160mm, 175mm, 185mm, and 195mm. Six EM sensors were installed in 3 different diameters (135mm, 155mm, and 165mm) of the total 18 cables. The sensor configuration is shown in Fig. 11.

The measurement results of six EM sensors which were installed in three different diameters (135mm, 155mm, and 165mm) together with their verified forced vibration test results are expressed in Fig. 12. By observing these results, it is confirmed that the EM sensors measurement results have good agreements with forced vibration test results and reliable to provide structural deformational information during the service life of the bridge.

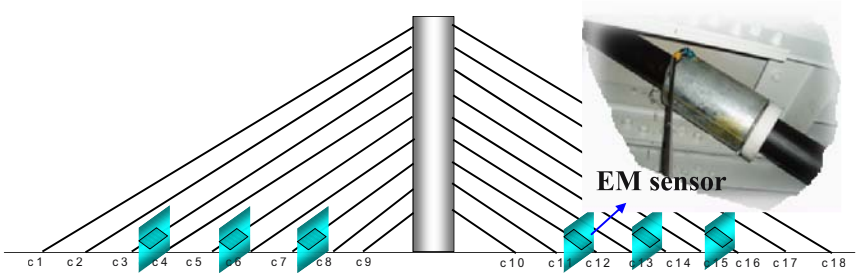

Figure 11. Sensor configuration.

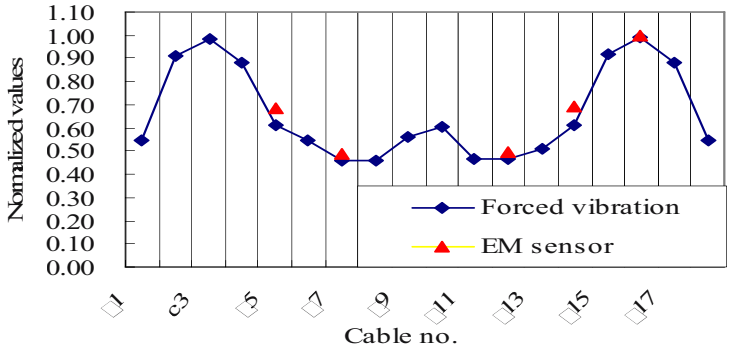

Figure 12. Comparison between EM sensor and forced vibration.

ACKNOWLEDGEMENTS

The authors would like to thank Prof. Andrej Jarosevic of Comenius University in Bratislava and Dr. Milan Chandoga of PROJSTAR PK s.r.o. at Bratislava for their collaborations in developing EM sensory technology.

NOTES

1. A sustainable structural health monitoring system with a digital network to acquire, process, store and transmit the measured data is discussed. The proposed sustainable monitoring system provides valuable information for directing timely maintenance relief to those areas of the structure most in need of repair, so the following items can be achieved:
   (1) Planned repair or replacement of the structure before catastrophic collapse;
   (2) Improved allocation of scarce maintenance funding for the highest risk structure member;
   (3) Determination of structural health after catastrophic events, such as earthquake, typhoon, fire, explosions and collision.
2. By observing numerous field measurement results, it is confirmed that EM sensory technology is a non-destructive, no-contact, easy to operate measurement system to measure actual stress of steel wires, bars and cables in many structural monitoring situations, even when other methods are inapplicable.

REFERENCES

1. Aktan E, Meystel A. "Real Time Intelligent Data Acquisition And Control Systems for Monitoring and Managing Infrastructure Networks", *Proc of the First fib Congress, Concrete Structures in the 21th Century*, Osaka, Japan, Oct. 13-19, 2002, pp. 205-214.
2. Frangopol M, Lin KY, Estes AC. " Life-Cycle Cost Design of Deteriorating Structures", *Journal of Structural Engineering*, **vol.**123, **no.**10, pp. 1390-1401, 1997.
3. Sumitro S, Tominaga M, Okamoto T, Kato Y, Kurokawa S. "Development of Monitoring Technology for Steel and Composite Structures", *Journal of Constructional Steel*, **vol.** 9, **no.**11, Nov., 2001, pp. 575-582.
4. Sumitro S. "True-stress measurement of PC steels by EM sensor", Special edition on Advance Technology, *Journal of Prestressed Concrete Japan (JPCEA)*, **vol.**43, **no.**6, pp.99-103, 2001. (in Japanese)
5. Sumitro S, Jarosevic A, Wang ML. "Elasto-Magnetic Sensor Utilization on Steel Cable Stress Measurement", *Proc of the First fib Congress, Concrete Structures in the 21th Century*, Osaka, Japan, Oct. 13-19, 2002, pp.79-86.

LONG-TERM MONITORING OPERATION OF THE TEST-ROAD IN KOREA HIGHWAY CORPORATION(KHC)

J. H. Jang[1], J.H. Jeong[2], S.M. Kwon[2], and H.G. Park[3]
[1] *EJtech Co., Ltd, Korea*
[2] *Korea Highway Corporation, Korea*
[3] *NewConsTech, Korea*

Abstract: This paper presents the monitoring system installed in a test-road built in 2002 to establish and develop pavement techniques and performances in Korea. The test-road, located 1 km far away from Yeoju IC in the central part of the peninsula, is a two-lane road of 7.7 km constituted by both concrete and asphalt pavements designed with 25 and 33 different sections, respectively. A total of 1,900 sensors of 11 types including strain gauges, soil pressure gauges and thermocouples were embedded in pavement sections to investigate their behavioral characteristics under environmental and traffic loadings. Both manual and automatic monitoring systems were installed. The automatic monitoring system stores and transmits regularly measured data to the server. The manual monitoring system is composed by a system storing temperature and water content data measured in the pavement sections and, a system constituted by a weigh-in-motion system, which provides information on the traffic crossing the test-road, and an automatic weather observation station. The manual monitoring system connects directly sensors embedded in the test-road to the data loggers installed on field so that users can easily acquire desired data obtained by experiments or field tests. Static and dynamic load tests as well as FWD impact load tests were performed for concrete pavement, and dynamic load and FWD impact load tests for asphalt pavement. Visual inspections were also carried out to investigate damages of pavement sections or unusual features. These automatic and manual monitoring systems will provide numerous and necessary information for researches on road pavement including the establishment of pavement design.

Key words: Automatic and manual monitoring systems, asphalt pavement, concrete pavement, field test, test-road, embedded sensor.

Farhad Ansari (ed.), Sensing Issues in Civil Structural Health Monitoring, 505–514.

1. INTRODUCTION

The concept of hometown is so deeply anchored in the mind of Korean people that one cannot separate the very intimate relationship between a Korean and the soil of his birthplace. This concept may also be applied for road pavement since its design should fit with the domestic environment as well as with the traffic and material characteristics. However, in spite of such peculiarity requirement, pavement design in Korea still remains based on foreign design methods. Currently, Korean pavement is designed according to the AASHTO Specifications, which is not only far from being able to reflect the unique environment, traffic and material characteristics of Korea but also leads to numerous examples of formal pavement design due to the difficulty encountered in applying design parameters. Such formal design may result in conservative design, which produces non-negligible rise of initial costs, or scanty design, which causes financial losses due to early damages. Following, a pavement design method appropriate to Korean conditions will undoubtedly lengthen the service life of pavement. Moreover, repair period will also be extended that will reduce the budget invested for maintenance and bring other economical benefits related to the diminution of accidents and traffic jams due to incessant repair works, or vehicle damages that may occur due to broken pavement.

Consequently, the test-road constructed in Korea will contribute significantly to researches on pavement design method appropriate to the domestic conditions as well as researches devoted to construction materials produced in the peninsula since it is subject to Korean climatic environment and traffic conditions corresponding to highway traffic volume. The research outcomes expected to result from this test-road are:

(1) Establishment of a Korean-type pavement design method,
(2) Development of durable pavement system,
(3) Provision of optimal pavement maintenance program, and
(4) Implementation of preventive maintenance concept.

2. TEST-ROAD

The test-road is constituted by two lanes of 7.7 km beginning at a distance of about 1 km in the southern direction far away from Yeoju IC and running in parallel to Jungbu Inland Expressway (Fig. 1), of which design began in March, 1997 and construction ended on December, 2002. Its official opening occurred on March, 2003. The test-road is managed by the Korea Highway Corporation (KHC). Fig. 2 depicts the overall composition of the test-road.

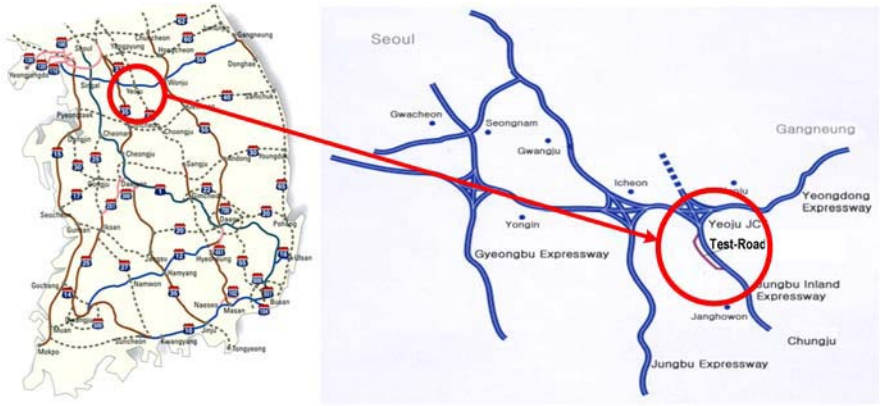

Figure 1. Location of the test-road, 1 km far away from Yeoju IC and parallel to Jungbu Inland Expressway

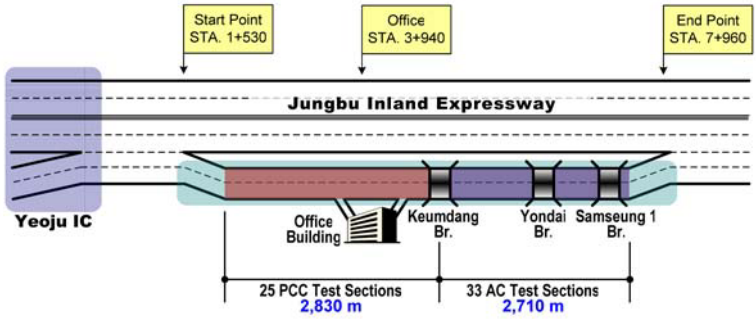

Figure 2. Overall view and composition of the test-road

The 7.7 km of the test-road are divided in two groups according to the type of pavement: asphalt and concrete. The concrete pavement group itself is composed by two types of pavement presenting a total of 25 sections: Jointed Plain Concrete Pavement (JPCP) and Continuously Reinforced Concrete Pavement (CRCP) with 22 and 3 sections, respectively.

The 22 JPCP sections were designed according to 3 design parameters: the concrete slab thickness (25, 30, 35 cm), the sub-base thickness (12, 15, 18 cm), and the sub-base material type (lean-concrete, aggregate, asphalt stabilizer).

Although 27 possible combinations may be obtained for these 3 parameters, the number of combinations has been reduced to the cases presenting a sub-base thickness of 15 cm applying aggregate and sub-base layer treated with asphalt stabilizer.

Three CRCP sections were designed according to a unique parameter that is the percentage of steel reinforcement (0.6, 0.7, 0.8 %). Additionally, steel-

fiber reinforced concrete, high-strength lean-concrete sub-base layer, cross-section without frost resistant layer, drainage base layer, and cross-section without dowel bar were also constructed in the test-road as functional pavement cross-sections. Fig. 3 illustrates the constitution of concrete pavement cross-sections.

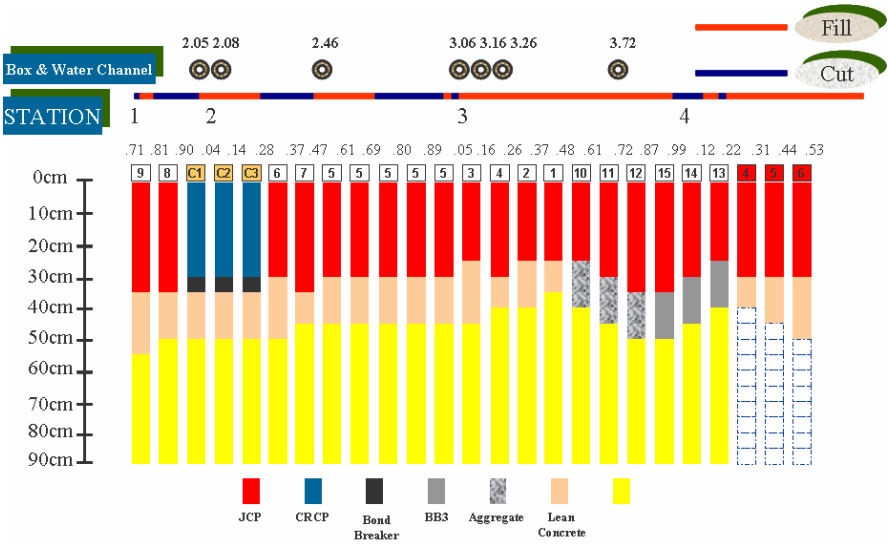

Figure 3. Layout of concrete pavement cross-sections applied in the test-road

Fifteen asphalt concrete pavement sections were selected with three design variables that are the base course thickness (15, 25, 35 cm), the base course material (asphalt with 25 mm aggregate, asphalt with 40 mm aggregate, aggregate), and the sub-base thickness (30 cm, 30 cm plus frost resistant layer, 40 cm). Here again, although 27 combinations may be obtained using these 3 parameters, asphalt stabilizer mixed with 25 mm aggregate, which is the basic design method of KHC, was applied in all cases, but 40 mm asphalt stabilizer and aggregate were applied only for the case of basic cross-section (sub-base of 30cm plus frost resistant layer). This reduced the number of possible combinations to a total of 15 different cross-sectional types. To examine the effect of materials used in the surface layer, the sub cross-sections were paved using PMA and SMA to the basic cross-section only. Consequently, a total of 33 cross-sections for the asphalt pavement were constructed (15 + 3 (base thickness) × 3 (sub-base thickness) × 2 (surface layer material)). Fig. 4 illustrates the constitution of asphalt pavement cross-sections.

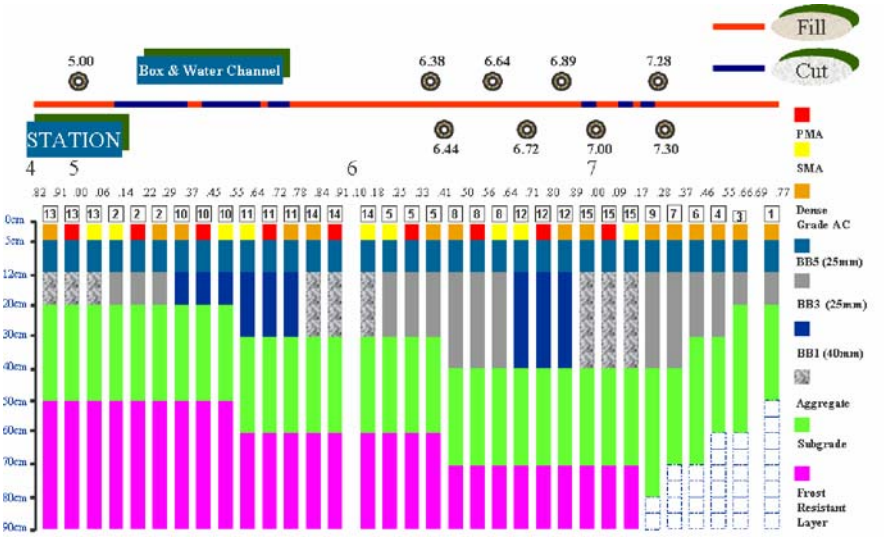

Figure 4. Layout of asphalt pavement cross-sections applied in the test-road

3. MEASUREMENT SENSORS

In order to monitor load-associated pavement responses and environment-associated long-term pavement performance, a total of 1,261 sensors of 11 types were installed in the concrete test pavement sections, and 636 sensors of 6 types in the asphalt pavement sections. These sensors are strain gauges, soil pressure gauges, thermocouples, crack measurement gauges and water content gauges.

About 1,900 sensors were installed in the KHC test-road to monitor the pavement behavior under traffic loads and environmental changes. These gauges are constituted by 11 types of sensors as shown in Fig. 5 and Table 1. In addition, Weigh-In-Motion (WIM) and Automatic Weather Station (AWS) are available and they provide the traffic and environmental data.

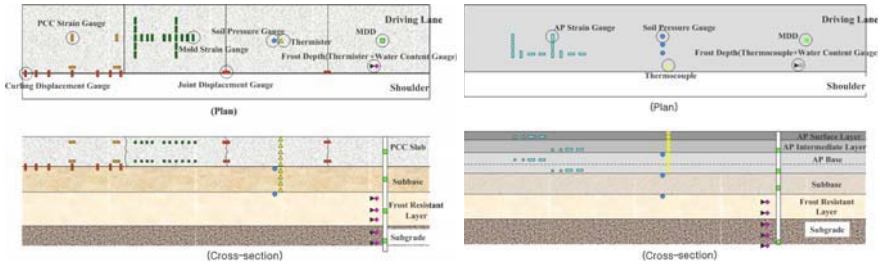

(a) (b)

Figure 5. Location of the sensors installed in the test-road: (a) Concrete pavement section; (b) Asphalt pavement section

Table 1. List of the gauges installed in the KHC test-road

Pavement type		PCC	AC
PCC strain gauge		638	–
Steel strain gauge		48	–
AC strain gauge		36	374
Mold strain gauge		132	–
Soil pressure gauge		34	66
MDD		4	6
Curling displacement gauge		51	–
Joint displacement gauge		120	–
Thermister or thermocouple		140	112
Frost depth gauge	Thermister	30	39
	Water content gauge	30	39

The following describes the measurands and locations of each type of sensor installed in the test-road.

- Concrete strain gauge: Embedded in the concrete slab to measure compression-tension behavior at the top of the test sections induced by traffic and environmental loadings.
- Asphalt strain gauge: Embedded in the surface, intermediate (BB5) and base (BB3) layers of asphalt sections to measure compression-tension behavior at the top of the test sections induced by traffic and environmental loadings.
- Soil pressure gauge: Embedded in the bottom of the test sections to measure compression forces transmitted to the bottom of the pavement sections and, following, to measure load distribution all along the depth.
- Water content gauge and thermister for the bottom of pavement: Estimate the frozen state of the pavement bottom by measuring the temperature and water content of the road surface according to the characteristics of the test section.

• Lean concrete thermister: Used to observe thermal variations per depth at the bottom of the pavement and the long-term evolution of temperature according to seasonal changes.

• Steel strain gauge: Installed by adhesion on the steel rebar of the CRCP to measure compression-tension behavior in steel induced by traffic and environmental loadings.

• Mould strain gauge: Embedded transversally and longitudinally in series at the bottom of the concrete slab to evaluate the stress distribution inside the test slab induced by traffic static loading.

• Crack and curling gauges: Measure the behavior of joints and curling development patterns in the concrete slab according to variations of temperature and humidity.

• Asphalt thermister/thermocouple: Used to observe thermal variations per depth at the bottom of the pavement and the long-term evolution of temperature according to seasonal changes.

4. MONITORING SYSTEM

Both automatic and manual monitoring systems have been considered for field data acquisition system installed in the KHC test-road in order to improve its efficiency and continuity.

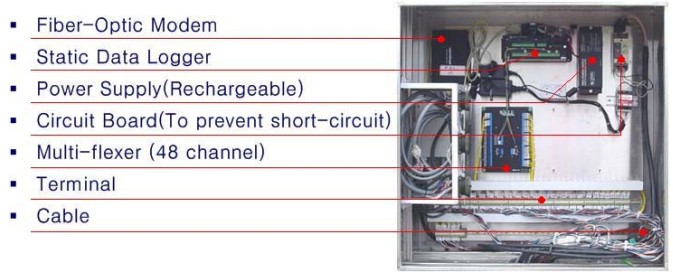

Figure 6. Automatic monitoring circuit box

Two types of automatic systems have been implemented. The first system exploits thermometer and water content gauges to measure the evolution of temperature and water content in the pavement layers according to weather changes. As depicted in Fig. 6, a fiber-optic communication network connecting the gauges to the server has been set up. The monitoring circuit boxes, consisting of static data logger and fiber-optic modem, are installed throughout a total of 15 cross-sections of the test road. The data logger is equipped with a rechargeable battery, so that measuring and storing of field data for a maximum period of one month can be performed even in

the case of power failure. Moreover, when the power is restored, the data logger can be connected again to retrieve the saved data and store them in the database of the test road.

The second system is composed of WIM system and automatic weather observation station. The WIM system has been installed to measure accurately cumulative passing-through traffic volume on the test road. It can gather such information as 11 vehicular types, vehicular axial weight, total vehicular weight, passing speed, distance between axles, distance between vehicles, etc.

Instruments like strain gauge, soil pressure gauge, curling and joint displacement gauge, etc., measure responses corresponding to particular loading or temperature change pattern. Following, the optimal exploitation of these instruments may be obtained through the manual monitoring system to control public traffic on the test road, to apply a particular loading or to measure responses at a given time. For this purpose, the manual monitoring system consists of a complex system: data gathering vehicle, loading control system to apply a particular loading, 58 manual monitoring circuit boxes connecting the gauges to the data gathering device, static data logger (which can measure continuously during a predetermined time), and driving information monitoring system to measure the driving (dynamic) information of testing vehicles. Fig. 7 illustrates the manual monitoring system.

Figure 7. Manual monitoring system

5. FIELD TEST

The following series of tests were performed using the manual monitoring system for the road section paved with concrete.

 Static loading test using vehicle load: Vehicle load has been applied on the concrete slab using a dump truck and the behavior of the pavement test section has been analyzed regard to the measured items that are the temperature, strain and soil pressure.

- Dynamic moving load test using vehicle load: The dynamic behavior of the pavement test section has been analyzed regard to the temperature, strain and soil pressure measured during the crossing of a dump truck moving at a constant speed. A wandering system has been also used to measure the moving speed of the vehicle and the elongation distance between the sensors and the vehicle wheels.
- FWD impact loading test: Analysis of the behavior of the pavement test section subject to impact load has been performed using FWD equipment. The measured items were the temperature, strain and soil pressure. The deflection of the surface of the slab and the FWD impact load were also measured in the vehicle carrying the FWD.
- Test for the acquisition of curling and joint behavior data: The transversal and longitudinal behaviors of the concrete slab subject to environmental loading have been measured at regular time intervals using a portable static data logger. Crack displacement gauges were used to measure joint and curling displacements.
- Traffic and environmental loading test: The behavior of the concrete slab subject to environmental and traffic loads has been analyzed using data measured every two hours during static loading test and FWD impact load test. The measured items were the temperature, strain and soil pressure. The deflection of the surface of the slab and the FWD impact load were also measured in the vehicle carrying the FWD.
- Test determining the radius of influence of load: A total of 142 strain gauges were embedded at a proportion of 44 gauges in a slab section to measure the area of influence of FWD impact loading. The measured items were the temperature and strain. The deflection of the surface of the slab and the FWD impact load were also measured in the vehicle carrying the FWD.

The following series of tests were performed using the manual monitoring system for the road section paved with asphalt.

- Dynamic moving load test using vehicle load: The dynamic behavior of the pavement test section has been analyzed regard to the temperature, strain and soil pressure measured during the crossing of a dump truck moving at a constant speed. A wandering system has been also used to measure the moving speed of the vehicle and the elongation distance between the sensors and the vehicle wheels.
- Evaluation test of the physical properties of asphalt using FWD: The asphalt pavement has been subject to FWD impact load test during 24 hours using the FWD equipment. And, the corresponding variations of the physical properties of asphalt pavement were measured according to thermal changes. A portable thermometer was used to measure the temperature at the pavement surface, and the deflection of the surface of the slab and the FWD impact load were also measured in the vehicle carrying the FWD.

6. CONCLUSIONS

Pavements in Korea are currently designed according to road pavement design specifications developed by USA and Japan, which produce pavement design that cannot reflect the unique domestic characteristics. To remedy the absence of appropriate pavement design, the KHC undertook, since 1997, researches on test-road for long-term development of pavement design specifications and improvement of pavement-related technologies, which resulted in the completion of a test-road in December, 2002 and its opening to traffic in March, 2004.

The KHC test-road, the first operational test-road in Korea as well as in Asia, will make it possible to design optimal pavement thickness and to select efficient pavement and maintenance materials by means of long-term monitoring data. The final objective is to extend the lifetime of pavement constructed in Korea and reduce the budget invested for its construction and maintenance.

REFERENCES

1. Kim DW, Kim JW, Kwon SM, and Yun KK "Installation and Application of Concrete Pavement Strain Gauges", *Proc. Of the KOSPE Conference*, KOREA, Oct. 2003, pp. 173-180
2. Kwon SM, Lee JW, Kim JW, and Ahn SS "The Present Condition of KHC Test Road Data Acquisition System" *Proc. Of the KOSPE Conference*, KOREA, Oct. 2003, pp. 327-332
3. Lee JH, Kim JW, Kim DH, and Lee KH "Improvement of field Installation Method for Asphalt Concrete Pavement Strain Gauge", *Journal of the Korean Society of Pavement Engineers*, Vol. 5, No. 3, pp. 31-42, 2003.

PIPELINE BUCKLING DETECTION BY THE DISTRIBUTED BRILLOUIN SENSOR

Fabien Ravet[1], Lufan Zou[1], Xiaoyi Bao[1], Liang Chen[1] ,
Rong Feng Huang[2], and Heng Aik Khoo[2]
[1]*Fiber Optic Group, University of Ottawa, 150 Louis-Pasteur, Ottawa, Ontario, Canada, K1N 6N5*
[2]*Department of Civil and Environmental Engineering, Carleton University, 1125 Colonel By Drive, Ottawa, Ontario, Canada, K1S 5B6*

Abstract: We conducted strain characterization experiment to monitor steel pipe buckling for the first time using distributed Brillouin sensor system. One specimen was prepared by locally thinning the inner wall to initiate buckling. An axial load was applied to the specimen and increased while compressive strain was measured by both Brillouin sensor and the strain gauges. With the Brillouin sensors, we observed compression in the whole specimen while elongation was detected in the neighbourhood of the thinned wall at onset of the buckling for the first time. The buckling was identified and localized with the Brillouin sensor measurement.

Key words: Distributed sensors, Brillouin scattering, pipeline, buckling, compression and tension

1. INTRODUCTION

In the past decade, the demand for safe infrastructure and power supply has dramatically increased in our society. The pressure on civil engineering, oil and utility industries has grown similarly. Our society requires not only a growth in the supply of the services but also improvement of the safety on the supplying chain. These requirements turn

Farhad Ansari (ed.), Sensing Issues in Civil Structural Health Monitoring, 515–524.

Structural Health Monitoring (SHM) into a key element of these industrial businesses. Current techniques used for SHM are localised devices giving only partial information on the stresses that affect the monitored structure. There is a need for a technique that allows distributed temperature and strain measurements in real time over lengths of a few meters to tenths of kilometres. The Brillouin Optical Fibre sensor (BOFS) technique has the advantage to combine all these characteristics [**1-5**].

Strain monitoring of steel structures with the Brillouin sensor has been reported in lab condition [**6**] (constant temperature) and field with temperature compensation [**7**]. These studies are of great interest. In fact, on the one end the environmental effects can degrade the pipeline structure [**8-9**] when operating temperatures and pressures for sub-sea oil and gas pipelines have dramatically increased. On the other end, the technology evolves to the use of larger diameter pipes. The combination of these two elements has increased the possibility for pipes to buckle. Buried land and offshore pipelines commonly suffer upheaval buckling where the pipe extricated vertically from protective trench, especially in northern regions where permafrost is encountered. Another mode of failure is for the pipe wall to buckle locally. Such environmental condition varies periodically inducing excessive constrains to the pipeline and generating buckling by combined effect of large temperature and pressure changes. Therefore pipeline integrity is threatened and must be monitored to prevent any leakage that can lead to costly situations: the energy supply chain is broken and affects services, the environment needs to be cleaned and the image of the industry is damaged.

The need for pipeline SHM is a critical issue that must be addressed. This paper demonstrates that Brillouin sensors are capable to fulfill such a task, and we identify the starting of pipe buckling in location and corresponded the compression and tension simultaneously for the first time.

2. BRILLOUIN SENSOR SYSTEM

The sensing medium of the BOFS is a standard single-mode fibre. Two laser columns are injected into this fibre in a counter-propagating configuration. An interaction between the two columns happens when the frequency difference of the two lasers matches the frequency of the acoustic phonons of the optical fibre. There is then a transfer of energy from the high frequency column (pump) to the low frequency column (probe). The amount of the loss of the pump is recorded at one end of the fibre as a function of the frequency difference in the form of Brillouin spectrum. The maximum loss occurs at the Brillouin frequency (ν_B), which is the phonon frequency. An experimental spectrum measured in the present trial is shown

in Figure 1 for pulses of 1.5ns. It has been taken from an unstressed part of the fibre to provide a reference. Two parameters are extracted from this spectrum: the Brillouin frequency (ν_B) and the relative peak power (RPP). The BOFS can record the Brillouin loss curve at different location along the fibre. The spatial resolution (w) is determined by the pulsewidth ($\Delta\tau$), which is 15ns in our case, with relation of $w = v_g \Delta\tau / 2$ where v_g is the pulse group velocity in the optical fibre. Measurement is taken every 5cm. The spatial resolution w may have the following consequence: if the defect size is smaller than w, the measured strain in this condition may be underestimated [**6**,**10**] .

The Brillouin Frequency changes linearly with temperature and strain [**1-5**]. The relationship between the Brillouin frequency variation and strain when temperature remains unchanged is $\varepsilon = (\nu_B - \nu_{0B}) / C_\varepsilon$ where ε is the tensile strain, ν_B is the Brillouin frequency shift when the fibre is strained, ν_{0B} is the Brillouin frequency shift of the unstrained fibre and C_ε is the strain proportionality coefficient [**1,3-5**] with $C_\varepsilon = 0.05941 MH / \mu\varepsilon$. The frequency step for the Brillouin spectrum measurement is 4MHz and the frequency range is 500-800MHz wide starting at 12500MHz.

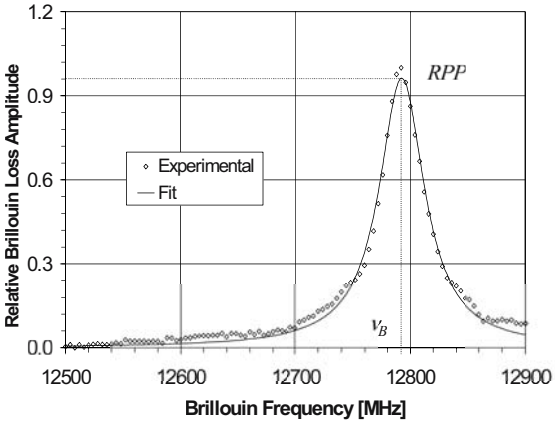

Figure.1. Brillouin spectrum measured on an unstressed part of the fibre. Peak is found to be 12792.56 MHz and the FWHM is 48.09 MHz. Curve fitting algorithm (Levenberg-Marquardt) is used to determine these values (R=0.99538522) by applying a Lorentzian profile fit.

3. EXPERIMENT DESCRIPTION

A steel specimen of 1m is tested with square end caps (20cm side length). The specimen has a cylinder shape with a diameter of 18cm. The location of buckling is controlled by thinning a small area of specimen inner walls at the mid-length, which induces weakness in the structure for buckling to occur at this region when an axial load is applied.

The specimen is instrumented with strain gauges and distributed Brillouin sensor. Figure2 shows the location of the fibres and strain gauges. The fibre is looped 8 times on the pipeline with 1m loose fibre separations. The strain gauges are distributed symmetrically about the mid-length of the specimen.

The specimen is placed on the test bench. The specimen is progressively compressed while the deformation is continuously monitored with the strain gauges and distributed sensor. The experiment is finished when the buckling happens. In the case of the pipeline, the buckling can be visually observed. In fact, the steel of the pipeline specimen starts to yield before buckling.

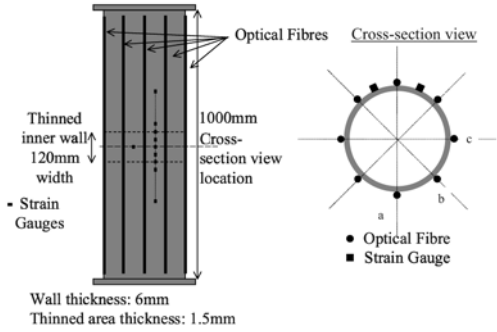

Figure 2. Pipeline specimen configuration and sensors layout.

4. MEASUREMENT RESULTS AND ANALYSIS

The pipeline is subjected to a gradual load increase from 0 to 730kN. The buckling happened after 730kN and the fibre was broken due to the small bending radius and rigid glue . Two load levels (350 and 700kN) were kept constant for 20 minutes in order to capture the Brillouin spectra distributions along the fibre. Figure 3 represents the Brillouin loss spectra measured in one of the 8 fibres section (b). The three curves show the effect

of the load increase: without load the Brillouin peak located at 12805MHz that is higher than the loose fibre Brillouin frequency. This is induced by the combination of small stress during the fibre installation and the drying of the glue. The peak frequency at 350kN configuration is downshifted from 12805MHz to 12750MHz corresponding to -220 $\mu\varepsilon$. The peak frequency is further reduced when 700kN is reached giving compression of -1296 $\mu\varepsilon$. The axial load to the structure causes this compression.

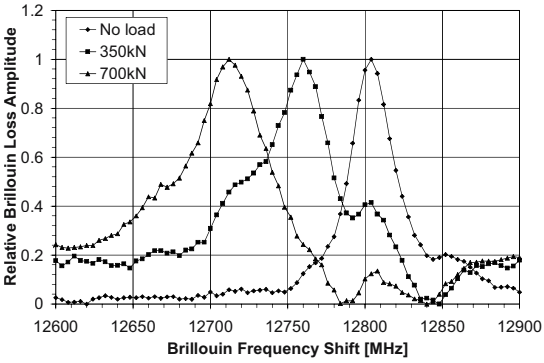

Figure 3. Brillouin Loss Spectra for three distinct loads measured at 244ns (section b), which is a located in the middle of the glued fibre section. The main peak is downshifted in frequency indicating that the pipeline is compressed.

Pipeline compression is confirmed by strain gauge, and comparison between strain gauge and the Brillouin sensor measurements shown in Figures 4 and 5 for various strips along the pipeline at 350kN and 700kN. Strain gauge readings and Brillouin sensor measurements appear to lie in the same strain range for a given load. Moreover the results indicate consistent behaviour for a load increase from 350kN to 700kN. As expected, the strain reading from distributed sensor is smaller than strain gauge reading, because the distributed sensor measures the average strain over 15cm (pulse length), while the strain gauge measured localized strain over 1cm. Due to non-uniform strain distribution as shown in Figure 3 for the spectrum at load 350 and 700kN, the spectrum is asymmetric and is broader than the unstressed Brillouin spectrum. The fitted central peak position is the convolution of all the different strains. The plotted strain is the averaged strain. The strain gauge reading corresponds only to one of the Brillouin spectrum at a specific location. Figures 3 and 6 represent the influence of strain gradient on the measured Brillouin spectrum.

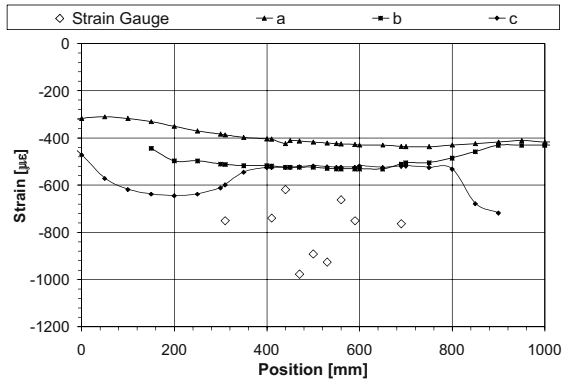

Figure 4. Pipeline Strain profiles obtained by Brillouin sensor and strain gauges measurement for the 350kN load applied. Labels a, b and c report the measurements obtained with the Brillouin sensor.

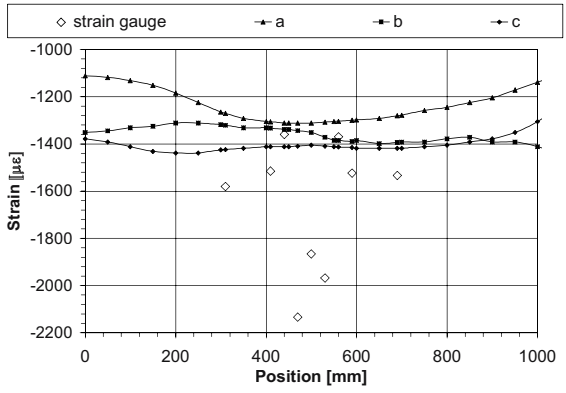

Figure 5. Pipeline Strain profiles obtained by Brillouin sensor and strain gauges measurement for the 700kN load applied. Labels a, b and c report the measurements obtained with the Brillouin sensor.

In the transition region between loose and glued fibre sections, spatial resolution covers loose and stressed fibres. It then leads to a spectrum composed of two and three peaks as illustrated by Figure 6. One peak corresponds to the loose fibre frequency peak while the other one is due to the load-induced strain. Both compressive and loose peaks have the same height, and the third peak represents tension at 700kN, which means that half of the pulse covers the strained section while the other half extends into the unstrained part of the fibre. This provides location between the loose and glued fibre, which can be used as a marker for our waveform location. Once a larger part of the pulse covers the strained section, the load induced peak power is higher than the unstrained peak. The detection of the transition region is improved by 5cm sampling period [**10**].

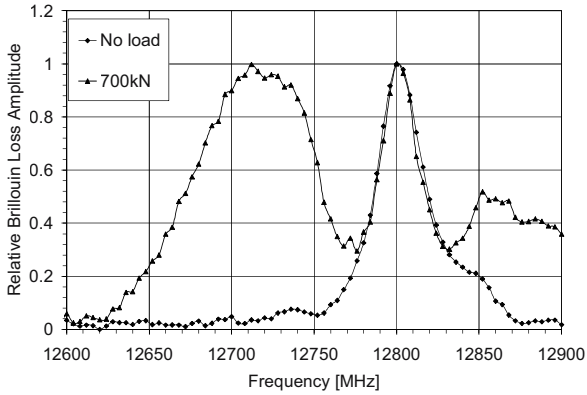

Figure 6. Brillouin Loss Spectra measured at 247.5ns (section b), which is located at the end of the glued fiber section. 700kN case has three peaks: Left (broad) and middle peaks characterize compression and loose fiber (unstrained contribution) with the same heights, while the right peak is the tension.

Compression is not the only effect we detected with the Brillouin sensor. In fact, we noticed the presence of a second peak, which has lower height representing short fibre length in the glued fibre regions as shown in Figure 7 and 8. These figures represent respectively three glued sections strain profiles. The load levels are 350 and 700 kN corresponding to the condition preceding the pipeline buckling. Peak 2 is associated with the compression (negative strain). As it appears in Figure 9 (spectrum measured at 220ns), the left peak (Peak 2) is bigger indicating that compression process is the major event for the pipe. Peak 1 (right peak) represents tension (positive strain). The tension increases as the applied load is raised as shown by the strain profiles in Figure 8, and the increasing amount of tension is not the same over the pipe, which indicates the non-uniform stress on the pipe. This may be due to the fact that the thinning of the inner wall is not perfectly uniform. So the buckling happened in position a and b first, and spread to position c finally. The interesting feature is that Peak 1 curve matches the unloaded curve value outside the stressed section but it becomes larger than the unloaded strain value in the middle of the stressed section (respectively at 220ns, 244ns and 264ns). Peak 1 RPP drops to 30% of the maximum spectrum amplitude indicating that the elongated length is very short. Obviously it is a very localized tension. We interpret such behavior as a signature of the buckling; the distributed location suggested it is in the thinned wall region. The whole pipeline suffers compression but a tiny part, axially distributed, must be extruded to elongate locally. The deformation is too small to be seen visually, but can be felt by pressing the hand on the surface. An inspection of Figure 9 confirms this point. This Figure shows three Brillouin Loss spectra around the stressed section. The 210 and 234 ns curves are associated with the loose fibre section with one peak at 12800MHz. Note that the Brillouin frequency shift measured here is higher

by 8 MHz when it is compared to the reference measurement of Figure 1. We attribute this shift to residual stresses induced by the fibre lay out between two glued sections because the fibre is taped and bent. The Brillouin spectrum at 220ns has two peaks: 1) compression (high loss); 2) elongation (low loss).

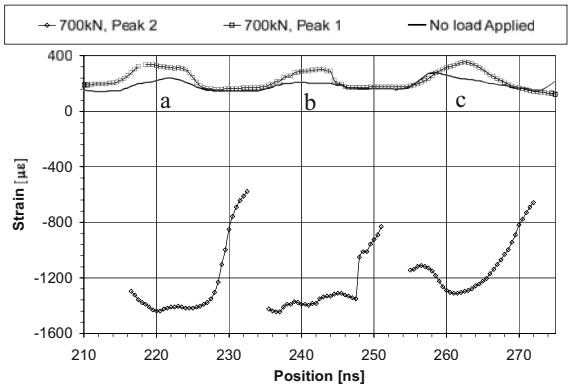

Figure 7. Strain profiles from Brillouin sensor measurements on three glued fibre sections for unloaded and (respectively sections a, b and c). 700kN and unloaded cases are reported.

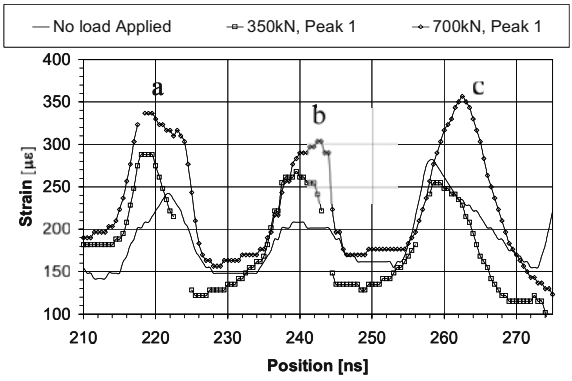

Figure 8. Strain profiles from Brillouin sensor measurements on three glued fibre sections for unloaded and (respectively sections a, b and c). 700kN, 350kN and unloaded cases are reported.

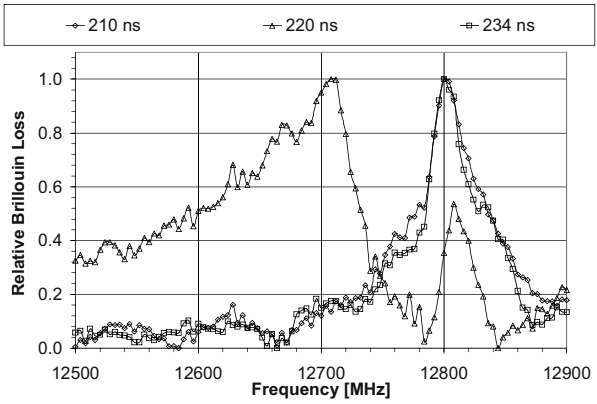

Figure 9. Brillouin Loss Spectra for three positions along the sensing fibre for a load of 700kN. 210 and 234 ns curves correspond the loose fibre section. Curve 220 ns is in the middle of the stressed section. In the 220 ns case, two peaks are observed. The left peak characterises compression while right peak is the tension contribution.

5. CONCLUSION

Buckling in a pipe has been detected and monitored successfully by the distributed Brillouin sensor system for the first time. The specimen was prepared by locally thinning the inner wall, which represents weakness to the pipe and induced buckling under the load. All the measurements showed a progressive increasing compression for the specimen as the load is increased. The Brillouin spectrum showed additional information: a small peak corresponds to the elongation of a short length element in the neighborhood of the thinned wall. The behavior was obvious for a load of 700kN, load preceding the buckling. Brillouin sensor is capable to monitor the buckling process and to localize the defect before it became visible. This is very important for warning of buckling and prevention of the costly disaster to the environment.

ACKNOWLEDGEMENT

The authors would like to acknowledge the financial support of ISIS Canada, Natural Science and Engineering Research Council of Canada. The discussions with Saeed Hadifaradji, Shahraam Afshar were of great help and much appreciated.

REFERENCES

1. M. Niklès, L. Thévenaz, P.A. Robert, "Brillouin Gain Spectrum Characterization in Single-Mode Optical Fibers", J. Lightwave Technol. 15, 1842-1851(1997).
2. X. Bao, J. Dhliwayo, N. Heron, D.J. Webb, D.A. Jackson, "Experimental and Theoretical Studies on a Distributed Temperature Sensor Based on Brillouin Scattering", J. Lightwave Technol. 13 (1995) 1340-1348.
3. J. Smith, M. DeMerchant, A. Brown, X. Bao, "Simultaneous Distributed Strain and Temperature Measurement", Applied Optics 38, No. 25, 5372-5377 (1999).
4. H. Naruse, M. Tateda, H. Ohno, A. Shimada, "Deformation of the Brillouin Gain Spectrum Caused by Parabolic Strain Distribution and Resulting Measurement Error in BOTDR Strain Measurement System", IEICE Trans. Electron., **E86-C**, 2111–2121 (2003).
5. T. Horigushi, K. Shimizu, T. Kurashima, M. Tateda, Y Koyamada, "Development of a Distributed Sensing Technique Using Brillouin Scattering", J. Lightwave Technol. **13**, 1296-1302 (1995).
6. L. Zou, G.A. Ferrier, S. Afshar V., Q. Yu, L. Chen, and X. Bao, "Distributed Brillouin scattering sensor for discrimination of wall-thinning defects in steel pipe under internal pressure", Appl. Opt. 43, 1583-1588 (2004).
7. X. Bao, M. DeMerchant, A. Brown, and T. Bremner, "Tensile and Compressive Strain Measurement in the Lab and Field With the Distributed Brillouin Scattering Sensor", J. Lightwave Tech. 19, 1698-1704 (2001).
8. R.A. Einsfeld, D.W. Murray, N. Yoosef-Ghodsi, "Buckling analysis of high-temperature pressurized pipelines with soil structure interaction", J. Brz. Soc. Mech. Sci. and Eng. **25**, 164-169 (2003)
9. A.C. Palmer, P.J. Williams, "Frost heave and pipeline upheaval buckling", Can. Geotech. J. **40**, 1033-1038 (2003).
10. D. Brown, M.D. DeMerchant, X. Bao, W.Bremner, "Spatial Resolution Enhancement of a Brillouin-Distributed Sensor Using a Novel Signal Processing Method in Single", J. Lightwave Technol. **17**, 1179-1183 (1999) .

SUBJECT INDEX